NASA CR-54680
RL-6278-SR

GPO PRICE $ _____
CFSTI PRICE(S) $ _____
Hard copy (HC) 9.26
Microfiche (MF) 3.00
ff 653 July 65

N66 26273 (ACCESSION NUMBER) (THRU)
626 (PAGES) 1 (CODE)
CR-54680 (NASA CR OR TMX OR AD NUMBER) 28 (CATEGORY)
FACILITY FORM 602

ION THRUSTOR ELECTRODE SURFACE PHYSICS STUDIES

by
R. G. WILSON

Prepared for
NATIONAL AERONAUTICS and SPACE ADMINISTRATION

CONTRACT NO. NAS 3-6278

HUGHES
HUGHES AIRCRAFT COMPANY
RESEARCH LABORATORIES
3011 MALIBU CANYON ROAD
MALIBU, CALIFORNIA

NASA CR-54680
HRL-6278-SR

SUMMARY REPORT

ION THRUSTOR ELECTRODE SURFACE PHYSICS STUDIES

by

R. G. Wilson

prepared for

NATIONAL AERONAUTICS AND SPACE ADMINISTRATION

CONTRACT NAS 3-6278

Technical Management
NASA Lewis Research Center
Cleveland, Ohio
John Ferrante

HUGHES RESEARCH LABORATORIES
Malibu, California

TABLE OF CONTENTS

LIST OF ILLUSTRATIONS v

ABSTRACT xiii

SUMMARY xiv

I. INTRODUCTION AND CONCLUSIONS 1

II. EXPERIMENTAL DESIGN AND TECHNIQUES 5

III. EXPERIMENTAL RESULTS 15

A. Vacuum Work Functions 15

B. Cesiated Electron Emission 44

C. Cesium Ion Emission 80

D. Emitter Fabrication 115

IV. THEORY AND ANALYTICAL CALCULATIONS 121

A. List of Symbols 121

B. Equilibrium Surface Coverage 123

C. Composite Surface Work Function 127

D. Atom and Ion Desorption Energies 180

E. Residence Times 189

F. Surface Diffusion Coefficient 189

G. Ion Critical Temperatures 197

H. Neutral Fraction 199

V. CONTRIBUTING PERSONNEL 201

REFERENCES 203

DISTRIBUTION LIST 205

LIST OF ILLUSTRATIONS

Fig. 1.	Experimental tube schematic	6
Fig. 2.	Experimental electronics block diagram	10
Fig. 3.	Electron emission from cesiated beryllium	45
Fig. 4.	Electron emission from cesiated titanium	47
Fig. 5.	Electron emission from cesiated chromium . . .	48
Fig. 6.	Electron emission from cesiated nickel	49
Fig. 7.	Electron emission from cesiated copper	51
Fig. 8.	Electron emission from cesiated niobium	52
Fig. 9.	Electron emission from cesiated tantalum	53
Fig. 10.	Electron emission from cesiated tungsten	56
Fig. 11.	Electron emission from cesiated rhenium	57
Fig. 12.	Electron emission from cesiated osmium	58
Fig. 13.	Electron emission from cesiated iridium	60
Fig. 14.	Electron emission from cesiated platinum	61
Fig. 15.	Electron emission from cesiated 304 stainless steel	62
Fig. 16.	Electron emission from cesiated tantalum boride	63
Fig. 17.	Electron emission from cesiated zirconium carbide (ZrC)	65
Fig. 18.	Electron emission from cesiated molybdenum carbide (Mo_2C)	66
Fig. 19.	Electron emission from cesiated tantalum silicide ($TaSi_2 \rightarrow Ta_5Si_3$)	67

Fig. 20. Electron emission from cesiated tungsten silicide ($WSi_2 \rightarrow 20\%\ WSi_2 + 80\%\ WSi_{0.7}$) 69

Fig. 21. Electron emission from cesiated Lucalox aluminum oxide (decreasing temperature) 70

Fig. 22. Electron emission from cesiated Lucalox aluminum oxide (increasing temperature) 71

Fig. 23. Electron emission from cesiated oxygenated copper 73

Fig. 24. Electron emission from cesiated oxygenated copper 74

Fig. 25. Electron emission from cesiated oxygenated copper 75

Fig. 26. Electron emission from cesiated oxygenated copper 76

Fig. 27. Electron emission from cesiated oxygenated copper 77

Fig. 28. Cesium ion emission from beryllium 82

Fig. 29. Cesium ion emission from titanium 84

Fig. 30. Cesium ion emission from chromium 85

Fig. 31. Cesium ion emission from nickel 87

Fig. 32. Cesium ion emission from copper 88

Fig. 33. Cesium ion emission from niobium 90

Fig. 34. Cesium ion emission from tantalum 91

Fig. 35. Cesium ion emission from tungsten (200) 93

Fig. 36. Cesium ion emission from rhenium 94

Fig. 37. Cesium ion emission from osmium 95

Fig. 38. Cesium ion emission from iridium 96

Fig. 39. Cesium ion emission from platinum 98

Fig. 40. Cesium ion emission from 304 stainless steel . . . 100

Fig. 41. Cesium ion emission from tantalum boride 101

Fig. 42. Cesium ion emission from zirconium carbide (ZrC) 102

Fig. 43. Cesium ion emission from molybdenum carbide (Mo_2C) 104

Fig. 44. Cesium ion emission from tantalum silicide ($TaSi_2 \rightarrow Ta_5Si_3$) 105

Fig. 45. Cesium ion emission from tungsten silicide 106

Fig. 46. Cesium ion emission from Lucalox aluminum oxide (actual data) 108

Fig. 47. Cesium ion emission from Lucalox aluminum oxide (smoothed-out data) 109

Fig. 48. Cesium ion emission from oxygenated OFHC copper (constant cesium arrival flux) 111

Fig. 49. Cesium ion emission from oxygenated OFHC copper (constant oxygen partial pressure) 112

Fig. 50. Surface ionization critical temperature envelopes for cesium on copper as a function of oxygen partial pressure 113

Fig. 51. Configuration entropy 125

Fig. 52. Vibration partition function (for cesium) 128

Fig. 53. Composite surface work function as a function of surface coverage for cesium on beryllium . . . 131

Fig. 54. Composite surface work function as a function of surface coverage for cesium on aluminum . . . 132

Fig. 55. Composite surface work function as a function of surface coverage for cesium on titanium 133

Fig. 56. Composite surface work function as a function of surface coverage for cesium on vanadium 134

Fig. 57. Composite surface work function as a function of surface coverage for cesium on chromium 135

Fig. 58. Composite surface work function as a function of surface coverage for cesium on manganese 136

Fig. 59. Composite surface work function as a function of surface coverage for cesium on iron 137

Fig. 60. Composite surface work function as a function of surface coverage for cesium on cobalt 138

Fig. 61. Composite surface work function as a function of surface coverage for cesium on nickel 139

Fig. 62. Composite surface work function as a function of surface coverage for cesium on copper 140

Fig. 63. Composite surface work function as a function of surface coverage for cesium on gallium 141

Fig. 64. Composite surface work function as a function of surface coverage for cesium on zirconium 142

Fig. 65. Composite surface work function as a function of surface coverage for cesium on niobium 143

Fig. 66. Composite surface work function as a function of surface coverage for cesium on molybdenum . . . 144

Fig. 67. Composite surface work function as a function of surface coverage for cesium on ruthenium 145

Fig. 68. Composite surface work function as a function of surface coverage for cesium on rhodium 146

Fig. 69. Composite surface work function as a function of surface coverage for cesium on palladium 147

Fig. 70. Composite surface work function as a function of surface coverage for cesium on indium 148

Fig. 71. Composite surface work function as a function of surface coverage for cesium on tin 149

Fig. 72. Composite surface work function as a function of surface coverage for cesium on hafnium 150

Fig. 73. Composite surface work function as a function of surface coverage for cesium on tantalum 151

Fig. 74. Composite surface work function as a function of surface coverage for cesium on tungsten 152

Fig. 75. Composite surface work function as a function of surface coverage for cesium on rhenium 153

Fig. 76. Composite surface work function as a function of surface coverage for cesium on osmium 154

Fig. 77. Composite surface work function as a function of surface coverage for cesium on iridium 155

Fig. 78. Composite surface work function as a function of surface coverage for cesium on platinum 156

Fig. 79. Composite surface work function as a function of surface coverage for cesium on lead 157

Fig. 80. Computer calculated composite surface work functions versus surface coverage for mannesium, strontium, calcium, cobalt, and vanadium on tungsten 158

Fig. 81. Computer calculated composite surface work functions versus surface coverage for boron, yttrium, scandium, lanthanum, antimony, and zinc on tungsten 159

Fig. 82. Computer calculated composite surface work functions versus surface coverage for palladium, rhodium, ruthenium, technetium, molybdenum, and niobium on tungsten 160

Fig. 83. Computer calculated composite surface work functions versus surface coverage for platinum, iridium, rhenium, osmium, tungsten, tantalum, and hafnium on tungsten 161

Fig. 84. Computer calculated composite surface work functions versus surface coverage for germanium, silver, gold, and thorium on tungsten 162

Fig. 85. Composite surface work function versus arrival flux for 22 adsorbate atoms on tungsten 164

Fig. 86. Composite surface work function versus arrival flux for 22 adsorbate atoms on iridium 165

Fig. 87. Composite surface work function versus arrival flux for 22 adsorbate atoms on rhenium 166

Fig. 88. Composite surface work function versus arrival flux for 22 adsorbate atoms on rhodium 167

Fig. 89. Composite surface work function versus arrival flux for 22 adsorbate atoms on nickel 169

Fig. 90. Composite surface work function versus arrival flux for 22 adsorbate atoms on platinum 170

Fig. 91. Composite surface work function versus arrival flux for 22 adsorbate atoms on osmium 171

Fig. 92. Composite surface work function versus arrival flux for 22 adsorbate atoms on molybdenum 173

Fig. 93. Composite surface work function versus arrival flux for 22 adsorbate atoms on tantalum 175

Fig. 94. Composite surface work function versus arrival flux for beryllium on nine substrate surfaces 176

Fig. 95. Composite surface work function versus arrival flux for copper on nine substrate surfaces 177

Fig. 96. Composite surface work function versus arrival flux for nickel on nine substrate surfaces 178

Fig. 97. Composite surface work function versus arrival flux for adsorbate atoms of aluminum, iron, copper, and nickel on tungsten surface at four surface temperatures 179

Fig. 98. Composite surface work function versus arrival flux for the five adsorbate atoms beryllium, aluminum, iron, nickel, and copper on a tungsten surface 181

Fig. 99. Composite surface work function versus arrival flux for the five adsorbate atoms beryllium, aluminum, iron, nickel, and copper on a rhenium surface 182

Fig. 100. Composite surface work function versus arrival flux for the five adsorbate atoms beryllium, aluminum, iron, nickel, and copper on an iridium surface 183

Fig. 101. Surface energy diagram. V_{v_i} is the energy required to raise an adatom to the i^{th} vibrational level. V_{m_i} is the energy required to raise an adatom into the migrational state, λ is the energy to desorb an adatom, and a is the mean distance between adsorption sites 192

ION THRUSTOR ELECTRODE SURFACE PHYSICS STUDIES

by

R. G. Wilson

ABSTRACT

Vacuum work functions, cesiated electron emission S curves, cesium ion emission curves, critical temperature envelopes, and cesium ion desorption energies are reported for 25 surfaces. Theoretical expressions and computer calculations are reported for composite surface work functions, cesium atom and ion desorption energies, residence times, and surface diffusions coefficients.

ION THRUSTOR ELECTRODE SURFACE PHYSICS STUDIES

by R. G. Wilson

Hughes Research Laboratories

SUMMARY

Experimental data concerning electron and ion emission from 25 cesiated and vacuum surfaces are reported. Included are vacuum work functions, electron emission S curves, cesium ion emission curves, critical temperature envelopes, and ion desorption energies. The range of cesium arrival flux is 10^{13} to 10^{17} atoms/cm^2-sec. Iridium and rhenium hold promise of being superior to tungsten as cesium contact ionizers: no material clearly superior to copper has yet been found for accel electrodes. Because aluminum oxide is an insulator and was studied in bulk form rather than as a thin film, the emission measurements have not unequivocably proved it a superior focus electrode material. Theoretical expressions and computer calculations are reported for composite surface work functions, cesium atom and ion desorption energies versus surface coverage for cesium adsorbed on 27 metal substrates, and for 21 other adsorbates on each of nine metal substrates. Residence times for 11 adsorbates on each of nine substrates versus surface temperature for six values of coverage from zero to one monolayer and the same residence times versus adsorbate arrival flux (10^8 to 10^{21} atoms/cm^2-sec) for several values of surface temperature are also included. Surface diffusion coefficients versus coverage are calculated for cesium on 31 substrates and for each of 20 other adsorbates on each of 9 substrates at each of 5 temperatures and versus temperature for 6 coverages.

I. INTRODUCTION AND CONCLUSIONS

The Final Summary Report on Contract NAS 3-6278 consists of four volumes: this volume contains the technical discussion, the experimental results, and some analytical results; three additional volumes contain supplementary analytical calculations: two of these accompanied the Semiannual Interim Report, and the third accompanies this report.

The objective of these two contracts was to improve the lifetime and efficiency of cesium surface contact ionization electrostatic thrustors by providing experimental and analytical information necessary for the selection of materials from which to fabricate improved thrustor electrodes.

The theoretical phase of the programs involved analytical calculations of composite surface work functions, atom and ion desorption energies, atom residence times, surface diffusion coefficients, and surface coverage as functions of substrate surface temperature and adsorbate arrival flux.

This contract program (including Contract NAS 3-5249) has led to the largest and most comprehensive study of the cesiated electron emission and cesium surface ionization characteristics of surfaces ever performed. A total of 25 surfaces were studied experimentally: 14 pure metals from beryllium to platinum, 2 metal alloys (304 stainless steel and iridium-tungsten), 6 refractory compounds (carbides, borides, and silicides), 2 insulator types, and one tertiary system, cesium-oxygen-copper. The materials studied experimentally under the combined contracts are listed in Table I.

The experimental measurements made were the vacuum work functions, electron emission versus surface temperature curves for cesium arrival fluxes between 10^{13} and 10^{17} atoms/cm^2-sec; and cesium surface ionization current densities versus surface temperature for the same cesium arrival fluxes. The last measurements yielded surface ionization critical temperature envelopes and cesium ion desorption energies at low (critical) coverage.

TABLE I

Materials Studied Experimentally

Material	Studied Under NAS 3-5249	Studied Under NAS 3-6278
beryllium		x
titanium		x
chromium	(x)	x
iron	x	
nickel		x
copper	x	x
niobium		x
molybdenum	x	
tantalum		x
tungsten		x
rhenium		x
osmium		x
iridium		x
platinum		x
304 stainless steel		x
tantalum boride	(x)	x
zirconium carbide		x
molybdenum carbide		x
molybdenum silicide	x	
tantalum silicide		x
tungsten silicide		x
aluminum oxide (sintered)	x	
aluminum oxide (Lucalox)		x
oxygenated copper		x
iridium-coated porous tungsten		x

Iridium (5.27 eV) and rhenium (4.96 eV) hold promise of being superior to tungsten for cesium surface contact ionization surfaces for application to cesium ion propulsion systems; a refractory high work function surface is desired, preferably one not having a high critical temperature. Osmium (4.83 eV), while slightly superior to tungsten in some fundamental parameters, is not a practical material because it cannot be worked. Platinum has the highest work function (5.3 to 5.8 eV), but its melting point temperature and sintering characteristics make it unsuitable.

A superior focus electrode surface (integral with the ionizer or independently suspended) is a stable, refractory surface with a low work function (at all cesium coverages) and/or a very high critical temperature; a low ionization efficiency for cesium is desired under operating cesium thrustor conditions. Only two pure metals, hafnium and thorium, appear to have suitable properties; however, the fabrication of electrode systems for large propulsion systems from either metal probably would be impractical. Two refractory compounds studied experimentally in this program (aluminum oxide and zirconium carbide) inhibit cesium ionization (low ionization efficiency) but not to the degree to offer tremendous improvements. Aluminum oxide is an insulator, and must be employed in thin films on a conducting surface to prevent the bulk insulator properties from predominating. As a thin layer, alumina offers the best improvement. Zirconium carbide is a very refractory and stable material, but it is only a fair cesium ionization inhibitor. (Electrodes would have to be fabricated from zirconium and then subsequently carbided.)

An accel electrode material must vaporize readily from the hot ionizer surface onto which it is sputtered by charge-exchange cesium ions. Because it resides momentarily on the ionizer and causes a degree of coverage (dependent upon the arrival flux, the desorption energy, and the surface temperature) of the ionizer, it should have a work function greater than that of the ionizer — certainly not much less. A low magnitude of back electron emission

from the cesiated accel electrode surfaces at their operation temperature is desirable. Therefore, materials may be judged by their relative cesiated electron emission in a given temperature range. These data are obtained satisfactorily only by direct experimental measurement. The necessary experimental data were obtained for all of the candidate metals in the appropriate range of cesium arrival flux and surface temperature. This comprised a major part of the comprehensive experimental program. A low sputtering rate is desirable for the accel electrode material, although this quantity varies only within a factor of about 5 among the candidate metals under identical conditions. No metal clearly superior to copper for combination with tungsten ionizer systems was found or can be predicted. If the higher-work-function and slightly higher-required-operating-temperature (higher critical temperatures) ionizing surfaces — iridium (coated on porous tungsten) and rhenium — are employed, then nickel, with its higher work function, lower sputtering yield, higher melting temperature, and slightly lower evaporation rate, may be superior to copper. The operating temperature of accel electrodes in high-thrust ion engines approaches the melting temperature of copper, and softening and loss of strength in large delicate structures has become a problem; therefore, a stronger, higher melting temperature material may be essential for higher current density systems.

II. EXPERIMENTAL DESIGN AND TECHNIQUES

This contract program required studying the influence of fractions of a monolayer of cesium on the electron and ion emission characteristics of a number of nonrefractory and refractory surfaces, including metals, semiconductors, and insulators. Therefore, a clean, ultrahigh vacuum environment was essential, and a method was required for quickly and efficiently studying electron and ion emission versus surface temperature, so that data could be obtained immediately after the emitter surface was cleaned and before any small partial pressures of any ambient gases could contaminate the emitter surfaces. Such a system was used, and techniques were developed for automating electron and ion emission measurements for all types of surfaces.

To simulate cesium ion thrustor electrode conditions as closely as possible, a plane parallel electrode geometry was chosen with about 1 mm spacing and with the capability of applying high electric fields of either polarity. All of the materials studied were practical polycrystalline "as received" or machined surfaces. Figure 1 is a schematic diagram of the experimental tube.

In the study of energetic cesium ion emission, the closely spaced planar collector surface material is sputtered back onto the emitter surface and can significantly alter the "apparent" characteristics of the surface, as shown by Chaikovskii and Ptitsyn.[1] Therefore, to maintain the basic nature and characteristics of the emitting surface during all emission measurements, the collector surfaces were also fabricated from the emitter material under study (unless this was electrically infeasible).

For the refractory materials, a ribbon emitter 0.001 or 0.002 in. thick and about 0.10 in. wide was used and was heated directly by ac current. A uniform temperature was created in the critical central region of the collector aperture and the thermocouple (see below), so that the cooling toward the ribbon ends was unimportant. The nonrefractory materials were heated indirectly by insulated central tungsten

E473-1

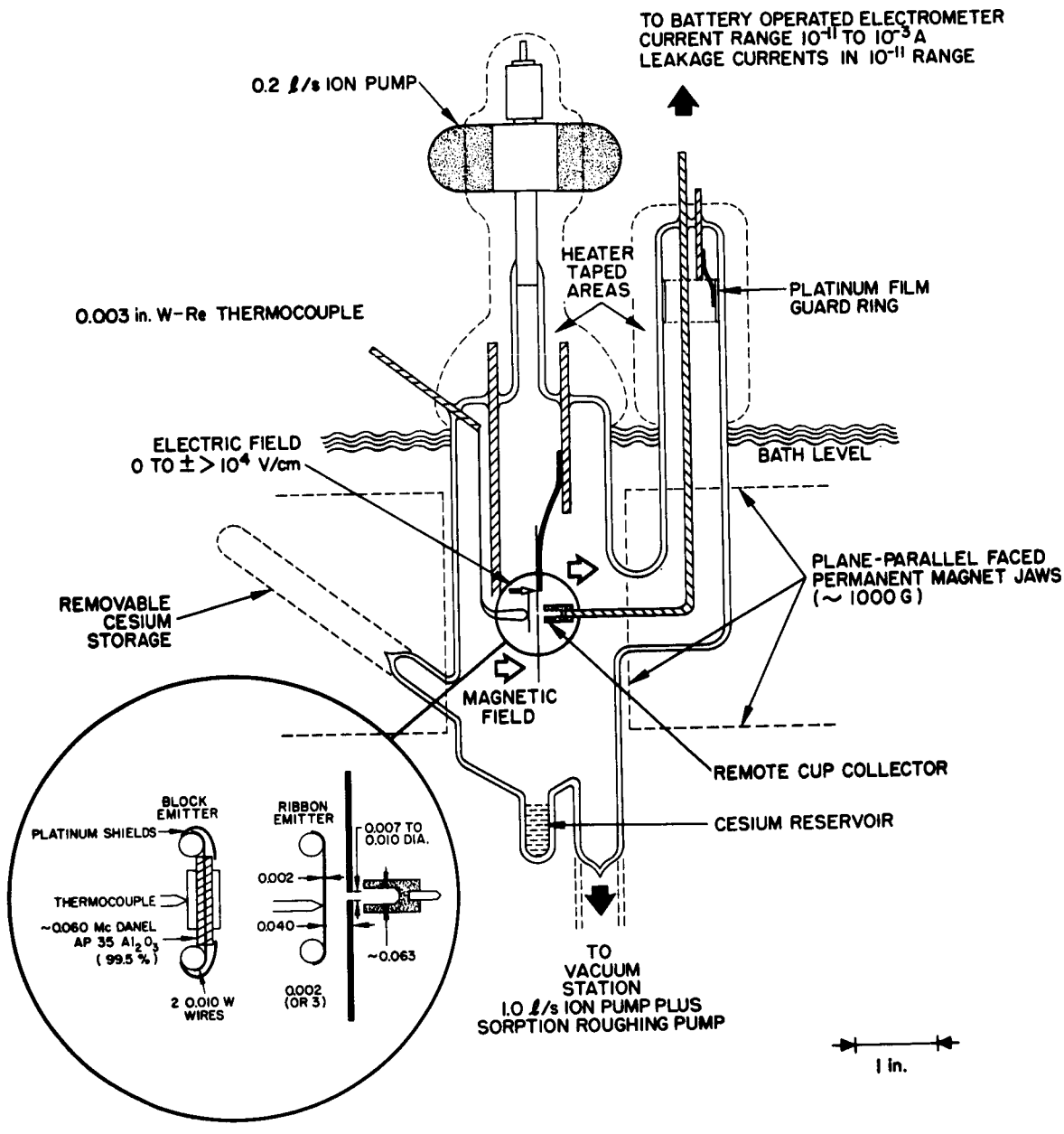

Fig. 1. Experimental tube schematic.

wires. The emitters were machined from square or round rods of high purity material. A high purity alumina insulator (AP 35 and McDanel 997) housing two 0.010-in. tungsten heater wires was fixed in the center of the emitter. These indirectly heated emitters assumed a very uniform temperature distribution over their entire surface. The alumina insulator protruded from each end, and it and the tungsten heater wires were shielded from the collectors by cool platinum or rhenium foils remotely mounted.

In order to measure as accurately as possible the electron and ion current densities and the associated emission surface temperatures, a double collector system (see Fig. 1) was employed; this consisted of a large area (~ 1-1/2 by 1-1/2 in.), thin (~ 0.002 in.) planar collector parallel to the emitter face, in which was machined a small aperture (0.007 to 0.012 in. diameter) located opposite the center of the emitter face. Behind the aperture was positioned a cup collector with an internal diameter several times the diaphragm aperture diameter (~ 0.060 in.). A potential difference applied between the emitter and diaphragm collector created a normal electric field in the region of the aperture and over most of the emitter face. To ensure additionally that the area from which the emitted electron current (passing through the diaphragm aperture and collected by the cup) was just the projected known area of the aperture, a normal magnetic field was always superimposed on the normal electric field by a permanent magnet with a field strength of about 1000 G (see Fig. 1). The area of the aperture was measured with an optical comparator at 100x.

The cup collector which monitored the small aperture currents was mounted remotely on a special side arm of the tube which extended out of the temperature bath (see Fig. 1). The leakage currents through the cesium layer adsorbed on the glass envelope walls were minimized by two methods. The glass walls of the collector arm were heated (by tapes) during measurements to reduce the cesium coverage, thereby increasing the leakage resistance. In addition, a platinum guard-ring

film was deposited on the inside arm walls. The film was grounded through an independent lead through the tube envelope (see Fig. 1). The background currents in this circuit were in the 10^{-11} A and sometimes in the 10^{-12} A scale, allowing emission currents to be measured through seven or eight orders of magnitude.

Two limiting factors in these measurements were the cesium film leakage currents and photoelectric emission currents from the collectors. To minimize photoelectric emission, the tubes were operated in the absence of external light. There was no convenient method of preventing the ultimate limitation of photoelectric emission resulting from radiation from the hot emitter which was incident on the collectors.

The temperature of the emitters was measured by 0.003-in. tungsten-rhenium thermocouples; these were spot welded to the emitters on the opposite side from the aperture so that they did not influence the emission from the small critical emitting area and yet accurately measured its temperature.

To provide the capability for controlling and varying the cesium arrival flux over a wide range of values, the experimental tubes were submerged in a large volume of liquid in a magnetic thermostatically controlled temperature bath. The bath was capable of maintaining a temperature to within 0.05C in the range from ambient to 300C. By using ice and water or dry ice and alcohol, the range could be extended to -30C with an accuracy of about 0.5C.

The cesiated electron emission S curves and the ion emission (critical temperature) curves were quickly and efficiently measured and recorded by feeding the dc millivolt output of the emitter thermocouple to the independent variable axis of an x-y recorder, and each of the two collector current outputs, in turn, through battery-operated electrometers to the dependent variable axis of the x-y recorder. This technique allowed electron emission S curves and cesium ion emission (critical temperature) curves to be measured and recorded continuously as the surface temperature was varied in either direction, and at various rates of temperature change.

The electronics of the experiment are shown in the block diagram of Fig. 2. The main units are the temperature bath; the experimental tube and magnet; the regulated and isolated emitter heater circuit to which the electric field producing voltage was applied from a well-regulated dc power supply; the two shielded electrometer collector circuits, each of which could be fed to the x-y recorder; the thermocouple-potentiometer circuit; the x-y recorder; and the ion pump and control circuit.

Calibrations of the x-y recorder traces were performed during each temperature sweep. Temperature and current level axis calibrations were never made independently of the data curves. The temperature axis was calibrated at appropriate points by a calibrated potentiometer through a switch, as shown in Fig. 2. The current level axis was frequently calibrated by having the recorder pen lift momentarily as it passed the major scale divisions on the electrometer scale.

Currents down to the 10^{-12} A range were recorded in the cesiated emission measurements, and currents down to the 10^{-13} and 10^{-14} A range were monitored in the vacuum emission measurements.

The rate of change of emitter temperature was controlled by regulating the rate of change of the emitter heater current. Therefore, by driving only the emitter heater current, it was possible to record a well-calibrated continuous plot of emission current versus surface temperature for temperature variation in either direction, to check reproducibility quickly and accurately, and to check for effects caused by variation of the rate of change of surface temperature. An important advantage of this technique was that electron emission curves were recorded graphically as continuous S curves with frequent calibration. Another important advantage was that the rapid automatic procedure made it possible to obtain emission data immediately following cleaning of the emitter surface, before any low partial pressures of ambient gases could significantly contaminate the surface. For example, at a pressure of 10^{-8} Torr of gases other than cesium vapor,

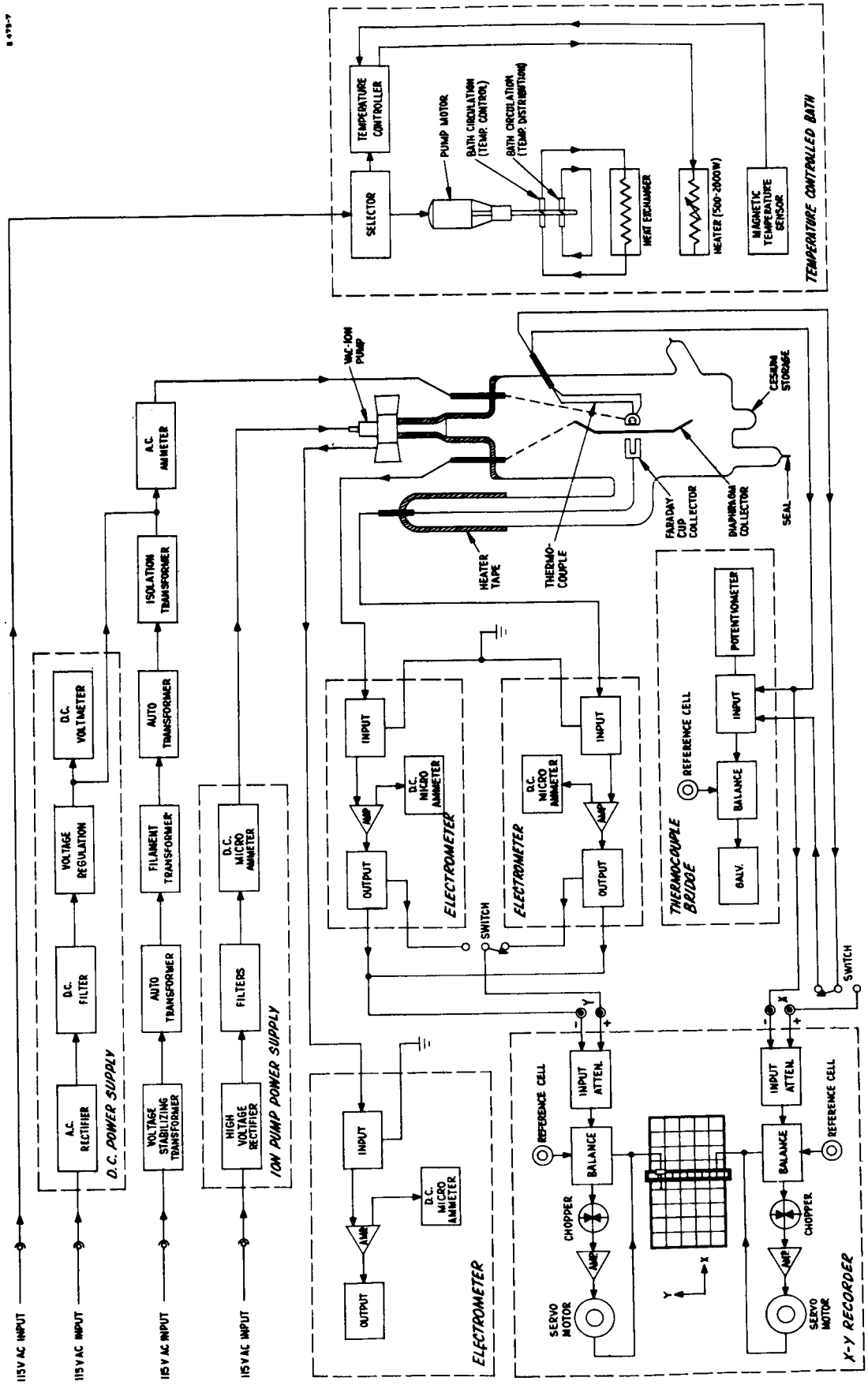

Fig. 2. Experimental electronics block diagram.

a monolayer is not formed for 100 sec; a complete current versus temperature plot from 500 to 2000K for a ribbon emitter could be obtained within this time. The only restriction on this technique was that only 500 V could be applied to the floating x-y recorder input terminals. This corresponded to an upper limit on the applied electric field of 5000 V/cm because the thermocouple output was at high voltage. Therefore, data could not be obtained by this technique for applied voltages in the kilovolt range.

Two techniques were employed in this work to determine the purity and/or composition of the emitter materials studied: spectrographic chemical analysis and x-ray diffraction. X-ray diffraction measurements, performed in our laboratory, were used especially for stoichiometric determinations in the fabrication of suitable high purity refractory compound emitters and to check the purity and stoichiometry of emitters after high temperature operation.

The vacuum work function measurements were made by recording the cup and diaphragm collector currents at a series of values of applied electric field at each of a series of emitter surface temperatures between the lower temperature limit, at which measurable currents were first observed, and the upper limit of either the melting point temperature or the temperature at which vaporization of the emitter became a serious problem. The emitter temperature was first raised to the upper limit where thermal cleaning occurred — thermal flash desorption for the refractories and vaporization of the outer emitter surface for the nonrefractories. The temperature was then lowered in a series of steps, at each of which a thermal equilibrium time was allowed. When a temperature dependence was observed, a second series of measurements was made for increasing temperature steps following the high temperature cleaning. At each temperature step, the applied field was varied from a few thousand volts per centimeter to zero in all cases, and in a few cases from between 10^4 and 10^5 V/cm to zero and back up (to check for high field effects). Usually the data were so flat (small

field dependence) that zero-field extrapolation could be accurately accomplished on a linear field plot, especially for the aperture-cup collector system. Occasionally, the data were transferred to a $\sqrt{E}$ plot for greater accuracy in the zero-field extrapolation in the Schottky emission region. All vacuum work function values quoted are zero-field-extrapolated effective thermionic work functions. That is, A was always used as 120.4 $A/cm^2\text{-}K^2$, and any resulting work function variation is given as a temperature dependence.

The study of thermionic emission (S curves) from cesiated nonrefractory metals, a major portion of this program, is a new field involving some special problems and techniques. Refractory metals can be thoroughly internally outgassed by high temperature processing, and surface contamination incident from the ambient pressure (vacuum) can be removed prior to measurements by thermal flashing. Neither of these techniques can be applied to metals which melt at temperatures below outgassing and flashing temperatures. Sputtering of the surfaces by ion bombardment can be utilized to clean the surface prior to short duration measurements; however, each time the surfaces are subsequently raised to high temperatures to desorb cesium or measure their high temperature emission characteristics dissolved or occluded impurities again diffuse onto the surface, resulting in surface contamination which can influence the emission measurements. This problem cannot be solved by sputtering. Oxygen is probably the contaminant species exerting the major influence because it is difficult to drive from the metals in this category, and because even a few atoms of an electronegative gas, such as oxygen, diffusing onto a surface, can act as adsorption centers for a number of cesium atoms; in turn, these reduce the surface work function and increase the electron emission. Contamination of this type generally reduces the "apparent" work function (increases the emission).

In this work, very high vacuums (10^{-9} and 10^{-10} Torr) and clean (fluidless) ion pumping techniques were combined with a tube design employing emitters and collectors of the same pure materials and fast automatic data collecting techniques, to aid in minimizing the influence of contamination. However, two problems were still encountered and the following two conclusions result. Some nonrefractory metals cannot be outgassed enough at temperatures below the limit imposed by complete evaporation of the emitter, and continual diffusion of small amounts of contaminants onto the surface at the maximum emission temperatures cannot be prevented. The high vapor pressure of these metals at these maximum emission temperatures and the resulting high atom density in the interelectrode region increase the electrical breakdown voltage threshold and result in discharges in the presence of high applied fields. These are both practical problems in terms of application to electrodes in cesium contact ion thrustors because high applied fields are essential, and because the electrodes are subject to the same contamination problems encountered in this work. Therefore the results of this work should be applicable to the practical problem.

Ambient background pressures of 10^{-9} Torr or less, and a pumping system free from any vapors were achieved with bakeable ultrahigh vacuum systems composed of ion pumps and chilled molecular sieve sorption pumps. Two identical vacuum systems each consisted of a chilled molecular sieve sorption pump, a high vacuum roughing valve, a bakeable ultrahigh vacuum valve, a 1-liter/sec ion pump, and a bakeout oven. Each experimental tube was sealed onto a glass manifold. Each tube included a 0.2-liter/sec appendage ion pump.

The pressure in the system was measured by monitoring the currents in the 1.0- and 0.2-liter/sec ion pumps. In order to measure the currents, which went below 10^{-7} A, a battery-operated electrometer was placed in the ground side of the ion pump circuit.

This lowers the background current by eliminating the leakage current in the control unit (power supply). To this end, the ion pumps were electrically isolated by insulating mounts. Even with this arrangement, it was difficult to obtain accurate measurements of pressures below about 1×10^{-9} Torr because of leakage currents across the ion pumps. Overnight bakeouts at 300 and 400C were used to clean the tubes initially. The emitters were then thoroughly outgassed, sometimes followed by another bakeout. Thermionic emission measurements were made on the vacuum station before distilling cesium. Following cesium distillation, the tubes were pinched off from the vacuum system, and baked out with the cesium reservoir in an ice bath. The appendage ion pumps were immediately ignited while the tubes were hot and pumped to ultimate pressure at least overnight (and often longer). The emitters were then again outgassed slowly, and again pumped to ultimate pressure. The tube was then mounted in the temperature bath. The appendage ion pumps were operated whenever possible thereafter, during measurements and between runs. They were not operated only when the emission currents were less than about 10^{-10} A; it was found that they have no influence on the data at higher currents.

III. EXPERIMENTAL RESULTS

The experimental measurements and the results obtained under this contract are divided into four areas: (1) vacuum work functions, (2) cesiated electron emission, (3) cesium ion emission, and (4) emitter fabrication.

A. VACUUM WORK FUNCTIONS

Before any cesiated emission measurements were made, vacuum work function data were obtained for each surface under study. The zero-field-extrapolated effective thermionic electron work functions of the polycrystalline surfaces studied are summarized in Table II. The following pertinent information regarding these polycrystalline surfaces is also included in Table II: purity, number of data points, temperature range of measurements, and work function values. The following tables give the work function values and the specific measurement temperatures for each of the surfaces studied.

1. Beryllium

The vacuum work function of beryllium was measured at 11 temperatures between 900 and 1200K. The results are shown in Table III. The measured value for the effective thermionic vacuum work function between 900 and 1200K for a 99.7% pure polycrystalline beryllium surface is 3.67 ± 0.03 eV. The upper temperature limit of 1200K was dictated by vaporization of the beryllium surface; the melting point is about 1550K.

2. Titanium

Measurements made for a first 99.6% pure 2-mil polycrystalline titanium ribbon between 1100 and 1600K indicated a negative temperature coefficient expressed by $\phi(T) = 5.14 - 6.9 \times 10^{-4} T$. The first

TABLE II

Summary of Effective Thermionic Vacuum Work Function Data

Surface	Purity	Melting Temperature, K	Number of Measurements	Temperature Range of Measurements, K	Work Function, eV (Including Temperature Dependence)[c]	ϕ (1200 K)	ϕ (1500 K)	ϕ (1900 K)
Beryllium	0.997	1551	17	900-1200	3.665 ± 0.03	3.67	—	—
Titanium	0.996	1950	38	1100-1600	3.55 to 4.25[b]	(3.55 to 4.25)	—	—
Chromium	0.9999	2173	28	1050-1450	3.90 ± 0.05	3.90	3.90	—
Iron[a]								
Nickel	0.995	1728	20	1150-1500	4.41 ± 0.03 T < 1250 $6.27 - 1.0 \times 10^{-3}$ T > 1380 1250 < T < 1380[b]	4.41	4.77	—
Copper	OFHC	1356	7	1100-1250	4.415 ± 0.03	4.42	—	—
Niobium	0.9999	2760	12	1050-2100	4.19 ± 0.04	4.19	4.19	4.19
Molybdenum[a]								
Tantalum	0.9995	3270	12	1100-2200	4.25 ± 0.05	4.25	4.25	4.25
Tungsten	0.99995	3653	22	1150-2200	4.50 ± 0.05	4.50	4.50	4.50
Rhenium	0.9999+	3453	18	1325-2250	4.96 ± 0.05	4.96	4.96	4.96
Osmium	0.999	~ 3000	11	1400-1650	$5.43 - 3.9 \times 10^{-4}$ T	4.96	4.84	4.69
Iridium	0.999	2727	22	1300-2100	5.27 ± 0.05	5.27	5.27	5.27
Platinum	0.9995	2042	28	1600-1950	5.79 ± 0.09 or $5.03 + 4.2 \times 10^{-4}$ T	—	5.66	5.83
304 Stainless Steel	alloy	~ 1700	10	1050-1400	4.34 ± 0.03 T < 1200 T > 1200, ϕ decreases[b]	4.32	(4.18)	—
Tantalum boride	$TaB_2 \rightarrow \gamma TaB+B$	3270?	14	1100-1550	4.27 ± 0.07	4.26	4.26	—
Zirconium carbide	ZrC	3448 or (3813?)	15	1000-1550	3.70; T > ~ 1400 $4.58 - 6.35 \times 10^{-4}$ T, T ~ 1400	3.82	3.70	—
Molybdenum carbide	Mo_2C	2690	12	1400-1650	$5.14 - 2.70 \times 10^{-4}$ T	4.82	4.73	—
Molybdenum silicide[a]								
Tantalum silicide	$TaSi_2 \rightarrow Ta_5Si_3$	2473	12	1180-1600	4.71 ± 0.03	4.71	4.71	—
Tungsten silicide	$WSi_2 \rightarrow WSi_{0.7}$	2438	9	1350-1610	4.62 ± 0.03	4.62	4.62	—
Al_2O_3 (sintered)[a]								
Al_2O_3 (Lucalox)	0.999	~ 2315	6	1550-1750	5.19 ± 0.09	—	5.19	5.19
Oxygenated copper[b]								
Iridium-coated porous tungsten			1	1517	5.25	—	5.25	—

[a] See R. G. Wilson, "Electrode Surface Physics Research," Summary Report, Contract NAS 3-5249, Hughes Research Laboratories, June 1965.
[b] See text.
[c] The negative temperature coefficients may be due to the desorption of small amounts of dissolved or occluded oxygen.

TABLE III

Vacuum Work Function of 99.7% Pure Polycrystalline Beryllium Surface

Surface Temperature, K	Effective Vacuum Work Function, eV	
	Diaphragm Collector	Aperture-Cup Collector
1180	3.65	3.65
1155	3.65	3.65
1133	3.66	3.66
1108	3.66	3.66
1083	3.68	3.67
1055	3.69	3.64
1032	3.70	Current $< 10^{-13}$ A
1005	3.69	
976	3.68	
957	3.70	
920	3.66	

titanium tube failed, and a replacement was fabricated. The first set of vacuum work function measurements for the replacement titanium ribbon emitter also indicated a negative temperature coefficient expressed by $\phi(T) = 5.09 - 7.4 \times 10^{-4}\ T$ for the diaphragm collector and $\phi(T) = 5.10 - 8.8 \times 10^{-4}\ T$ for the cup collector. Because of the difference between these data and those for the first surface, the vacuum work function was checked after the titanium ribbon had been outgassed at 1585K for 10 min. A shift to lower work function was observed for both collector systems, which exhibited a negative temperature coefficient of $\phi(T) = 5.18 - 8.8 \times 10^{-4}\ T$ for the diaphragm collector and $\phi(T) = 6.14 - 1.91 \times 10^{-3}\ T$ for the cup collector. These measurements started at a maximum temperature and decreased to lower temperatures. A third set of measurements for the vacuum work function was recorded on another day, starting at a minimum temperature

and increasing to a maximum value, but without further degassing. The vacuum work function for both collector systems yielded the same results as those recorded for the decreasing temperature measurements made after outgassing. The previous drift toward a lower work function probably resulted from gettered substances and/or changes in the crystalline structure of the ribbon produced by processing at elevated temperatures, both characteristic of titanium. Titanium contains quantities of hydrogen and oxygen which change with the temperature and with the heat treatment history. The amounts decrease with increasing temperature in the thermionic emission temperature range, and degassing at 1585K drives both impurities out. The data above indicate a reduction in work function by degassing. Therefore, it is implied that the presence of hydrogen and oxygen in titanium increases the work function; this is a logical conclusion because both are electronegative gases. It is concluded that the work function of titanium is at least as low as 3.6 to 3.8 eV, the actual work function of a titanium surface is dependent upon the amount of dissolved (and adsorbed) gases, the influence of these gases is to increase the work function, the work function will change with temperature and heat treatment history, and work function values of titanium above 3.9 eV are probably for contaminated surfaces. The upper temperature limit was imposed by vaporization; the melting point is about 1950K. The results are presented in Table IV.

3. Chromium

Three experimental tubes were fabricated with indirectly heated chromium emitters and chromium collectors. The emitters were formed by machining two opposing flat surfaces on 99.99% pure polycrystalline chromium tubules. The diaphragm collector (same for all emitters) was constructed by plating a 0.010-in. copper foil with about 0.003 in. of chromium on the side facing the emitter. A 0.010-in. diameter hole was then drilled for the collector cup aperture, and the copper was removed in the vicinity of the hole edge.

TABLE IV

Vacuum Work Function of a 99.6% Pure Polycrystalline Titanium Surface

Surface Temperature, K	Effective Vacuum Work Function, eV			
	Diaphragm Collector		Aperture-Cup Collector	
	New Data	Old Data	New Data	Old Data
1586	3.80		3.60	
1585		4.09		4.10
1545	3.78		3.50	
1535		4.12		4.12
1488		4.16		4.16
1445	3.93		3.69	
1442		4.18		4.17
1432	4.05		3.93	
1395		4.20		4.19
1347		4.22		4.21
1320	4.11		4.02	
1304	4.02		3.84	
1300		4.27		4.26
1270	4.16		4.08	
1253		4.30		4.30
1218	4.20		4.15	
1205		4.32		$<10^{-13}$ A
1165	4.15		4.06	
1160	4.23			
1156		4.36		$<10^{-13}$ A
1113	4.26			

The effective vacuum work function was measured for the first chromium tube at seven temperatures between 1100 and 1400K. The result was an unexpected 3.90 ± 0.03 eV, independent of temperature in this range, as shown in Table V. This value is termed "unexpected" because the values quoted in the Handbook of Chemistry and Physics are much higher — in the range 4.4 to 4.7 eV, with 4.6 the preferred value. Because of this substantial disagreement, the measurements were repeated under several different conditions and for more than one experimental tube.

A second series of measurements was made later with the first chromium tube; immediately preceding the measurements the emitter temperature was raised to a value at which a substantial layer of chromium was evaporated (at 10^{-9} Torr), thereby insuring a fresh, clean chromium surface. The first few measurements were then actually made at temperatures at which chromium was being vaporized, and the results were in agreement with those reported above (see Table V).

Just as these measurements were completed, one of the thermocouple wires changed its position enough to contact the diaphragm collector, thereby shorting out the emitter and preventing the application of a potential difference. Consequently, a second experimental tube was fabricated. This second tube was carefully processed like the first one, including vaporization of the emitter surface. The work function was measured at eight temperatures between 1080 and 1420K (also given in Table V). The results were in agreement with those of the first tube, 3.90 ± 0.03 eV. Following these measurements, the tube was maintained overnight at this ultrahigh vacuum, and a single measurement was made on the following day, not preceded by any vaporization. The value obtained was 3.89 eV.

In order to aid in the substantiation of a pure chromium specimen, the emitter was removed from the first tube and was subjected to an x-ray diffraction measurement. The results of this measurement prove that the emitter was essentially randomly oriented pure

TABLE V

Vacuum Work Function of Three 99.99% Pure Polycrystalline Chromium Surfaces

Surface Temperature, K	Effective Work Function	
	Diaphragm Collector	Aperture-Cup Collector
1059	—	3.86
1087	3.90	—
1099	3.89	—
1130	3.88	3.94
1143	3.91	—
1158	3.93	—
1164	3.88	3.91
1206	3.92	—
1212	3.91	—
1214	3.87	3.90
1232	—	3.84
1254	3.93	—
1255	3.86	3.90
1280	3.96	—
1308	3.86	3.89
1310	3.94	—
1350	3.90	3.91
1355	3.86	3.90
1356	3.87	3.90
1357	3.94	—
1395	3.86	3.87
1397	3.88	—
1397	—	3.82
1403	3.86	3.86

chromium — to within the detection sensitivity of the instrument. Following the cesiated emission measurements another x-ray diffraction run was made on the chromium emitter face. The emitter surface was found to have become oriented strongly in the (110) direction during the extended cesiated measurements.

4. Iron

The data for iron were reported completely in the Final Report for Contract NAS 3-5249.

5. Nickel

The vacuum work function of a well outgassed nickel ribbon was measured at 20 temperatures (at three different times and for increasing and decreasing temperatures) between 1150 and 1500K. The upper temperature limit was imposed by vaporization; the melting temperature is about 1730K. The results are given in Table VI.

Two distinct work function values were reproducibly observed:

$$\phi(T) = 6.27 - 1.0 \times 10^{-3} T \quad \text{for} \quad 1380 < T < (1500)$$

$$\phi(T) = 4.41 \pm 0.01 \quad \text{for} \quad (1170) < T < 1250 .$$

Between 1250 and 1380 K, a very nearly constant emission current was observed. The constant current decreased slightly with each subsequent series of measurements. Nickel is known to be very difficult to free of dissolved oxygen. Oxygen diffusing onto a nickel surface would tend to make the apparent work function anomalously high. These data may indicate that a contaminant such as oxygen was diffusing onto the nickel surface between 1250 and 1380K and being desorbed more rapidly for higher temperatures, and that the clean work function is actually 4.41 eV. It is noted that the work functions measured for the elements near nickel (28) are: iron (26) 4.47 eV, copper (29) 4.42 eV, and quoted is cobalt (27) 4.40 eV.

TABLE VI

Vacuum Work Function of a 99.5% Pure Polycrystalline Nickel Surface

Surface Temperature, K			Effective Vacuum Work Function, eV	
Run No. 1	Run No. 2	Run No. 3	Diaphragm Collector	Aperture-Cup Collector
1490			4.80	4.79
	1487		4.78	4.77
	1462		4.80	4.79
1443			4.81	4.82
	1439		4.82	current
		1417	4.85	less than
	1415		4.86	10^{-13} A
1409			4.83	↓
		1392	4.85	
	1390		4.89	
		1370	4.73	
1358			4.80	
1319			4.75	
		1311	4.65	
		1272	4.54	
		1257	4.49	
		1222	4.40	
1217			4.42	
1178			4.41	
		1172	4.41	

6. Copper

The vacuum work function of an oxygen-free copper surface was measured at seven temperatures between 1100 and 1300K, as seen in Table VII. The result was 4.42 ± 0.03 eV. The upper temperature limit was dictated by the melting point, 1356K.

TABLE VII

Vacuum Work Function of an OFHC Copper Surface

Surface Temperature, K	Effective Vacuum Work Function, eV
1100	4.40
1123	4.40
1158	4.40
1180	4.40
1205	4.40
1230	4.42
1255	4.43

7. Niobium

The vacuum work function of a 2-mil, 99.99% pure niobium ribbon, outgassed at 2100K for 2.5 hours, was measured at 12 temperatures between 1050 and 2100K. The upper temperature limit was imposed by vaporization of the emitter support posts. The results are tabulated in Table VIII.

The measured value for the effective thermionic vacuum work function for a pure polycrystalline niobium surface is 4.19 ± 0.04 eV. (The lowest temperature value for the cup collector was not used in the vacuum work function calculation.)

8. Molybdenum

The data for molybdenum were reported completely in the Final Report for Contract NAS 3-5249.

TABLE VIII

Vacuum Work Function of a 2-mil, 99.99% Pure Niobium Ribbon

Surface Temperature, K	Effective Vacuum Work Function, eV	
	Diaphragm Collector	Aperture-Cup Collector
2073	4.15	4.20
1970	4.19	4.19
1865	4.20	4.20
1768	4.16	4.20
1678	4.17	4.18
1570	4.18	4.20
1485	4.17	4.21
1400	4.19	4.24
1323	4.20	(4.28)
1237	4.20	$I < 10^{-13}$ A
1155	4.20	
1078	4.21	

9. Tantalum

The vacuum work function of a 99.95% pure 0.003-in. tantalum ribbon was measured at 12 temperatures between 1100 and 2200K. The ribbon had been outgassed at 2375K for 21 hours. The results are shown in Table IX. The effective vacuum work function for a well-outgassed polycrystalline tantalum ribbon is 4.25 ± 0.05 eV. X-ray diffraction measurements on the tantalum ribbon after the measurements were completed showed that the surface was almost entirely (211) oriented.

TABLE IX

Vacuum Work Function of a 3-mil, 99.95% Pure Tantalum Ribbon

Surface Temperature, K	Effective Vacuum Work Function, eV	
	Diaphragm Collector	Aperture-Cup Collector
2150	4.15	4.23
2045	4.23	4.25
1940	4.30	4.21
1835	4.25	4.28
1735	4.30	4.30
1635	4.20	4.27
1545	4.28	4.28
1460	4.29	4.25
1375	4.29	4.25
1293	4.25	4.20
1213	4.25	4.23
1133	4.20	$I < 10^{-13}$ A

10. Tungsten

Vacuum work function measurements were recorded for two 99.995% pure 0.003-in. tungsten ribbons at 22 temperatures (decreasing and increasing temperatures) between 1150 and 2200K. The first ribbon was outgassed at 2400K for 15 hours, and the second for 18 hours at 2400K. Heating a tungsten emitter to 2400K for extended periods of time can yield two results: (1) elimination of minute traces of contaminants, and (2) stabilization of the crystal structure. The upper temperature limit was established by the vaporization of the ribbon support posts. The measurements are shown in Table X for each of the tungsten ribbons. X-ray diffraction measurements on the tungsten ribbons showed that the surface studied after outgassing was essentially entirely (100) oriented.

TABLE X

Vacuum Work Function Data for a 99.995% Pure Tungsten (100) Surface

Surface Temperature, K	Effective Vacuum Work Function, eV		Emitter Number	Direction of Temperature Change
	Diaphragm Collector	Aperture-Cup Collector		
2185	4.50	4.51	1	Decrease
2145	4.50	4.43	2	Decrease
2077	4.43	4.45	1	Decrease
2008	4.55	4.47	2	Decrease
1975	4.48	4.48	1	Increase
1970	4.47	4.47	1	Decrease
1940	4.60	4.49	2	Decrease
1870	4.50	4.45	1	Decrease
1803	4.63	4.55	2	Decrease
1772	4.55	4.50	2	Decrease
1770	4.49	4.48	1	Decrease
1737	4.68	4.59	2	Decrease
1673	4.51	4.45	1	Increase
1670	4.51	4.49	1	Decrease
1640	4.50	4.45	2	Decrease
1577	4.48	4.44	1	Decrease
1545	4.50	4.43	2	Decrease
1490	4.50	4.45	1	Decrease
1431	4.60	4.55	2	Decrease
1407	4.50	4.45	1	Decrease
1407	4.50	4.46	1	Increase
1320	4.48	4.40	1	Decrease
1239	4.55	$I < 10^{-13}$ A	1	Decrease

Thus, these results are for a "polycrystalline" single crystal face. The measured value for the effective thermionic vacuum work function for a well outgassed pure polycrystalline tungsten surface of (100) preferred orientation is 4.50 ± 0.07 eV.

11. Rhenium

The vacuum work function of a 2-mil 99.99+% pure rhenium ribbon was measured at 10 temperatures between 1325 and 2250K. The upper temperature limit was imposed by vaporization of the emitter support posts. The results are presented in Table XI. The measured value for the effective thermionic vacuum work function for a pure polycrystalline rhenium surface is 4.96 ± 0.05 eV. (The two lowest temperature values for the diaphragm collector are not weighted heavily.)

TABLE XI

Vacuum Work Function of a 99.99+% Pure Polycrystalline Rhenium Surface

Surface Temperature, K	Effective Vacuum Work Function, eV	
	Diaphragm Collector	Aperture-Cup Collector
2225	4.92	4.92
2115	4.94	4.94
2009	4.99	4.96
1905	5.00	4.96
1803	5.00	4.95
1704	5.01	4.95
1606	4.99	4.90
1515	5.00	4.90
1430	5.05	Current $< 10^{-13}$ A
1348	5.10	

12. Osmium

An osmium emitter was fabricated by hot pressing and sintering a disc of osmium to 95% of theoretical density from high purity osmium powder. The disc was polished, cut, and bored into a standard square emitter with a central hole for indirect heating. (Osmium cannot be rolled into a foil for a directly heated emitter.) A berllyia insulator was used to allow this refractory metal to be heated hotter than most indirectly heated emitters. The osmium emitter was outgassed at 1570K for 3.8 hours, followed by 2.3 hours at 1610K, followed by 1.4 hours at 1680K. The processing at the highest temperature was continued until the electron emission stabilized — it decreased during the processing. When the emission had stabilized, the vacuum work function was measured at 11 temperatures in both decreasing and increasing sequences between 1400 and 1650K. The results, taken from the collector cup only, are shown in Table XII. The zero-field-extrapolated, effective thermionic work function of a polycrystalline osmium surface is (4.83 ± 0.05) eV between 1400 and 1650K with a distinct negative temperature coefficient expressed by $\phi = 5.43 - 3.9 \times 10^{-4} T$ eV (± 0.03 eV). X-ray diffraction measurements on the osmium surface prior to these measurements showed a random orientation. X-ray diffraction measurements on the same surface following the vacuum and cesiated emission measurements showed the identical random osmium orientation.

13. Iridium

The vacuum work function of a 2-mil 99.9% pure iridium ribbon was measured at 13 temperatures between 1300 and 2100K. The results are tabulated in Table XIII. Combining these results, the measured value for the effective thermionic vacuum work function between 1300 and 2100K for a 99.9% pure polycrystalline iridium surface is 5.27 ± 0.05 eV.

TABLE XII

Vacuum Work Function for Osmium

Surface Temperature, K	Work Function, eV	Surface Temperature, K	Work Function, eV
1413	4.88	1553	4.81
1437	4.88	1566	4.80
1465	4.86	1585	4.80
1495	4.84	1614	4.81
1523	4.82	1640	4.78
1535	4.81		

TABLE XIII

Vacuum Work Function of a 99.9% Pure Polycrystalline Iridium Surface

Surface Temperature, K	Effective Vacuum Work Function, eV	
	Diaphragm Collector	Aperture-Cup Collector
2076	5.27	5.27
2008	5.29	5.29
1941	5.32	5.31
1868	5.30	5.30
1802	5.31	5.31
1737	5.28	5.28
1667	5.25	5.23
1607	5.23	5.23
1545	5.25	5.23
1488	5.26	Current $< 10^{-13}$ A
1433	5.28	
1374	5.28	
1317	5.28	

14. Platinum

The vacuum work function of a 99.95% pure platinum ribbon emitter was measured at 16 temperatures between 1600 and 1950K. The melting point of platinum is 2046K. A necessary safety factor below this value established the upper temperature limit. The data obtained with the aperture-cup collector system are shown in Table XIV as "new" data. The diaphragm currents yielded inconsistent and different work function values, and were therefore discarded in favor of the more reliable cup data. The cup collector currents were below 10^{-13} A for temperatures below 1650K.

For comparison, platinum vacuum work function measurements for both collector systems taken from earlier data for a different platinum emitter and tube are included in Table XIV as "old" data. The two sets of cup collector measurements are in good agreement. There is excellent correlation between the data point temperature for old and new data; this is worth noting because the former temperatures were obtained by corrected optical measurements while the latter utilized a W(5% Re) - W(26% Re) thermocouple. When the 28 work function measurements of Table XIV are averaged, independent of any temperature dependence, a value of 5.79 ± 0.09 eV is obtained for the effective vacuum thermionic work function of platinum. When the cup collector values are plotted and a straight line is drawn in the temperature range of the observations, the temperature dependent expression is $\phi(T) = 5.03 + 4.2 \times 10^{-4}\ T$ in electron volts.

15. 304 Stainless Steel

The effective vacuum work function of a machined 304 stainless steel surface was measured at 10 temperatures between 1050 and 1400K. The results are given in Table XV. The upper temperature limit was imposed by vaporization (primarily chromium); the melting point is about 1730K.

TABLE XIV

Vacuum Work Function of a 99.95% Pure Polycrystalline Platinum Surface

Surface Temperature, K	Effective Vacuum Work Function, eV		
	Aperture-Cup Collector		Diaphragm Collector
	New Data	Old Data	Old Data
1946		5.89	5.85
1913		5.85	5.80
1880		5.83	5.80
1850		5.80	5.80
1846	5.80		
1818		5.78	5.79
1813	5.82		
1783		5.78	5.83
1781	5.81		
1752		5.76	5.82
1748	5.81		
1717		5.73	5.81
1714	5.75		
1686		5.70	5.80
1650	5.70		
1654		5.70	5.80
1620		5.72	5.79

For 304 stainless steel, a value of 4.34 eV is exhibited at the lower temperatures. This value is in agreement with the lowest values previously obtained for pure iron under Contract NAS 3-5249, but is slightly lower than most of the iron data. Because the work function of chromium is 3.90 eV and because 304 stainless steel is 18% chromium,

TABLE XV

Vacuum Work Function of a Polycrystalline
304 Stainless Steel Surface

Temperature, K	Effective Work Function, eV
1395	4.22
1350	4.28
1321	4.30
1300	4.28
1274	4.29
1250	4.30
1212	4.32
1170	4.34
1127	4.34
1085	4.34

a somewhat lower work function would be predicted. The 8% of nickel should not influence the effective polycrystalline thermionic work function because the effective work function of nickel is greater than that of iron. The tendency toward a decreased function at higher temperatures may be attributed to the higher vapor pressure of chromium. Chromium may be diffusing onto the surface and evaporating, resulting in a higher surface concentration of chromium than the approximately 18% in the bulk. Therefore, the data shown above may indicate a vacuum work function for 304 stainless steel of 4.34 eV at temperatures below 1200K, which then decreases toward the work function of chromium (3.9 eV) as the temperature is raised above 1200K.

16. Tantalum Boride

Vacuum work function measurements were made for a surface originally shown by x-ray diffraction to be vary largely TaB_2. The surface was outgassed at 1515K for 15 hours. This surface was fabricated on an indirectly heated block of tantalum by a technique which prevents diffusion of boron into the tantalum substrate. The upper temperature was imposed by both the fabrication temperature of the TaB_2 surface and the heater system. The work function was measured at 14 temperatures between 1100 and 1550K. The results are shown in Table XVI. These data indicate a value of effective

TABLE XVI

Vacuum Work Function of a Tantalum Boride Surface

Surface Temperature, K	Effective Vacuum Work Function, eV	
	Diaphragm Collector	Aperture-Cup Collector
1523	4.30[a]	4.32
1489	4.24	4.32
1458	4.24	4.32
1432	4.24	4.33
1403	4.25	4.32
1377	4.24	4.32
1349	4.19	4.32
1320	4.22	4.33
1293	4.23	4.32
1265	4.19	4.30
1239	4.19	4.26[a]
1193	4.20	$I < 10^{-13}$ A
1145	4.25	
1110	4.25	

[a]Not used in vacuum work function calculation

vacuum thermionic work function of a polycrystalline surface of tantalum boride of 4.26 ± 0.07 eV when both diaphragm and cup collectors are considered. If treated individually, the diaphragm yields 4.22 ± 0.03 eV and the cup collector gives 4.32 ± 0.03 eV, with the cup value favored. (The highest temperature value for the diaphragm collector and the lowest temperature value for the cup collector were not used in the vacuum work function calculation.) When the cesiated emission measurements were completed, the surface was checked by x-ray diffraction. A change in stoichiometry was observed. Essentially no TaB_2 was found, but the lines of γTaB and those of rhombohedral free boron were present. As in the case of $TaSi_2$, it cannot be stated with certainty whether the vacuum work function data apply to a TaB_2, a TaB + B, or a changing surface. It is possible that in the cases of both $TaSi_2$ and TaB_2, the stoichiometry changes are initiated by the high temperature operation in cesium vapor.

17. Zirconium Carbide

The vacuum work function of an indirectly heated block emitter of zirconium carbide (ZrC) was measured at 15 temperatures between 1000 and 1550K. The upper temperature limit was dictated by the melting point of the insulator containing the heater wires. The results are shown in Table XVII for both the diaphragm and cup collector systems.

The measured value for the effective thermionic vacuum work function of a polycrystalline ZrC surface exhibits a negative temperature coefficient expressed by $\phi(T) = 4.58 - 6.35 \times 10^{-4} T$ eV for $T < \sim 1400$K; for $T > \sim 1400$K, the work function is constant and equal to 3.70 ± 0.03 eV.

TABLE XVII

Vacuum Work Function of a Zirconium Carbide (ZrC) Surface

Surface Temperature, K	Effective Vacuum Work Function, eV	
	Diaphragm Collector	Aperture-cup Collector
1545	3.70	3.70
1503	3.70	3.70
1460	3.70	3.67
1440	3.75	3.70
1418	3.71	3.69
1380	3.77	3.70
1334	3.77	3.74
1293	3.80	3.76
1253	3.80	3.78
1213	3.85	3.83
1173	3.87	3.84
1131	3.86	3.87
1095	3.91	$I < 10^{-13}$ A
1053	3.90	
1015	3.94	

18. Molybdenum Carbide

The vacuum work function of a 2-mil carbided molybdenum ribbon (Mo_2C by x-ray diffraction) was measured at 12 temperatures between 1400 and 1650K. The upper temperature limit was established as the maximum temperature reached in the fabrication of the Mo_2C surface. A vacuum work function measurement was made following degassing for 4 hours at 1600K. A re-check of the vacuum work function was made following an additional bakeout of the tube and degassing of the emitter for two additional hours at 1600K. Both measurements are included in Table XVIII and show good agreement.

TABLE XVIII

Vacuum Work Function of a Molybdenum Carbide (Mo_2C) Surface

Surface Temperature, K	Effective Vacuum Work Function, eV		
	Aperture-Cup Collector		Diaphragm Collector
	First Measurement	Re-check	
1642	4.70		4.73
1610		4.69	
1605	4.69		4.75
1574	4.70		4.70
1549		4.72	
1545	4.70		4.75
1520	4.74		4.74
1491		4.75	
1485	4.80		
1457	4.77		
1434		4.78	
1430	4.80		

When the cup and diaphragm collector values are plotted, and a straight line is drawn in the temperature range of the observations, the effective thermionic vacuum work function of a polycrystalline Mo_2C surface is expressed by $\phi(T) = 5.14 - 2.70 \times 10^{-4}$ T eV.

19. Molybdenum Silicide

The data for molybdenum silicide were reported completely in the Final Report on Contract NAS 3-5249.

20. Tantalum Silicide

The vacuum work function of a silicided 0.002-in. tantalum ribbon, shown by x-ray diffraction measurements prior to emission measurements) to be $TaSi_2$, was measured at 12 temperatures between 1180 and 1600K. The upper temperature limitation was imposed by the maximum temperature reached during the fabrication of the $TaSi_2$ surface. The emitter surface was outgassed for approximately 13 hours at an average temperature of 1500K prior to the vacuum work function measurements. The results are given in Table XIX. Combining these results, the measured value for the effective thermionic vacuum work function between 1180 and 1600K for the polycrystalline tantalum silicide surface is 4.71 ± 0.03 eV.

Upon completion of the cesiated emission measurements, x-ray diffraction measurements indicated a change in stoichiometry to predominantly Ta_5Si_3. (This same change had occurred for $MoSi_2$, $MoSi_2 \rightarrow Mo_5Si_3$.) It is not known when, at what rate, or under what conditions the chage occurred — during outgassing, vacuum measurements, or cesiated emission measurements. It may have occurred gradually throughout all the operations. Therefore, it cannot be stated with certainty whether the data are for a purely $TaSi_2$ surface or a composite of $TaSi_2$ and Ta_5Si_3. However, the 4.71 eV value should correspond to the lower work function value if it was composite. Silicon probably diffuses onto the tantalum substrate during the change, although some could evaporate from the surface.

TABLE XIX

Vacuum Work Function Data for a Tantalum Silicide ($TaSi_2 \rightarrow Ta_1Si_3$) Surface

Surface Temperature, K	Effective Vacuum Work Function, eV	
	Diaphragm Collector	Aperture-Cup Collector
1585	4.72	4.72
1553	4.71	4.70
1523	4.75	4.74
1495	4.71	4.70
1465	4.71	4.69
1438	4.71	4.70
1410	4.71	4.71
1382	4.70	4.70
1354	4.70	$I < 10^{-13}$ A
1300	4.72	
1246	4.71	
1192	4.73	

21. Tungsten Silicide

Vacuum work function measurements were made for a surface originally shown by x-ray diffraction to be WSi_2. The surface was outgassed at an average temperature of 1500K for 14 hours. The surface was fabricated on a 3-mil tungsten ribbon. The upper temperature was limited by the fabrication temperature of the tungsten silicide surface. The effective work function was measured at nine temperatures between 1350 and 1610K. The results are shown in Table XX.

TABLE XX

Vacuum Work Function of a Tungsten Silicide Surface

Surface Temperature, K	Effective Vacuum Work Function, eV
1607	4.61
1577	4.63
1544	4.61
1517	4.60
1488	4.63
1460	4.62
1430	4.60
1400	4.64
1371	4.63

The effective thermionic vacuum work function of a polycrystalline tungsten silicide surface is 4.62 ± 0.03 eV. After the cesiated emission measurements were completed, the surface was checked by x-ray diffraction. The composition of the surface had changed to 20% WSi_2 plus 80% $WSi_{0.7}$, a lower silicon content. The M_5Si_3 compound

apparently does not exist for tungsten, as it does for molybdenum and tantalum. Again, the vacuum work function data may be for some combination of WSi_2 and $WSi_{0.7}$. However, because these data were measured before the extended cesiated measurements, and the final surface still had 20% WSi_2 remaining it is likely that when the vacuum measurements were made, the surface was predominantly WSi_2.

22. Aluminum Oxide (Sintered)

The data for sintered alumina were reported completely in the Final Report for Contract NAS 3-5249.

23. Aluminum Oxide (Lucalox)

The vacuum work function of a well outgassed block of Lucalox was measured at 10 temperatures between 1300 and 1750K. The upper temperature limit was dictated by the melting point of the alumina insert containing the heater wire. The high electric fields applied between the emitter and the diaphragm collector, which are required to draw saturated electron emission from the Lucalox emitter, also draw electron emission from other sources (such as the Kovar supporting posts and the rhenium shielding, both of which were at thermionic emission temperatures). If the electric field penetrates deep enough, electrons could be pulled from the tungsten heater wires. These factors probably caused the diaphragm collector currents to be too high and the apparent work function to be too low. Therefore, only the cup collector data are tabulated in Table XXI. The cup collector currents were below 10^{-13} A for temperatures below 1550K. The measured value of the effective thermionic vacuum work function between 1550 and 1750K for a 99.9% pure polycrystalline aluminum oxide (Lucalox) surface is 5.19 ± 0.09. When the possible temperature coefficient is included, the result is $\phi(T = 3.83 + 8 \times 10^{-4} T$.

TABLE XXI

Vacuum Work Function of 99.9% Pure Polycrystalline Aluminum Oxide (Lucalox) Surface

Surface Temperature, K	Effective Vacuum Work Function, eV
	Aperture-Cup Collector
1551	5.10
1600	5.13
1617	5.14
1666	5.20
1707	5.28
1743	5.26

24. Oxygenated Copper

The work function data for oxygenated polycrystalline (OFHC) copper are shown in Table XXII. The copper emitter was initially outgassed at 975K for 17.5 hours, plus 1110K for 6.5 hours, plus 1240K for 15 min. Values were measured at six temperatures between 1050 and 1220K. Included are work function measurements at four oxygen partial pressures from 2×10^{-7} to 2×10^{-4} Torr for five temperatures between 1050 and 1220K. Because of the low melting point and high vapor pressure of the copper emitter, the maximum emitter temperature was limited to a value for which the uncesiated emission currents were very low for the diaphragm collector and unmeasurable ($< 10^{-13}$ A) for the collector cup. The effective thermionic vacuum work function for a polycrystalline OFHC copper surface is 4.45 ± 0.05 eV, which compares well with our previously reported values. The oxygenated condition results in an increase in the work function of the copper surface, except for the lowest oxygen partial pressure. Measured values were 4.45 ± 0.05 eV, 5.02 ± 0.08 eV, 6.6 ± 0.2 eV, and greater than 7 or 8 eV for oxygen partial pressures of 2×10^{-7}, 2×10^{-6}, 2×10^{-5}

TABLE XXII

Work Functions of Oxygenated (OFHC) Copper Surfaces

Oxygen Partial Pressure, Torr	Surface Temperature, K	Effective Work Function, eV
No Oxygen	1108	4.50 ± 0.05
	1165	4.45
	1214	4.40
	1104	4.45
	1161	4.40
2×10^{-7}	1053	4.45 ± 0.05
2×10^{-6}	1053	5.08 ± 0.08
	1107	4.99
	1160	4.99
2×10^{-5}	1159	6.6 ± 0.2
	1213	6.6
2×10^{-4}	1213	>7 or 8

and 2×10^{-4} Torr, respectively. The combination of a work function of 4.4 eV or greater and a low melting point made it difficult to measure the thermionic work function even for the vacuum condition. Therefore, the electron emission was even more difficult to measure with increasing oxygen partial pressures and resulting increased work function. This explains why so few data points are reported in Table XXII. At the highest oxygen partial pressure, no emission could be measured. The work function shown for this oxygenated condition is simply a lower limit; values this high could not be measured.

25. Iridium-Coated Porous Tungsten

An indirectly-heated iridium-coated porous tungsten block emitter was fabricated and vacuum work function measurements were made. The maximum temperature was limited by the melting point of the alumina insulator containing the tungsten heater wires. The emitter was outgassed for 6 hours at 1490K. The value measured for the effective vacuum work function is 5.25 eV at 1517K.

B. CESIATED ELECTRON EMISSION

The experimentally measured electron emission current density versus surface temperature curves at six cesium arrival fluxes (in general) between 10^{13} and 10^{17} atoms/cm^2-sec for cesiated surfaces of beryllium, titanium, chromium, nickel, copper, niobium, tantalum, tungsten, rhenium, osmium, iridium, platinum, 304 stainless steel, tantalum boride, zirconium carbide, molybdenum carbide, tantalum silicide, tungsten silicide, aluminum oxide (Lucalox), oxygenated copper, and iridium-coated porous tungsten are shown in this section. These curves correspond to essentially the zero-field extrapolated condition. The influence of applied field was reported in the Final Report on Contract NAS 3-5249, and no significant variations from the results of that work have been observed. It was concluded that the influence of applied field for a clean surface is just the Schottky effect. For contaminated surfaces, however, the field effect is greatly enhanced, so that at applied fields of the order of 10^5 V/cm, the minima in the S curves can be destroyed.

1. Beryllium

The emission levels from beryllium (Fig. 3) are low. No minimum work function is observed. The final value of work function is 1.94 eV.* This may mean that the vacuum work function of cesium is actually 1.94 eV rather than 1.85 eV. This is the first such measurement known to this author for cesium on a substrate which is an alkaline earth metal.

*The cesium coverage is estimated to be between 1 and 2 monolayers where the 1.94 eV work function is measured. The value 1.94 eV is consistent with photoelectric values of the work function of cesium.

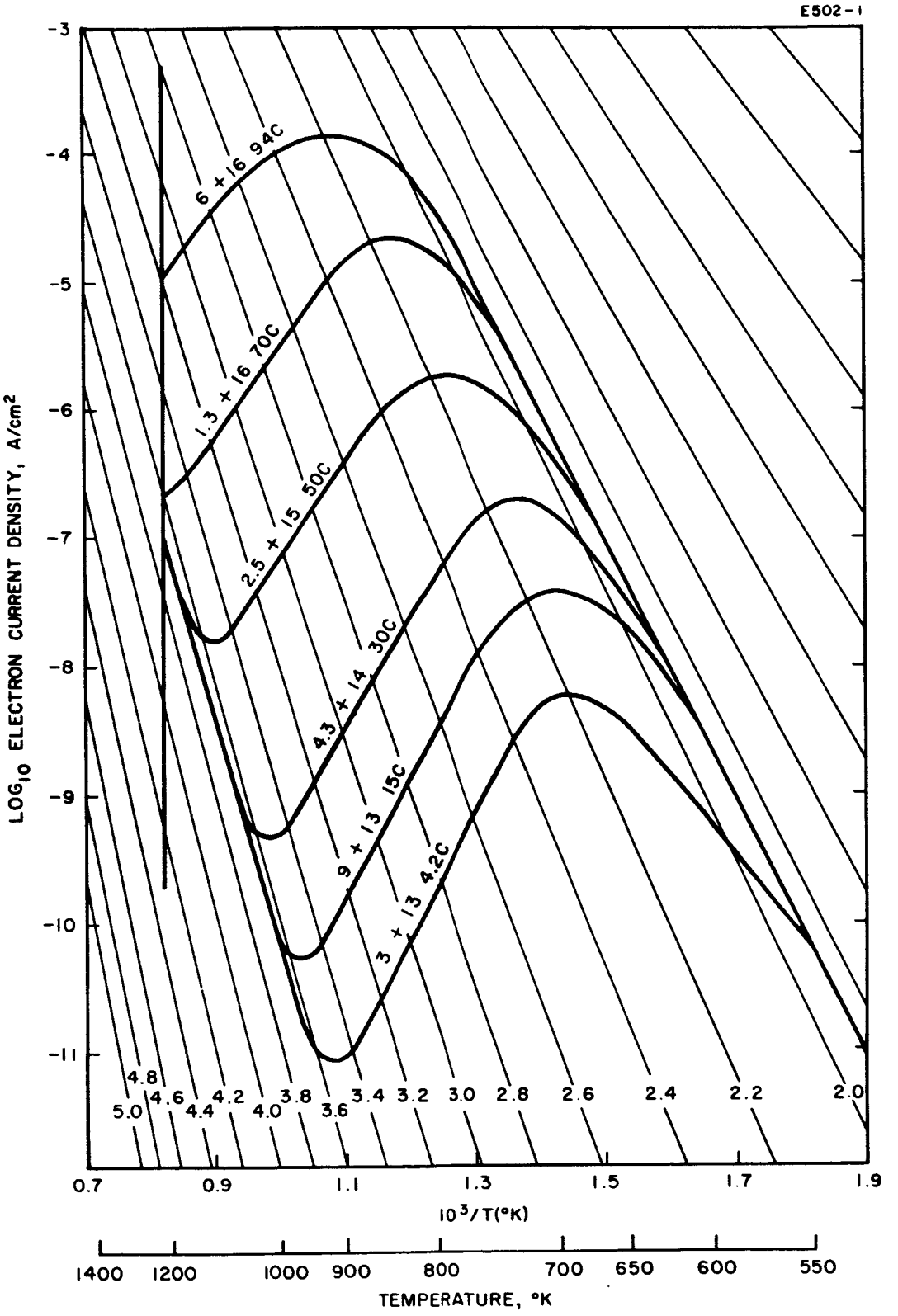

Fig. 3. Electron emission from cesiated beryllium.

2. Titanium

The cesiated electron emission curves for titanium (Fig. 4) are notably different from the others. The emission peaks occur at lower temperatures and the associated work function is lower, although the emission levels are low. The data are sharp and uniform. The minimum work function is about 1.32 eV, and the heavily cesiated work function is about 1.44 eV. A heater failure terminated the cesiated emission measurements before the highest arrival fluxes were completed.

3. Chromium

The curves for chromium (Fig. 5) are rather similar to those for tungsten for lower temperatures. A minimum work function of about 1.7 eV is observed. The lower vacuum work function of chromium causes differences at higher temperatures. The "clean" cesiated work function for chromium is seen to be about 3.55 eV, whereas its vacuum work function is about 3.9 eV.

4. Iron

The cesiated electron emission data for iron were reported in the Final Report on Contract NAS 3-5249.

5. Nickel

The data for nickel (Fig. 6) exhibit several different characteristics. The heavily cesiated work functions are relatively high for increasing temperature runs (2.0 to 1.75 eV), and they increase with increasing cesium arrival flux, an unusual observation. A phenomenon which has the characteristics of a contamination is exhibited at higher temperatures. For the increasing temperature curves, a tendency for the emission to follow a work function of 3.6 eV is consistently exhibited, but with an eventual wandering over to higher work function. The net result is very shallow minima in the S curves. It is not known whether

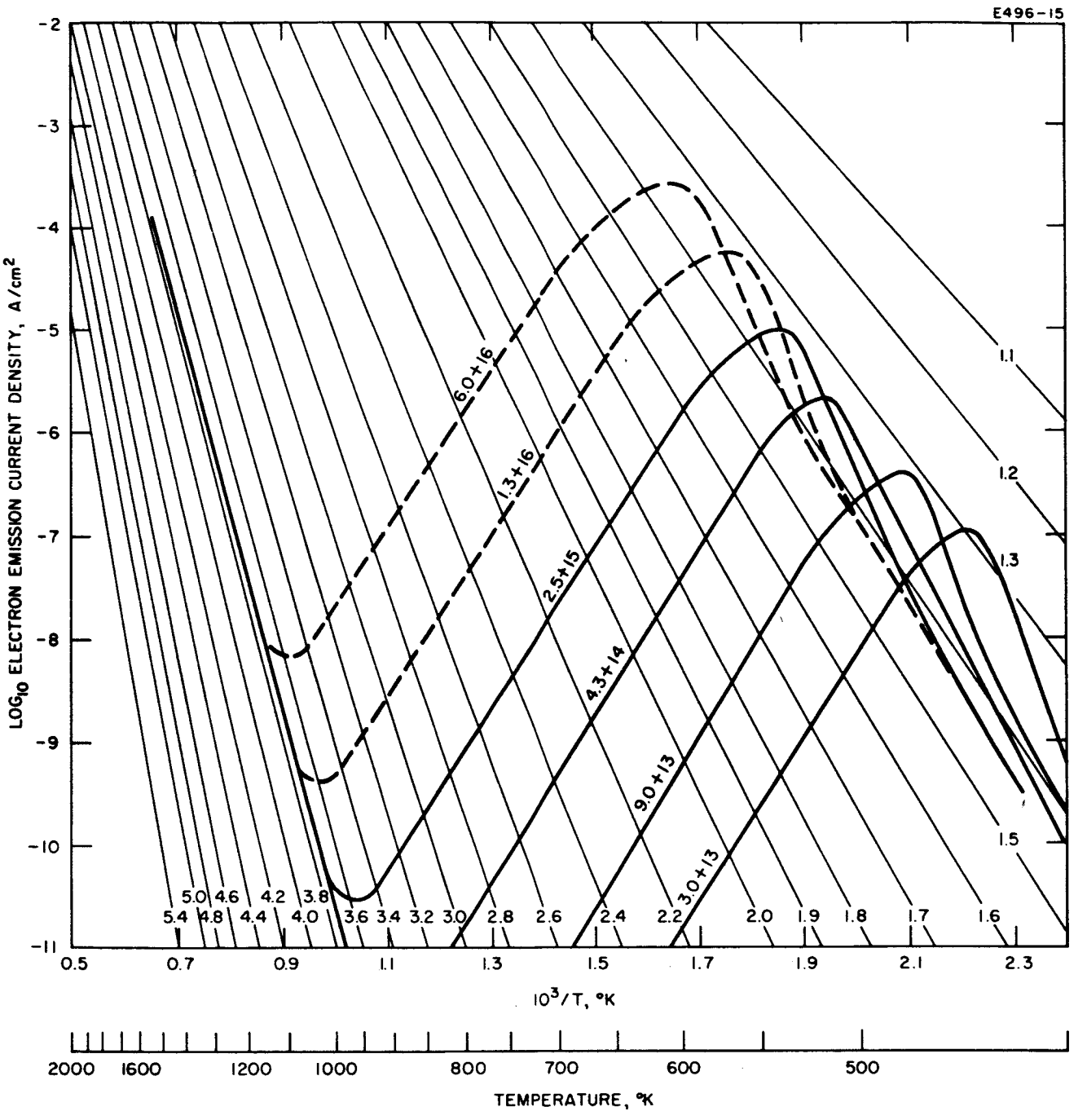

Fig. 4. Electron emission from cesiated titanium.

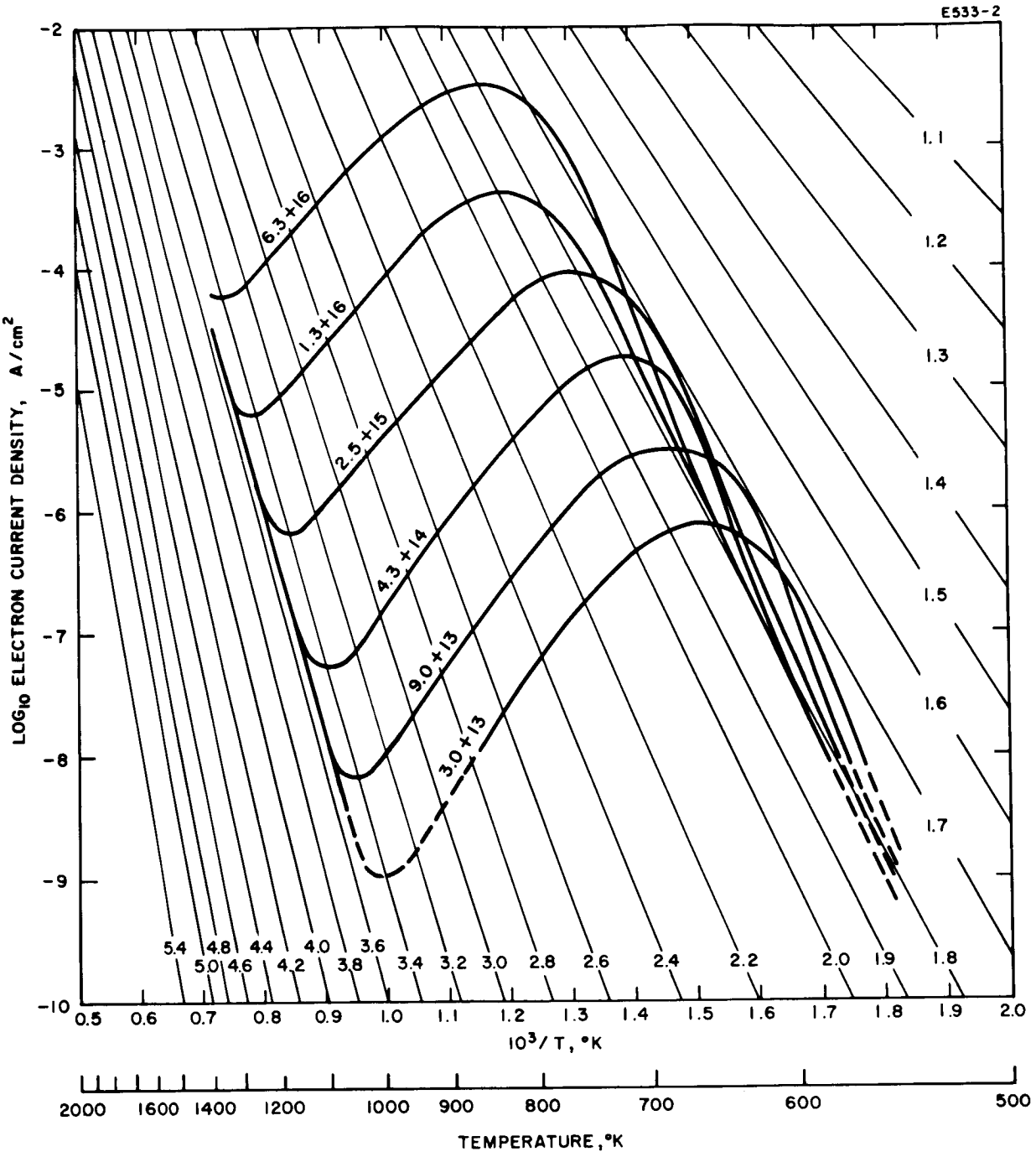

Fig. 5. Electron emission from cesiated chromium.

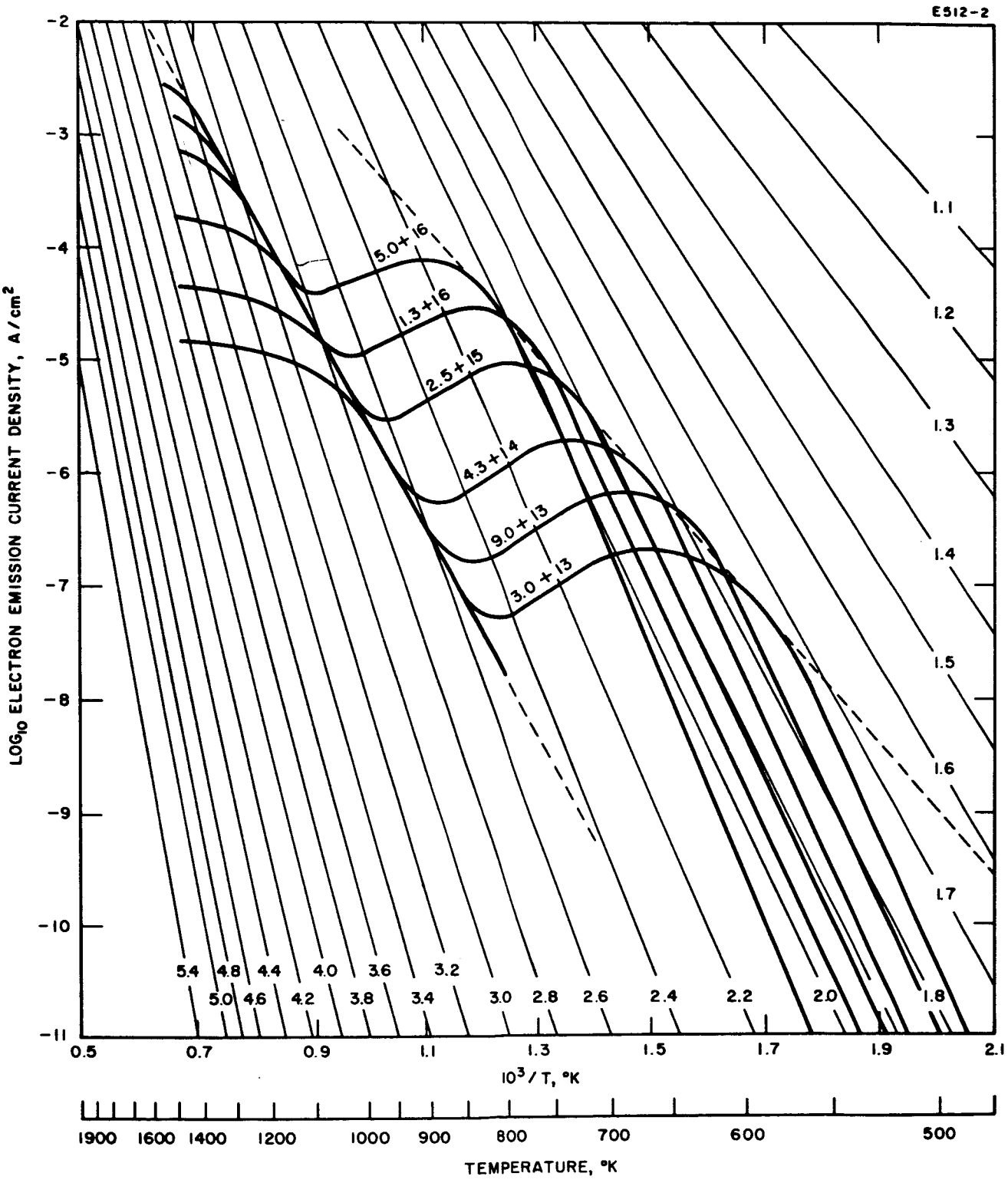

Fig. 6. Electron emission from cesiated nickel.

these characteristics are caused by some impurity gas adsorbed in the nickel which gradually diffuses to the surface, or by some fundamental work function variation in the nickel surface. Two facts are known: the vacuum work function of the nickel surface exhibited two distinct work functions which were reversible with temperature change; and, if a contamination is responsible, it cannot be removed by lengthy processing at temperatures at which nickel is noticeably vaporizing.

6. Copper

The curves for copper (Fig. 7) show a slight dissimilarity with those reported under Contract NAS 3-5249. The cesiated work functions are higher and the minima are deeper, indicating a cleaner surface. The emission maxima agree fairly well.

7. Niobium

The curves for niobium shown in Fig. 8 are typical of the refractory metals. The "clean" work function is about 4.1 eV, the heavily cesiated work function is about 1.62 eV, and a "roll over" is exhibited with a minimum work function of about 1.44 eV. The emission levels are high and the cesiated work function is quite low.

8. Molybdenum

The cesiated electron emission data for molybdenum were reported in the Final Report on Contract NAS 3-5249.

9. Tantalum

In Fig. 9, for pure tantalum, the emission maxima for four extra curves corresponding to the lowest four cesium arrival fluxes are added. These curves were anomalous and temporary. That is, they were unstable and did not represent emission from tantalum except under very special conditions. Corresponding curves at the two highest cesium arrival fluxes could not even be obtained. This

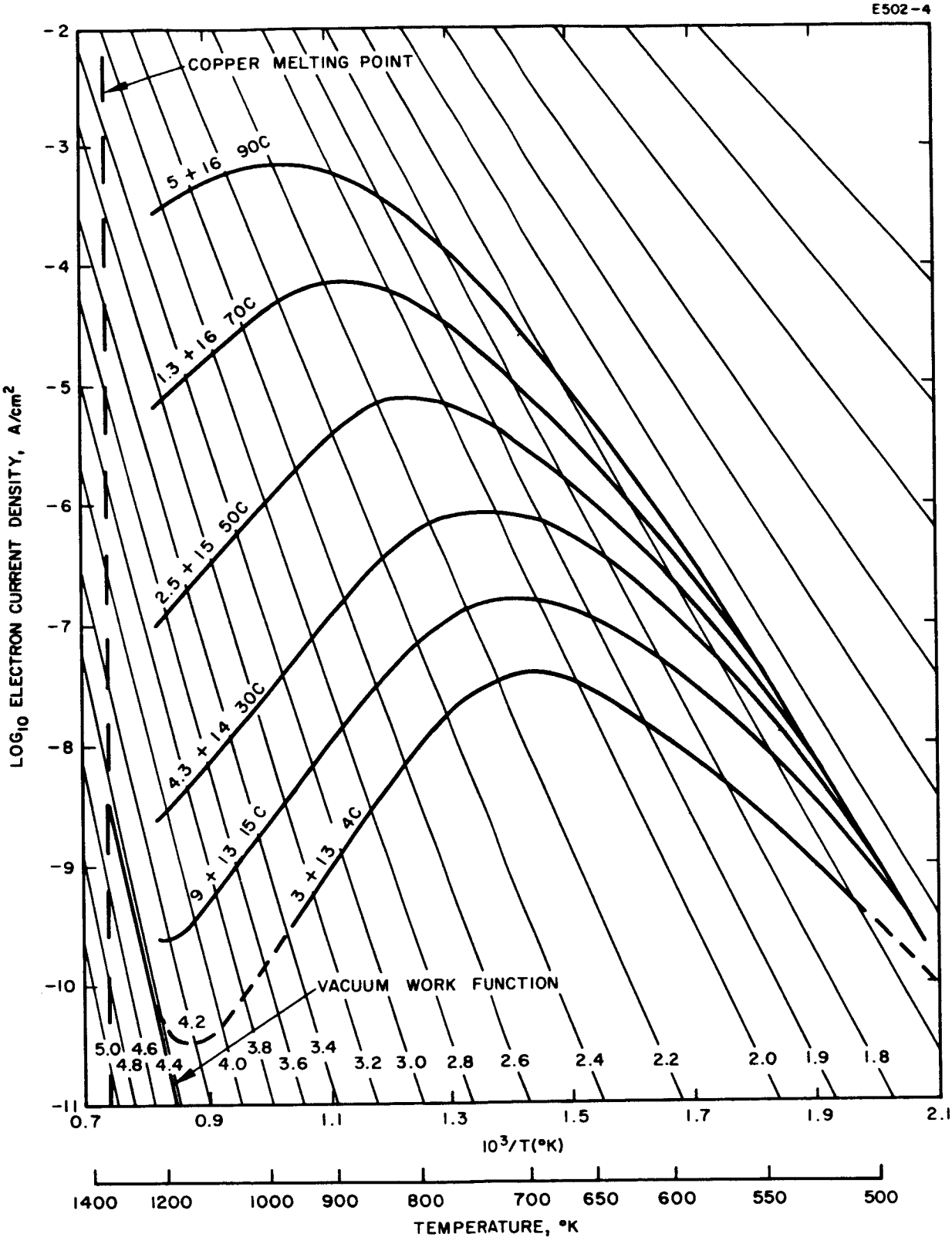

Fig. 7. Electron emission from cesiated copper.

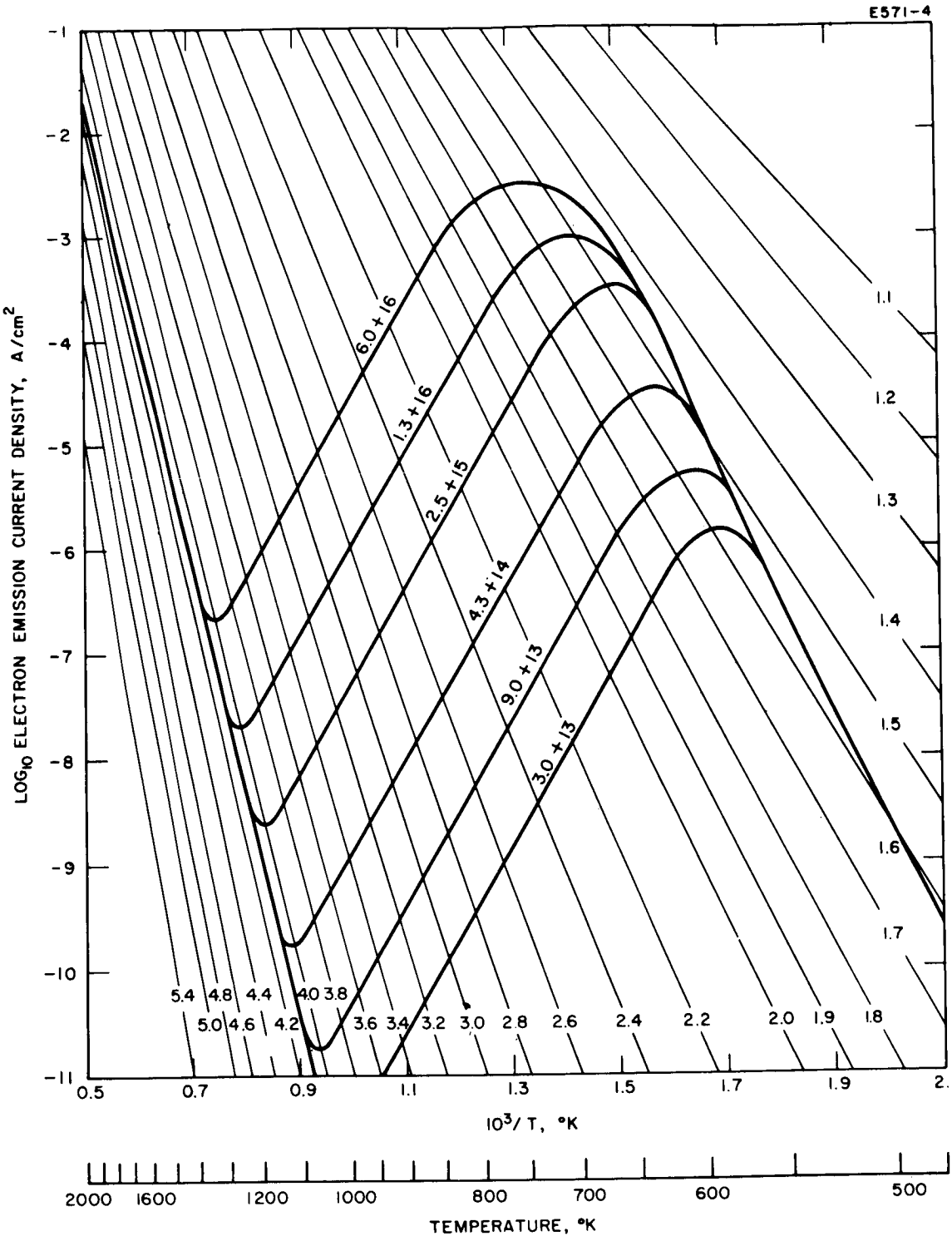

Fig. 8. Electron emission from cesiated niobium.

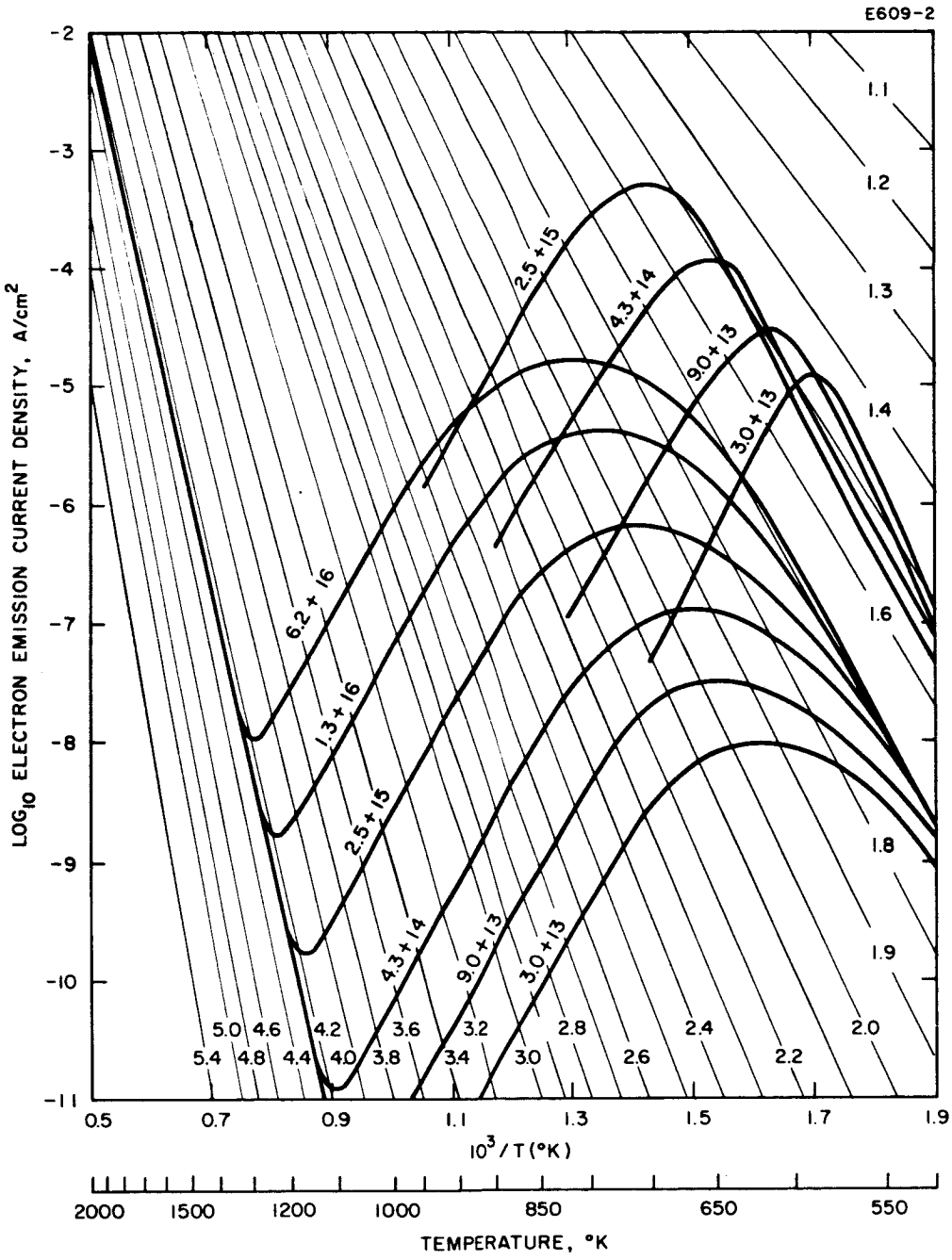

Fig. 9. Electron emission from cesiated tantalum.

anomalously high emission mode (see Fig. 9) exhibited a heavily cesiated work function of about 1.55 eV and a minimum work function of about 1.47 eV. The emission maxima are seen to be much higher and sharper or narrower in temperature. Double peaked curves were not observed – only one mode or the other. However, oscillations between two modes were observed later, as described below.

The anomalously high emission mode existed as the cesium arrival flux was increased until 1.3×10^{16} atoms/cm^2-sec was reached, at which time the low emission mode occurred for the highest two arrival fluxes. A return to the four lowest arrival fluxes then gave the consistent full set of curves seen in Fig. 9. The high emission mode could not be re-attained for a full temperature sweep – increasing or decreasing. Neither high temperature flashing nor periods of time at ambient (room) temperature would cause the re-appearance of the high emission mode at any arrival flux. However, when the electron emission curve corresponding to an arrival flux of 9.0×10^{13} atoms/cm^2-sec was rechecked, certain anomalous qualities were observed with variations in the emitter temperature and applied potential, as described in the following example. The emitter temperature was held constant such that the electron emission current at the S curve maximum could be observed. The applied potential was then varied from 0 to 200 V. The electron emission increased with the applied voltage by two orders of magnitude. Oscillations of about 2 cps and an order of magnitude change were observed in the electron emission peak value at 75 and 160 to 175 V applied potential.

With the applied potential held constant (200V), the temperature of the emitter was varied across the emission maximum region. The high emission mode was immediately destroyed and could not be recovered, except by reducing the applied potential to 5 V, heating the emitter to $\sim$ 2300K for a few minutes, then cooling rapidly to the peak region temperature and returning the voltage to $\sim$ 200 V. Hours at 2300K and low cesium arrival flux resulted only in the low emission mode for a normal full temperature scan.

For the normal emission mode, the full set of reproducible curves in Fig. 9, the curves are typical of refractory metals. The minimum and heavily cesiated work functions are about 1.7 eV.

10. Tungsten

For tungsten, the "clean" work function is 4.47 eV, the heavily cesiated work function is 1.63 eV, and the minimum work function is 1.61 eV, as seen in Fig. 10. The emission levels are fairly high and can be compared to similar data obtained by other different techniques reported in the literature.

11. Rhenium

For rhenium (Fig. 11) the minimum work function is about 1.53 eV and the heavily cesiated work function is 1.57 eV. The curves are well spread out on the current density axis, resulting in relatively high emission at high arrival flux and relatively low emission at low flux. The "clean" work function for rhenium is about 4.8 eV, which is close to the 4.9 to 5.0 eV value measured for the vacuum work function. The emission peaks are relatively broad, broader than those for tungsten, but narrower than that for iridium.

12. Osmium

The cesiated electron emission S curves for osmium are shown in Fig. 12. The emission maxima are the highest observed. The minimum and heavily cesiated work functions are both about 1.45 eV. Osmium was the only refractory metal not used as a ribbon and outgassed at $\sim$ 2000K; it was a block emitter outgassed at $\sim$ 1700K. There is, therefore, a chance that it is less clean than the others. The low, heavily cesiated work function and the lack of a distinct minimum may be related to the lower outgassing temperature.

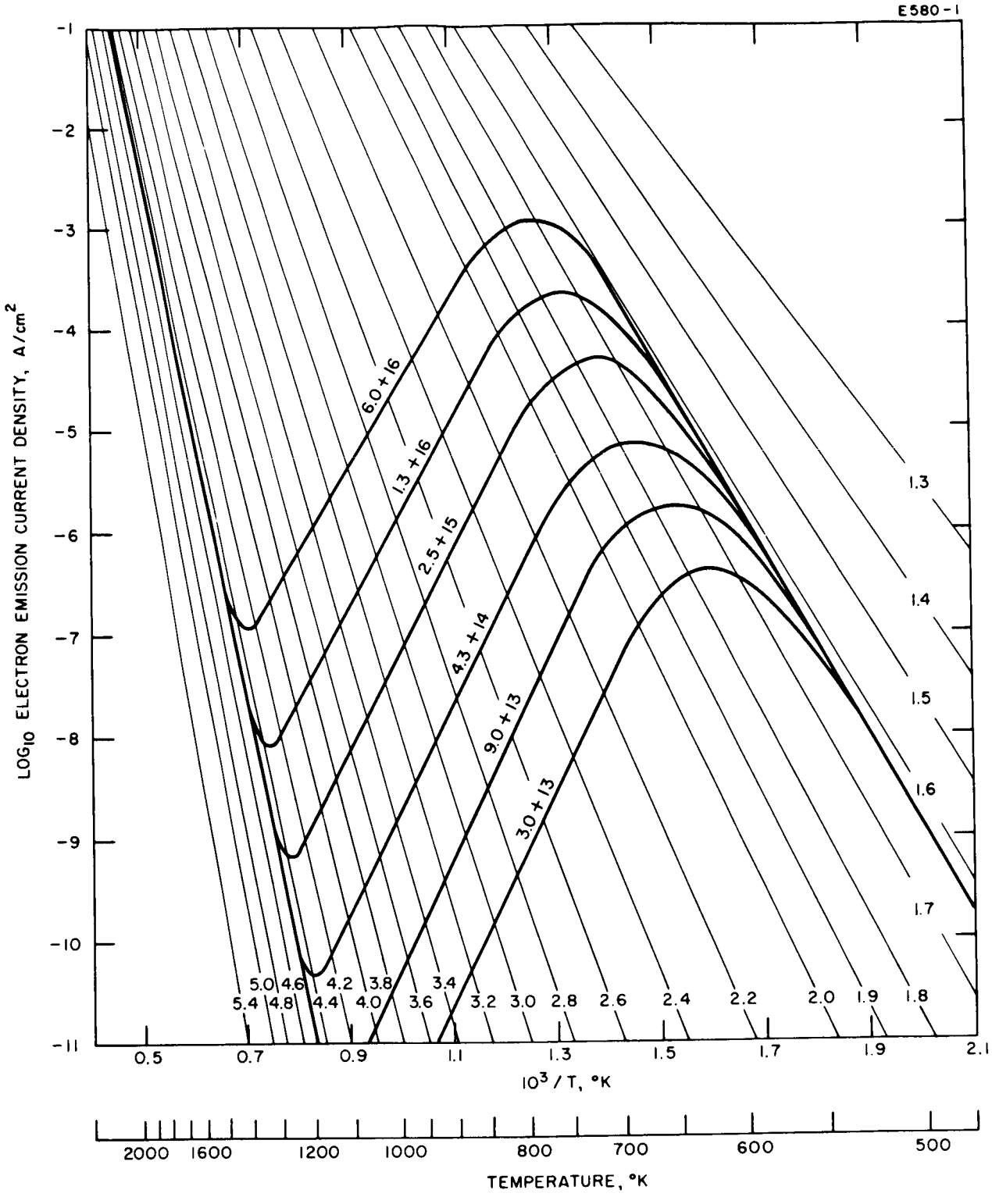

Fig. 10. Electron emission from cesiated tungsten.

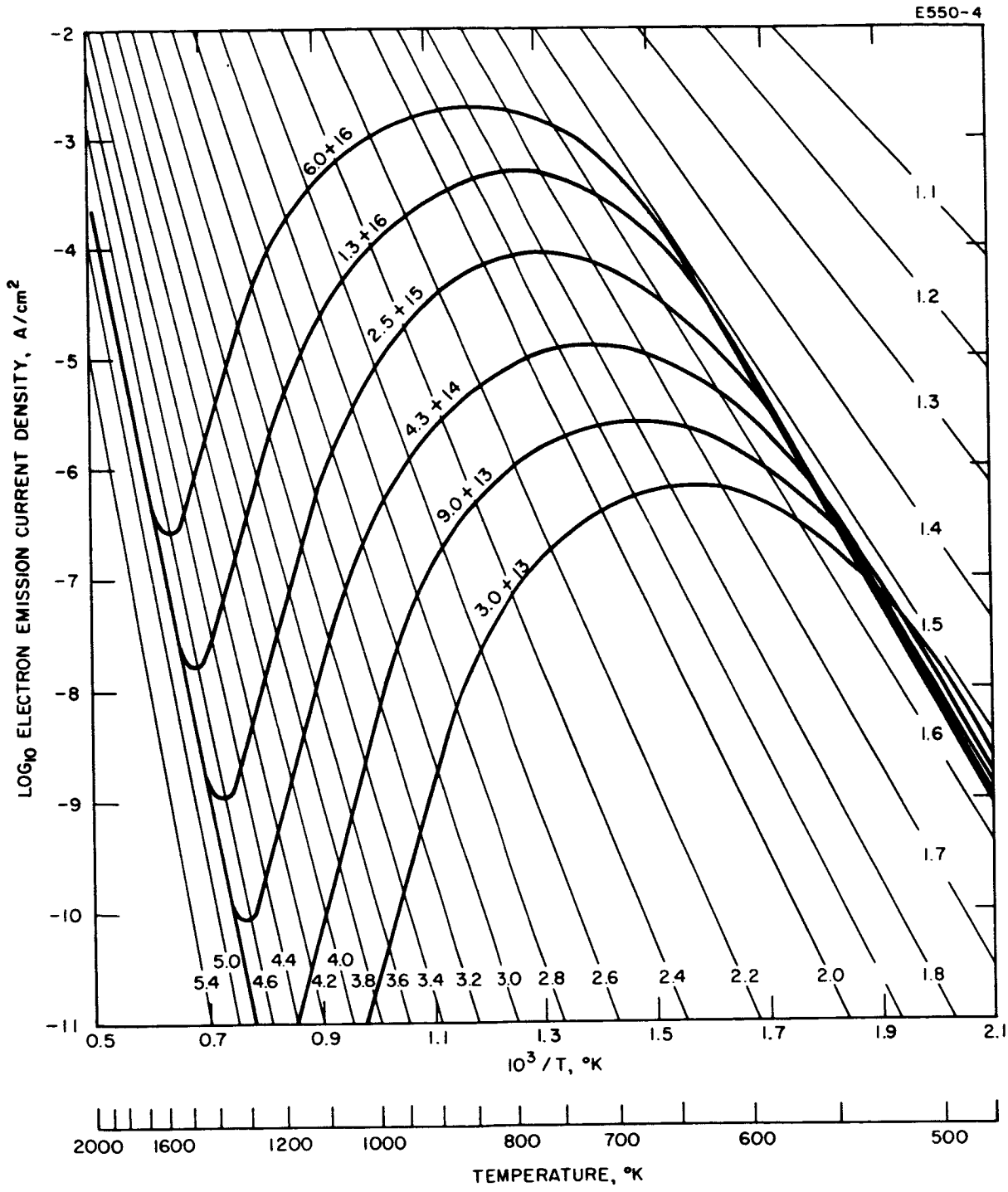

Fig. 11. Electron emission from cesiated rhenium.

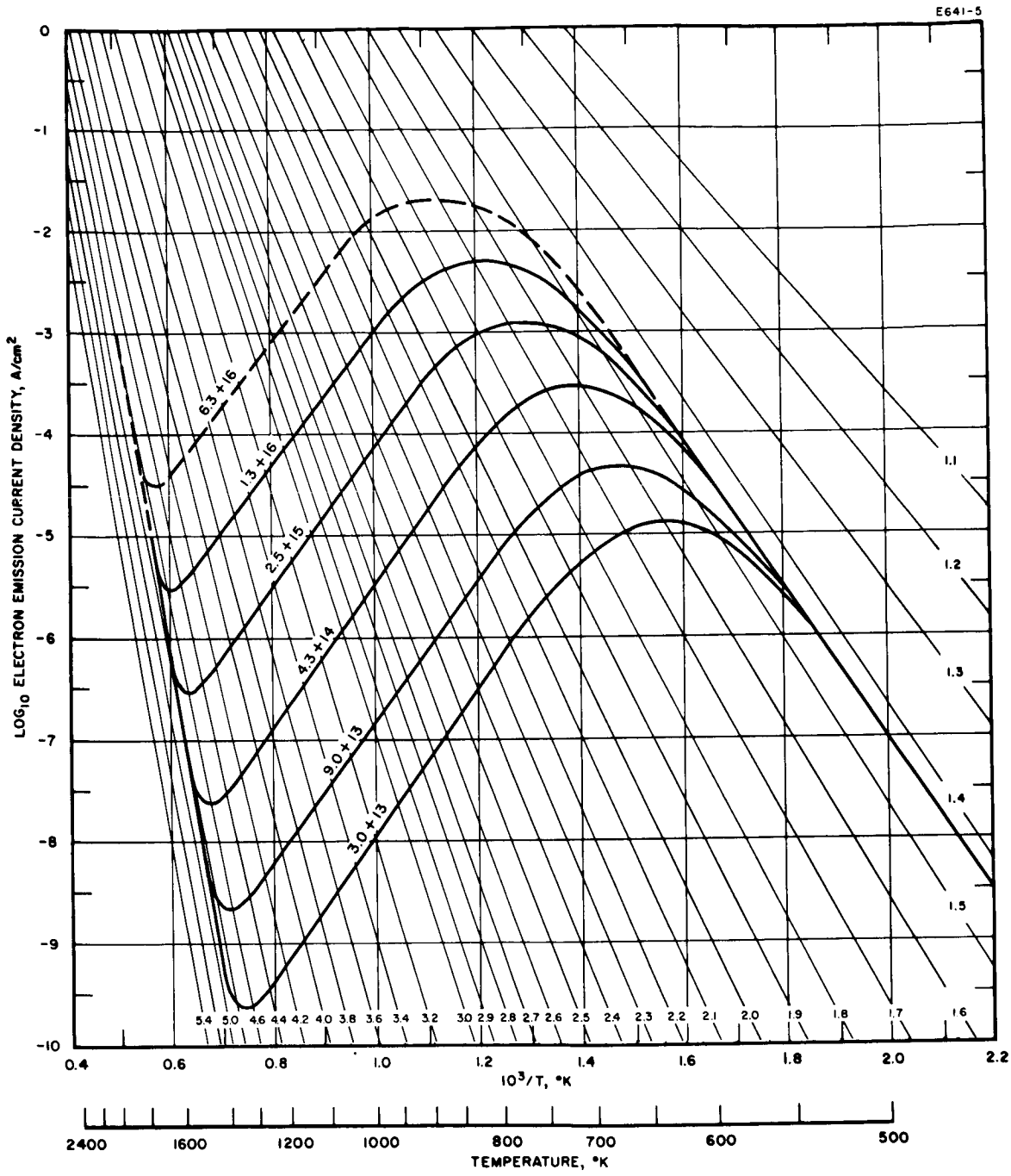

Fig. 12. Electron emission from cesiated osmium.

13. Iridium

The emission levels for iridium (Fig. 13) are comparatively high in the medium temperature range. The minimum work function (large θ) is about 1.8 eV and coincides with a number of others. The "clean" cesiated function agrees with the vacuum work function (5.1 to 5.3 eV). The emission peak is very broad.

14. Platinum

Platinum (Fig. 14) exhibits the broadest emission peak of all surfaces studied, and has a low minimum work function, 1.59 eV. The emission maxima are moderate.

15. 304 Stainless Steel

The emission levels for stainless steel (Fig. 15) are relatively high. The minimum work function is 1.52 eV and the heavily cesiated work function is 1.60 eV. The "clean" work function is 3.5 eV, somewhat lower than the vacuum work function.

16. Tantalum Boride

Cesiated emission data for tantalum boride were obtained at only the lowest four cesium arrival fluxes before the tube failed completely. The four actual data traces are shown in Fig. 16. The inconsistencies are attributed to the erratic behavior of the emitter heater. It was difficult to obtain any data at all, and it is guessed that the heater was shorting out and influencing the thermocouple readings. The four curves do progress uniformly to higher emission levels with increasing cesium arrival flux, but they are somewhat irregular. The minimum cesiated work function is about 1.5 eV and the heavily cesiated work function may be 1.67 eV.

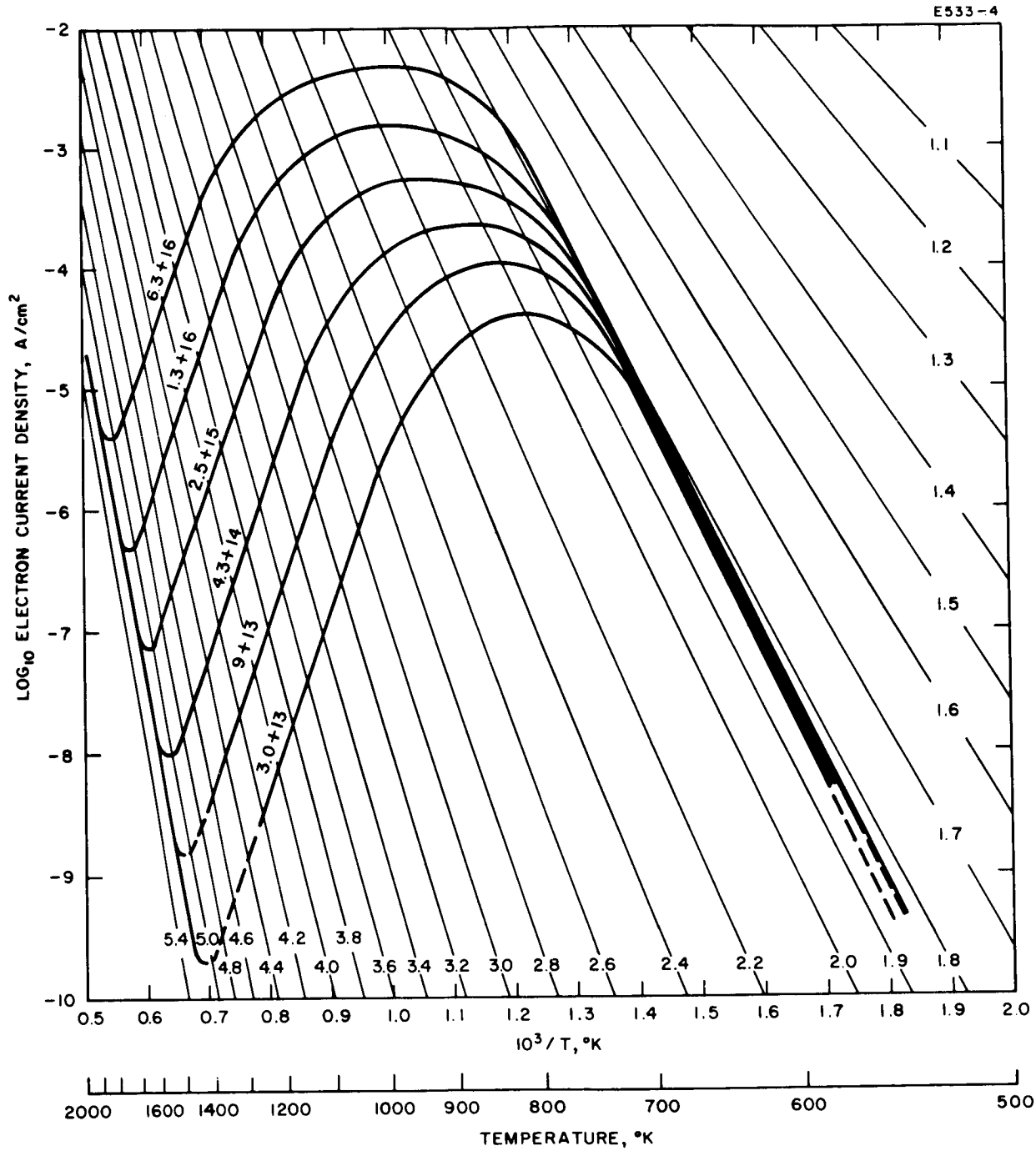

Fig. 13. Electron emission from cesiated iridium.

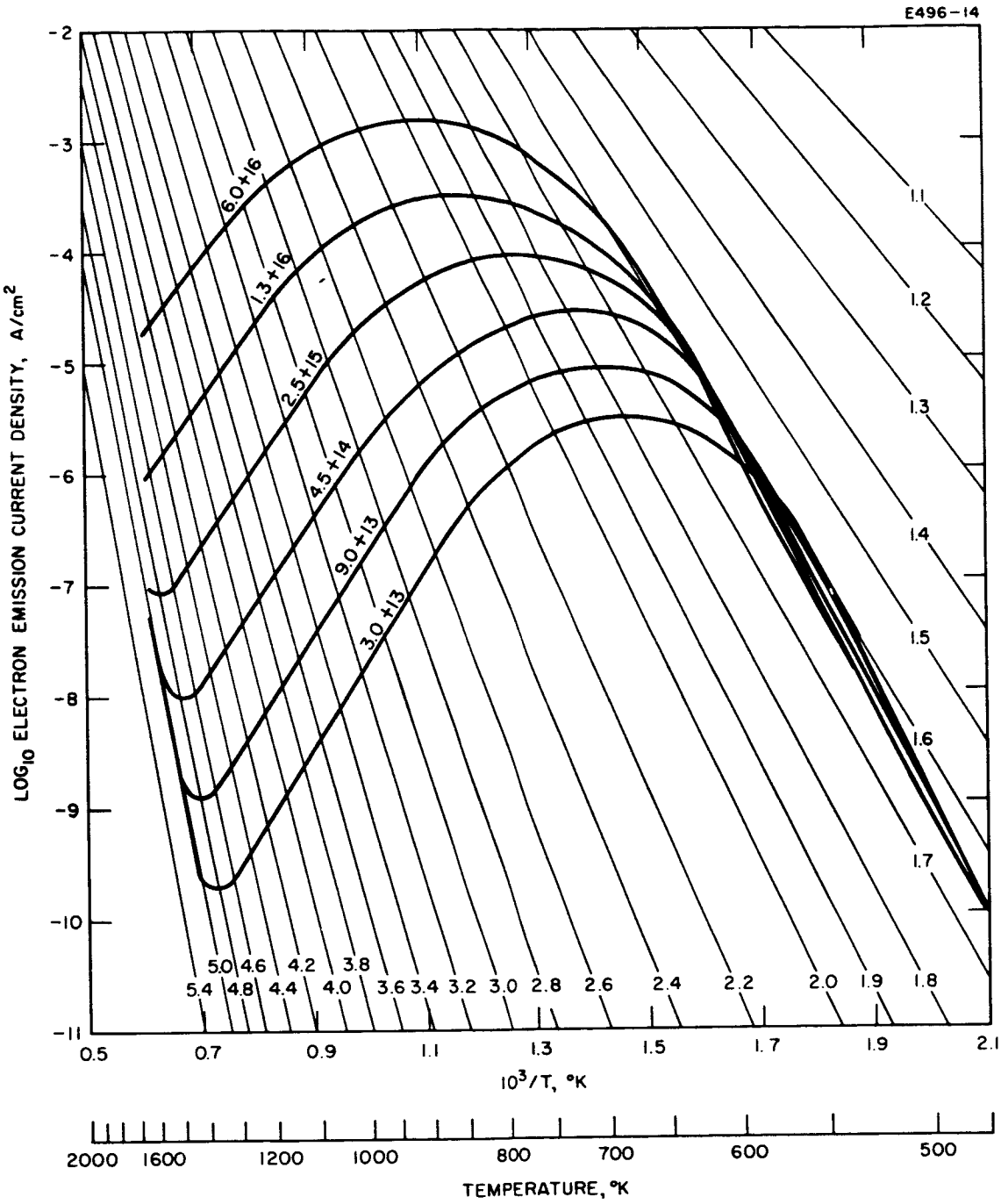

Fig. 14. Electron emission from cesiated platinum.

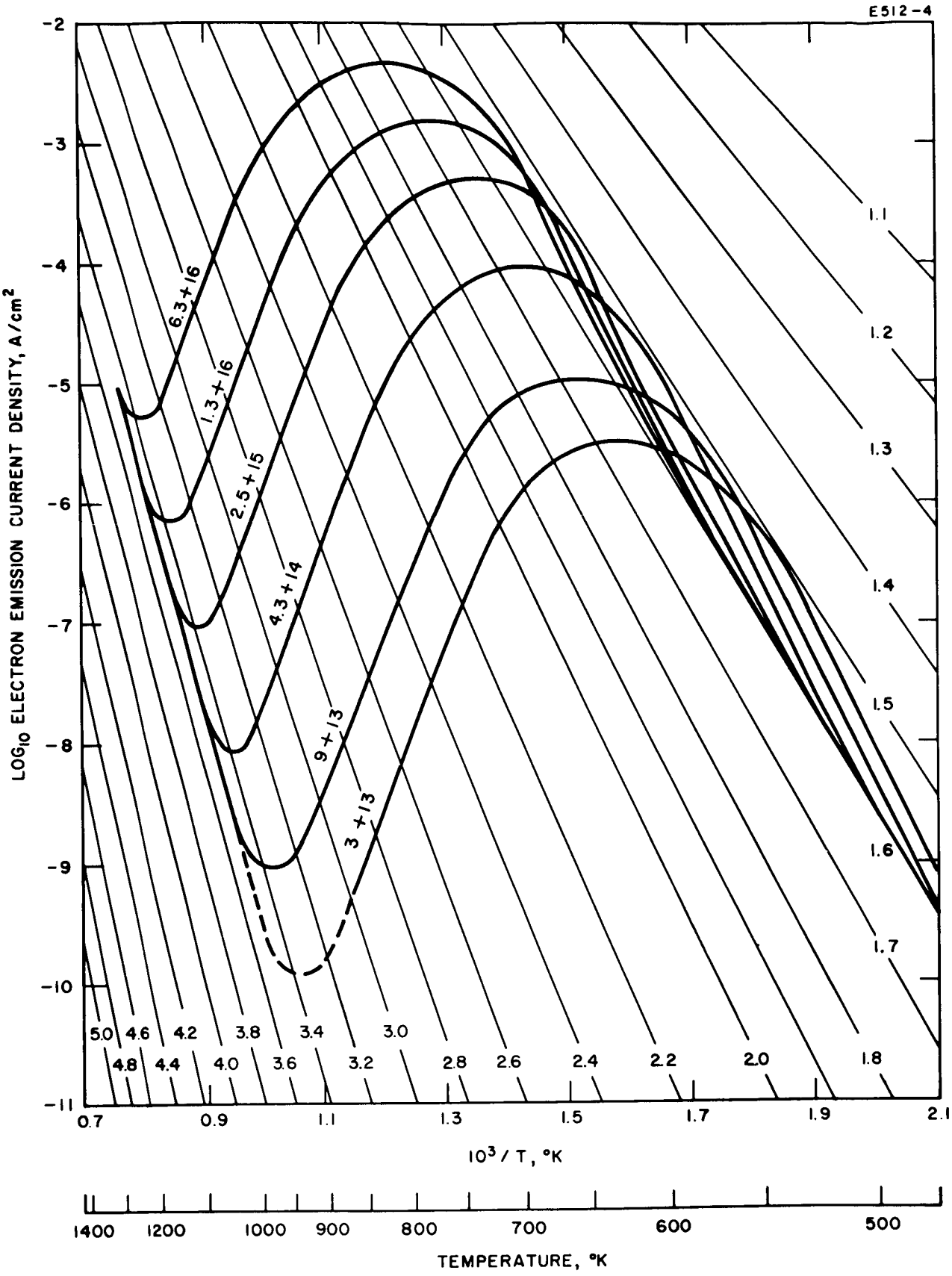

Fig. 15. Electron emission from cesiated 304 stainless steel.

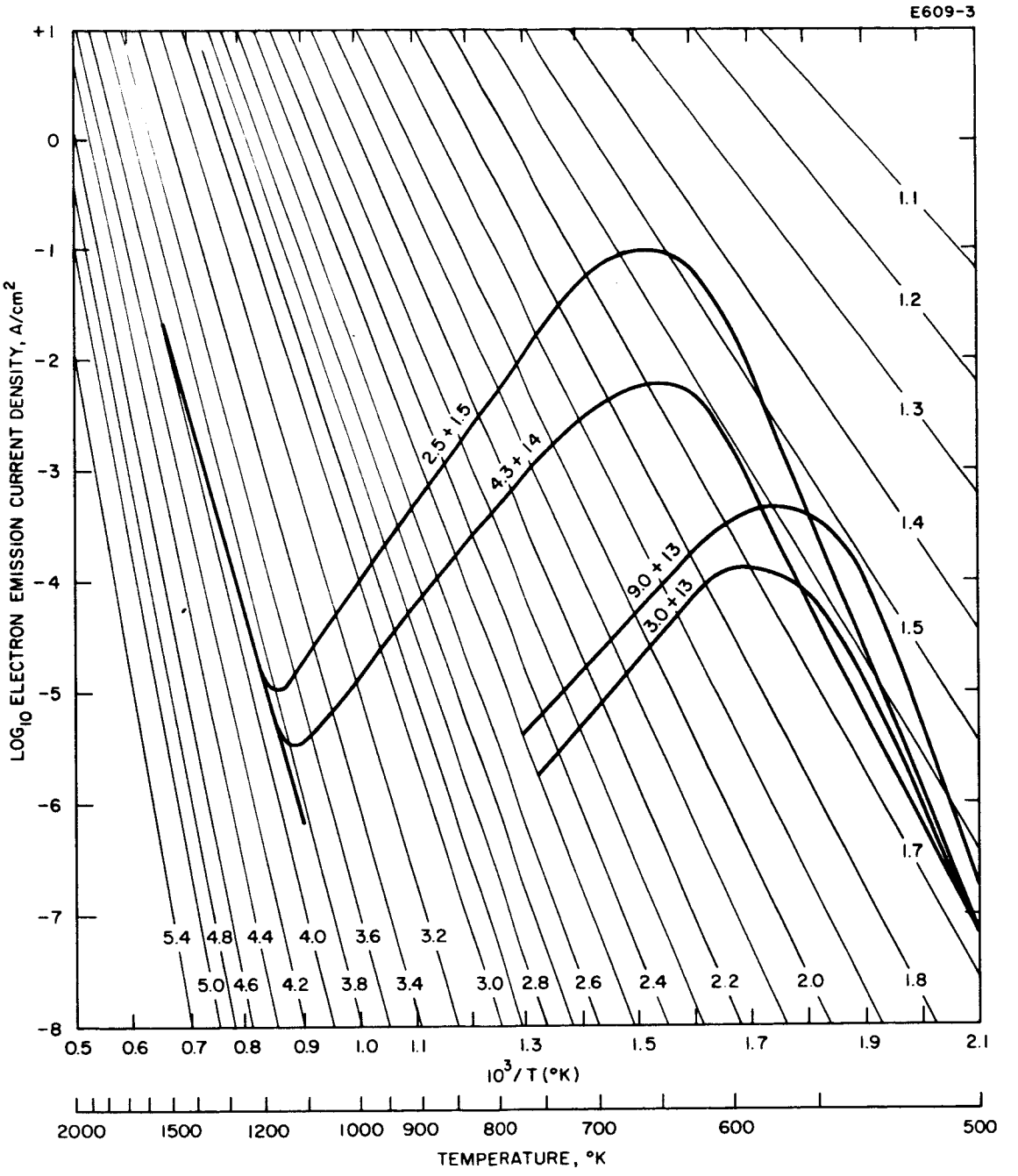

Fig. 16. Electron emission from cesiated tantalum boride ($TaB_2 \rightarrow \gamma TaB + B$).

17. Zirconium Carbide

The curves for zirconium carbide are interesting and significant to this program. In most cases, electron emission peaks could not be found (above leakage background currents) at all with the cup collector, and those observed with the aperture (diaphragm) collector (Fig. 17) are very low. The values of heavily cesiated work function, ~ 1.68 eV, and of the minimum cesiated work function, 1.60 eV, are similar to other materials; the emission magnitude is low at the maxima and minima. The peaks for 3.0×10^{13} and 9.0×10^{13} atoms/cm^2-sec were barely observed above the leakage current background. As seen in Fig. 17 they are found in the 10^{-12} and 10^{-11} A/cm^2 ranges. Comparing the data at 2.5×10^{15} atoms/cm^2-sec of cesium, at 850K, the emission is six orders lower than for copper, 1-1/2 orders below titanium, the next lowest, and 8 orders below a group of the highest emission surfaces.

18. Molybdenum Carbide

The electron emission S curves for cesiated molybdenum carbide (Mo_2C) are shown in Fig. 18. The curves are typical of refractory metals with work functions in the 4.5 to 4.7 eV range. The "clean" work function is about 4.3 eV, the heavily cesiated work function is about 1.48 eV, and the minimum work function is about 1.45 eV.

19. Molybdenum Silicide

The cesiated electron emission data for molybdenum silicide were reported in the Final Report on Contract NAS 3-5249.

20. Tantalum Silicide

The electron emission S curves for cesiated tantalum silicide ($TaSi_2 \rightarrow Ta_5Si_3$) are shown in Fig. 19. The "clean" work function is about 4.7 eV, the heavily cesiated work function is about 1.53 eV, and the minimum work function is about 1.47 eV.

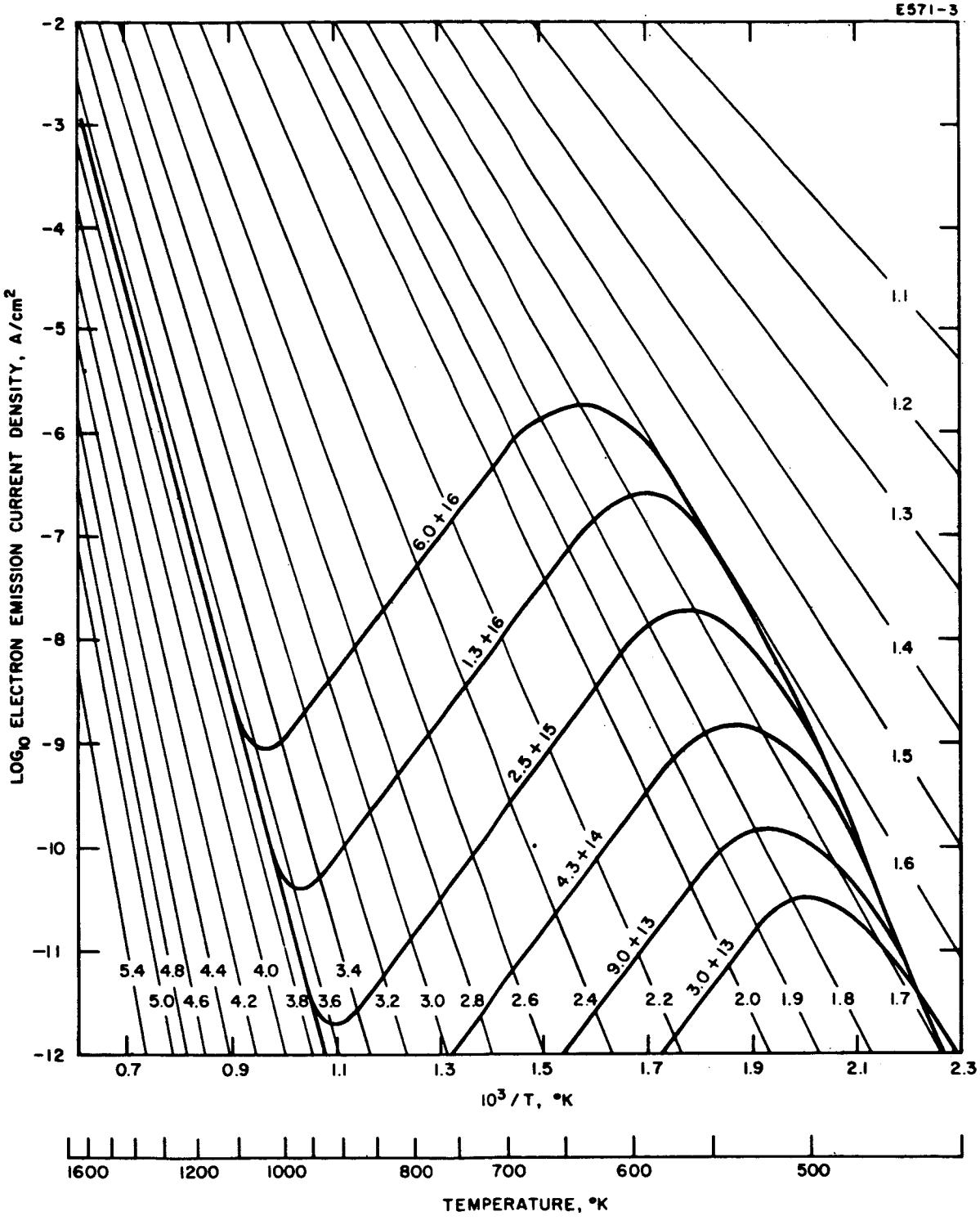

Fig. 17. Electron emission from cesiated zirconium carbide (ZrC).

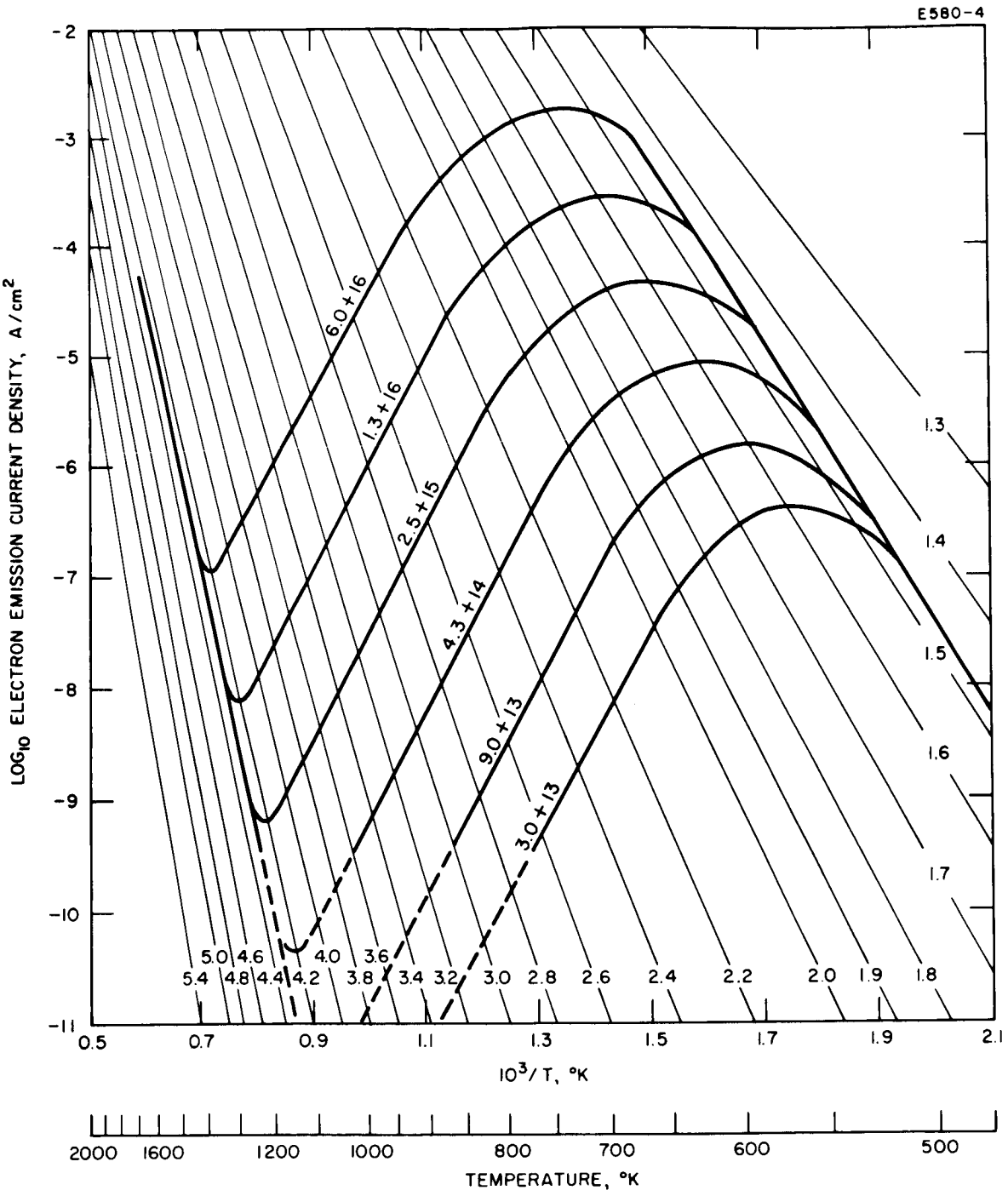

Fig. 18. Electron emission from cesiated molybdenum carbide (Mo_2C).

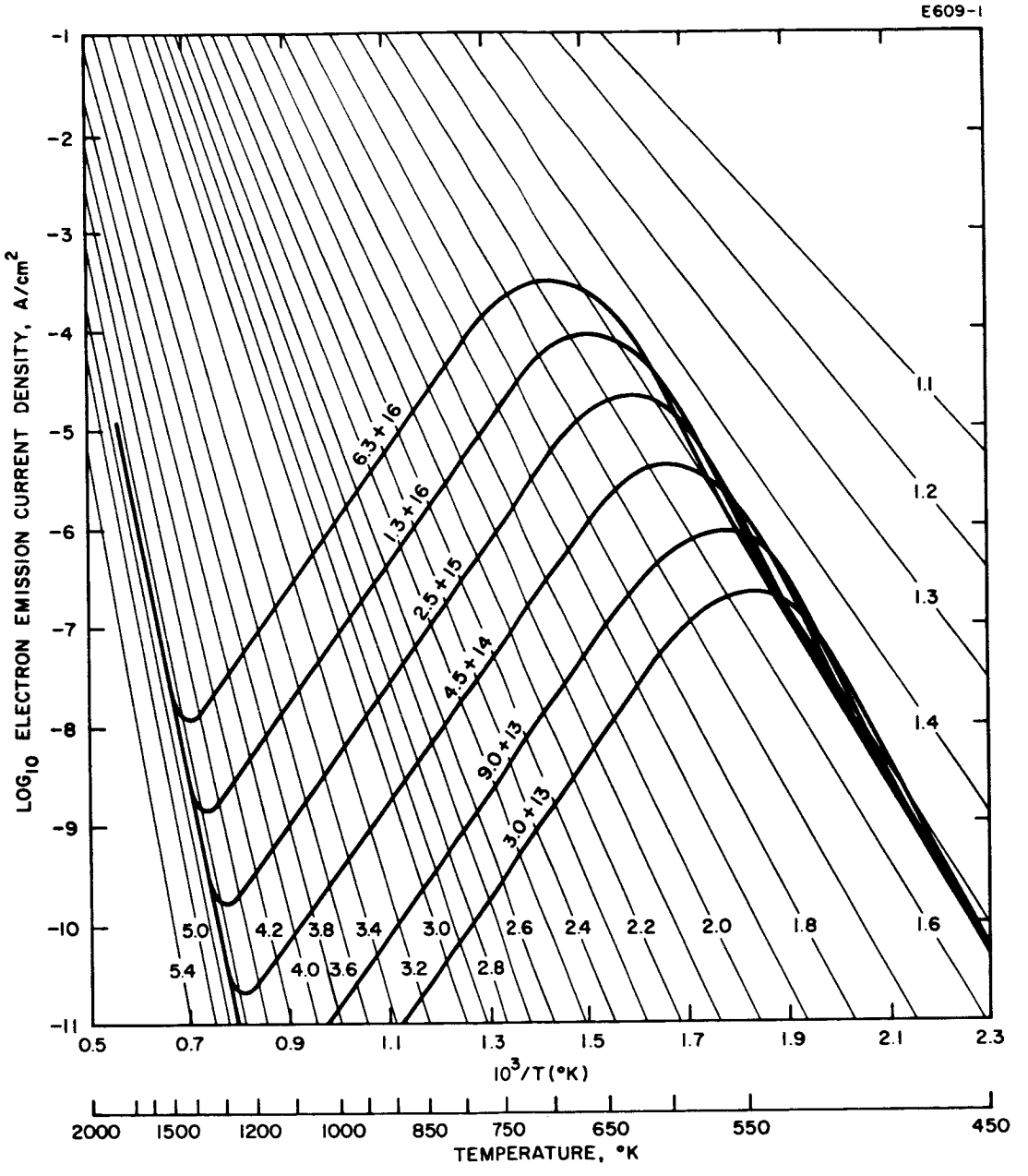

Fig. 19. Electron emission from cesiated tantalum silicide ($TaSi_2 \rightarrow Ta_5Si_3$).

21. Tungsten Silicide

The electron emission S curves for tungsten silicide ($WSi_2 \rightarrow$ 20% WSi_2 + 80% $WSi_{0.7}$) are shown in Fig. 20. The "clean" work function varies from 4.6 to 3.6 eV depending upon the temperature and the cesium arrival flux, the minimum work function is about 1.46 eV, and the heavily cesiated work function is about 1.50 eV.

22. Aluminum Oxide (Sintered)

The cesiated electron emission data for sintered aluminum oxide were reported in the Final Report on Contract NAS 3-5249.

23. Aluminum Oxide (Lucalox)

The curves for Lucalox aluminum oxide (shown in Figs. 21 and 22) are somewhat anomalous, irregular, inconsistent, and non-reproducible. Figure 21 is a representative full set of matching data obtained by starting from maximum temperature. A resemblance to a normal set of S curves is seen, with some exceptions. The "clean" work function varied with arrival flux from about 4.0 to about 3.5 eV, whereas the vacuum work function was about 5.0 eV. The curves for various arrival flux are spread out rather strangely. The values of heavily cesiated work function or minimum work function vary widely and anomalously between 1.75 and 1.35 eV. The corresponding set of electron emission curves obtained by increasing the temperature from room temperature at each flux is shown in Fig. 22. They are seen to be completely anomalous, exhibiting no emission maxima, but having regions of nearly constant emission and some surface-ionization-like discontinuities. The results for Lucalox alumina were nonreproducible in detail, but were reproducible in general shape and characteristics. One fundamental problem in the experimental design of the alumina tube, or any other insulator surface, should be recalled when these data are interpreted: a conductor (in this case copper foil)

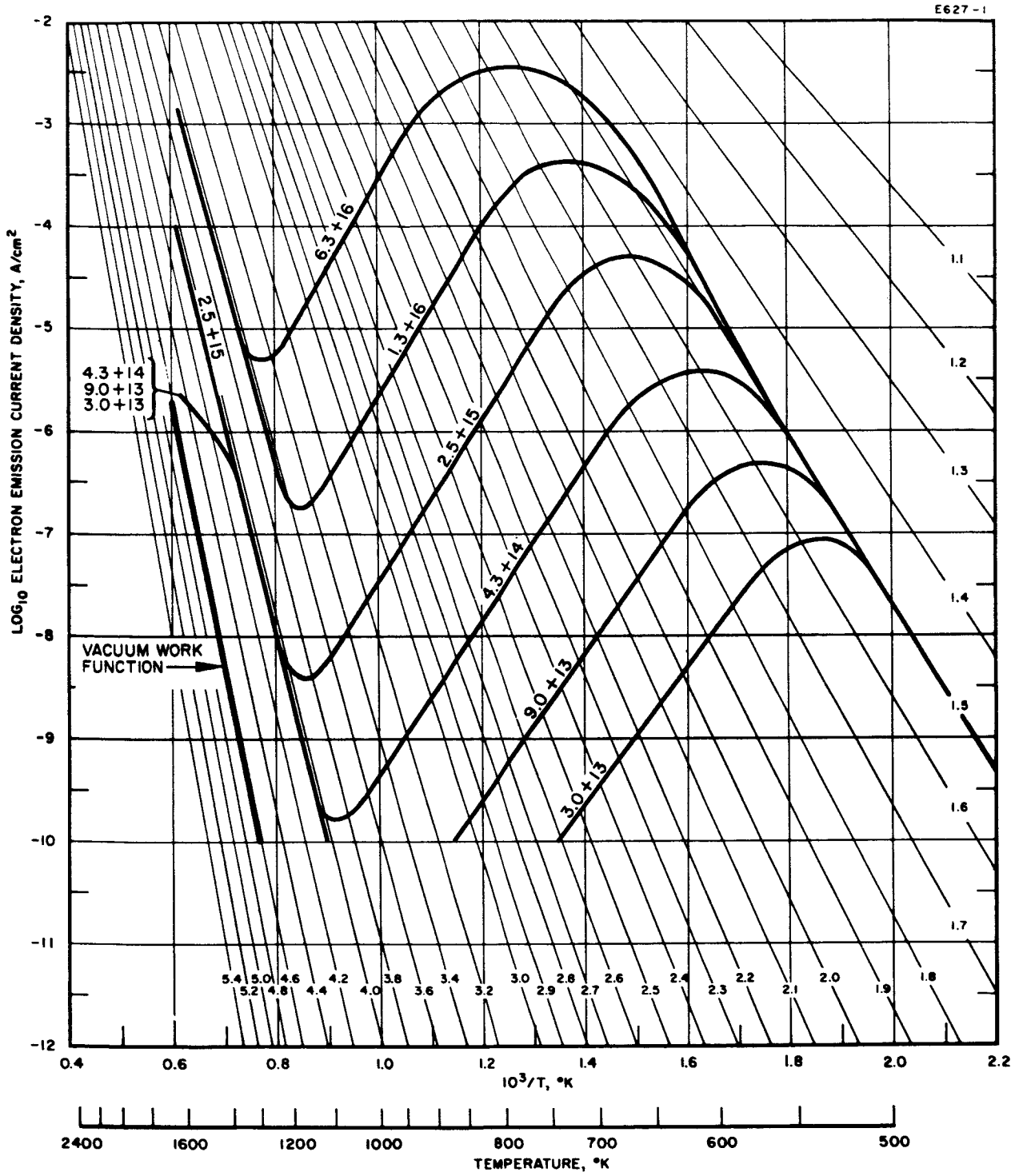

Fig. 20. Electron emission from cesiated tungsten silicide ($WSi_2 \rightarrow$ 20% WSi_2 + 80% $WSi_{0.7}$).

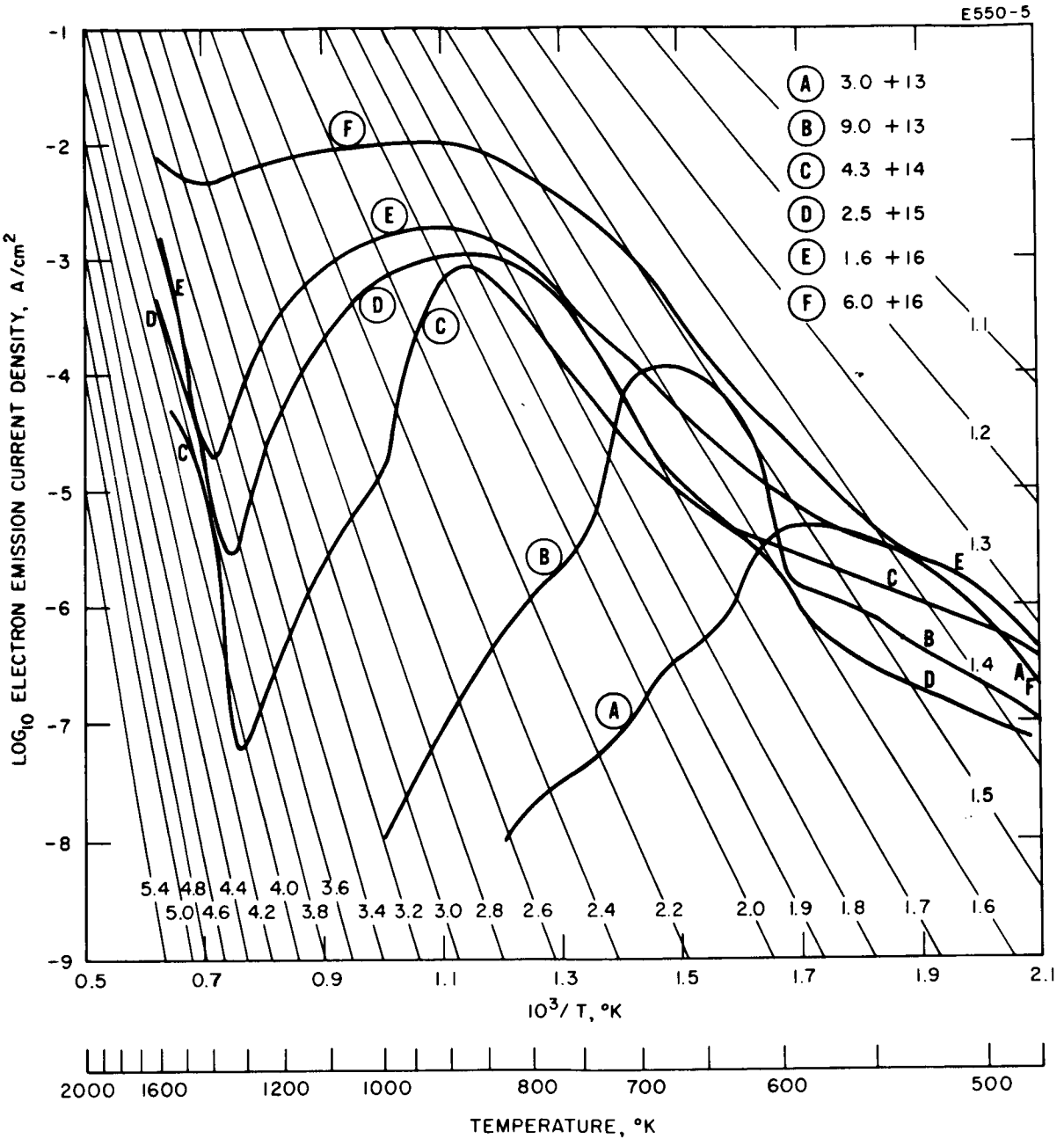

Fig. 21. Electron emission from cesiated Lucalox aluminum oxide (decreasing temperature).

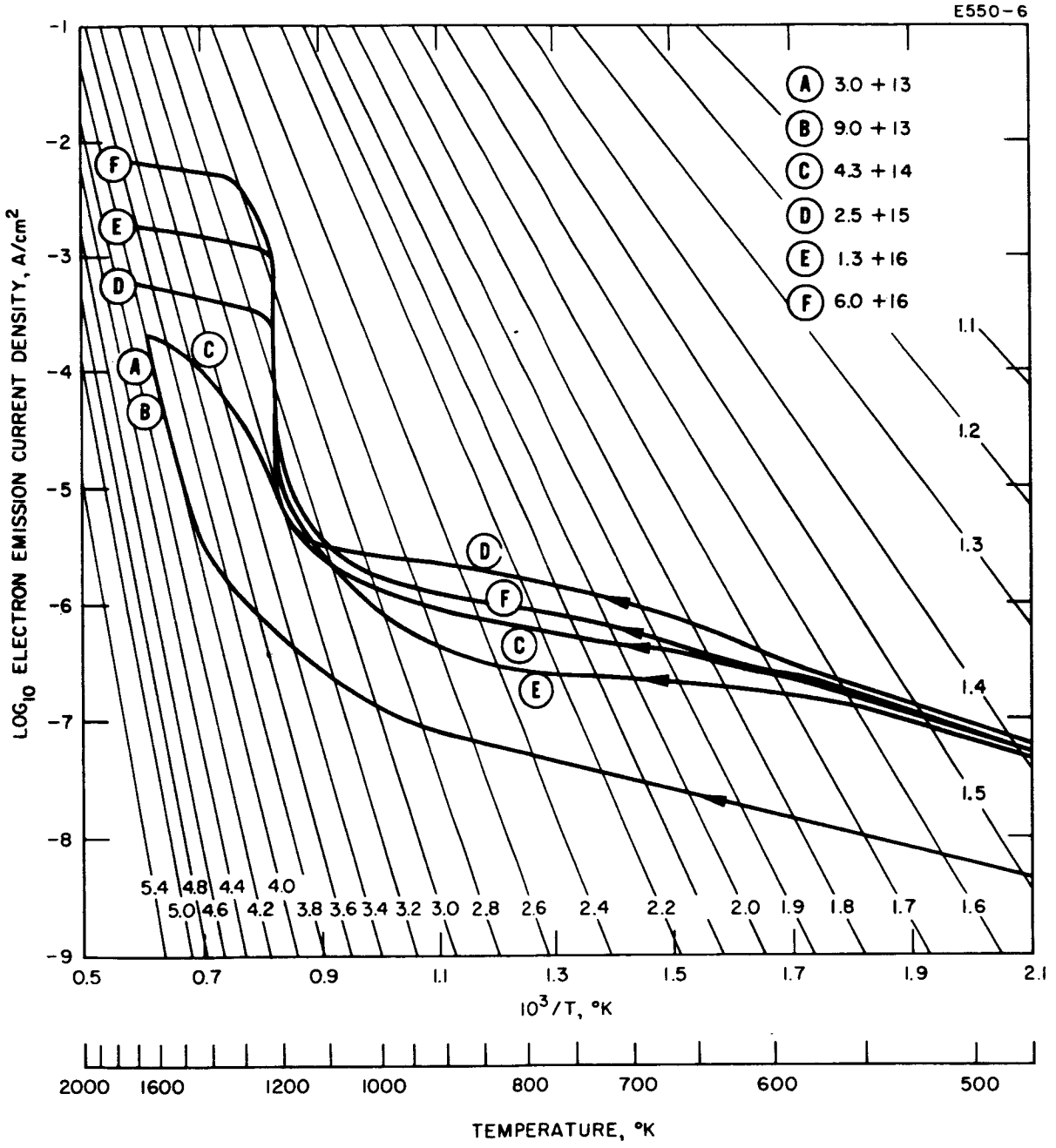

Fig. 22. Electron emission from cesiated Lucalox aluminum oxide (increasing temperature).

must be used as the collector to oppose the insulator surface. It is expected, however, that any copper sputtered onto the emitter is vaporized off when the emitter is flashed to high temperature before each new descending temperature run is started. These curves are significantly different from those for a porous and relatively impure alumina insulator surface reported under Contract NAS 3-5249. The anomalies may also be attributed to the fact that this emitter is an insulator, which allows several possible arguments and explantations.

24. Oxygenated Copper

The electron emission S curves obtained for four oxygenated conditions of copper at three cesium arrival fluxes are shown in Figs. 23 through 27. Figures 23, 24, and 25 show the curves for each of the three cesium arrival fluxes separately, together with the previously obtained corresponding curves of unoxygenated copper. The three lowest oxygen partial pressures are shown as one curve in each case; some minor deviations from the composite curve occurred, but they were random and no consistent pattern was exhibited. Figures 26 and 27 are the same data plotted at two conditions of oxygen pressure at the three cesium arrival fluxes. The following observations are made. For oxygen pressures (measured in the oxygen side arm) of zero, 2×10^{-6} and 2×10^{-5} Torr, essentially no difference was observed. At an oxygen pressure of 2×10^{-4} Torr, a change did occur; the emission level decreased at the normal low temperature maximum and a second higher temperature emission maximum with a higher emission level appeared (or increased). The second or higher temperature emission maximum did exist (at a reduced level) at the lowest cesium arrival flux. In all cases, the oxygenated emission curves, including the one for no oxygen release into the cesiated copper region, are higher and sharper than those previously obtained for cesiated copper in the absence of any oxygen introduction. The increase is about

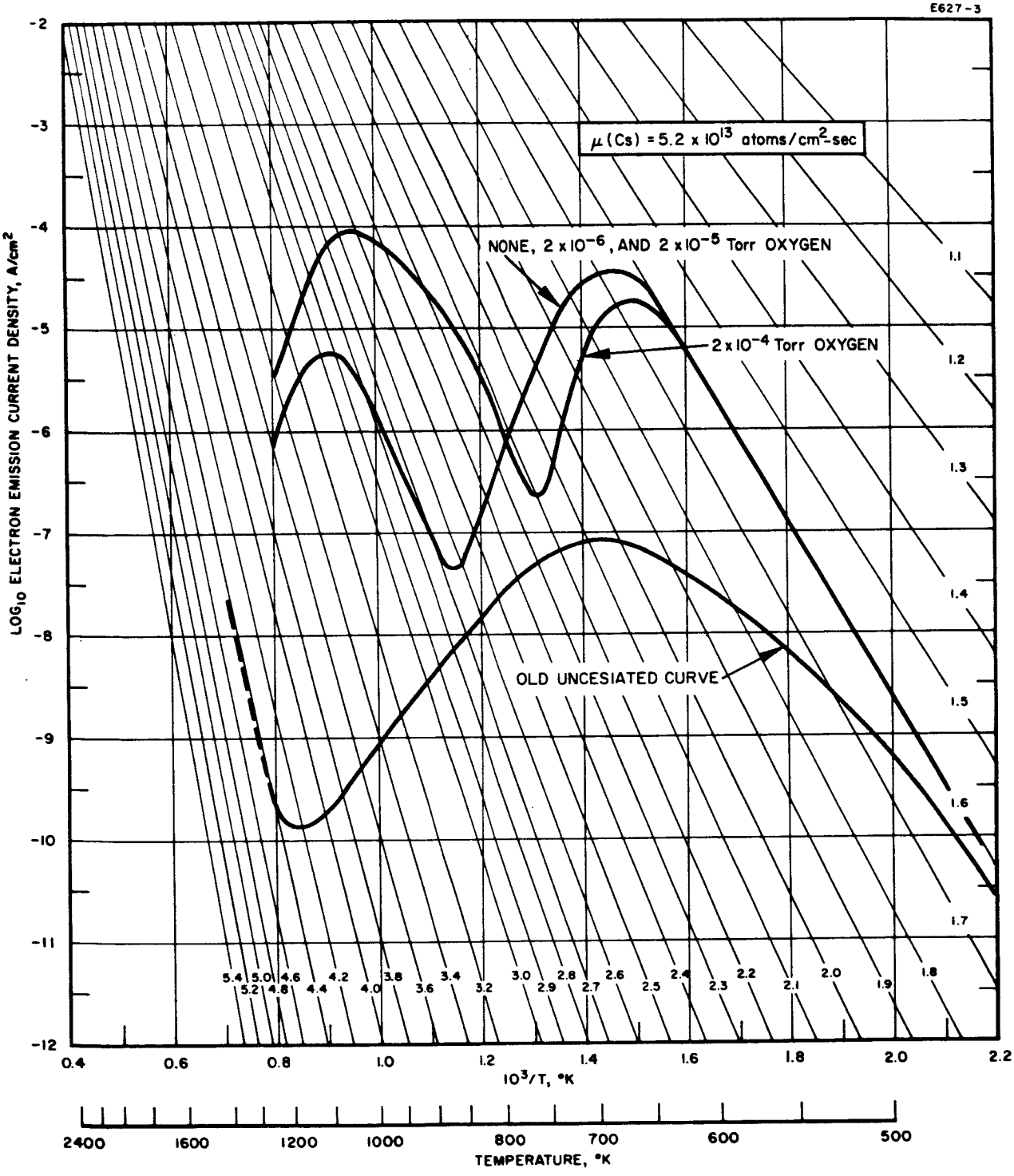

Fig. 23. Electron emission from cesiated, oxygenated copper. μ(Cs) = 5.2 x 10^{13} atoms/cm^2-sec.

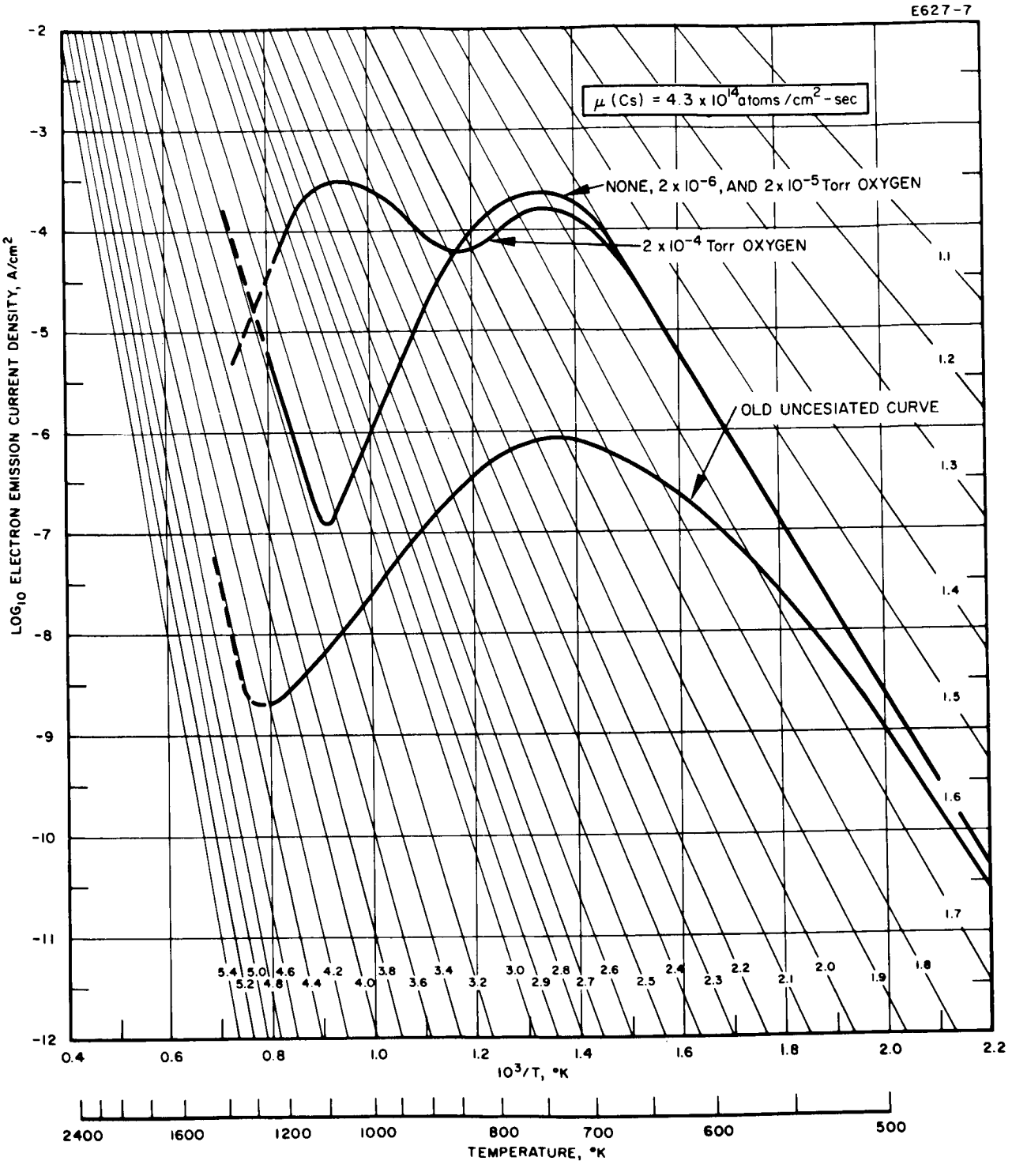

Fig. 24. Electron emission from cesiated, oxygenated copper. $\mu(Cs) = 4.3 \times 10^{14}$ atoms/cm^2-sec.

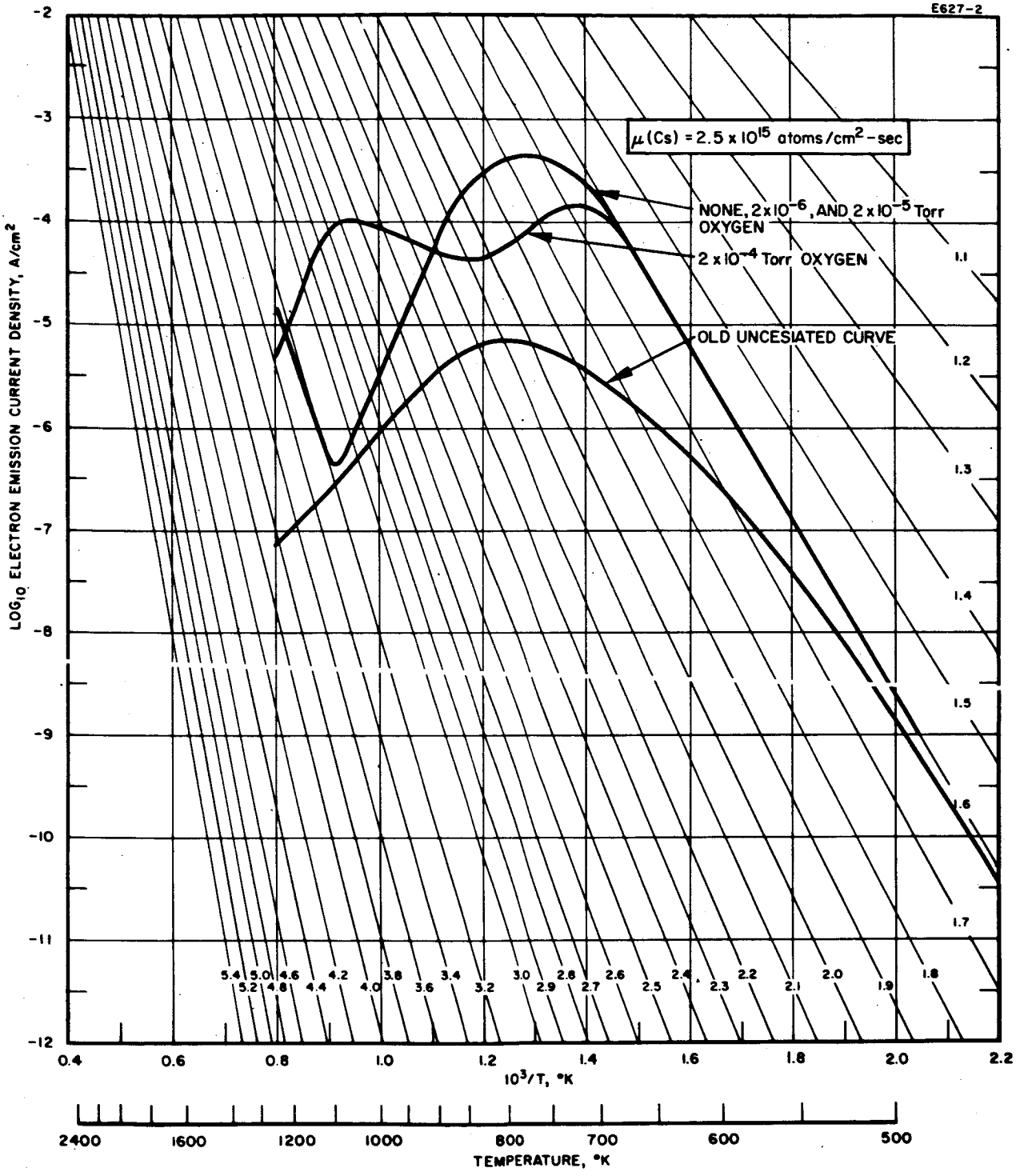

Fig. 25. Electron emission from cesiated, oxygenated copper. μ(Cs) = 2.5 x 10^{15} atoms/cm^2-sec.

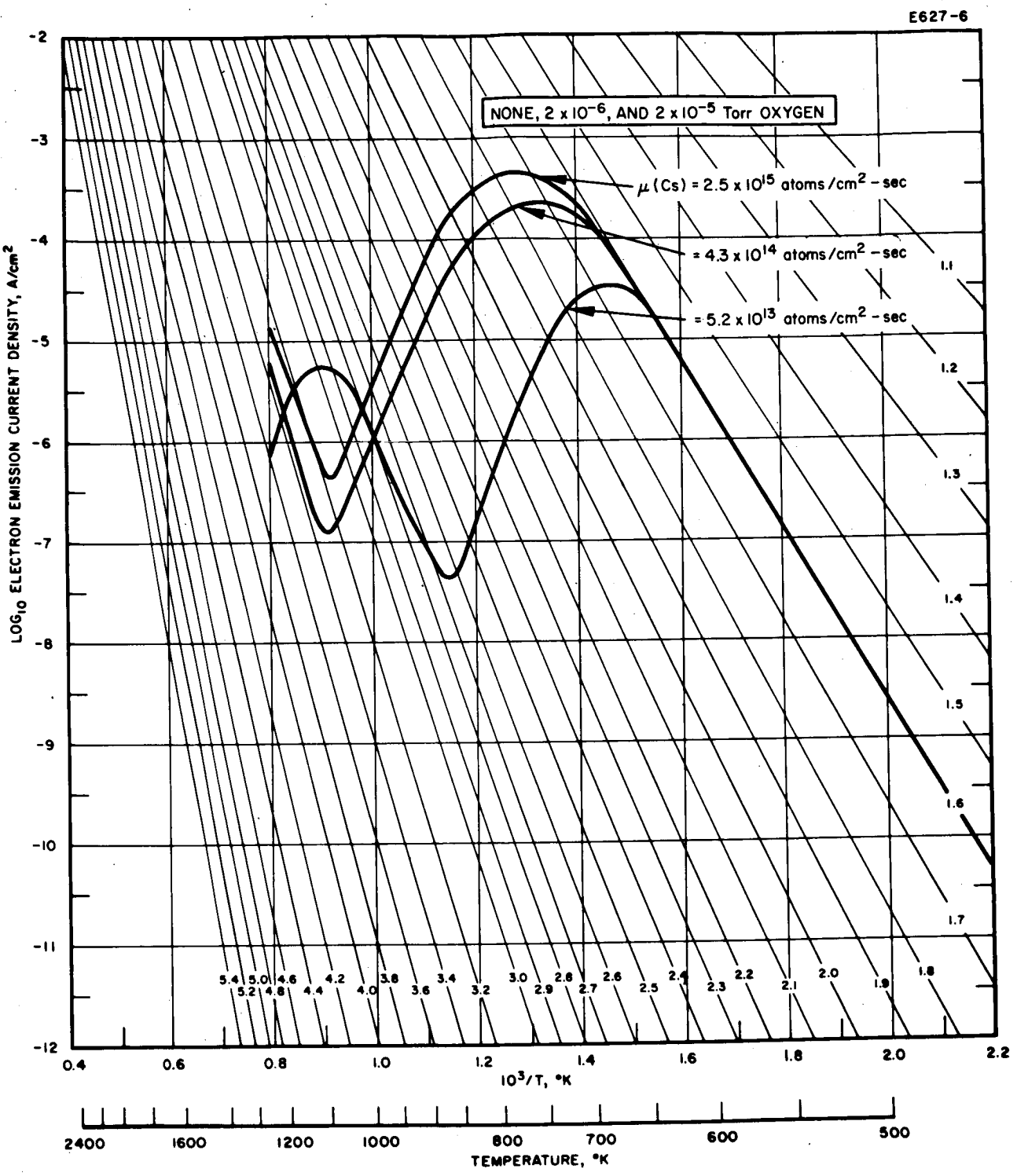

Fig. 26. Electron emission from cesiated, oxygenated copper. None, 2×10^{-6}, and 2×10^{-5} Torr oxygen.

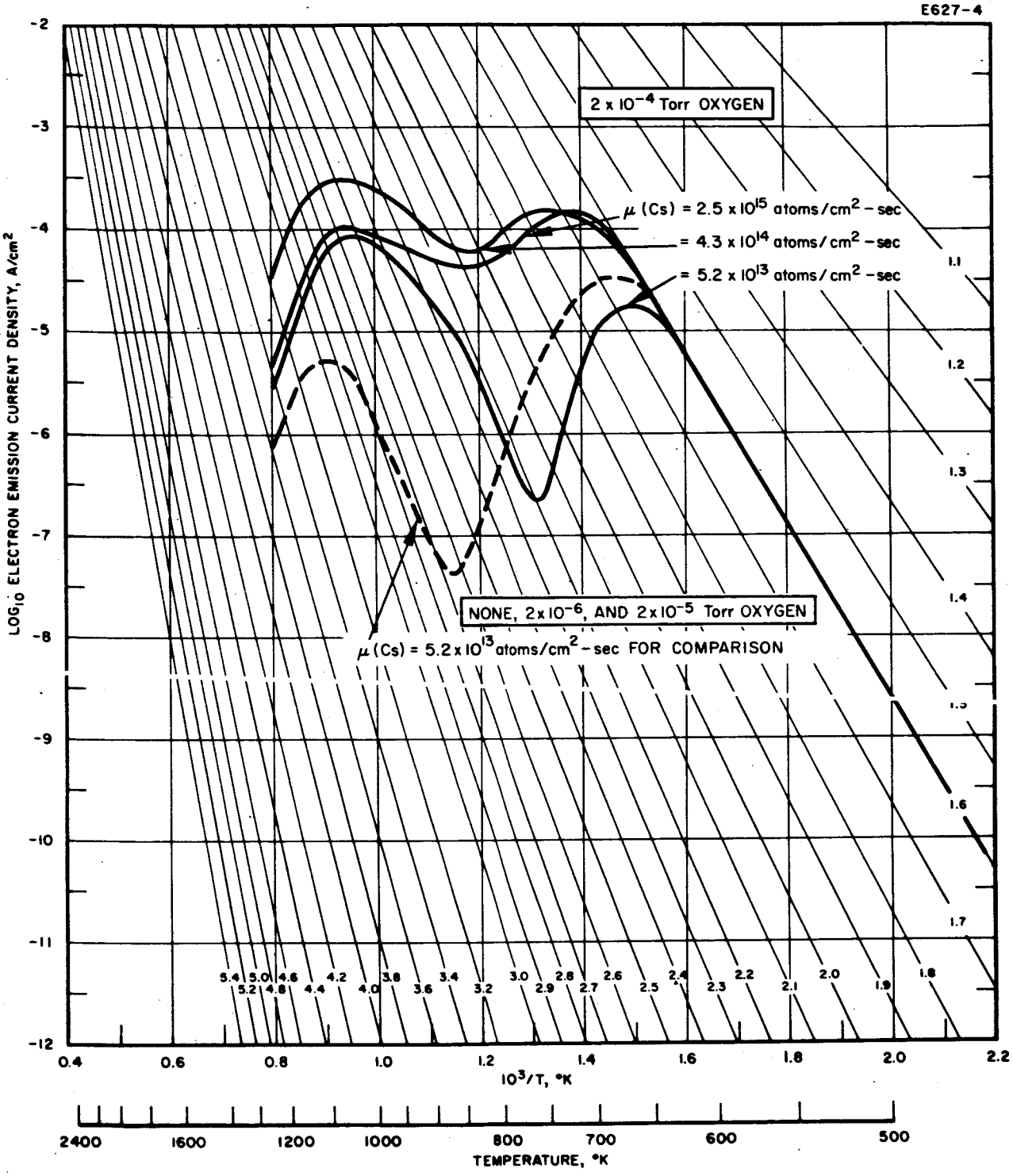

Fig. 27. Electron emission from cesiated, oxygenated copper. 2 x 10^{-4} Torr oxygen.

two orders of magnitude, with a tendency to decrease with increasing cesium arrival flux. The second emission maximum occurs near the minimum in the previous curves, resulting in a rather flat emission curve. Some interchange of maximum emission levels occurred at both high cesium and high oxygen pressure (Fig. 27). A curve exhibiting two emission maximum for cesiated and oxygenated copper occur and can definitely be attributed to the presence of oxygen. However, the data indicate that once oxygen has been introduced in fairly large quantities, the emission curve does not (at least soon) revert to the clean or never oxygenated emission condition, even though no oxygen is being introduced. That is, a permanent or semipermanent oxygen "poisoning" occurs which is characterized by increase emission (about two orders at the maximum).

The minimum work function and heavily cesiated work function for the oxygenated conditions are the same and are about 1.60 eV, which is the value ultimately approached by the previous unoxygenated curves. In Figs. 24 and 25, "clean" work function lines (for the oxygenated and cesiated condition) show at about 3.35 and 3.25 eV, while the second emission maximum completely obscures such a portion of the curves in Fig. 23 and for the highest oxygen condition in all cases (that is, when the second emission maximum occurs).

The oxygen was introduced from a second side arm by heating BaO_2, which decomposes to $BaO + O_2$. Cesium is known to getter oxygen to form various cesium oxides. The copper surface had been heavily oxygenated, but later cleaned up to cause the return of the vacuum copper condition, prior to the distillation of cesium into the tube. Because the emission curves for no oxygen release from the BaO_2 arm are the same as for the two lowest oxygen conditions, but all of these curves are different from the previous unoxygenated curves, it is concluded that for low oxygen pressures and even for no oxygen release, a minimum oxygenation level is maintained (either by the arrival of cesium oxide formed from prior oxygenation conditions, or bound on the copper surface) until the oxygen

pressure is increased to about 10^{-4} Torr, at which time the effects seen in the figures occur.. This raises the question as to how much of the oxygen being released into the cesium filled copper emitter volume reaches the copper emitter surface, any reduction being attributed to tying up of oxygen by the cesium on the walls of the tube.

An x-ray diffraction measurement was performed on the copper emitter following the measurements described above. The results showed randomly oriented copper with a small but definite series of lines for monoclinic CuO. This small amount of CuO could correspond to a larger relative surface concentration assuming it is all on the surface, while the copper lines also result from a deeper (bulk) penetration of x-rays. Furthermore, when the emitter was removed from the experimental tube, pockets of green coloration could be clearly seen on the copper emitter surfaces. This indicates that a semipermanent oxygenated (actually CuO) condition existed, and therefore probably accounts for the changed emission even for the condition of no oxygen release. This leads to the conclusion that the data described above are for an "oxidized" copper surface, rather than for an "oxygenated" copper surface, the implication being that for an "oxidized" surface, the oxygen is not adsorbed in a partial monolayer which desorbs easily upon heating, but rather a strong chemical bond exists between the oxygen and copper — a CuO bond and surface.

25. Iridium-Coated Porous Tungsten

Data were obtained for iridium coated porous tungsten at four cesium arrival fluxes corresponding to 10, 30, 50, and 70C cesium vapor temperatures. The data had to be recorded for very slow rates of temperature change for this emitter, apparently because cesium diffused into the porous structure and extra time was required to reach kinetic equilibrium while cesium diffused in or out from the pores as the surface temperature was lowered or raised. The data were qualitatively the same as for pure iridium and therefore are not included.

As a summary and comparison, the cesiated work functions for all of the materials are listed in Table XXIII. The "clean" cesiated work function is the constant work function approached as the surface temperature is increased above that where the emission minimum occurs; supposedly where the surface coverage is small enough the surface work function is not affected measurably. Under these conditions, however, the surface has been repeatedly heated and cooled in a cesium atmosphere.

C. CESIUM ION EMISSION

The cesium ion emission current density versus surface temperature curves have been measured, in general, at six cesium arrival fluxes between 10^{13} and 10^{17} atoms/cm^2-sec for surfaces of beryllium, titanium, chromium, nickel, copper, niobium, tantalum, tungsten, rhenium, osmium, iridium, platinum, 304 stainless steel, tantalum boride, zirconium carbide, molybdenum carbide, tantalum silicide, tungsten silicide, aluminum oxide (Lucalox), oxygenated copper, and iridium coated porous tungsten. The values of applied voltage are just greater than those required to draw saturated ion emission, that is, just above the "knee."

1. Beryllium

For beryllium (Fig. 28), all of the increasing temperature curves fall on the same line, which corresponds to low emission levels and low ionization efficiencies at higher arrival fluxes, compatible with the low vacuum work function measured for beryllium (3.67 eV). The decreasing temperature curves exhibit an irregular and large hysteresis effect which increases with increasing arrival flux. This type of structure has also been observed for chromium. The two metals have one important common characteristic — low work function — and it may be

TABLE XXIII

Cesiated Work Functions

Surface Material	Vacuum Work Function, eV	"Clean" Cesiated Work Function, eV	Heavily Cesiated Work Function ($\theta > 1$), eV	Minimum Cesiated Work Function ($\theta \approx 0.7$),[a] eV
Beryllium	3.67	3.67	1.94	1.94
Titanium	3.8	3.75	1.44	1.32
Chromium	3.90	3.55	1.81	1.70
Iron	4.5	3.7	1.85	1.8
Nickel	4.7	> 4.0	1.7 - 2.0	1.7 - 2.0
Copper	4.42	4.4	1.64	1.64
Niobium	4.19	4.1	1.62	1.44
Molybdenum	4.2 - 4.3	4.35	1.74	1.62
Tantalum	4.25	4.25	1.55	1.47
Tungsten	4.50	4.47	1.63	1.61
Rhenium	4.96	4.80	1.57	1.53
Osmium	4.84	4.75	1.48	1.48
Iridium	5.27	5.2	1.85	1.79
Platinum	5.7	5.0	1.66	1.59
304 Stainless Steel	4.3	3.5	1.60	1.52
Tantalum Boride	4.26	3.9	1.67	1.5
Zirconium Carbide	3.70	3.70	1.60	1.68
Molybdenum Carbide	4.73	4.3	1.48	1.45
Molybdenum Silicide	4.72	4.7	1.84	1.73
Tantalum Silicide	4.71	4.7	1.53	1.47
Tungsten Silicide	4.62	4.6	1.50	1.46
Alumina (sintered)	4.91	5.0	1.84	1.84
Alumina (Lucalox)	5.19	~4	1.6 - 1.8	1.6 - 1.8
Oxygenated Copper	4.5 to >8	3.4 and up	1.60	1.60
Iridium-Coated Porous Tungsten	5.25	(5.2)	(1.8)	(1.8)

[a] $\theta \approx 0.7$ assumed at ϕ_{min} from Taylor and Langmuir.

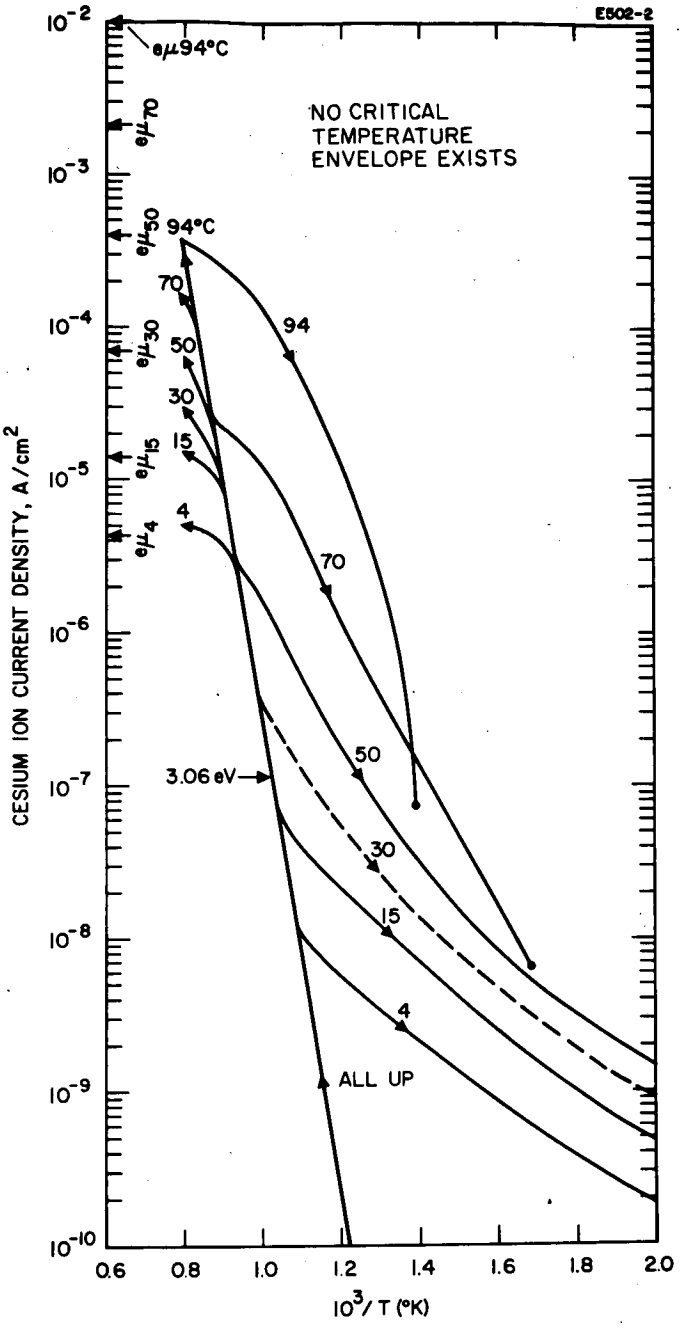

Fig. 28. Cesium ion emission from beryllium.

speculated that curves of this shape may be characteristic of low work function surfaces. A critical temperature envelope cannot be drawn clearly for beryllium, but the slope of the straight line in Fig. 28 yields 3.06 eV for a desorption energy for cesium from beryllium at low coverage.

2. Titanium

The cesium ion emission curves for titanium (Fig. 29) are uniform and sharp. Small temperature hysteresis occurs at low arrival fluxes and disappears above 10^{-3} A/cm^2. The critical temperature envelope (increasing temperature) for titanium is the lowest observed for all of the materials studied to date or known to have been studied elsewhere. At 10 mA/cm^2, the critical temperature for titanium is 170K lower than that for tungsten. A heater failure terminated the cesiated emission measurements before the highest cesium arrival fluxes were completed.

3. Chromium

Cesium ion emission data for chromium were previously reported in the Final Report on Contract NAS 3-5249. Some anomalies, including very large hysteresis and two kinds of saturated ion emission, led to the statement that those data were questionable and therefore tentative and subject to remeasurement. The anomalies were attributed to a high pressure in the experimental tube. The measurements for chromium have been repeated (Fig. 30) under suitable pressure conditions, and the curves are not anomalous. Previously only two curves with a well defined critical temperature were observed. These two curves are included in Fig. 30. Although an extremely large anomalous temperature hysteresis effect was measured previously, only small conventional ones occurred during these measurements. However, an indication of the same high ion current emission at lower temperatures appears at a very low level in Fig. 30, and it

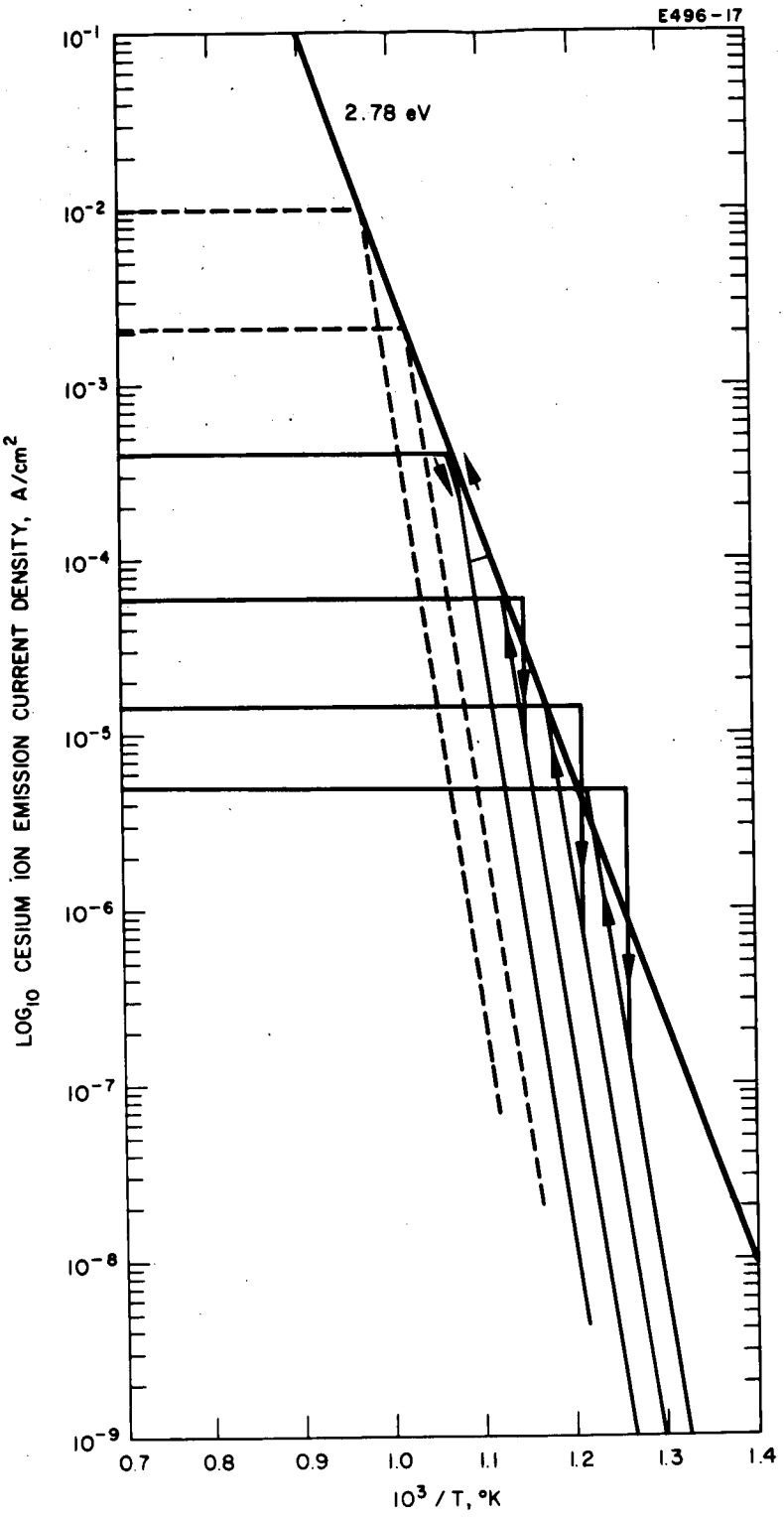

Fig. 29.
Cesium ion emission from titanium.

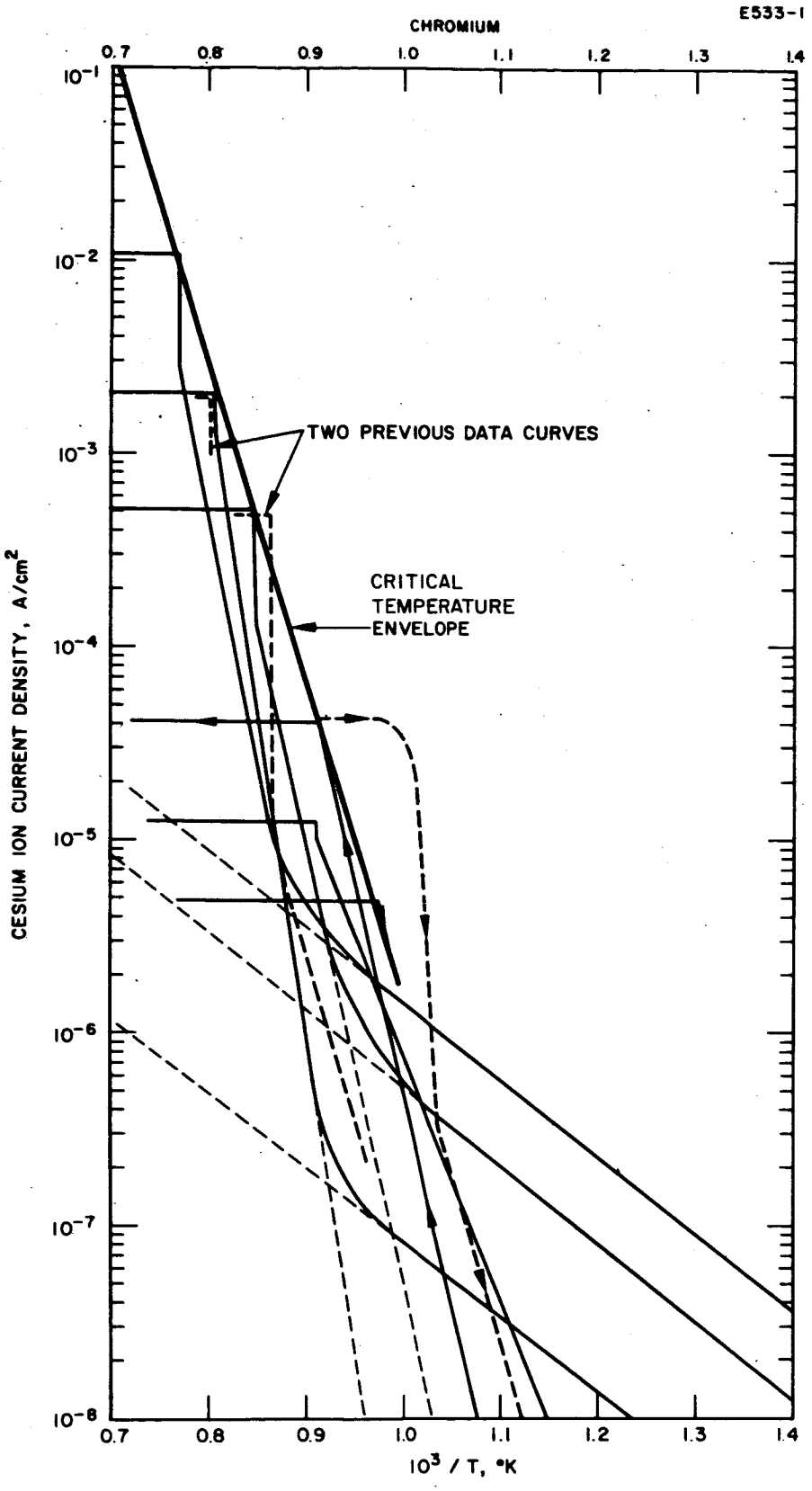

Fig. 30. Cesium ion emission from chromium.

increases with increasing cesium pressure. The subtractions of the two kinds of curves are shown. The two previously measured "normal" critical temperatures are seen to be in reasonable agreement with the new envelope. The ion desorption energy obtained from the chromium critical temperature envelope is 3.28 eV.

4. Iron

The cesium ion emission data for iron were reported in the Final Report on Contract NAS 3-5249.

5. Nickel

The cesium ion emission data for nickel (Fig. 31) result in a low critical temperature envelope. The curves are sharp and distinct. The ion and electron emission data for nickel when considered together may be indicative of an unusually wide range of work function distribution for nickel. The slope of the critical temperature envelope gives a value of 2.26 eV for the cesium ion desorption energy at critical coverage for nickel.

6. Copper

The curves for copper (Fig. 32) are normal. A more usual form of temperature hysteresis is observed. The effect decreases with increasing cesium arrival flux, as usual, probably disappearing just above 10 mA/cm^2 of cesium ions. The same S-shaped curve (reported in the Final Report on Contract NAS 3-5249) in the nonsaturated region for increasing temperature at low arrival fluxes was observed this time. A very good critical temperature envelope can be drawn for the copper data. Its slope yields the value 2.85 eV for the desorption energy of cesium from copper at low coverage.

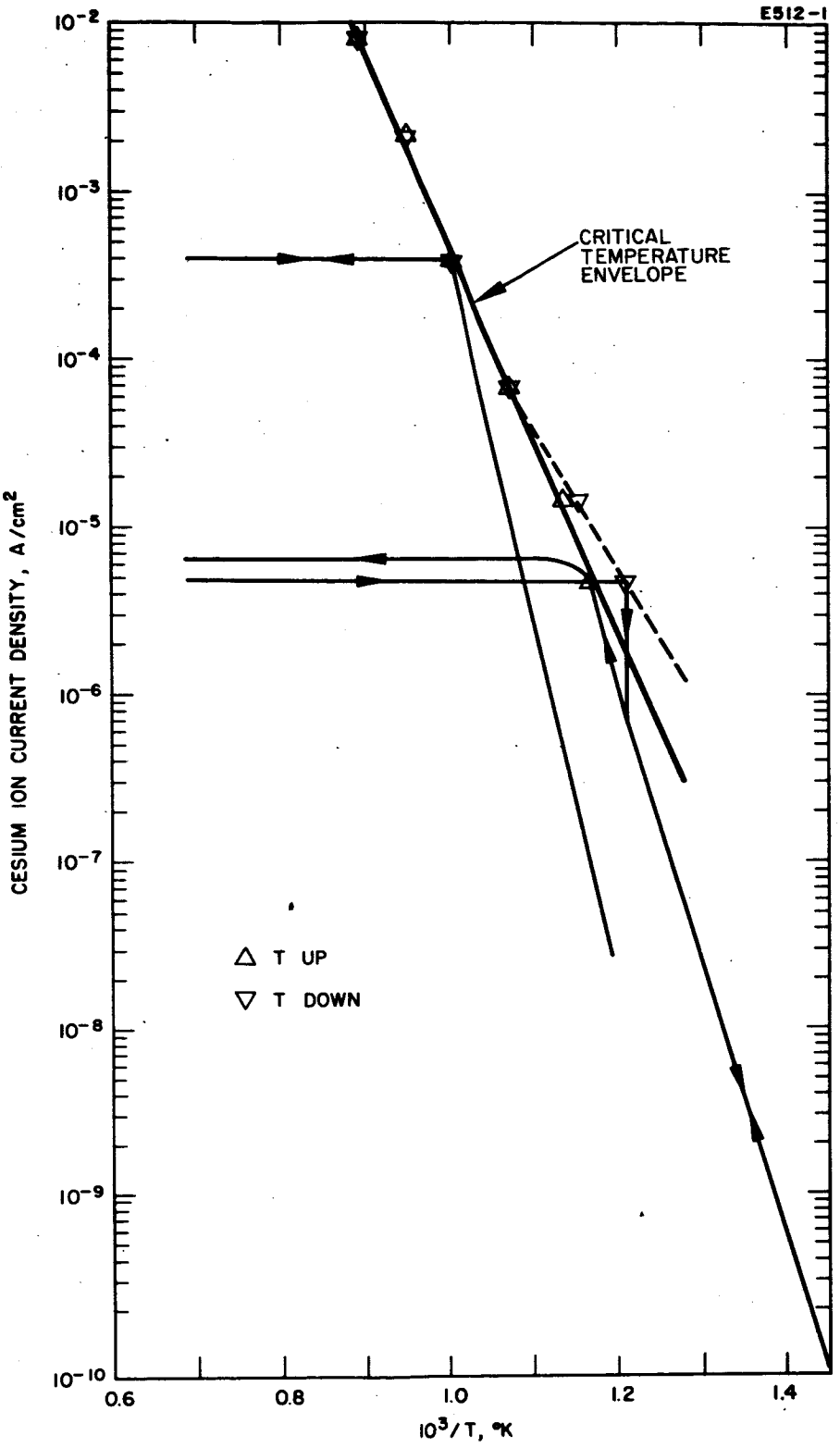

Fig. 31. Cesium ion emission from nickel.

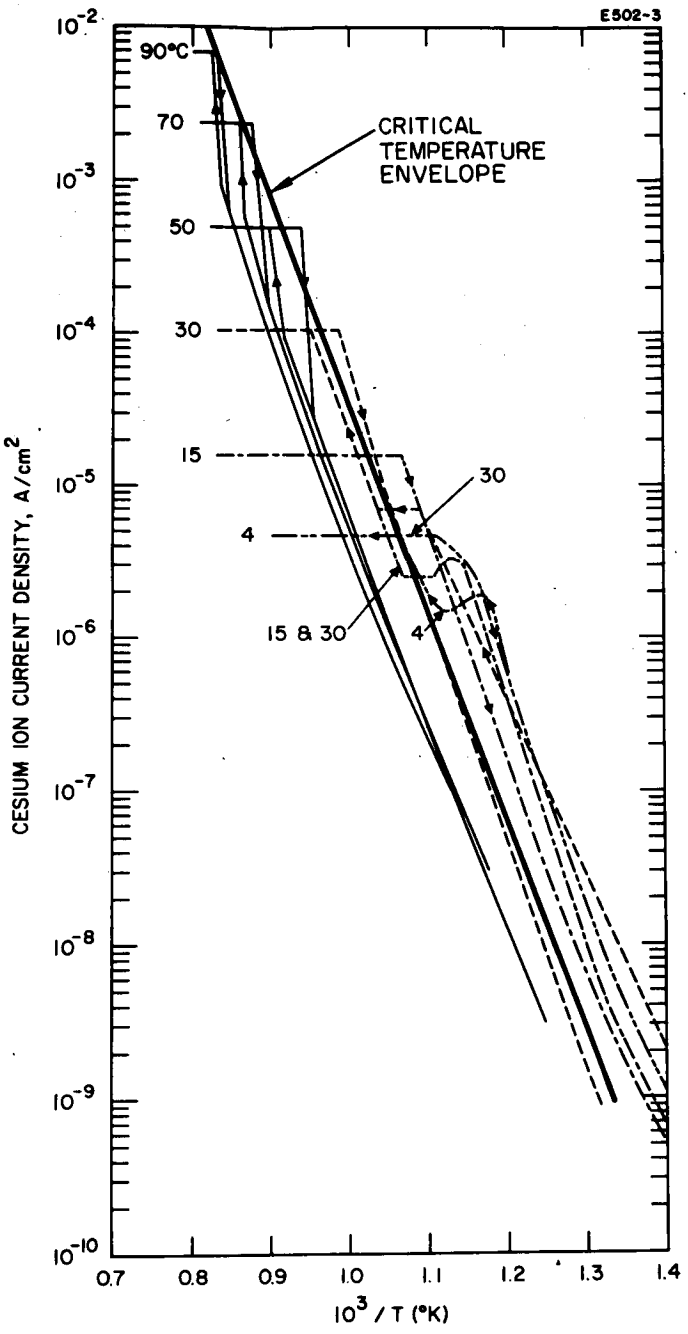

Fig. 32. Cesium ion emission from copper. The experimental data curves for cesium temperatures of 4, 15, and 30 C are done in different symbols because of overlapping.

7. Niobium

The cesium ion emission curves for niobium are shown in Fig. 33. The curves for niobium exhibit no sharp critical temperature break but rather a continuous rise to saturation. Full ionization is achieved for niobium. The average value of the cesium ion desorption energy obtained from the critical temperature slope is 2.85 eV.

8. Molybdenum

The cesium ion emission data for molybdenum were reported in the Final Report on Contract NAS 3-6278.

9. Tantalum

The data for tantalum are somewhat anomalous. A set of curves with somewhat poor consistency and uniformly low ionization efficiencies (24 to 42%) are shown in Fig. 34. These curves were all obtained early, while the anomalous electron emission data described above were being obtained. The two consistent curves at 4.3×10^{14} and 2.5×10^{15} atoms/cm^2-sec with higher ionization efficiencies (83 and 87%) were obtained after the anomalously high electron emission mode had been permanently destroyed. These curves are assumed to be the correct ones for the finally stable and reproducible tantalum surface. The cesium ion desorption energy obtained from the slope of the envelope is quite high, 3.96 eV. The 83 and 87% ionization efficiencies are consistent with the measured vacuum work function of 4.25 eV. The desorption energy is rather unusually high and may be related to the anomalous emission effects. Tantalum is known to be a good getter for certain gases, especially hydrogen, and such effects may be the cause for all of the problems encountered for tantalum and even for the tantalum compounds.

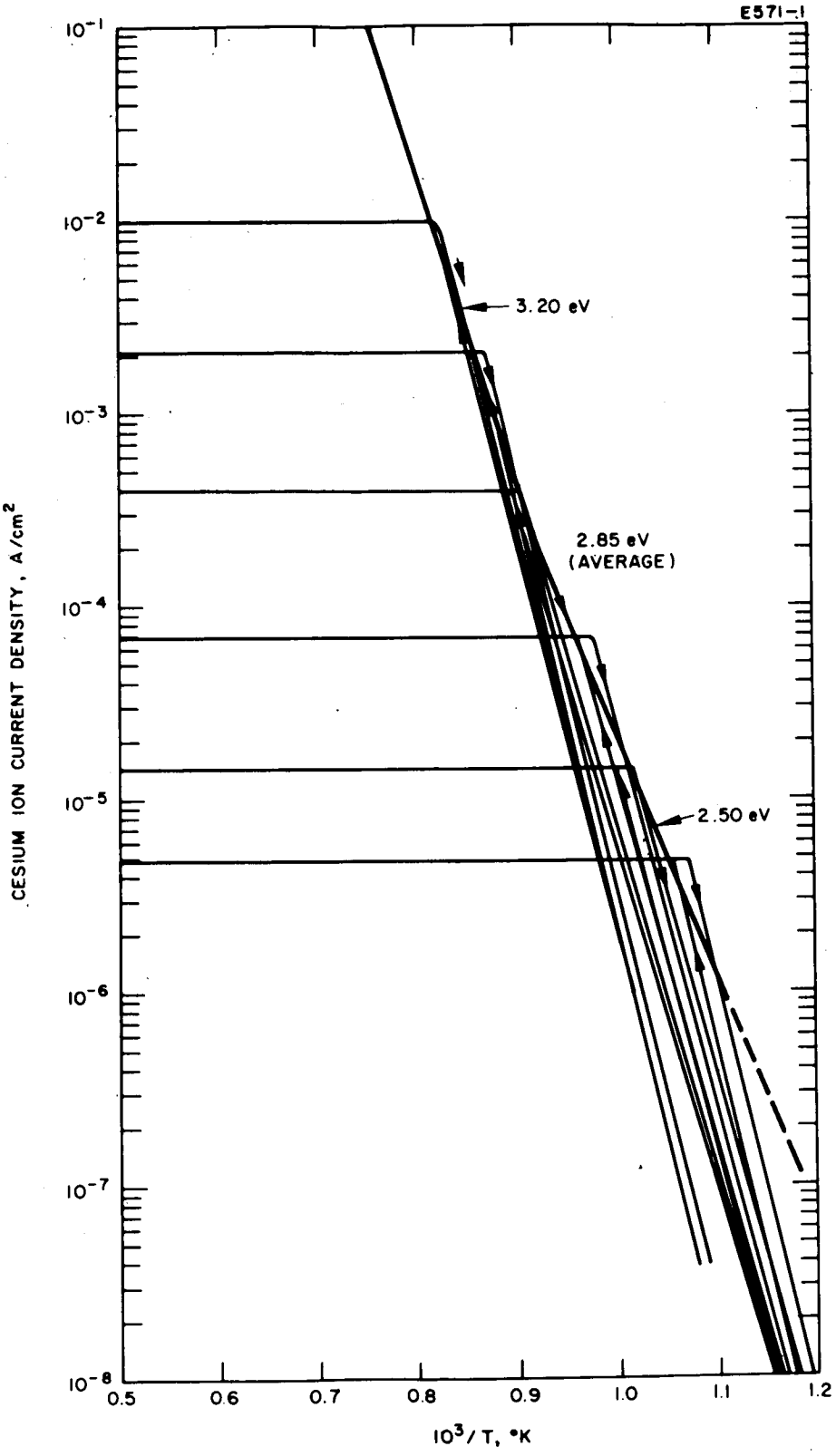

Fig. 33. Cesium ion emission from niobium.

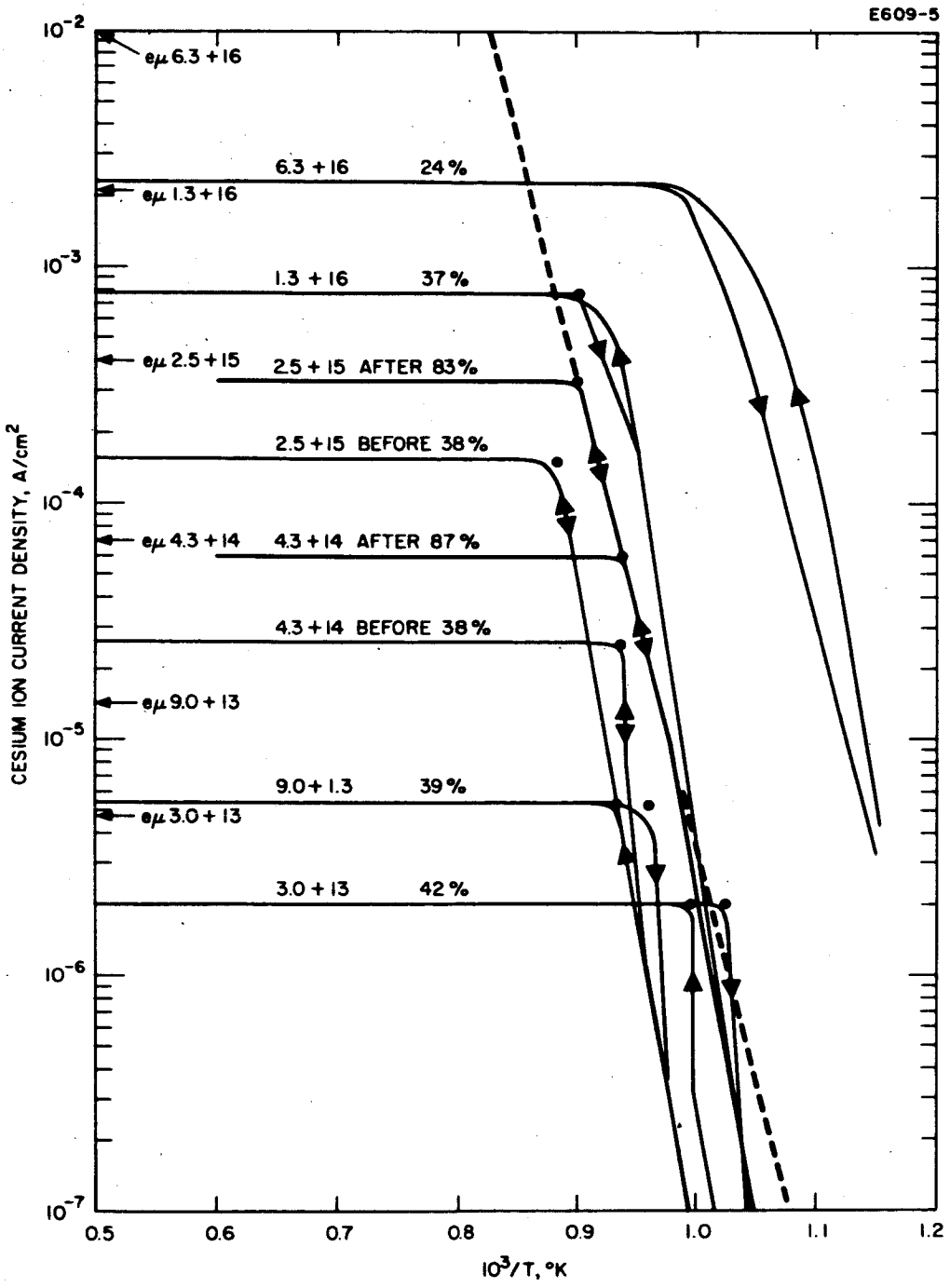

Fig. 34. Cesium ion emission from tantalum.

10. Tungsten

The cesium ion emission curves for tungsten are shown in Fig. 35. Sharp critical temperature breaks to saturated emission are exhibited. Full ionization is attained. The value of cesium ion desorption energy at the critical coverage obtained from the slope of the critical temperature envelope is 2.68 eV.

11. Rhenium

The ion emission curves for rhenium (Fig. 36) are sharp and normal and are similar to those for tungsten. The increasing temperature critical temperature envelope is just slightly higher than that for tungsten, about 20K. A relatively small temperature hysteresis effect is exhibited which disappears at about 10 mA/cm^2. The slope of the critical temperature envelope yields a value of 2.75 eV for the desorption energy of cesium ions from rhenium at low critical coverage.

12. Osmium

The cesium ion emission curves for osmium are shown in Fig. 37. Full ionization and sharp critical temperature breaks are exhibited. Sizable temperature hysteresis occurs at low current density, but decreases rapidly to disappear at about 2 mA/cm^2, above which the single critical temperature envelope appears to follow the decreasing temperature envelope for lower current densities. The two cesium ion desorption energies determined from the two critical temperature slopes are 5.67 and 2.25 eV.

13. Iridium

For iridium (Fig. 38), data from two sets of increasing temperature runs are included. A very large temperature hysteresis effect is observed for iridium. The critical temperatures exhibit rather large current discontinuities and are therefore clearly defined. The slope of

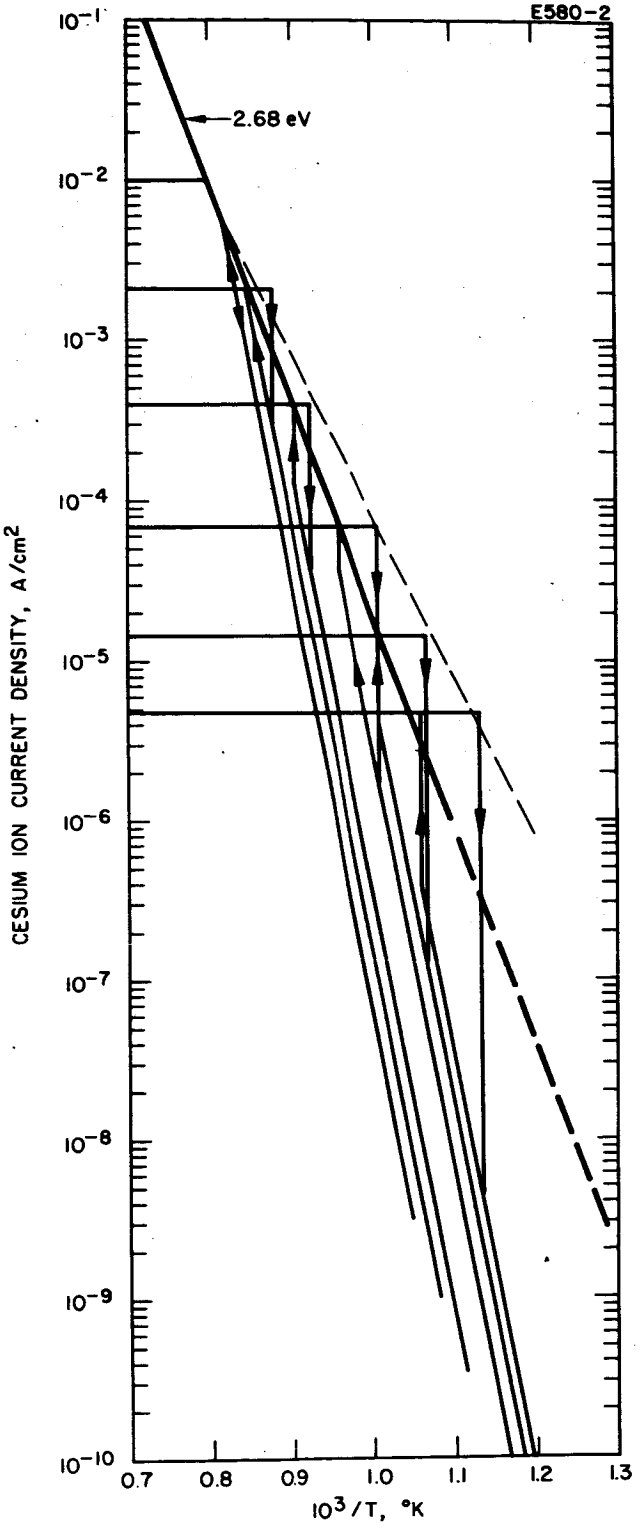

Fig. 35. Cesium ion emission from tungsten (200).

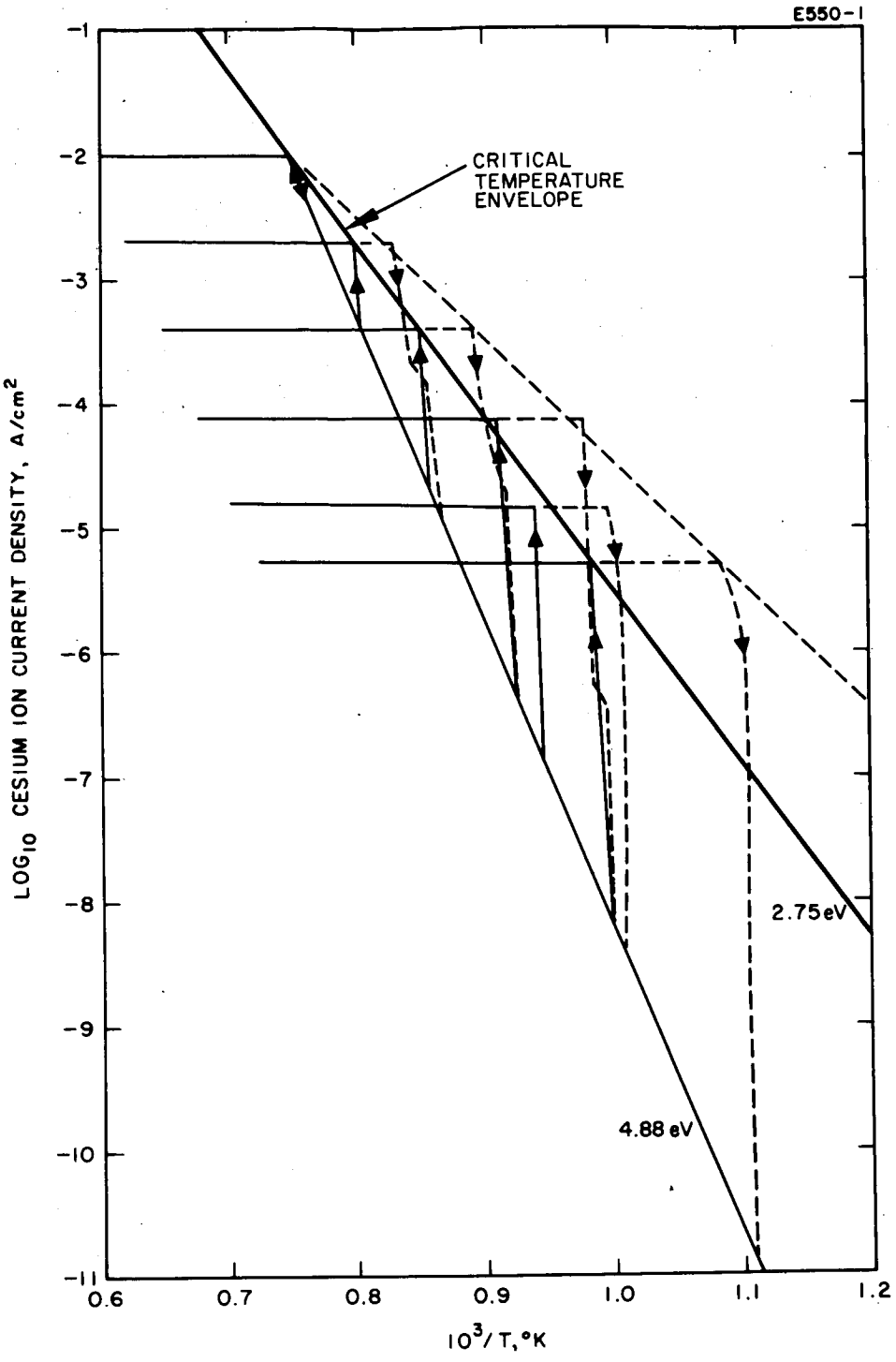

Fig. 36. Cesium ion emission from rhenium.

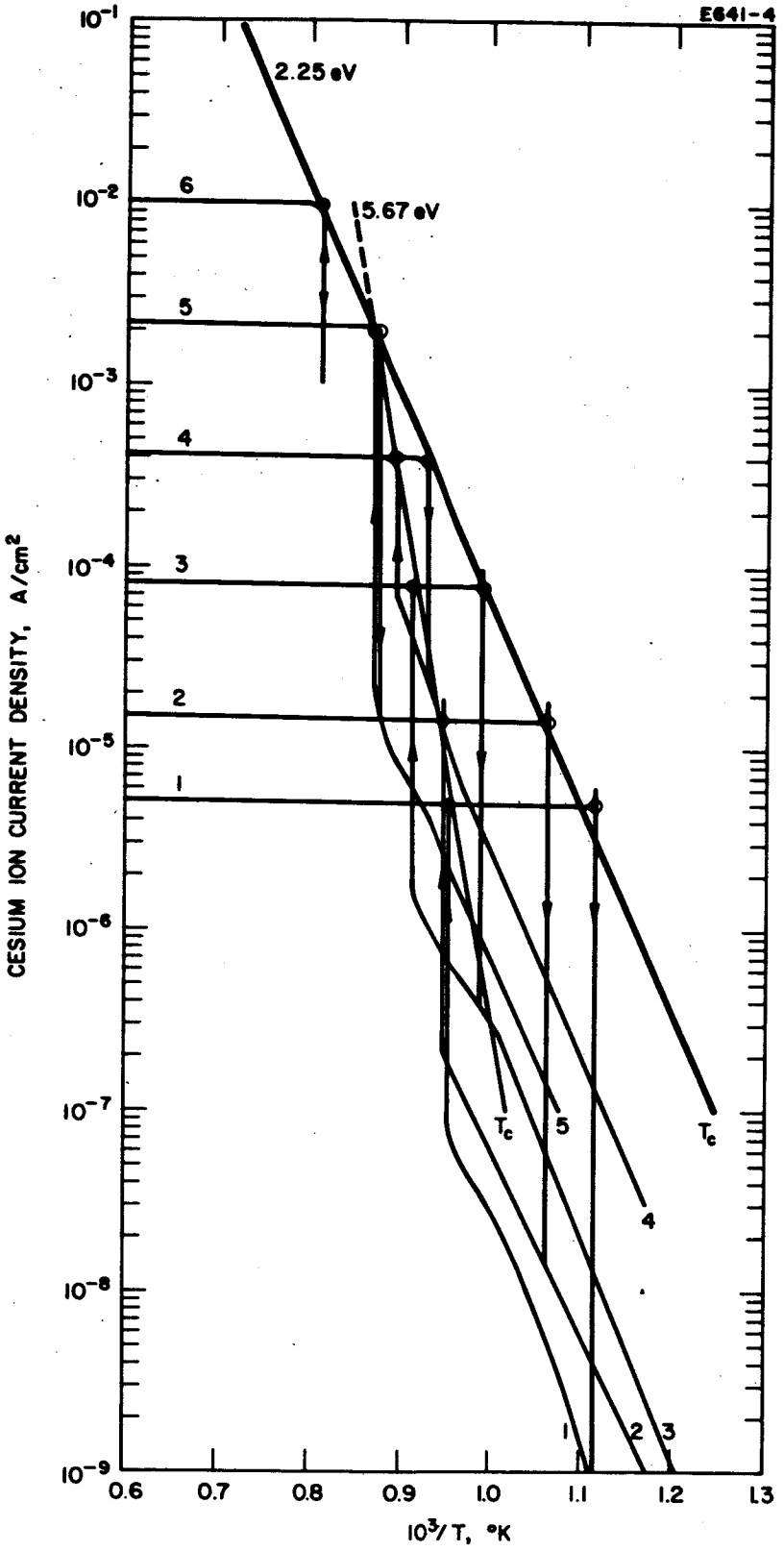

Fig. 37. Cesium ion emission from osmium.

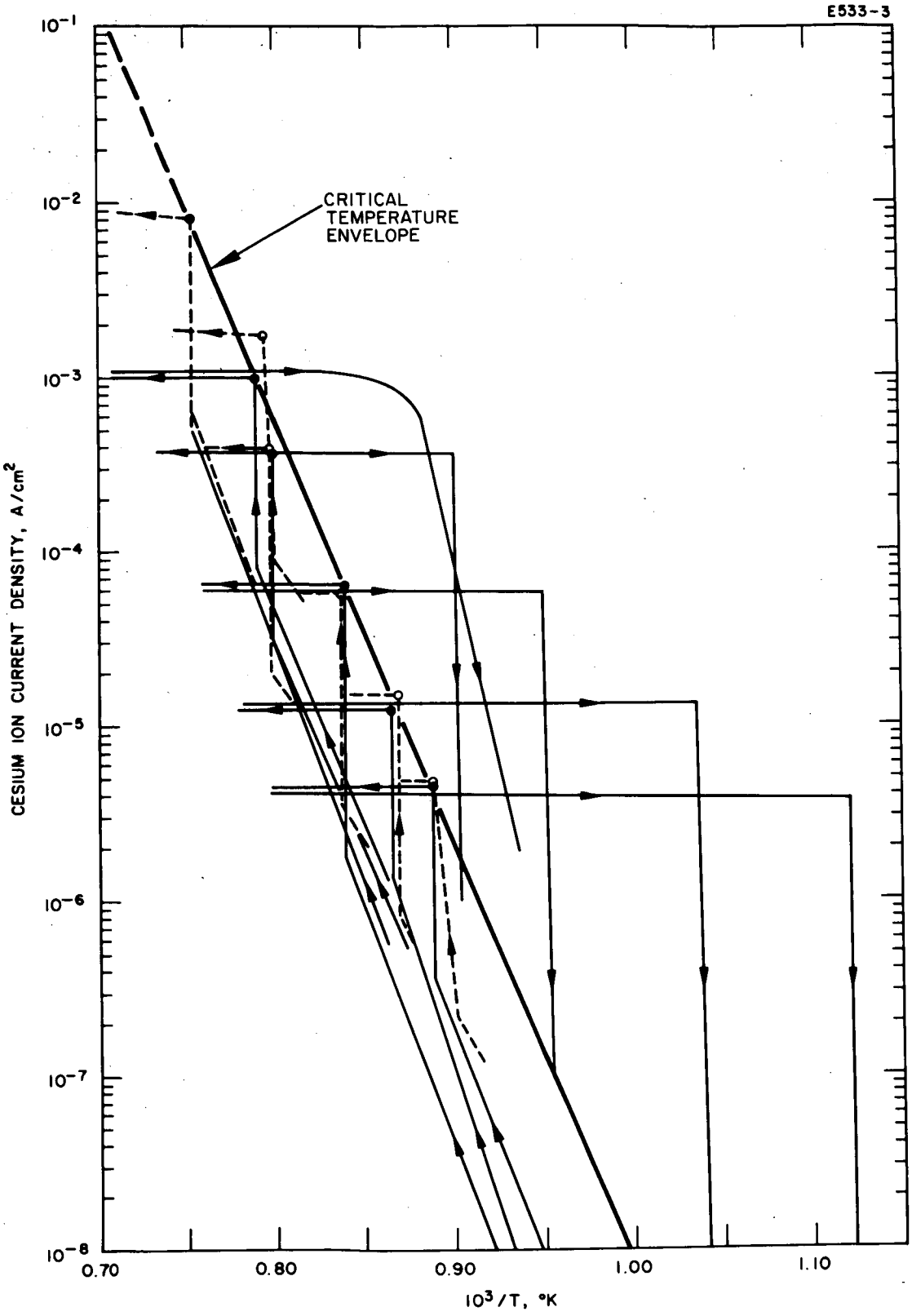

Fig. 38. Cesium ion emission from iridium.

the increasing temperature critical temperature envelope for iridium yields a value of 4.83 eV for the low coverage cesium ion desorption energy. The difference between the critical temperature of iridium and tungsten (iridium always greater) as a function of cesium ion current density is summarized in Table XXIV.

TABLE XXIV

Difference Between the Critical Temperatures of Iridium and Tungsten

J_+, A/cm^2	T_c, K
10^{-2}	32
10^{-3}	75
10^{-4}	105
10^{-5}	128
10^{-6}	146
10^{-7}	158
10^{-8}	171

14. Platinum

Platinum (Fig. 39) exhibits the highest (normal) cesium ion critical temperatures of all materials studied to date. The saturation discontinuities are comparatively large at high current density. The slope of the envelope yields 3.61 eV for the desorption energy for cesium ions.

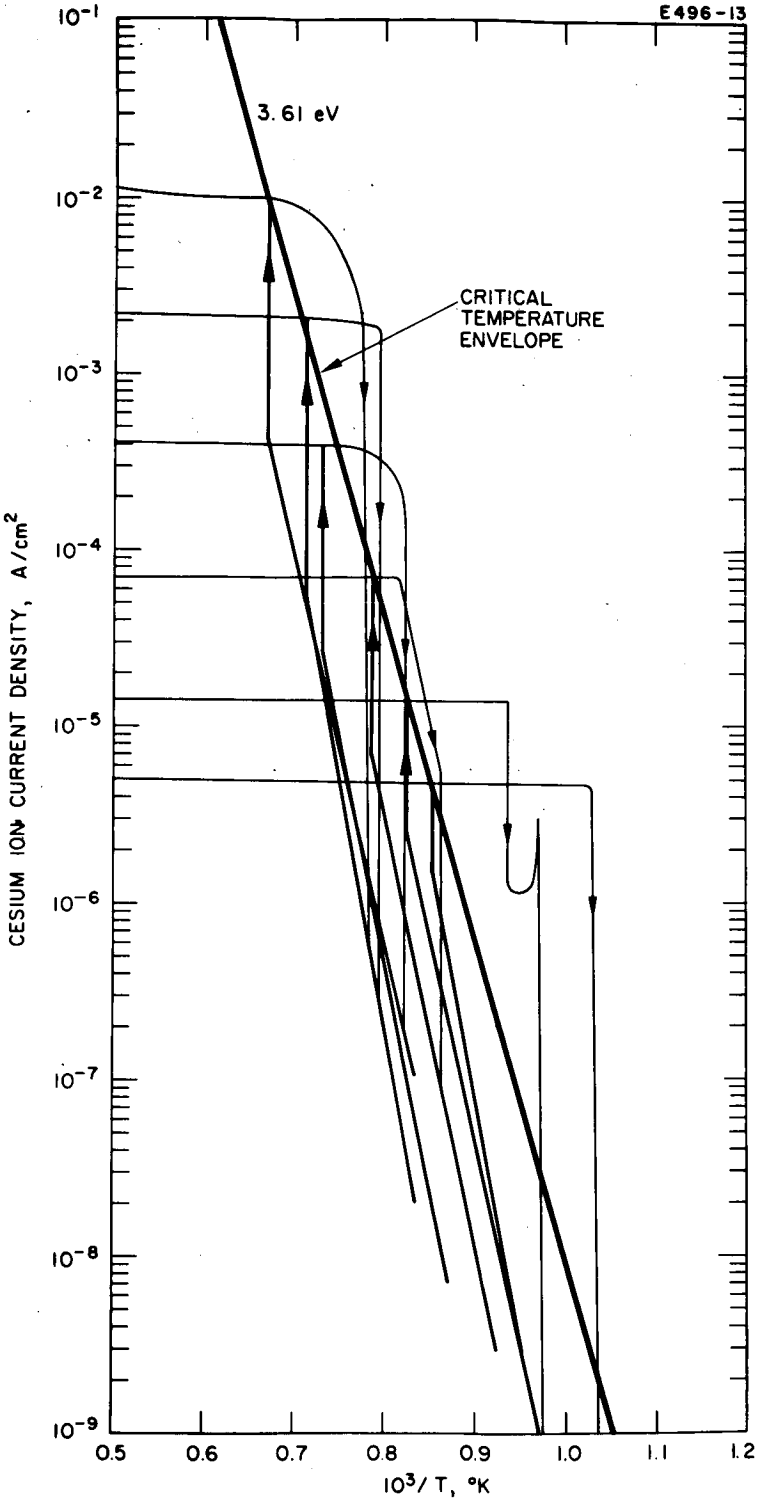

Fig. 39. Cesium ion emission from platinum.

15. Stainless Steel

The cesium ion emission from 304 stainless steel (Fig. 40) is conventional. It shows rather large temperature hysteresis, probably disappearing just above 10 mA/cm^2. The increasing temperature critical temperature envelope falls slightly above that for tungsten, among many others. Its slope yields a value of 3.15 eV for the cesium ion desorption energy at critical coverage.

16. Tantalum Boride

The ion emission data for tantalum boride were even more irregular than the electron emission data. Data were obtained for only the lowest four cesium arrival fluxes. The broad band shown in Fig. 41 has been drawn to include the meanderings of the eight curves (four for each collector). The critical temperature envelope must lie somewhere within the band, and the approximate corresponding ion desorption energy is about 3.0 to 3.1 eV.

17. Zirconium Carbide

For zirconium carbide (ZrC), cesium ionization characteristics consistent with a measured vacuum work function below the ionization potential of cesium are observed (Fig. 42). Ionization efficiencies of 4 to 6% are observed; when substituted into the equation

$$\phi_{ion}(\theta_c) = V_i - kT_c \left[\frac{1}{2} \ell n \left(\frac{1}{\beta} - 1\right)\right]$$

(which is the Saha-Langmuir equation solved for ϕ and is the definition of ϕ_{ion}), these yield values of 3.7 eV for the ion work function of zirconium carbide. This is the same value as the electron work function of the "clean" arm of the cesiated S curves and of the measured vacuum work function. The fact that the electron and ion work functions are nearly the same implies that the work function distribution of a polycrystalline ZrC surface is very narrow, if not single valued. No

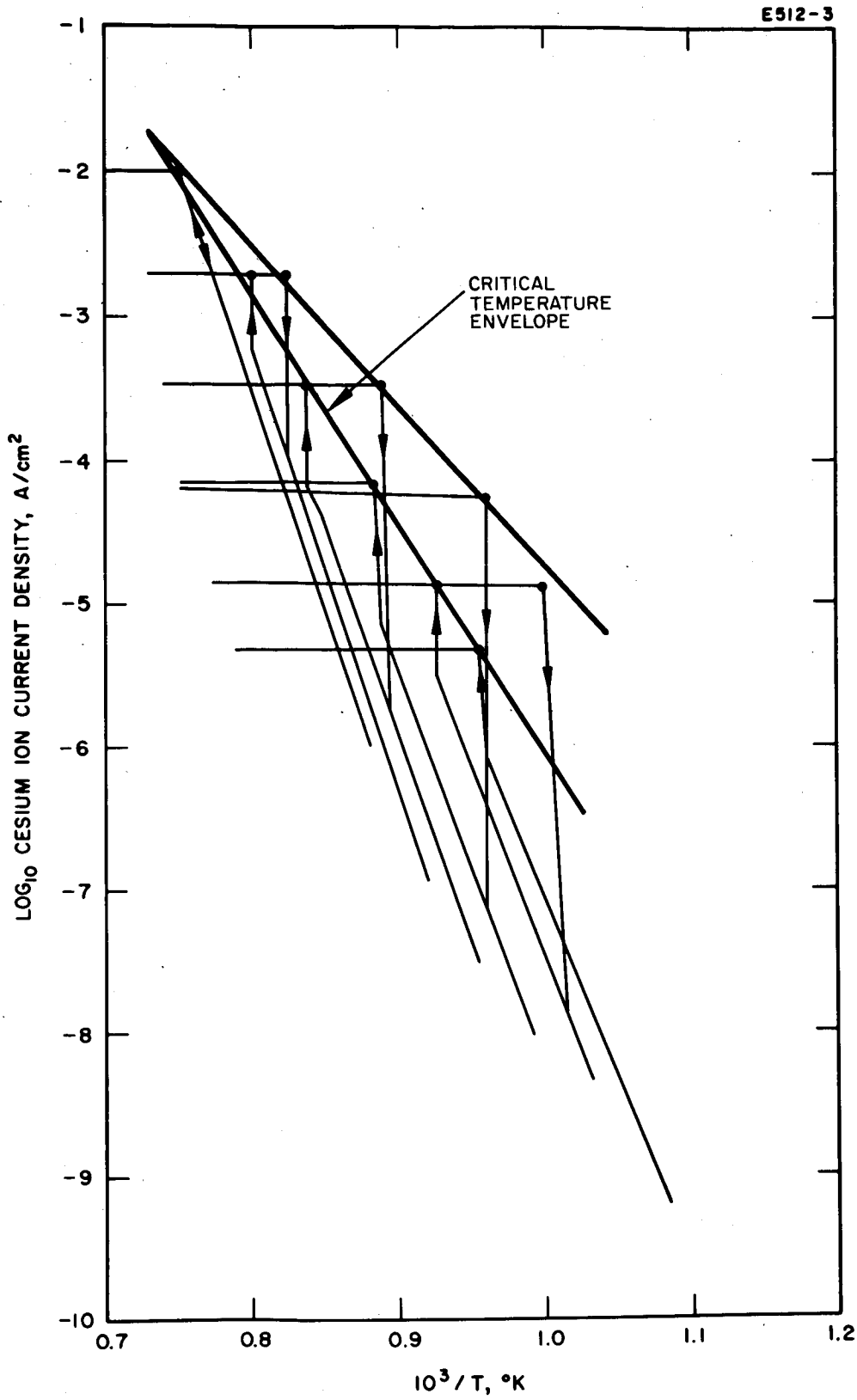

Fig. 40. Cesium ion emission from 304 stainless steel.

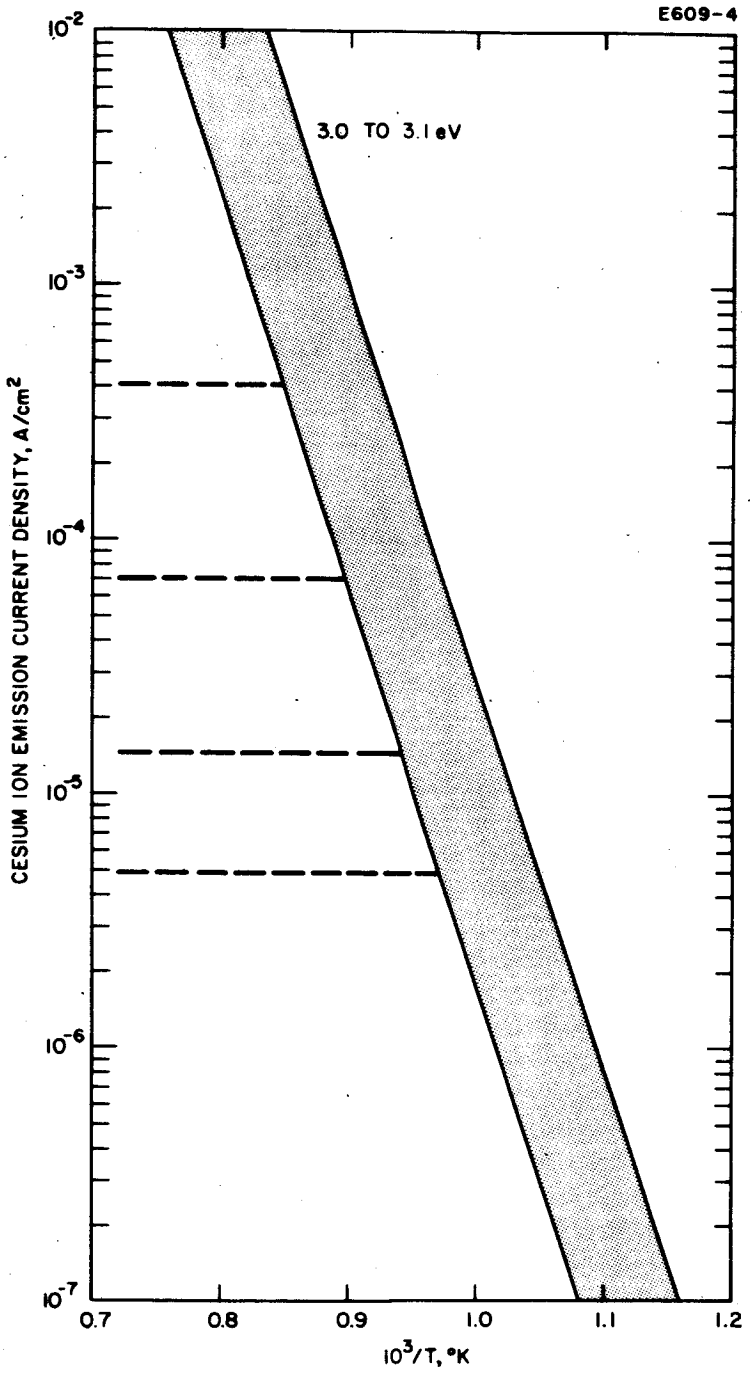

Fig. 41. Cesium ion emission from tantalum boride ($TaB_2 \rightarrow TaB + B$).

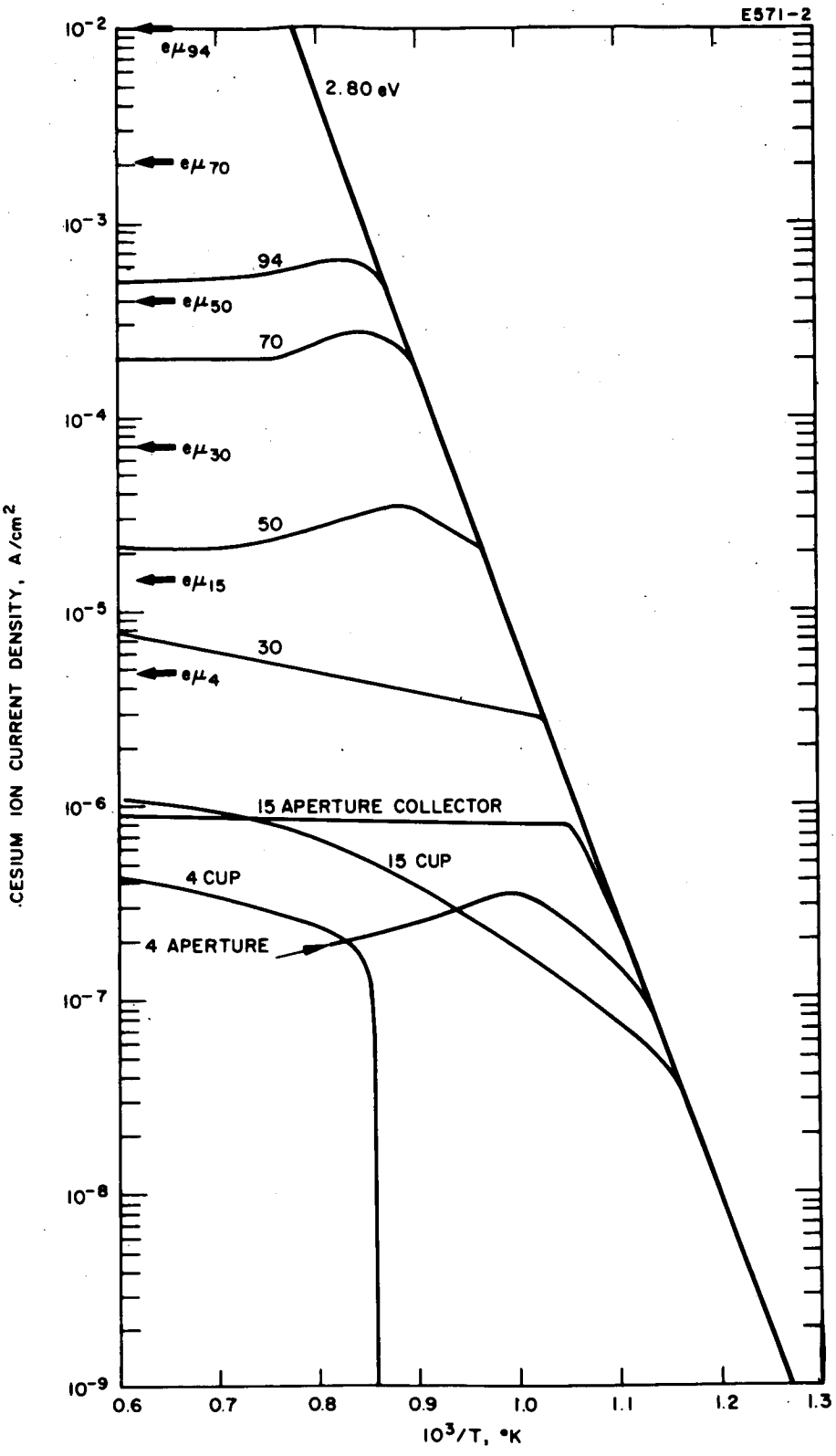

Fig. 42. Cesium ion emission from zirconium carbide (ZrC).

critical temperature envelope exists but the cesium ion current densities traverse the same exponential curve, the slope of which yields a value of 2.80 eV for the desorption energy of cesium ions under the conditions of this situation, which is for higher surface coverage.

18. Molybdenum Carbide

The cesium ion emission curves for molybdenum carbide (Mo_2C) are shown in Fig. 43. Small sharp critical temperature breaks to saturation occur. Full ionization is attained. The value of cesium ion desorption energy obtained from the slope of the critical temperature envelope is 2.50 eV.

19. Molybdenum Silicide

The cesium ion emission data for molybdenum silicide ($MoSi_2 \rightarrow Mo_5Si_3$) were reported in the Final Report on Contract NAS 3-5249.

20. Tantalum Silicide

The cesium ion emission curves for tantalum silicide ($TaSi_2 \rightarrow Ta_5Si_3$) are shown in Fig. 44. The curves for tantalum silicide are fairly normal, and the cesium ion desorption energy measured from the slope of the critical temperature envelope is 2.98 eV.

21. Tungsten Silicide

The cesium ion emission curves for tungsten silicide are shown in Fig. 45. Sharp critical temperature breaks are exhibited. A large degree of structure occurs in the critical temperature hysteresis, including spikes and multiple sharp breaks. Three critical temperature envelopes are drawn in Fig. 45; two are upper and lower limits, and the third is a weighted average with a value of 2.26 eV for the corresponding cesium ion desorption energy.

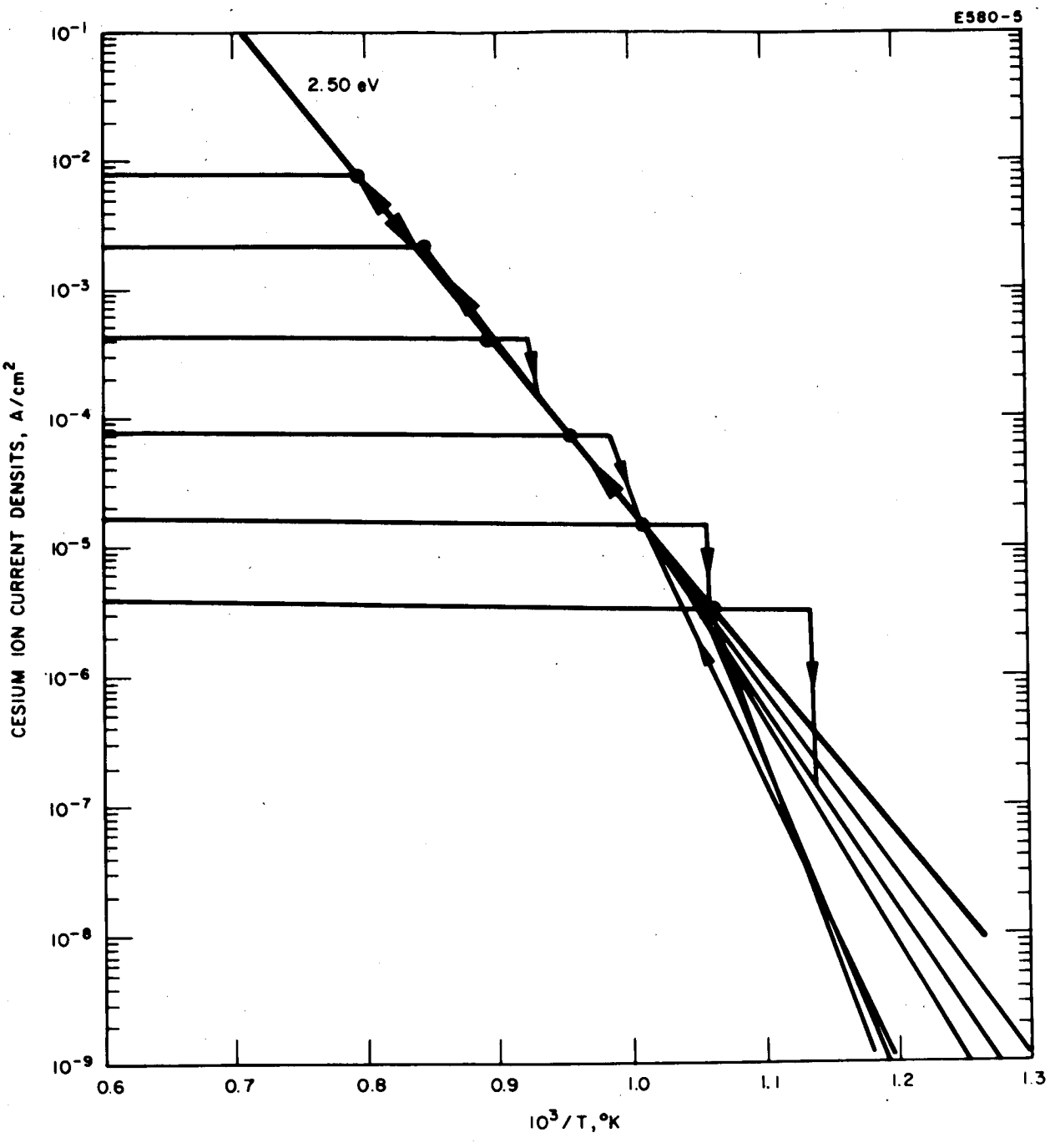

Fig. 43. Cesium ion emission from molybdenum carbide (Mo_2C).

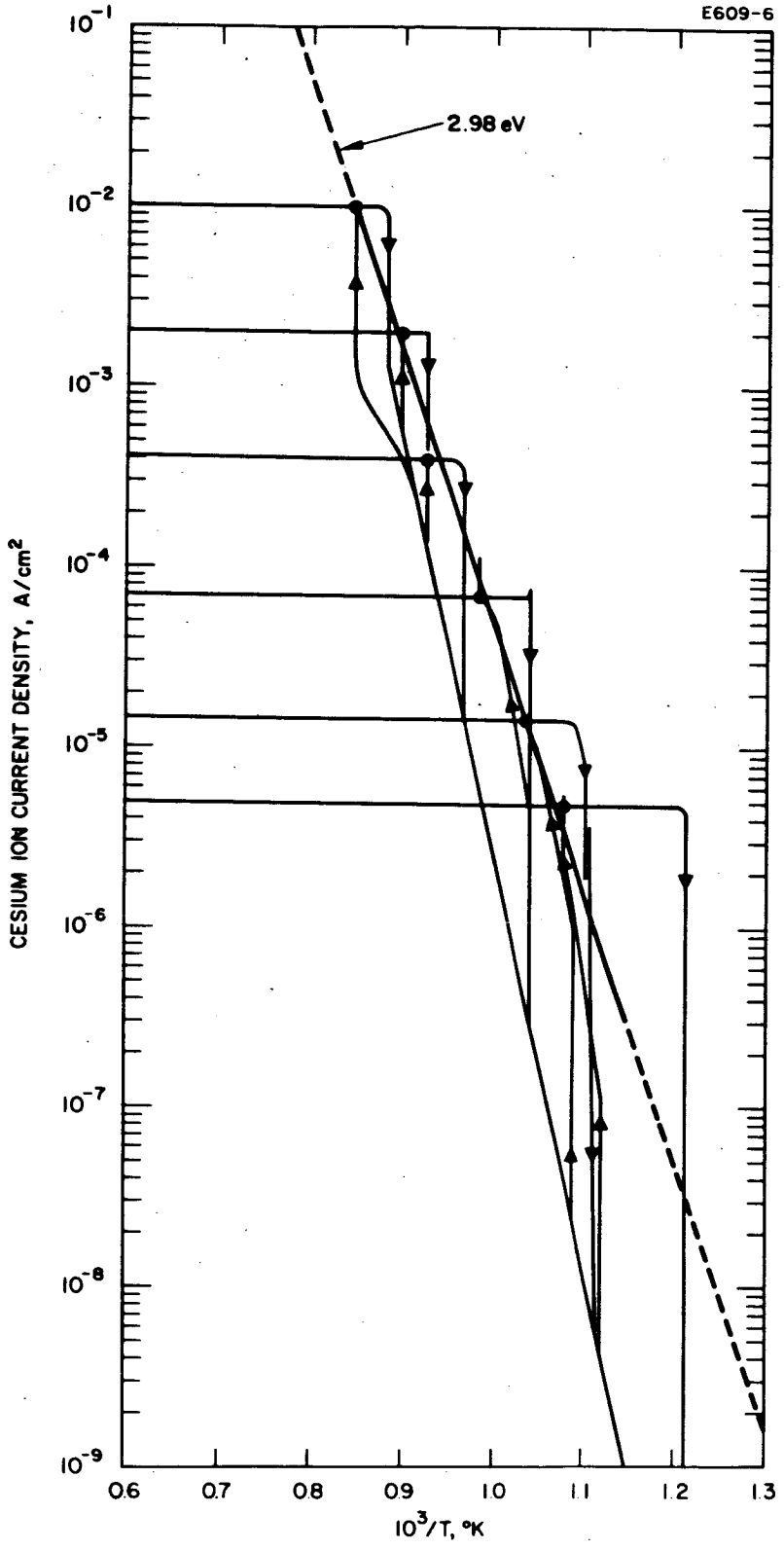

Fig. 44.
Cesium ion emission from tantalum silicide ($TaSi_2 \rightarrow Ta_5Si_3$).

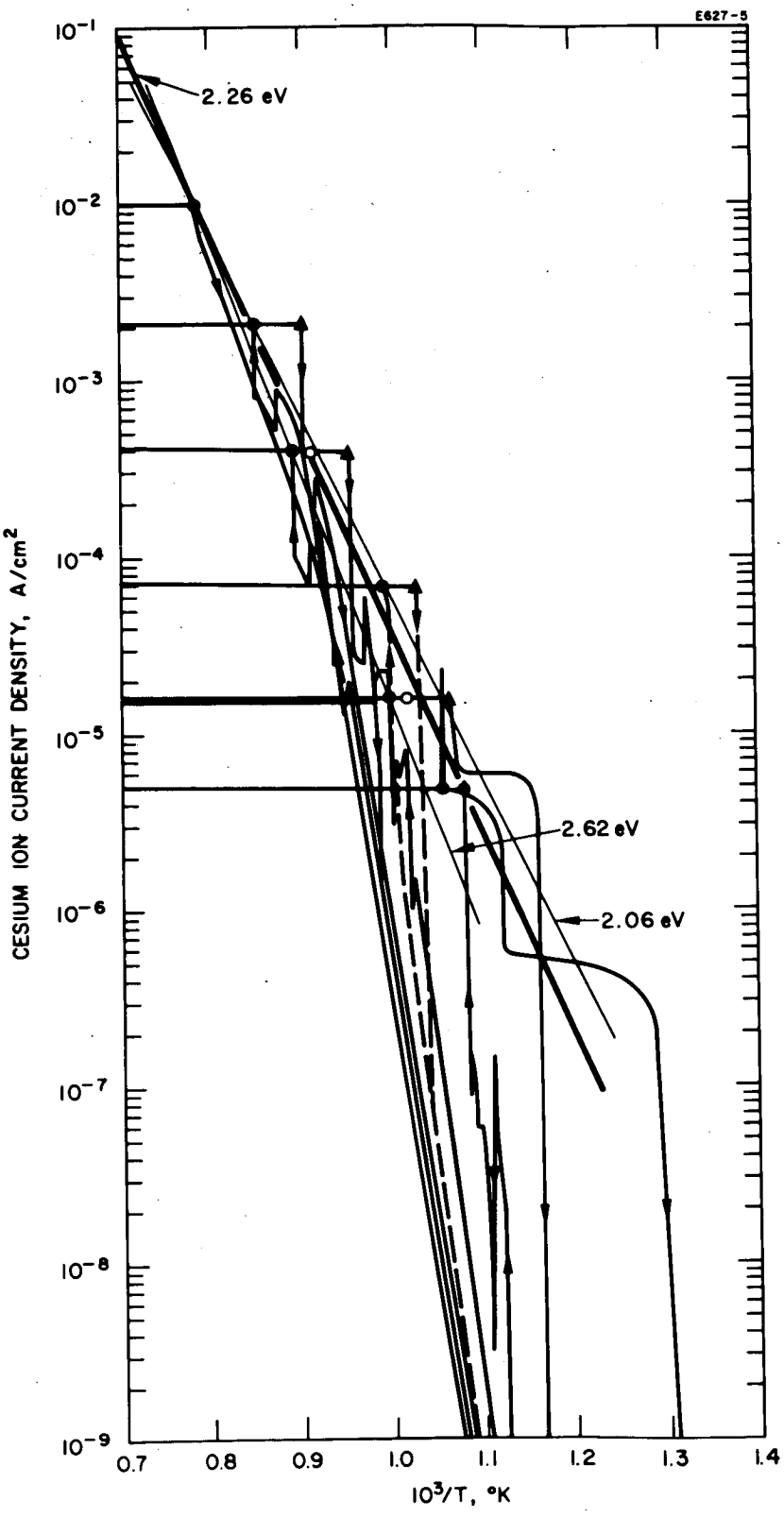

Fig. 45.
Cesium ion emission from tungsten silicide.

22. Aluminum Oxide (Sintered)

The cesium ion emission data for sintered alumina were reported in the Final Report on Contract NAS 3-5249.

23. Aluminum Oxide (Lucalox)

The ion emission data for aluminum oxide are plotted in Fig. 46 as recorded with slow time variation along the temperature axis. The curves are seen to be somewhat anomalous, inconsistent, and are non-reproducible in detail. Two facts are pointed out, as mentioned earlier. First, the collector cannot be an insulator, so copper is used. At lower emitter temperatures, therefore, there is the possibility that the emitter is covered with more copper atoms sputtered back from the collector by the cesium ions than for hotter surface temperature. Second (and very important), the emitter is an insulator, much more pure than in the previous case of porous sintered alumina. The possibility therefore exists for charge buildup effects and long equilibration times. Surface charging and other insulator effects may account for the inconsistency and nonreproducibility effects. The curves shown in Fig. 46 are representative for Lucalox, but are not unique. A number of curves were recorded at different rates of temperature change, and some reproducibility checks were made at the same time rate of temperature change. Detailed reproducibility was not possible, and significant variations with rate of temperature change were observed. In Fig. 47, a set of curves is shown which has been made self consistent and made to fit most of the data for Lucalox. The value of the cesium ion desorption energy obtained from the slope of the increasing temperature envelope is about 1.34 eV, much lower than for any metals. This is not surprising because although alumina exhibits an electron work function similar to that of metals, it is an insulator and the bonding mechanisms for adsorbed cesium may be different. For example, ionic and covalent bonding may be impossible because of the lack of

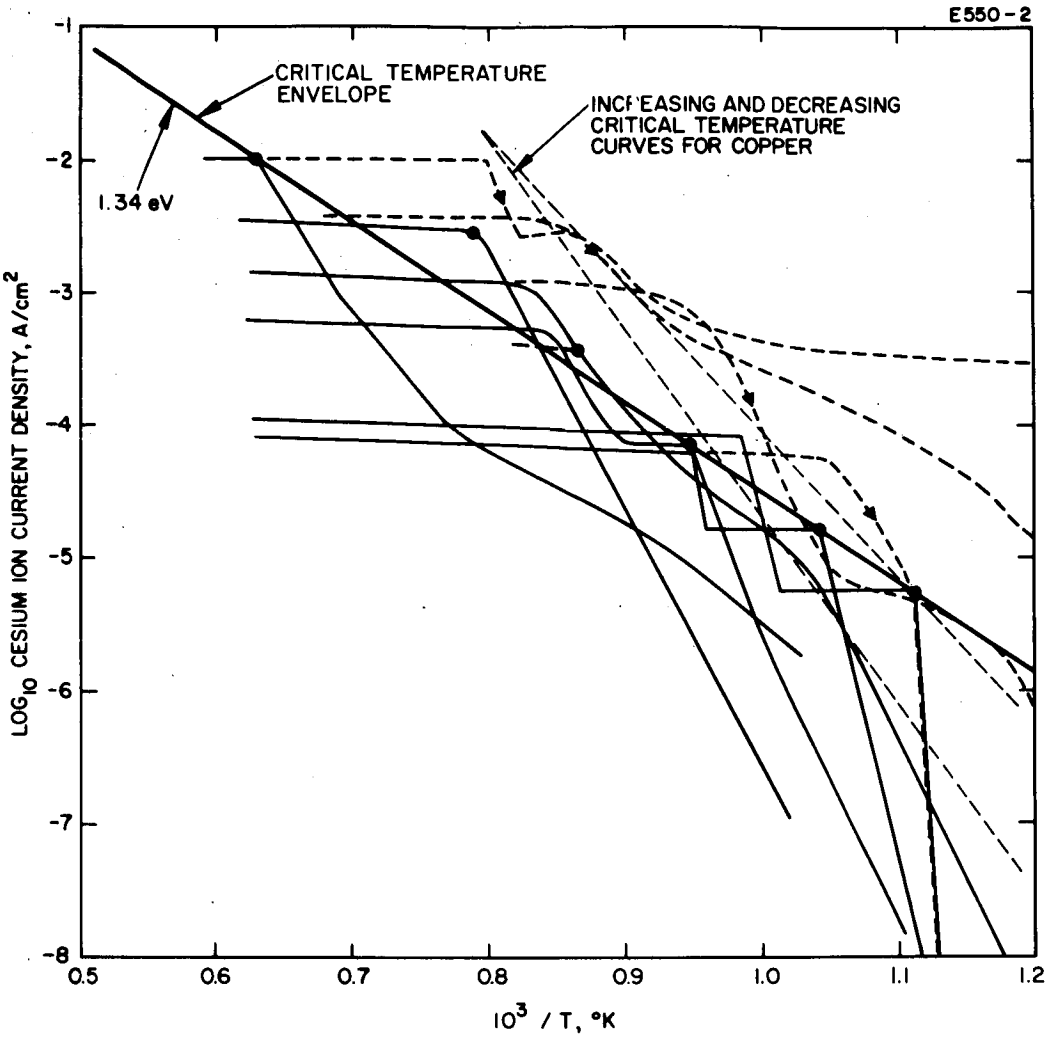

Fig. 46. Cesium ion emission from Lucalox aluminum oxide (actual data).

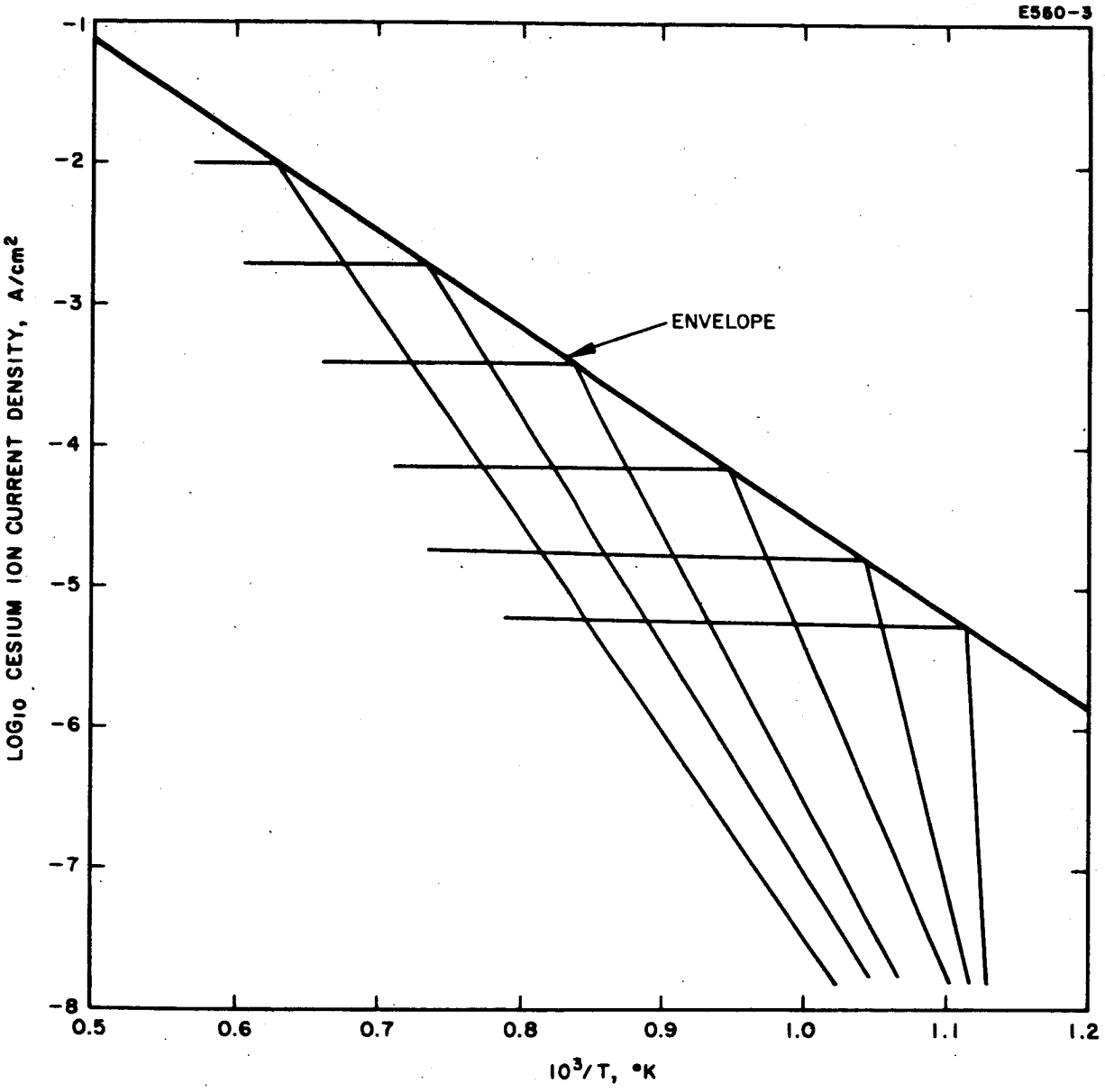

Fig. 47. Cesium ion emission from Lucalox aluminum oxide (smoothed-out data).

available electrons for this process in the substrate, leaving only an image charge force to comprise the bond. However, the substrate is an insulator and the concept of an image charge is probably invalid. Thus, the bonding mechanism is probably different, and it is not surprising that the binding energy is less.

24. Oxygenated Copper

The ion emission data measured for cesiated oxygenated copper (polycrystalline OFHC) are shown in Fig. 48, where the four oxygen conditions are plotted together at each of the three cesium arrival fluxes. Figure 49 is the same data plotted with the three cesium arrival fluxes grouped at each of the four oxygen conditions. In these groupings, the critical temperature envelopes for various oxygen conditions are drawn, and the cesium ion desorption energies obtained from the slopes are indicated. The temperature hysteresis effect was observed only for the lowest cesium arrival flux. In Fig. 50, the four critical temperature curves are plotted together. A general increase in slope with increasing oxygen partial pressure is observed. Three of the envelopes pass through a common point and the fourth is displaced slightly toward low cesium fluxes. If this curve is moved slightly to cause it also to pass through the common intersection point, a uniform progression in desorption energies (slopes) results. This has been done in Fig. 50 with the dashed curve. The measured desorption energies bear a possible relationship to the work functions measured for the oxygenated copper surface as a function of oxygen partial pressure in the absence of cesium. This comparison is shown in Table XXV, where the increases in cesium ion desorption energy and the increases in uncesiated surface work function are tabulated as a function of oxygen partial pressure. In both cases, a strong dependence on oxygen is exhibited.

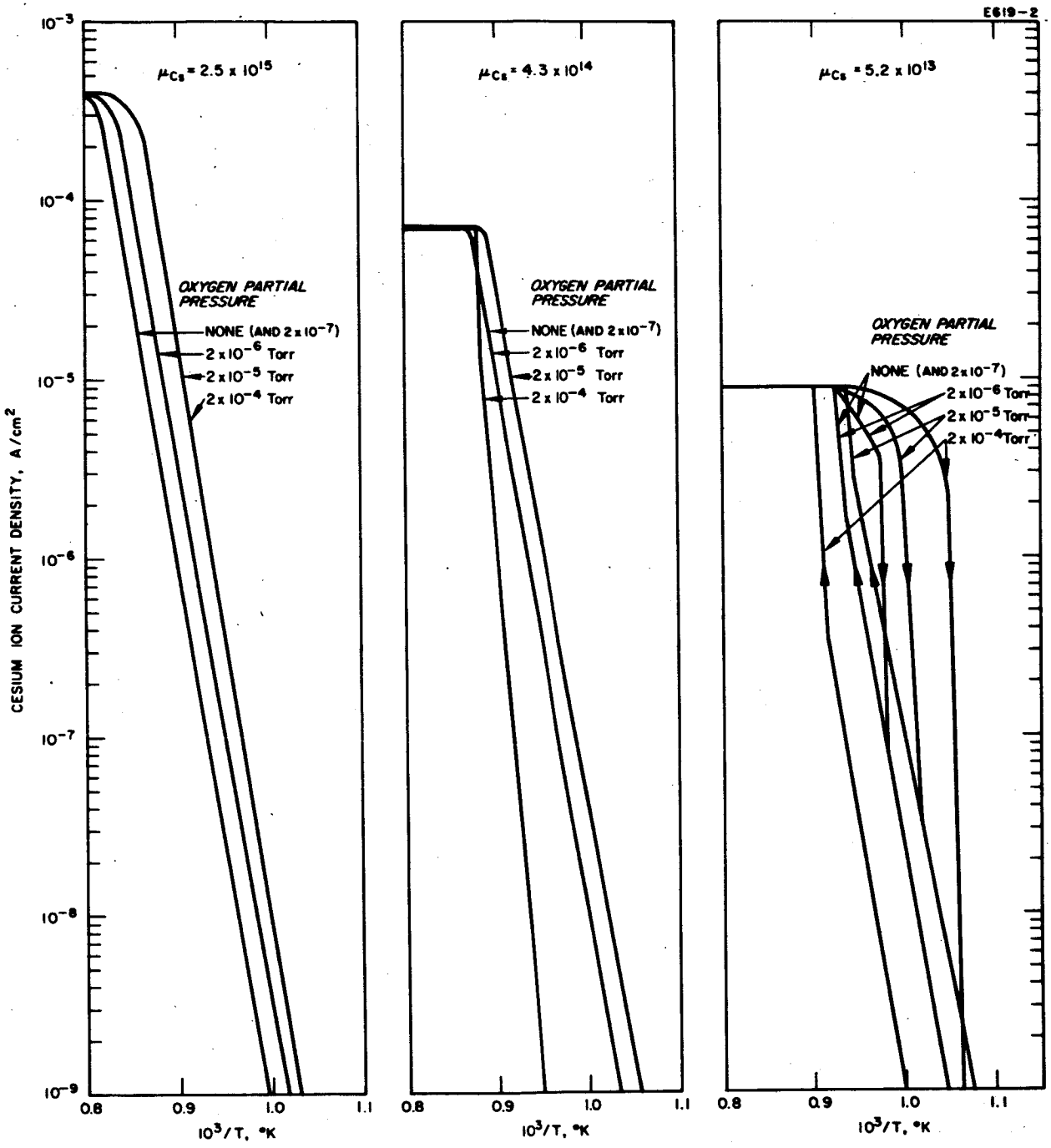

Fig. 48. Cesium ion emission from oxygenated OFHC copper (constant cesium arrival flux).

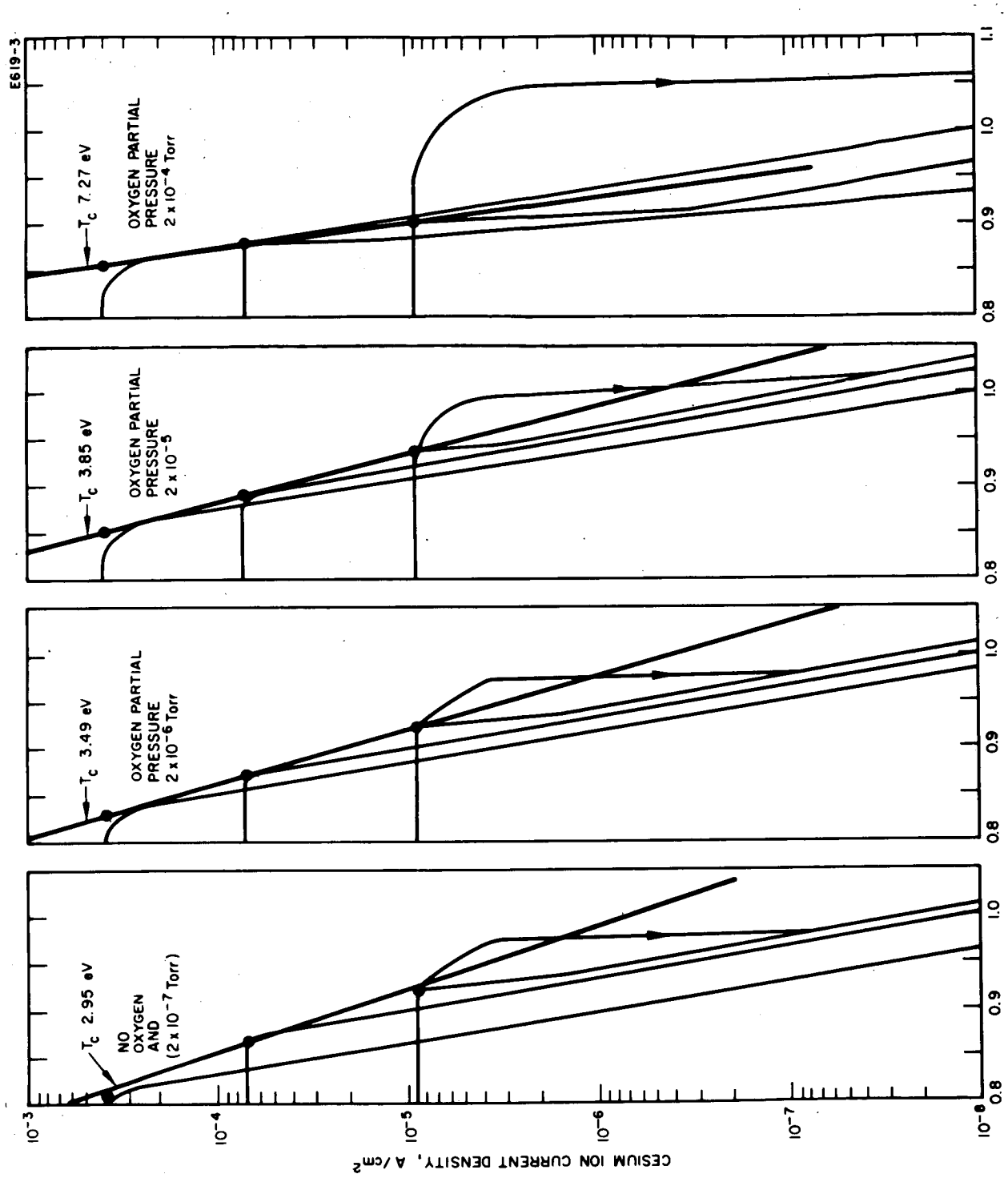

Fig. 49 Cesium ion emission from oxygenated QEHC

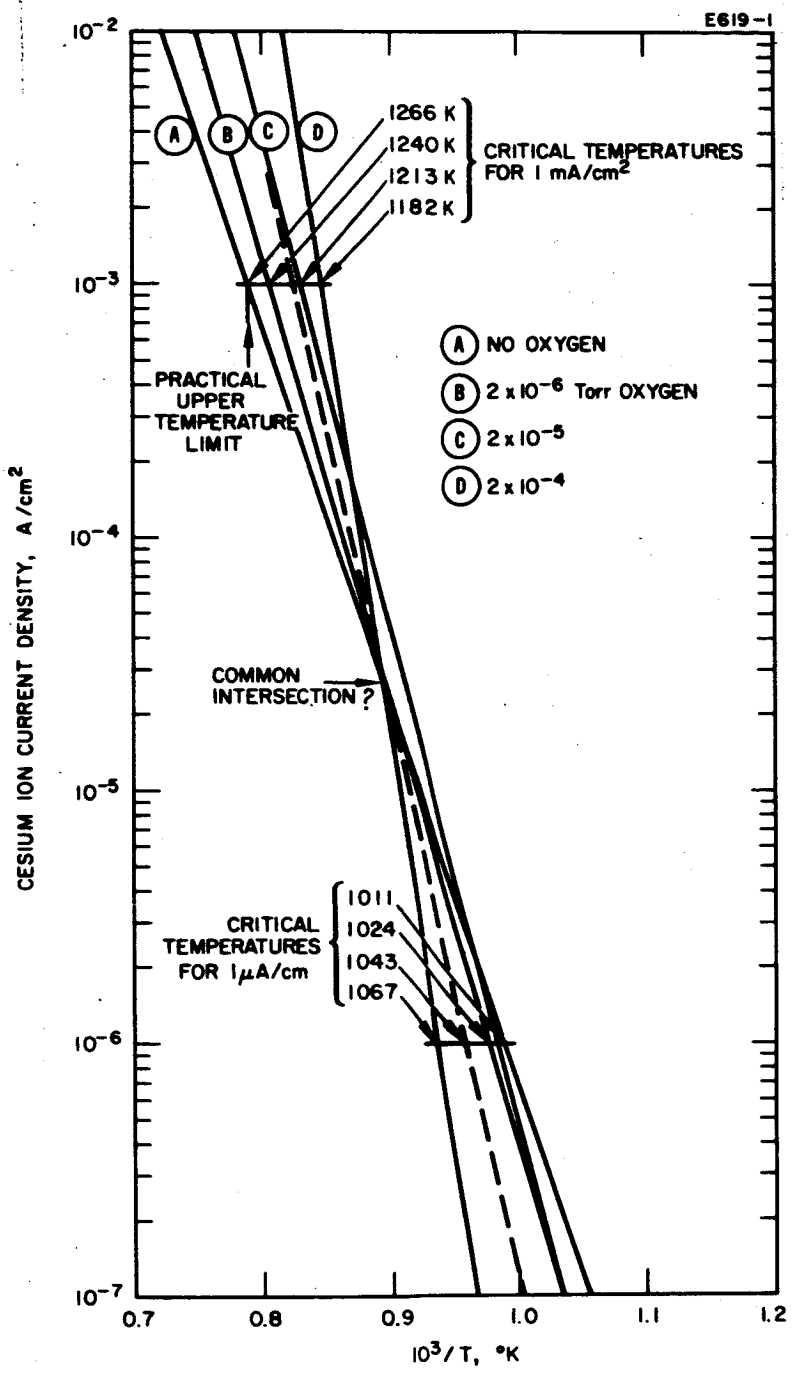

Fig. 50. Surface ionization critical temperature envelopes for cesium on copper as a function of oxygen partial pressure.

TABLE XXV

Comparison of Experimental Cesium Desorption Energies with Surface Work Functions for Oxygenated Copper

Oxygen Partial Pressure, Torr	Cesium Ion Desorption Energy, eV	Oxygenated Surface Work Function, eV	Increase In Desorption Energy, eV	Increase In Surface Work Function
None	2.95	4.45	—	—
2×10^{-6}	3.49	5.02	0.54	0.57
2×10^{-5}	4.40	6.60	1.45	2.15
2×10^{-4}	7.27	> 7 or 8	4.32	> 2.5 or 3.5

The influence of oxygen on the cesium surface ionization critical temperature is shown in Fig. 50. The influence of oxygen on the critical temperature is seen to reverse with the magnitude of the ion current density with a region of no dependence (intersection of envelopes) at about 2 or 3 $\times 10^{-5}$ A/cm^2. For reference, the critical temperatures at 1 mA/cm^2 and 1 μA/cm^2 are shown in Fig. 50. The critical temperatures vary over about 80K at 1 mA/cm^2, and it is evident that a considerable increase in the cesium ion current density obtainable from copper is possible for an oxygenated surface if rather high oxygen pressures (arrival fluxes) can be employed.

Full ionization is obtained even for the unoxygenated condition, and lower neutral fractions of cesium are probably possible for the higher work function oxygenated surfaces. Sharp critical temperature breaks are exhibited only at the lowest cesium arrival flux.

25. Iridium-Coated Porous Tungsten

Ion emission curves for iridium-coated porous tungsten were recorded at the same four cesium arrival fluxes mentioned in the preceding section. Again, long times were required to collect the

temperature varying data to ensure equilibrium conditions. Even then the curves were less sharp and not so well defined as for iridium or tungsten. The critical temperatures did agree with those obtained for pure iridium. The sharp current density breaks to saturation were not evidenced as they were for pure iridium. As for the electron curves, this is attributedto diffusion of cesium in an out of the porous structure.

As a summary and comparison, the cesium ion desorption energies (at critical coverage) as measured from the slopes of the critical temperature envelopes are listed in Table XXVI, together with the vacuum work functions and "clean" cesiated work functions. The expression used to calculate the desorption energies from the experimental data is

$$\lambda_+(\theta_c) = \frac{k \ln(J_{+_1}/J_{+_2})}{(1/T_2 - 1/T_1)} \quad \text{in eV} \qquad (1)$$

which is a solution of $J_+ = A \exp(\lambda_+/kT)$ for λ_+ where (J_{+_1}, T_1) and (J_{+_2}, T_2) are two points on the critical temperature envelope.

D. EMITTER FABRICATION

During the year, approximately 50 experimental tubes were fabricated. In many cases, a variety of failures required a number of extra tubes to be built. In most cases, the failures were routine; in others, success could be achieved only be design modifications. These modifications and the nonroutine materials problems are described below as information for this technology.

The materials for which the standard ribbon emitter design was attempted were beryllium, titanium, nickel, niobium, molybdenum, tantalum, tungsten, rhenium, iridium, and platinum. For beryllium and titanium, ribbons proved to be unsatisfactory, because of hot spots, thinning, grain growth, and severe distortion; for this reason, solid

TABLE XXVI

Cesium Ion Desorption Energies (at critical coverage)

Surface Material	Vacuum Work Function, eV	"Clean" Cesiated Work Function, eV	Cesium Ion Desorption Energy (at θ_c), eV
Beryllium	3.67	3.67	3.06
Titanium	3.8	3.75	2.78
Chromium	3.90	3.55	3.28
Iron	4.5	3.7	(5.95)
Nickel	4.7	> 4.0	2.26
Copper	4.42	4.4	2.85
Niobium	4.19	4.1	2.85
Molybdenum	4.2 - 4.3	4.35	2.45
Tantalum	4.25	4.25	3.96
Tungsten	4.50	4.47	2.68
Rhenium	4.96	4.80	2.75
Osmium	4.84	4.75	5.67
Iridium	5.27	5.0	4.83
Platinum	5.7	5.0	3.61
304 Stainless Steel	4.3	3.5	3.15
Tantalum Boride	4.26	3.9	3.0 - 3.1
Zirconium Carbide	3.70	3.70	2.80
Molybdenum Carbide	4.73	4.3	2.50
Molybdenum Silicide	4.72	4.7	2.62
Tantalum Silicide	4.71	4.7	2.98
Tungsten Silicide	4.62	4.6	2.26
Alumina (Sintered)	4.91	5.0	3.31
Alumina (Lucalox)	5.19	~ 4	(1.34)
Oxygenated Copper	4.5 to > 8	3.4 and up	2.95 to 7.27
Iridium-Coated Porous Tungsten	5.25	(5.2)	(4.8)

block emitters had to be employed. All of the other materials were satisfactory as ribbons. The total list for which block emitters were used is beryllium, titanium, chromium, iron, copper, osmium, 304 stainless steel, Al_2O_3 (Lucalox), oxygenated copper, and iridium-coated porous tungsten. The six refractory compounds will be discussed separately. Two of the metals, chromium and osmium, are not easily machinable with regular tool bits; consequently, they were cut, ground, and polished with diamond tools.

The tungsten-26% rhenium and tungsten-5% rhenium thermocouple wires were successfully welded and held through thermal cycling to all of the materials except copper, osmium, iridium, Al_2O_3, and tungsten silicide. The thermocouples were imbedded in the copper emitters, and squeezed between two concentric cylinders for Al_2O_3. In the case of iridium and tungsten silicide initial welds were made, but failure occurred during temperature cycling. The final technique used to attach the thermocouple wires to the 99.9% pure iridium ribbon was the incorporation into the weld of a small "patch" of iridium foil. Since iridium welds well to itself (and to niobium), this patch served to fuse the thermocouple with the emitter surface, and eliminated failures of the junction. For tungsten silicide and osmium, a patch of niobium was used.

For Lucalox, the emitter design incorporated four 0.010-in. tungsten heater wires instead of a single wire. These heater wires were contained in a 0.060-in. diameter Al 997 alumina rod with four parallel holes running through its length. This rod was placed inside a square machined Lucalox emitter and was grooved on the outside (5 mils) to receive the thermocouple wires laid parallel to the emitter. This allowed the thermocouple junction to be pressed against the inside surface of the Lucalox emitter, midway between the ends and facing toward the collector just 0.018 in. from the portion of the emitter facing the collector aperture. It is assumed that this method yielded accurate thermocouple temperature measurements, which were required because

it is impossible to use optical measuring procedures on a translucent material, such as Lucalox, which transmits about 95% of visible light (from the central tungsten heater, in this case) and for which no reliable emissivity data were available. Optical temperature measurements were compared with the thermocouple readings and found to be high by hundreds of degrees. The thermocouple indicated the maximum emitter temperature for this design.

One ribbon emitter, tungsten silicide, could not be reliably welded to the Kovar support posts; ruptures occurred during temperature cycling. WSi_2 is a very brittle material, and fracturing was a serious hazard. A successful technique was found after many tries. A piece of niobium foil between WSi_2 and Kovar resulted in a satisfactory bond.

Considerable effort was expended in trying to create an osmium coating on a tantalum ribbon by decomposition of $OsCl_4$ on the hot tantalum surface. Partial success was achieved; an x-ray diffraction measurement of the final surface did show the spectrum of osmium, but it was rather weak, indicating that the osmium layer was dangerously thin. Because a parallel effort produced an entirely satisfactory osmium emitter, the vapor deposition technique was abandoned. The major problem with the plating technique seemed to be the critical temperature limits required to cause the $OsCl_4$ to vaporize but not decompose. The technique appears to work, but long deposition times are required. The $OsCl_4$ was made by an outside chemical laboratory from very pure osmium powder supplied by this laboratory. Apparently it is difficult to make $OsCl_4$ without also making $OsCl_3$ and other chlorides, all of which decompose at temperatures below those for significant evaporation.

The successful alternative technique which produced an osmium emitter was performed by R. Turk of this laboratory, and our machine shop. Very pure osmium powder was hot pressed and sintered to 95% density, ground and polished, and machined into a standard, indirectly heated configuration – that is, a square bar with a central hole. Photomicrographs indicated a very satisfactory polycrystalline surface.

A series of experiments were required to produce suitable emitters of ZrC and of Mo_2C. W. E. McKee and J. M. Hammond of this laboratory experimented with these two materials until satisfactory surfaces of each were obtained. The technique used to determine the chemistry and stoichiometric quality of the surfaces was, as usual, x-ray diffraction.

For ZrC, the carbiding of directly heated ribbons of two different thicknesses, 0.0008 and 0.008 in., resulted in severe distortion caused by swelling of the lattice associated with formation of the carbide. This problem was solved by changing to an indirectly heated block emitter machined from pure zirconium, which was then carbided. After several carbiding runs, followed by x-ray diffraction checks, a satisfactory surface of ZrC was obtained. The ZrC surface is very stable. Ten hours at 1600K and repeated heating and cooling to 1600K in a cesium atmosphere (10^{-6} to 10^{-2} Torr) had no influence. It is not attacked by hot cesium, and its melting point is very high.

There are two carbides of molybdenum — Mo_2C and MoC. Mo_2C forms first (light carbiding) followed by MoC as the process progresses. Beyond this step, a pure carbon deposit is detected on MoC. Fabrication employing a directly heated ribbon was successful for Mo_2C. Several carbiding runs followed by x-ray diffraction measurements resulted in the ability to control the degree of carbon reaction to produce a surface for which the x-ray diffraction lines of Mo_2C were present and those of MoC were not.

Both the ZrC and the Mo_2C surfaces were checked by x-ray diffraction following completion of all experimental measurements. The "before" and "after" spectra were identical in both cases, indicating no stoichiometry changes under the conditions of the experiments.

Several tantalum diboride ribbon emitters were fabricated by W. E. McKee of this laboratory, starting with a 0.005-in. tantalum ribbon. The ribbons were first carbided; a layer of tantalum was deposited and was then borided. The carbide layer under the boride

surface layer prevented diffusion of the boron from the surface layer to the interior metallic tantalum, a process which was found to occur readily at a temperature in the range required for the cesiated measurements. X-ray diffraction measurements on these ribbons showed them to be of large TaB_2 stoichiometry with some small amounts of lower boron tantalum borides. However, these ribbons were observed to be extremely brittle and fragile, and it was impossible to successfully fabricate even one ribbon emitter tube from them. Consequently, a block emitter of tantalum was machined and successfully subjected to the same boriding process. Even in this case, however, the TaB_2 layer was found to be very brittle, and it flaked off easily from the TaC sublayer if subjected to any mechanical strain or shock. This problem was encountered with the first tantalum boride tube used in Contract NAS 3-5249. Another TaB_2 emitter surface was satisfactorily fabricated and successfully studied under Contract NAS 3-6278.

Disilicide surfaces of molybdenum, tantalum, and tungsten were satisfactorily fabricated on ribbons of the base metal by a powder pack technique. These three surfaces were found by McKee to be thermally unstable at 1400C, in agreement with x-ray diffraction measurements made after the cesiated emission measurements were completed.

IV. THEORY AND ANALYTICAL CALCULATIONS

Of significant value to this surface physics program, which involves the comparison of a wide variety of metal adsorbate-metal substrate systems, would be generalized, analytical expressions for certain basic adsorption system parameters; these could then be programmed for computer calculation of a large number of adsorbate-substrate combinations to aid in the selection of optimum electrode materials. Such expressions have been developed and used in extensive computer calculations under this program for atom and ion adsorption/desorption energies for cesium on a variety of metal surfaces, nonrefractory as well as refractory; for atom and ion desorption energies for a variety of metals from substrates of tungsten and eight other refractory metals; for the equilibrium surface coverage of any one metal on another as a function of arrival flux, surface temperature, and atom and ion desorption energy; for the variation of composite surface work function of various adsorbate-substrate combinations as a function of surface coverage, and therefore indirectly as a function of arrival flux and surface temperature; for atom residence times as a function of coverage, surface temperature, and arrival flux; and for surface diffusion coefficients as a function of coverage, temperature, and arrival flux (indirectly). The expressions and the computer calculations which have been performed are described in the following sections.

A. LIST OF SYMBOLS

α	polarizability, cm^3 or $Å^3$
$\bar{\alpha}$	reflection coefficient or sticking probability, unitless
β	surface ionization efficiency, unitless
θ	surface coverage, unitless
λ	desorption energy, eV

μ	arrival flux, atoms/cm^2-sec
ν	desorption flux, atoms/cm^2-sec
σ	surface concentration, atoms/cm^2
τ	mean residence time, sec
ϕ	effective work function, eV
χ	electronegativity, eV
χ_o	distance of adatom from substrate at which probability of electron transition vanishes, approximately r, cm or Å
ψ	angle, unitless
ω	fundamental vibration frequency, sec^{-1}
d	diameter, cm or Å
D_s	surface diffusion coefficient, cm^2/sec
E	applied surface electric field, V/cm
g	statistical weight, unitless
G	shape factor (nonarbitrary), unitless
$H_s, \Delta H_s$	sublimation energy per atom, eV/atom or kcal/mole
j^v	vibration partition function, unitless
J	current density, A/cm^2
k	Boltzmann constant, eV/atom-^oK
m	effective dipole moment, coul-m
M	dipole moment, coul-m
NF	neutral fraction, unitless
r	covalent radius, cm or Å
S	orbital strength, entropy (ΔS is change in entropy), unitless; eV/atom-^oK
T	surface temperature, degrees
v	valence, unitless
V_i	ionization potential (energy), eV

subscripts

o	atom
+	ion
-	electron
c	ion critical (temperature) point

NOTE: All parentheses indicate the value of θ for which the function is evaluated; (0) corresponds to the bare substrate and (1) refers to the bulk adsorbate.

B. EQUILIBRIUM SURFACE COVERAGE

The dependent variable in all of the expressions for the fundamental (not applied, as are T and E) surface physics quantities, ϕ, λ_o, λ_+, τ, and D_s is the surface coverage θ. The most general expression for θ, including the influence of all strengths of applied field and an ion component of incident flux, is

$$\theta = \frac{\bar{\alpha}\mu_o + \mu_+}{\sigma(1)} \left(\frac{h}{kT}\right)\left[1 - e^{-\left(\frac{h\omega}{kT}\right)}\right]^{-1} \exp\left[-\frac{\Delta S(\theta)}{k}\right]$$

$$\left\{\exp - \left[\frac{\lambda_o(\theta) + \frac{1}{2}\alpha_o(1)\,E^2 + eE\,\chi_o}{kT}\right] + \frac{g_o(1)}{g_+(1)}\right.$$

$$\left.\exp - \left[\frac{\lambda_+(\theta) + \frac{1}{2}\alpha_+(1)\,E^2 - e\sqrt{eE}}{kT}\right]\right\}^{-1} . \qquad (2)$$

This expression results from the fundamental definition of θ,

$$\theta \equiv \frac{\sigma}{\sigma(1)} = \frac{\mu_{total}\,\tau_{total}}{\sigma(1)} . \qquad (3)$$

The total arrival flux may be composed of an ion component and a neutral component. In general, there is a reflection coefficient or a sticking probability which reduces the effective neutral component.

$$\mu = \bar{\alpha}\,\mu_o + \mu_+ . \qquad (4)$$

In the most general case, when both atomic and ionic states of the adsorbate are considered, the general expression for the adsorbate mean residence time is

$$\tau = \left[\frac{1}{\tau_o} + \frac{g_o(1)}{g_+(1)} \frac{1}{\tau_+} \right]^{-1} . \qquad (5)$$

g_+/g_o is the statistical weight ratio of the adsorbate ionic to atomic states.

For a metal substrate, the activation energy for surface migration (or diffusion) is low compared with that for evaporation. Surface migration therefore maintains equilibrium among the adsorbate particles. Under these conditions τ_i is obtained from the isotherm of the adsorbate particles

$$\tau_i(\theta, E, T) = g_i \left(\frac{h}{kT} \right) \left[1 - \exp\left(- \frac{h\omega}{kT} \right) \right]^{-1} \exp \left[\frac{\lambda_i(\theta, E, T)}{kT} - \frac{\Delta S(\theta)}{k} \right] . \qquad (6)$$

In this equation,

$$\left[1 - \exp\left(- \frac{h\omega}{kT} \right) \right]^{-1}$$

is the vibration partition function in any number of dimensions. Here $\exp - [\Delta S(\theta)/k]$ is an entropy term discussed in more detail in Ref. 2. It is related to the statistical population density in the adsorbed layer and is influenced by the population and depopulation of the adsorbed layer by the adsorption-desorption process. Its value is unity at $\theta = 0$ and increases with increasing θ, as shown in Fig. 51, where the expression

$$\exp \left[\frac{\Delta S(\theta)}{k} \right] = A_f^{-1}(\theta) \exp \left[\theta \frac{\partial}{\partial \theta} \ln A_f(\theta) \right] \qquad (7)$$

with

$$A_f(\theta) = (1 - \theta)^{1/2} (1 - \theta^{1/2})$$

is plotted.

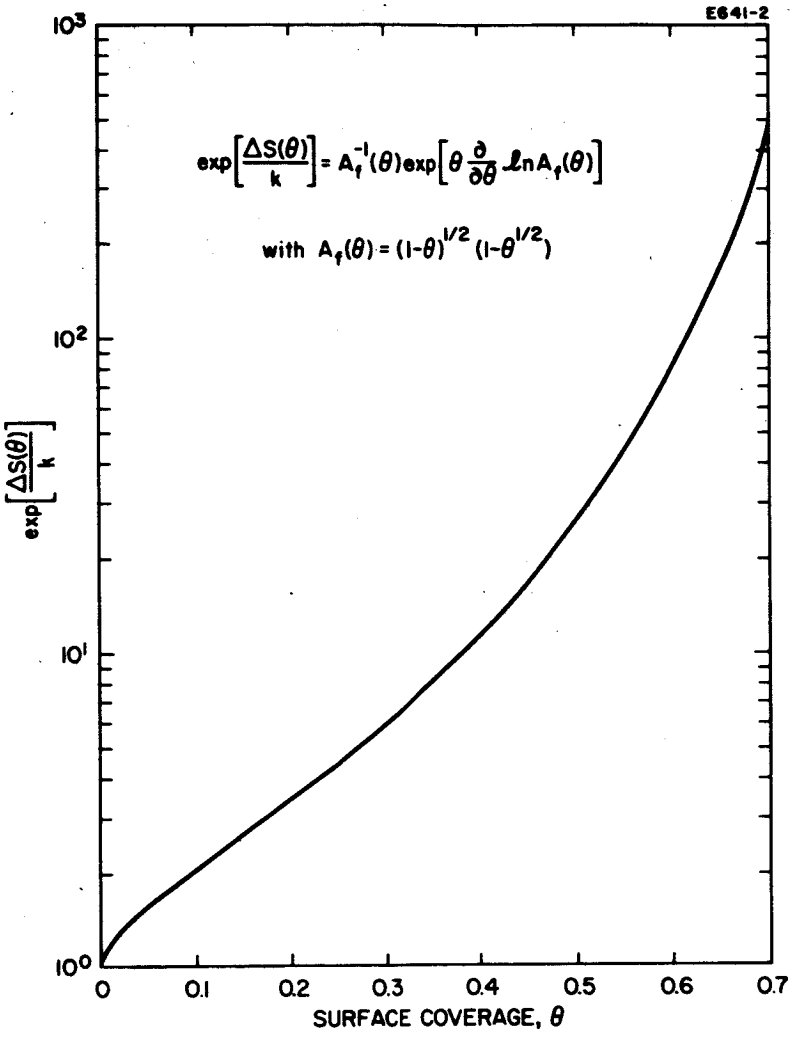

Fig. 51. Configuration entropy.

However, its magnitude is limited by the formation of multiple layers, which starts to occur well before the first monolayer is completed (about 0.6). Therefore it never reaches the potentially large values as $\theta \rightarrow 1$, because, at $\theta \approx 0.6$, multiple layers form at some locations and the mass condensation mode sets in. The term is near unity for small θ, such as in the region of the critical coverage θ_c which is below 0.05. This term can account for differences between experiment and theory for non-zero values of θ and should be calculated when a rigorous comparison is desired.

The θ and E dependences of λ_o and λ_+ can be written explicitly. The θ dependences are discussed at length in subsequent sections. The electric field dependences are

$$\lambda_o(\theta, E) = \lambda_o(\theta) + \frac{1}{2}\, a_o(1)\, E^2 + eE\,\chi_o \qquad (8)$$

and

$$\lambda_+(\theta, E) = \lambda_+(\theta) + \frac{1}{2}\, a_+(1)\, E^2 - e\sqrt{eE} \qquad (9)$$

where the $+(1/2)aE^2$ terms are increases resulting from the interaction of an inhomogeneous field with the polarized adsorbate, $E\chi_o$ is the shift in the ionization energy caused by the presence of the electric field, and $-e\sqrt{eE}$ is a reduction in λ_+ only, resulting from the same reduction in the image charge forces between the ion and the substrate surface. If μ_+ is negligible or nonexistent, and if $E \lesssim 10^6$ V/cm, as they are in the case under consideration (and in most cases), eq. (2) reduces to

$$\theta = \frac{\bar{a}\mu}{\sigma(1)} \left(\frac{h}{kT}\right) \left[1 - \exp\left(-\frac{h\omega}{kT}\right)\right]^{-1} \exp\left[\frac{\Delta S(\theta)}{k}\right] \left\{\exp\left(-\frac{\lambda_o(\theta)}{kT}\right) + \frac{g_o(1)}{g_+(1)} \exp\left[\frac{\lambda_+(\theta) + e\sqrt{eE}}{kT}\right]\right\}^{-1}, \qquad (10)$$

which is the expression applicable in this analysis. It is noted that θ itself occurs as an independent variable in two exponents. Therefore, θ cannot be independently solved for. However, once $\lambda_o(\theta)$ and $\lambda_+(\theta)$ curves are calculated from the expressions in the subsequent sections, an iterative process can be used to find a value of θ which satisfies (10). This can be done conveniently with a fast computer.

In Fig. 52,

$$\left(\frac{h}{kT}\right)\left[1 - \exp\left(-\frac{h\omega}{kT}\right)\right]^{-1}$$

is plotted versus T (for ω of cesium, as a numerical example), and it is seen that this expression can be replaced by $1/\omega$ for $T > 1000K$, which is the case for the ionizer surfaces in a cesium ion thrustor.

C. COMPOSITE SURFACE WORK FUNCTION

The expression

$$\phi(\theta) = \phi(0) - [\phi(0) - \phi(1)]\ [1 - G(\theta)]$$

$$- \frac{C_1\, \theta\, G(\theta)\, \sigma(1)\, [\phi(0) - \phi(1)] \left\{1 - \dfrac{1}{2\sigma(0)\,[r(0) + r(1)]^2}\right\}^{1/2}}{\left\{1 + \dfrac{a(1)}{[r(0) + r(1)]^3}\right\}\left\{1 + 9\, a(1)\, [\sigma(1)\, \theta]^{3/2}\right\}} \tag{11}$$

is written with the aid of Gyftopoulos and Levine.[3] This expression results from the superposition of a dipole barrier and electronegativity barrier. The electronegativity barrier $\phi_e(\theta)$ is assumed proportional to the electronegativity of the composite surface

$$\phi_e(\theta) = C_2 + C_3\, \chi(\theta) \quad . \tag{12}$$

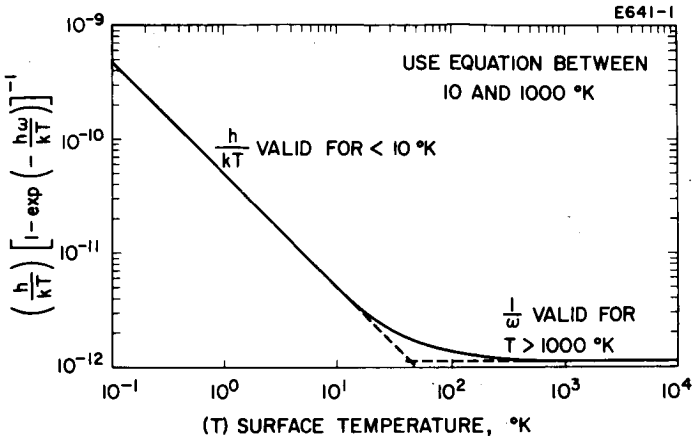

Fig. 52. Vibration partition function (for cesium).

The application of appropriate boundary conditions on $\phi_e(\theta)$ and $d\phi_e(\theta)/d\theta$ at $\theta = 0$ and 1 results in

$$\phi_e(\theta) = \phi(1) - [\phi(0) - \phi(1)]\, G(\theta) \tag{13}$$

where $G(\theta)$ is a polynomial in θ which is given by the boundary conditions or may be known empirically from contact potential measurements. This polynomial has been recently derived by an independent technique.[4]

The dipole barrier $\phi_d(\theta)$ results from polarization of both the adsorbate and substrate atoms resulting from interelectron bonding which is partly ionic and partly covalent, and is related to the electronegativity. The dipole moment of a single adatom-substrate dipole $M(0)$ is calculated. A square array of adatoms and therefore of dipoles is assumed, and the depolarizing field and the effective dipole moment $m(\theta)$ are calculated.

$$\phi_d(\theta) = -\frac{m(\theta)\,\sigma(1)\,\theta}{\epsilon_o} = -\frac{\theta\, G(\theta)\,\sigma(1)\, M(0)}{\epsilon_o\left\{1 + \dfrac{9a(1)\,[\sigma(1)\,\theta]^{3/2}}{4\pi\,\epsilon_o}\right\}} \tag{14}$$

where

$$M(0) = 4\, M(0\text{-}1)\cos\psi = \frac{C_4[\chi(0) - \chi(1)]\left\{1 - \dfrac{1}{2\sigma(0)[r(0) + r(1)]^2}\right\}^{1/2}}{\left\{1 + \dfrac{a(1)}{4\pi\epsilon_o[r(0) + r(1)]^3}\right\}} . \tag{15}$$

C_1 and all other constants to be used are functions only of the system of units employed.

Equation (11) has been used to calculate the composite surface work functions as a function of surface coverage for cesium on 27 substrates (the solid line (PHI) curves of Figs. 53 through 79), for 21 adsorbates on each of 9 substrates (189 combinations), the solid line (PHI) curves in the figures which comprise the supplementary volume entitled "Work Functions and Adsorption Energy Calculations," plus 28 additional adsorbates on tungsten only (Figs. 80 through 84). All of these curves are especially sensitive to the value of the vacuum work function of the adsorbate and may require modification for particular surfaces for which the work function is known to be different from that used in these calculations.

The 27 substrates for cesium are, together with the corresponding figure numbers in parentheses: beryllium (53), aluminum (54), titanium (55), vanadium (56), chromium (57), manganese (58), iron (59), cobalt (60), nickel (61), copper (62), gallium (63), zirconium (64), niobium (65), molybdenum (66), ruthenium (67), rhodium (68), palladium (69), indium (70), tin (71), hafnium (72), tantalum (73), tungsten (74), rhenium (75), osmium (76), iridium (77), platinum (78), and lead (79). The 21 adsorbates and 9 substrates which comprise the supplement are: lithium, beryllium, carbon, sodium, aluminum, silicon, potassium, titanium, chromium, manganese, iron, nickel, copper, rubidium, gallium, indium, tin, cesium, barium, mercury, and lead; and tungsten, iridium, rhenium, rhodium, nickel, platinum, osmium, molybdenum, and tantalum. The additional 28 adsorbates done for just a tungsten substrate are (with figure numbers) magnesium (80), strontium (80), calcium (80), cobalt (80), vanadium (80), boron (81), yttrium (81), scandium (81), lanthanum (81), antimony (81), zinc (81), palladium (82), rhodium (82), ruthenium (82), technetium (82), molybdenum (82), niobium (82), platinum (83), iridium (83), rhenium (83), osmium (83), tungsten (83), tantalum (83), hafnium (83), germanium (84), silver (84), gold (84), and thorium (84).

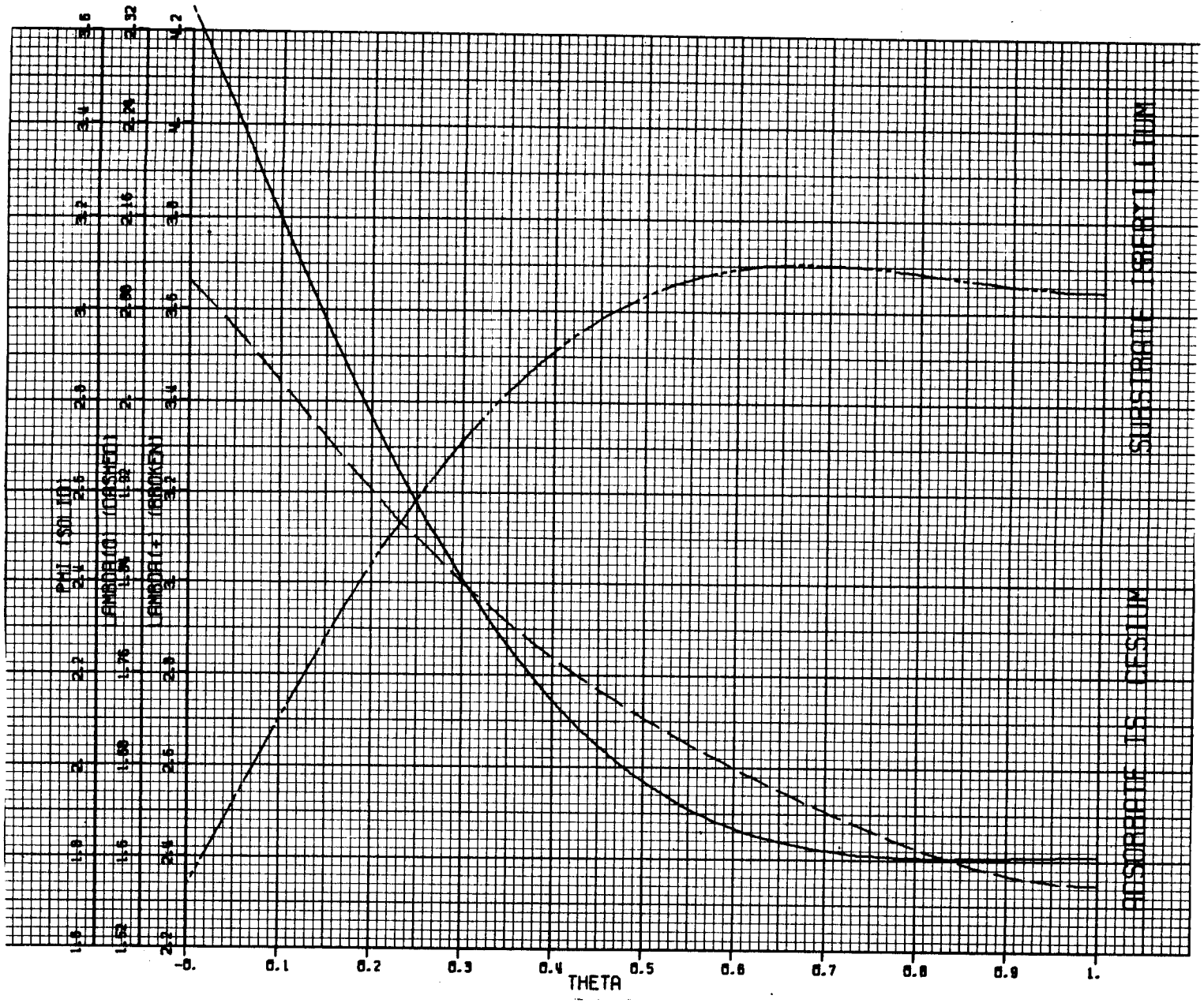

Fig. 53. Composite surface work function as a function of surface coverage for cesium on beryllium.

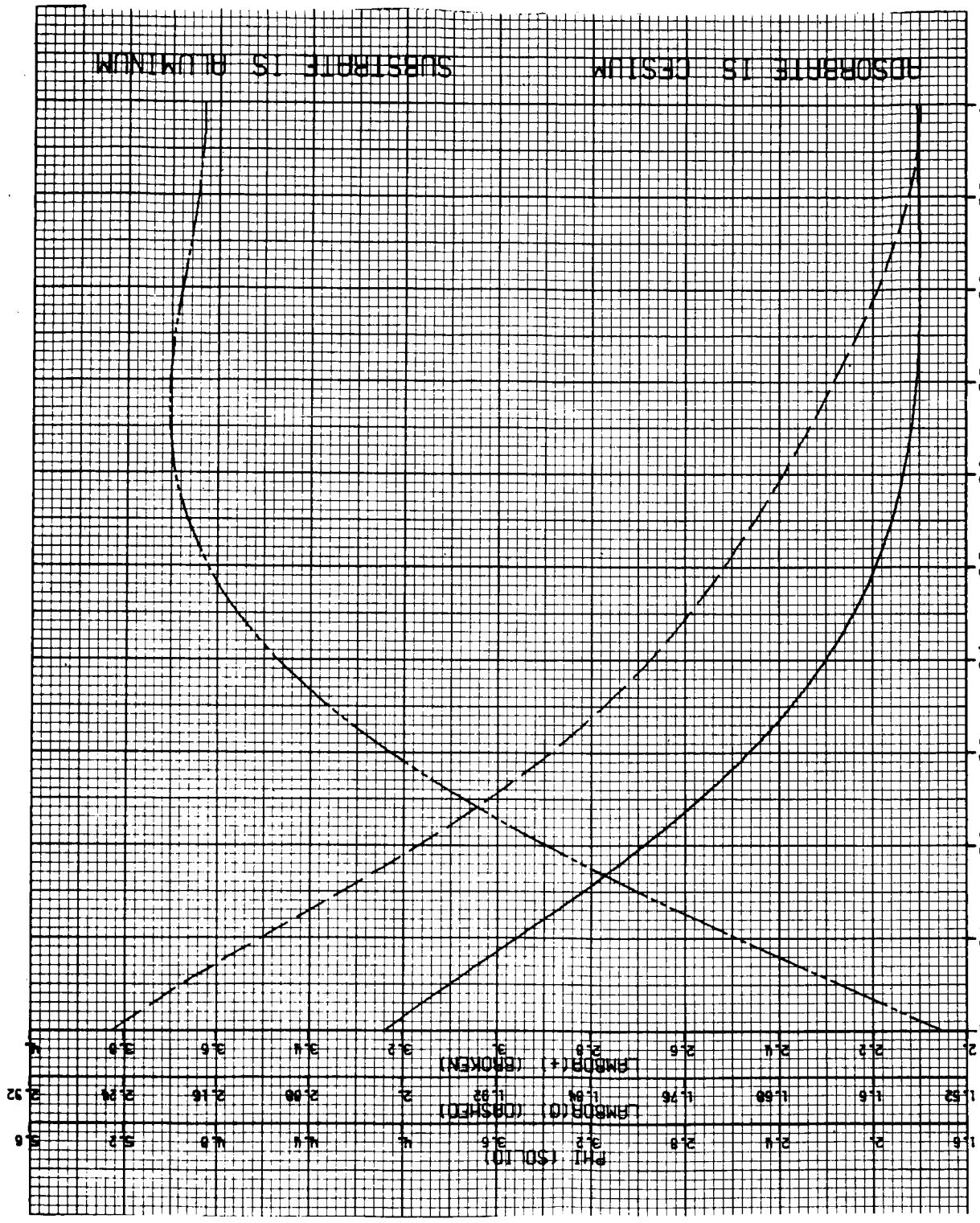

Fig. 54. Composite surface work function as a function of surface coverage for cesium on aluminum.

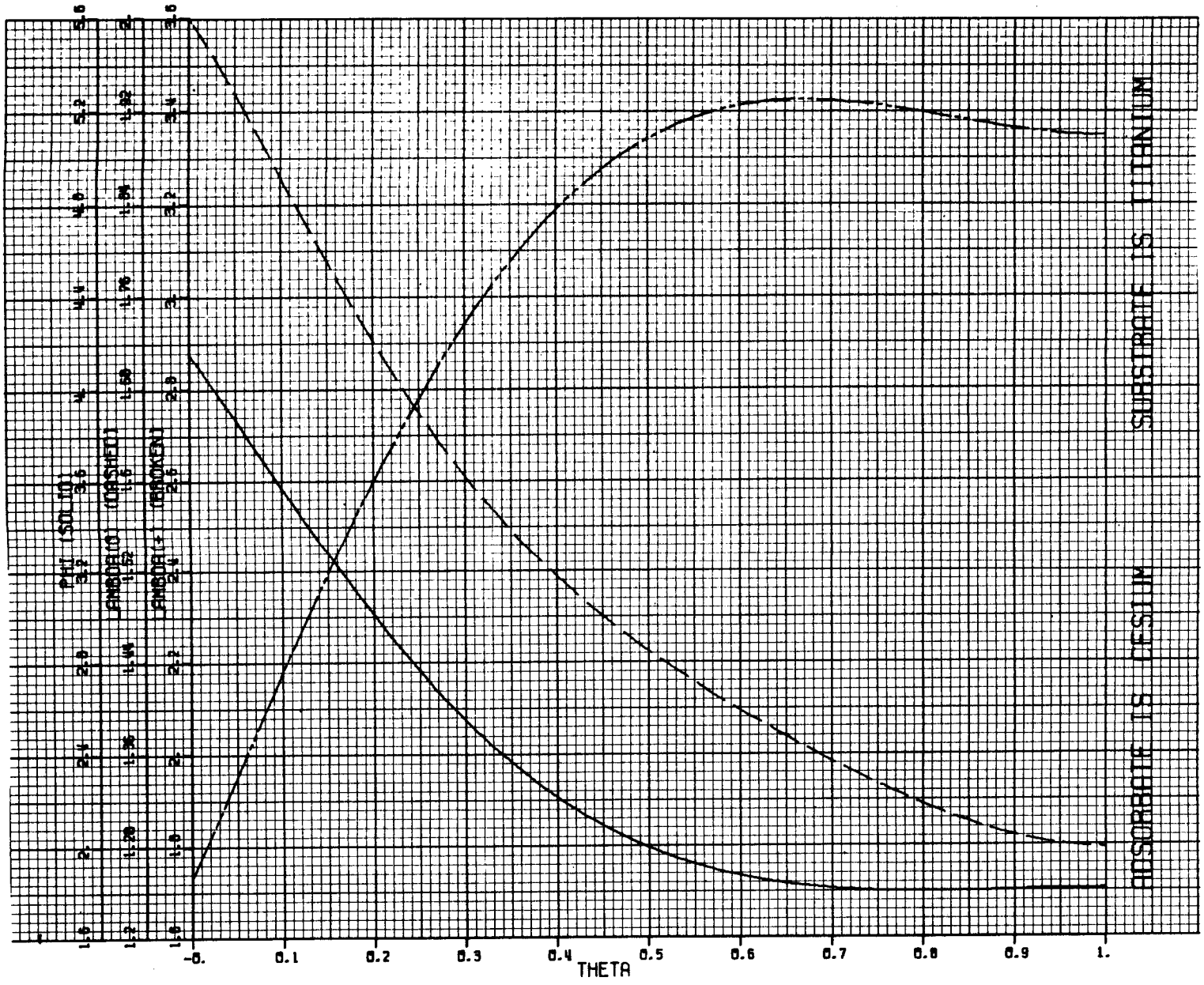

Fig. 55. Composite surface work function as a function of surface coverage for cesium on titanium.

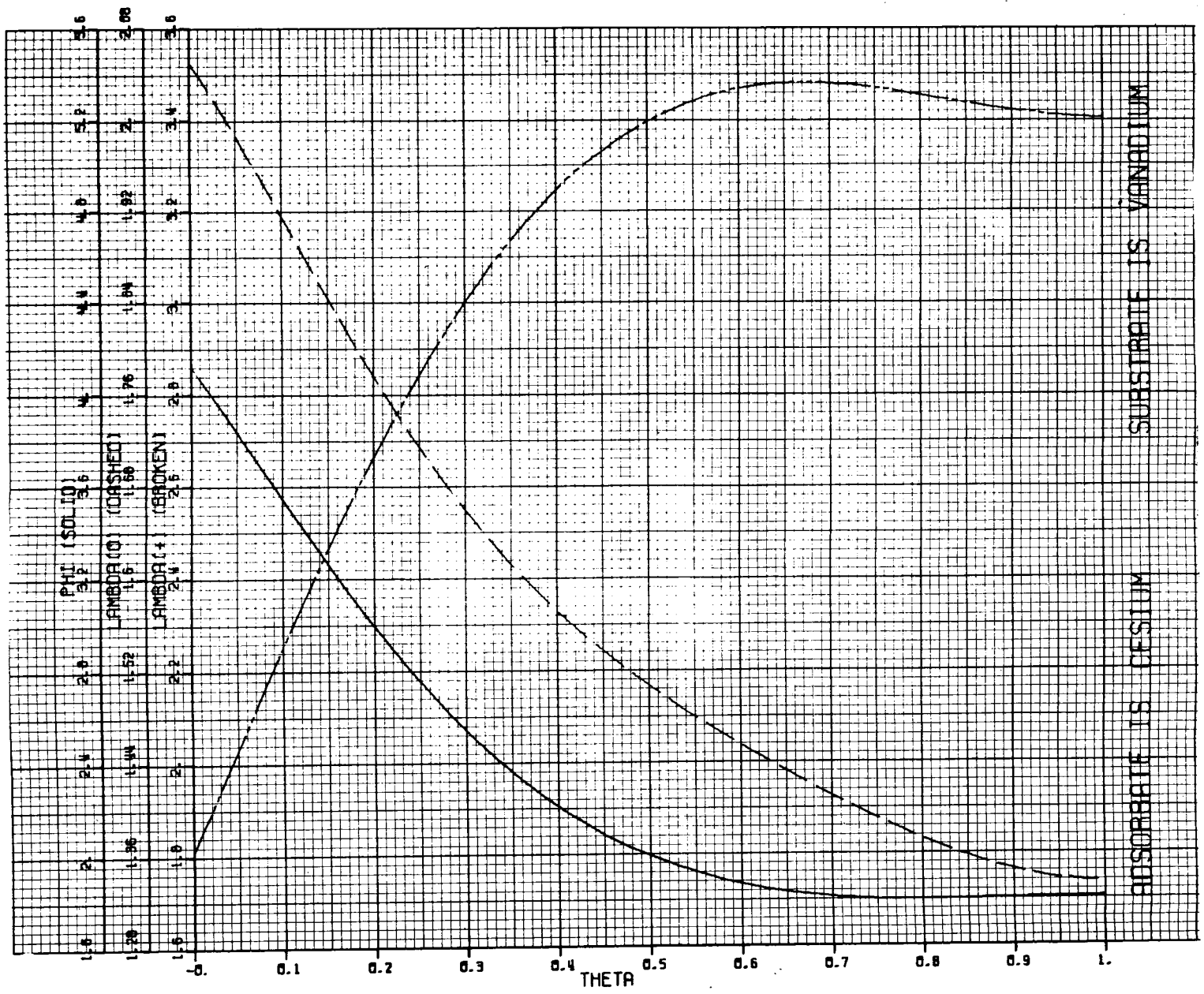

Fig. 56. Composite surface work function as a function of surface coverage for cesium on vanadium.

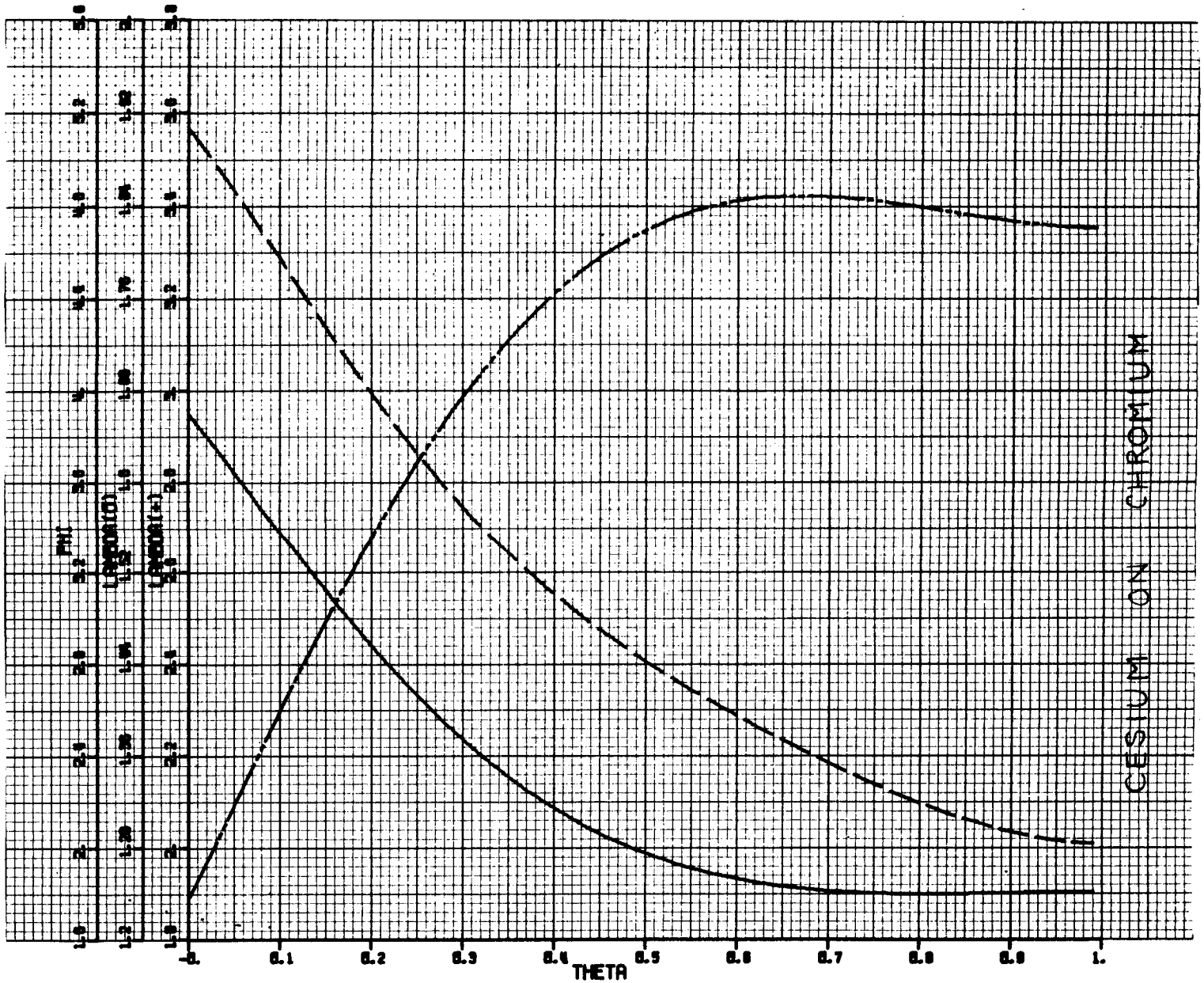

Fig. 57. Composite surface work function as a function of surface coverage for cesium on chromium.

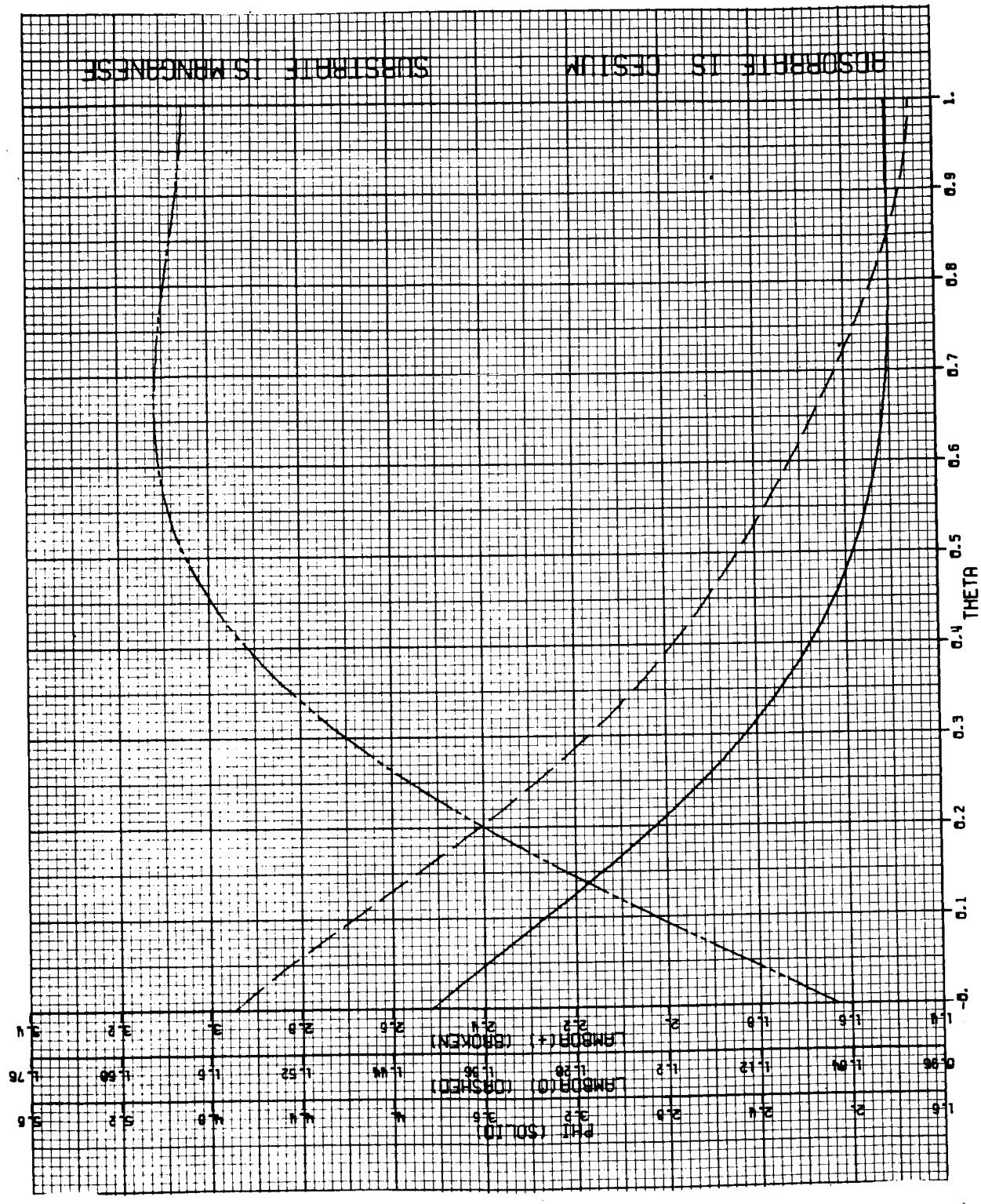

Fig. 58. Composite surface work function as a function of surface coverage for cesium on manganese.

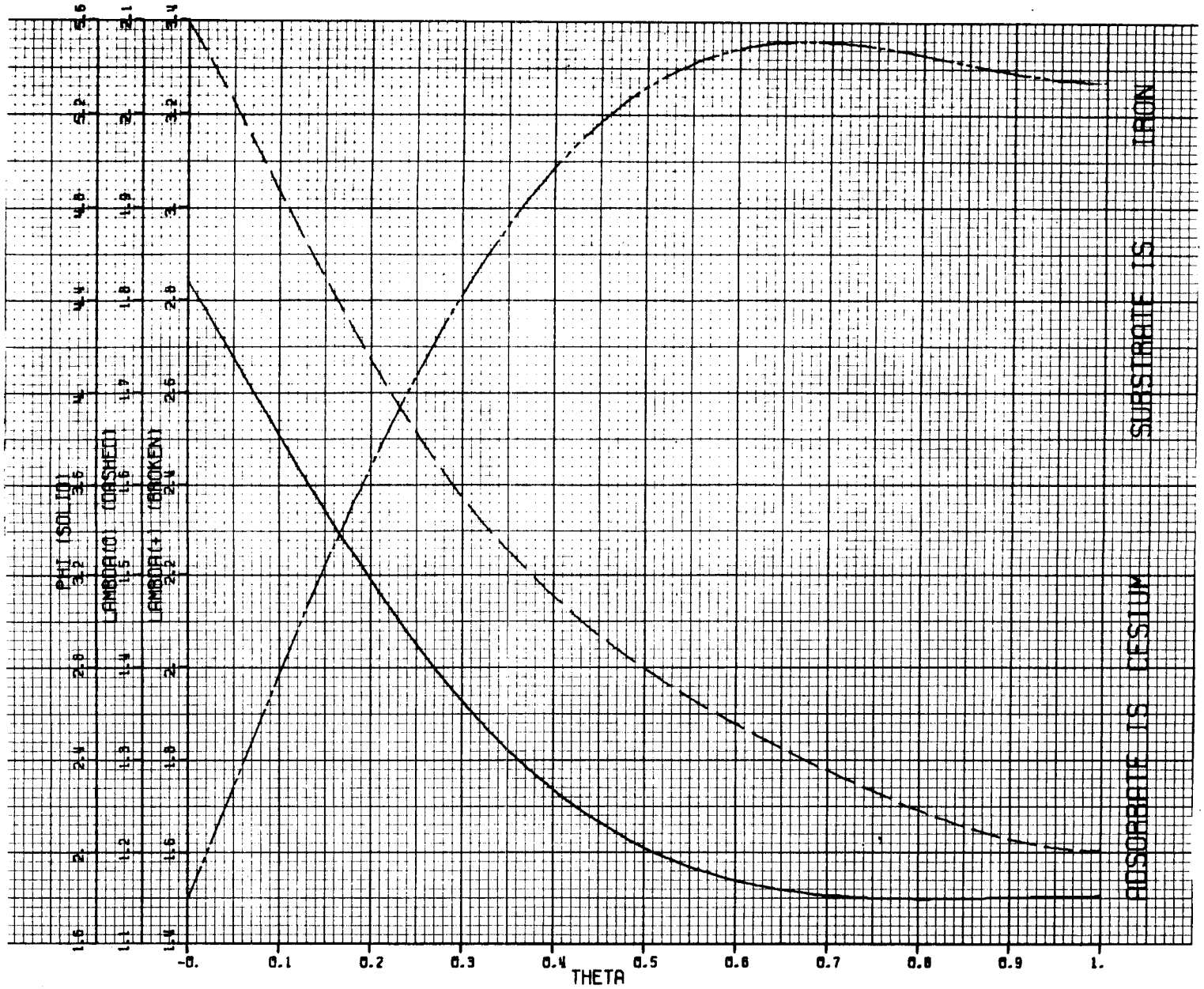

Fig. 59. Composite surface work function as a function of surface coverage for cesium on iron.

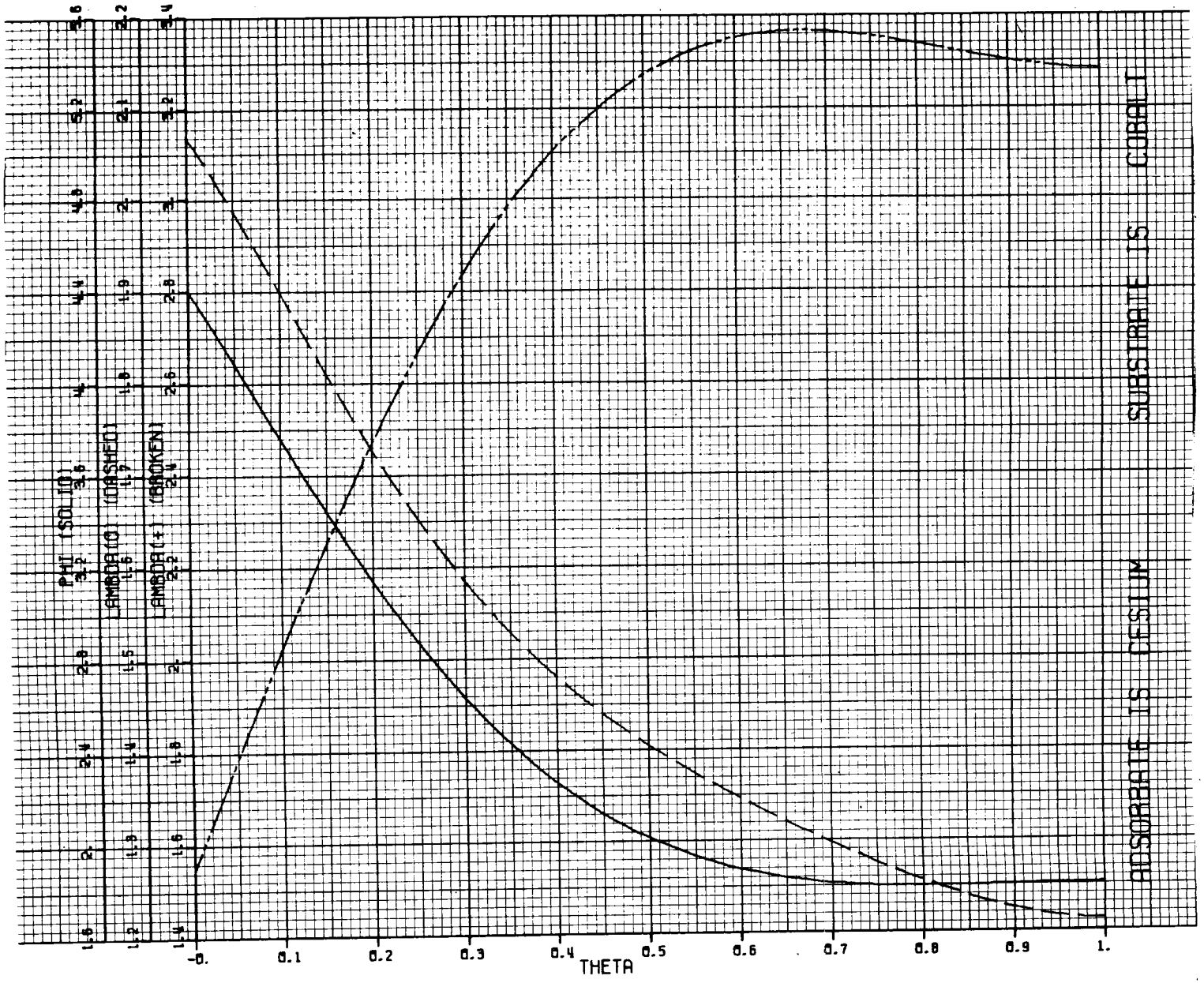

Fig. 60. Composite surface work function as a function of surface coverage for cesium on cobalt.

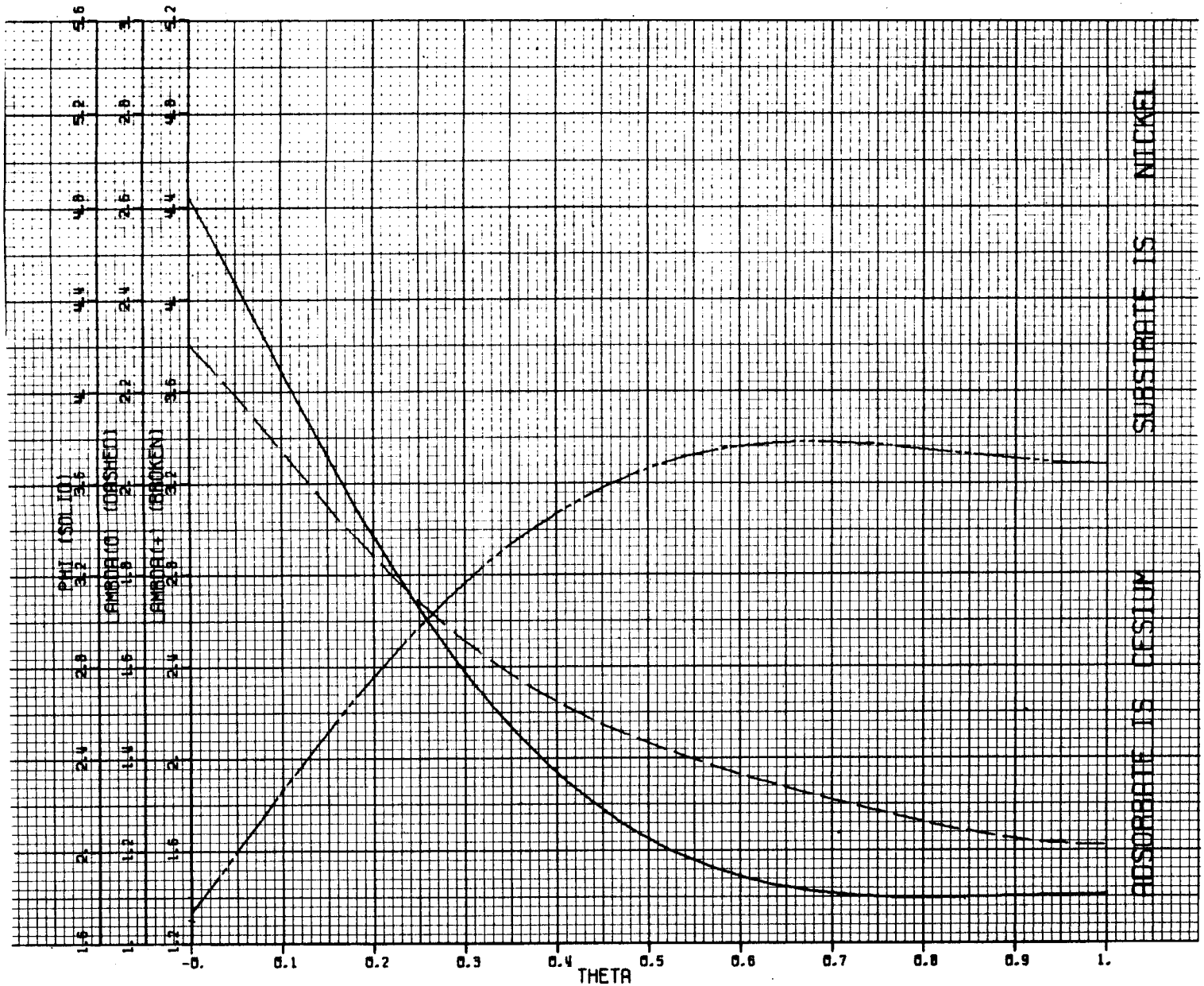

Fig. 61. Composite surface work function as a function of surface coverage for cesium on nickel.

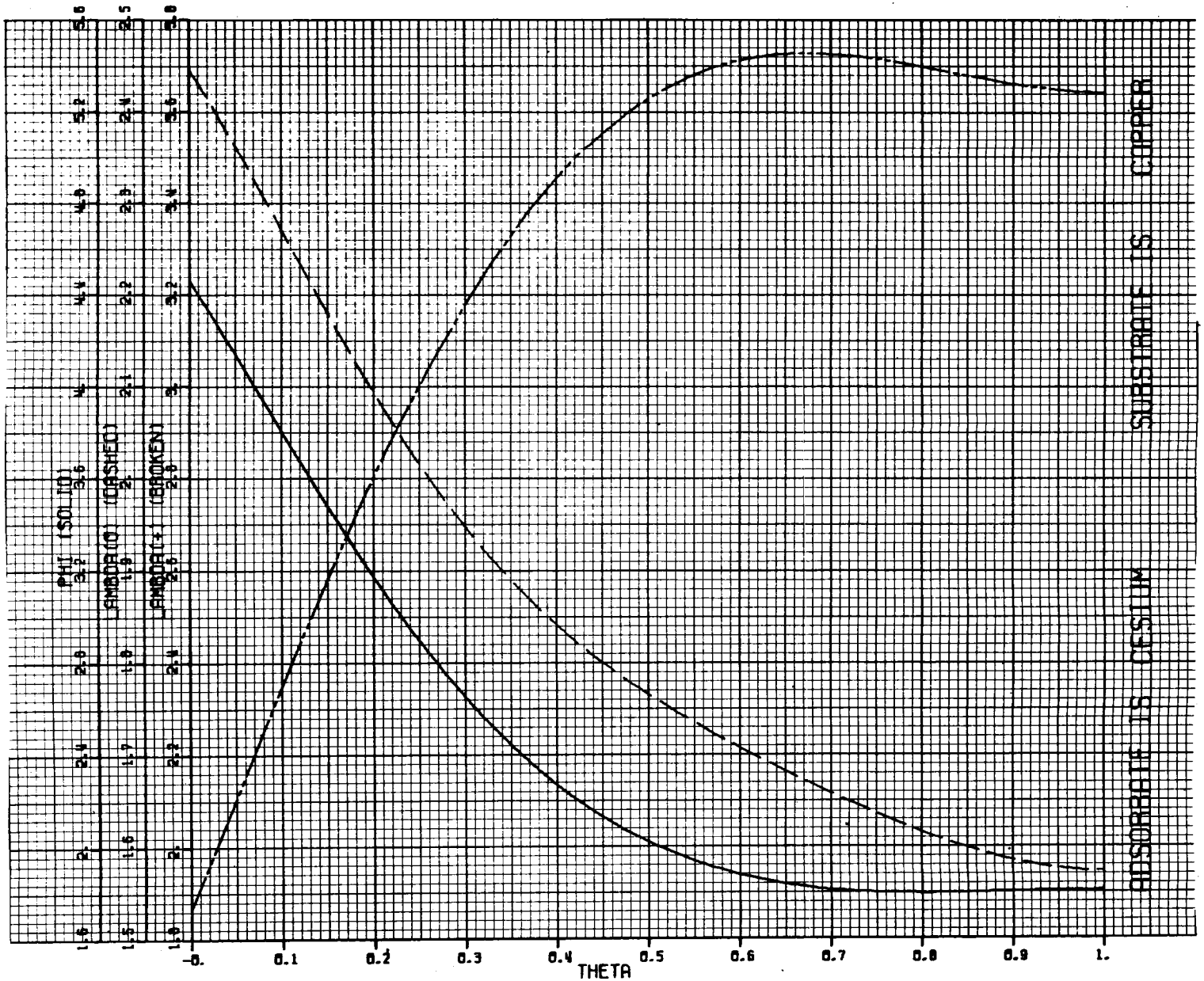

Fig. 62. Composite surface work function as a function of surface coverage for cesium on copper.

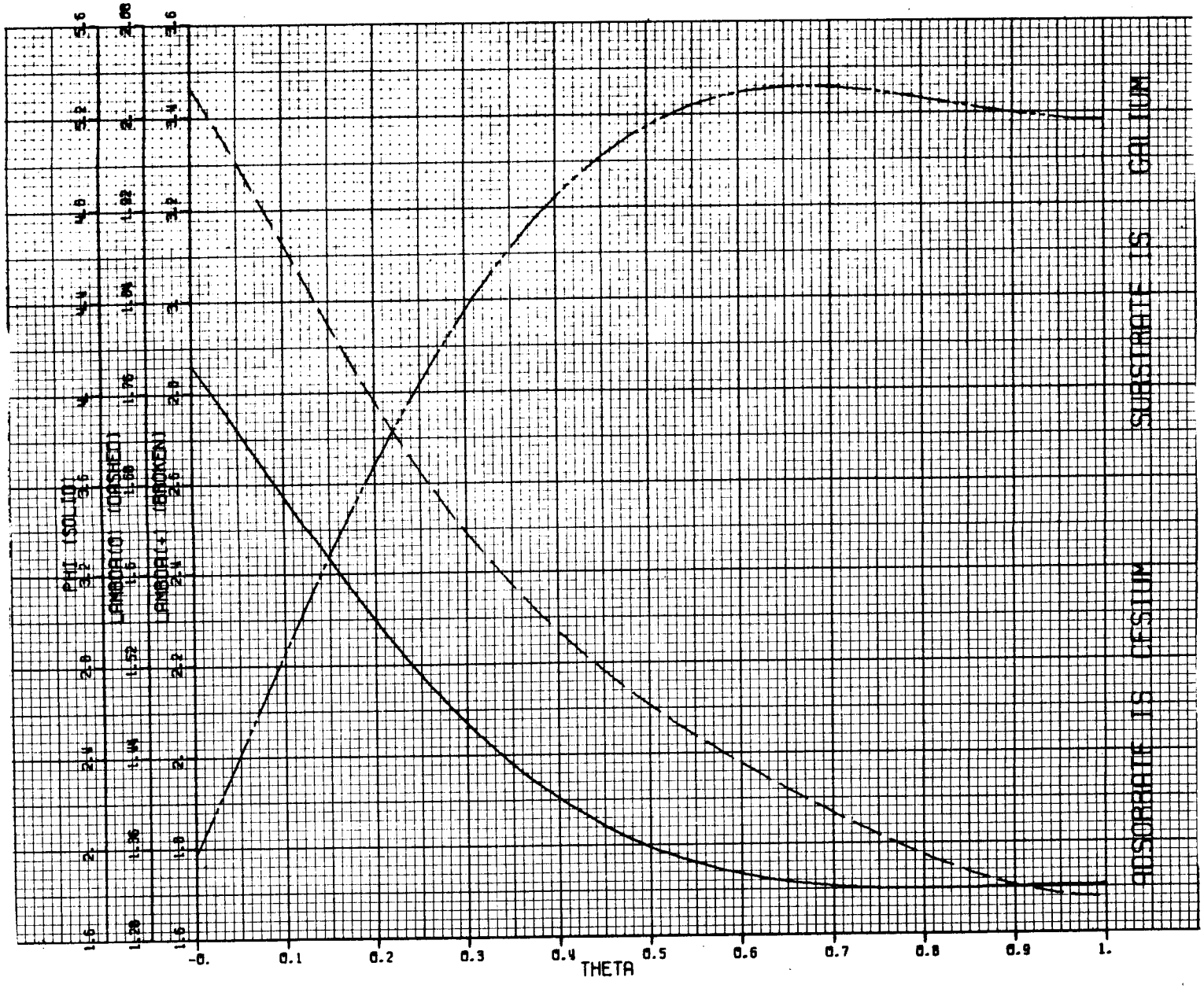

Fig. 63. Composite surface work function as a function of surface coverage for cesium on gallium.

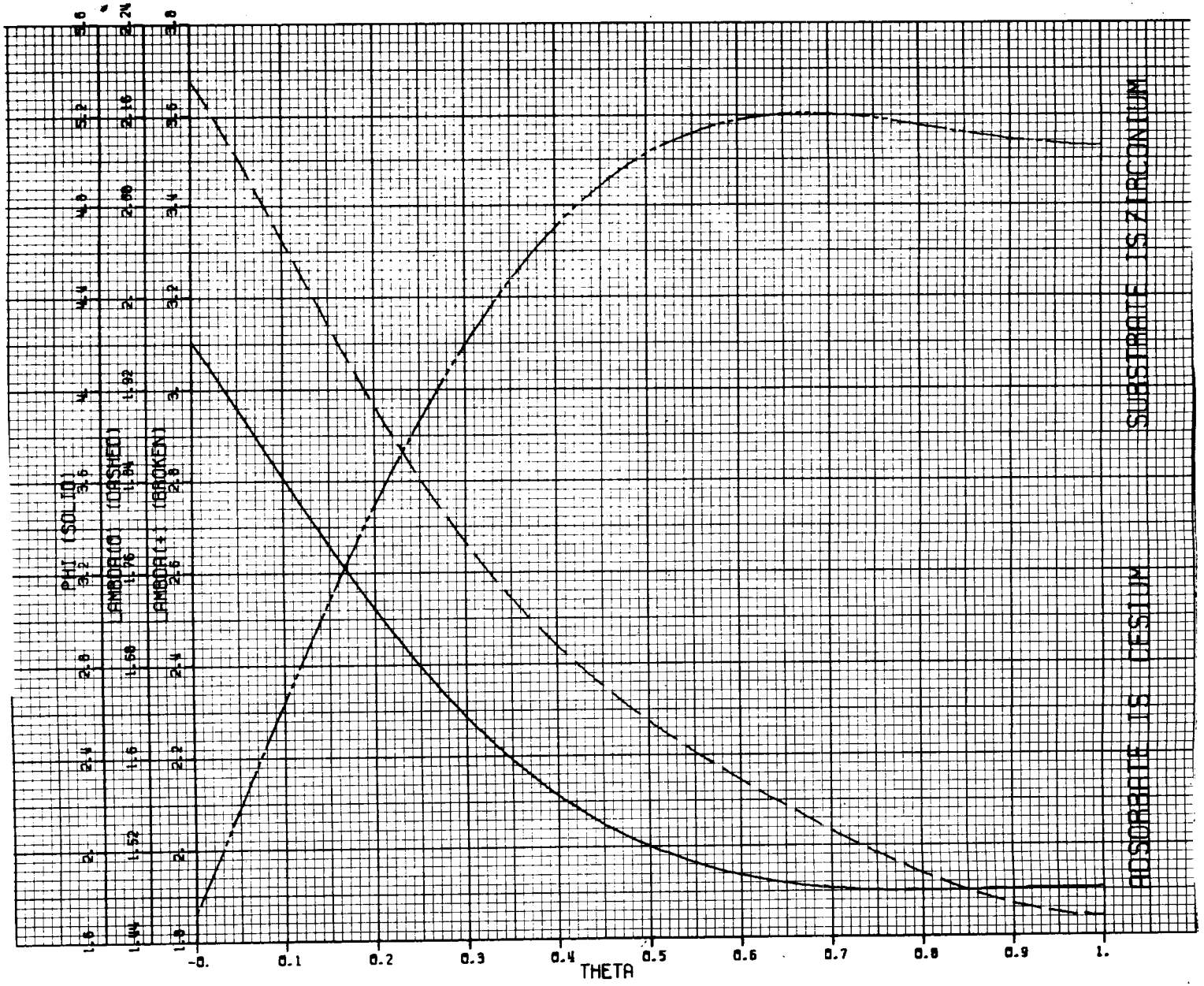

Fig. 64. Composite surface work function as a function of surface coverage for cesium on zirconium.

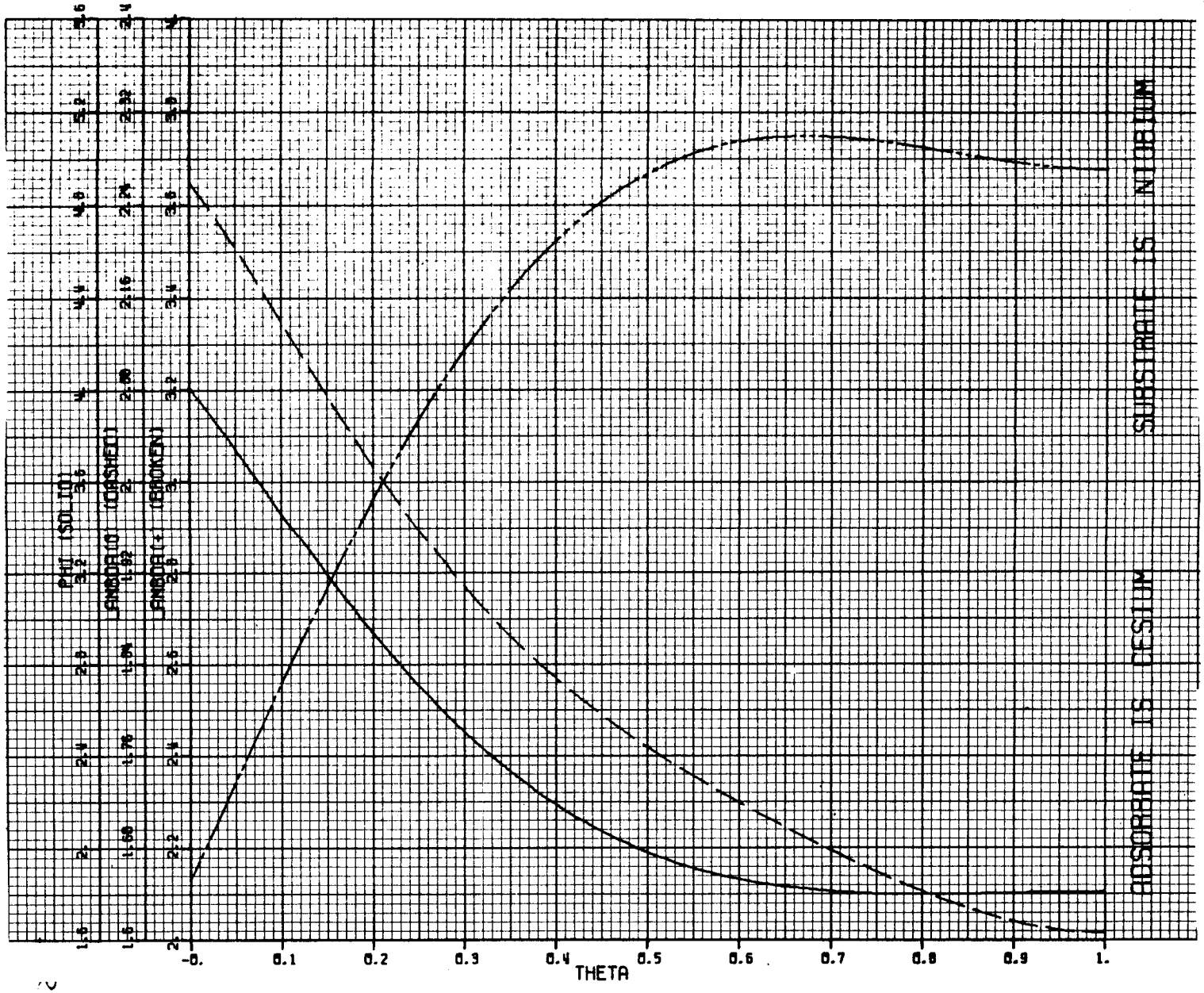

Fig. 65. Composite surface work function as a function of surface coverage for cesium on niobium.

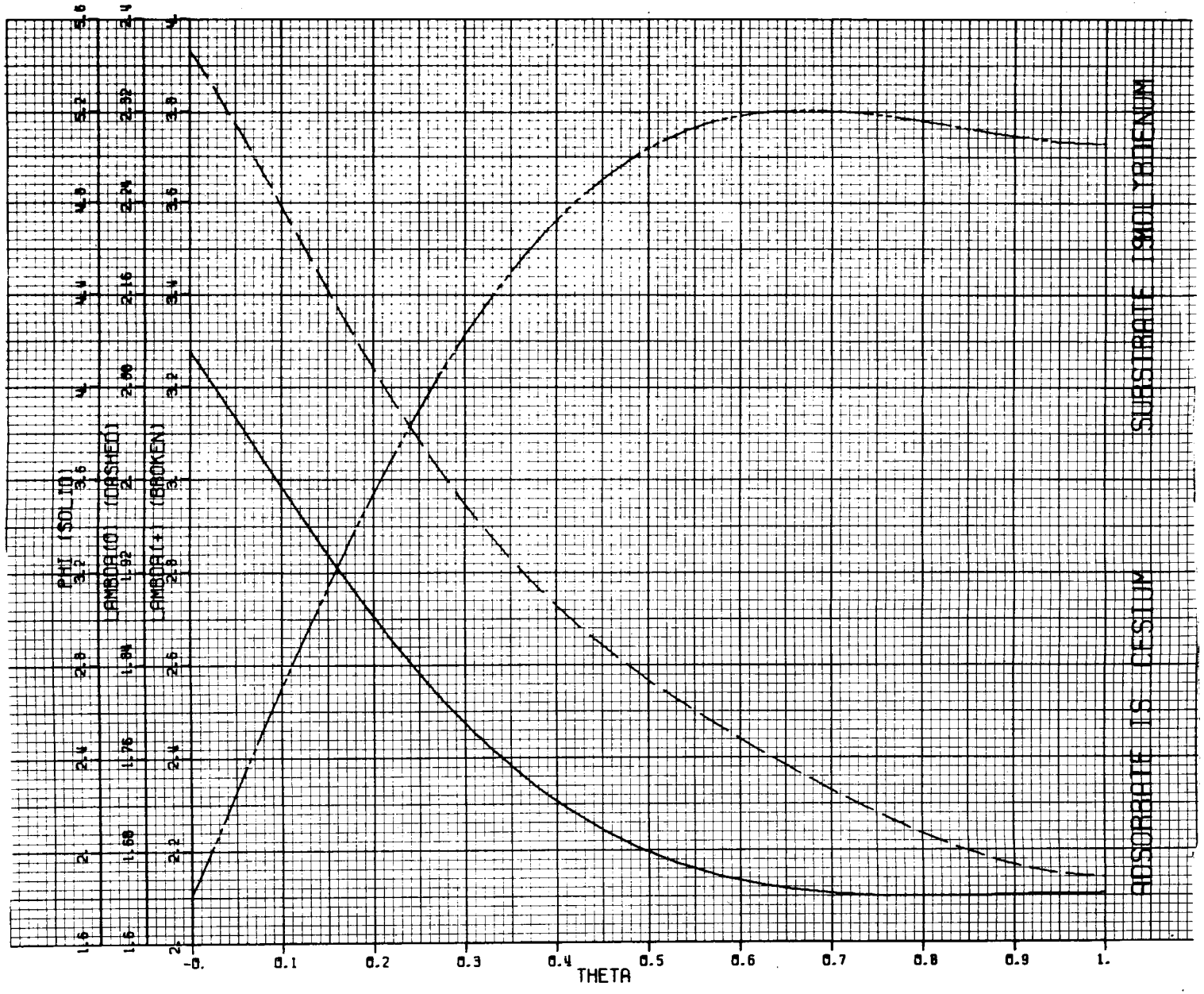

Fig. 66. Composite surface work function as a function of surface coverage for cesium on molybdenum.

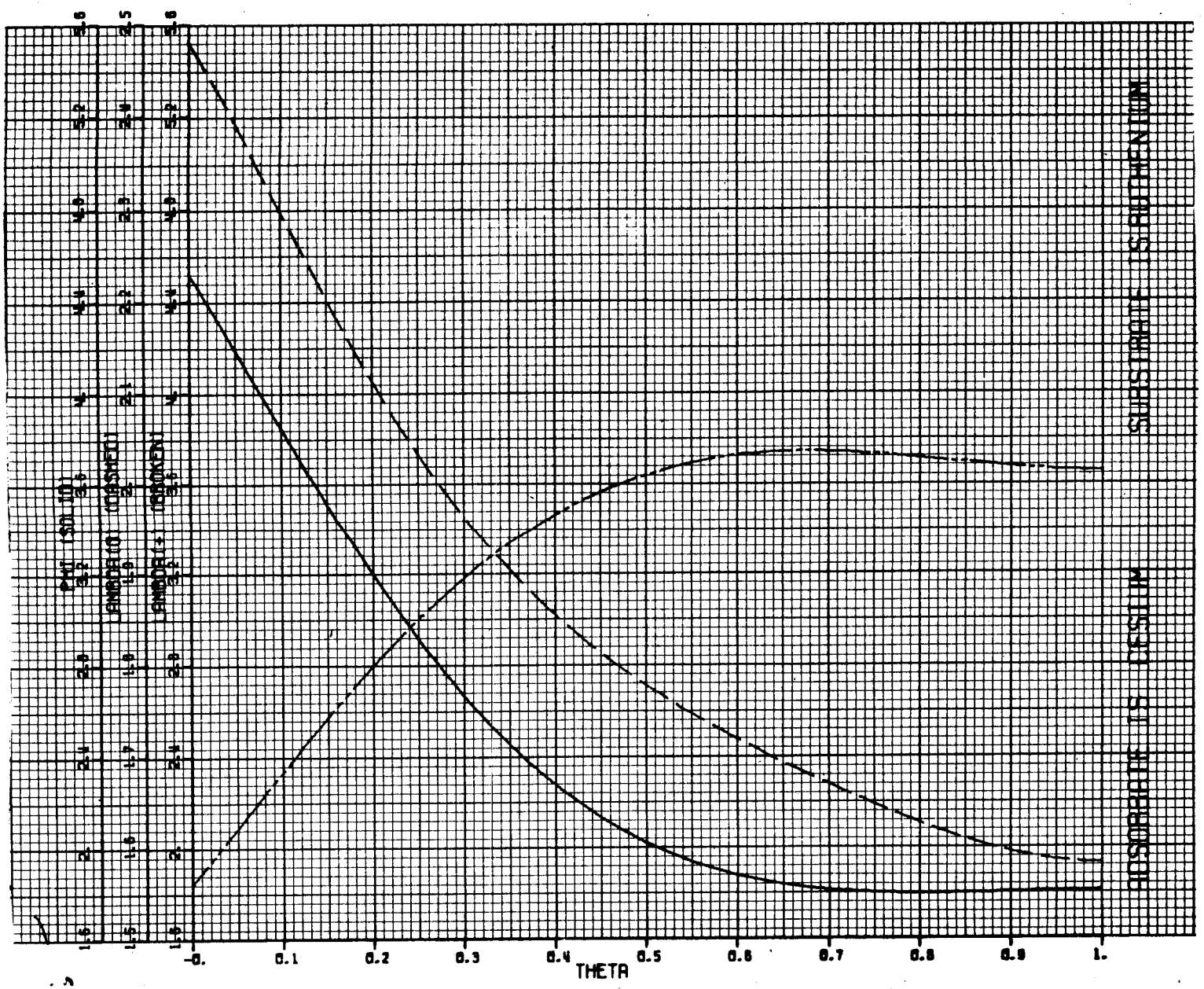

Fig. 67. Composite surface work function as a function of surface coverage for cesium on ruthenium.

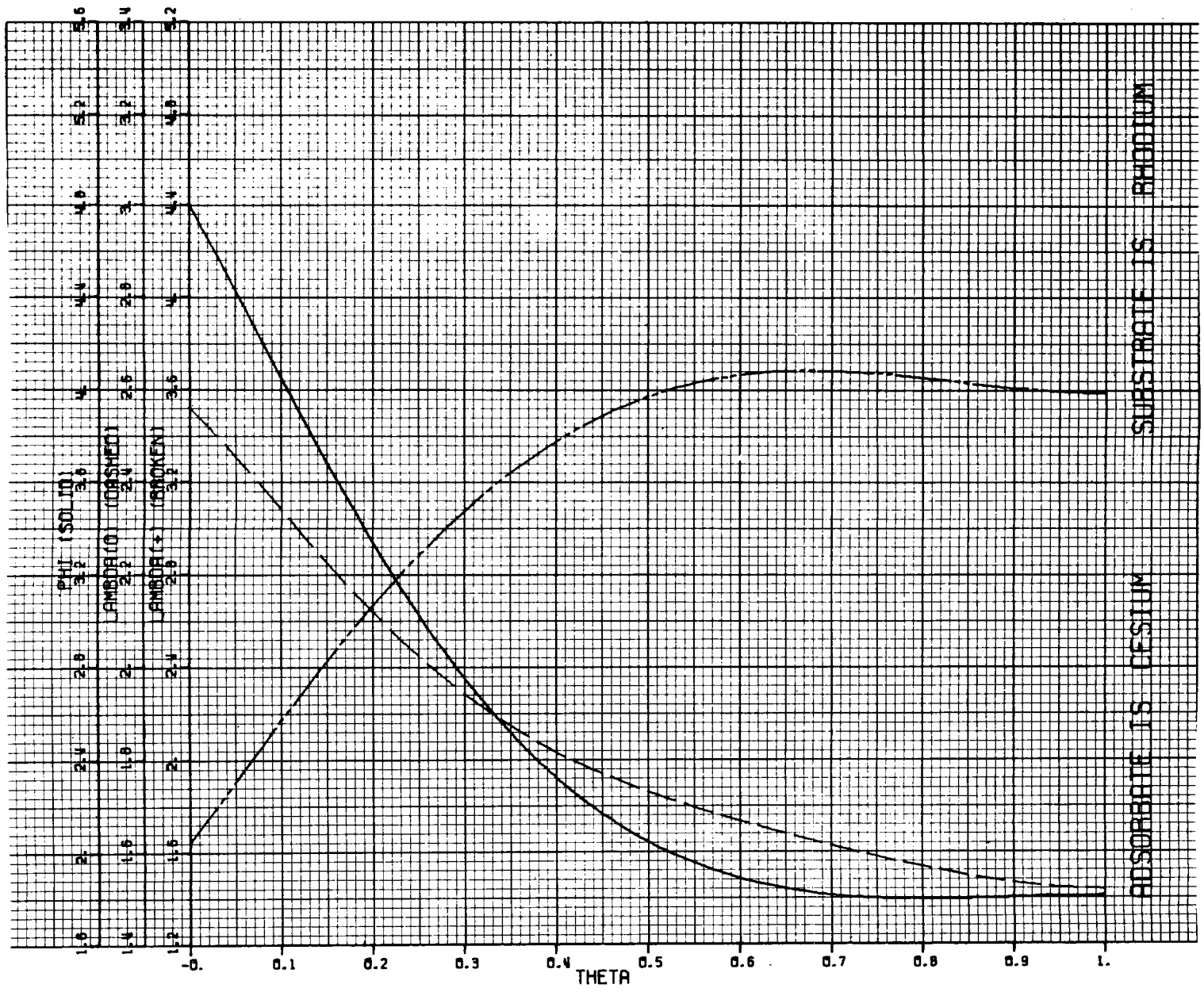

Fig. 68. Composite surface work function as a function of surface coverage for cesium on rhodium.

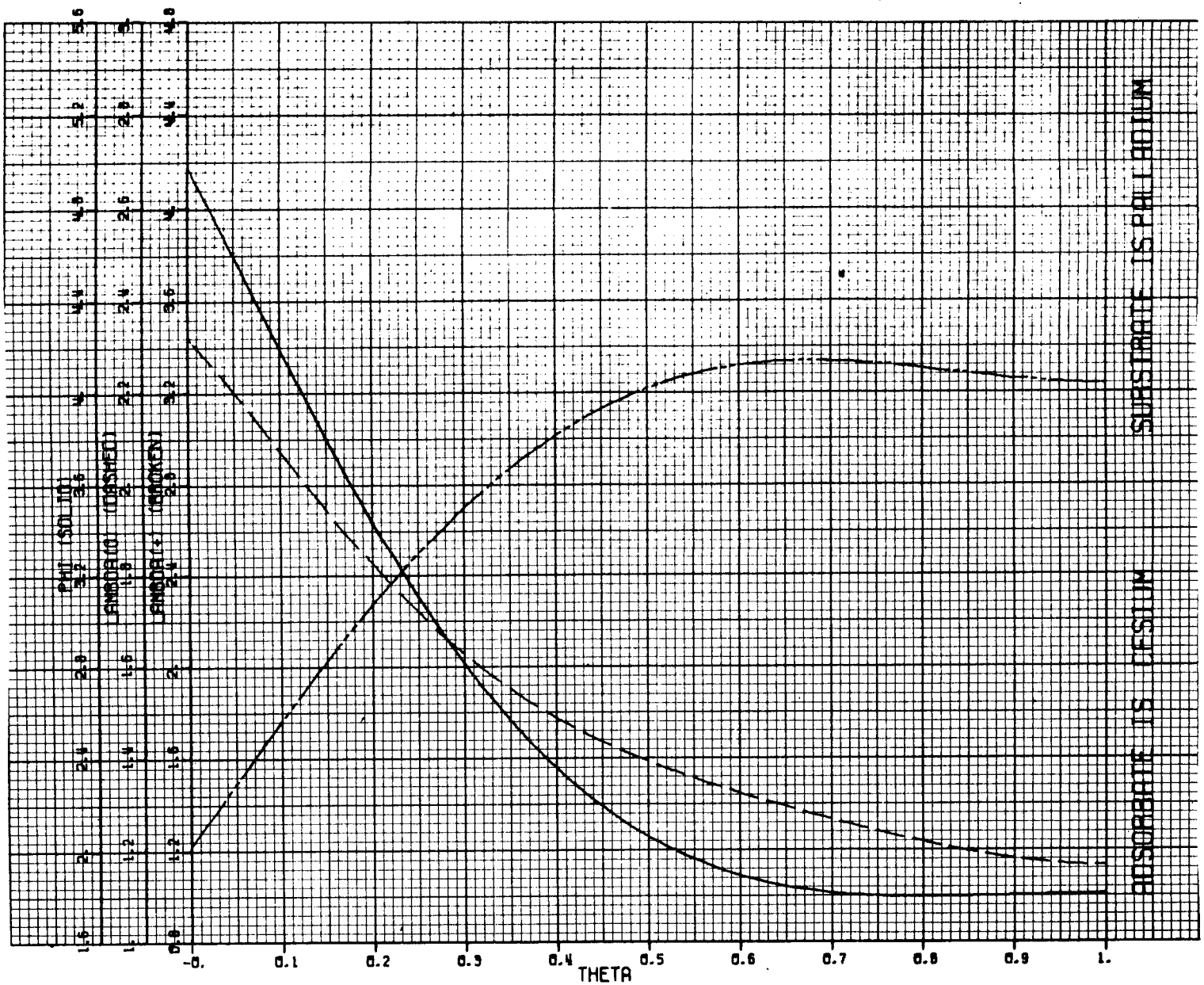

Fig. 69. Composite surface work function as a function of surface coverage for cesium on palladium.

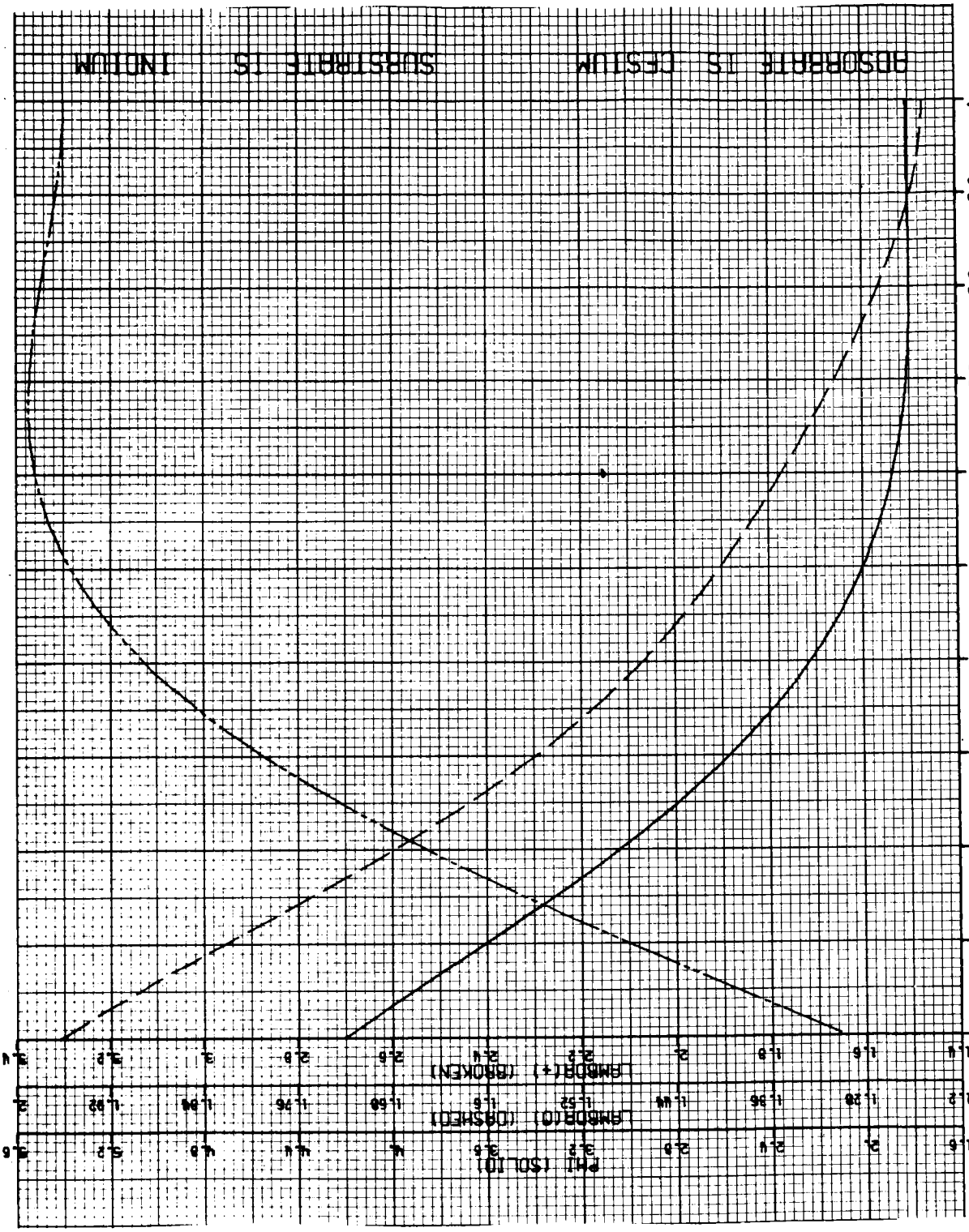

Fig. 70. Composite surface work function as a function of surface coverage for cesium on indium.

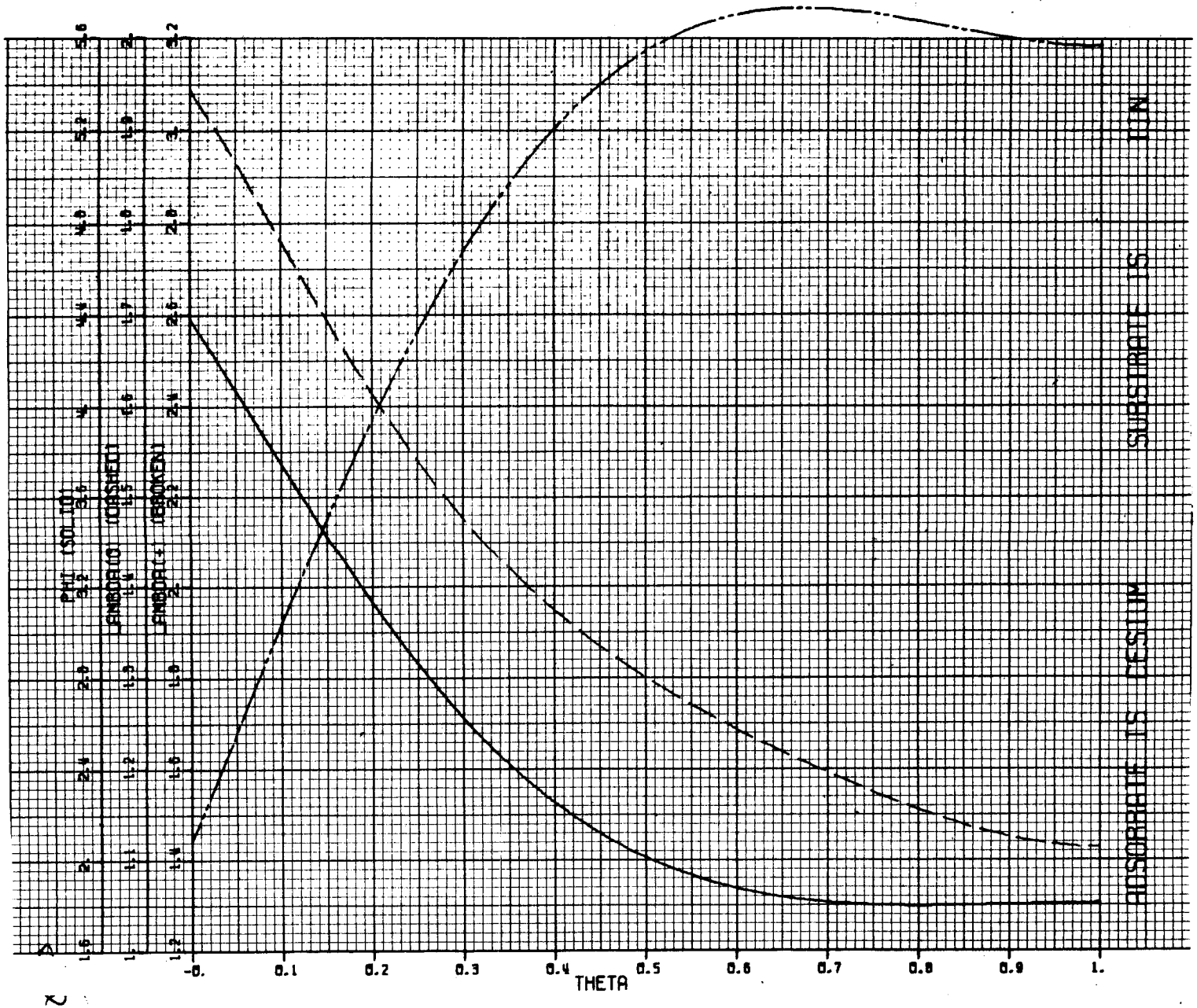

Fig. 71. Composite surface work function as a function of surface coverage for cesium on tin.

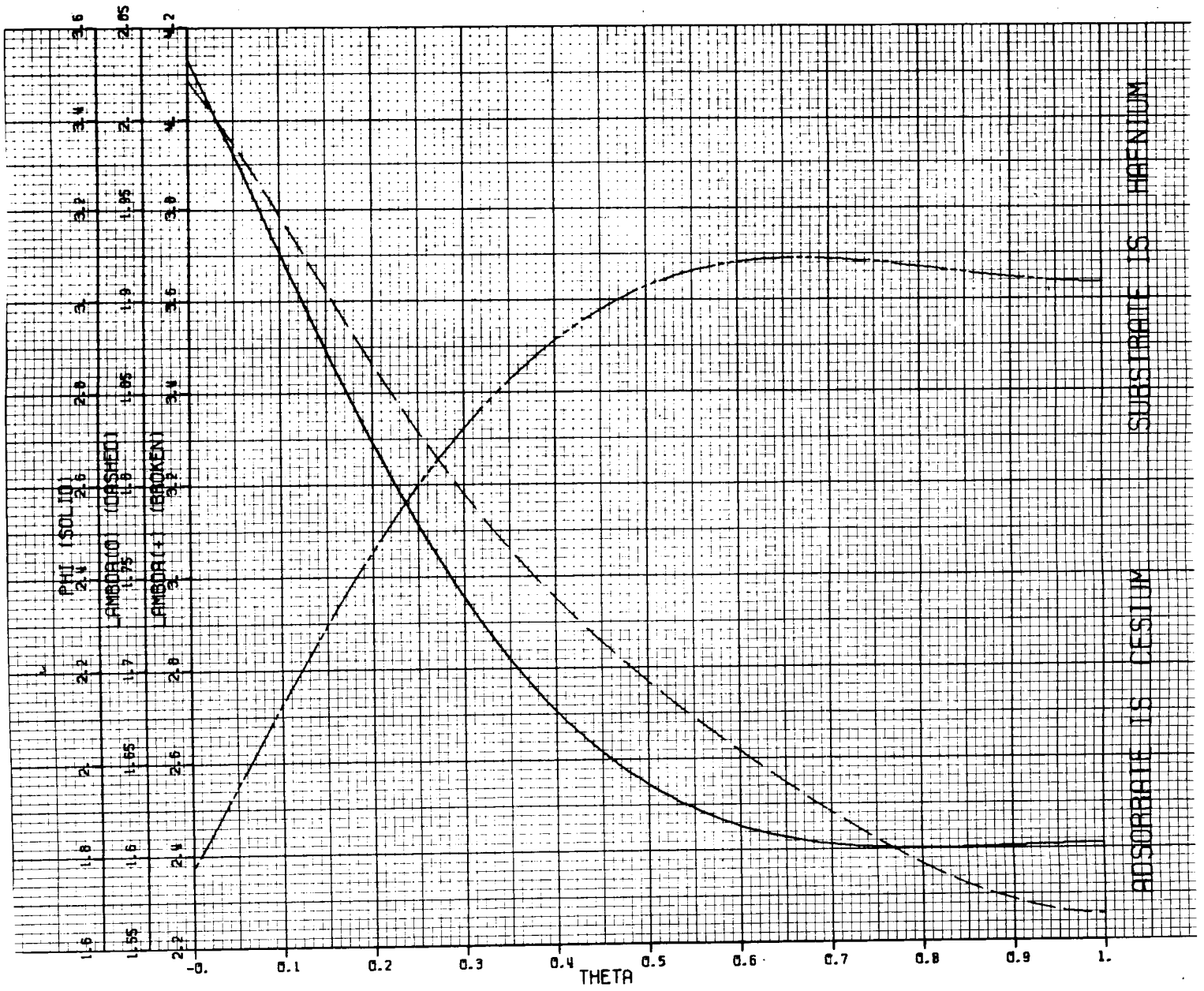

Fig. 72. Composite surface work function as a function of surface coverage for cesium on hafnium.

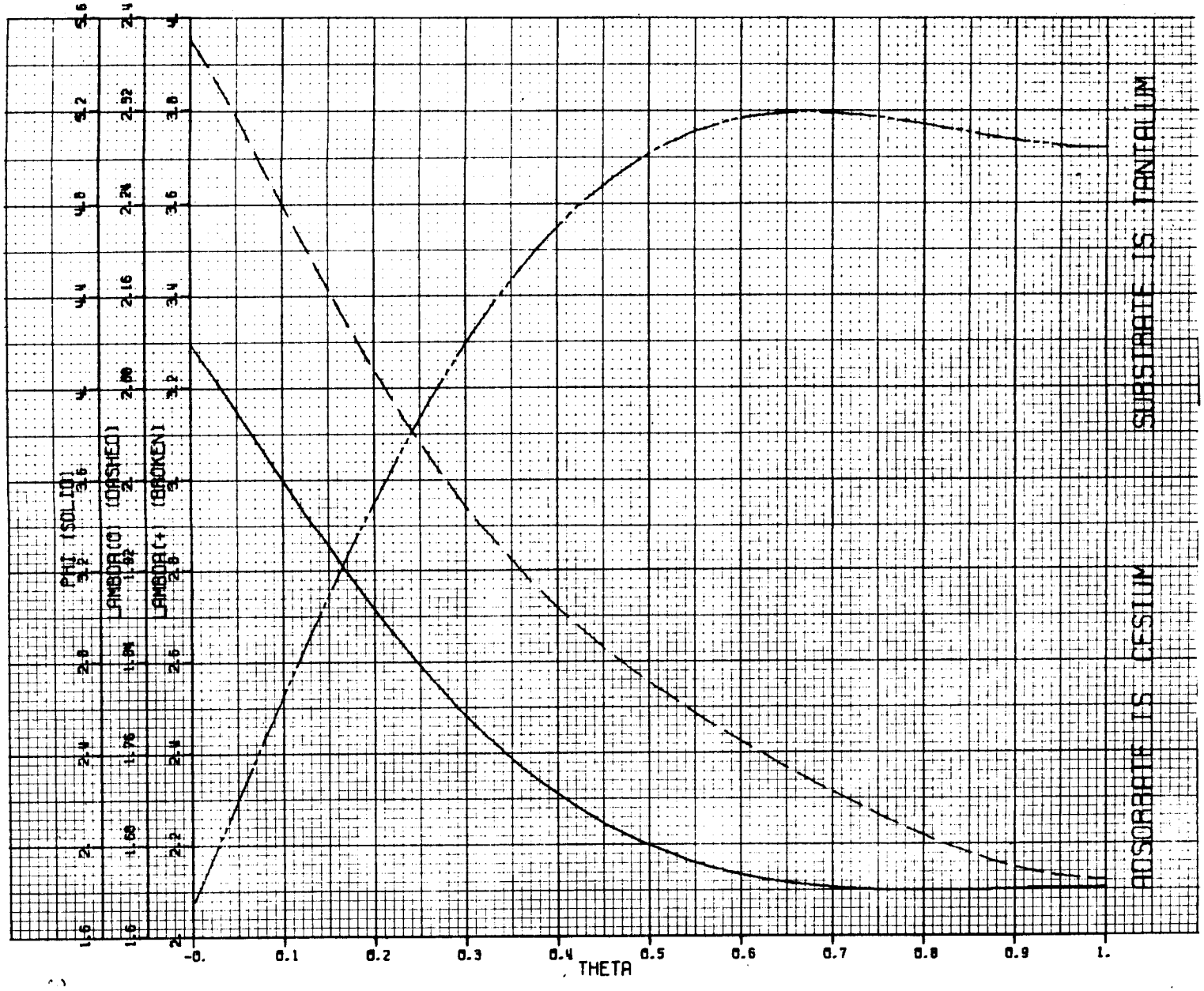

Fig. 73. Composite surface work function as a function of surface coverage for cesium on tantalum.

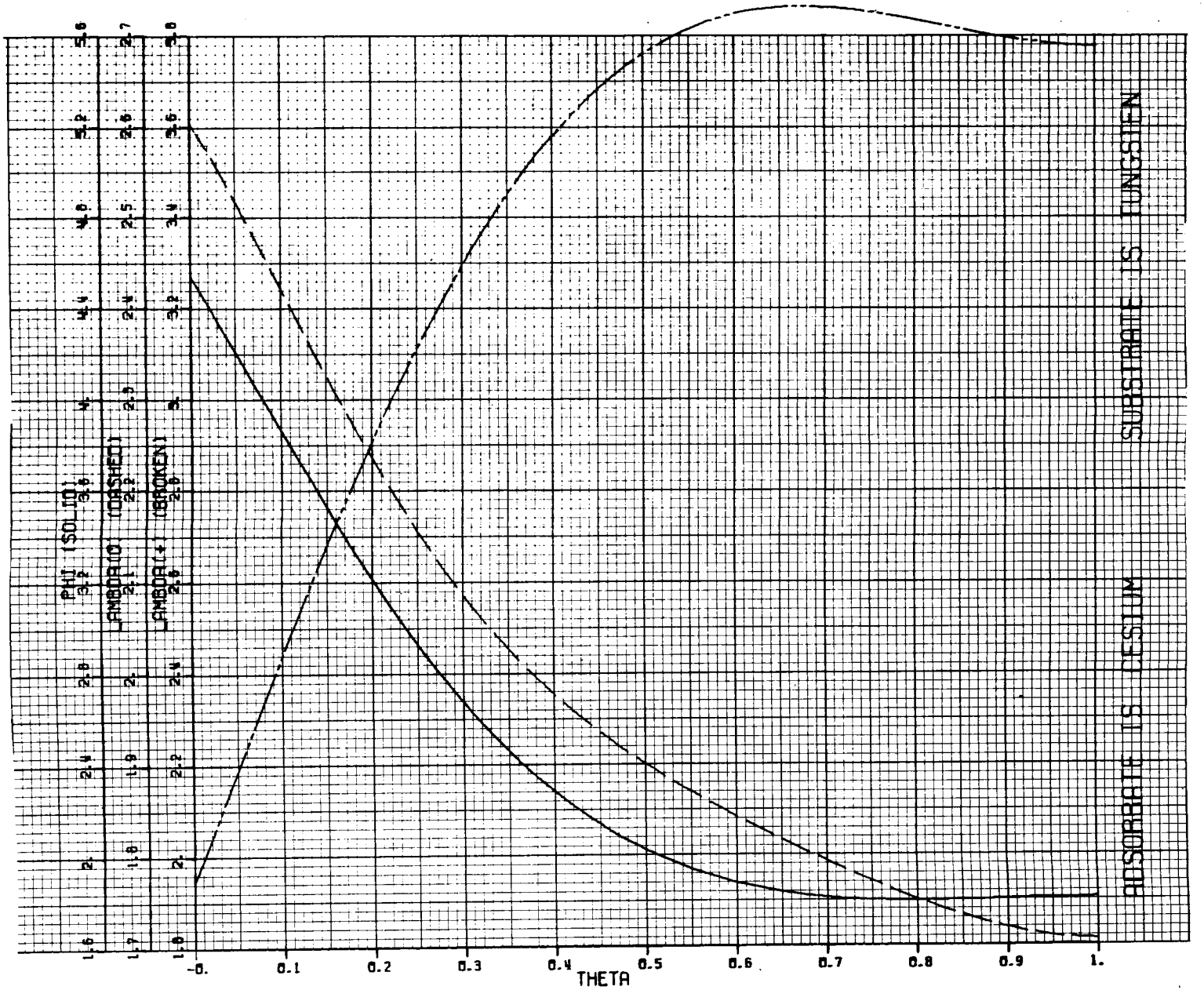

Fig. 74. Composite surface work function as a function of surface coverage for cesium on tungsten.

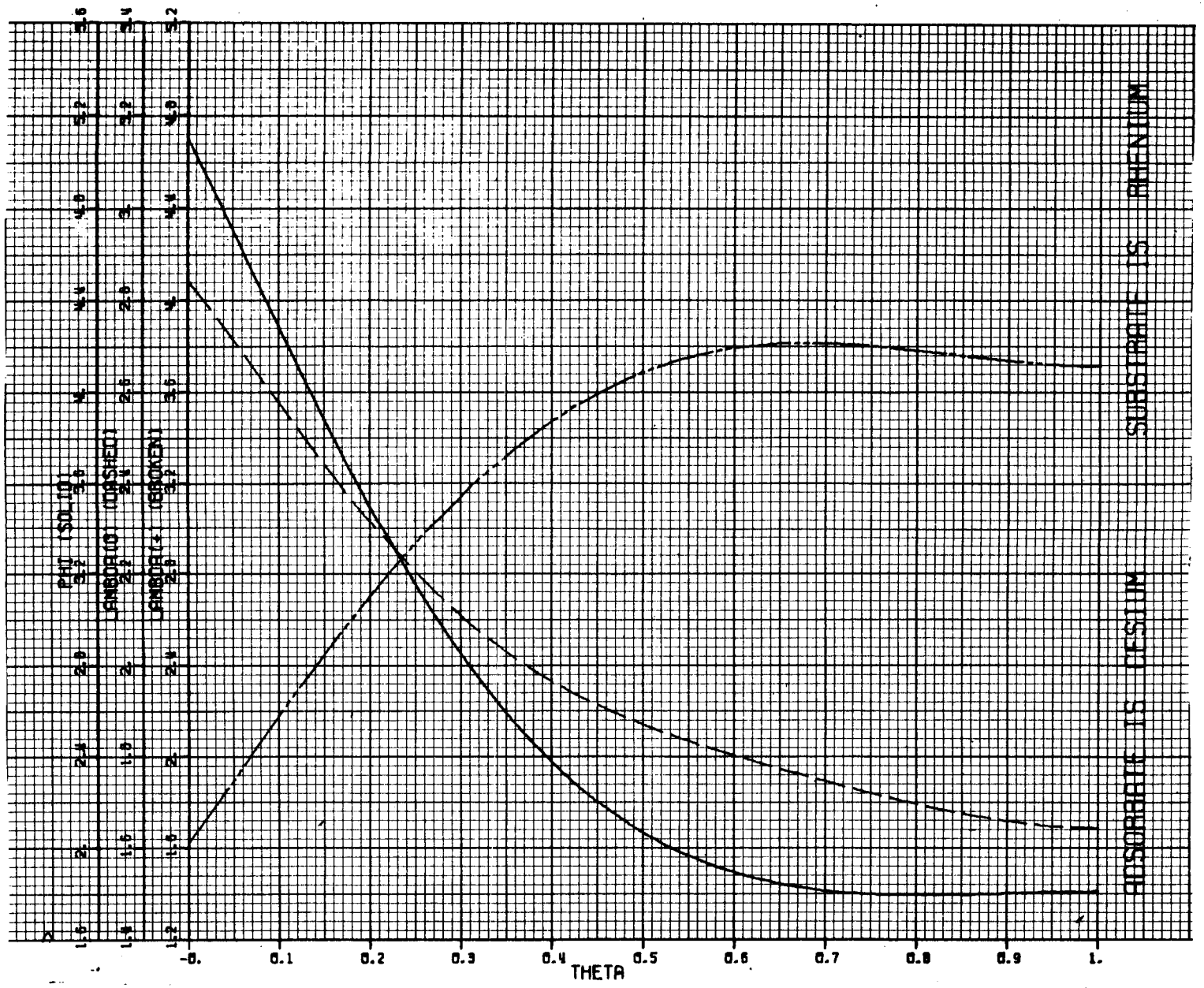

Fig. 75. Composite surface work function as a function of surface coverage for cesium on rhenium.

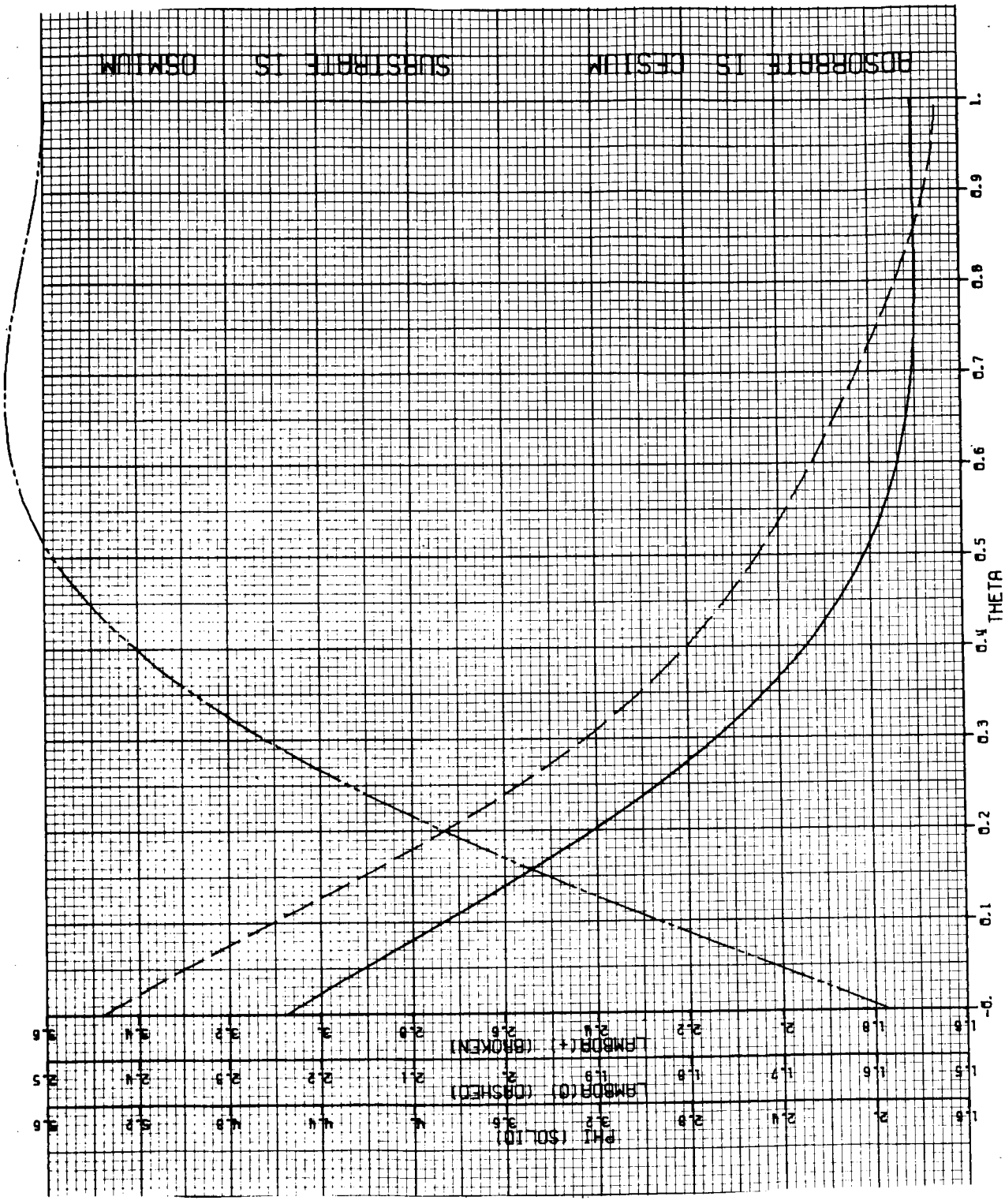

Fig. 76. Composite surface work function as a function of surface coverage for cesium on osmium.

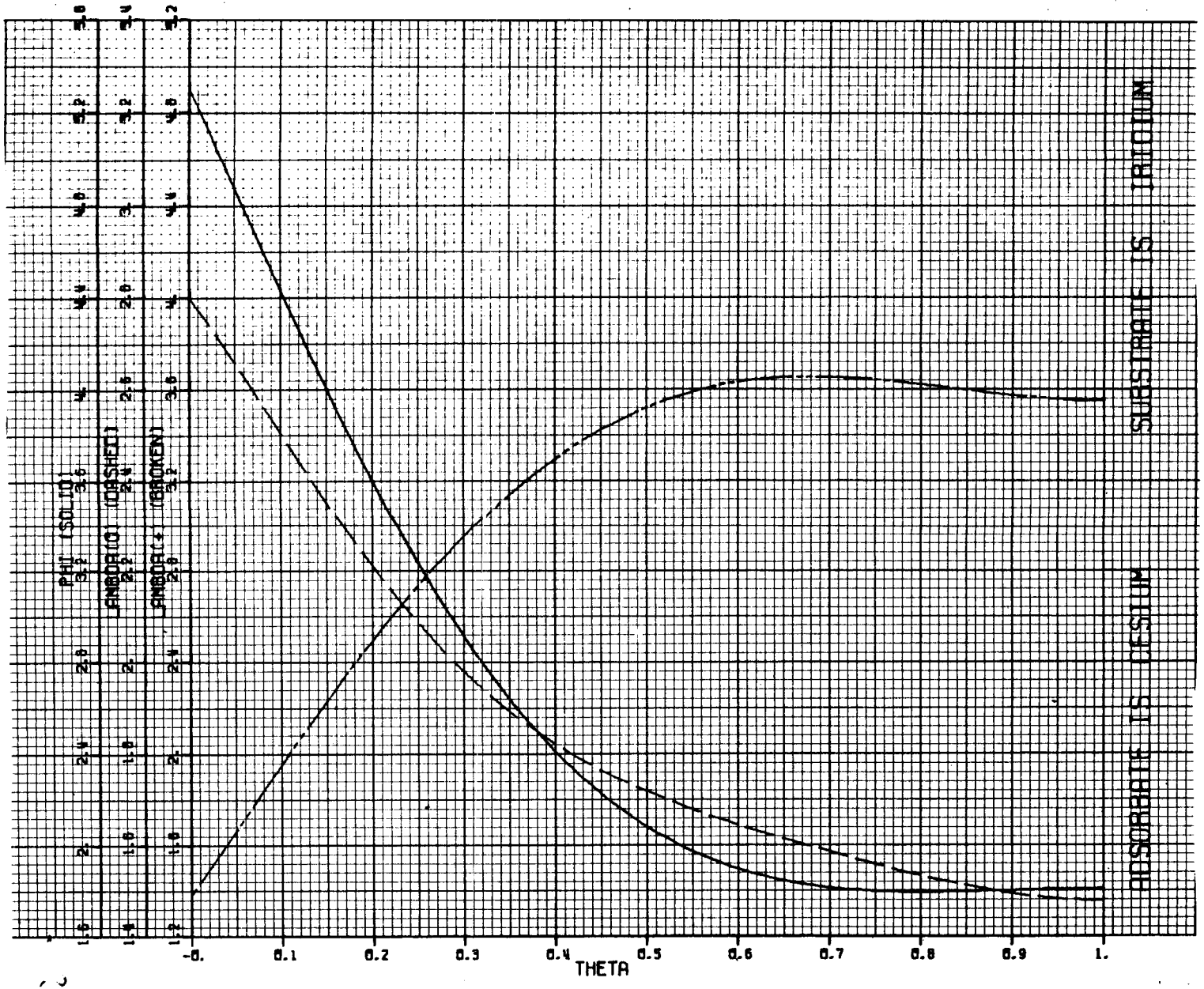

Fig. 77. Composite surface work function as a function of surface coverage for cesium on iridium.

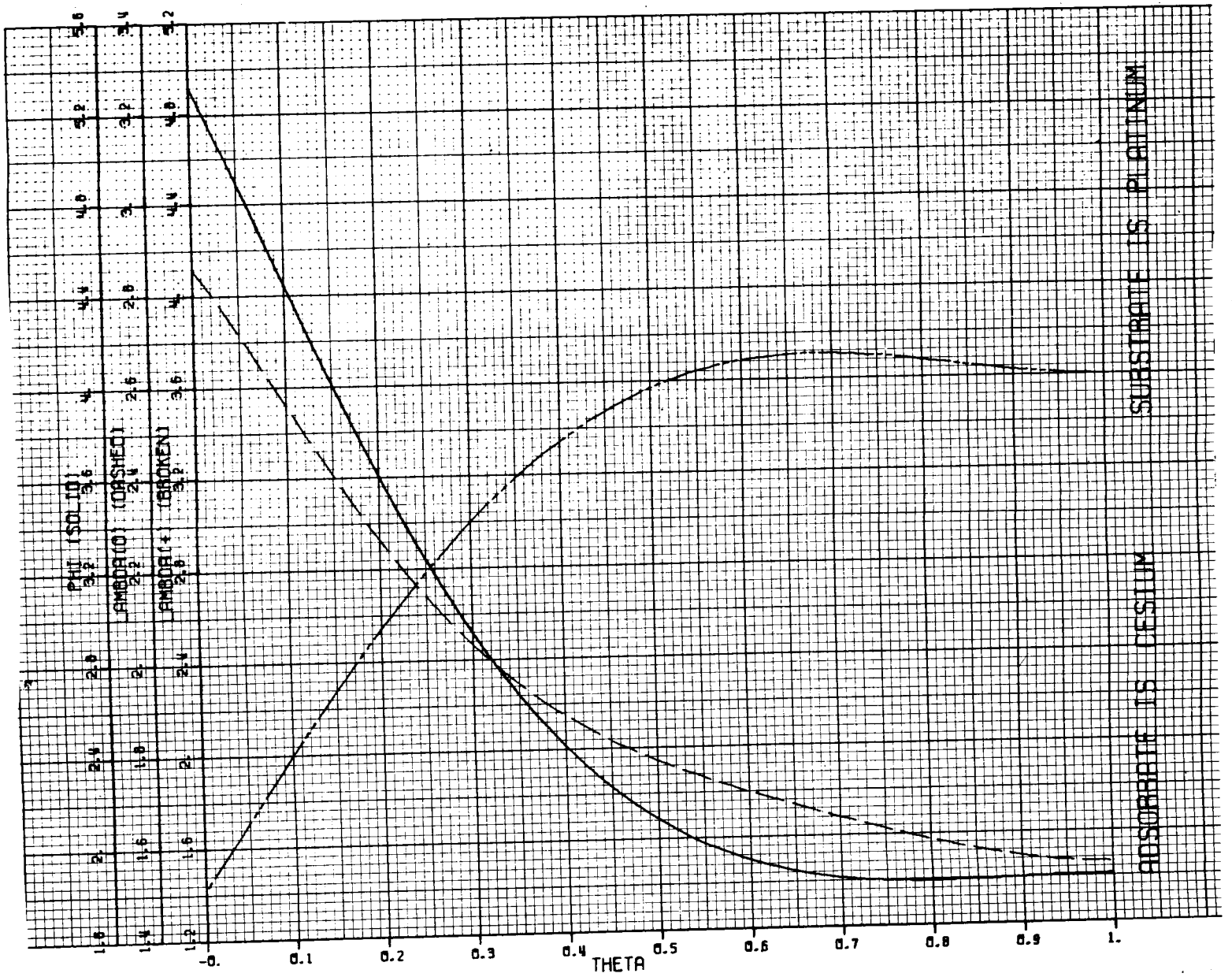

Fig. 78. Composite surface work function as a function of surface coverage for cesium on platinum.

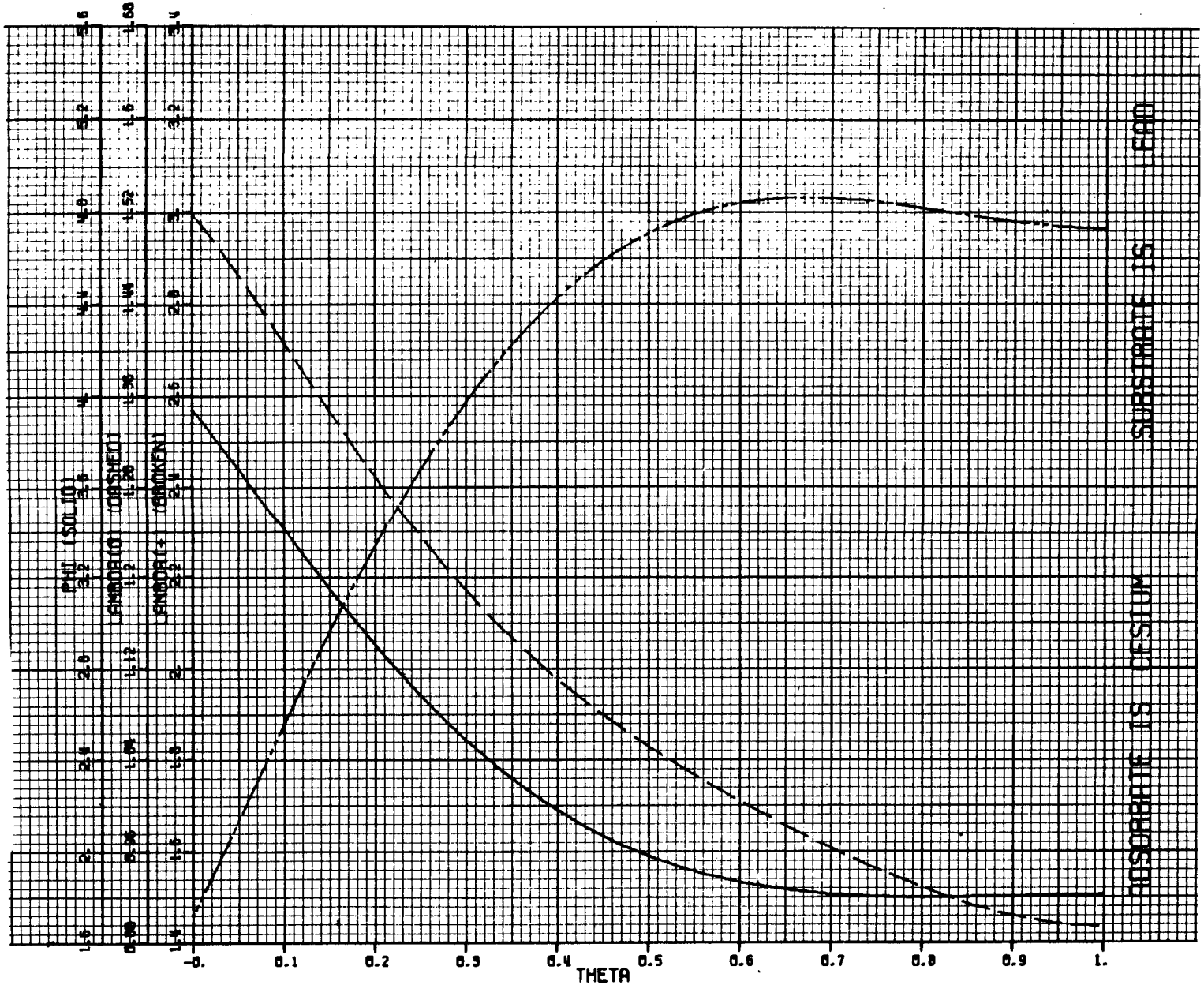

Fig. 79. Composite surface work function as a function of surface coverage for cesium on lead.

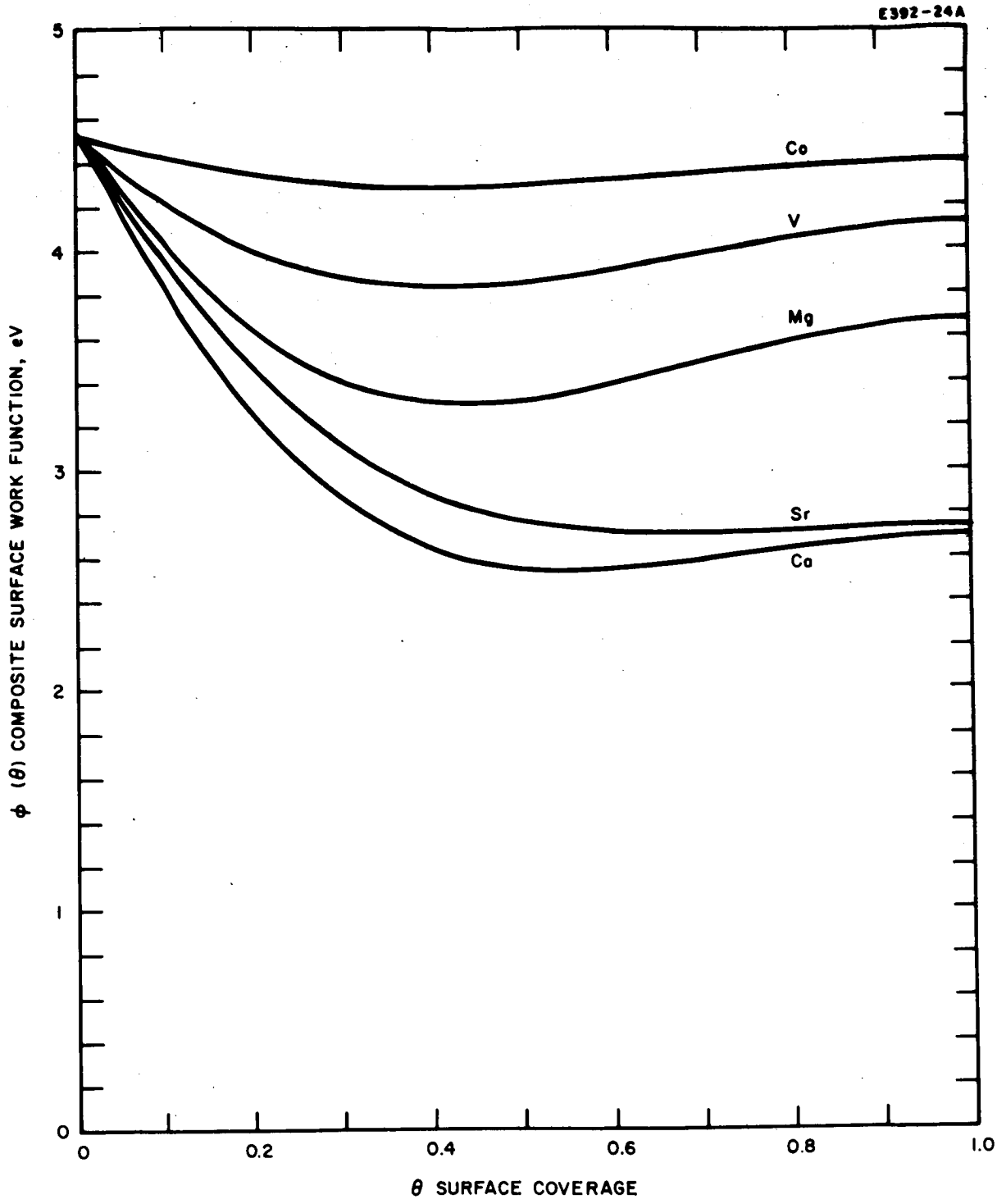

Fig. 80. Computer calculated composite surface work functions versus surface coverage for magnesium, strontium, calcium, cobalt, and vanadium on tungsten.

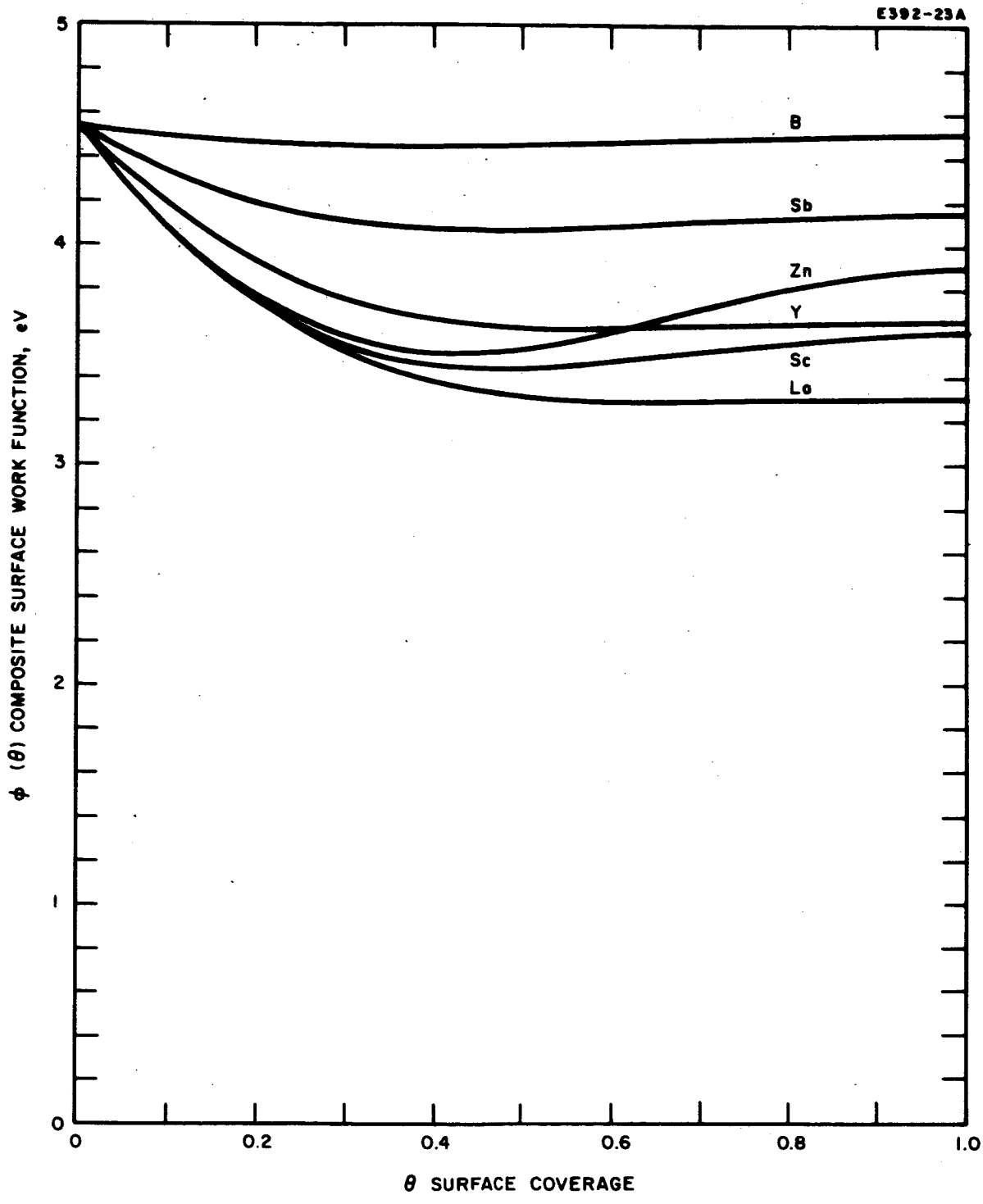

Fig. 81. Computer calculated composite surface work functions versus surface coverage for boron, yttrium, scandium, lanthanum, antimony, and zinc on tungsten.

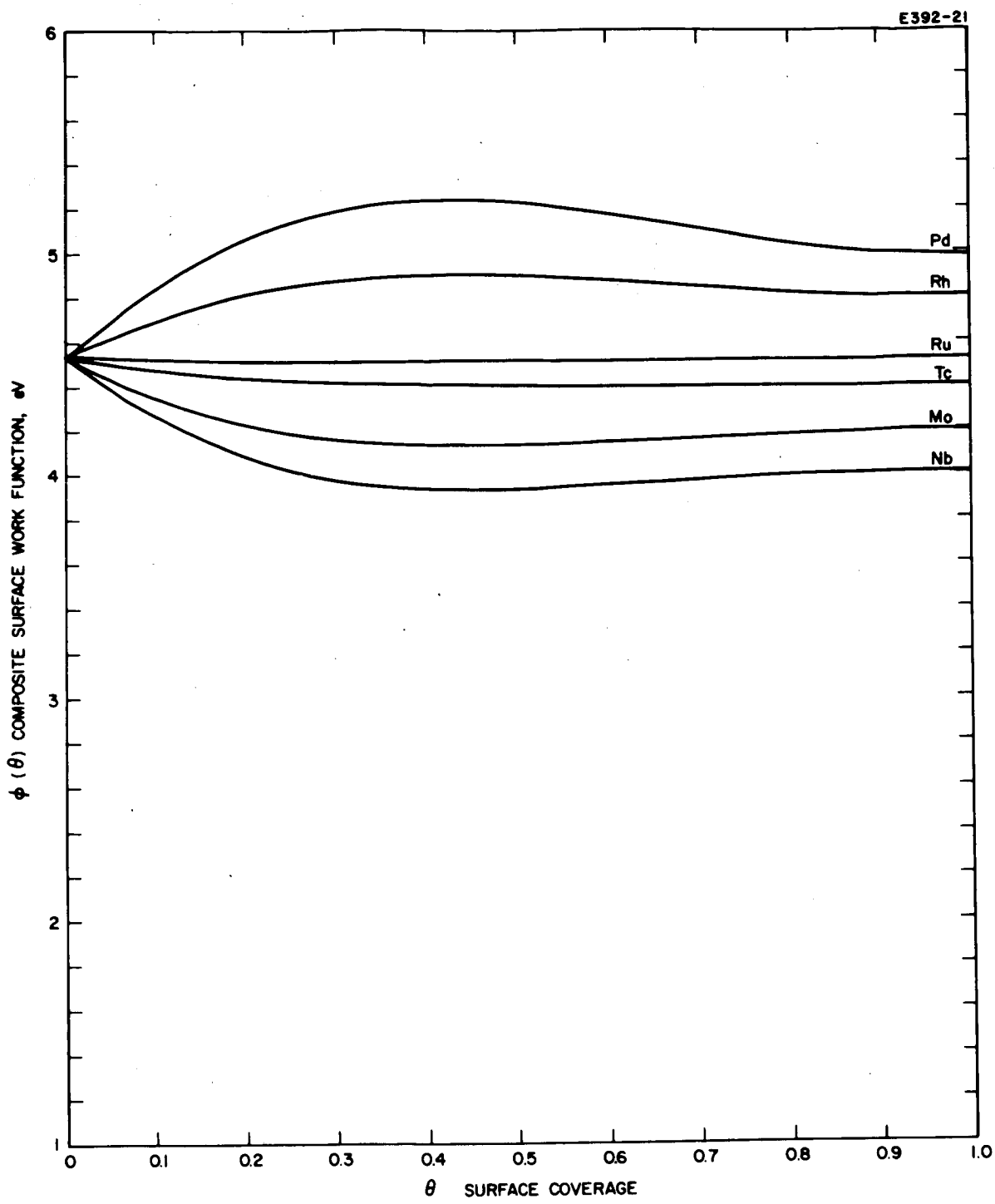

Fig. 82. Computer calculated composite surface work functions versus surface coverage for palladium, rhodium, ruthenium, technetium, molybdenum, and niobium on tungsten.

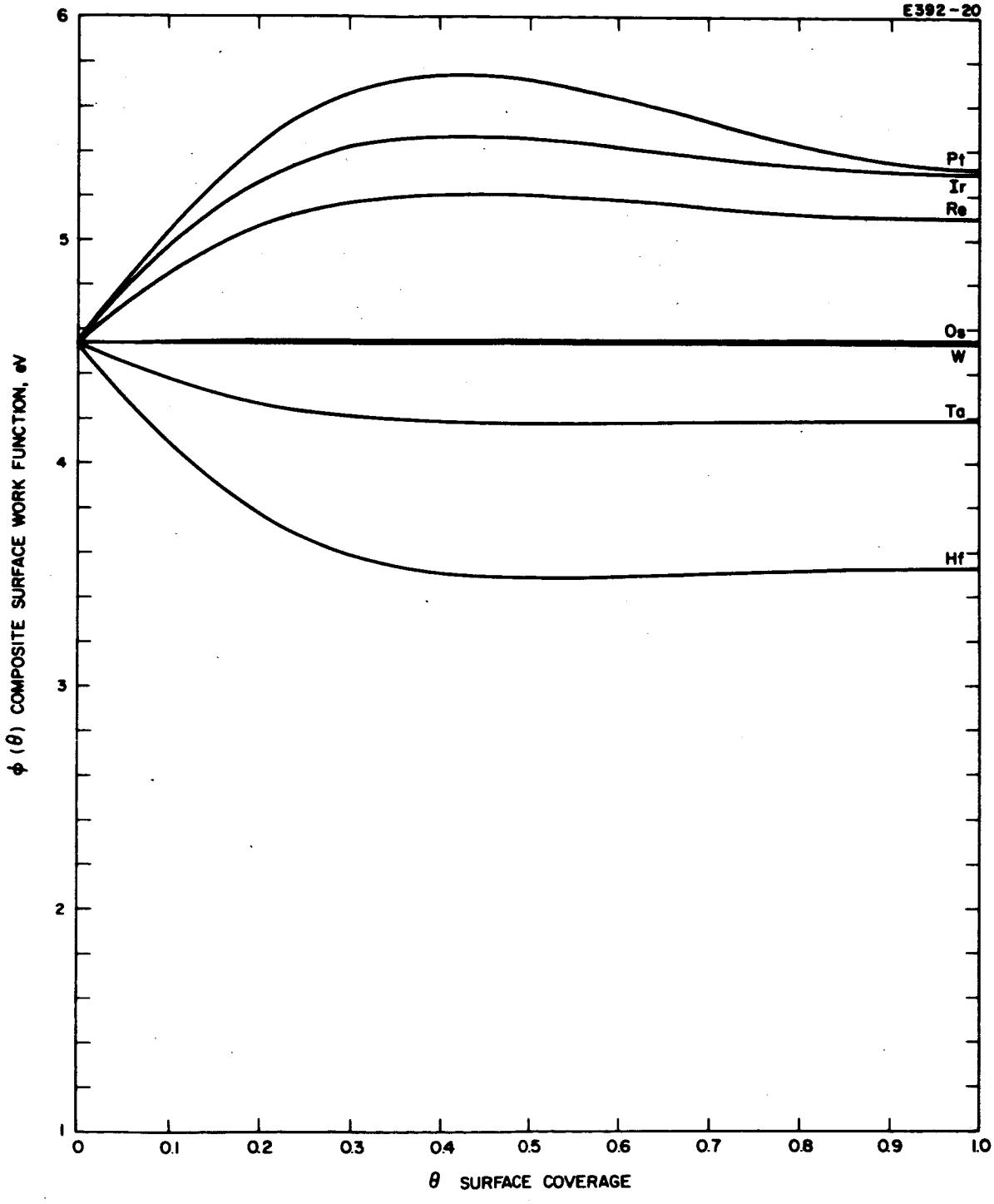

Fig. 83. Computer calculated composite surface work functions versus surface coverage for platinum, iridium, rhenium, osmium, tungsten, tantalum, and hafnium on tungsten.

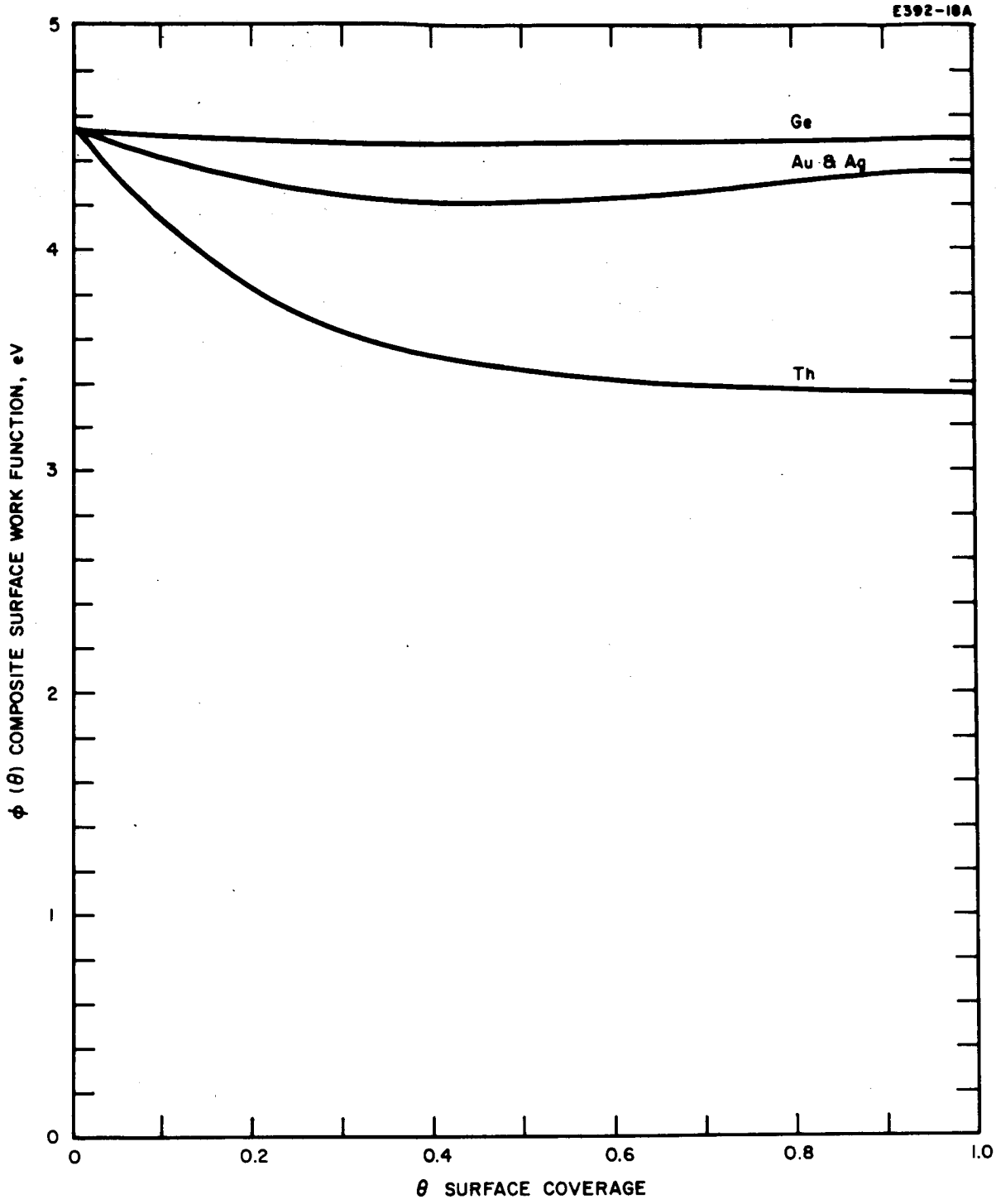

Fig. 84. Computer calculated composite surface work functions versus surface coverage for germanium, silver, gold, and thorium on tungsten.

Also calculated, using a computer program but plotted by hand, were composite surface work functions and corresponding surface coverages as functions of the arrival flux of 27 adsorbates on the same nine substrates listed above. These calculations were made using a small coverage approximation. The results are accurate only to about 0.05 of a monolayer of surface coverage, which is probably too large a coverage to be tolerated in a cesium ion thrustor. These curves are plotted to $\theta = 0.1$ in Figs. 85 through 93. The calculations and curves cover the range of arrival flux from 10^8 to 10^{21} atoms/cm^2-sec. These calculations assume only natural atom evaporation (no extracted ion currents) in the determination of the adsorption-desorption equilibrium. The 27 adsorbates are lithium, beryllium, carbon, sodium, aluminum, silicon, potassium, calcium, titanium, chromium, manganese, iron, nickel, copper, zinc, gallium, rubidium, strontium, silver, cadmium, indium, tin, cesium, barium, lanthanum, mercury, and lead.

To show more clearly the variations among the nine substrates, three particular adsorbates with a wide range of work functions — beryllium (3.7 eV), copper (4.4 eV), and nickel (5.0 eV, which has since been shown to be about 4.86 eV) — were selected, and the composite surface work function versus arrival flux curves for the nine substrates have been plotted on separate graphs (Figs. 94 through 96). As before, these curves are for the small coverage approximation, and are plotted to $\theta = 0.1$. To show the influence of surface temperature, composite surface work function versus arrival flux curves for four adsorbates (aluminum, copper, iron, and nickel) on tungsten are plotted in Fig. 97 for surface temperatures of 1300, 1400, 1500, and 1600K. These curves are also for the small coverage approximation.

A computer program was formulated for composite surface work function versus adsorbate arrival flux for several adsorbate metals on tungsten with the full θ dependence rather than with the small surface coverage approximations. Such calculations involve lengthy iterative processes to some chosen degree of accuracy, but result in full curves

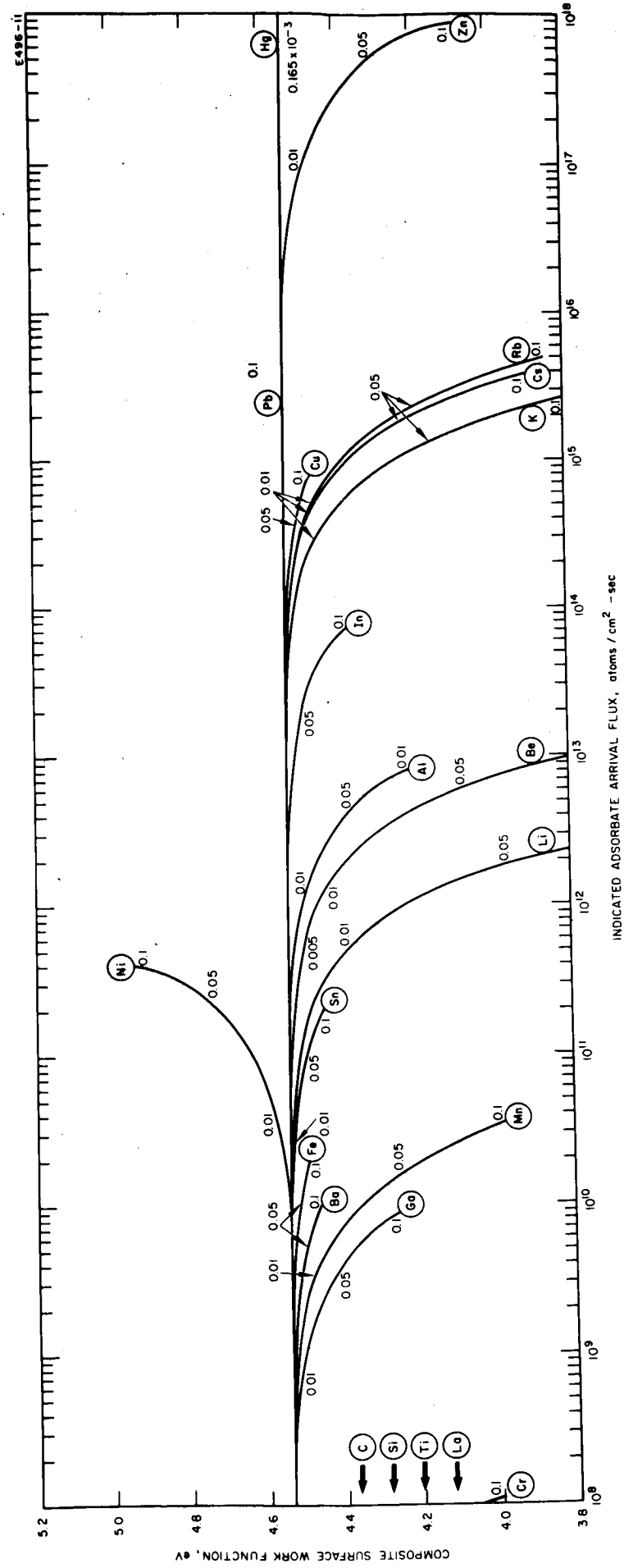

Fig. 85. Composite surface work function versus arrival flux for 22 adsorbate atoms on tungsten. The numbers along the curves are the values of the coverage.

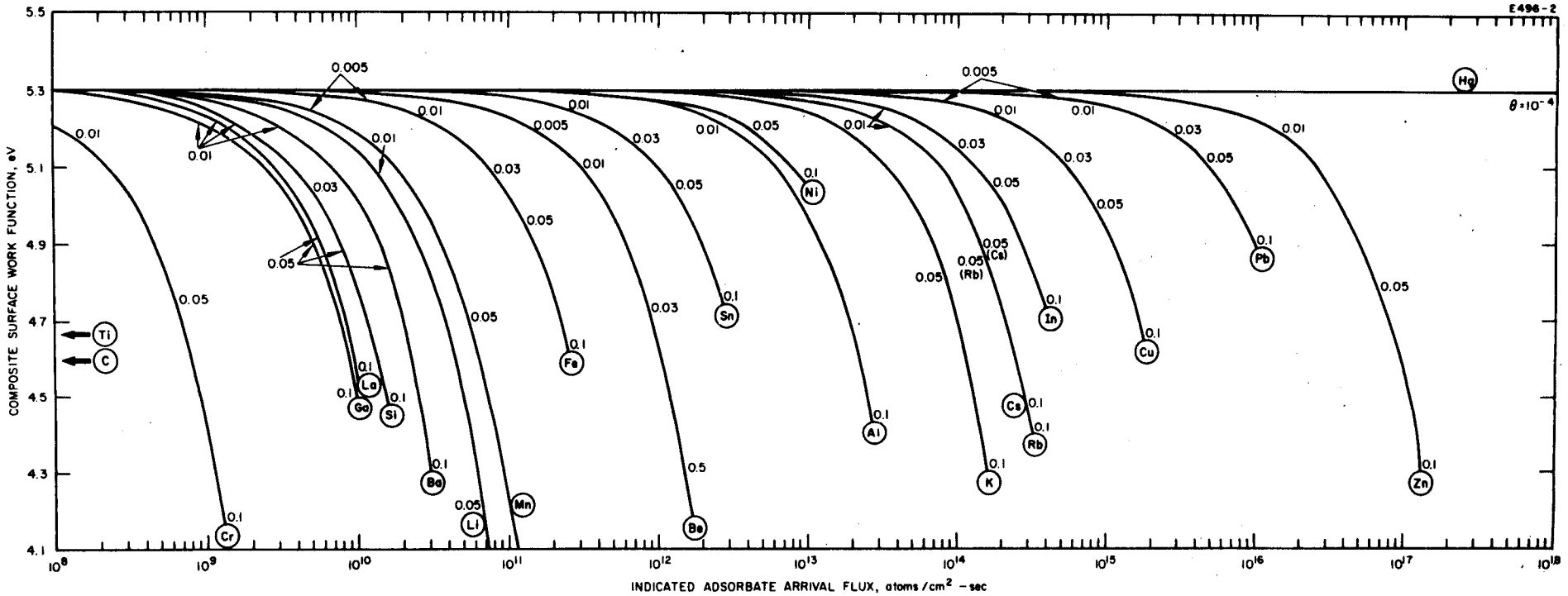

Fig. 86. Composite surface work function versus arrival flux for 22 adsorbate atoms on iridium. The numbers along the curves are the values of the coverage.

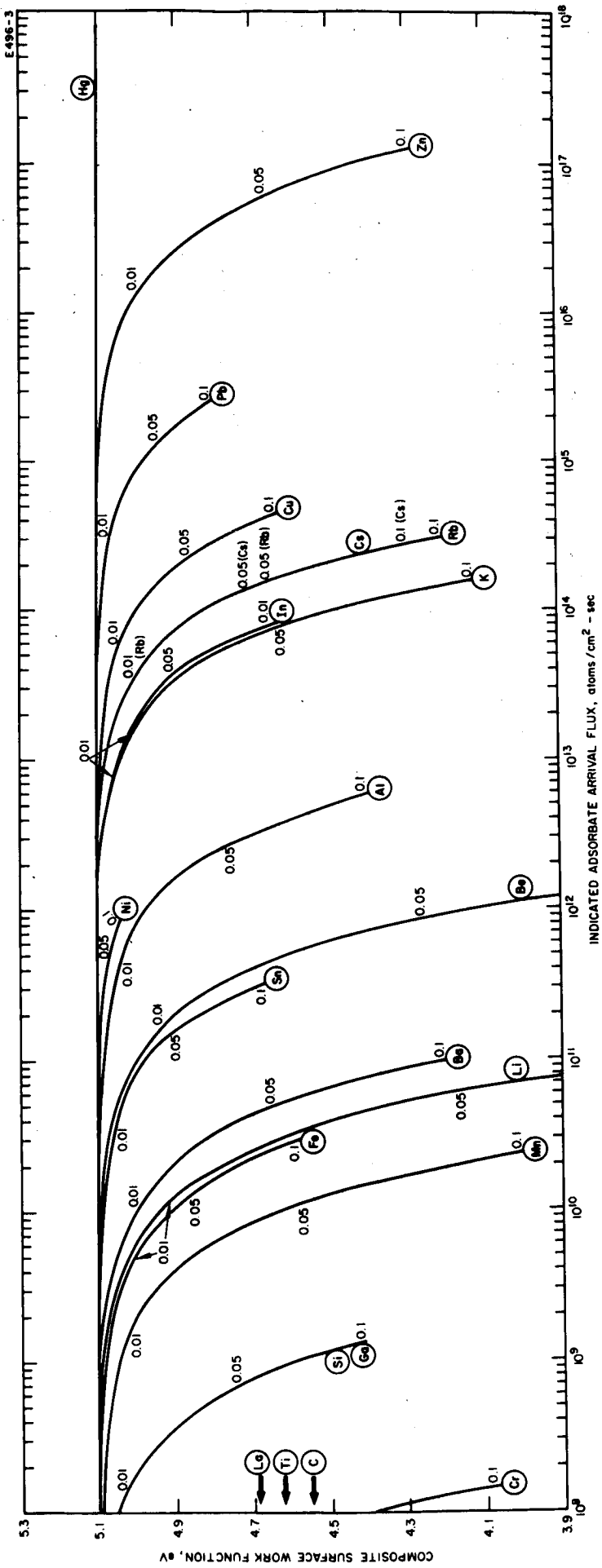

Fig. 87. Composite surface work function versus arrival flux for 22 adsorbate atoms on rhenium. The numbers along the curves are the values of the coverage.

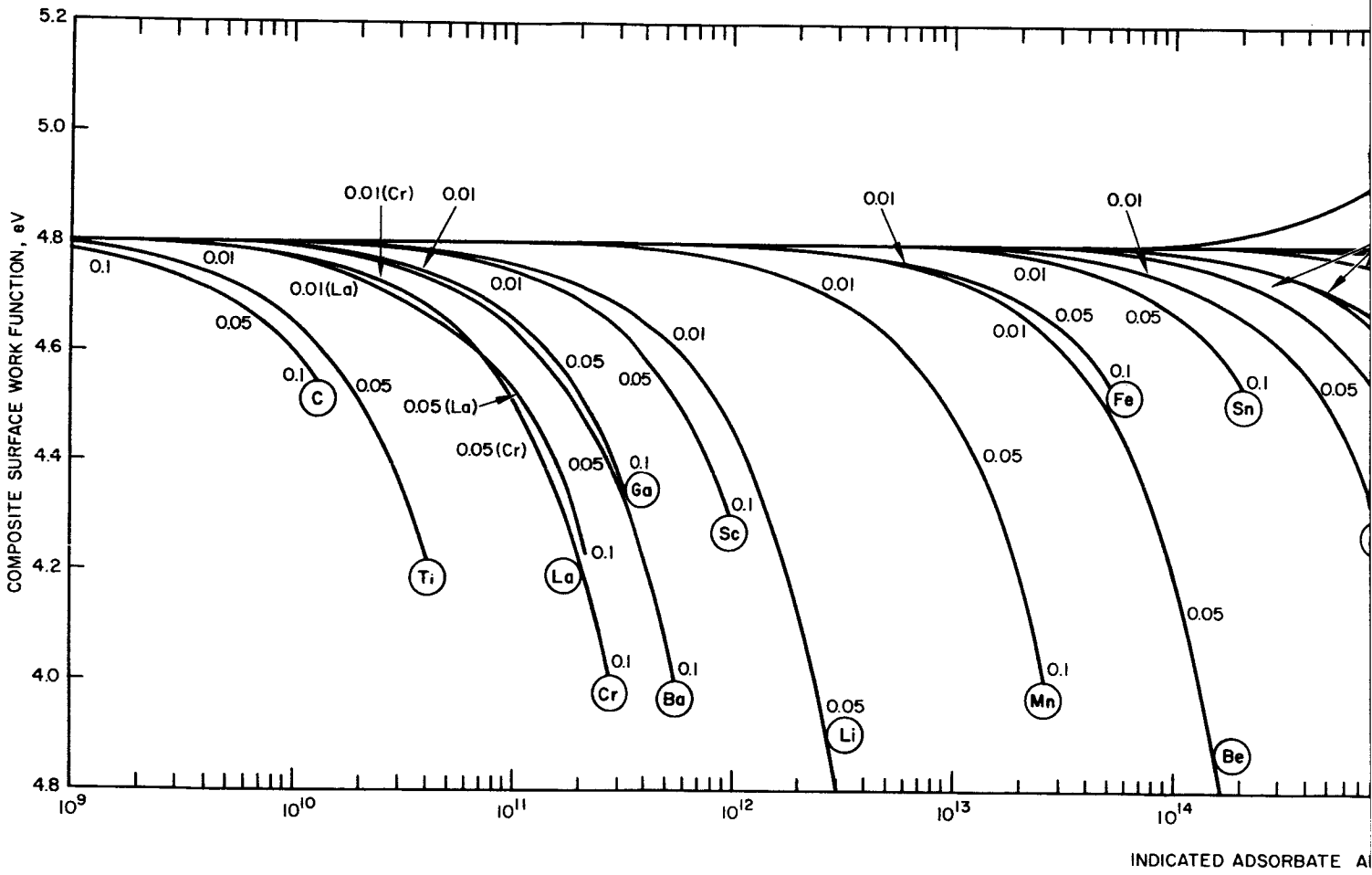
COMPOSITE SURFACE WORK FUNCTION, eV
5.2
5.0
4.8
4.6
4.4
4.2
4.0
4.8
10^9
10^{10}
10^{11}
10^{12}
10^{13}
10^{14}
INDICATED ADSORBATE A
0.01(Cr)
0.01
0.01(La)
0.05(La)
0.05(Cr)
0.1
0.05
C
Ti
La
Cr
Ga
Ba
Sc
Li
Mn
Fe
Be
Sn

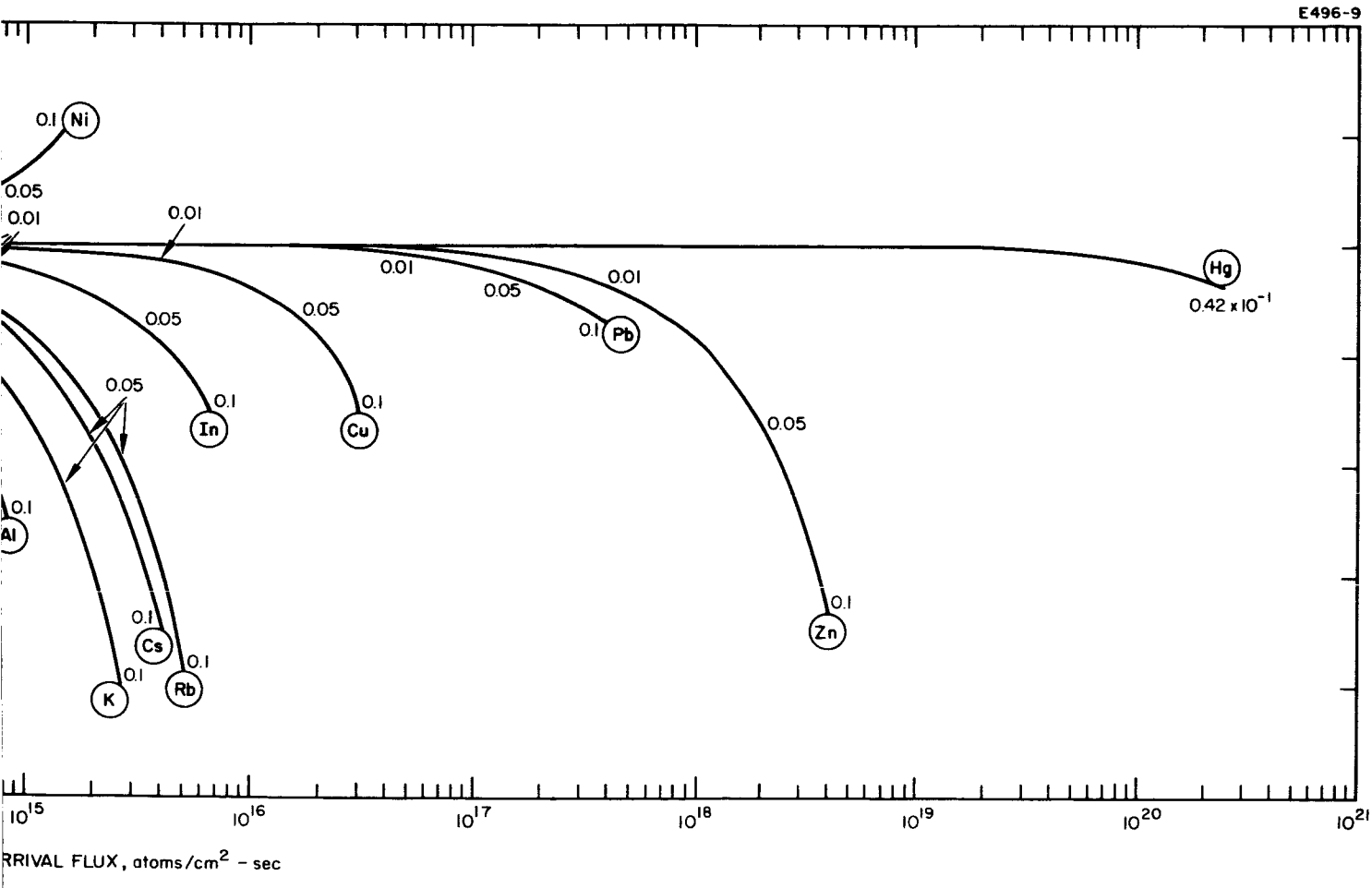

Fig. 88. Composite surface work function versus arrival flux for 22 adsorbate atoms on rhodium. The numbers along the curves are the values of the coverage.

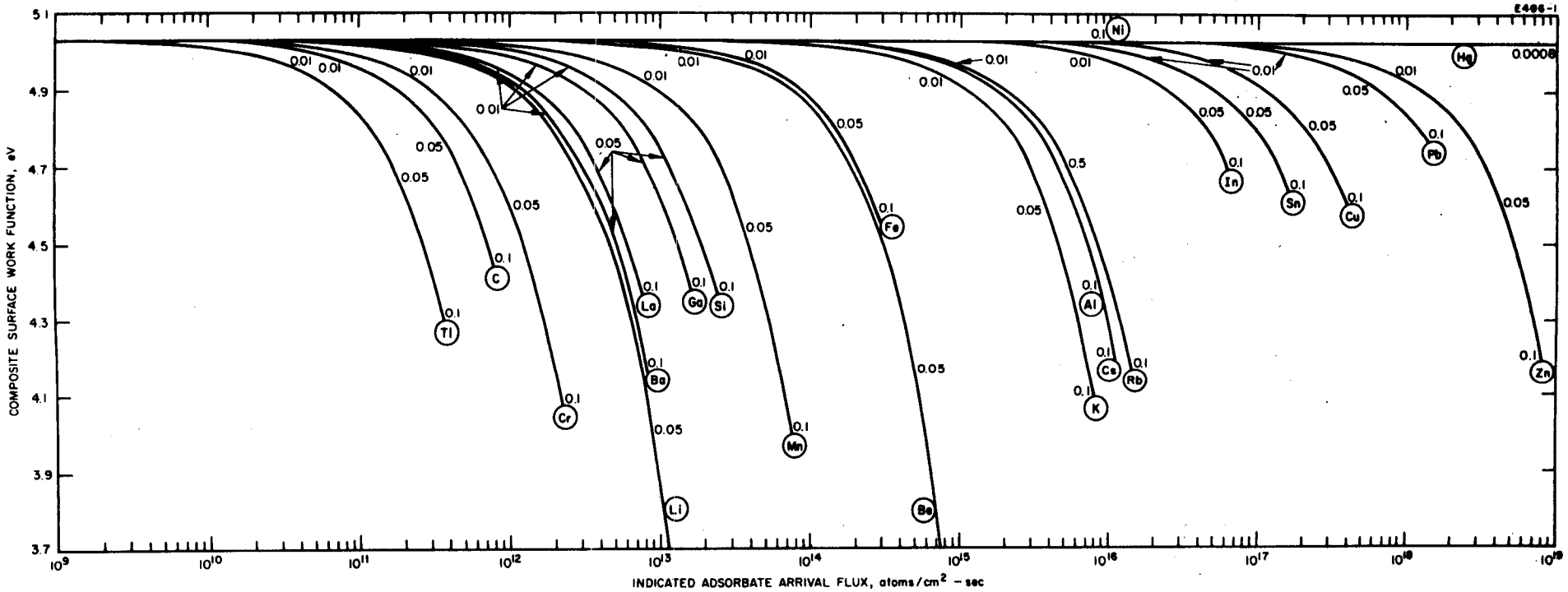

Fig. 89. Composite surface work function versus arrival flux for 22 adsorbate atoms on nickel. The numbers along the curves are the values of the coverage.

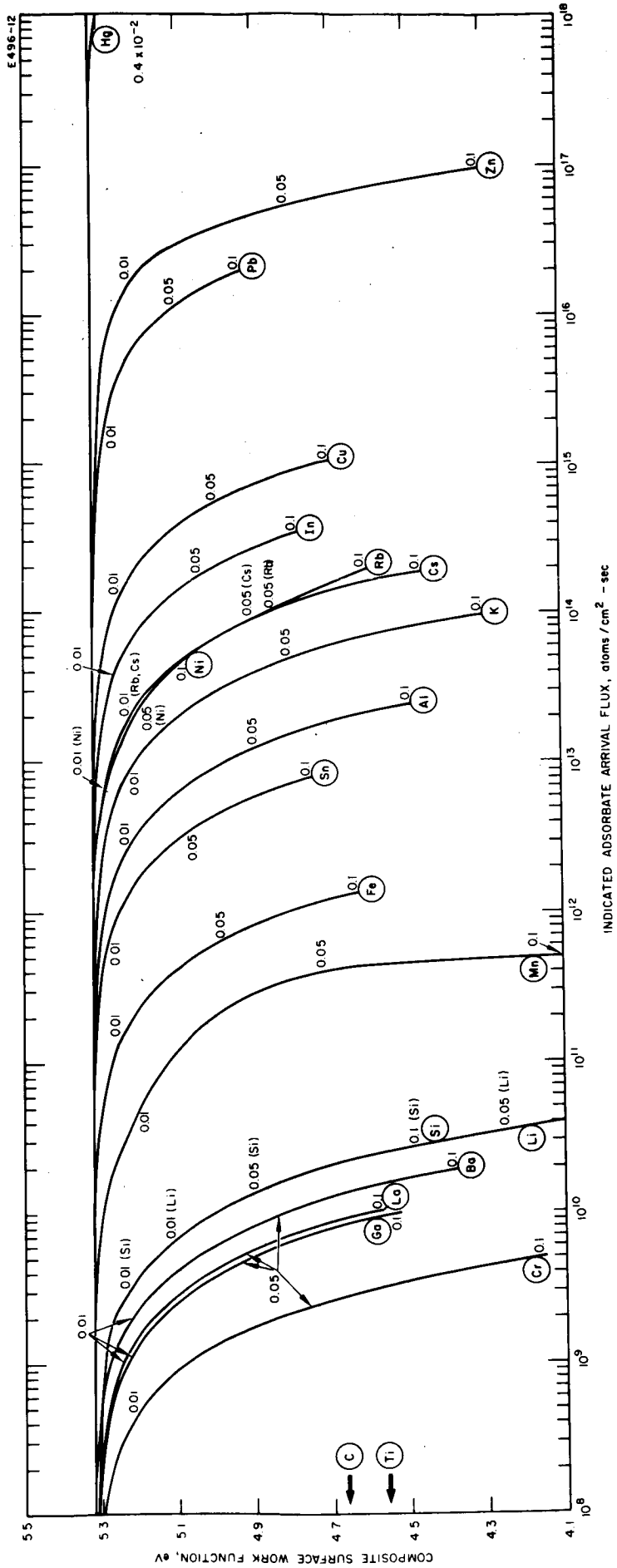

Fig. 90. Composite surface work function versus arrival flux for 22 adsorbate atoms on platinum. The numbers along the curves are the values of the coverage.

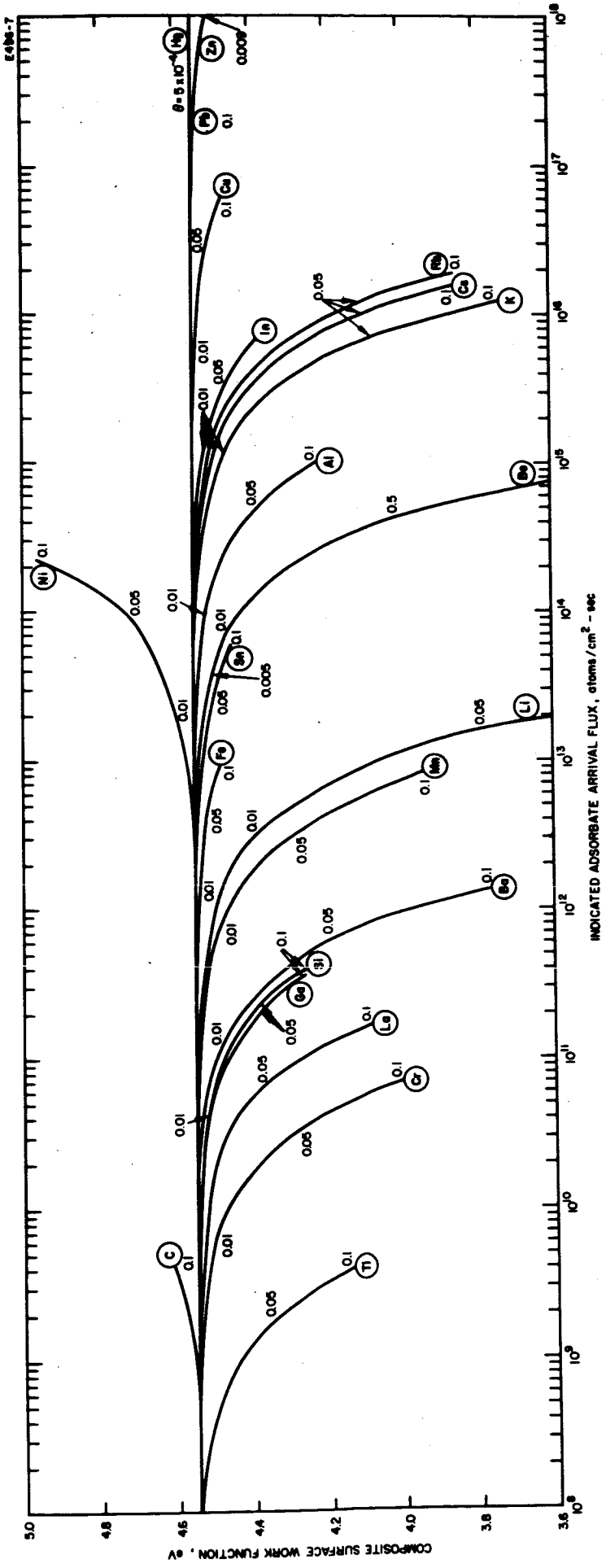

Fig. 91. Composite surface work function versus arrival flux for 22 adsorbate atoms on osmium. The numbers along the curves are the values of the coverage.

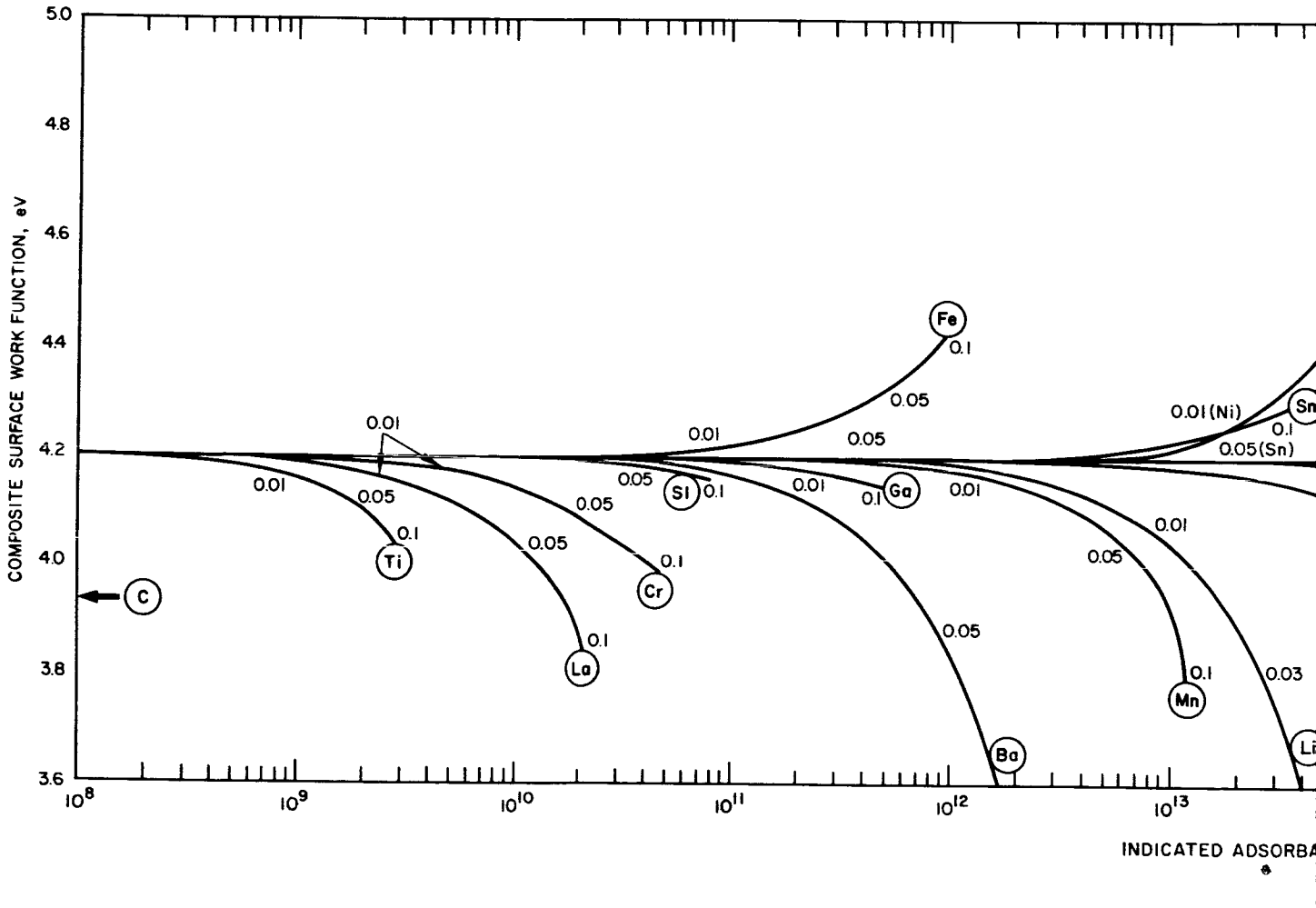
COMPOSITE SURFACE WORK FUNCTION, eV
5.0
4.8
4.6
4.4
4.2
4.0
3.8
3.6
10^8
10^9
10^{10}
10^{11}
10^{12}
10^{13}
INDICATED ADSORBA
C
Ti
La
Cr
Si
Ga
Fe
Ba
Mn
Sn
Li
0.01
0.05
0.1
0.01(Ni)
0.05(Sn)
0.03

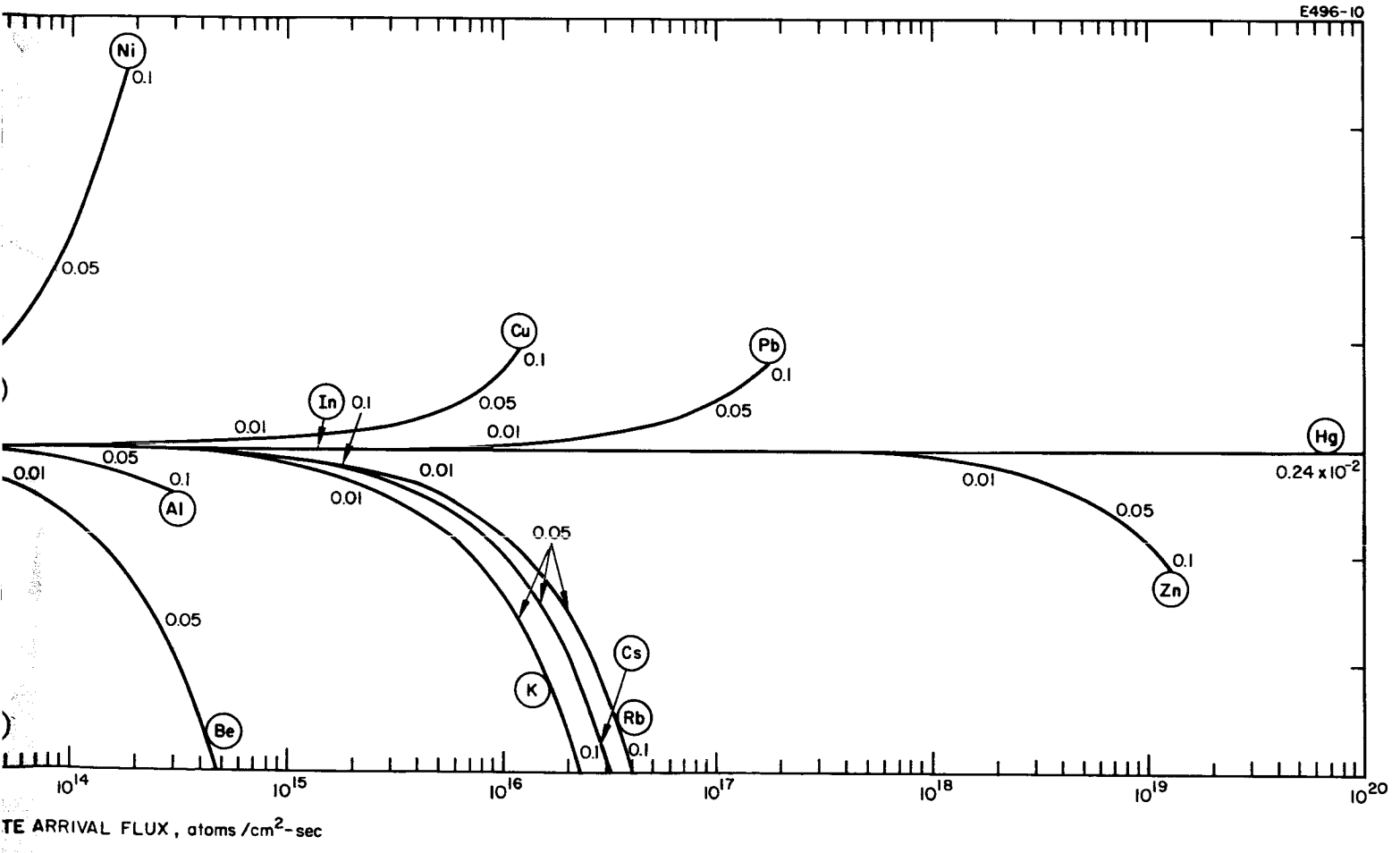

Fig. 92. Composite surface work function versus arrival flux for 22 adsorbate atoms on molybdenum. The numbers along the curves are the values of the coverage.

174 (2)

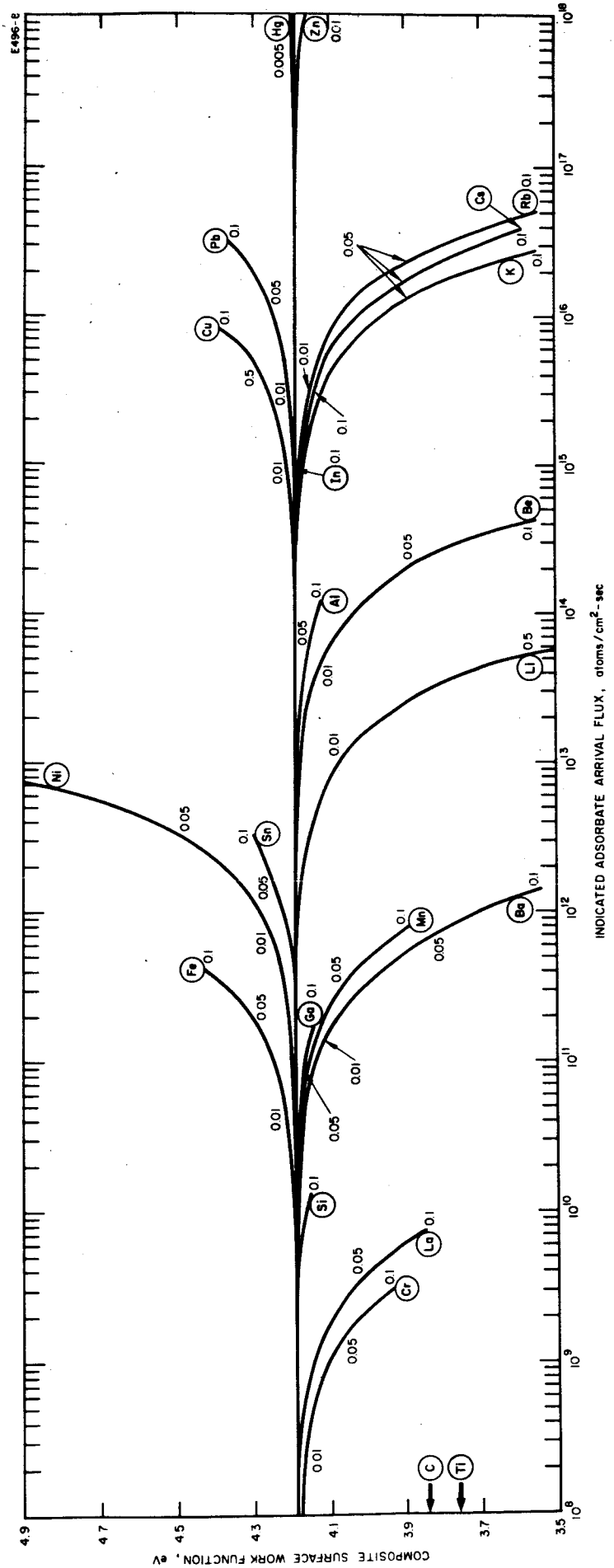

Fig. 93. Composite surface work function versus arrival flux for 22 adsorbate atoms on tantalum. The numbers along the curves are the values of the coverage.

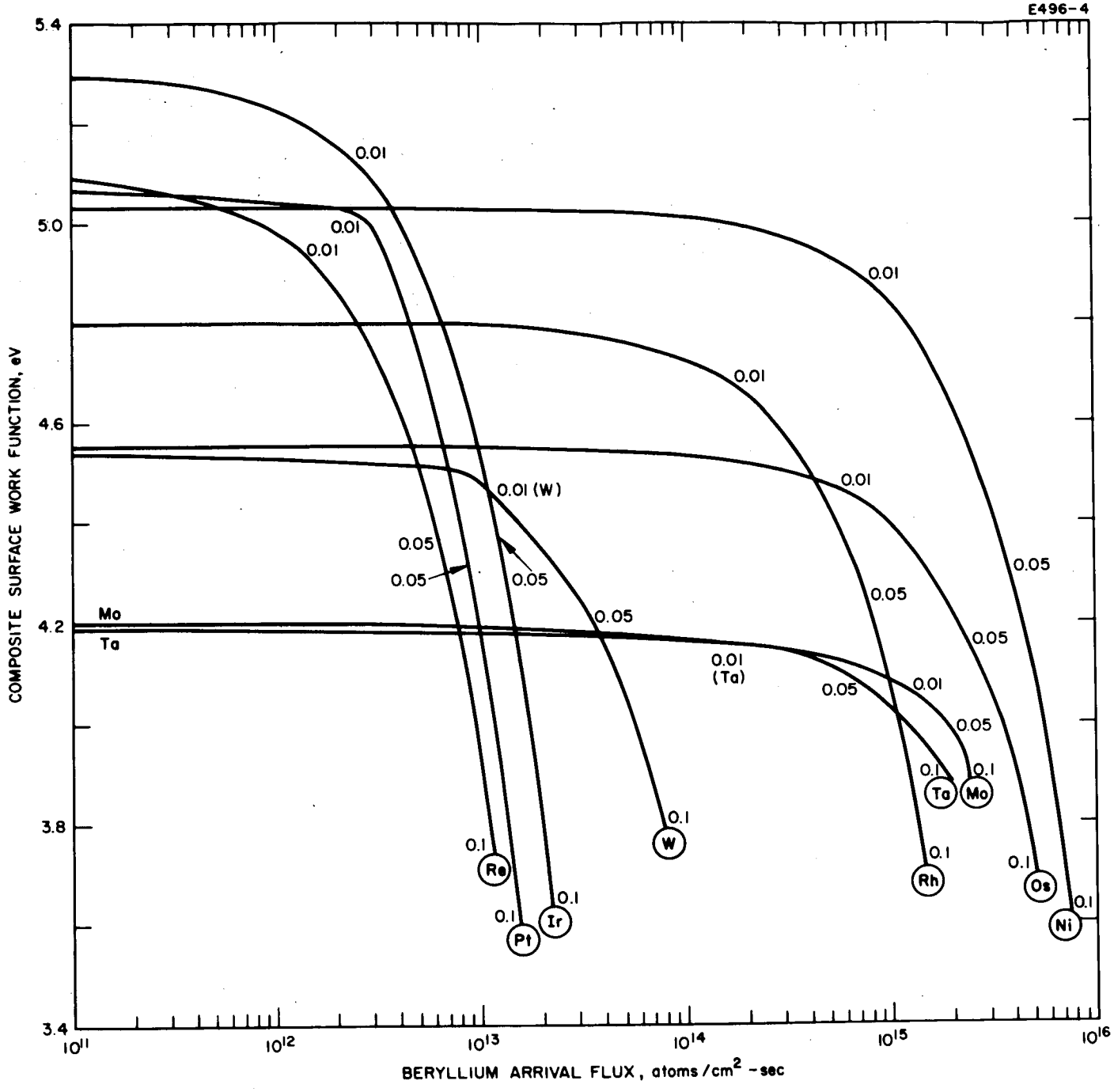

Fig. 94. Composite surface work function versus arrival flux for beryllium on nine substrate surfaces. The numbers along the curves are the values of the coverage.

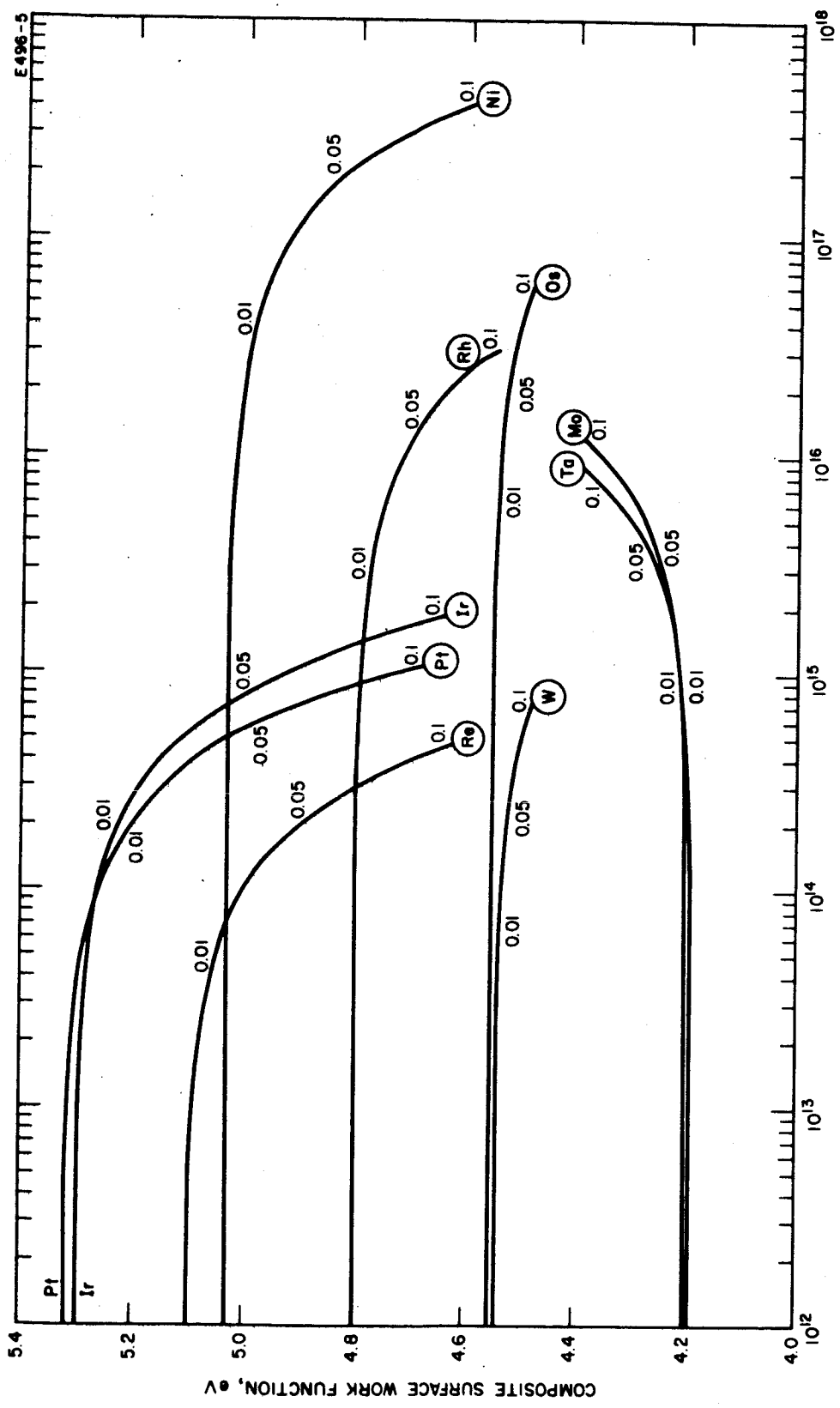

Fig. 95. Composite surface work function versus arrival flux for copper on nine substrate surfaces. The numbers along the curves are the values of the coverage.

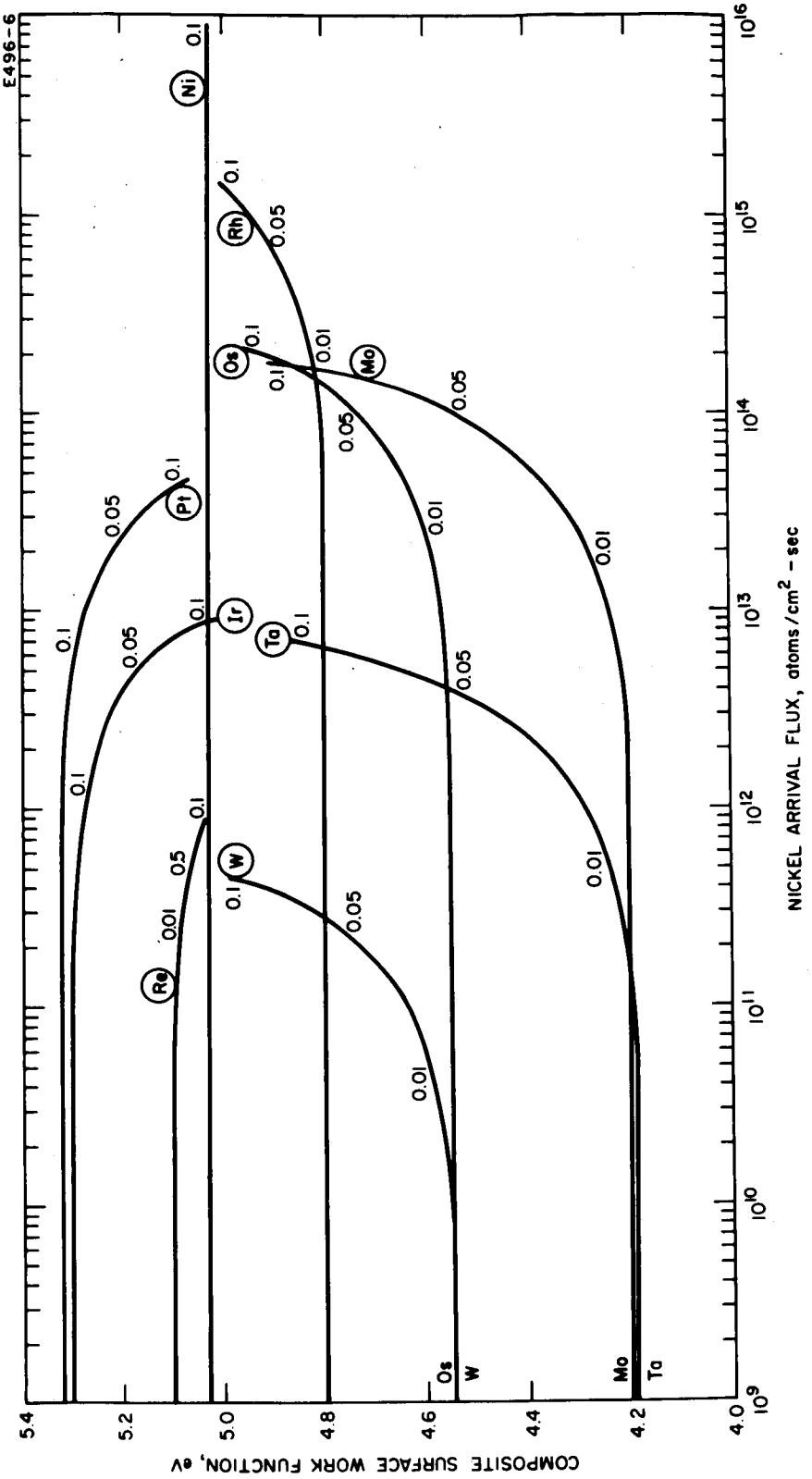

Fig. 96. Composite surface work function versus arrival flux for nickel on nine substrate surfaces. The numbers along the curves are the values of the coverage.

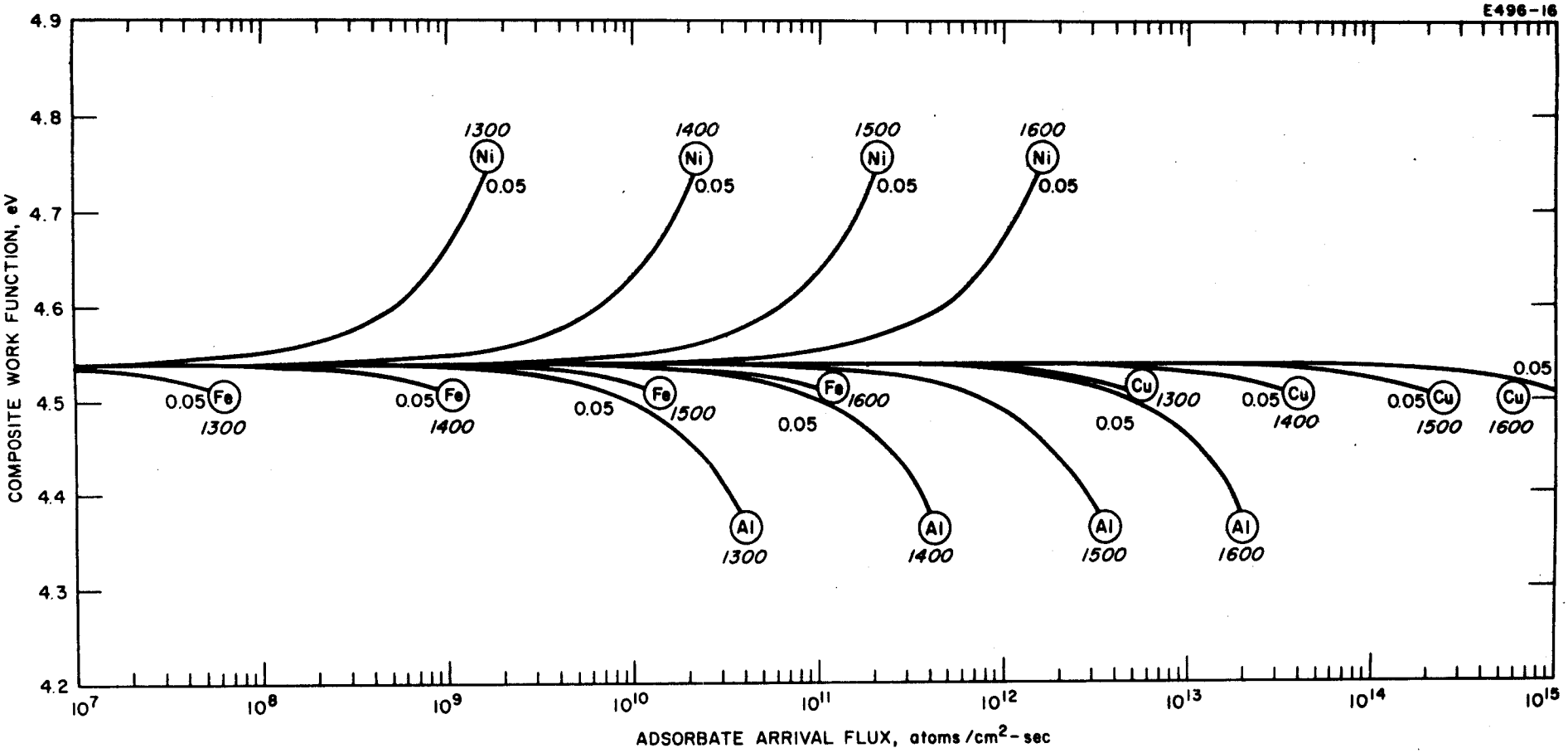

Fig. 97. Composite surface work function versus arrival flux for adsorbate atoms of aluminum, iron, copper, and nickel on tungsten surface at four surface temperatures: 1300, 1400, 1500, and 1600 K.

of $\phi[\theta(\mu)]$ versus μ. Calculations of this type were run for each of five adsorbates on each of three substrates throughout the arrival flux range from 10^8 to 10^{21} atoms/cm^2-sec. These curves are included as Figs. 98 through 100. The five adsorbates are beryllium, aluminum, iron, nickel, and copper, and the three substrates are tungsten, rhenium, and iridium. More curves of this type were not calculated because the iterations required by the fact that the expression for θ (eq. (2)) involves functions of θ itself, require long, expensive computer computation times. The existing computer programs can easily be used for other adsorbate-substrate combinations in the future.

D. ATOM AND ION DESORPTION ENERGIES

The expression for the ion desorption energy

$$\lambda_+(\theta) = \lambda_o(\theta) + V_i(1) - \phi(\theta) \tag{16}$$

derived from application of the Born-Haber energy cycle is commonly used when $\lambda_o(\theta)$ can be obtained by explicit calculation. It should be realized that in this expression the surface ionization potential V_s, which occurs in the energy cycle, is implicit within $\lambda_o(\theta)$. This expression is used herein because $\lambda_o(\theta)$ and $\phi(\theta)$ are calculated explicitly.

The explicit expression for $\lambda_o(\theta)$ is written with the aid of Ref. 2.

$$\lambda_o(\theta) = \underbrace{F(\theta)\,\phi\,(\theta)\,[1 + \delta(\theta)]}_{\text{ionic part}} + \underbrace{[H_s(0)H_s(1)]^{1/2}\left[\frac{2}{\frac{S(0)}{S(1)} + \frac{S(1)}{S(0)}}\right]\left[1 - \frac{F^2(\theta)}{v^2}\right]^{1/2}}_{\text{covalent part}} \tag{17}$$

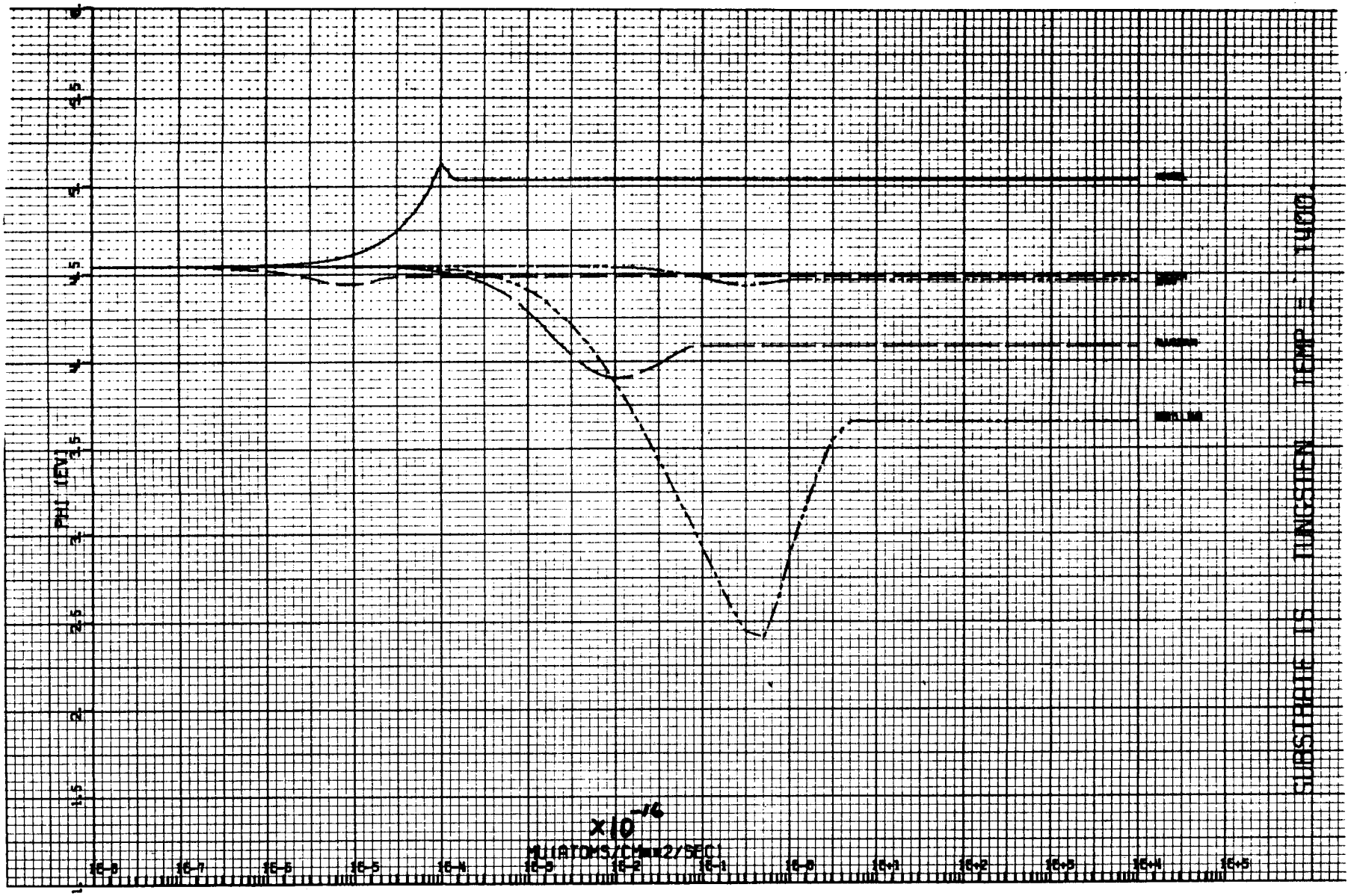

Fig. 98. Composite surface work function versus arrival flux for the five adsorbate atoms beryllium, aluminum, iron, nickel, and copper on a tungsten surface (no surface coverage limitation).

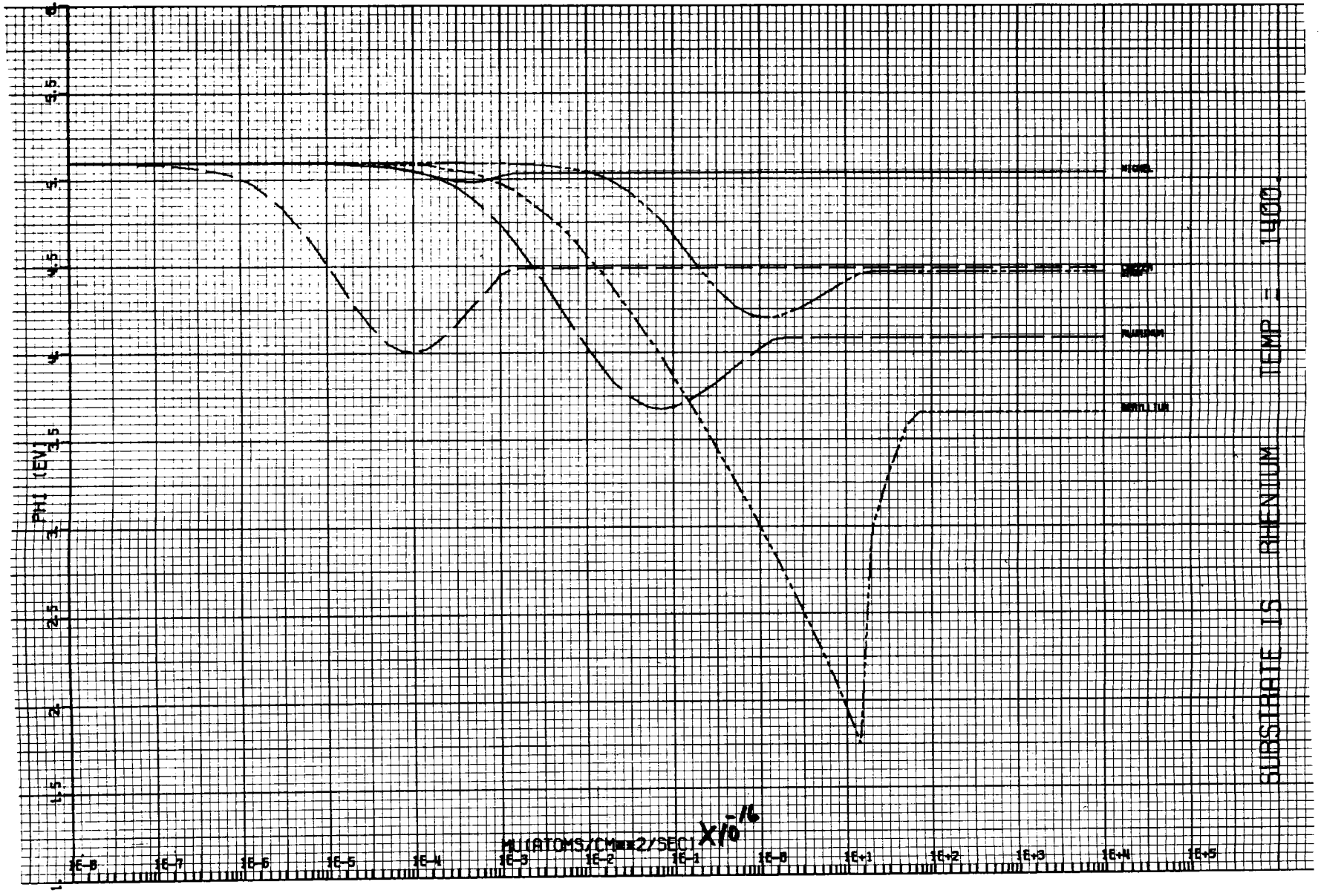

Fig. 99. Composite surface work function versus arrival flux for the five adsorbate atoms beryllium, aluminum, iron, nickel, and copper on a rhenium surface (no surface coverage limitation).

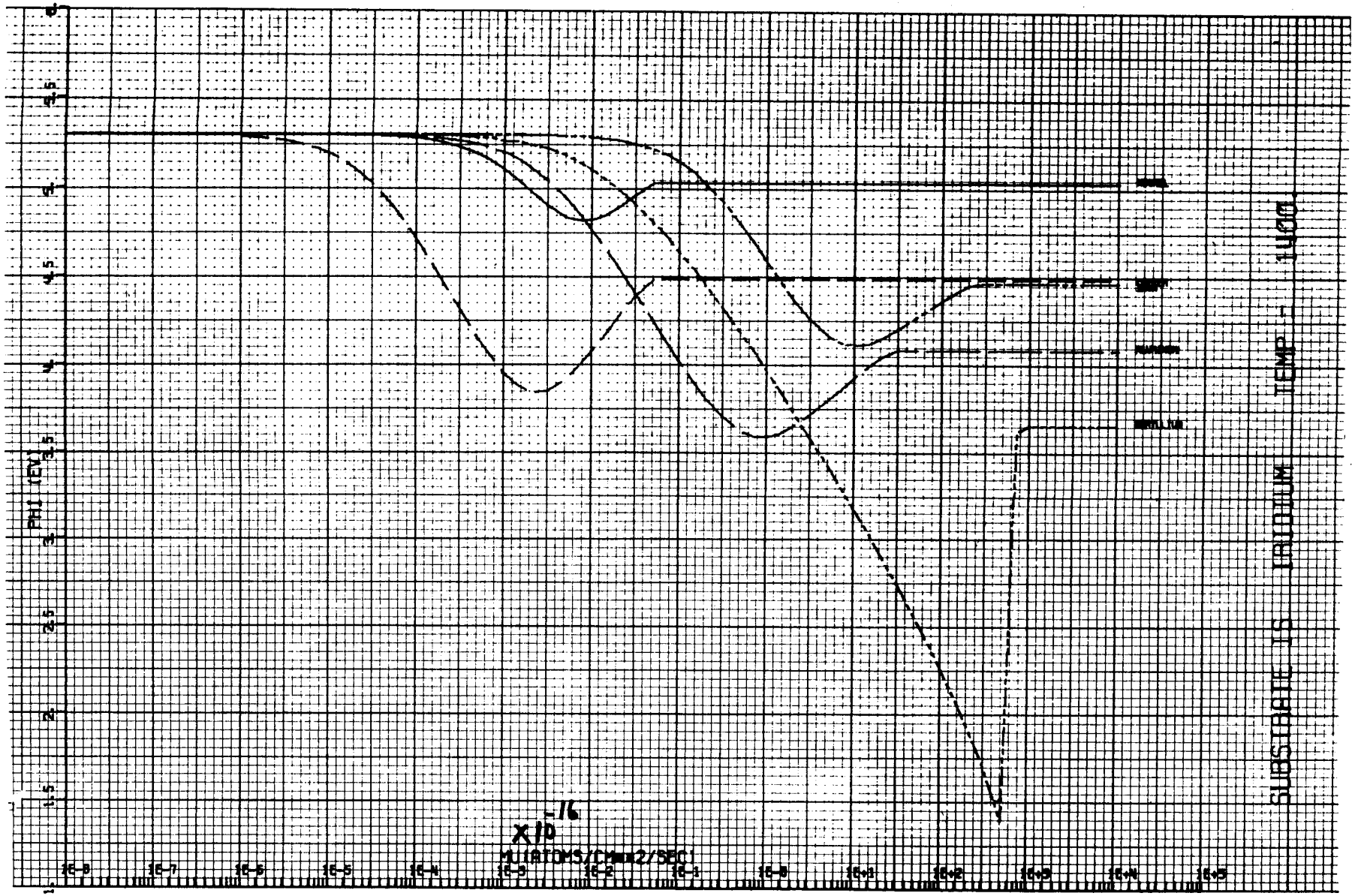

Fig. 100. Composite surface work function versus arrival flux for the five adsorbate atoms beryllium, aluminum, iron, nickel, and copper on an iridium surface (no surface coverage limitation).

where

$$F(\theta) = \frac{C_5 \left[\phi(0) - \phi(1)\right] G(\theta)}{\left[r(0) + r(1)\right] \left\{1 + \frac{a(1)}{\left[r(0) + r(1)\right]^3}\right\}} \qquad (18)$$

and

$$\delta(\theta) = \frac{F(\theta)}{\phi(\theta)} \left\{\frac{C_6}{\left[r(0) + r(1)\right]} - V_i(1)\right\} \qquad (19)$$

C_5 and C_6 again depend only on the system of units employed.

This expression for $\lambda_o(\theta)$ is derived from a treatment of intermetallic surface bonding as a combination of ionic and covalent forces based on a surface model which assumes a single polarized species which may be desorbed as either atoms or ions, rather than the existence of two distinct adsorbed species, adatoms and adions, on a conductor, thereby avoiding a number of fundamental shortcomings of the latter model. A number of analogies are drawn from molecular adsorption physics.

$\lambda_o(\theta)$ is written as the superposition of ionic and covalent parts. The ionic part is assumed to result from a coulomb interaction between opposite charges at opposite ends of the bonds, and the covalent part from pairing of valence electrons contributed by the atoms in the bond. A purely ionic bond is characterized by a dipole moment equal to the product of the charges and the internuclear distance. A purely covalent bond has no dipole moment. The ionic part is assumed to result from a fraction of charge $F(\theta)$ transferred from the adsorbate to the substrate, which determines the ionic character of the bond and which is associated with the surface dipole moment. The ionic part reduces to zero when no dipole moment exists and the bond is purely covalent ($F = 0$) and to the energy required to remove an adsorbed ion from the surface of a conductor when $F = 1$. The fraction of charge F results from a surface double layer of thickness equal to the internuclear distance in which self-depolarization is accounted for.

The covalent contribution to $\lambda_o(\theta)$ is assumed to result from mutual pairing of valence spins of adsorbate and substrate particles. This covalent portion is estimated as the geometric mean of the product of three terms, each of which is the product of a component for the adsorbate and for the substrate. This expression reduces to the proper limiting values when the all-ionic or all-covalent, or the pure adsorbate or the pure substrate extremes are chosen. The first term is the heat of sublimation and is the major contributor. The second is the square of the orbital strength, because as the eccentricity of the wave function of the valence orbital increases, the overlapping of the electron clouds of the surface particles increases, and the covalent bond becomes stronger. The last term is the valence charge participating in the covalent bond and is the smallest contributer, included to insure that when the bond is purely ionic, the covalent term vanishes. The second and third factors may be interpreted as the angular efficiency of the orbitals and the charge efficiency, respectively. These two terms are consistent in indicating that perfect covalent electron pairing occurs only when the pairing orbitals are identical and have equal charges.

In the calculation of equilibrium surface coverage, mean atom and ion residence times, and composite surface work function, the atomic desorption energy λ_o occurs in a sensitive exponent. Small changes or inaccuracies in λ_o therefore have a large effect on the values of the above quantities. The major contributing term in the expression for λ_o in (17) is $[H_s(0)\, H_s(1)]^{1/2}$. It is therefore very important to use the proper values for the H_s's.

The values of $H_s(0)$ and $H_s(1)$ called for in the equation for the atomic desorption energy $\lambda_o(\theta)$ are the desorption energies of a substrate atom from its own surface (lattice) and of an adsorbate atom from its own bulk solid surface. These quantities are not strictly the heats of sublimation ΔH_s of the two species, although they are closely related to them. The heat of sublimation is the energy required to

remove an atom from within the surface of a (metal) lattice (i.e., completely bound in the metal lattice). More nearest neighbor and next nearest neighbor bonds must be broken in this case than for desorption from an adsorption site on the surface of the lattice. Therefore, the heat of sublimation per atom is larger than the atomic desorption energy (by a factor of less than two). The actual surface desorption energy varies with the crystal face from which desorption occurs and therefore it depends on the crystal structure of the substrate. An investigation of the nearest-neighbor and next-nearest-neighbor bonding for the various crystal faces of the three principal crystal structures encountered in the work to which this problem is being applied (body-centered cubic, face-centered cubic, and hexagonal close-packed) has been made in order to solve this problem.

Assuming that the interactions between neighboring atoms in a crystal can be described as occurring between pairs of nearest neighbors with a bond energy E_1, and between next nearest neighbors, with a bond energy E_2, the desorption energies can be written for the various crystal faces of the various crystal types from knowledge of the crystal structure. These can then be related to the expression for an atom removed from within the crystal structure (i.e., the experimentally measured sublimation energy). Ratios of these can then be taken to obtain the desired result. As an example, Table XXVII gives the nearest-neighbor plus next-nearest-neighbor bonding sums for the three principal planes of the three primary crystal structures, the ratios of the strengths of the next-nearest-neighbor bonds to the nearest-neighbor bonds E_2/E_1, the corresponding total sublimation energy expression, and the ratio of surface desorption energy to sublimation energy.

TABLE XXVII

Influence of Crystallography on Sublimation Energies

Crystal Structure Type	$\Delta H_s + \frac{kT}{2}$	H_s (100) or (001)	H_s (110) or (010)	H_s (111) or (110)	$\frac{E_2}{E_1}$	Average Ratio of $H_s / \Delta H_s$
Face-centered cubic	$6E_1+3E_2$	$4E_1+1E_2$	$5E_1+2E_2$	$3E_1+3E_2$	1/10	0.667
Body-centered cubic	$4E_1+3E_2$	$4E_1+1E_2$	$2E_1+2E_2$	$4E_1+3E_2$	1/2	0.788
Hexagonal close packed	$6E_1+3E_2$	$3E_1+3E_2$	$4E_1+4E_2$	$5E_1+2E_2$	1/10	0.682

A further correction is required in the calculation of H_s to account for the temperature dependence of ΔH_s. The sublimation energy decreases with increasing surface temperature as

$$\Delta H_s(T) = \Delta H_s(0) - \frac{kT}{2} \tag{20}$$

or

$$\Delta H_s(T_x) = \Delta H_s(T_m) + \frac{k}{2}(T_m - T_x) \tag{21}$$

where $\Delta H_s(T_m)$ is the sublimation energy measured (or quoted) at T_m, and T_x is the temperature at which ΔH_s is desired. Values for ΔH_s are often quoted at 25C. Therefore, for a substrate surface temperature of 1400K the correction factor, when ΔH_s is quoted at 25C, is 0.047 eV.

The values of H_s used in the expression for $\lambda_o(\theta)$ are then obtained from the expression

$$H_s(T_x) = \left(\frac{H_s}{\Delta H_s}\right)\left[\Delta H_s(T_m) + \frac{k}{2}(T_m - T_x)\right] \tag{22}$$

where the ratio $(H_s/\Delta H_s)$ is calculated for the appropriate crystal structure type at T_x by the technique described above and illustrated in Table XXVII.

Equations (17) and (16) with (17) substituted for $\lambda_o(\theta)$ were programmed and used to calculate the atom adsorption/desorption energy (the dashed curves) and the ion adsorption/desorption energies (the broken curves) for cesium on 27 substrates, shown in Fig. 53 through 79; and for 21 adsorbates on each of 9 substrates (189 combinations), which comprise the supplementary volume entitled "Work Functions and Adsorption Energy Calculations." The substrate temperature assumed for all of these calculations was 1400K, although any

other temperature from 0 to 2000K would make little difference in the numerical results. The corrections for crystallography were made where believed appropriate. The 27 cesium substrates and the 21 adsorbate-9 substrate combinations for which the calculated curves were made are listed in Section IV-C.

E. RESIDENCE TIMES

Equation (6) was programmed and used to calculate the atom residence times for a variety of adsorbate-substrate combinations. Two programs and two types of calculations were made. The residence times versus (reciprocal) substrate temperature were calculated for the series of surface coverages: 0.00, 0.01, 0.05, 0.10, 0.25, 0.50, and 1.00 ($\theta = 1.00$ is invalid for the reason described earlier). Also calculated and plotted were the residence times versus adsorbate arrival flux for the series of surface temperatures 1300 to 1900K, by hundreds of degrees (or for fewer temperatures in some cases). These residence times were calculated in the range between 10^{-5} and 10^{+5} sec in the first case, and for the range of arrival fluxes between 10^{8} and 10^{21} atoms/cm^{2}-sec in the second case, for the 11 adsorbates (beryllium, carbon, aluminum, silicon, titanium, chromium, iron, nickel, copper, tin, and cesium) on 9 substrates (tungsten, iridium, rhenium, rhodium, platinum, osmium, molybdenum, tantalum, and nickel). The resulting 198 graphs (812 curves) were bound and distributed as the supplemental volume entitled "Residence Time Calculations."

F. SURFACE DIFFUSION COEFFICIENT

The surface physics problem dealt with here is to develop a practical theoretical expression for a surface diffusion coefficient for atoms adsorbed on a real, generalized surface which is consistent with certain experimental observations and which can be used to make

comparison calculations for various adsorbate-substrate combinations. Most real and practical surfaces are polycrystalline and rough, resulting in a variety of kinds of adsorption sites and in a distribution in adsorption energies. The adsorption energies and concentration of sites are functions of the degree of coverage.

While we are concerned with a surface phenomenon, the motion is not just in two dimensions; the atoms comprising the surface (substrate) and the migrating (diffusing) atoms are vibrating (thermal energy) and the latter may also desorb from the surface. Various degrees of sophistication can be introduced into the theory, starting with simple two-dimensional gas motion in which the surface plays no role other than to define the plane of motion, and the only collisions which the diffusing atoms undergo are with other diffusing atoms, i.e., collisions with surface atoms are not considered. In this case, there are no stable adsorption "sites" and the surface diffusion coefficient can be written simply as

$$D_s = \left(\frac{1}{2N}\right) v_{th}\, \ell_s = \frac{1}{4}\left(\frac{\pi k T}{2m}\right)^{1/2} \ell_s \qquad (23)$$

where N is the number of degrees of freedom, v_{th} is the mean thermal velocity of the diffusing atoms defined by the "gas" equilibrium temperature T (the surface temperature), and m is the mass of the diffusing atom species. The mean free path ℓ_s can be calculated from the collision diameter of the adsorbed atoms and is very dependent on the surface concentration of adatoms σ or the surface coverage θ, and can be quite large for low coverages. In this situation, there are no adsorption sites, and no activation energy is required to dissociate an adatom from one site to allow it to move to another site. The arguments against this oversimplified concept are (1) that calculated values of are at least two orders of magnitude below experimental values and (2) that the theoretical temperature coefficients is in disagreement with experiment as follows: $v_{th} \propto T^{1/2}$ and $D_s \propto T^n$ where $n \approx 1$.

Thus log D_s versus T^{-1} indicates an "apparent" activation energy of nRT or nkT which is considerably below observed values; experimental values indicate a large activation energy for migration.

The next logical step is to consider a surface which is composed of thermally vibrating atoms in a uniform array, i.e., in a crystal lattice. This situation is characterized by a uniform pattern of identical adsorption sites with spacing equal to the lattice constant a. The adsorption energy is identical at every site and an activation energy for migration between sites can now be introduced. Furthermore, the collisions of the migrating atoms now may not be limited to other migrating adatoms but collisions can be allowed with the substrate lattice atoms which are vibrating normally to the surface upon which the adatoms migrate. ℓ_s is now predominantly influenced by collisions with the substrate lattice atoms and is far less dependent upon σ or θ of the adatoms, and ℓ_s is therefore much smaller.

Activated surface migration involves three-dimensional vibration while adsorbed at a site, followed by activation into a momentary two-dimensional gas state, until readsorption occurs. This continual switching between a three-dimensional vibrator and a two-dimensional gas implies an increase in entropy. An entropy term is required and will be introduced later in the expression combining the vibration and migration motion via the lifetime.

If sufficient energy is supplied to the adsorbed atoms, they may be desorbed completely from the surface. The total binding energy of the adatoms must be supplied in this case. The magnitude of desorption energies λ is approximately five times the corresponding migration activation energies V_m. This accounts for the fact that the equilibrium surface coverage conditions are governed by diffusion rather than be desorption.

For a generalized practical surface, a potential energy diagram such as that shown in Fig. 101, may be representative. In Fig. 101, only two types of surface "patches" or adsorption sites are illustrated, but the concept can readily be generalized to an arbitrary number of different types of surface adsorption sites. In Fig. 101, vibrational

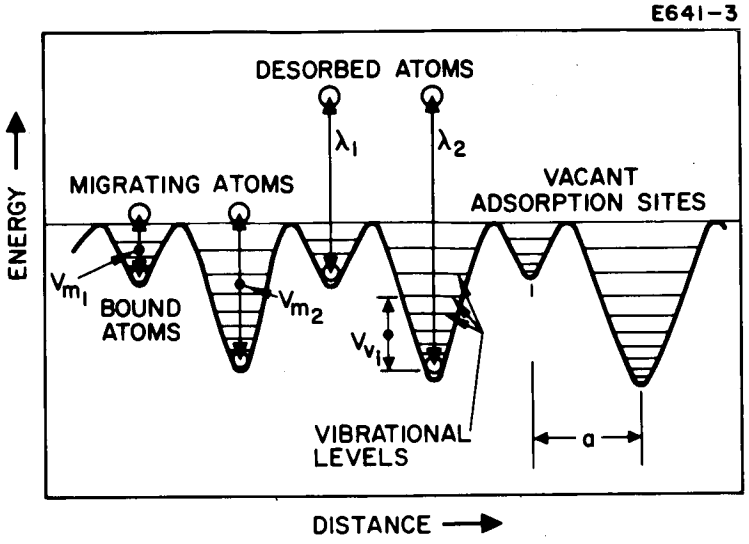

Fig. 101. Surface energy diagram. V_{v_i} is the energy required to raise an adatom to the i^{th} vibrational level. V_{m_i} is the energy required to raise an adatom into the migrational state, λ is the energy to desorb an adatom, and a is the mean distance between adsorption sites.

states are shown within each adsorption site. The energies associated with the vibrational states in the i^{th} kind of site are V_{v_i}. The migrational activation energies are V_{m_i}, and the desorption energies are λ_i.

Let us now begin a mathematical development with a simplified generalized expression for a diffusion coefficient

$$D = \frac{1}{2N} \frac{\ell^2}{\tau} \tag{24}$$

where N is the number of degrees of freedom, ℓ is the mean free path length or distance between adsorption sites, and τ is the mean time spent by a migrating atom between adsorptions or migrations (which involves the times spent in vibrational states while in adsorption sites τ_v and the times spent in migrations τ_m).

For surface diffusion or migration, $N = 2$; let us employ the subscript s, leading to

$$D_s = \frac{\ell_s^2}{4} \cdot \frac{1}{\tau_s} \quad . \tag{25}$$

This is the same expression as (23) using the relationship between ℓ_s and τ_s: $\tau_s = \ell_s / v_{th}$.

The mean time associated with one complete migration event τ_s involves the time to excite an adatom through vibrational energy states until its energy exceeds that required for activation into a migrational state V_m plus the time required to migrate to another adsorption site.

$$\tau_s = \tau_v + \tau_m = \tau_o \left[\exp\left(\frac{h\omega}{kT}\right) + \exp\left(\frac{V_m(\theta)}{kT}\right) \right] \tag{26}$$

$$\tau_o = \frac{h}{kT} \left[1 - \exp\left(-\frac{h\omega}{kT}\right) \right]^{-1} \tag{27}$$

where $\exp(h\omega/kT)$ is the vibrational Boltzmann term, $\exp(V_m(\theta)/kT)$ is the migrational Boltzmann term, ω is the fundamental or characteristic vibrational frequency of the atom, and $[1 - \exp(-h\omega/kT)]^{-1}$ is the vibration partition function (in any number of dimensions).

Substituting (26) and (27) in (25) with a for ℓ_s and introducing the configuration entropy difference term $(\Delta s(\theta)/k)$, yields

$$D_s(\theta) = \frac{a^2}{4}\left(\frac{kT}{h}\right)\left[1 - \exp\left(-\frac{h\omega}{kT}\right)\right] \exp\left[\frac{\Delta s(\theta)}{k}\right]\left[\exp\left(\frac{h\omega}{kT}\right) + \exp\left(\frac{V_m(\theta)}{kT}\right)\right]^{-1} \tag{28}$$

$\Delta S(\theta)$ is the configuration entropy term mentioned earlier to account for the entropy increase resulting from the transitions between the three-dimensional vibrator and the two-dimensional gas states.

$$\exp\left(\frac{\Delta S}{k}\right) = A_f^{-1}(\theta) \exp\left[\theta \frac{\partial}{\partial\theta} \ell n\, A_f^{-1}(\theta)\right] \tag{29}$$

where A_f, the free area, is the fraction of the total surface area available for migration. A_f decreases with increasing θ. Levine and Gyftopoulos[5] have chosen to write $\Delta S/k$ as the geometrical mean between the Van der Waal and cage models (with $\gamma = 1$ in each case) in an effort to equalize the over and under estimates of these two models. We have chosen to use their expression for A_f and hence for $\Delta S/k$:

$$A_f = (1 - \theta)^{1/2} \quad (1 - \theta^{1/2}) \quad , \tag{30}$$

leading to

$$\exp\left[\frac{\Delta S(\theta)}{k}\right] = (1 - \theta)^{-1/2} (1 - \theta^{1/2})^{-1} \exp\left[\frac{\theta}{2} (1 - \theta)^{-1} + \frac{\theta^{1/2}}{2} (1 - \theta^{1/2})^{-1}\right]. \tag{31}$$

Equation (31) is plotted in Fig. 51 as a function of θ from $\theta = 0$ to $\theta = 0.7$. As described in some detail by Levine and Gyftopoulos, the expressions for $\Delta S/k$ are not valid above θ equal to about 0.6, because the second monolayer is beginning to form. The calculation made here for $D_s(\theta)$ is not valid above $\theta \simeq 0.6$ for the same reason.

$V_m(0)$ is just the activation energy for surface migration for an isolated adatom. As θ increases, the magnitude of V_m is influenced by the interaction of each adatom with its neighboring adatoms in addition to the substrate surface. For a number of adsorbate-substrate combinations, including some cases where the adatom is an atom of the substrate, values of V_m have been determined. In some cases, V_m has been measured for several values of θ.[6] V_m will also vary with the particular crystal plane or direction comprising the substrate or the make-up of a polycrystalline surface.

For most of the combinations for which V_m has been measured, the desorption energy λ has also been measured. λ is also a function of θ. A comparison of the measured values of V_m and λ for a variety of adsorbate-substrate combinations shows that

$$V_m \approx 0.22\,\lambda \quad . \tag{32}$$

Therefore, for combinations for which $V_m(\theta)$ has not been measured (which includes most of them), this empirical relationship can be used; together with an expression for $\lambda(\theta)$, it allows calculations of $D_s(\theta)$ to be made for new systems. Equation (17) is such an expression for $\lambda(\theta)$, which requires in turn the use of (11) for $\phi(\theta)$.

All of these equations have been combined into one large computer program to calculate some curves for $D_s(\theta)$ through the use of the empirical relationship of (32). Curves of $D_s(\theta)$ versus θ from 0 to 0.6 have been calculated at T = 1000, 1400, 1600, and 2000K for cesium on 31 substrates and for each of 20 other adsorbates on each of 9 substrates; curves of $D_s(\theta)$ versus T from 100 to 2000K have

been calculated at $\theta = 0.00$, 0.01, 0.03, 0.10, and 0.30, and 0.70 for the same adsorbate-substrate combinations. These curves have been bound into a separate supplementary volume entitled "Diffusion Coefficient Calculations." The 31 substrates for cesium are beryllium, carbon, aluminum, silicon, titanium, vanadium, chromium, manganese, iron, cobalt, nickel, copper, gallium, germanium, zirconium, niobium, molybdenum, ruthenium, rhodium, palladium, indium, tin, antimony, hafnium, tantalum, tungsten, rhenium, osmium, iridium, platinum, and lead; the 21 adsorbates and 9 substrates are listed in Section III-C.

Simplifications can be made in two temperature regimes. If T is equal to or less than approximately 10 K, the vibration partition function can be approximated by (h/kT) and

$$D_s(\theta) = \frac{a^2 h}{4KT} \exp-\left[\frac{\Delta S(\theta)}{k}\right] \left[\exp\left(\frac{h\omega}{kT}\right) + \exp\left(\frac{V_m(\theta)}{kT}\right)\right]^{-1} . \tag{33}$$

If T is equal to or greater than approximately 1000K, the partition function may be approximated by $(1/\omega)$ and

$$D_s(\theta) = \frac{a^2 \omega}{4} \exp-\left[\frac{\Delta S(\theta)}{k}\right] \left[\exp\left(\frac{h\omega}{kT}\right) + \exp\left(\frac{V_m(\theta)}{kT}\right)\right]^{-1} . \tag{34}$$

Furthermore, if $\theta \leqq 10^{-2}$,

$$\exp\left[\frac{\Delta S(\theta)}{k}\right] \approx 1$$

and

$$D_s(\theta) = \frac{a^2 \omega}{4} \left[\exp\left(\frac{h\omega}{kT}\right) + \exp\left(\frac{V_m(\theta)}{kT}\right)\right]^{-1} ; \tag{35}$$

furthermore, if $V_m(\theta) >> h\omega$,

$$D_s(\theta) = \frac{a^2\omega}{4} \exp\left[-\frac{V_m(\theta)}{kT}\right] . \qquad (36)$$

The value of a used in these calculations was $\sqrt{10}$ Å, in all cases. This is a minimum possible value and the curves are, therefore, lower limits. Experimental values are expected to be above these curves by the square of the ratio of actual a to the assumed value. Larger values of a can result from not all lattice sites being available for adsorption sites, from various causes, for example, surface contamination or defects.

G. ION CRITICAL TEMPERATURES

Because the measurement of critical temperatures for saturated cesium ion emission from a variety of metal substrates is one of the major goals of this contract, a theoretical investigation of the subject is in order so that the experimental data may be related to a satisfactory theory. A theoretical expression for all surfaces relating T_c to J_+ or μ which gives good agreement with the experimental data for cesium on solid and porous tungsten is developed below. Combination of the expression with a form of the Saha-Langmuir equation shows the theoretical relationship between β_c and J_+ (or μ) which is in good agreement with experimental data.

The ionization efficiency and ion current density are shown to be slightly dependent on the applied electric field. The expressions originally expressed are simplified forms of more complex ones (e.g., involving the explicit forms for patchy surfaces). For this application, the range of E is taken as 10^4 to 10^5 V/cm. θ is not assumed to be zero but rather a small value θ_c, the value of the coverage at the critical point. The explicit dependences of the desorption energies on θ are used. The analysis is made specifically for cesium but can be extended to other adsorbates.

$$J_+ = e\mu\beta \tag{37}$$

$$\beta = \frac{\nu_+}{\mu} \quad . \tag{38}$$

The ratio of desorbing ion flux to the total incident flux

$$\nu_+ = \frac{\sigma}{\tau_+} = \frac{\theta\,\sigma\,(1)}{2} \left(\frac{kT}{h}\right)\left[1 - e^{-\left(\frac{h\omega}{kT}\right)}\right] \exp\left[\frac{\Delta S(\theta)}{k}\right] \exp - \left[\frac{\lambda_+(\theta) - e\sqrt{eE}}{kT}\right] \tag{39}$$

where τ_+ is discussed in a previous section.

For the critical temperature condition, $T = T_c$, $\beta = \beta_c$, $\theta = \theta_c$ and E is greater than the magnitude required to extract the saturated ion current density. Because θ is small (probably less than 10^{-2}) in the critical region, $\exp[\Delta S(\theta)/k]$ may be approximated by unity. Thus

$$\beta_c = \left(\frac{\theta_c\,\sigma(1)}{2\mu}\right)\left(\frac{kT_c}{h}\right) \quad 1 - e^{-\left(\frac{h\omega}{kT_c}\right)} \exp - \left[\frac{\lambda_+(\theta_c) - e\sqrt{eE}}{kT_c}\right] \tag{40}$$

and

$$J_+ = \left(\frac{e\theta_c\,\sigma(1)}{2}\right)\left(\frac{kT_c}{h}\right)\left[1 - e^{-\left(\frac{h\omega}{kT}\right)}\right] \exp - \left[\frac{\lambda_+(\theta_c) - e\sqrt{eE}}{kT_c}\right] . \tag{41}$$

It will be seen that β (and J_+) vary with certain parameters above the critical point.

The [ ] term, the statistical mechanics vibration partition function was discussed in a previous section where it was shown that for T > 1000K, its value was $h\omega/kT$. Therefore, (39) and (40) become

$$\beta_c = \left(\frac{\theta_c \sigma(1) \omega}{2\mu}\right) \exp - \left[\frac{\lambda_+ (\theta_c) - e\sqrt{eE}}{kT_c}\right] \qquad (42)$$

$$J_+ = \left(\frac{e\theta_c \sigma(1)\omega}{2}\right) \exp - \left[\frac{\lambda_+(\theta_c) - e\sqrt{eE}}{kT_c}\right] . \qquad (43)$$

For saturated ion current density extraction, E must be greater than the space-charge-limited — emission-limited knee value. For $J_+ > \sim 10^{-4}$ A/cm^2, the term $e\sqrt{eE}$ is not negligible. For $E = 1.3 \times 10^4$ and 1.0×10^5 V/cm, the corresponding values of $e\sqrt{eE}$ are 0.04 and 0.12 eV.

Equation (42) can be written

$$\ell n\, J_+ = \ell n \left(\frac{e\theta_c \sigma(1)\omega}{2}\right) - \left[\frac{\lambda_+ (\theta_c) - e\sqrt{eE}}{kT_c}\right] \qquad (44)$$

or

$$\ell n\, J_+ = A - \frac{B}{T_c} . \qquad (45)$$

H. NEUTRAL FRACTION

By introducing a simplified form of the Saha-Langmuir equation at the critical point

$$\beta_c = \left\{1 + 2 \exp \left[\frac{V_i - \phi(\theta_c) - e\sqrt{eE}}{kT_c}\right]\right\}^{-1} \qquad (46)$$

and combination of (41) and (45), T_c can be eliminated and an expression derived which relates β_c and μ:

$$\beta_c = \left[\frac{\theta_c \sigma(1)\omega}{2\mu}\right]\left(\frac{\beta_c^{-1} - 1}{2}\right)^{\left[\frac{\lambda_+(\theta_c) - e\sqrt{eE}}{\phi(\theta_c) + e\sqrt{eE} - V_i}\right]} . \qquad (47)$$

β_c cannot be conveniently solved for, but we can solve for μ (and J_+) in terms of β_c, plot the expression, and obtain graphically β_c as a function of μ.

$$\mu = \left[\frac{\theta_c \sigma(1)\omega}{2\beta_c}\right]\left(\frac{\beta_c^{-1} - 1}{2}\right)^{\left[\frac{\lambda_+(\theta_c) - e\sqrt{eE}}{\phi(\theta_c) + e\sqrt{eE} - V_i}\right]} . \qquad (48)$$

Substituting $J_+ \equiv e\beta_c\mu$ and $\beta_c = 1 - NF$,

$$J_+ = \left[\frac{e\theta_c \sigma(1)\omega}{2}\right]\left[\frac{NF}{2(1 - NF)}\right]^{\left[\frac{\lambda_+(\theta_c) - e\sqrt{eE}}{\phi(\theta_c) + e\sqrt{eE} - V_i}\right]} . \qquad (49)$$

Equation (49) gives the relationship between ion current density and neutral fraction.

V. CONTRIBUTING PERSONNEL

The persons associated with the research program carried out under this contract, and their contributions, were

R. G. Wilson	Project Scientist
P. J. Coane	Fabrication and operation of the vacuum system, emission measurements, and data reduction and analysis
J. D. Montross	Fabrication and processing of experimental tubes and special materials procurement and handling
G. H. Guss	Computer Programmer
C. H. Fetters	Glass blowing associated with experimental tubes and vacuum system
W. E. McKee and J. M. Hammond	Refractory compound surface fabrication
E. Senkovits	X-ray diffraction measurements

REFERENCES

1. E. F. Chaikovskii and G. V. Ptitsyn, Soviet Phys. – Tech. Phys. 10, 410 (1965).

2. J. D. Levine and E. P. Gyftopoulos, Surface Science 1, 171 (1964).

3. E. P. Gyftopoulos and J. D. Levine, J. Appl. Phys. 33, 67 (1962).

4. J. D. Levine, private communication.

5. J. D. Levine and E. P. Gyftopoulos, Surface Science 1, 225 (1964).

6. C. J. Bennette, R. W. Strayer, and L. W. Swanson, Quarterly Progress Report No. 2, Contract NAS 3-5902, 22 December 1964, pp. 17-21.

DISTRIBUTION LIST

	Addressee	Number of Copies
1.	Spacecraft Technology Procurement Section NASA-Lewis Research Center 21000 Brookpark Road Cleveland, Ohio 44135 Attn: John H. Deford	1
	Technology Utilization Office NASA-Lewis Research Center 21000 Brookpark Road Cleveland, Ohio 44135 Attn: John Weber	1
	Office of Reliability & Quality Assurace NASA-Lewis Research Center 21000 Brookpark Road Cleveland, Ohio 44135	1
	Office of Reliability & Quality Assurance NASA-Lewis Research Center 21000 Brookpark Road Cleveland, Ohio 44135 Attn: W. Rayle	1
	Spacecraft Technology Division NASA-Lewis Research Center 21000 Brookpark Road Cleveland, Ohio 44135 Attn: J. H. Childs	2
	Spacecraft Technology Division NASA-Lewis Research Center 21000 Brookpark Road Cleveland, Ohio 44135 Attn: D. L. Lockwood	2
	Spacecraft Technology Division NASA-Lewis Research Center 21000 Brookpark Road Cleveland, Ohio 44135 Attn: John Ferrante	3

	Addressee	Number of Copies
	Spacecraft Technology Division NASA-Lewis Research Center 21000 Brookpark Road Cleveland, Ohio 44135 Attn: Y. E. Strausser	2
	Electromagnetic Propulsion Division NASA-Lewis Research Center 21000 Brookpark Road Cleveland, Ohio 44135 Attn: W. Moeckel	1
	Electromagnetic Propulsion Division NASA-Lewis Research Center 21000 Brookpark Road Cleveland, Ohio 44135 Attn: E. Richley	1
	Electromagnetic Propulsion Division NASA-Lewis Research Center 21000 Brookpark Road Cleveland, Ohio 44135 Attn: Library	2
	Electromagnetic Propulsion Division NASA-Lewis Research Center 21000 Brookpark Road Cleveland, Ohio 44135 Attn: Reports Control Office	1
	Electromagnetic Propulsion Division NASA-Lewis Research Center 21000 Brookpark Road Cleveland, Ohio 44135 Attn: H. E. Nastelin	1
2.	NASA-Headquarters FOB-10B 600 Independence Avenue, S. W. Washington, D. C. 20546 Attn: RNT/James Lazar	1

	Addressee	Number of Copies
3.	Commander Aeronautical Systems Division Wright-Patterson Air Force Base, Ohio Attn: AFAPL (APIE) Robert Supp	1
4.	Jet Propulsion Laboratory 4800 Oak Grove Drive Pasadena, California Attn: J. J. Paulson	1
5.	NASA-Langley Research Center Technical Library Langley Field, Virginia	1
6.	Electro-Optical Systems, Inc. 125 North Vinedo Avenue Pasadena, California Attn: Dr. A. T. Forrester	1
7.	Space Technology Laboratories 8433 Fallbrook Avenue Canoga Park, California Attn: Dr. D. Langmuir	2
8.	Headquarters, USAF Air Force Office of Scientific Research Washington 25, D.C. Attn: Dr. M. Slawsky	2
9.	United Aircraft Corporation Research Department East Hartford, Connecticut Attn: Dr. R. G. Meyerand, Jr.	1
10.	Field Emission Corporation McMinnville, Oregon Attn: Dr. F. Charbonnier	2
11.	Lockheed Aircraft Corporation Missile and Space Company Palo Alto, California Attn: Dr. G. B. Shook	1

	Addressee	Number of Copies
12.	Oak Ridge National Laboratory Thermonuclear Project Oak Ridge, Tennessee Attn: Dr. A. Weinberg	1
13.	Stanford University Hansen Microwave Laboratory Stanford, California Attn: Dr. G. S. Kino	1
14.	General Electric Company General Engineering Laboratories Schenectady, New York Attn: Dr. Lynn Stauffer	1
15.	Marshall Space Flight Center Huntsville, Alabama Attn: Dr. E. Stuhlinger (M-RP-DIR)	1
16.	MSA Research Corporation Callery, Pennsylvania Attn: J. W. Meusteller	1
17.	Aerospace Corporation P.O. Box 95085 Los Angeles 45, California Attn: Technical Library Documents Group	1
18.	U.S. Atomic Energy Commission Office of Technical Information Extension P.O. Box 62 Oak Ridge, Tennessee	1
19.	National Research Corporation 70 Memorial Drive Cambridge, Massachusetts 02142 Attn: R. W. Diehl	1
20.	AFPR, Hughes Aircraft Company Florence Avenue and Teale Street Culver City, California Attn: RWRAAC-2-D. Fisher	1

	Addressee	Number of Copies
	AFPR, Hughes Aircraft Company Florence Avenue and Teale Street Culver City, California Attn: RWRAPS-9-Mr. Weldon	1
21.	Litton Industries Electron Tube Division 960 Industrial Road San Carlos, California Attn: Dr. Rajindar Wadhwa	1
22.	AFWL - Kirtland Air Force Base, New Mexico Attn: Capt. C. F. Ellis/WLPC	1
23.	Electrical Propulsion Laboratory Westinghouse Astronuclear Laboratories Pittsburgh 35, Pennsylvania Attn: Mr. H. W. Szymanowski, Mgr.	1
24.	NASA-Scientific and Technical Information Facility P.O. Box 33 College Park, Maryland 20740 Attn: NASA Representative RQT-2448	6
25.	Radio Corporation of America David Sarnoff Research Center Princeton, New Jersey Attn: K. G. Hernqvist	1
26.	Hiram College Department of Physics Hiram, Ohio Attn: Prof. Lawrence Shaffer	1

SUPPLEMENT

NAS 3-6278

SUMMARY REPORT

FOREWORD

This supplement to the Final Report on Contract NAS 3-6278 contains the results of 7094 digital computer calculations plotted by the use of a Cal Comp plotter. The theory and equations on which these calculations are based are described in the Final Report. The quantities plotted here are the surface diffusion coefficient versus temperature for six values of surface coverage and the surface diffusion coefficient versus surface coverage for four values of temperature, for each of 21 adsorbates on each of nine substrates, 378 graphs and 1890 curves in all. The six values of surface coverage and their corresponding curve symbols are (1) zero, ————; (2) 0.01, ————————; (3) 0.03, ———— ————; (4) 0.10, ————————; (5) 0.30, ————————————; and (6) 0.70, ————————————. The four values of temperature and their corresponding curve symbols are (1) 1000K, ———; (2) 1400K, ————————; (3) 1600K, ————————————; and (4) 2000K, ——— ———. The 21 adsorbates are lithium, beryllium, carbon, sodium, aluminum, silicon, potassium, titanium, chromium, manganese, iron, nickel, copper, gallium, rubidium, indium, tin, cesium, barium, magnesium, and lead; the nine substrates are tungsten, rhenium, osmium, iridium, platinum, rhodium, molybdenum, tantalum, and nickel.

The value of a used in these calculations was $\sqrt{10}$ Å, in all cases. This is a minimum possible value and the curves are, therefore, lower limits. Experimental values are expected to lie above these curves by the square of the ratio of actual a to the assumed value. Layer values of a can result from not all lattice sites being available for adsorption sites, from various causes, for example, surface contamination or defects.

DIFFUSION COEFFICIENT (M)
1E-4
1E-5
1E-6
1E-7
1E-8
1E-9
1E-10
1E-11
1E-12
1E-13
TEMPERATURE (K) (*10²)
80.
120.
160.
200.
SUBSTRATE IS TUNGSTEN ADSORBATE IS LITHIUM

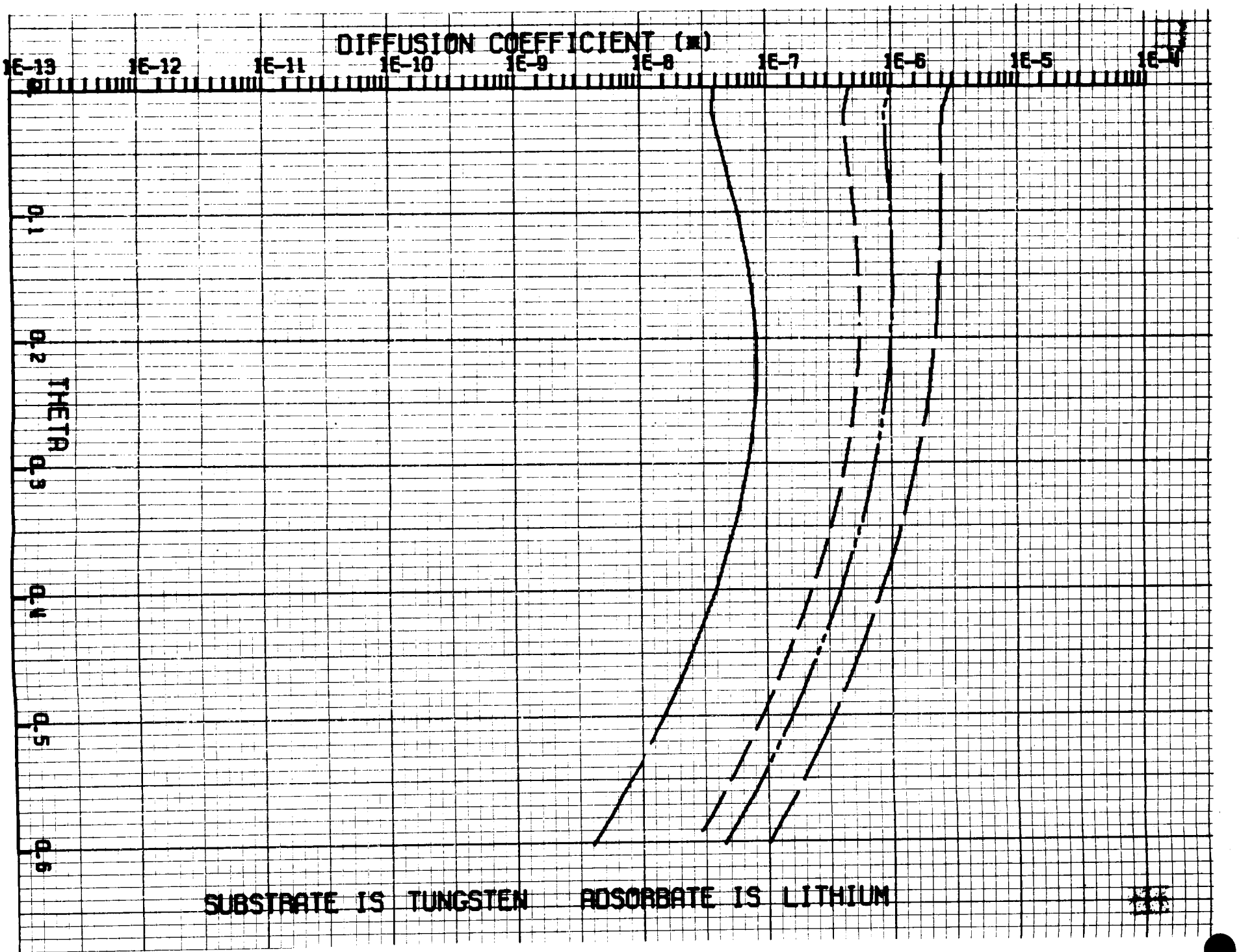
DIFFUSION COEFFICIENT (m)
1E-13
1E-12
1E-11
1E-10
1E-9
1E-8
1E-7
1E-6
1E-5
1E-4
θ1
θ1.1
θ1.2
θ1.3
θ1.4
θ1.5
θ1.6
THETA
SUBSTRATE IS TUNGSTEN ADSORBATE IS LITHIUM

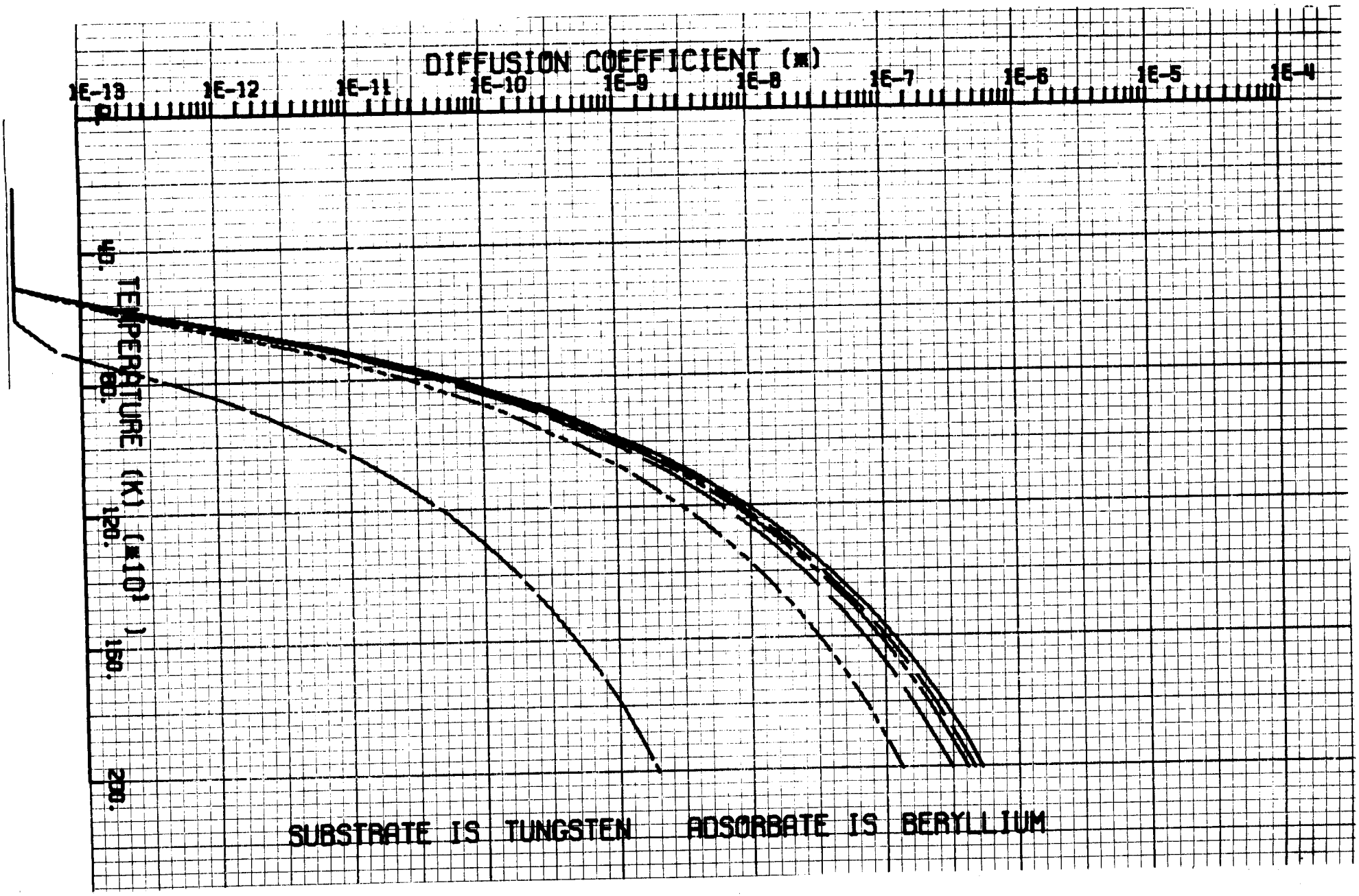
DIFFUSION COEFFICIENT (m)
1E-13
1E-12
1E-11
1E-10
1E-9
1E-8
1E-7
1E-6
1E-5
1E-4
TEMPERATURE (K) (m10³)
200.
160.
120.
80.
40.
SUBSTRATE IS TUNGSTEN ADSORBATE IS BERYLLIUM

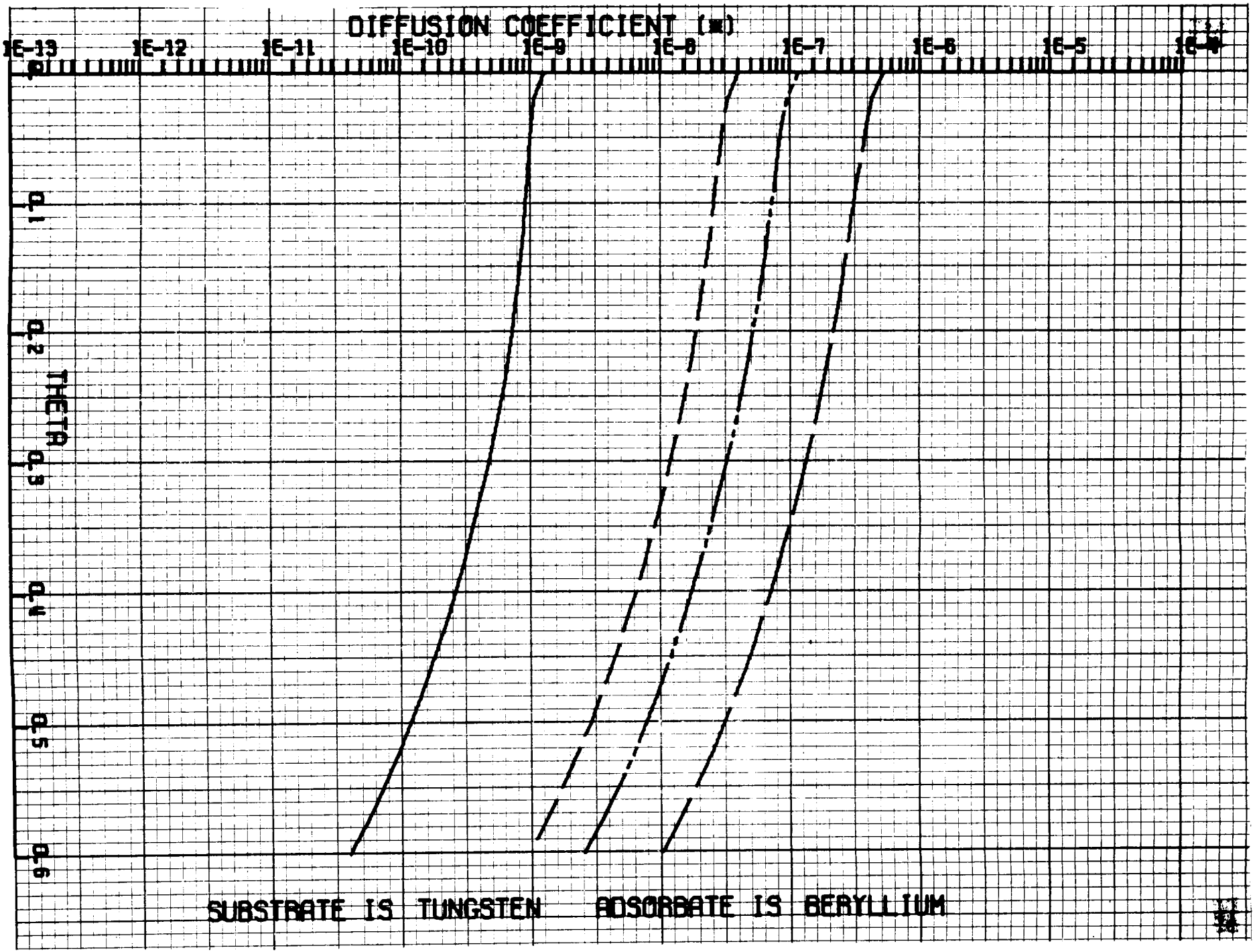
DIFFUSION COEFFICIENT (m)
1E-13
1E-12
1E-11
1E-10
1E-9
1E-8
1E-7
1E-6
1E-5
1E-4
THETA
0.1
0.2
0.3
0.4
0.5
0.6
SUBSTRATE IS TUNGSTEN ADSORBATE IS BERYLLIUM

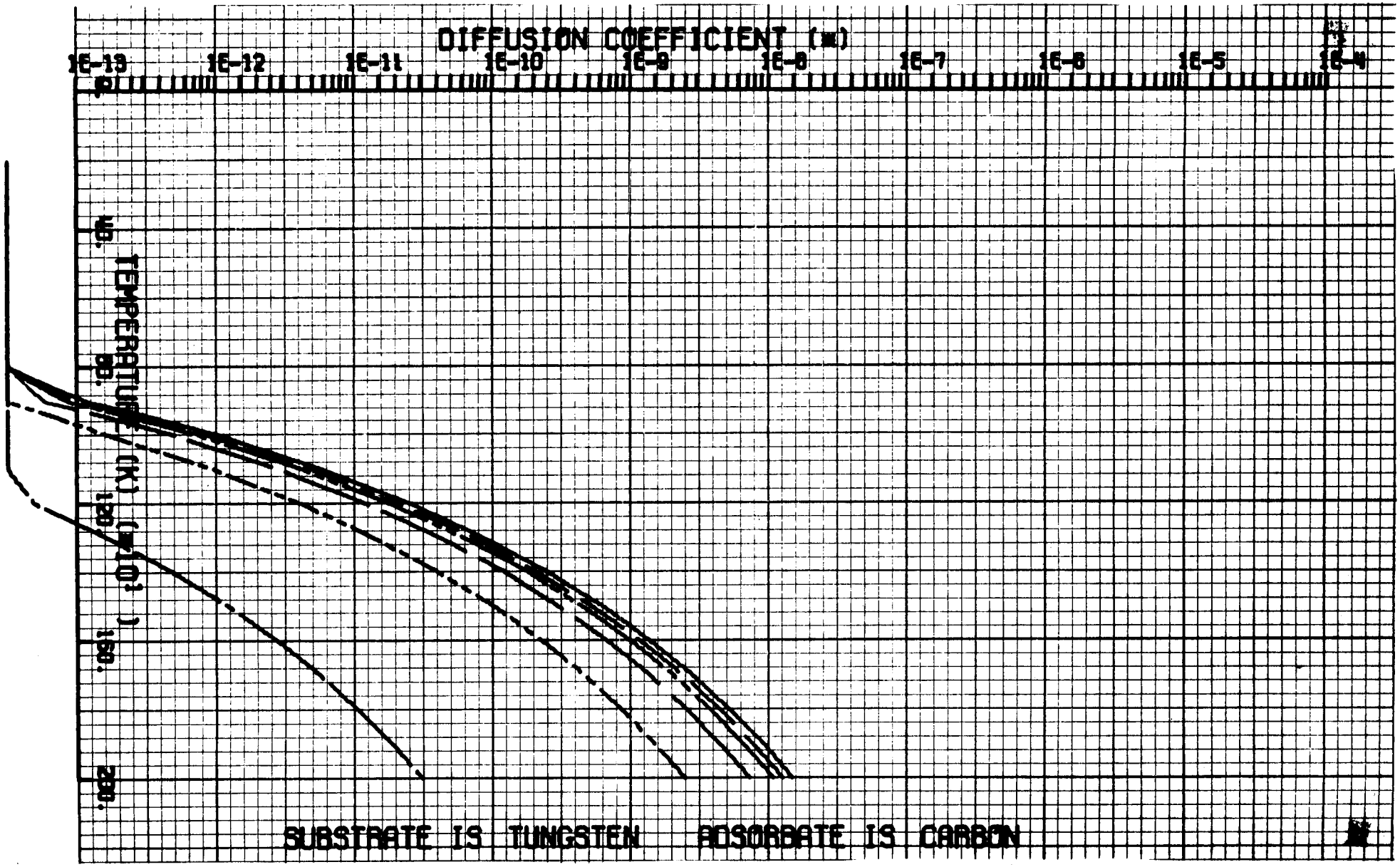
DIFFUSION COEFFICIENT (m)
1E-13
1E-12
1E-11
1E-10
1E-9
1E-8
1E-7
1E-6
1E-5
1E-4
TEMPERATURE (K)
SUBSTRATE IS TUNGSTEN ADSORBATE IS CARBON

DIFFUSION COEFFICIENT (cm²)
1E-4
1E-5
1E-6
1E-7
1E-8
1E-9
1E-10
1E-11
1E-12
1E-13
0
0.1
0.2
0.3
0.4
0.5
0.6
THETA
SUBSTRATE IS TUNGSTEN ADSORBATE IS CARBON

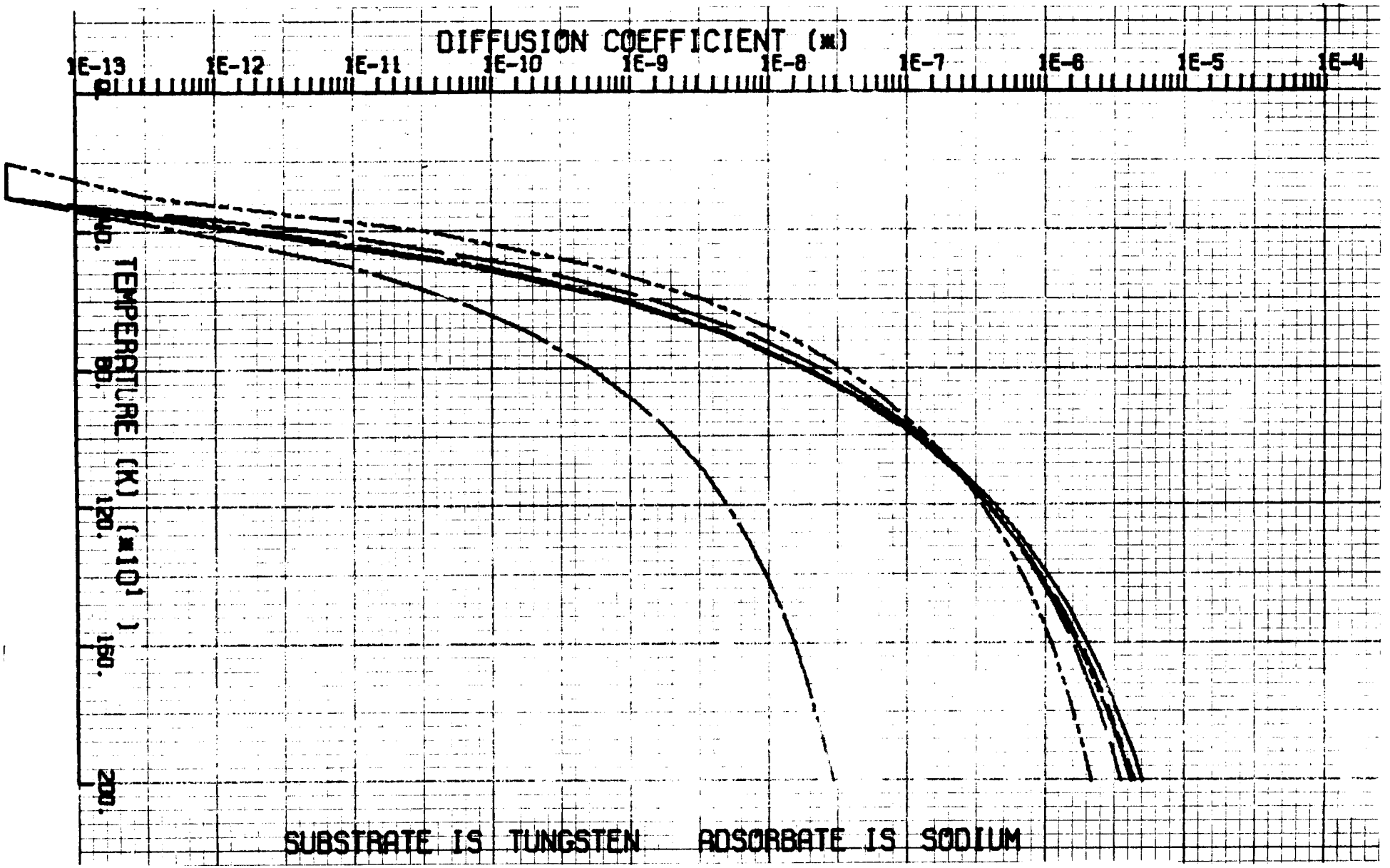
DIFFUSION COEFFICIENT (*)
1E-13
1E-12
1E-11
1E-10
1E-9
1E-8
1E-7
1E-6
1E-5
1E-4
40.
TEMPERATURE (K) (*10^1)
80.
120.
160.
200.
SUBSTRATE IS TUNGSTEN ADSORBATE IS SODIUM

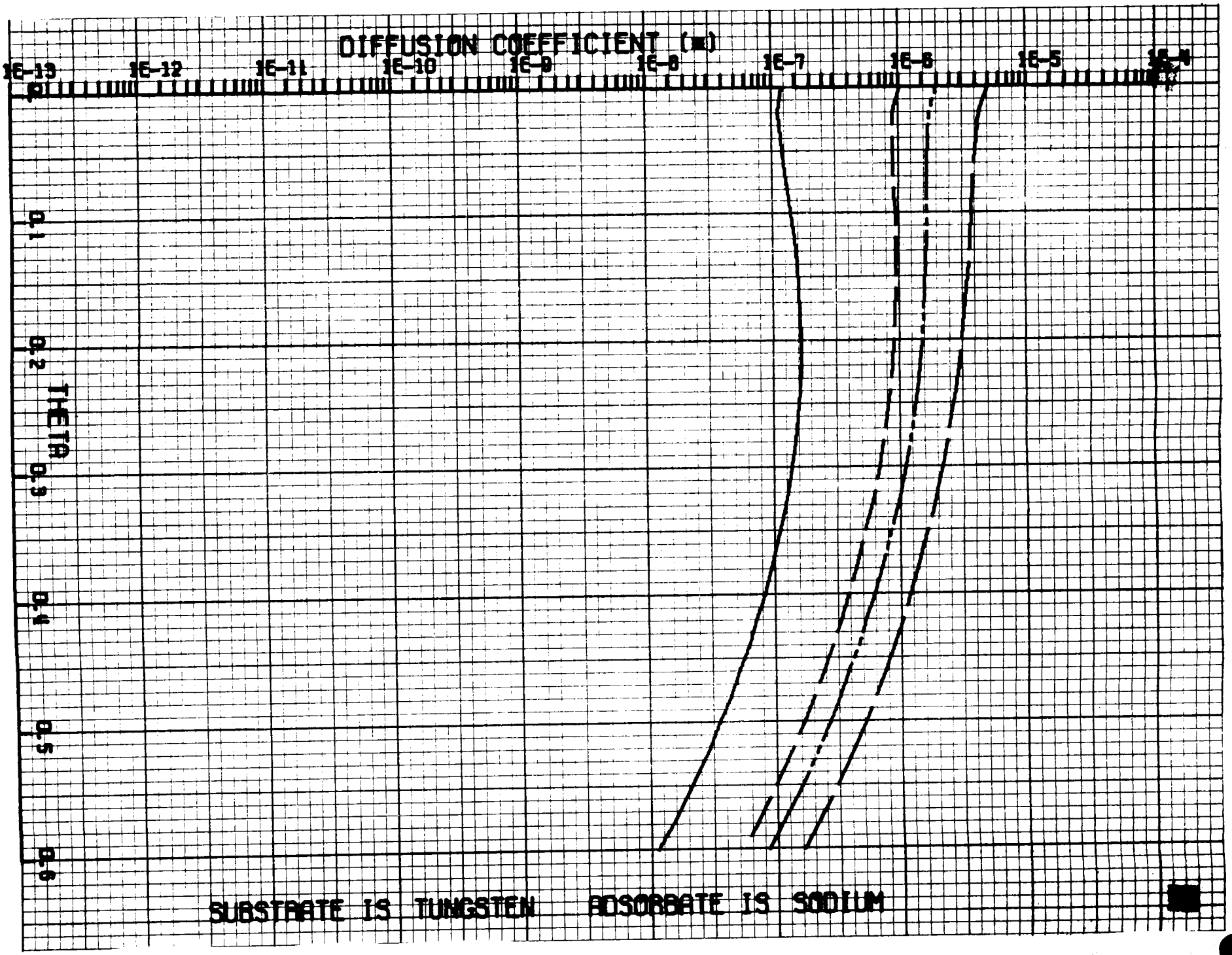
DIFFUSION COEFFICIENT (■)
1E-13
1E-12
1E-11
1E-10
1E-9
1E-8
1E-7
1E-6
1E-5
1E-4
0.1
0.2
THETA
0.3
0.4
0.5
0.6
SUBSTRATE IS TUNGSTEN ADSORBATE IS SODIUM

DIFFUSION COEFFICIENT (cm²)
1E-4
1E-5
1E-6
1E-7
1E-8
1E-9
1E-10
1E-11
1E-12
1E-13
TEMPERATURE (K) (×10¹)
40.
80.
120.
160.
200.
SUBSTRATE IS TUNGSTEN ADSORBATE IS ALUMINUM
13

DIFFUSION COEFFICIENT (M²)
1E-4
1E-5
1E-6
1E-7
1E-8
1E-9
1E-10
1E-11
1E-12
1E-13
0.1
0.2
0.3
0.4
0.5
0.6
THETA
SUBSTRATE IS TUNGSTEN ADSORBATE IS ALUMINUM

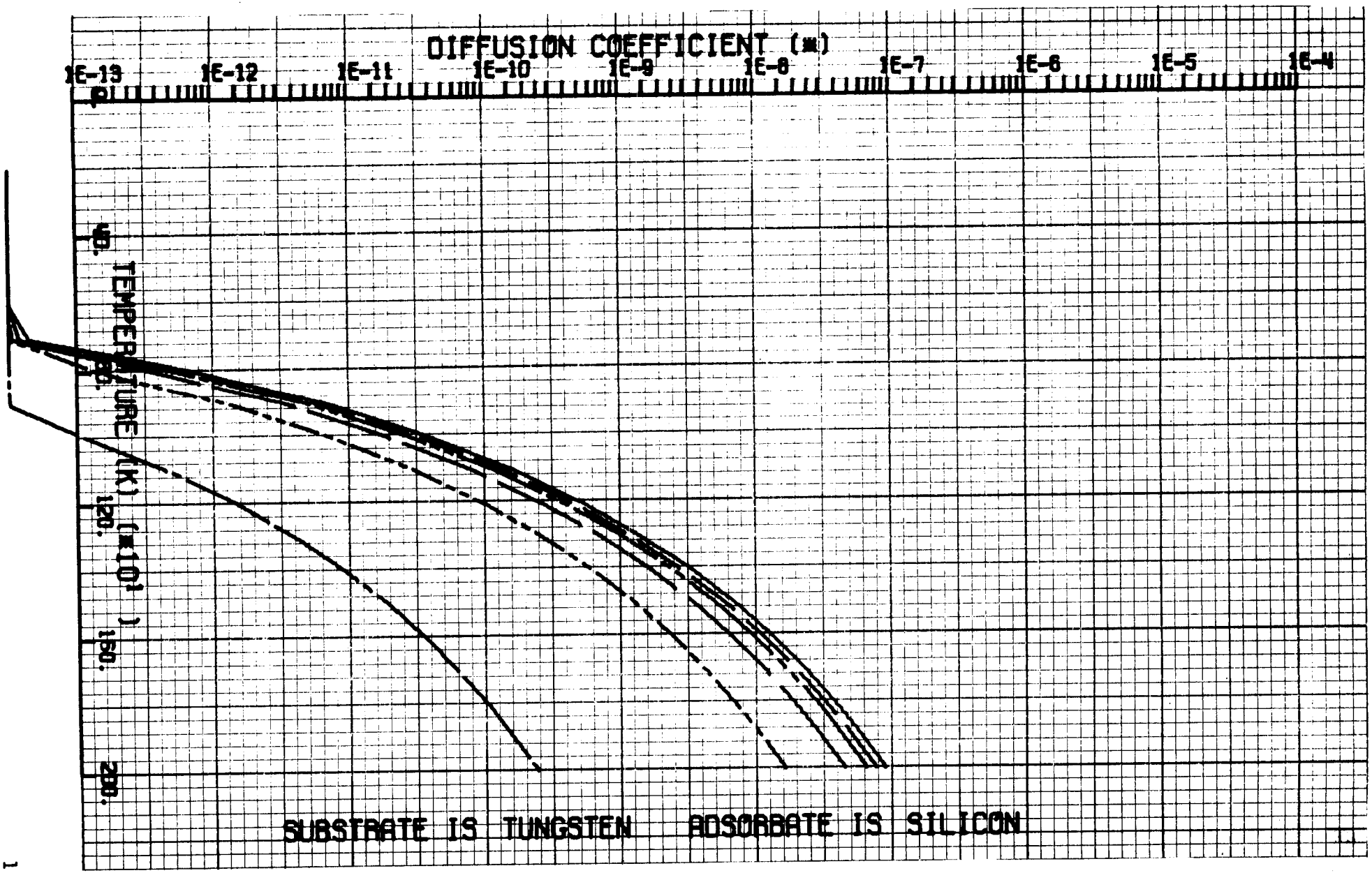
DIFFUSION COEFFICIENT (m)
1E-13
1E-12
1E-11
1E-10
1E-9
1E-8
1E-7
1E-6
1E-5
1E-4
TEMPERATURE (K) (x10¹)
SUBSTRATE IS TUNGSTEN ADSORBATE IS SILICON

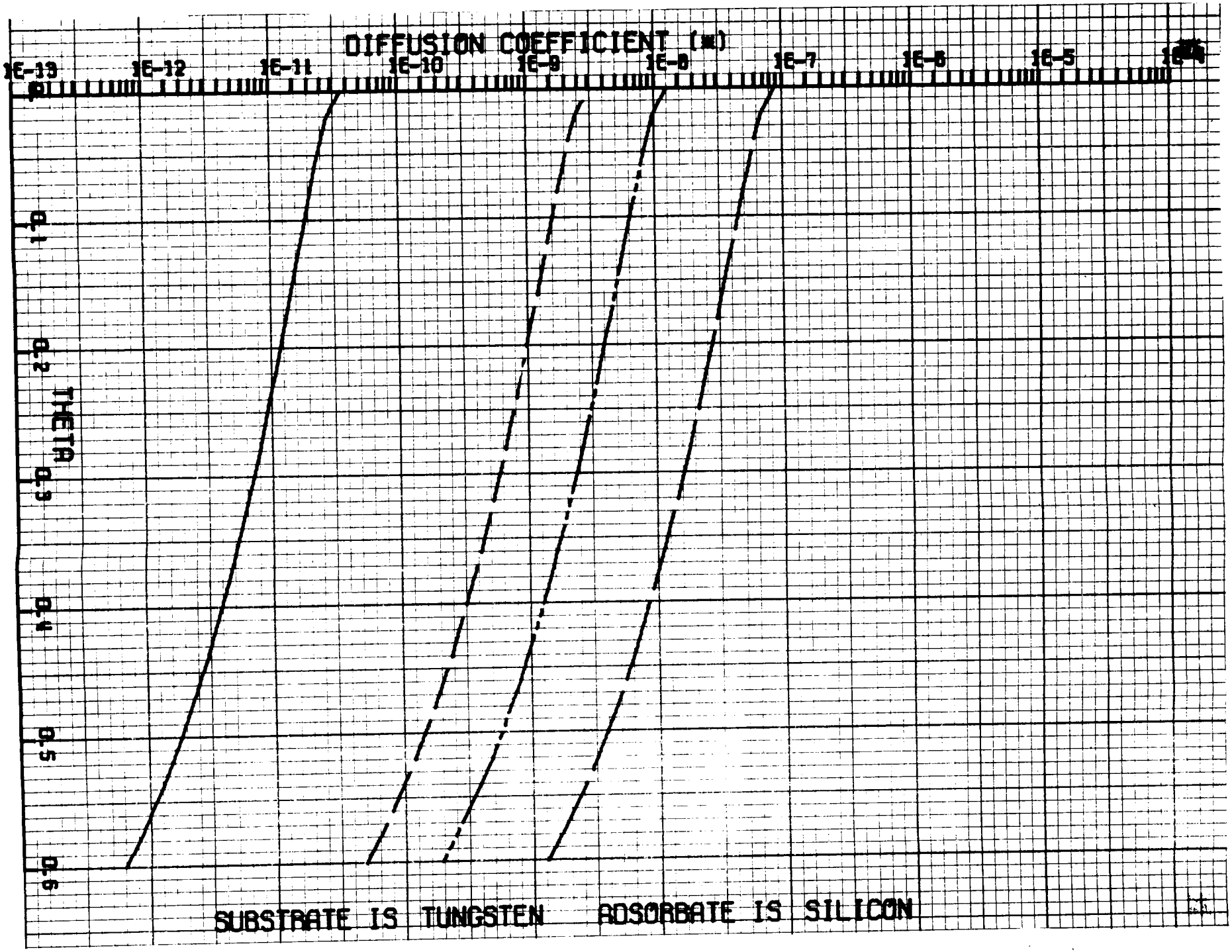
DIFFUSION COEFFICIENT (m)
1E-13
1E-12
1E-11
1E-10
1E-9
1E-8
1E-7
1E-6
1E-5
THETA
0.1
0.2
0.3
0.4
0.5
0.6
SUBSTRATE IS TUNGSTEN ADSORBATE IS SILICON

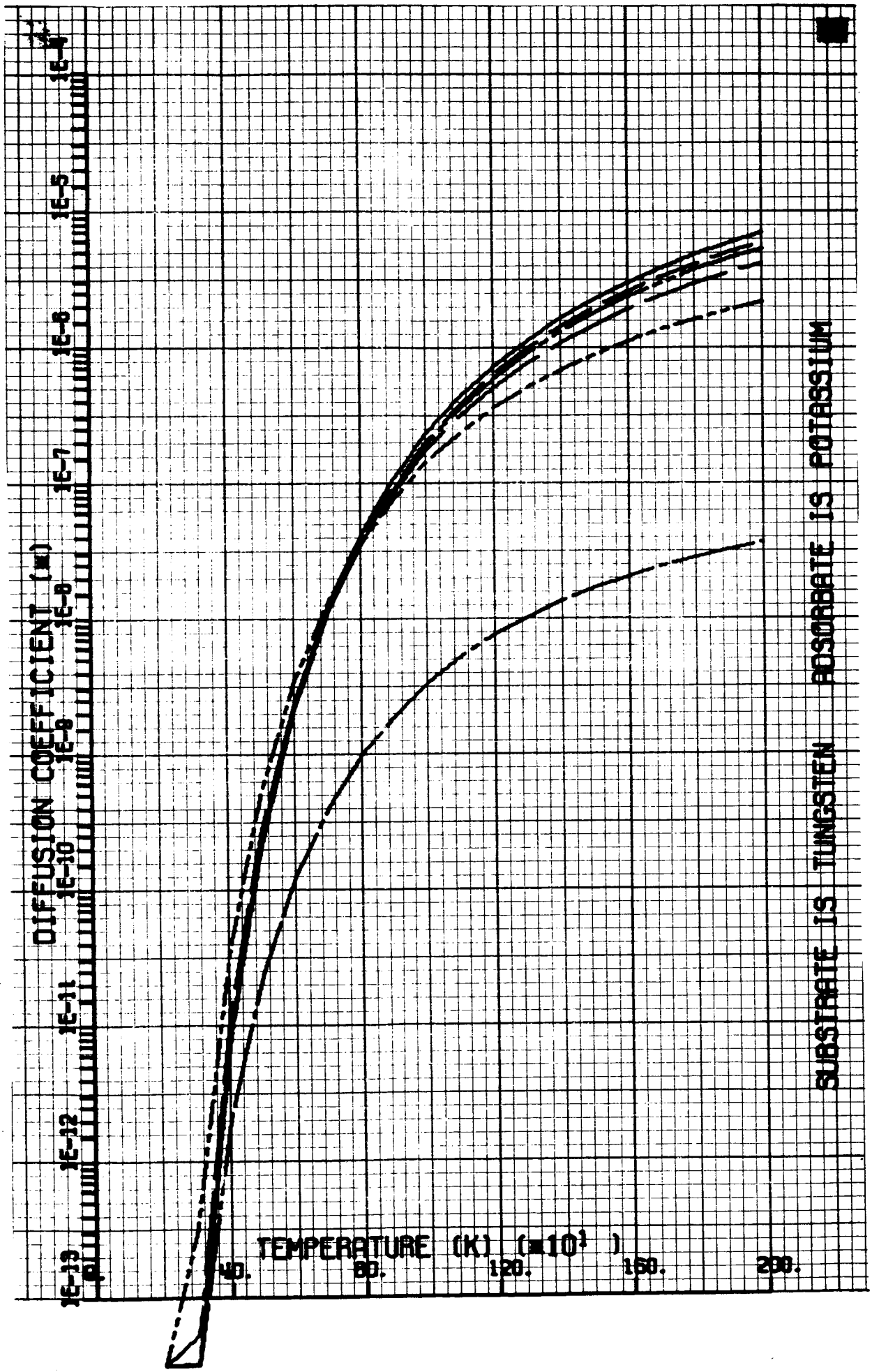
DIFFUSION COEFFICIENT (m²)
1E-4
1E-5
1E-6
1E-7
1E-8
1E-9
1E-10
1E-11
1E-12
1E-13
40.
80.
120.
160.
200.
TEMPERATURE (K) (×10¹)
SUBSTRATE IS TUNGSTEN ADSORBATE IS POTASSIUM

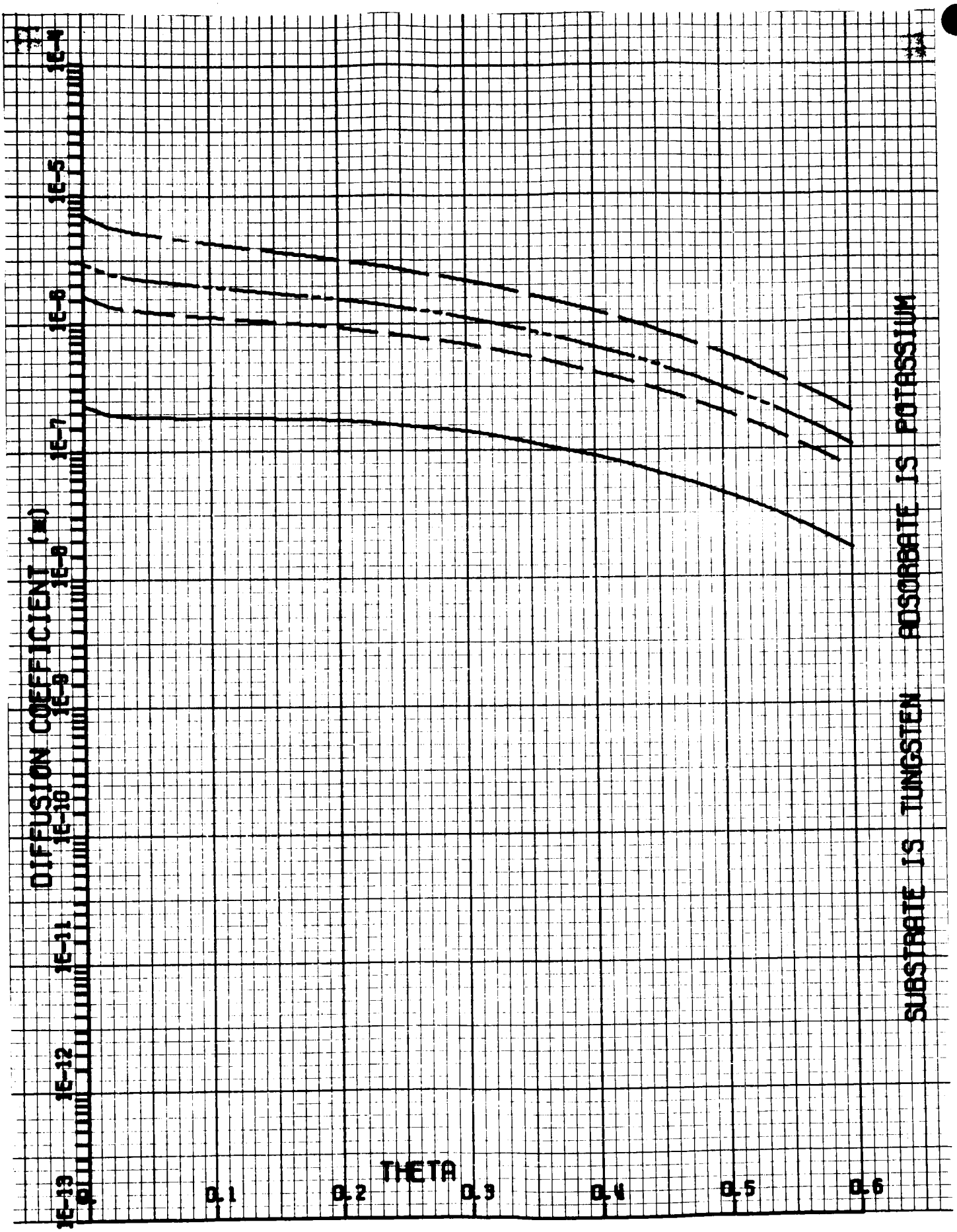
DIFFUSION COEFFICIENT (M²)
1E-4
1E-5
1E-6
1E-7
1E-8
1E-9
1E-10
1E-11
1E-12
1E-13
0
0.1
0.2
0.3
0.4
0.5
0.6
THETA
SUBSTRATE IS TUNGSTEN - ADSORBATE IS POTASSIUM

DIFFUSION COEFFICIENT (m²)
1E-4
1E-5
1E-6
1E-7
1E-8
1E-9
1E-10
1E-11
1E-12
1E-13
TEMPERATURE (K) (×10¹)
40.
80.
120.
160.
200.
SUBSTRATE IS TUNGSTEN ADSORBATE IS TITANIUM

DIFFUSION COEFFICIENT (M²)
1E-5
1E-6
1E-7
1E-8
1E-9
1E-10
1E-11
1E-12
1E-13
0
0.1
0.2
0.3
0.4
0.5
0.6
THETA
SUBSTRATE IS TUNGSTEN ADSORBATE IS TITANIUM

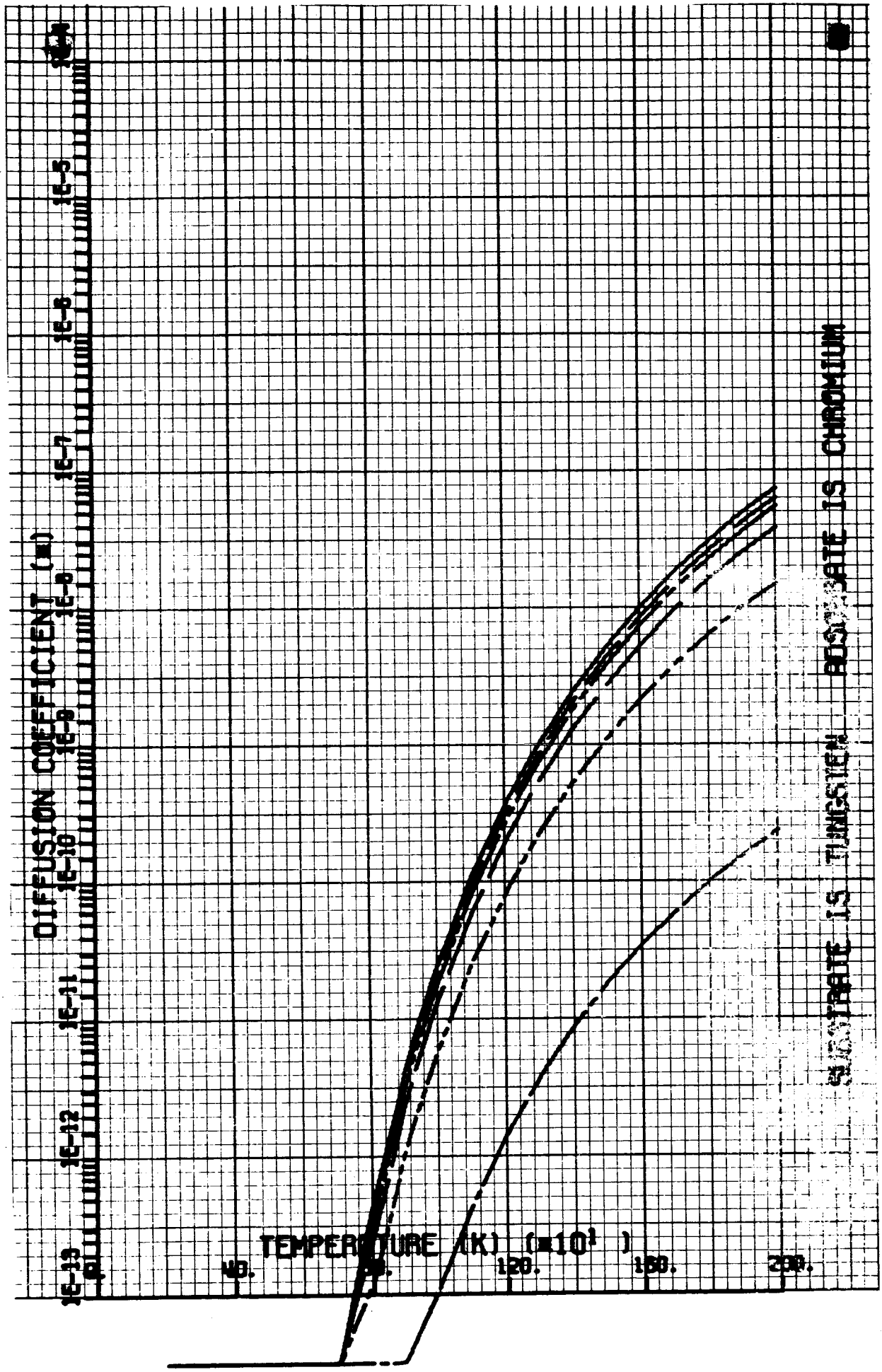
DIFFUSION COEFFICIENT (cm²)
1E-3
1E-5
1E-7
1E-9
1E-11
1E-12
1E-13
TEMPERATURE (K) (×10¹)
120.
160.
200.
SILICIDE IS TUNGSTEN DISILICATE IS CHROMIUM

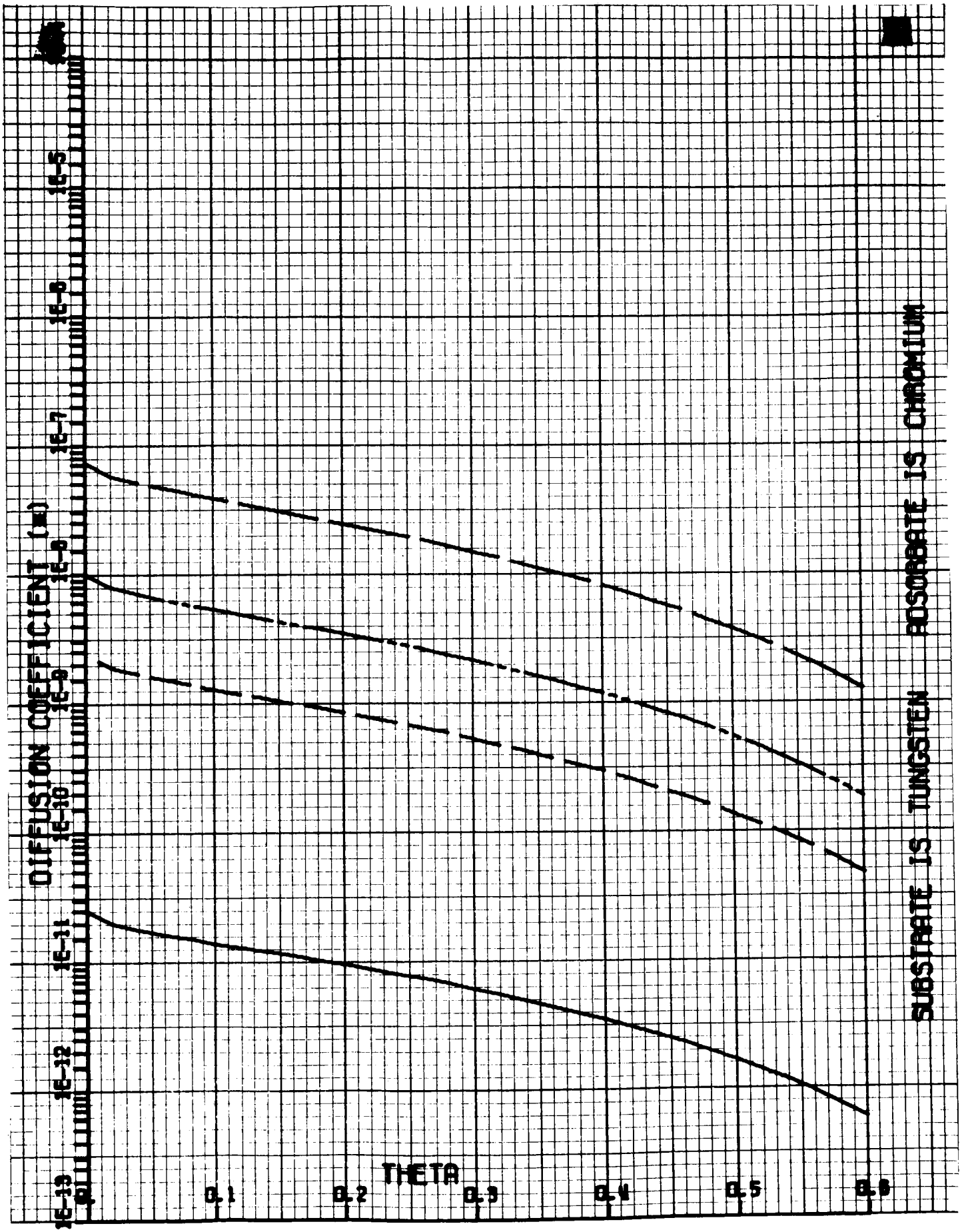
DIFFUSION COEFFICIENT (D)
1E-5
1E-6
1E-7
1E-8
1E-9
1E-10
1E-11
1E-12
1E-13
0
0.1
0.2
0.3
0.4
0.5
0.6
THETA
SUBSTRATE IS TUNGSTEN ADSORBATE IS CHROMIUM

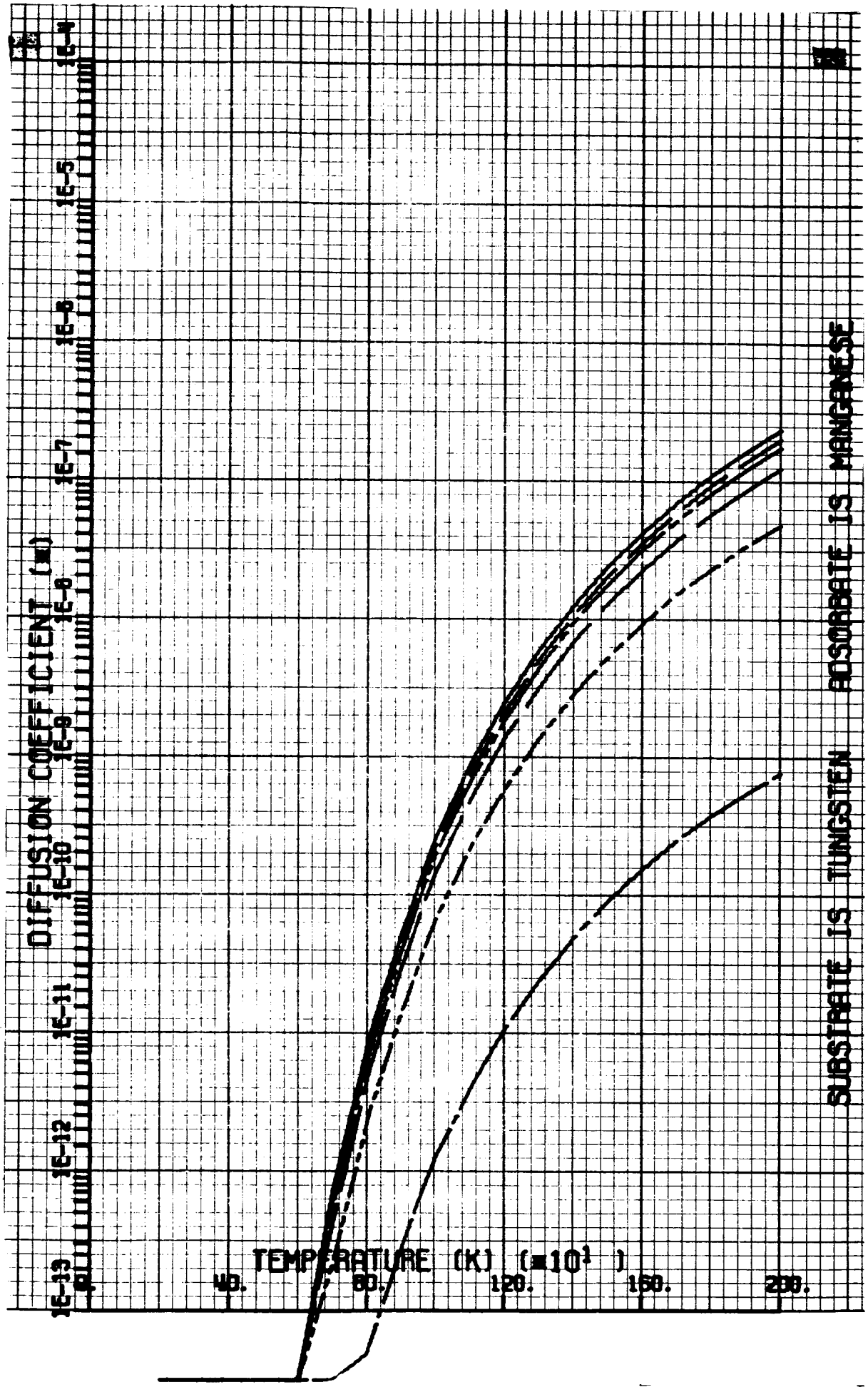
DIFFUSION COEFFICIENT (cm²)
1E-4
1E-5
1E-6
1E-7
1E-8
1E-9
1E-10
1E-11
1E-12
1E-13
TEMPERATURE (K) (×10¹)
40.
80.
120.
160.
200.
SUBSTRATE IS TUNGSTEN ADSORBATE IS MANGANESE

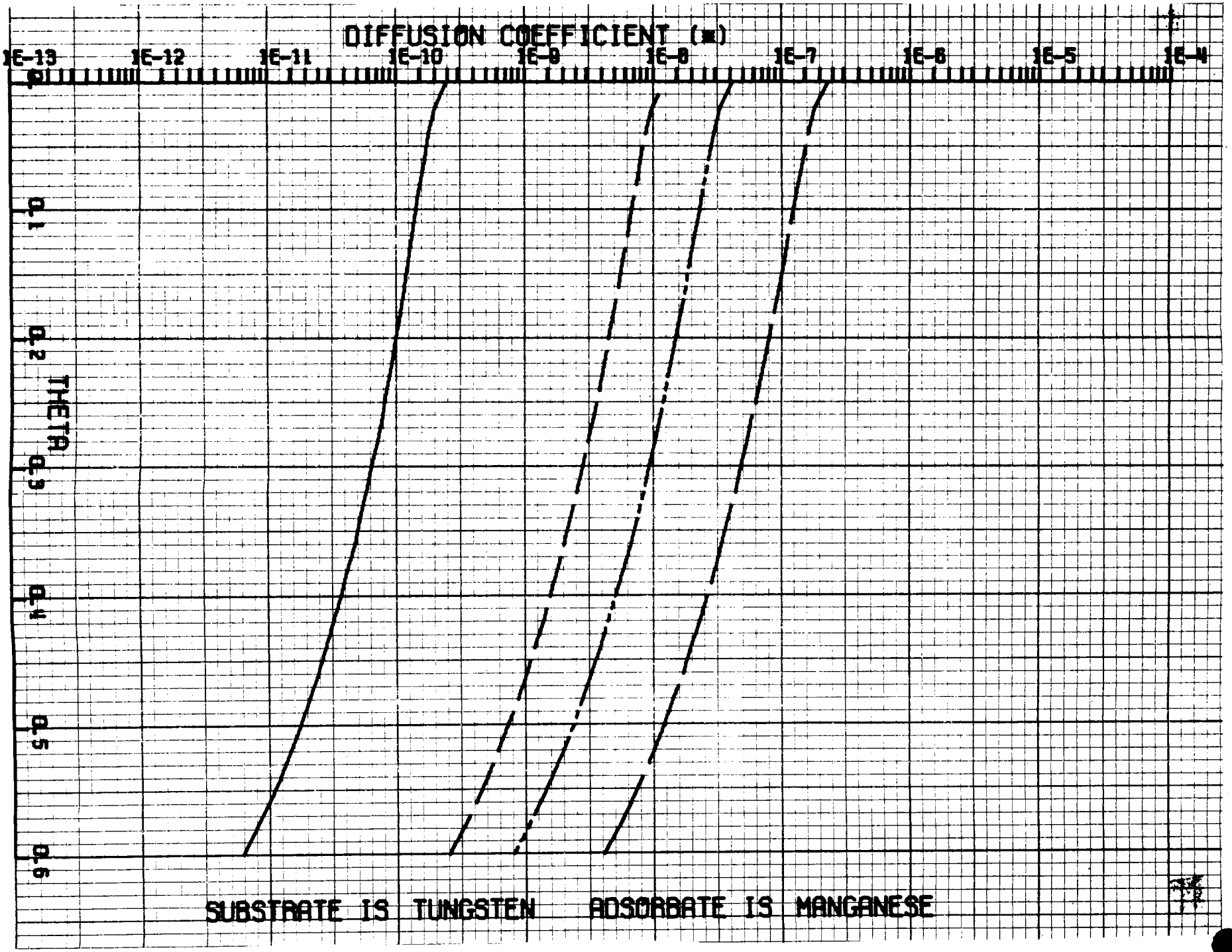
DIFFUSION COEFFICIENT (*)
1E-13
1E-12
1E-11
1E-10
1E-9
1E-8
1E-7
1E-6
1E-5
1E-4
THETA
SUBSTRATE IS TUNGSTEN ADSORBATE IS MANGANESE

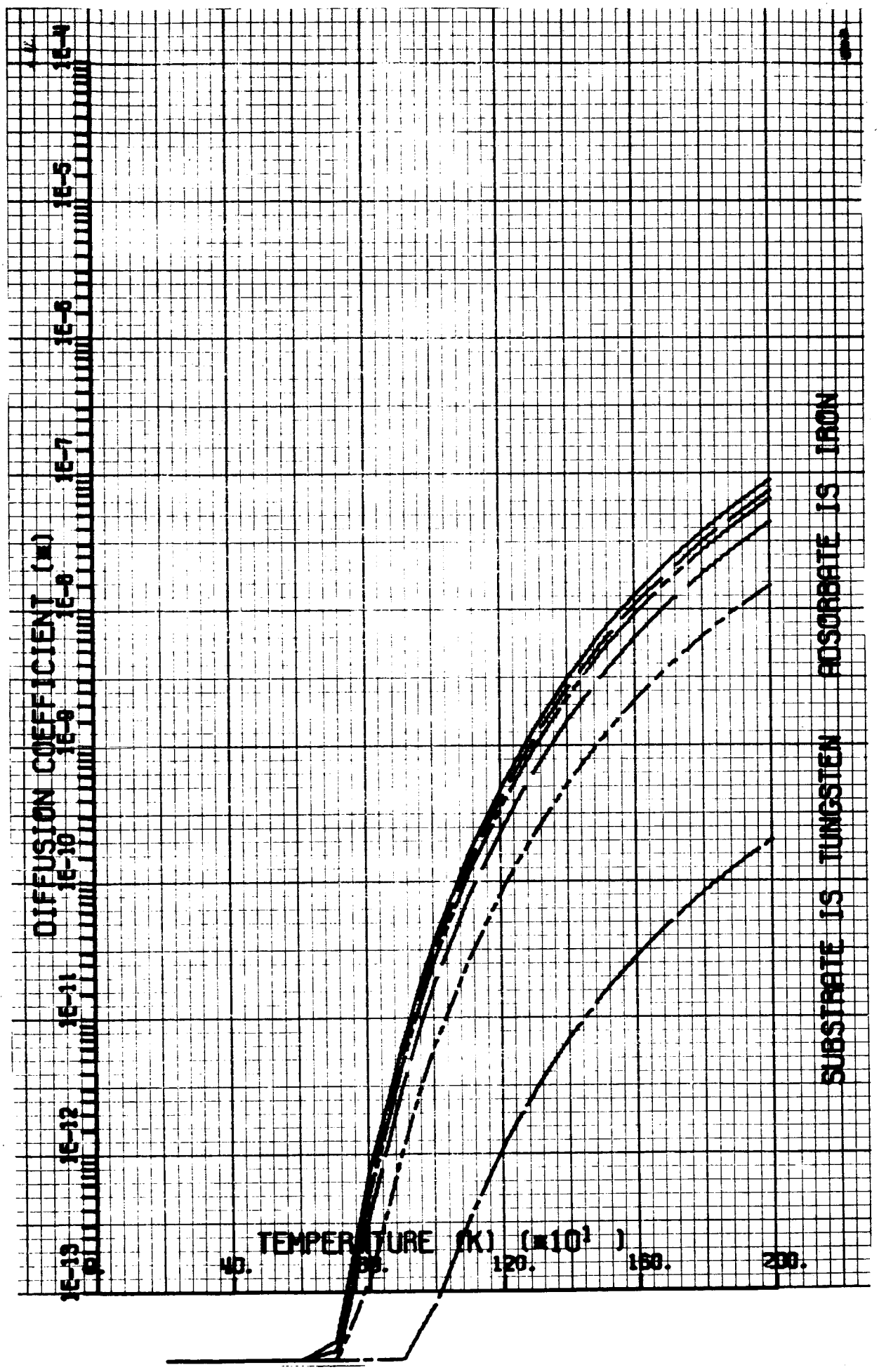
DIFFUSION COEFFICIENT (M²)
1E-4
1E-5
1E-6
1E-7
1E-8
1E-9
1E-10
1E-11
1E-12
1E-13
TEMPERATURE (K) (×10¹)
40.
80.
120.
160.
200.
SUBSTRATE IS TUNGSTEN ADSORBATE IS IRON

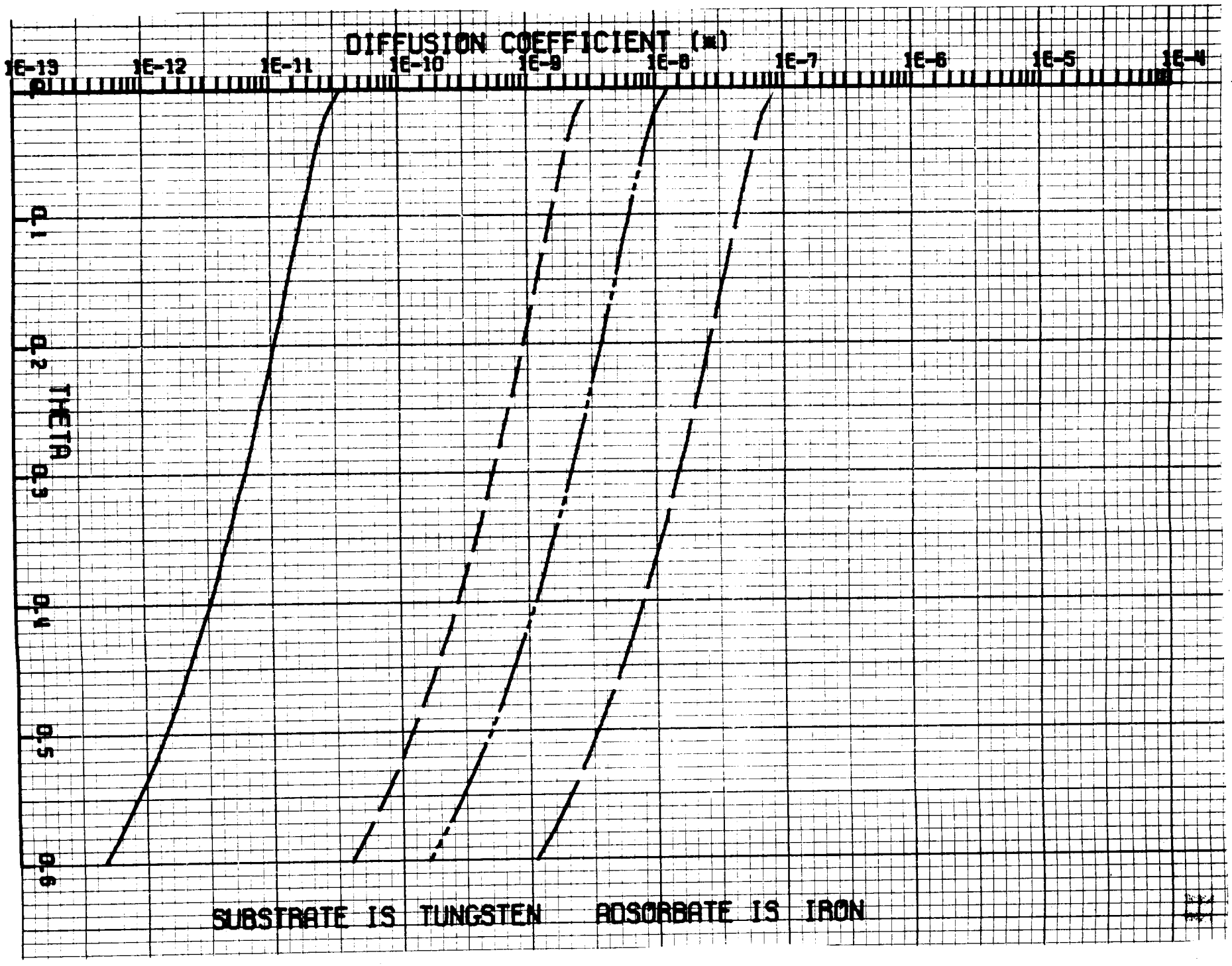
DIFFUSION COEFFICIENT (*)
1E-13
1E-12
1E-11
1E-10
1E-9
1E-8
1E-7
1E-6
1E-5
1E-4
THETA
0
0.1
0.2
0.3
0.4
0.5
0.6
SUBSTRATE IS TUNGSTEN ADSORBATE IS IRON

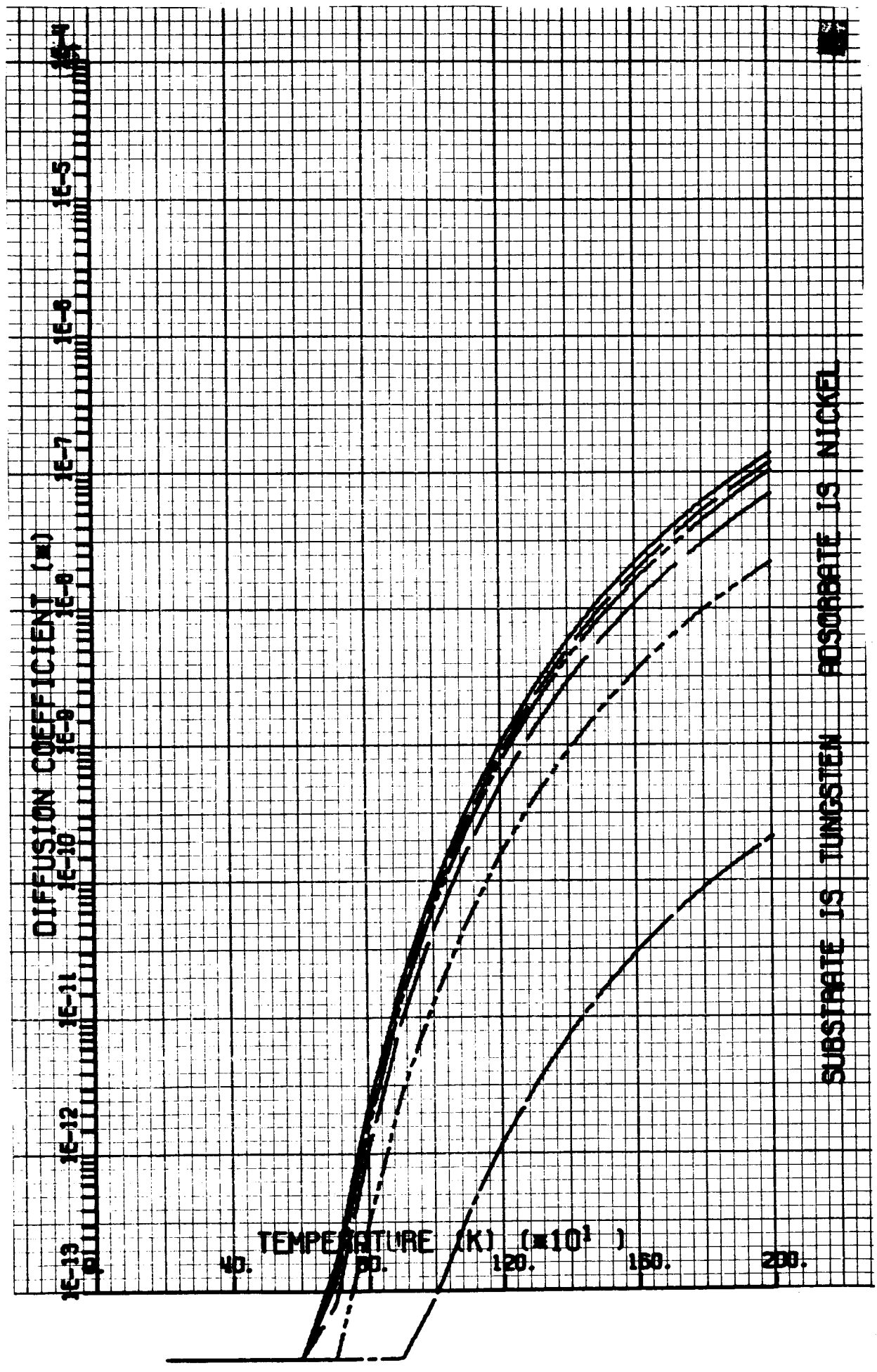
DIFFUSION COEFFICIENT (cm²)
1E-4
1E-5
1E-6
1E-7
1E-8
1E-9
1E-10
1E-11
1E-12
1E-13
TEMPERATURE (K) (×10¹)
40.
80.
120.
160.
200.
SUBSTRATE IS TUNGSTEN ADSORBATE IS NICKEL

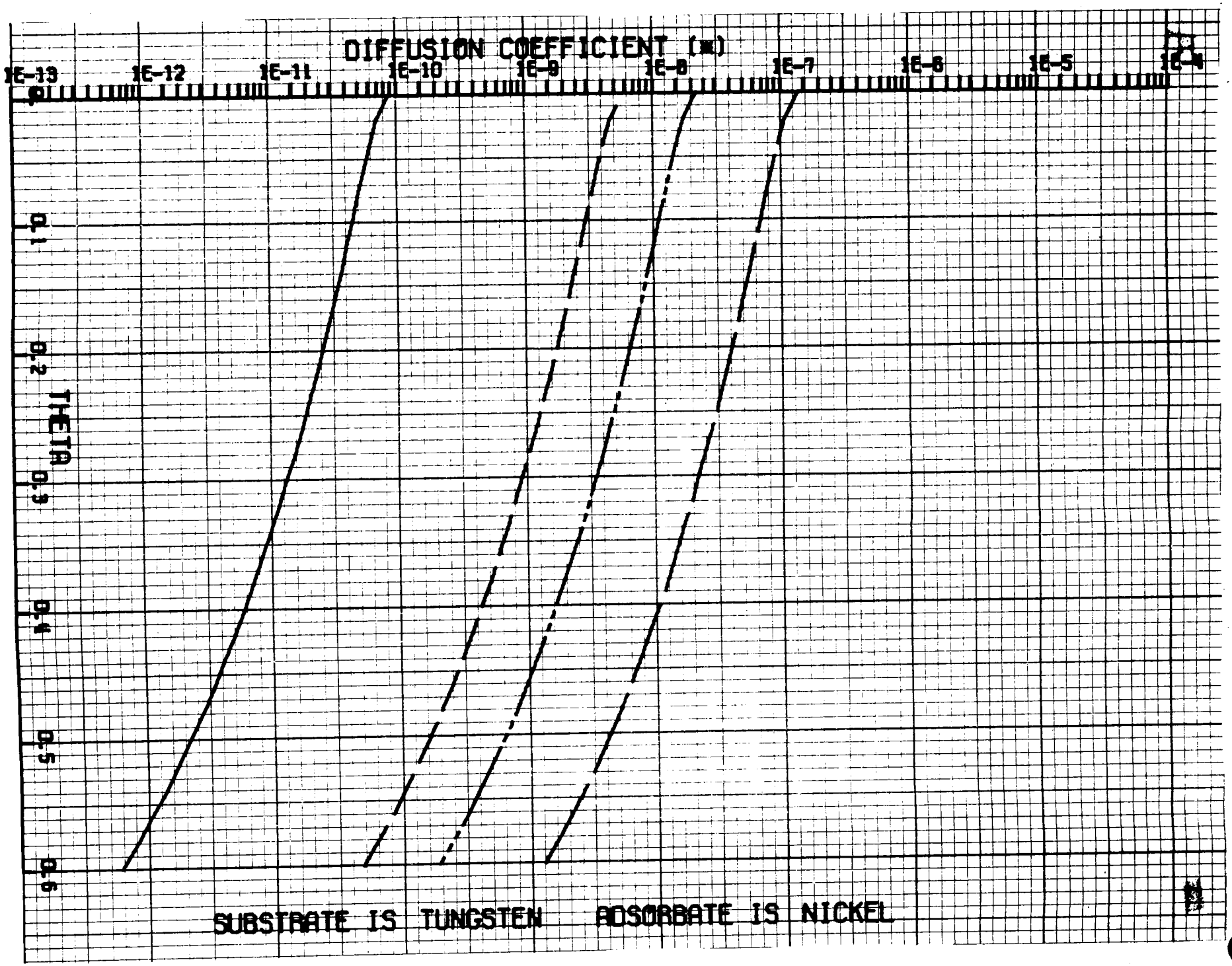
DIFFUSION COEFFICIENT (M)
1E-13
1E-12
1E-11
1E-10
1E-9
1E-8
1E-7
1E-6
1E-5
1E-4
THETA
0.1
0.2
0.3
0.4
0.5
0.6
SUBSTRATE IS TUNGSTEN ADSORBATE IS NICKEL

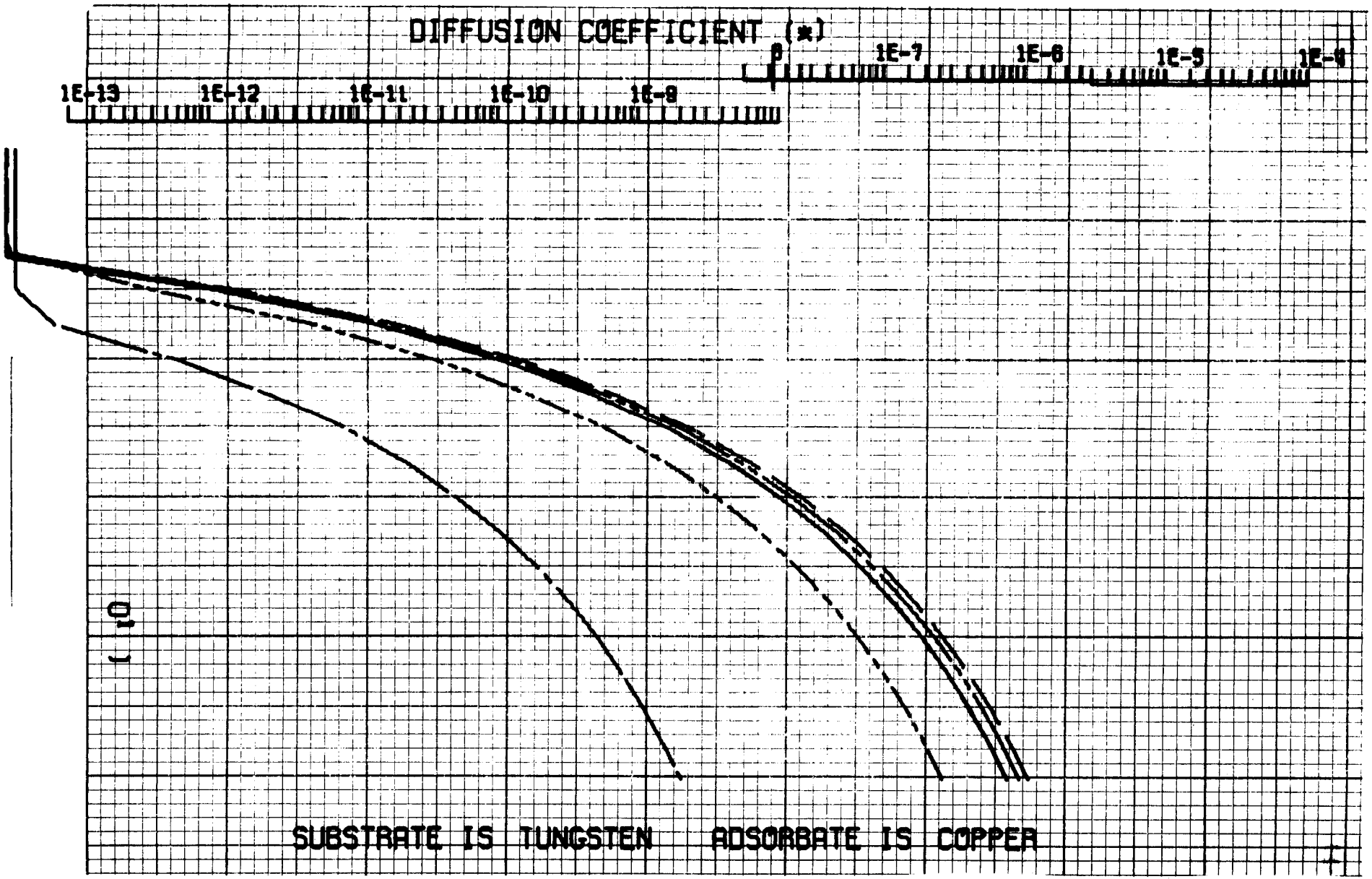
DIFFUSION COEFFICIENT (*)
1E-13
1E-12
1E-11
1E-10
1E-9
0
1E-7
1E-6
1E-5
1E-4
f(D)
SUBSTRATE IS TUNGSTEN ADSORBATE IS COPPER

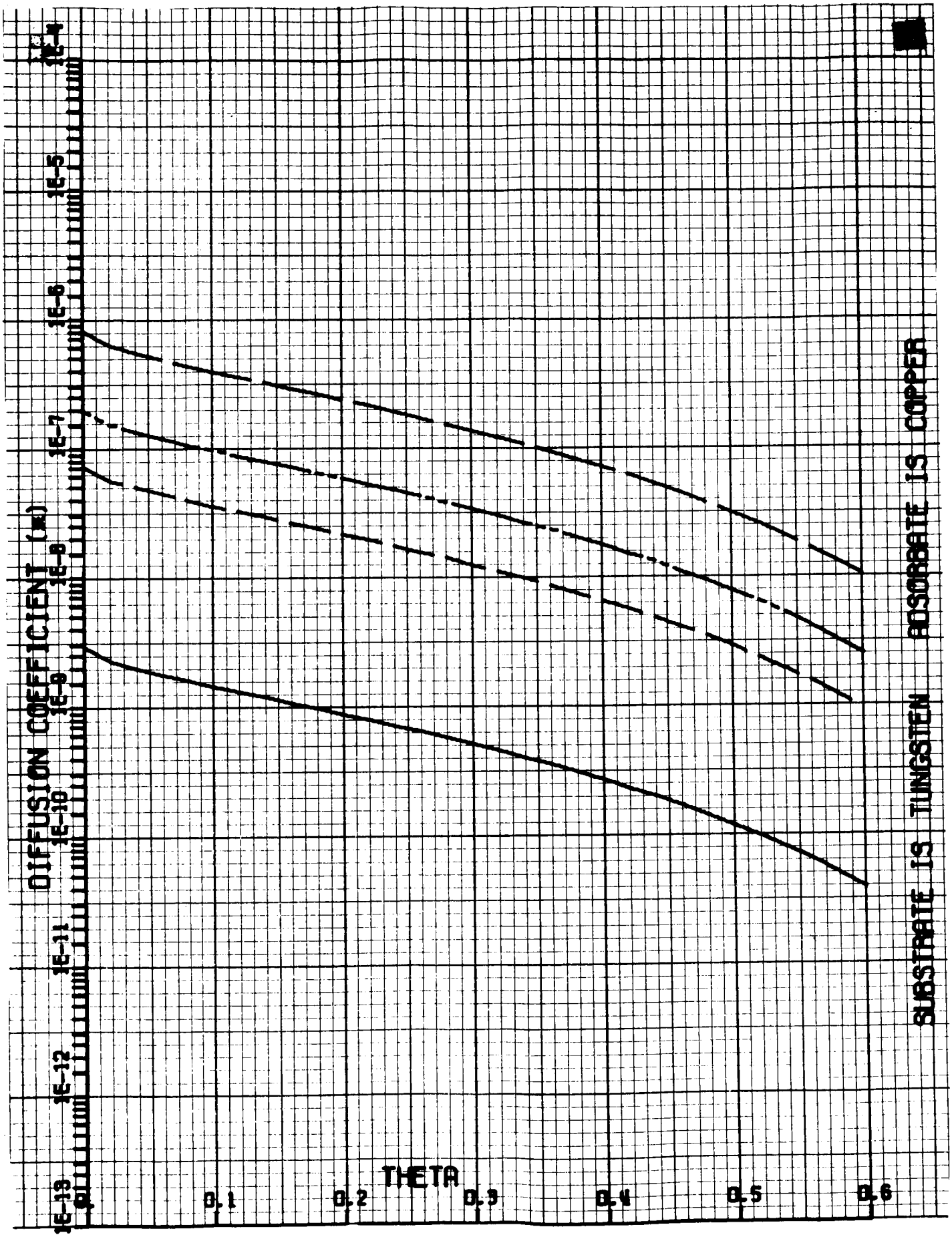
DIFFUSION COEFFICIENT (cm²)
1E-4
1E-5
1E-6
1E-7
1E-8
1E-9
1E-10
1E-11
1E-12
1E-13
0
0.1
0.2
0.3
0.4
0.5
0.6
THETA
SUBSTRATE IS TUNGSTEN ADSORBATE IS COPPER

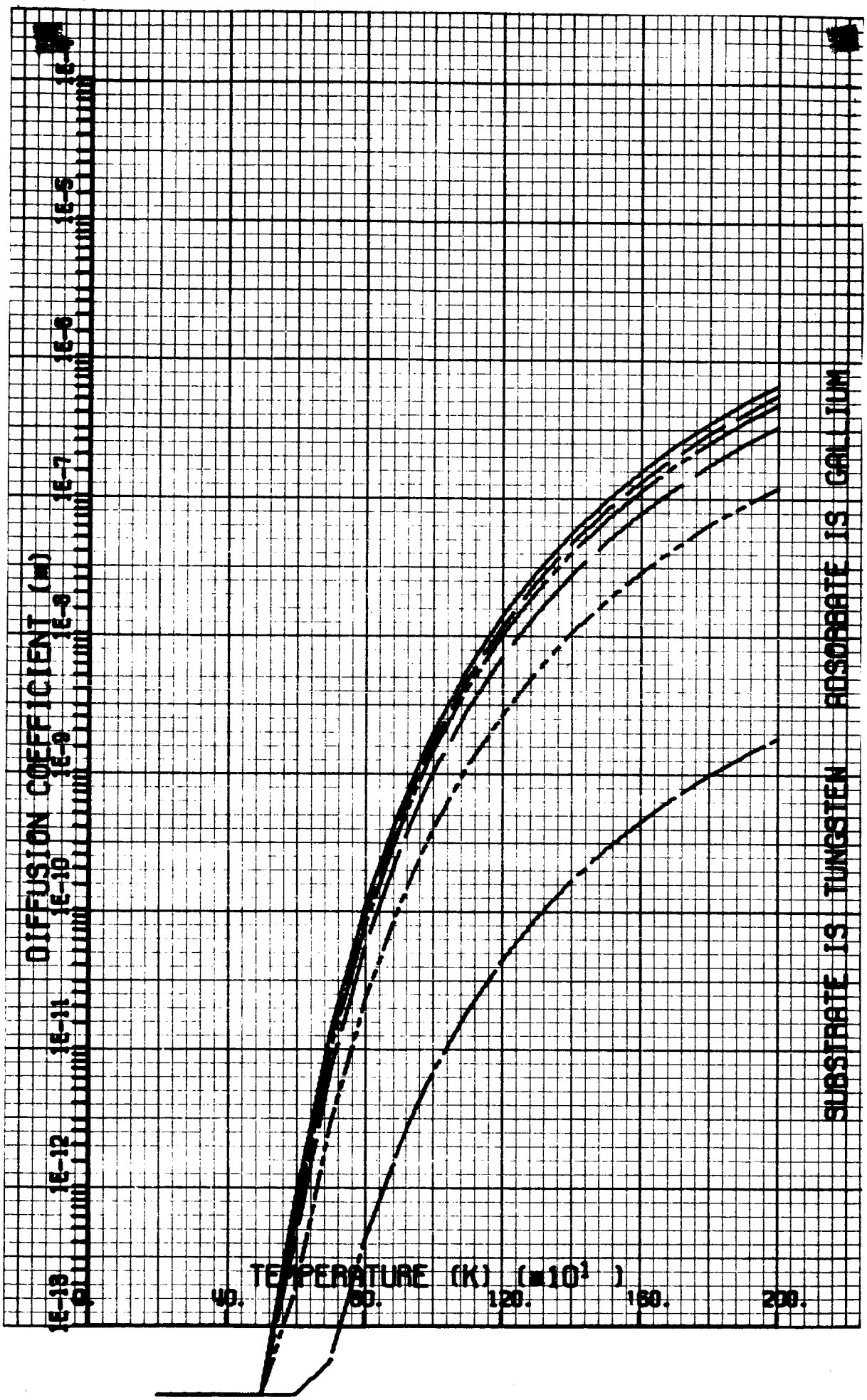
DIFFUSION COEFFICIENT (m²)
1E-4
1E-5
1E-6
1E-7
1E-8
1E-9
1E-10
1E-11
1E-12
1E-13
TEMPERATURE (K) (×10¹)
40.
80.
120.
160.
200.
SUBSTRATE IS TUNGSTEN ADSORBATE IS GALLIUM

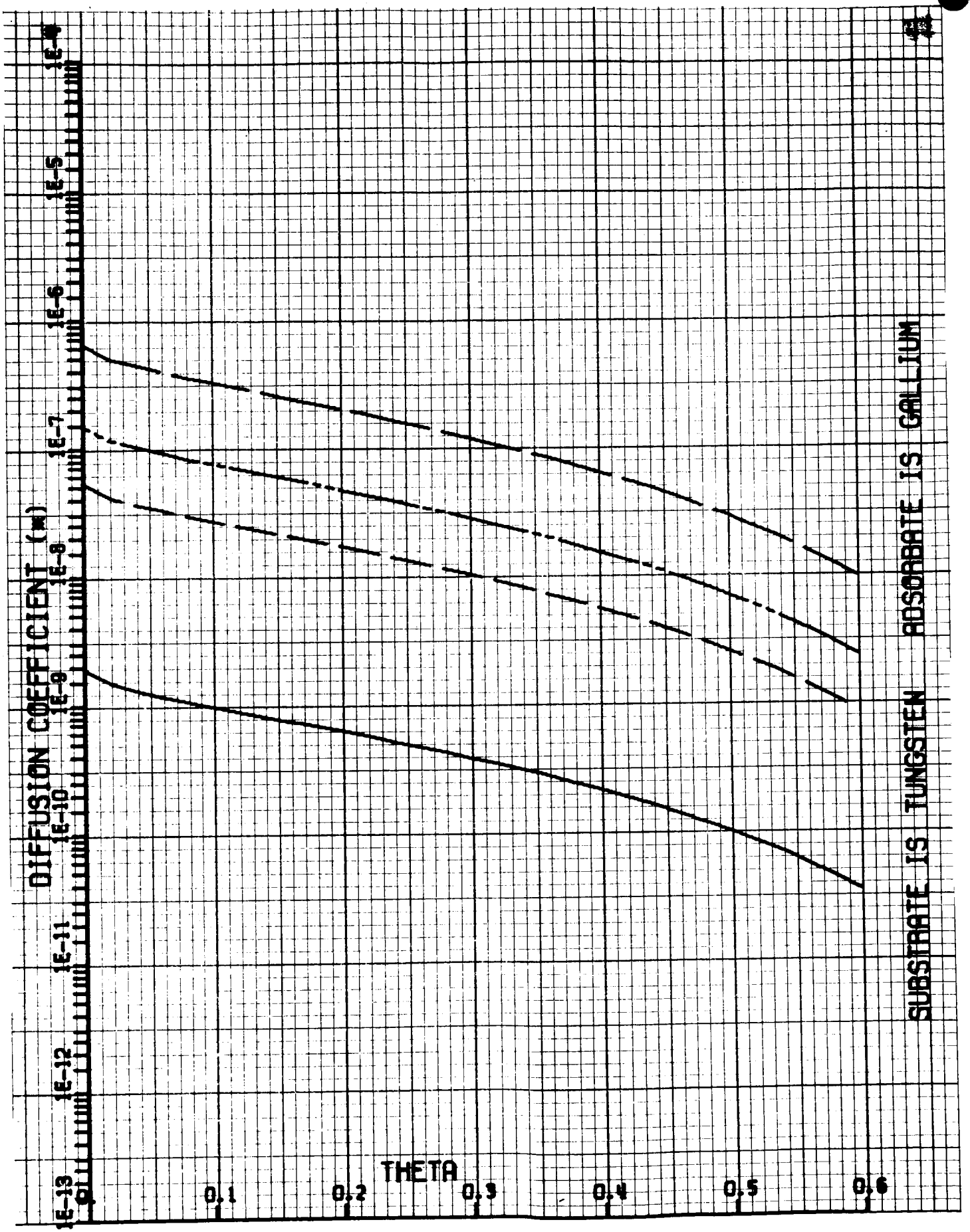
DIFFUSION COEFFICIENT (m)
1E-4
1E-5
1E-6
1E-7
1E-8
1E-9
1E-10
1E-11
1E-12
1E-13
THETA
0.1
0.2
0.3
0.4
0.5
0.6
SUBSTRATE IS TUNGSTEN ADSORBATE IS GALLIUM

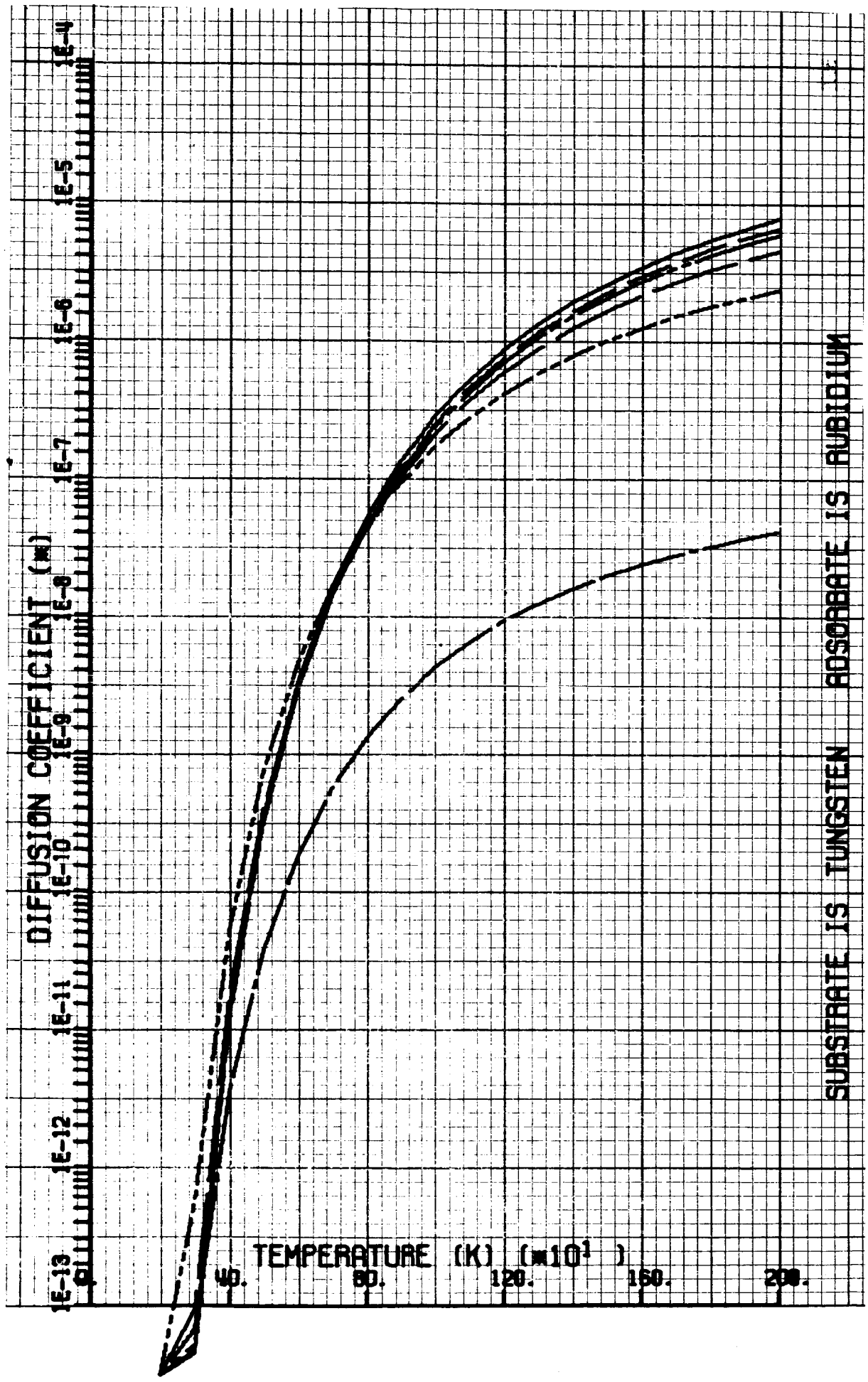
DIFFUSION COEFFICIENT (m)
1E-4
1E-5
1E-6
1E-7
1E-8
1E-9
1E-10
1E-11
1E-12
1E-13
TEMPERATURE (K) (*10¹)
40.
80.
120.
160.
200.
SUBSTRATE IS TUNGSTEN ADSORBATE IS RUBIDIUM

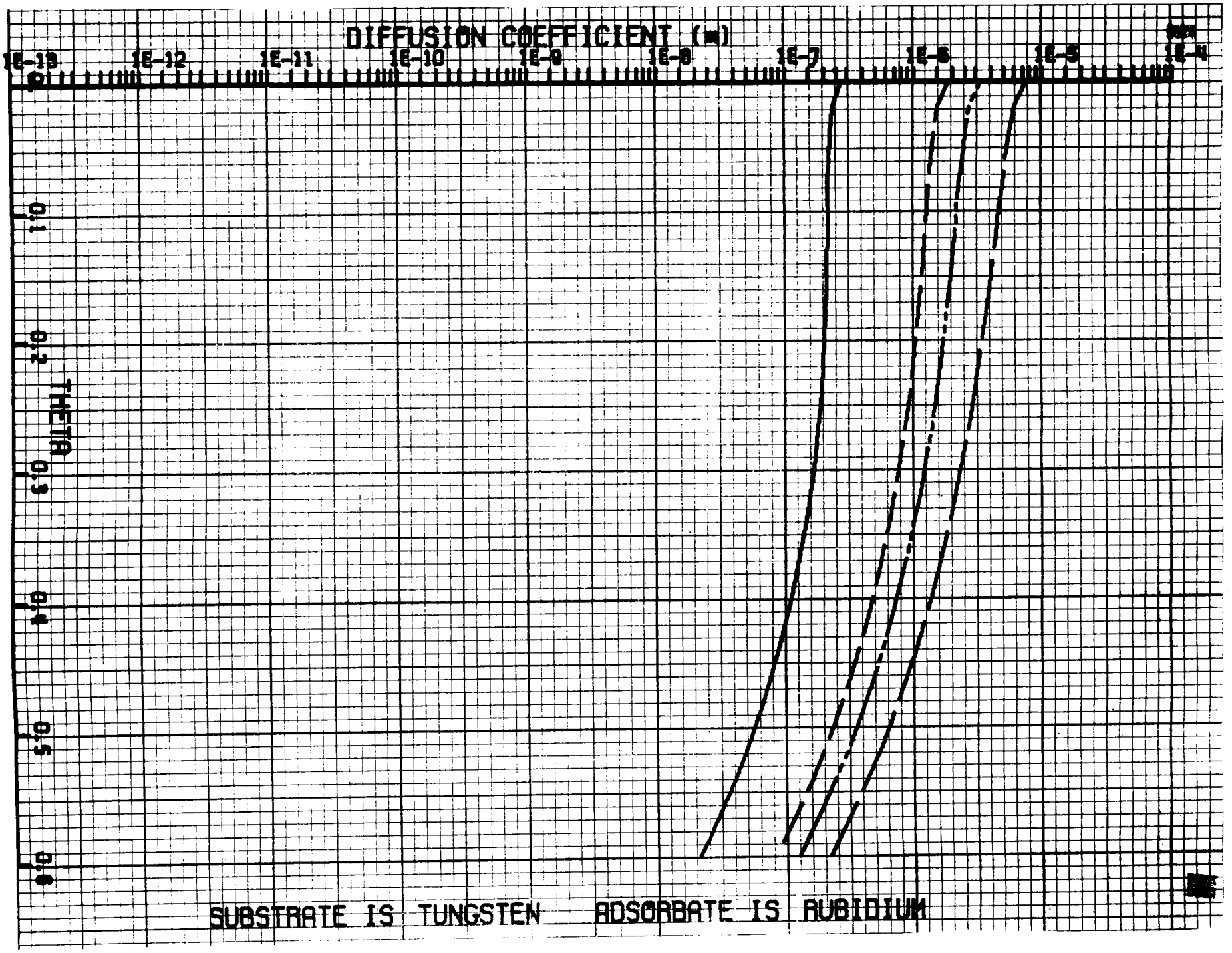
DIFFUSION COEFFICIENT (m)
1E-13
1E-12
1E-11
1E-10
1E-9
1E-8
1E-7
1E-6
1E-5
1E-4
THETA
0.1
0.2
0.3
0.4
0.5
0.6
SUBSTRATE IS TUNGSTEN ADSORBATE IS RUBIDIUM

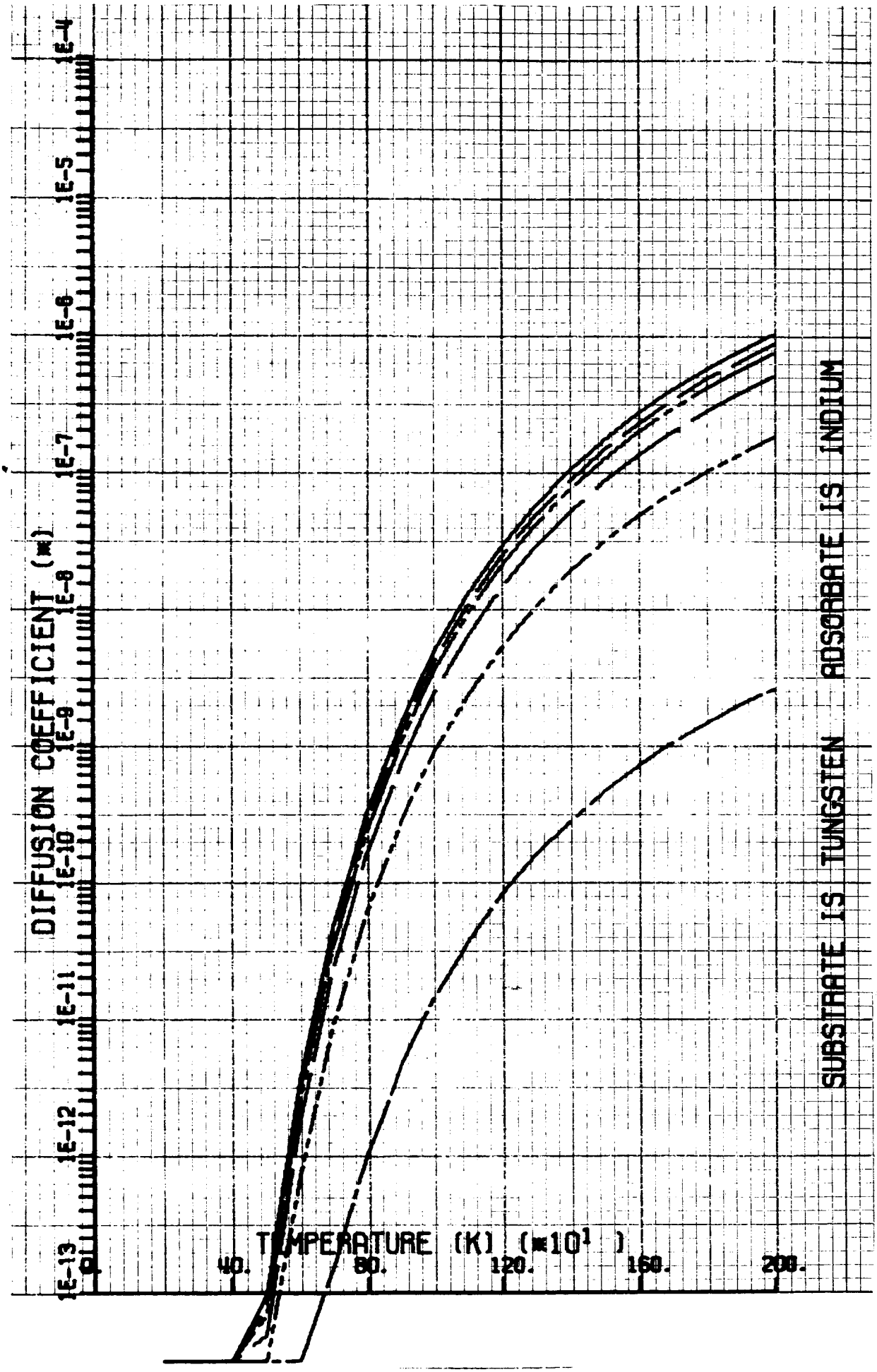
DIFFUSION COEFFICIENT (*)
1E-4
1E-5
1E-6
1E-7
1E-8
1E-9
1E-10
1E-11
1E-12
1E-13
TEMPERATURE (K) (*10^1)
40.
80.
120.
160.
200.
SUBSTRATE IS TUNGSTEN ADSORBATE IS INDIUM

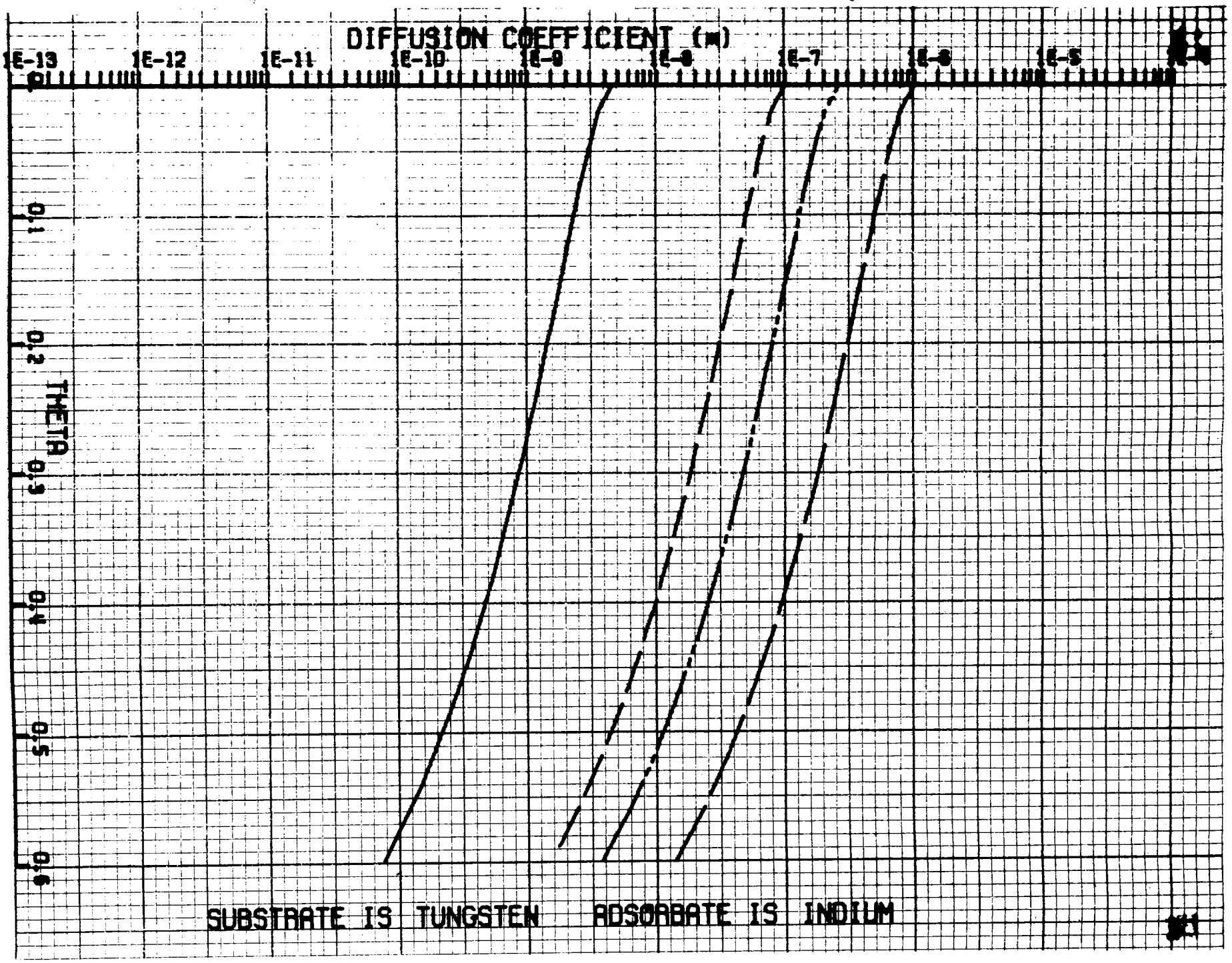
DIFFUSION COEFFICIENT (m)
1E-13
1E-12
1E-11
1E-10
1E-9
1E-8
1E-7
1E-6
1E-5
0.1
0.2
THETA
0.3
0.4
0.5
0.6
SUBSTRATE IS TUNGSTEN ADSORBATE IS INDIUM

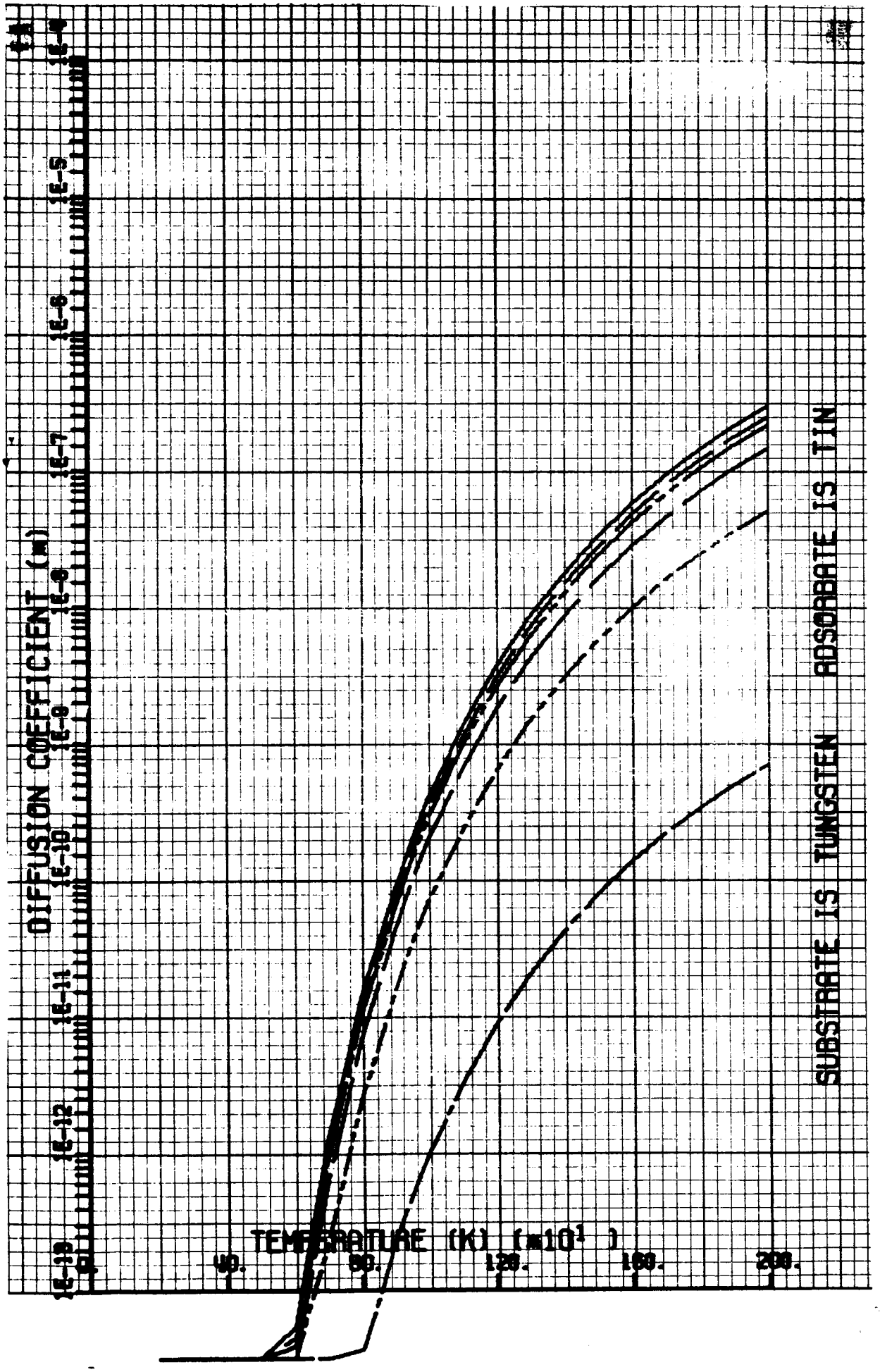
DIFFUSION COEFFICIENT (m)
1E-4
1E-5
1E-6
1E-7
1E-8
1E-9
1E-10
1E-11
1E-12
1E-13
40.
80.
120.
160.
200.
TEMPERATURE (K) (*10¹)
SUBSTRATE IS TUNGSTEN ADSORBATE IS TIN

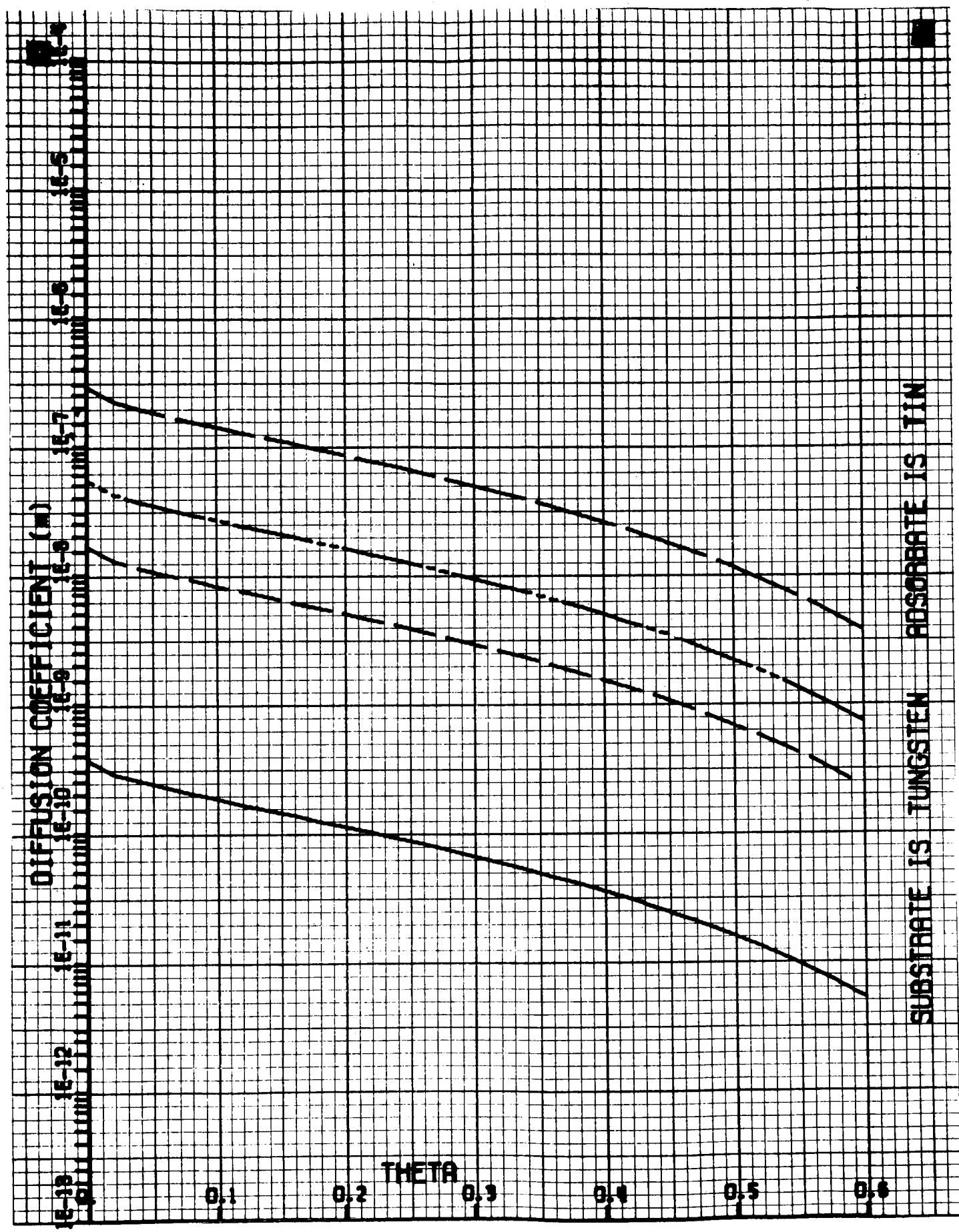
DIFFUSION COEFFICIENT (m)
1E-13
1E-12
1E-11
1E-10
1E-9
1E-8
1E-7
1E-6
1E-5
1E-4
0
0.1
0.2
0.3
0.4
0.5
0.6
THETA
SUBSTRATE IS TUNGSTEN ADSORBATE IS TIN

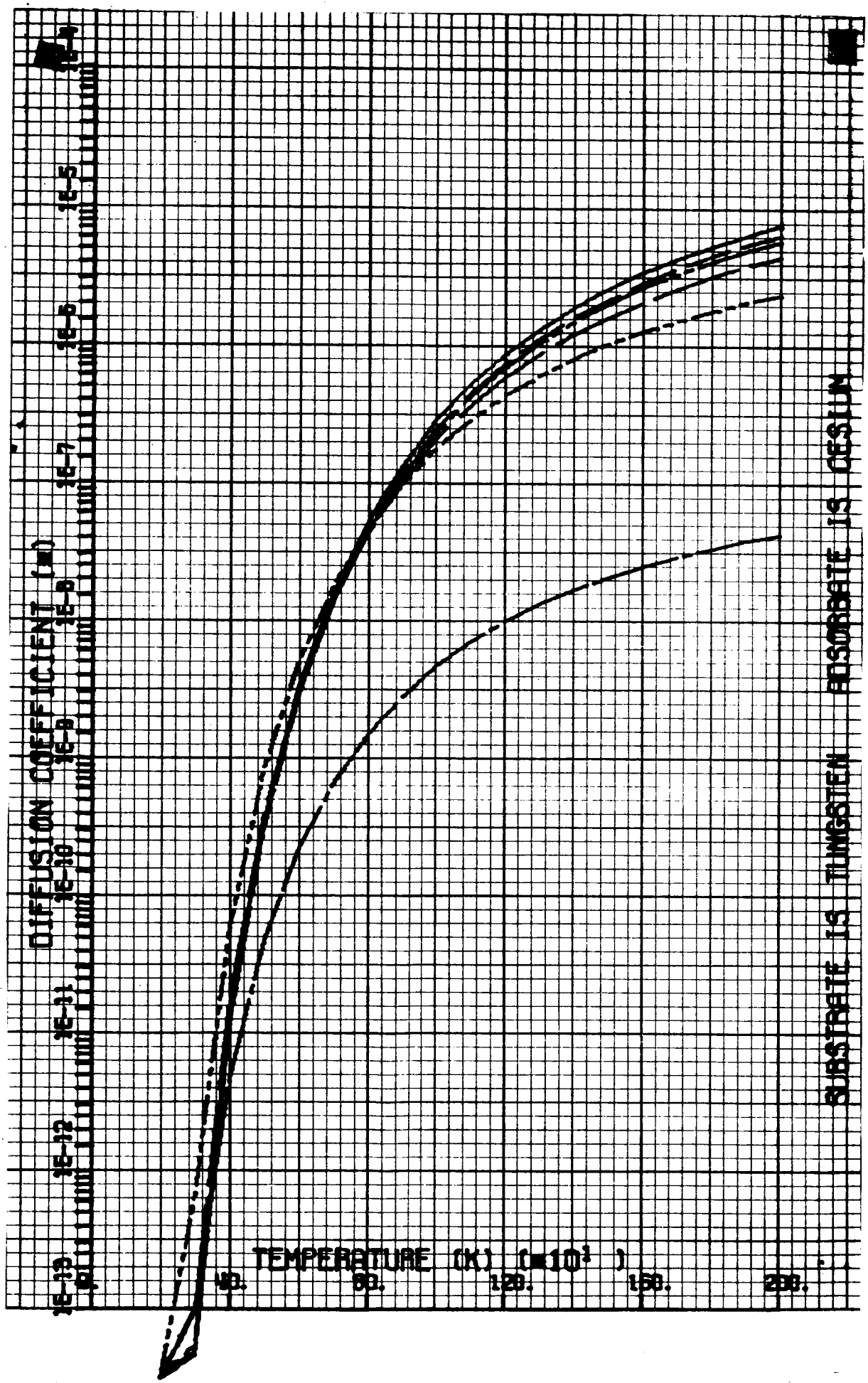
DIFFUSION COEFFICIENT (M²)
1E-3
1E-4
1E-5
1E-6
1E-7
1E-8
1E-9
1E-10
1E-11
1E-12
1E-13
TEMPERATURE (K) (×10³)
40.
80.
120.
160.
200.
SUBSTRATE IS TUNGSTEN ADSORBATE IS OESLIN

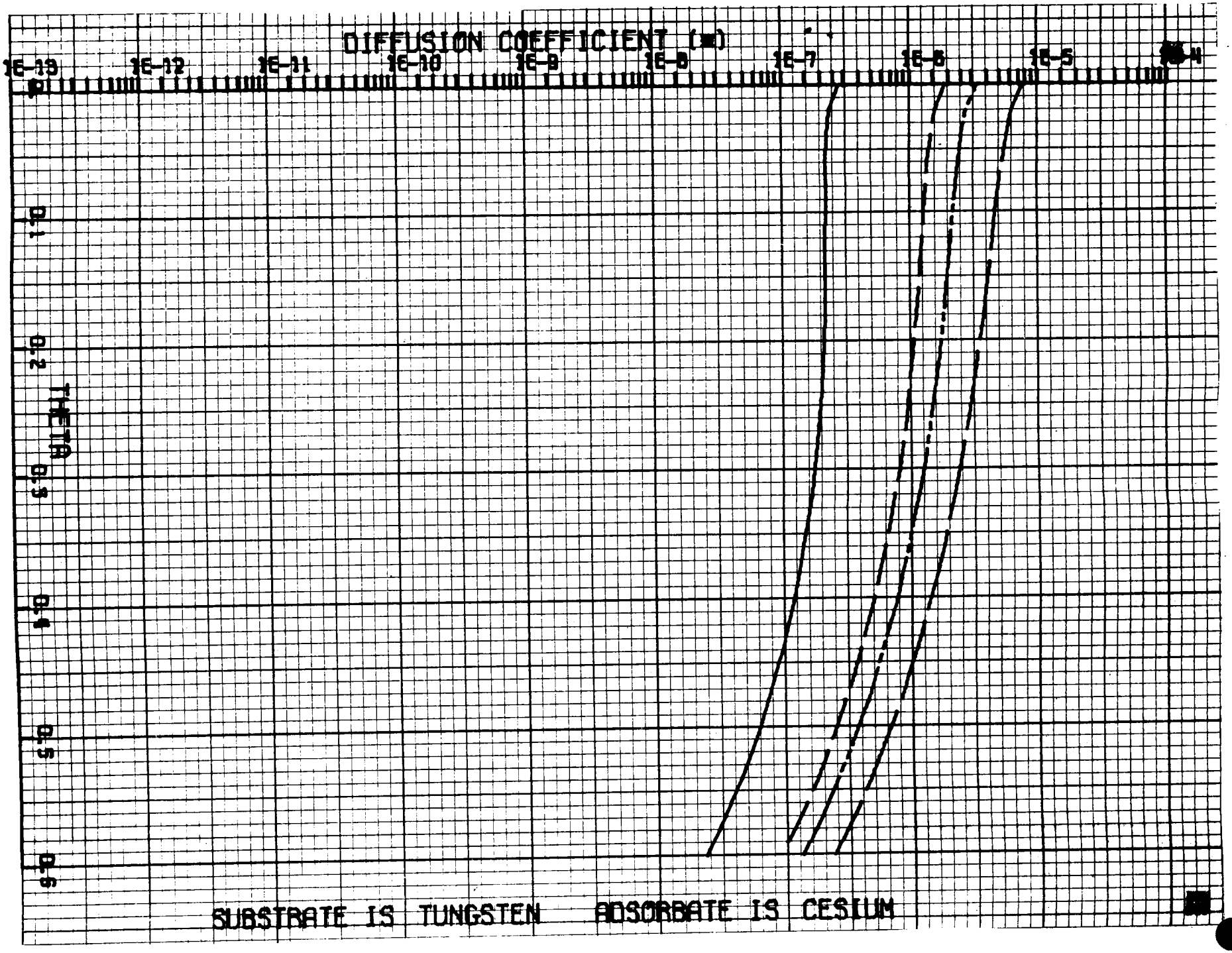
DIFFUSION COEFFICIENT (
1E-13
1E-12
1E-11
1E-10
1E-9
1E-8
1E-7
1E-6
1E-5
THETA
0.1
0.2
0.3
0.4
0.5
0.6
SUBSTRATE IS TUNGSTEN ADSORBATE IS CESIUM

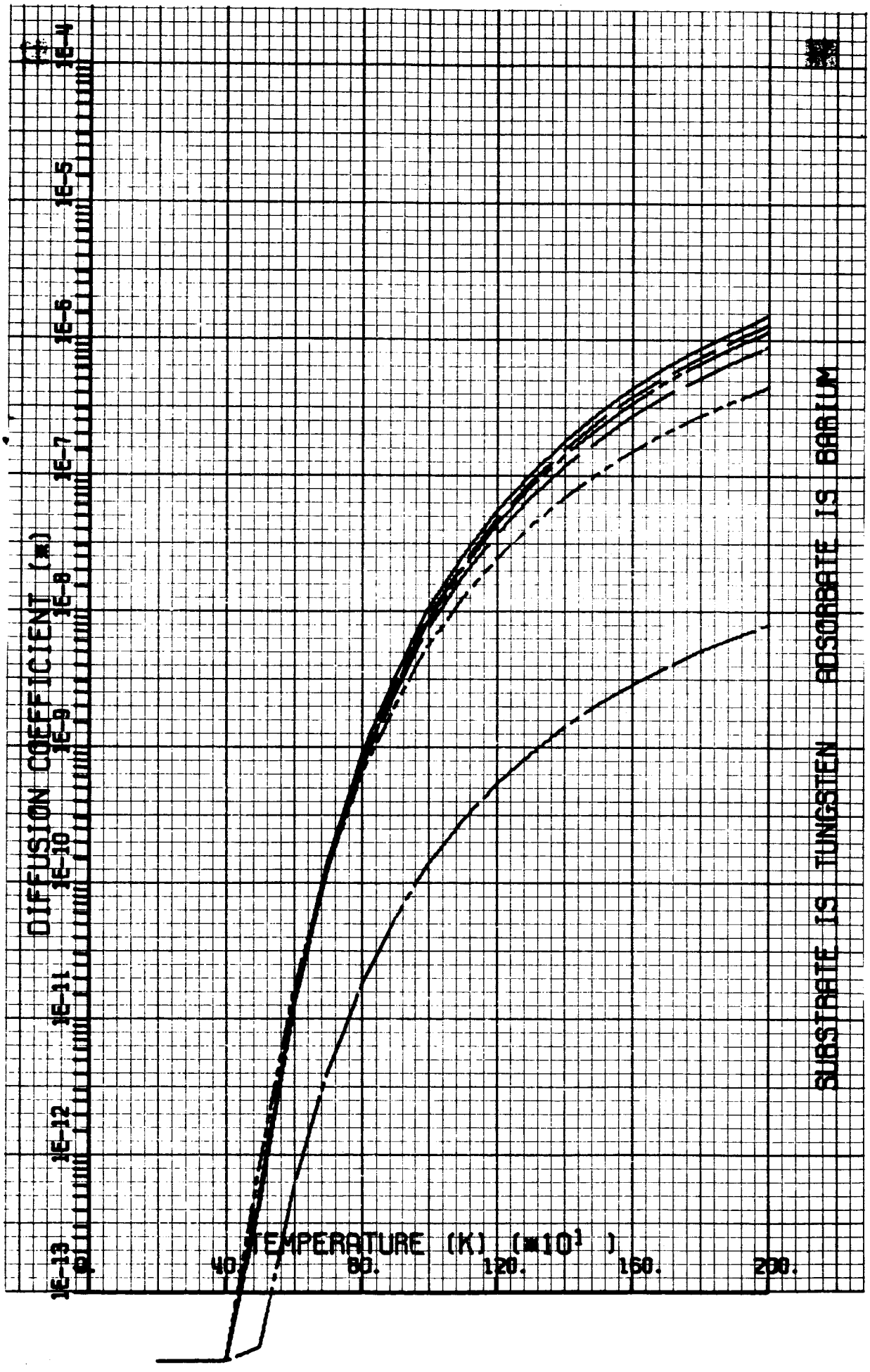
DIFFUSION COEFFICIENT (cm²)
1E-4
1E-5
1E-6
1E-7
1E-8
1E-9
1E-10
1E-11
1E-12
1E-13
TEMPERATURE (K) (×10¹)
40.
80.
120.
160.
200.
SUBSTRATE IS TUNGSTEN ADSORBATE IS BARIUM

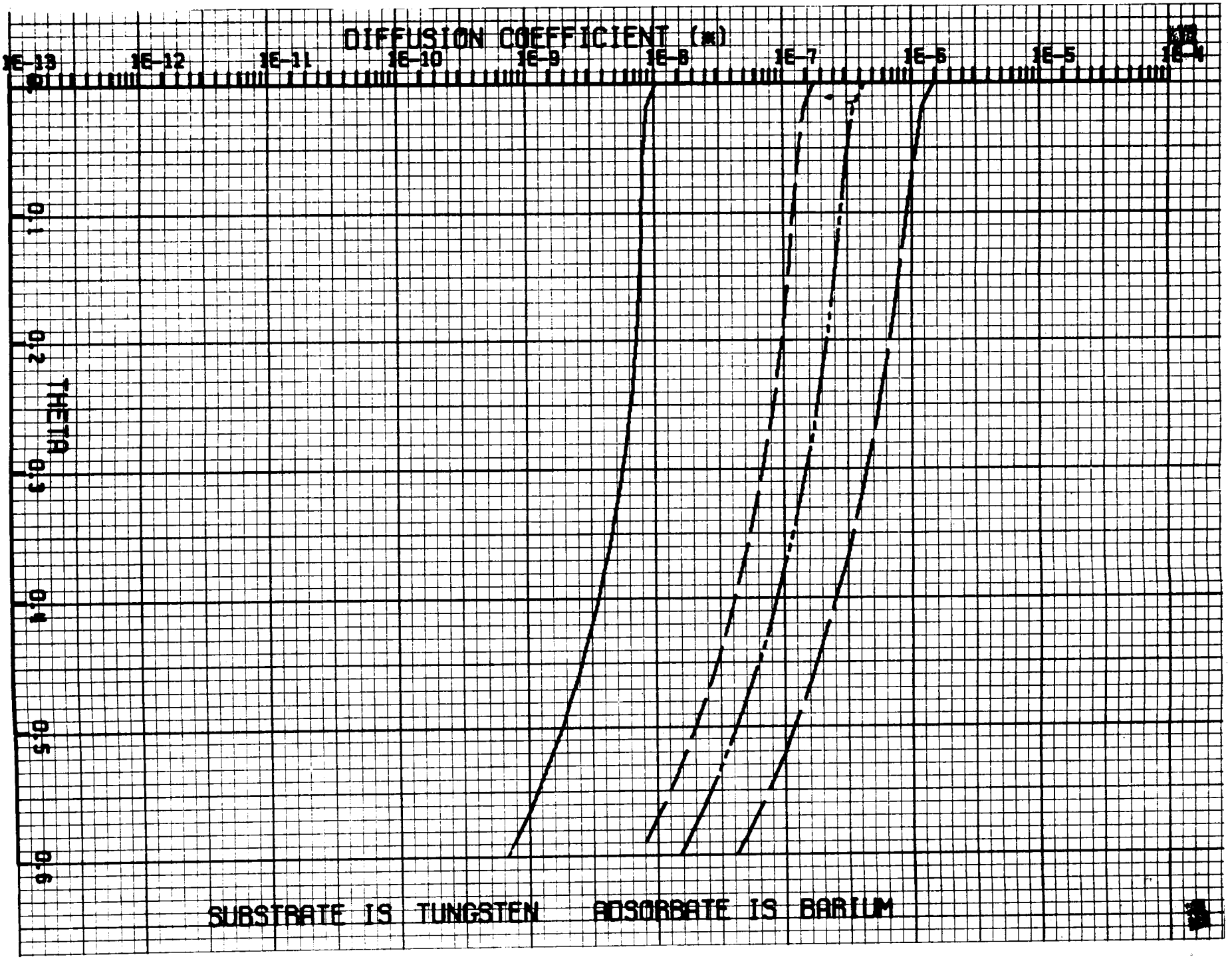
DIFFUSION COEFFICIENT (m)
1E-13
1E-12
1E-11
1E-10
1E-9
1E-8
1E-7
1E-6
1E-5
1E-4
0.1
0.2
0.3
0.4
0.5
0.6
THETA
SUBSTRATE IS TUNGSTEN ADSORBATE IS BARIUM

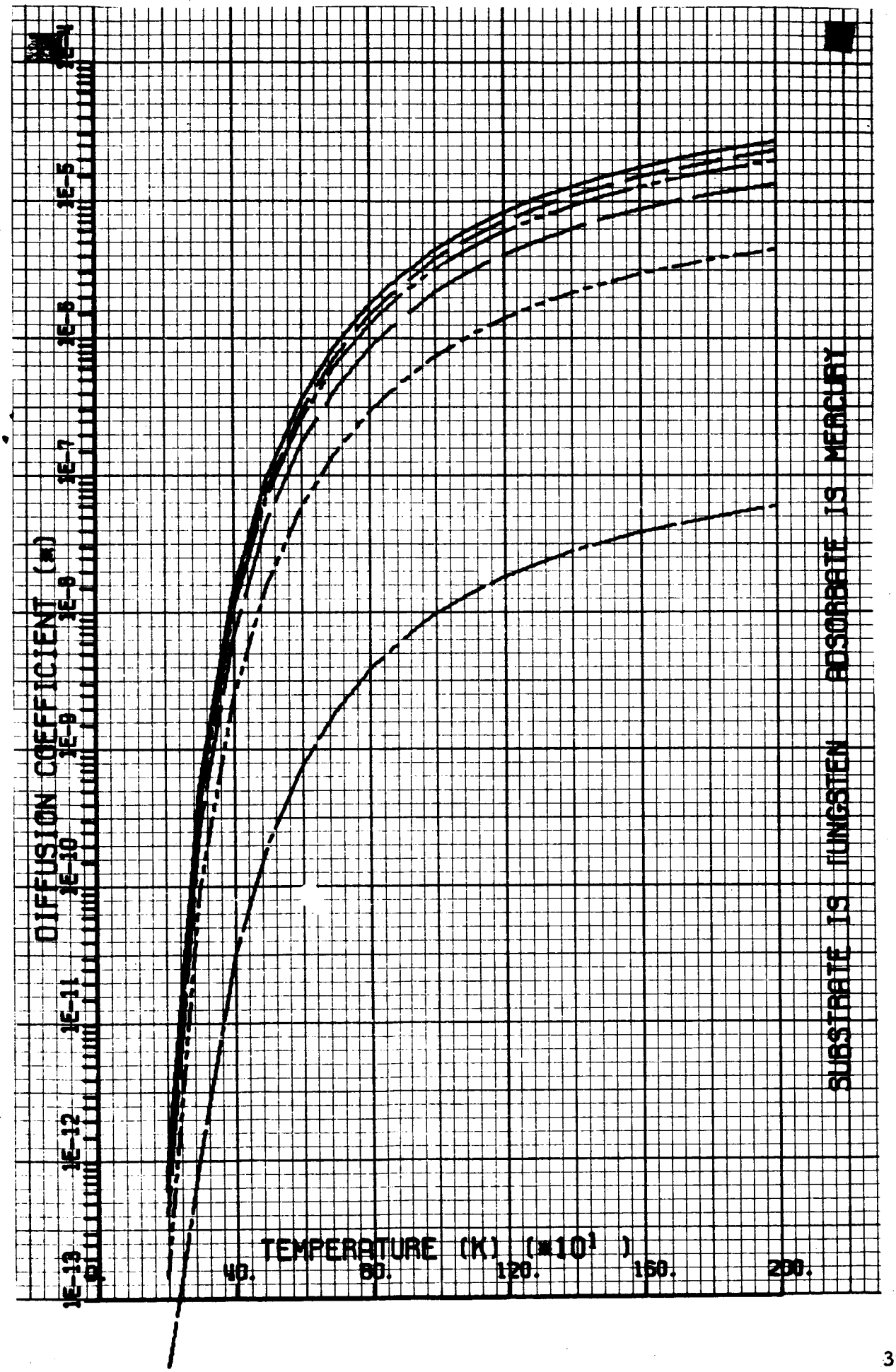
DIFFUSION COEFFICIENT (m)
1E-5
1E-6
1E-7
1E-8
1E-9
1E-10
1E-11
1E-12
1E-13
TEMPERATURE (K) (*10¹)
40.
80.
120.
160.
200.
SUBSTRATE IS TUNGSTEN ADSORBATE IS MERCURY

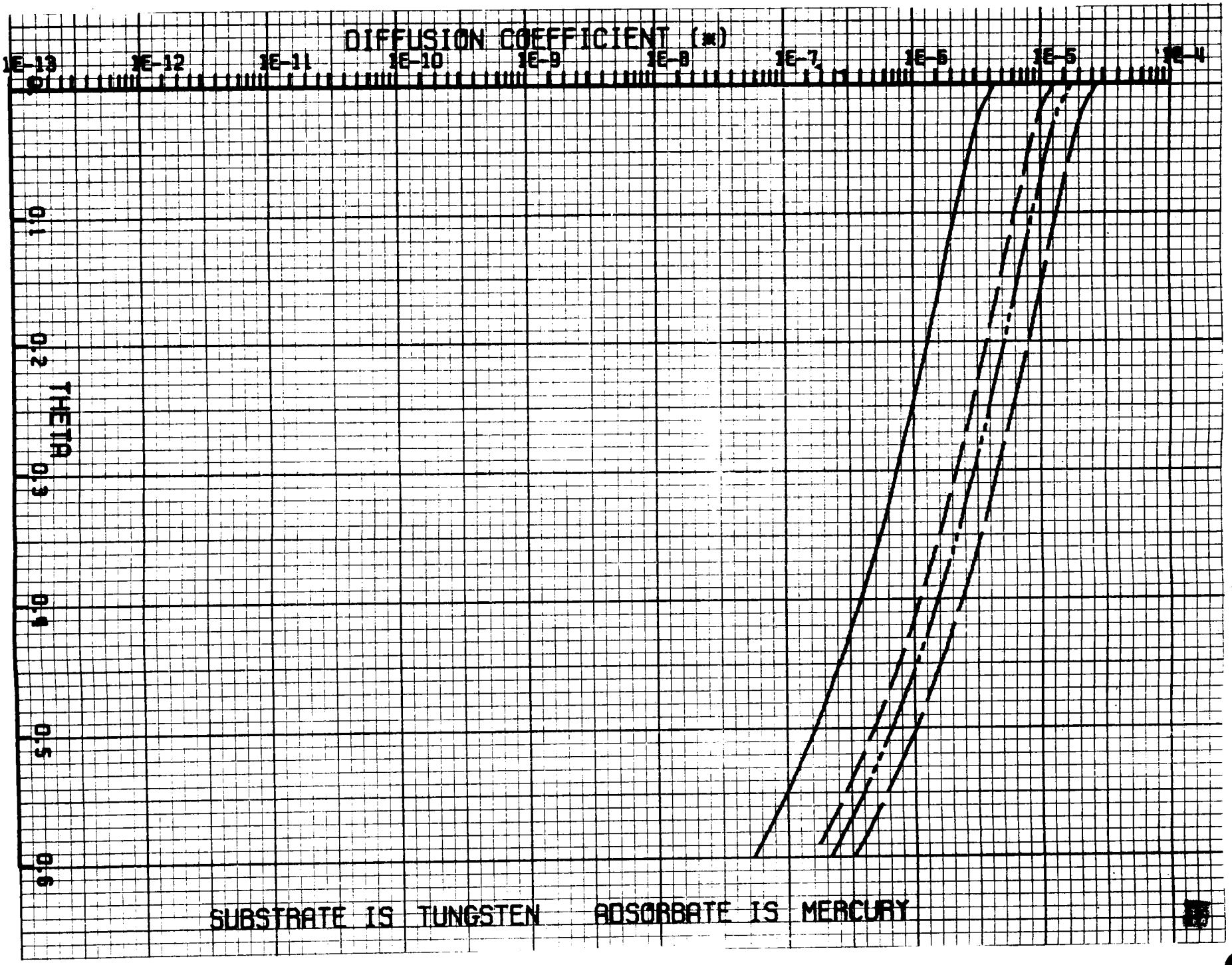
DIFFUSION COEFFICIENT (*)
1E-13
1E-12
1E-11
1E-10
1E-9
1E-8
1E-7
1E-6
1E-5
1E-4
THETA
0.1
0.2
0.3
0.4
0.5
0.6
SUBSTRATE IS TUNGSTEN ADSORBATE IS MERCURY

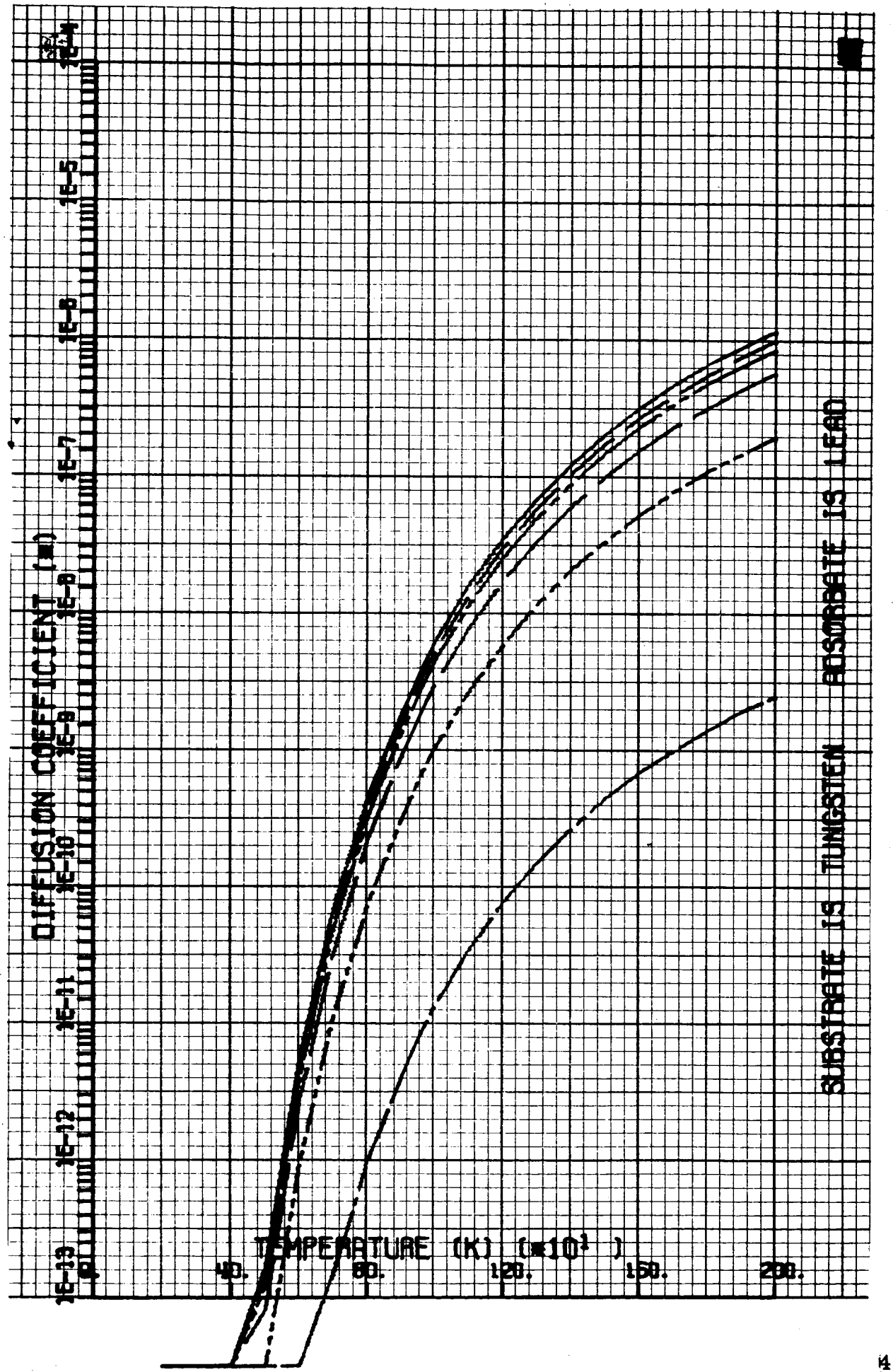
DIFFUSION COEFFICIENT (M²)
1E-4
1E-5
1E-6
1E-7
1E-8
1E-9
1E-10
1E-11
1E-12
1E-13
TEMPERATURE (K) (×10¹)
40.
80.
120.
150.
200.
SUBSTRATE IS TUNGSTEN ADSORBATE IS LEAD

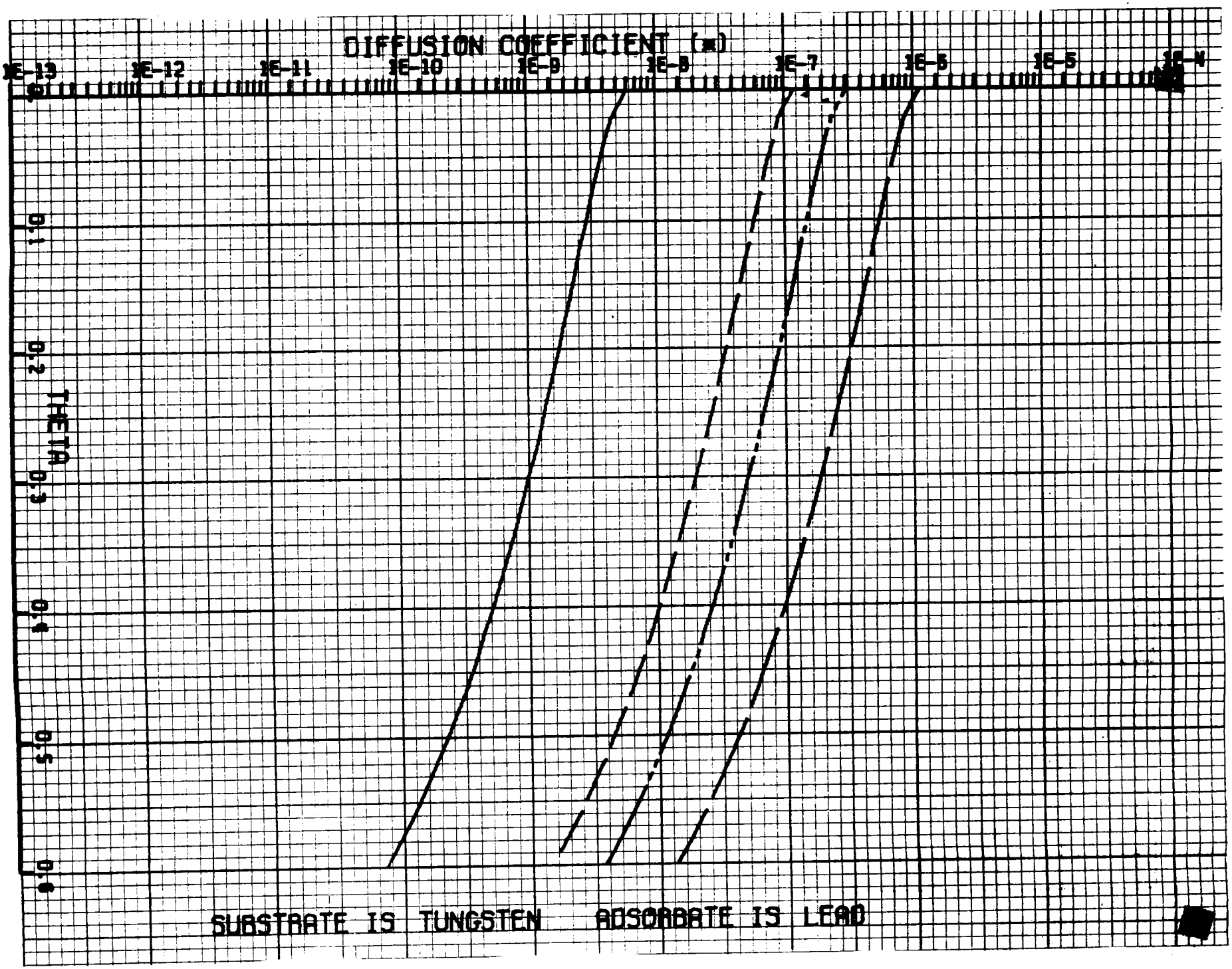
DIFFUSION COEFFICIENT (m)
1E-13
1E-12
1E-11
1E-10
1E-9
1E-8
1E-7
1E-6
1E-5
1E-4
THETA
0.1
0.2
0.3
0.4
0.5
0.6
SUBSTRATE IS TUNGSTEN ADSORBATE IS LEAD

DIFFUSION COEFFICIENT (M²)
1E-4
1E-5
1E-6
1E-7
1E-8
1E-9
1E-10
1E-11
1E-12
1E-13
TEMPERATURE (K) (*10¹)
60.
120.
160.
200.
SUBSTRATE IS RHENIUM ADSORBATE IS LITHIUM

DIFFUSION COEFFICIENT (M²)
1E-4
1E-5
1E-6
1E-7
1E-8
1E-9
1E-10
1E-11
1E-12
1E-13
0.1
0.2
0.3
0.4
0.5
0.6
THETA
SUBSTRATE IS RHENIUM
ADSORBATE IS LITHIUM

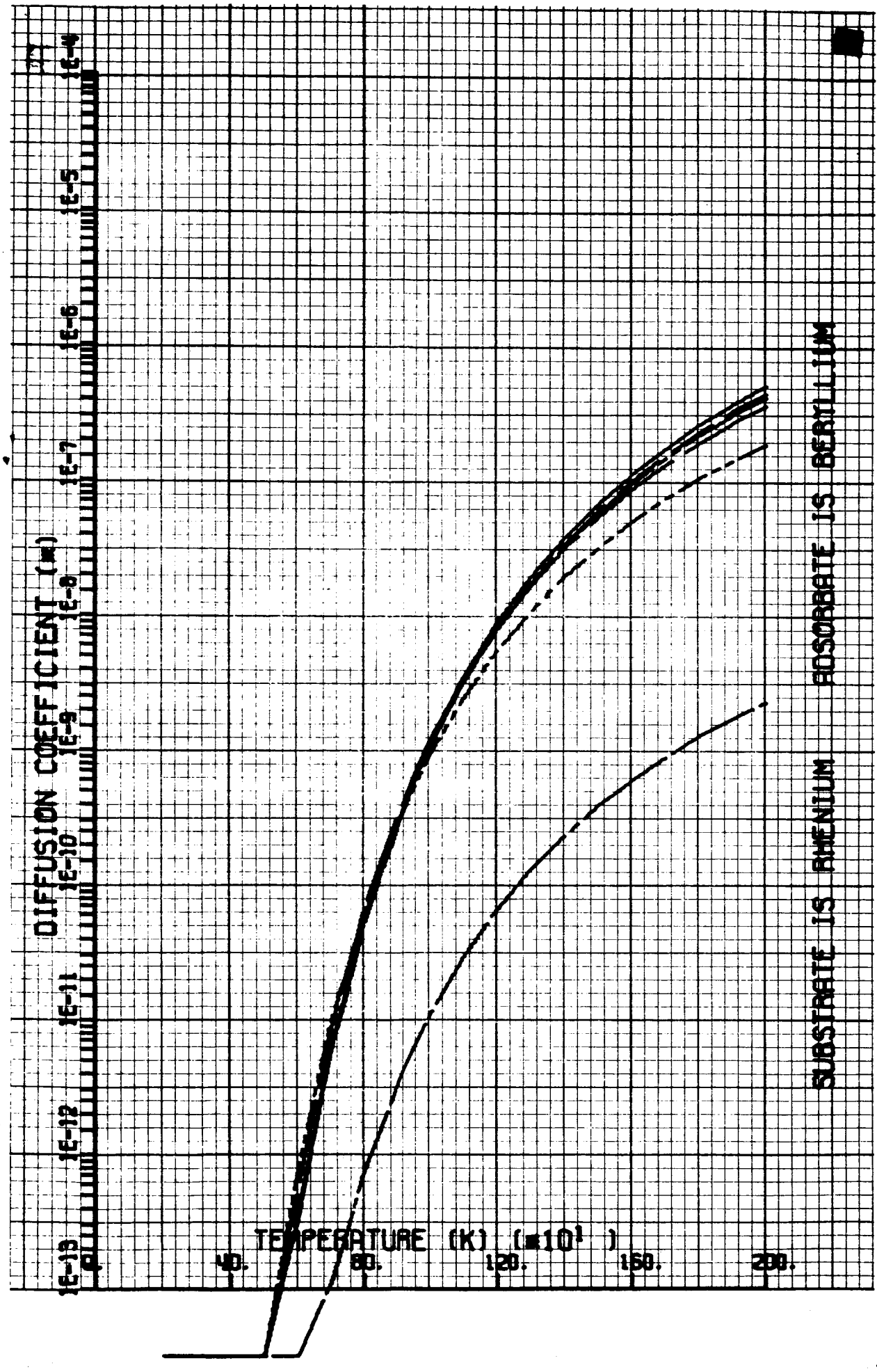
DIFFUSION COEFFICIENT (M²)
1E-4
1E-5
1E-6
1E-7
1E-8
1E-9
1E-10
1E-11
1E-12
1E-13
TEMPERATURE (K) (*10¹)
40.
80.
120.
160.
200.
SUBSTRATE IS RHENIUM ADSORBATE IS BERYLLIUM

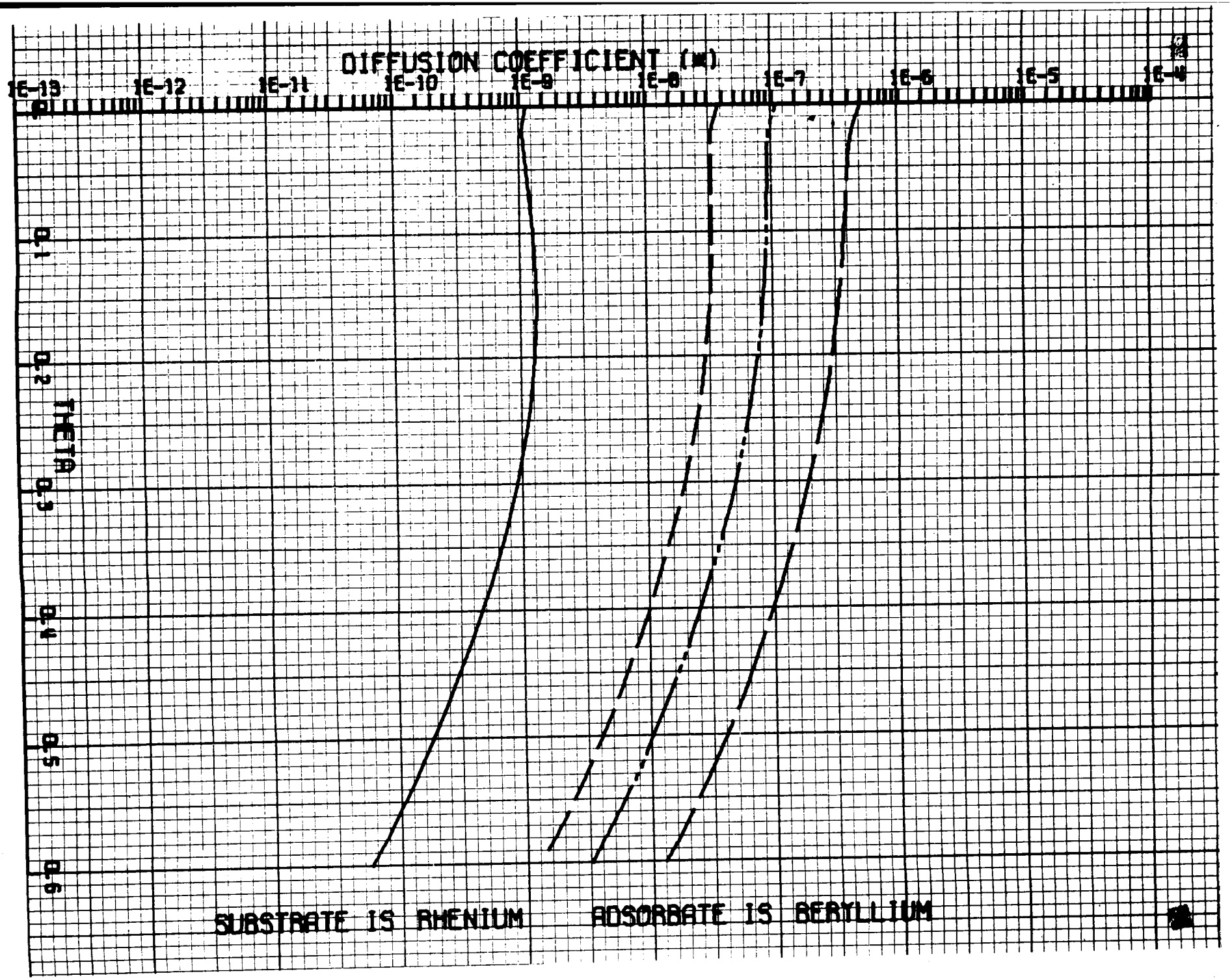
DIFFUSION COEFFICIENT (M)
1E-13
1E-12
1E-11
1E-10
1E-9
1E-8
1E-7
1E-6
1E-5
1E-4
THETA
0.1
0.2
0.3
0.4
0.5
0.6
SUBSTRATE IS RHENIUM
ADSORBATE IS BERYLLIUM

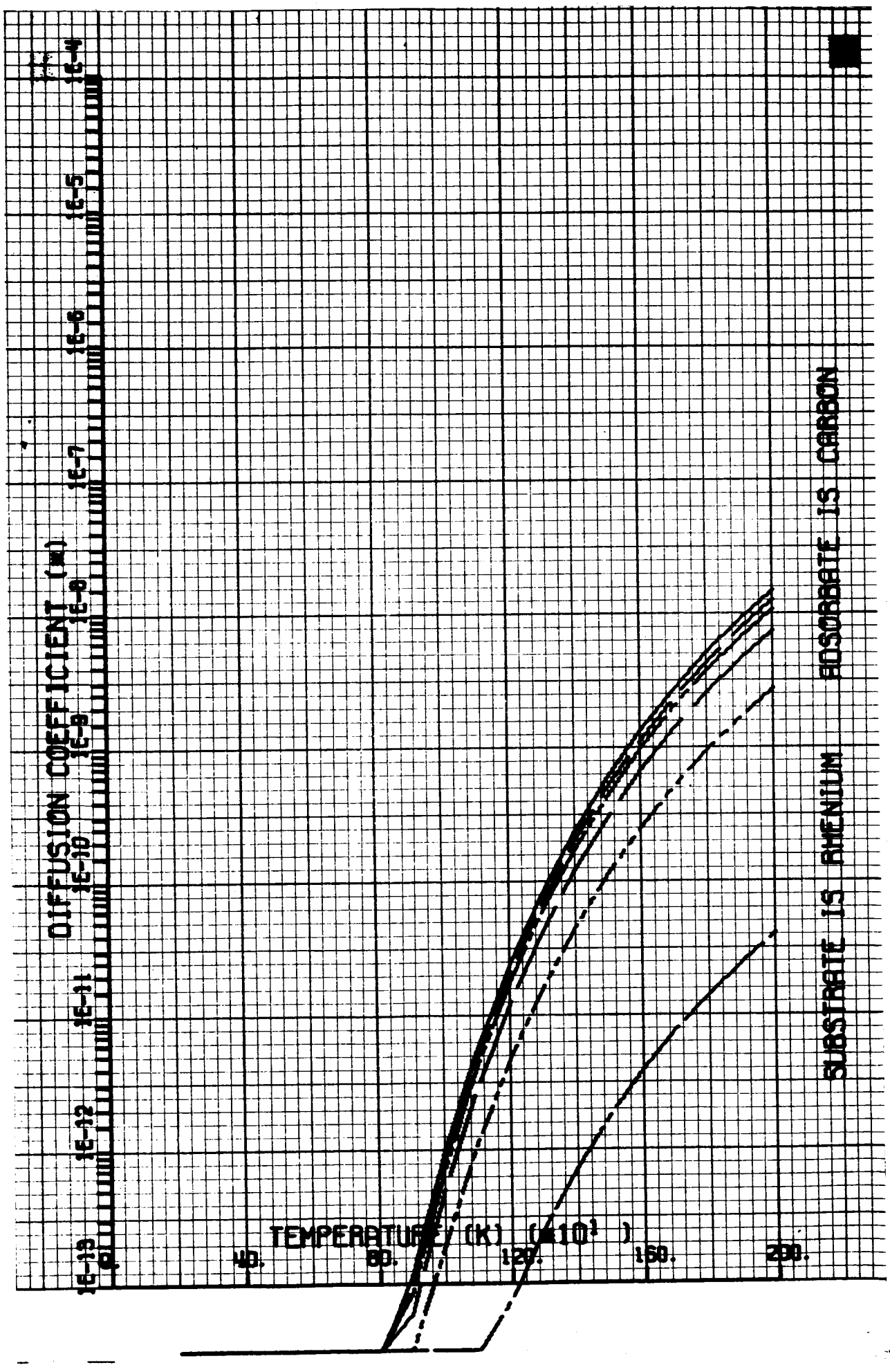
DIFFUSION COEFFICIENT (M)
1E-4
1E-5
1E-6
1E-7
1E-8
1E-9
1E-10
1E-11
1E-12
1E-13
TEMPERATURE (K) (X10³)
40.
80.
120.
160.
200.
SUBSTRATE IS ARGENTUM ADSORBATE IS CARBON

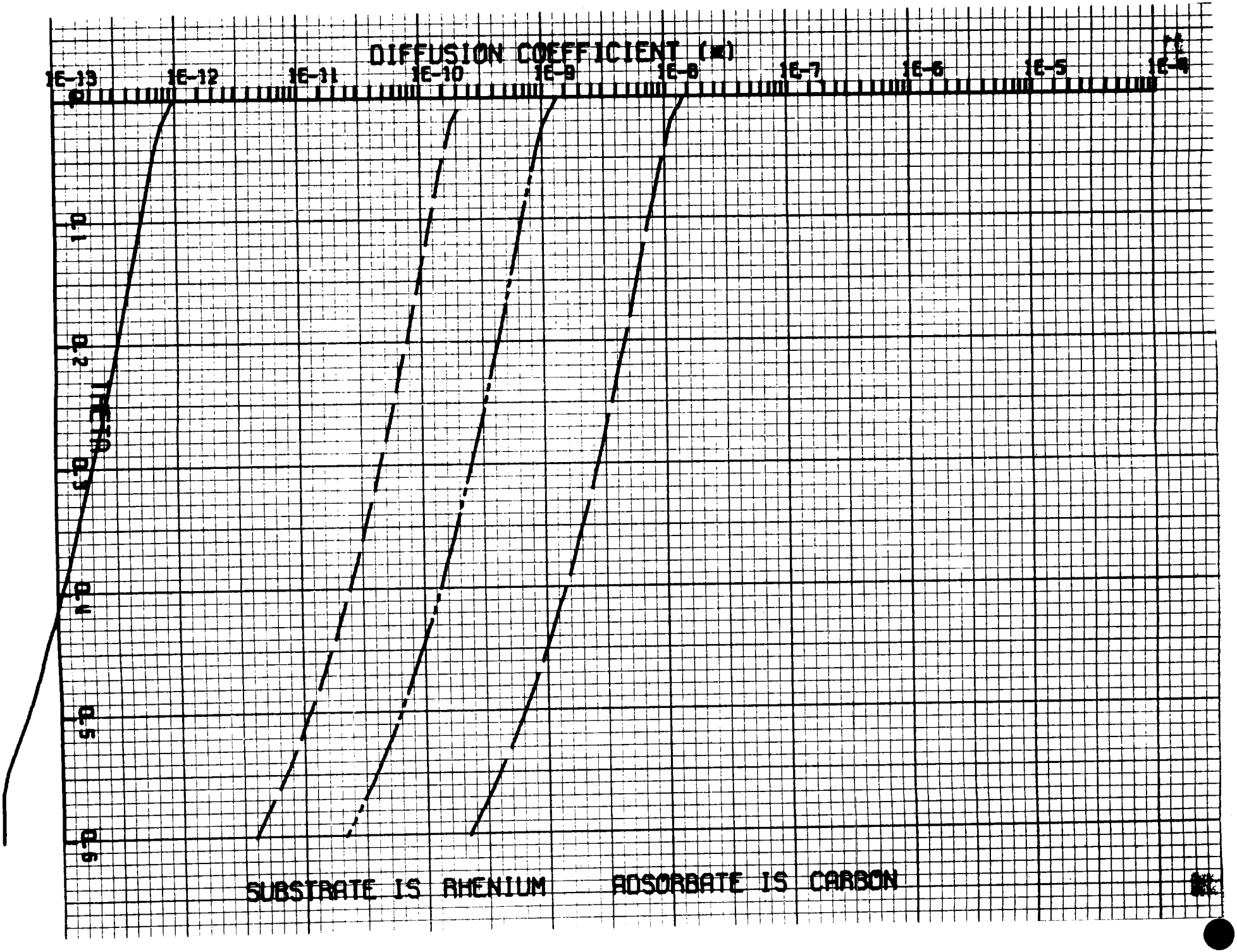
DIFFUSION COEFFICIENT (m)
1E-13
1E-12
1E-11
1E-10
1E-9
1E-8
1E-7
1E-6
1E-5
1E-4
0.1
0.2
0.3
0.4
0.5
0.6
FRACTION
SUBSTRATE IS RHENIUM
ADSORBATE IS CARBON

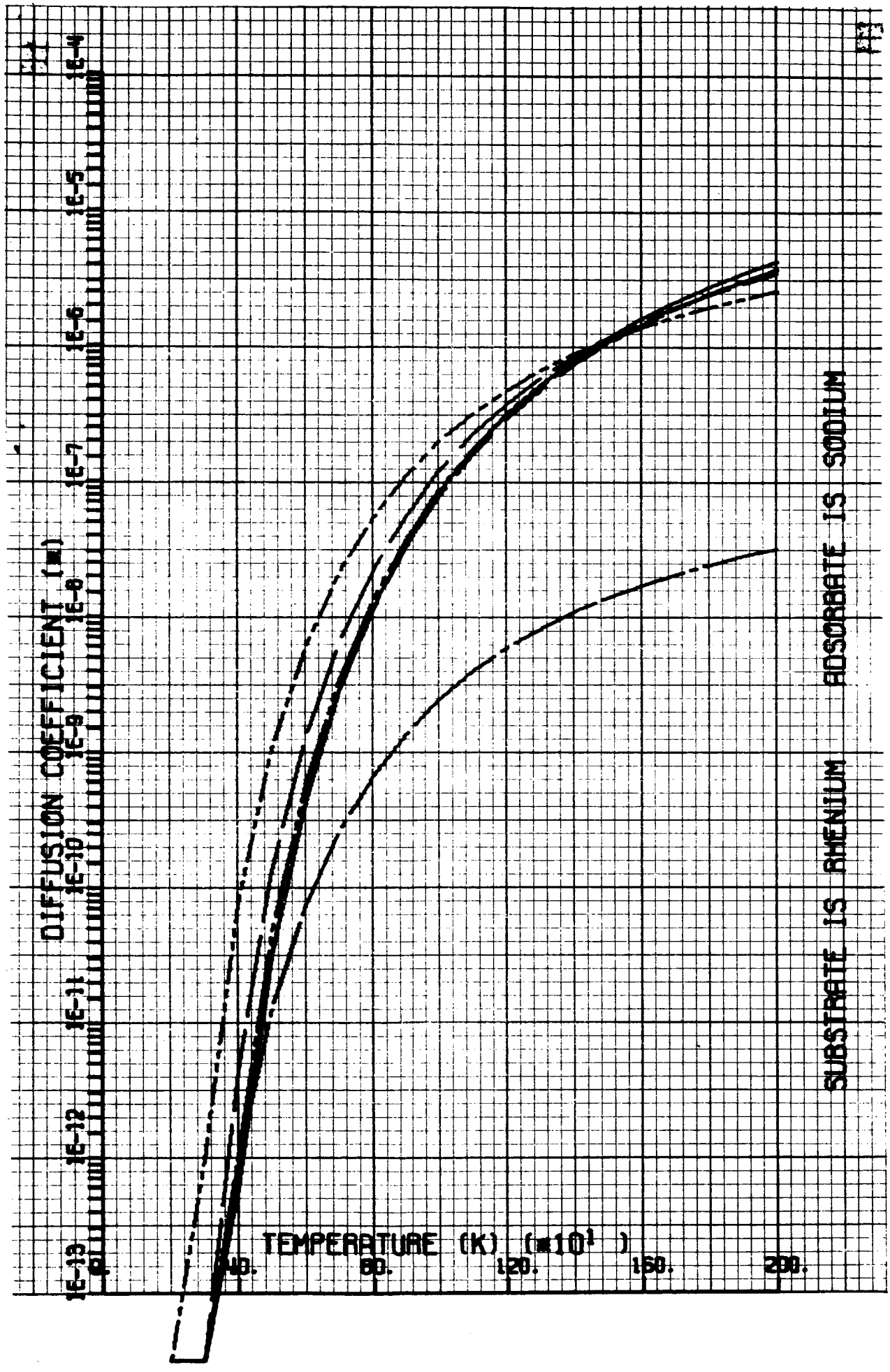
DIFFUSION COEFFICIENT (M)
1E-4
1E-5
1E-6
1E-7
1E-8
1E-9
1E-10
1E-11
1E-12
1E-13
TEMPERATURE (K) (*10¹)
40.
80.
120.
160.
200.
SUBSTRATE IS RHENIUM ADSORBATE IS SODIUM

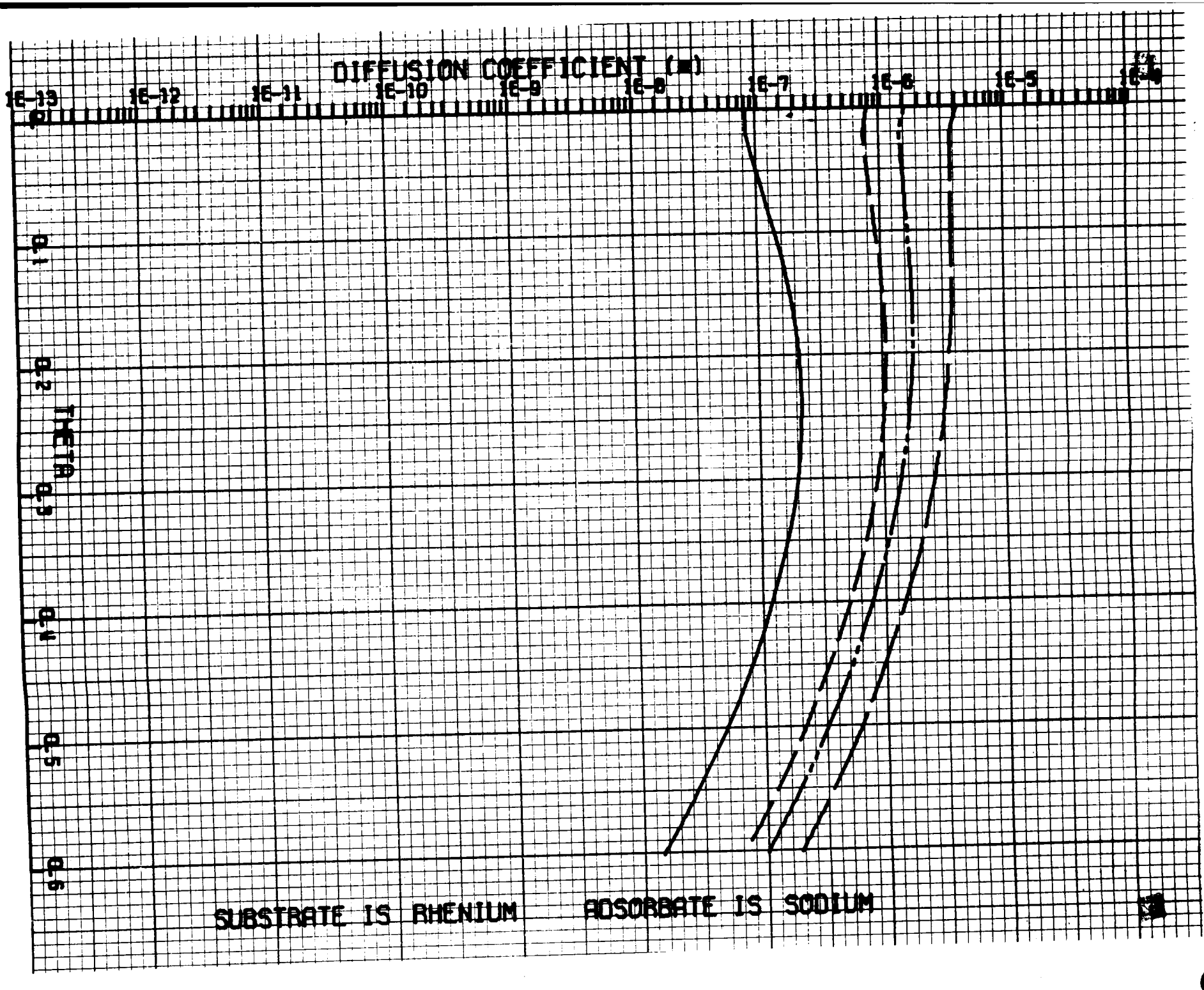
DIFFUSION COEFFICIENT (m)
1E-13
1E-12
1E-11
1E-10
1E-9
1E-8
1E-7
1E-6
1E-5
1E-4
THETA
0.1
0.2
0.3
0.4
0.5
0.6
SUBSTRATE IS RHENIUM
ADSORBATE IS SODIUM

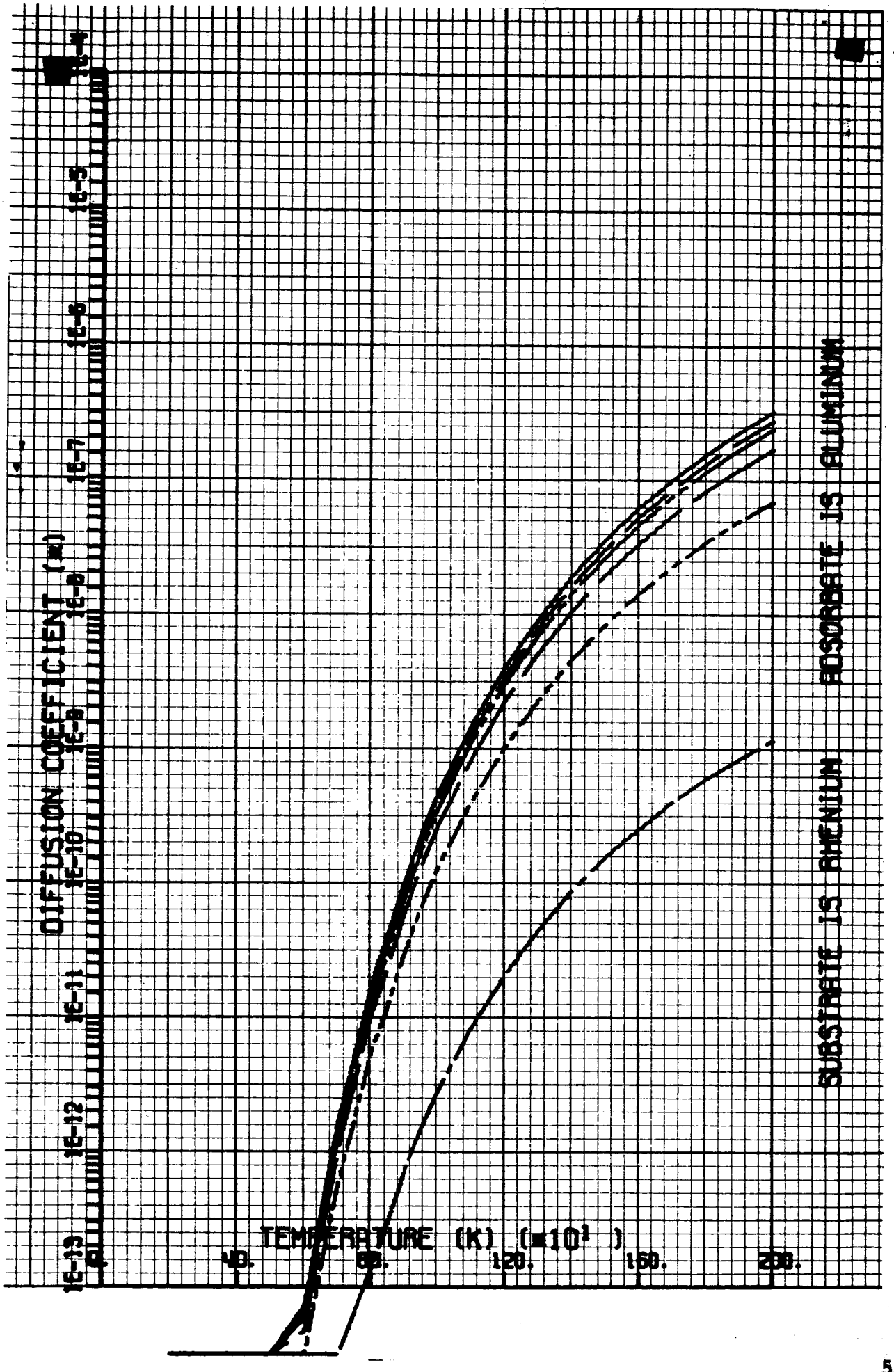
DIFFUSION COEFFICIENT (M²)
1E-4
1E-5
1E-6
1E-7
1E-8
1E-9
1E-10
1E-11
1E-12
1E-13
TEMPERATURE (K) (*10¹)
40.
80.
120.
160.
200.
SUBSTRATE IS RHENIUM ADSORBATE IS ALUMINUM

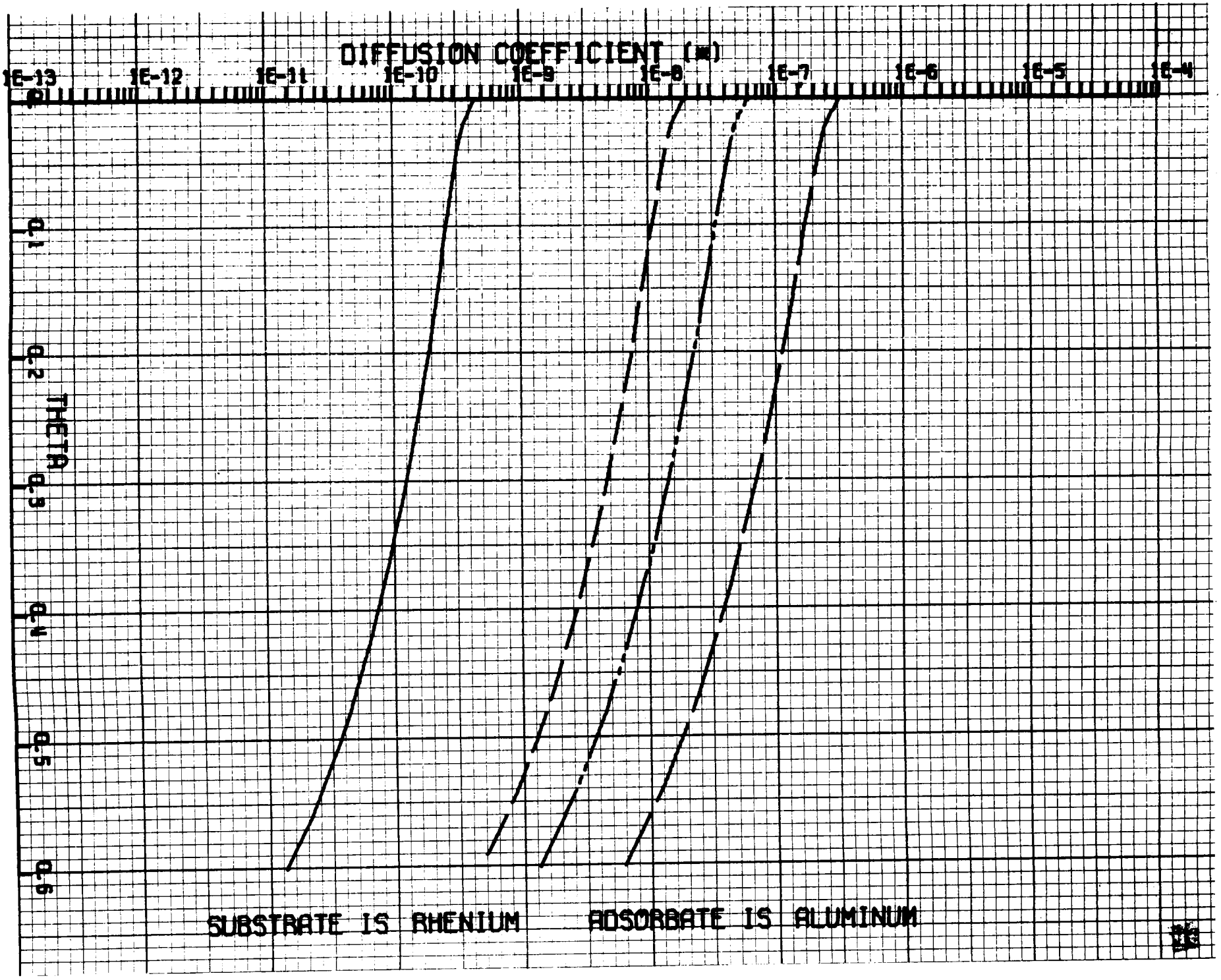
DIFFUSION COEFFICIENT (M)
1E-13
1E-12
1E-11
1E-10
1E-9
1E-8
1E-7
1E-6
1E-5
1E-4
THETA
0.1
0.2
0.3
0.4
0.5
0.6
SUBSTRATE IS RHENIUM
ADSORBATE IS ALUMINUM

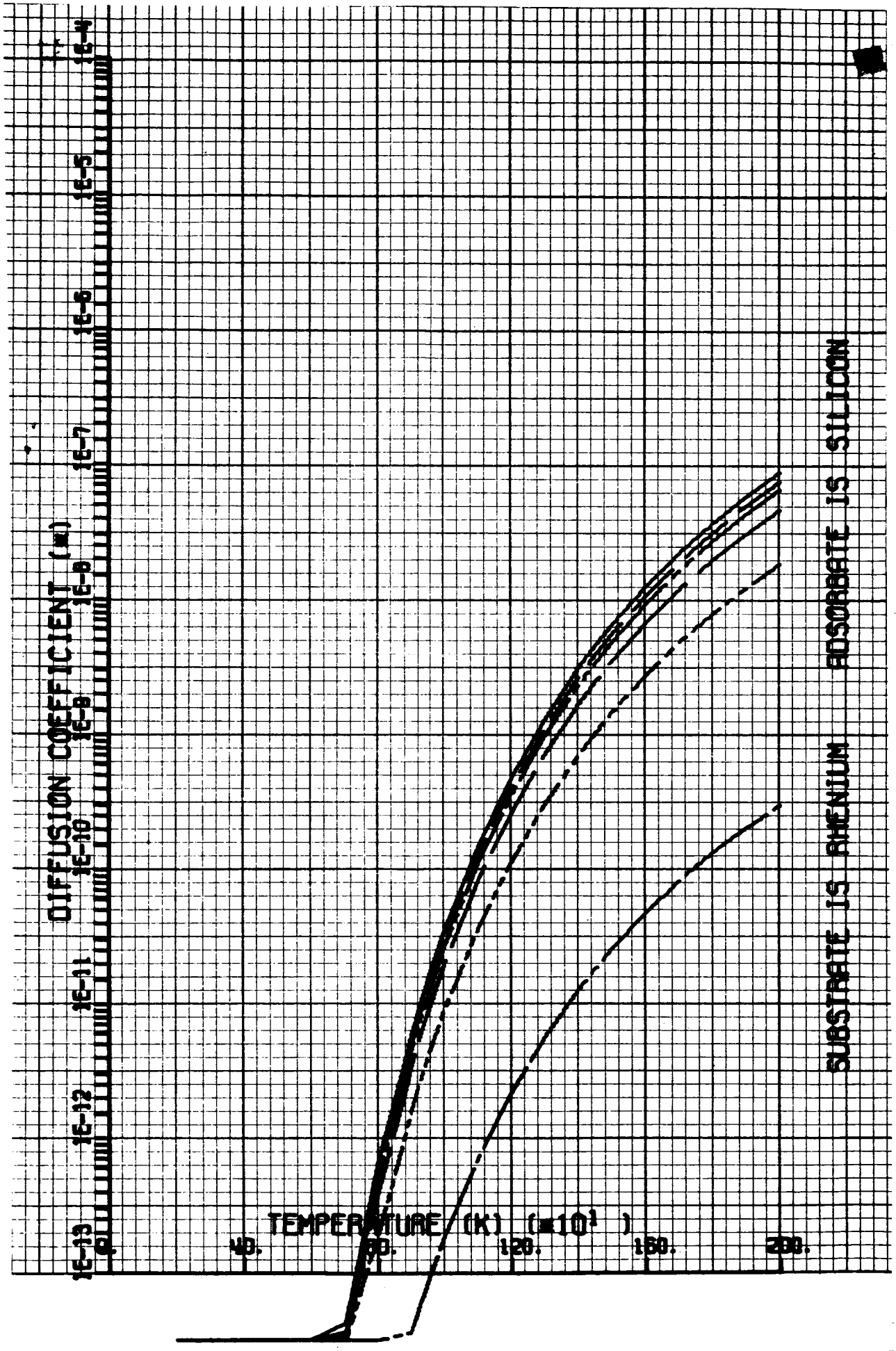
DIFFUSION COEFFICIENT (M²)
1E-4
1E-5
1E-6
1E-7
1E-8
1E-9
1E-10
1E-11
1E-12
1E-13
TEMPERATURE (K) (*10¹)
40.
80.
120.
160.
200.
SUBSTRATE IS RHENIUM ADSORBATE IS SILICON

DIFFUSION COEFFICIENT (cm)
1E-4
1E-5
1E-6
1E-7
1E-8
1E-9
1E-10
1E-11
1E-12
1E-13
0
0.1
0.2
0.3
0.4
0.5
0.6
THETA
SUBSTRATE IS RHENIUM ADSORBATE IS SILICON

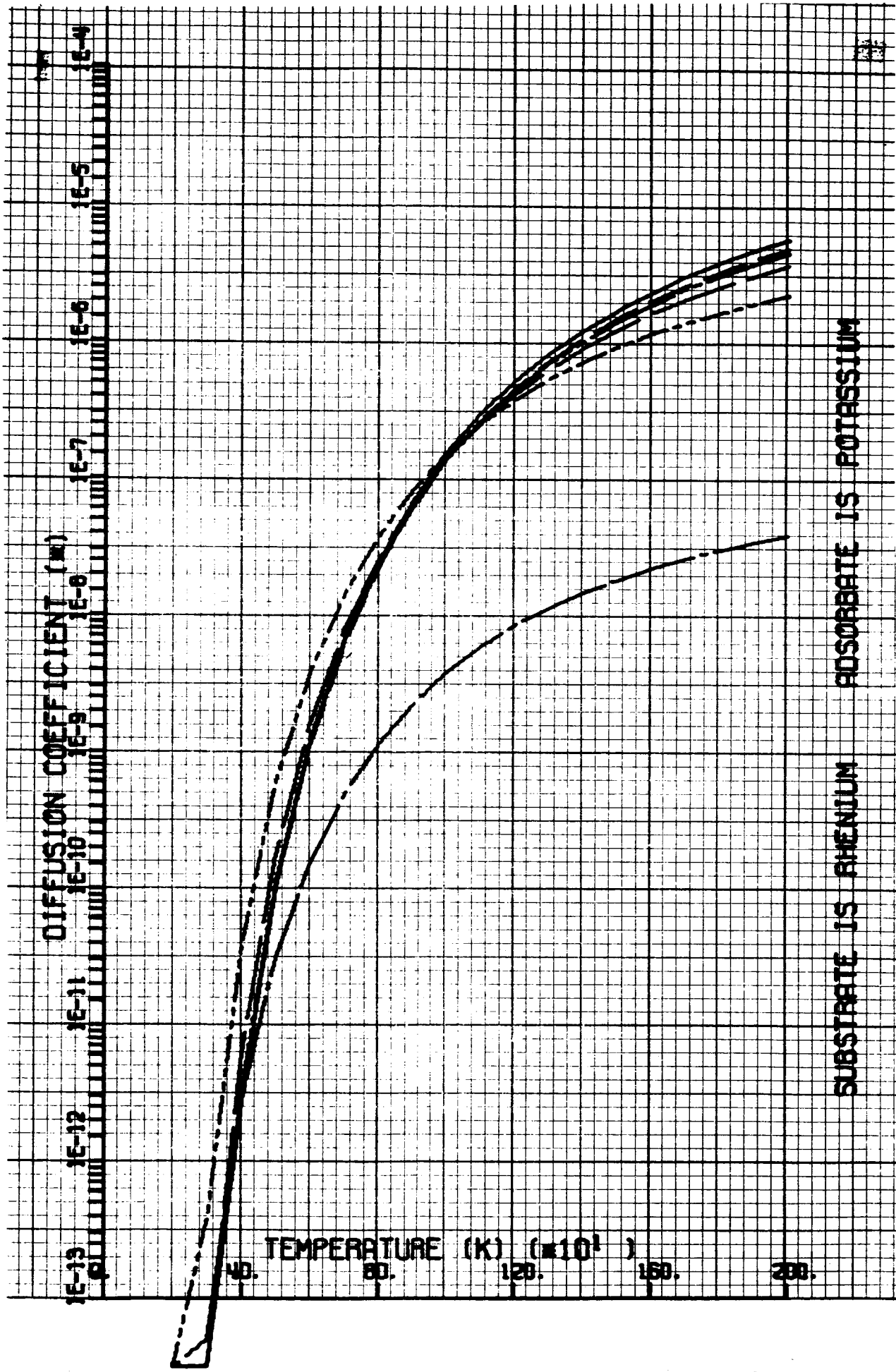
DIFFUSION COEFFICIENT (M²)
1E-4
1E-5
1E-6
1E-7
1E-8
1E-9
1E-10
1E-11
1E-12
1E-13
TEMPERATURE (K) (×10¹)
40.
80.
120.
160.
200.
SUBSTRATE IS ARGENTUM ADSORBATE IS POTASSIUM

DIFFUSION COEFFICIENT (m²)
1E-4
1E-5
1E-6
1E-7
1E-8
1E-9
1E-10
1E-11
1E-12
1E-13
0.1
0.2
0.3
0.4
0.5
0.6
THETA
SUBSTRATE IS RHENIUM ADSORBATE IS POTASSIUM

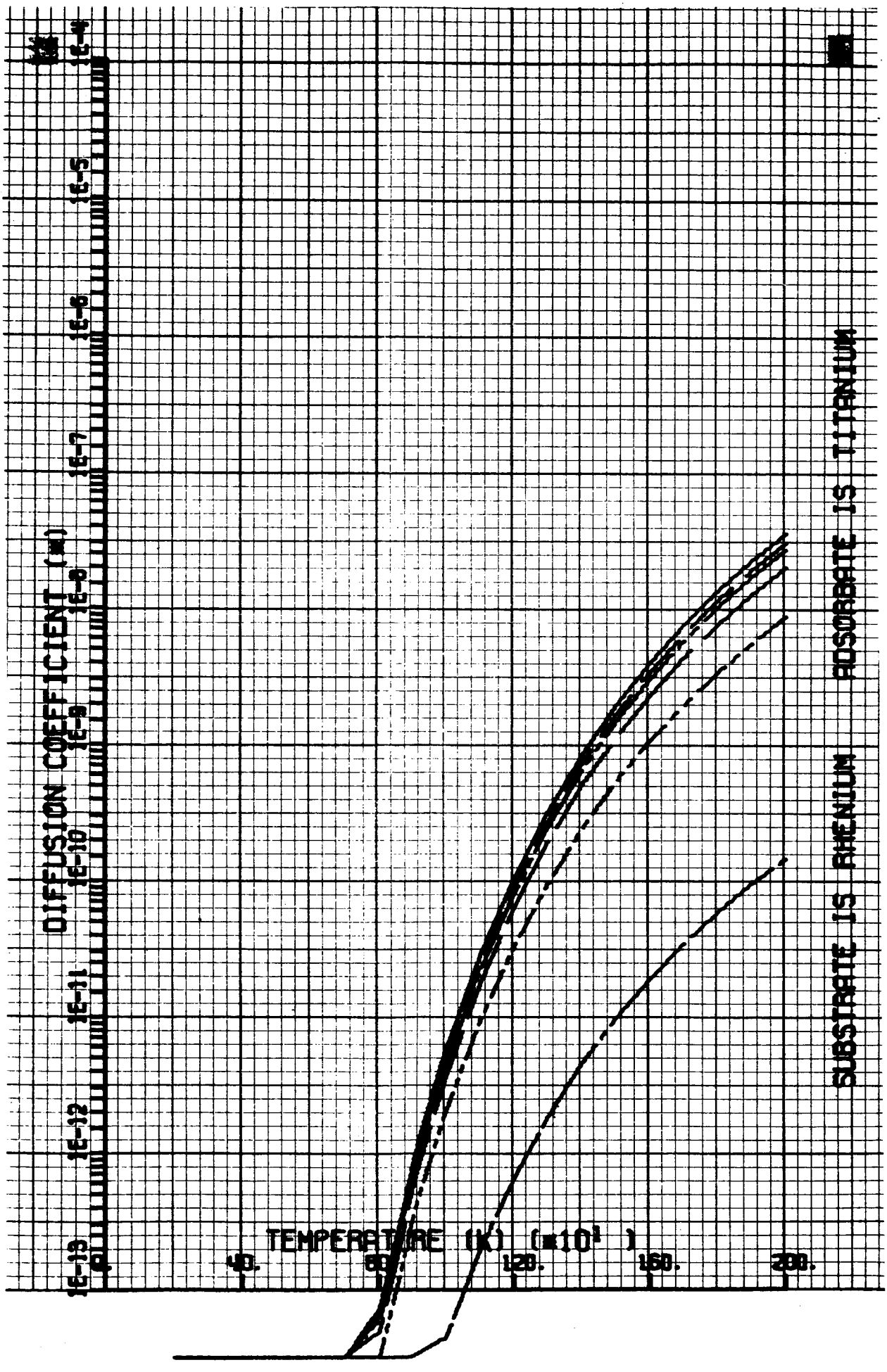
DIFFUSION COEFFICIENT (M²)
1E-4
1E-5
1E-6
1E-7
1E-8
1E-9
1E-10
1E-11
1E-12
1E-13
TEMPERATURE (K) (×10¹)
40.
80.
120.
160.
200.
SUBSTRATE IS RHENIUM ADSORBATE IS TITANIUM

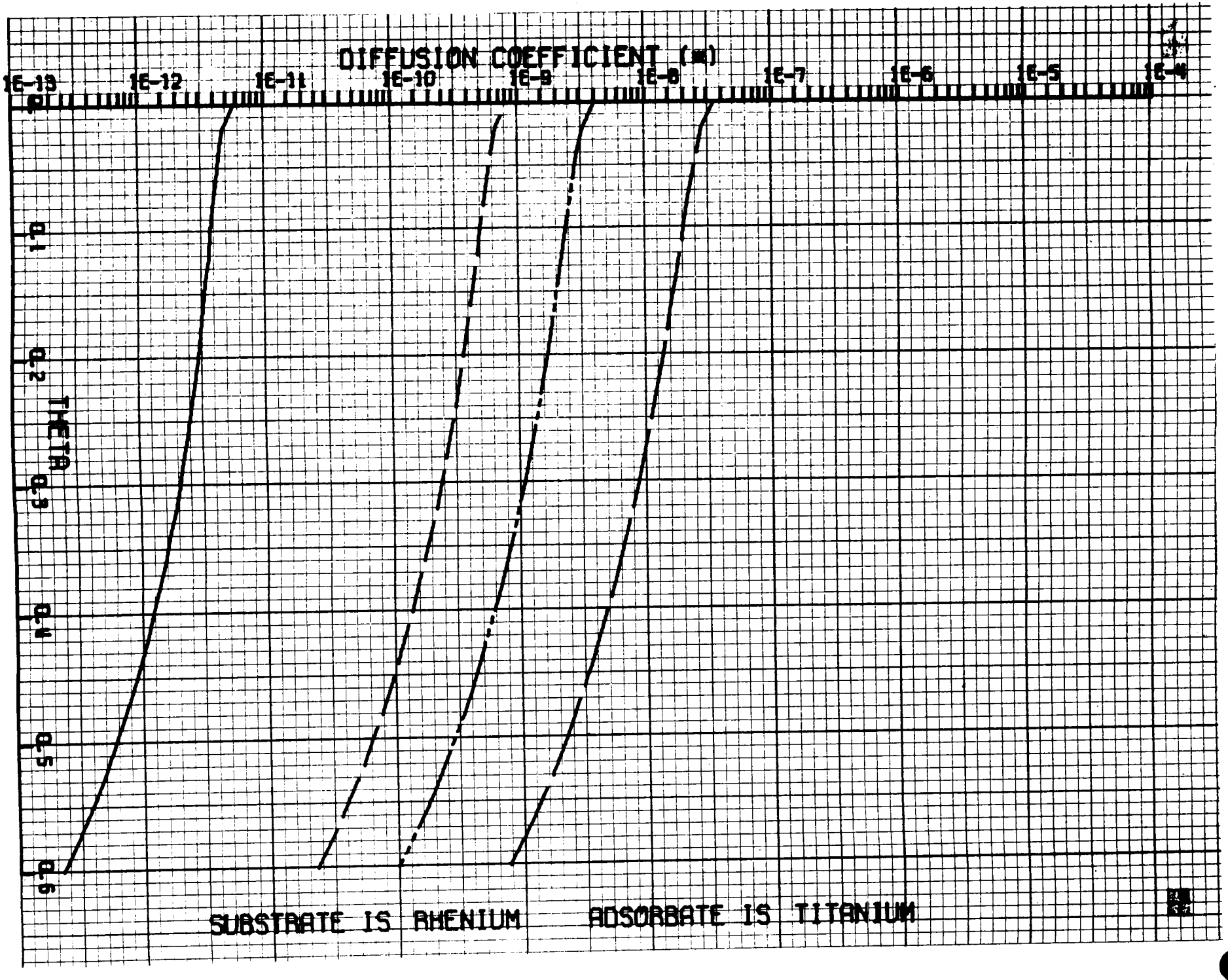
DIFFUSION COEFFICIENT (m)
1E-13
1E-12
1E-11
1E-10
1E-9
1E-8
1E-7
1E-6
1E-5
1E-4
THETA
0.1
0.2
0.3
0.4
0.5
0.6
SUBSTRATE IS RHENIUM
ADSORBATE IS TITANIUM

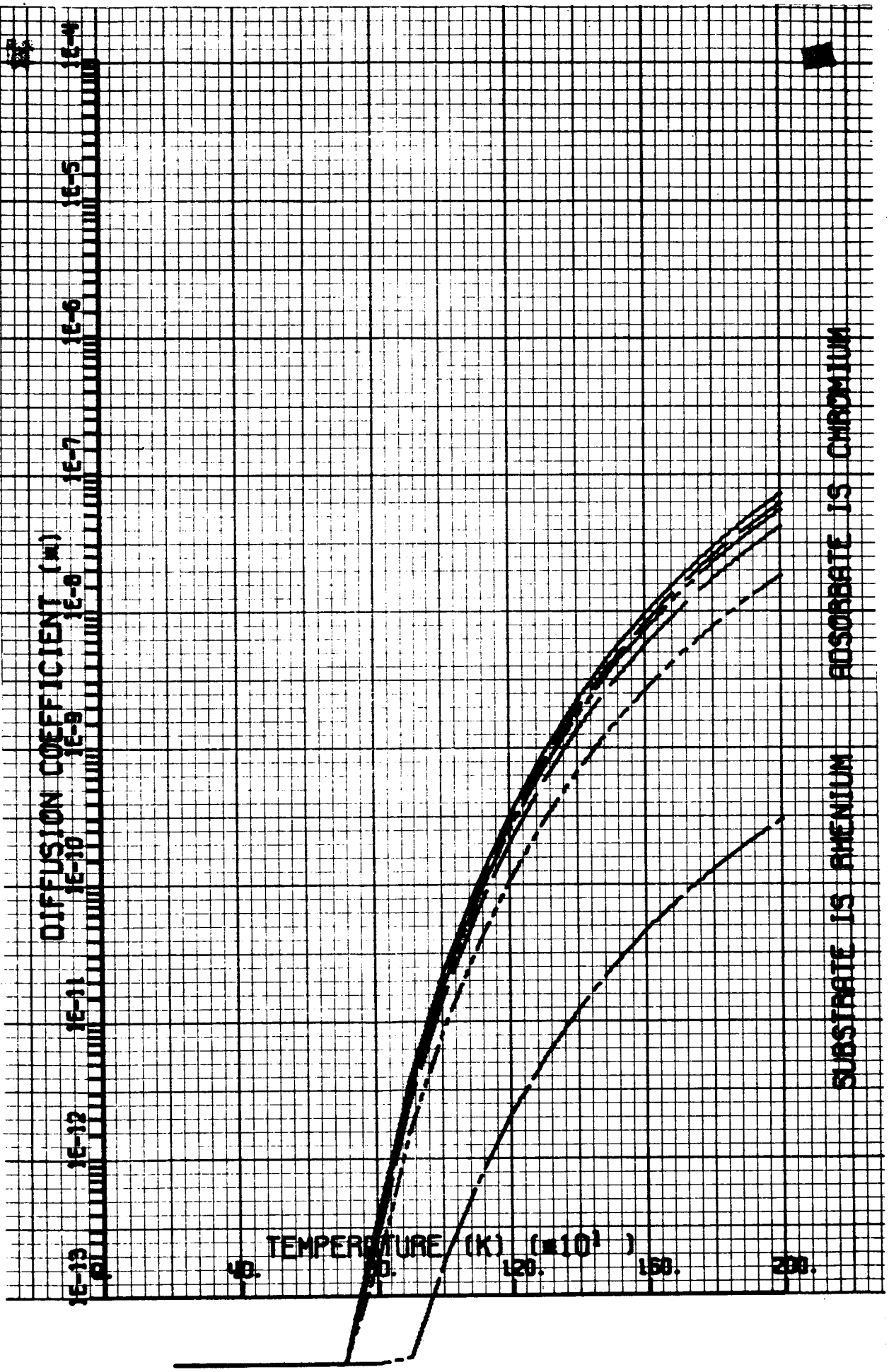
DIFFUSION COEFFICIENT (M)
1E-4
1E-5
1E-6
1E-7
1E-8
1E-9
1E-10
1E-11
1E-12
1E-13
TEMPERATURE (K) (*10¹)
40.
80.
120.
160.
200.
SUBSTRATE IS RHENIUM ADSORBATE IS CHROMIUM

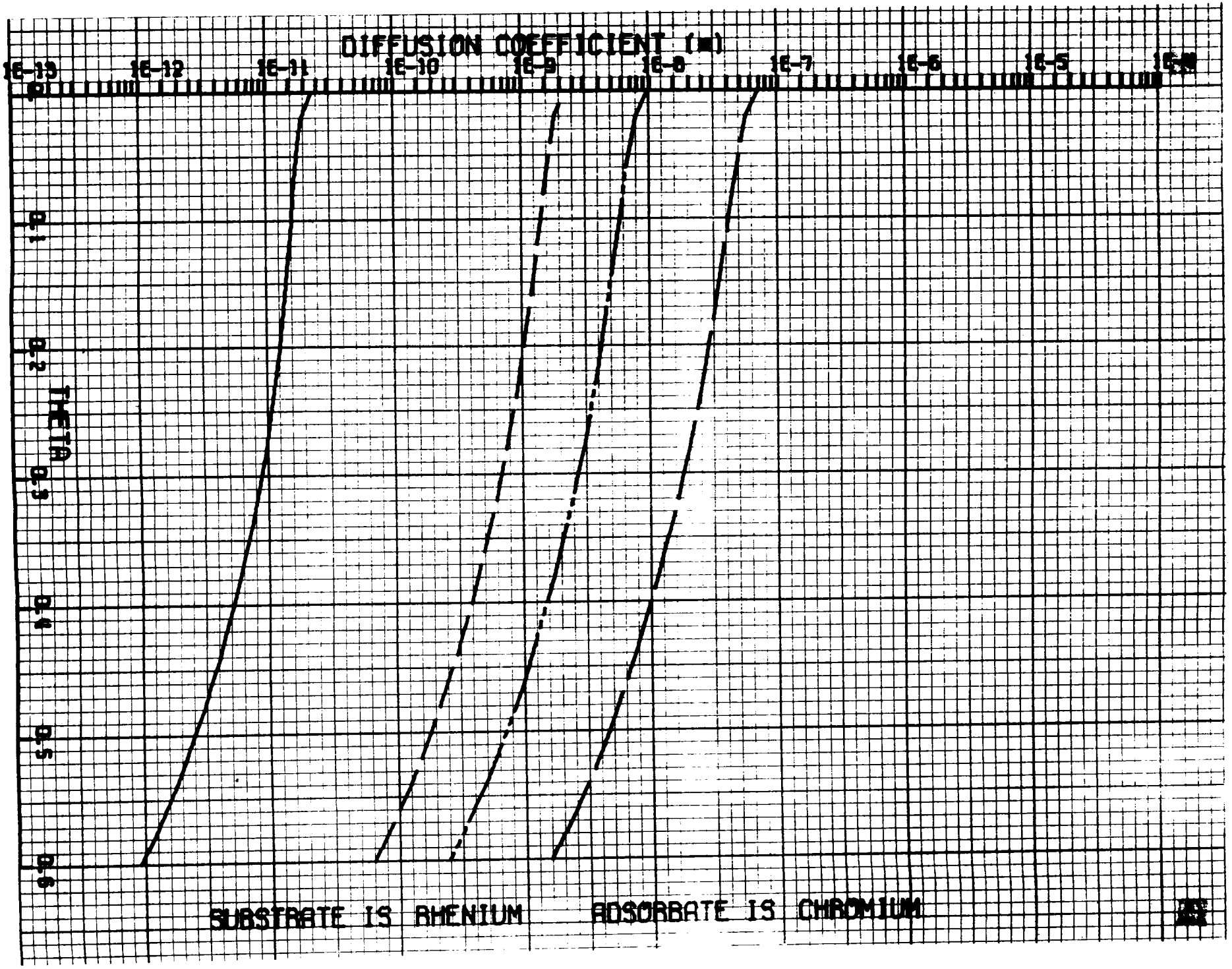
DIFFUSION COEFFICIENT (m)
1E-13
1E-12
1E-11
1E-10
1E-9
1E-8
1E-7
1E-6
1E-5
1E-4
0.1
0.2
0.3
0.4
0.5
0.6
HEIGHT
SUBSTRATE IS RHENIUM
ADSORBATE IS CHROMIUM

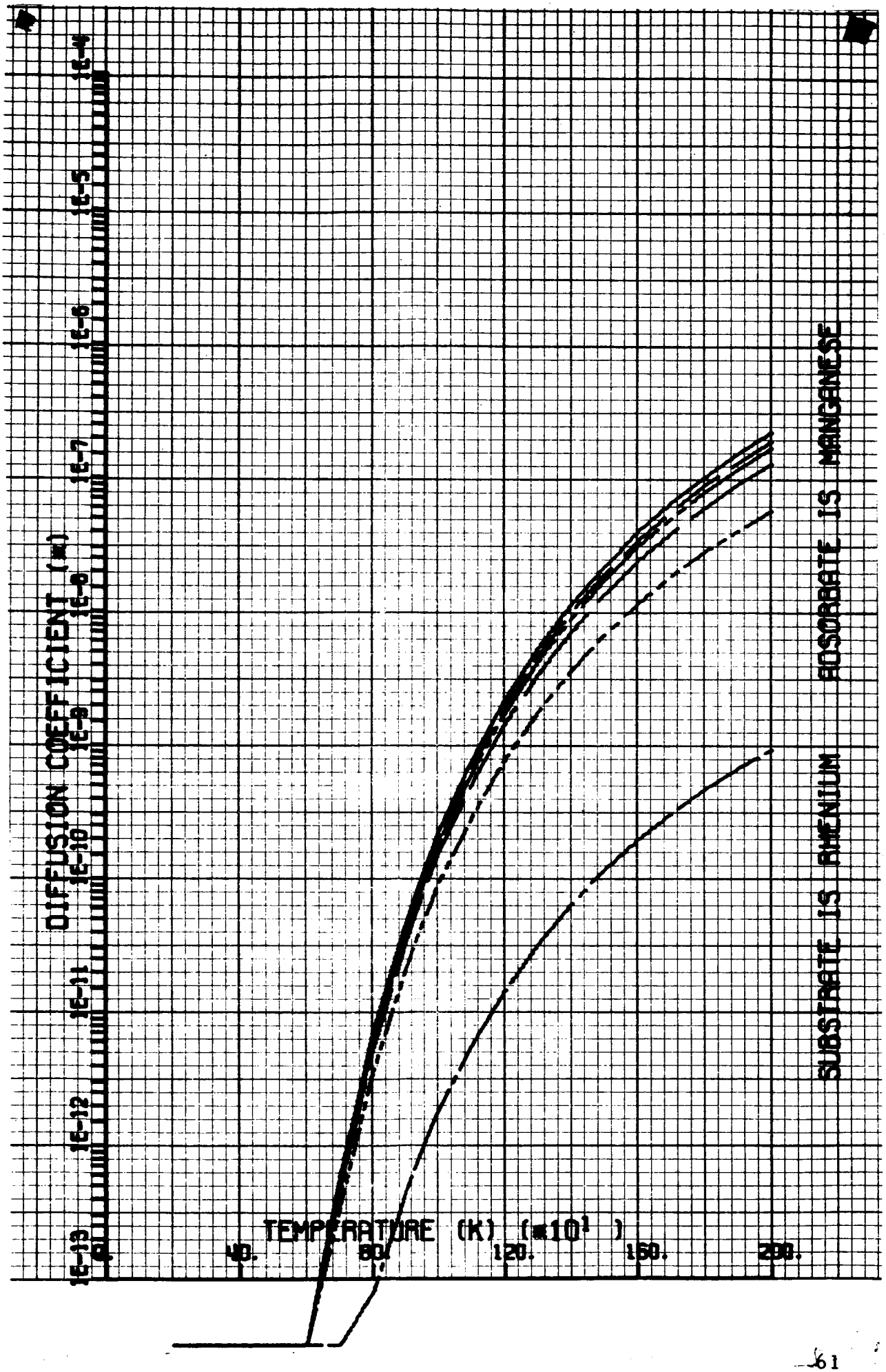
DIFFUSION COEFFICIENT (M²)
1E-4
1E-5
1E-6
1E-7
1E-8
1E-9
1E-10
1E-11
1E-12
1E-13
TEMPERATURE (K) (×10¹)
40.
80.
120.
150.
200.
SUBSTRATE IS AMENIUM EOSORBATE IS MANGANESE

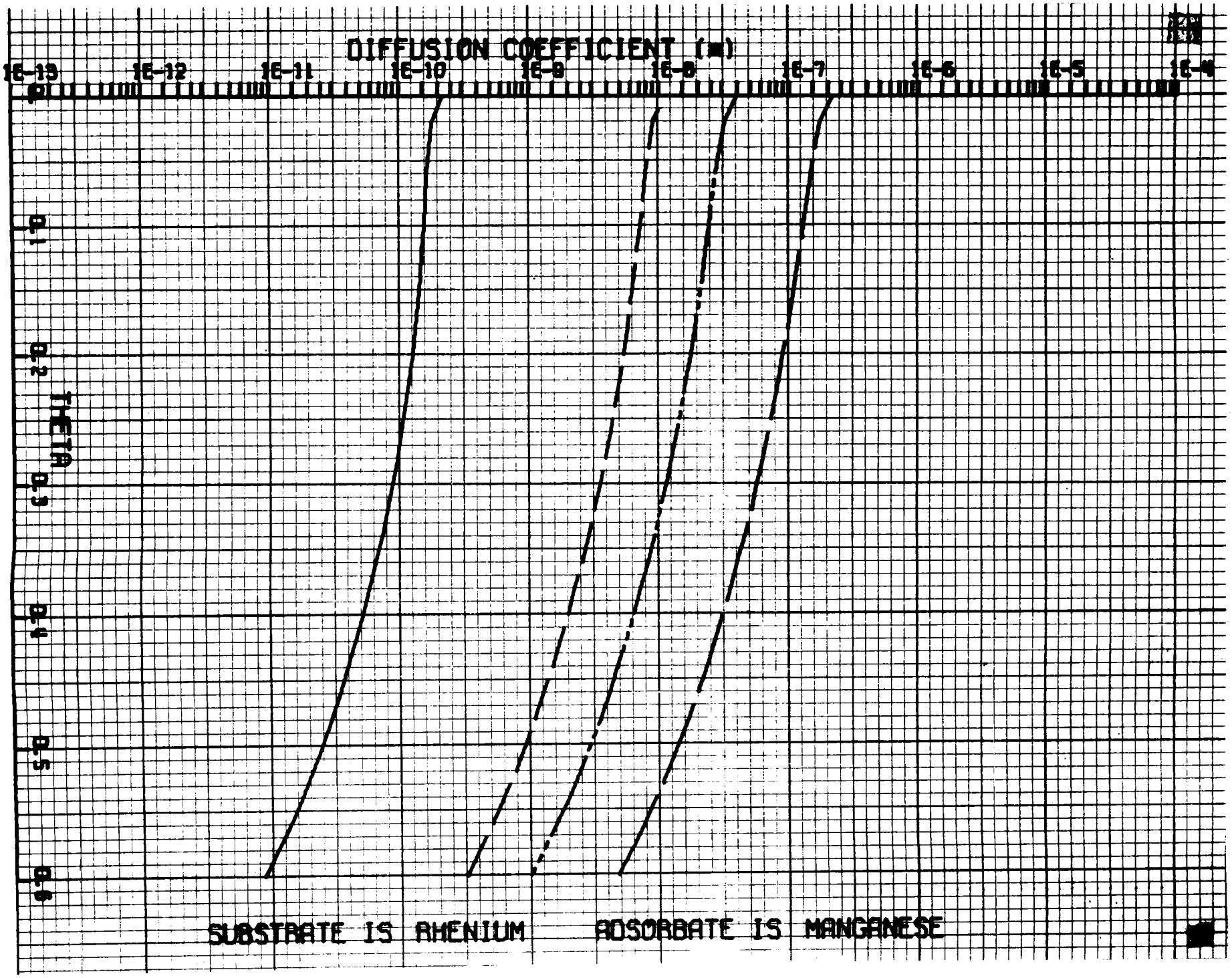
DIFFUSION COEFFICIENT (m)
1E-13
1E-12
1E-11
1E-10
1E-9
1E-8
1E-7
1E-6
1E-5
1E-4
THETA
0.1
0.2
0.3
0.4
0.5
0.6
SUBSTRATE IS RHENIUM ADSORBATE IS MANGANESE

DIFFUSION COEFFICIENT (M²)
1E-4
1E-5
1E-6
1E-7
1E-8
1E-9
1E-10
1E-11
1E-12
1E-13
TEMPERATURE (K) (×10¹)
40.
80.
120.
160.
200.
SUBSTRATE IS RHENIUM ADSORBATE IS IRON

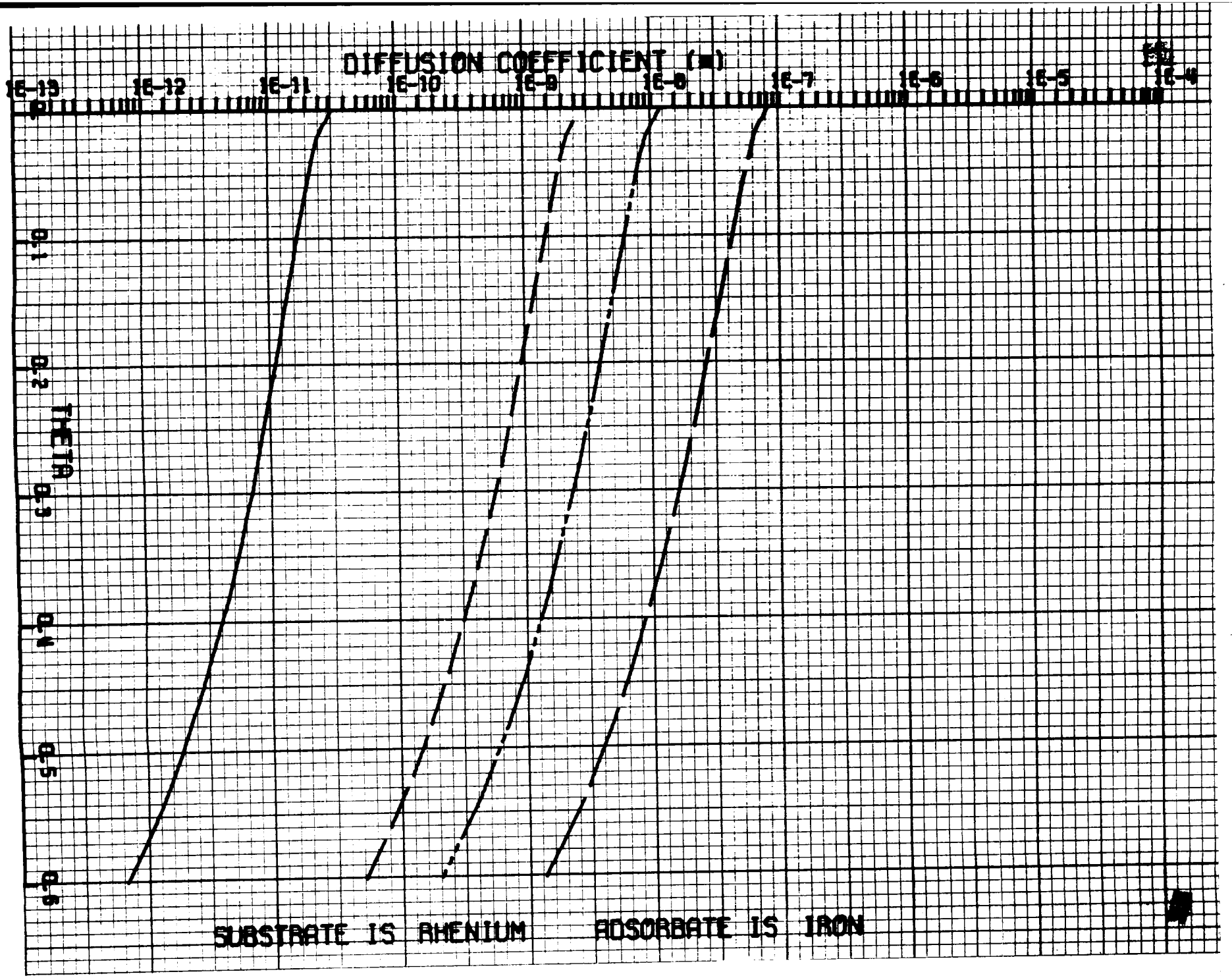
DIFFUSION COEFFICIENT (cm)
1E-13
1E-12
1E-11
1E-10
1E-9
1E-8
1E-7
1E-6
1E-5
1E-4
THETA
0.1
0.2
0.3
0.4
0.5
0.6
SUBSTRATE IS RHENIUM ADSORBATE IS IRON

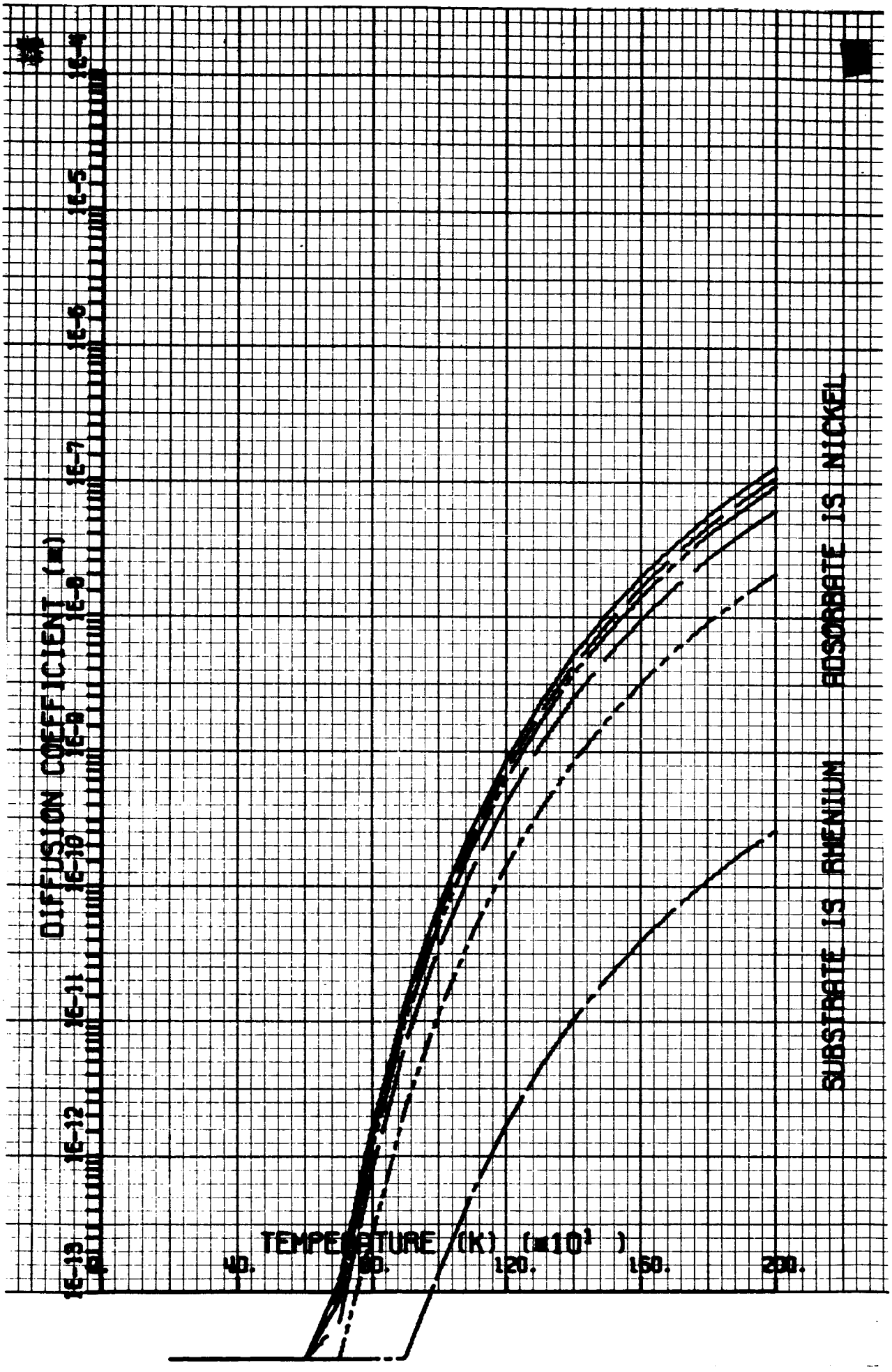
DIFFUSION COEFFICIENT (m²)
1E-4
1E-5
1E-6
1E-7
1E-8
1E-9
1E-10
1E-11
1E-12
1E-13
TEMPERATURE (K) (×10¹)
40.
80.
120.
160.
200.
SUBSTRATE IS RHENIUM ADSORBATE IS NICKEL

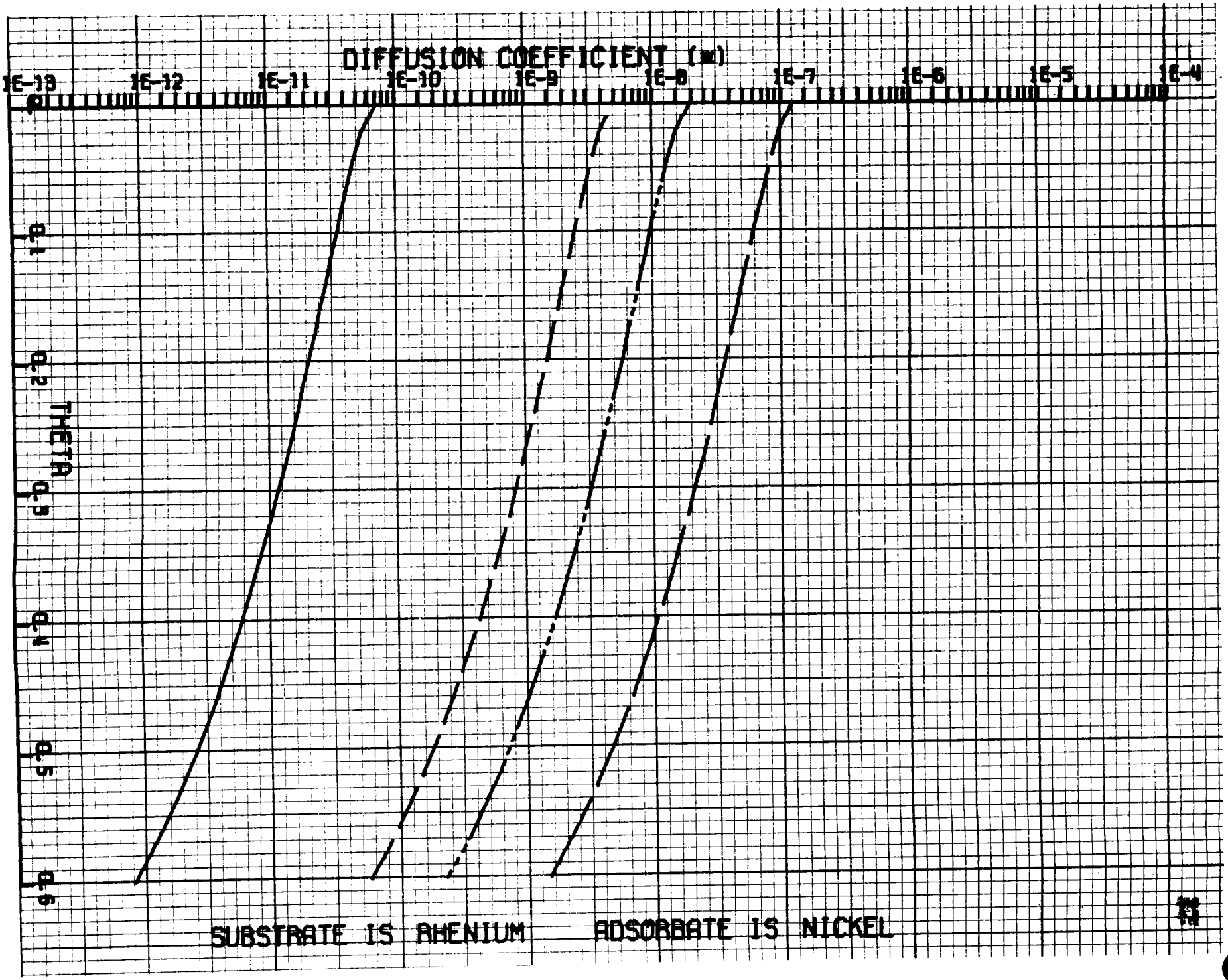
DIFFUSION COEFFICIENT (m)
1E-13
1E-12
1E-11
1E-10
1E-9
1E-8
1E-7
1E-6
1E-5
1E-4
THETA
θ1
θ2
θ3
θ4
θ5
θ6
SUBSTRATE IS RHENIUM
ADSORBATE IS NICKEL

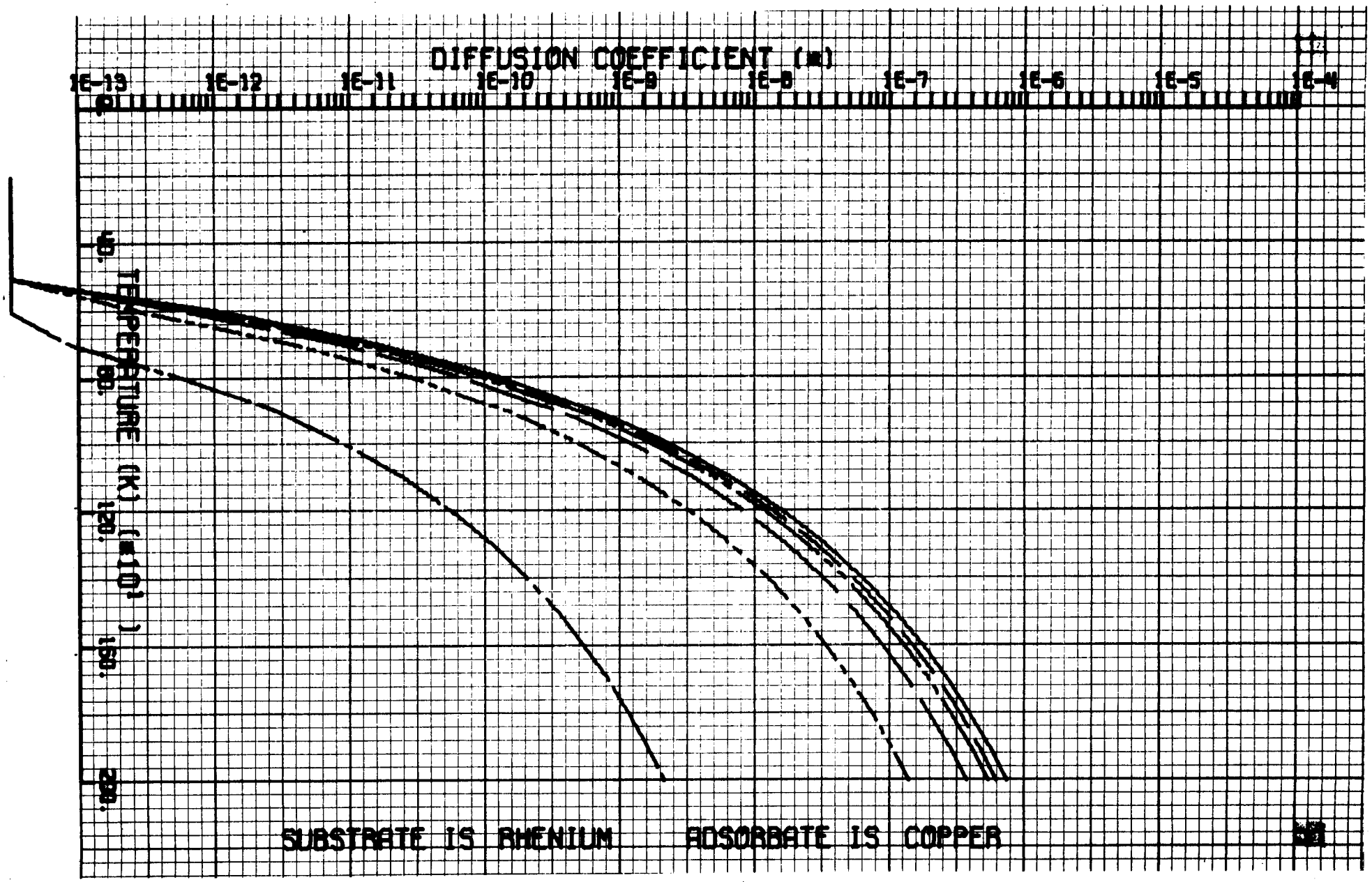
DIFFUSION COEFFICIENT (m)
1E-13
1E-12
1E-11
1E-10
1E-9
1E-8
1E-7
1E-6
1E-5
1E-4
TEMPERATURE (K) (10^)
SUBSTRATE IS RHENIUM
ADSORBATE IS COPPER

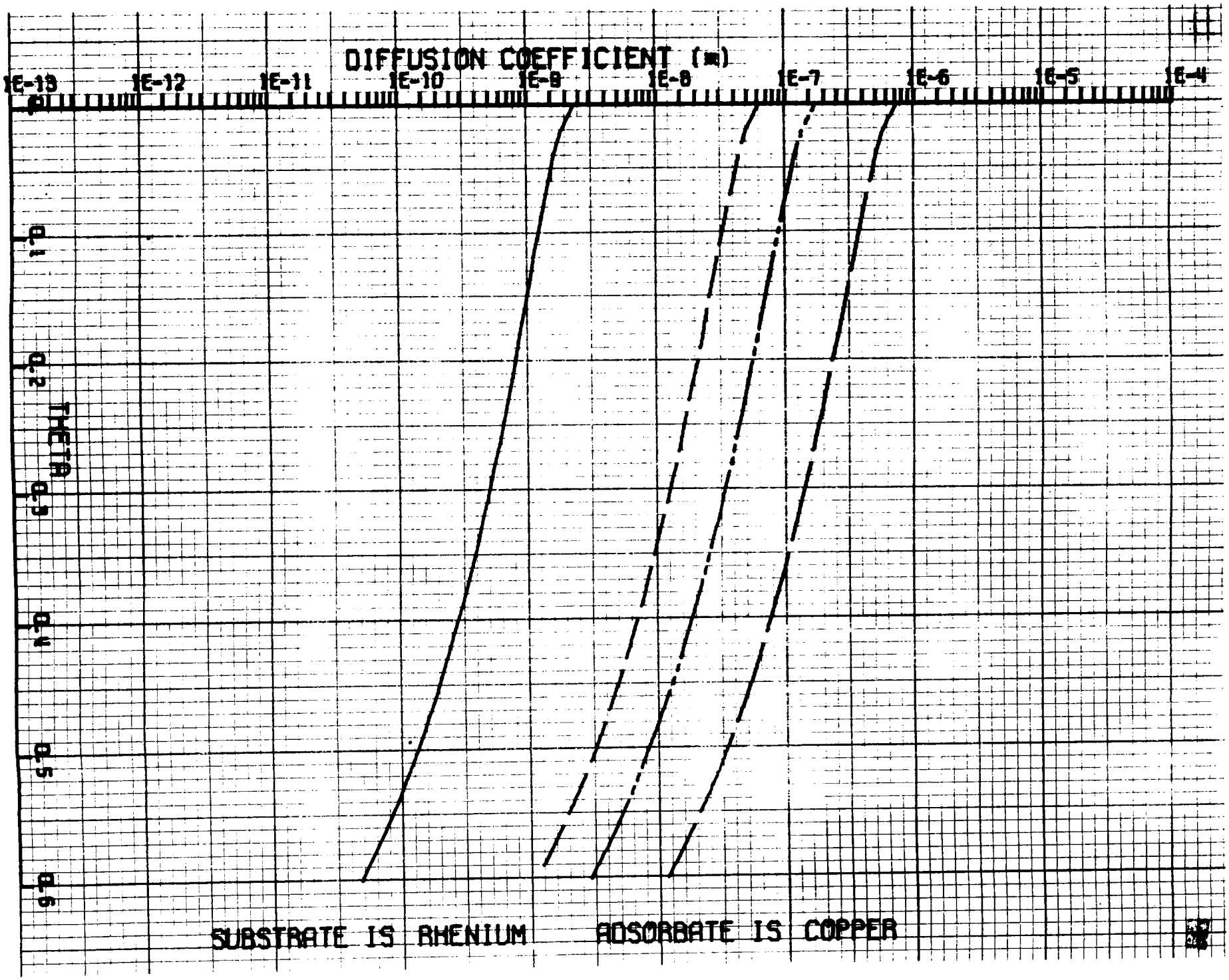
DIFFUSION COEFFICIENT (m)
1E-13
1E-12
1E-11
1E-10
1E-9
1E-8
1E-7
1E-6
1E-5
1E-4
THETA
0.1
0.2
0.3
0.4
0.5
0.6
SUBSTRATE IS RHENIUM
ADSORBATE IS COPPER

DIFFUSION COEFFICIENT (m²)
1E-13
1E-12
1E-11
1E-10
1E-9
1E-8
1E-7
1E-6
1E-5
1E-4
TEMPERATURE (K) (×10¹)
40.
80.
120.
160.
200.
SUBSTRATE IS RHENIUM ADSORBATE IS GALLIUM

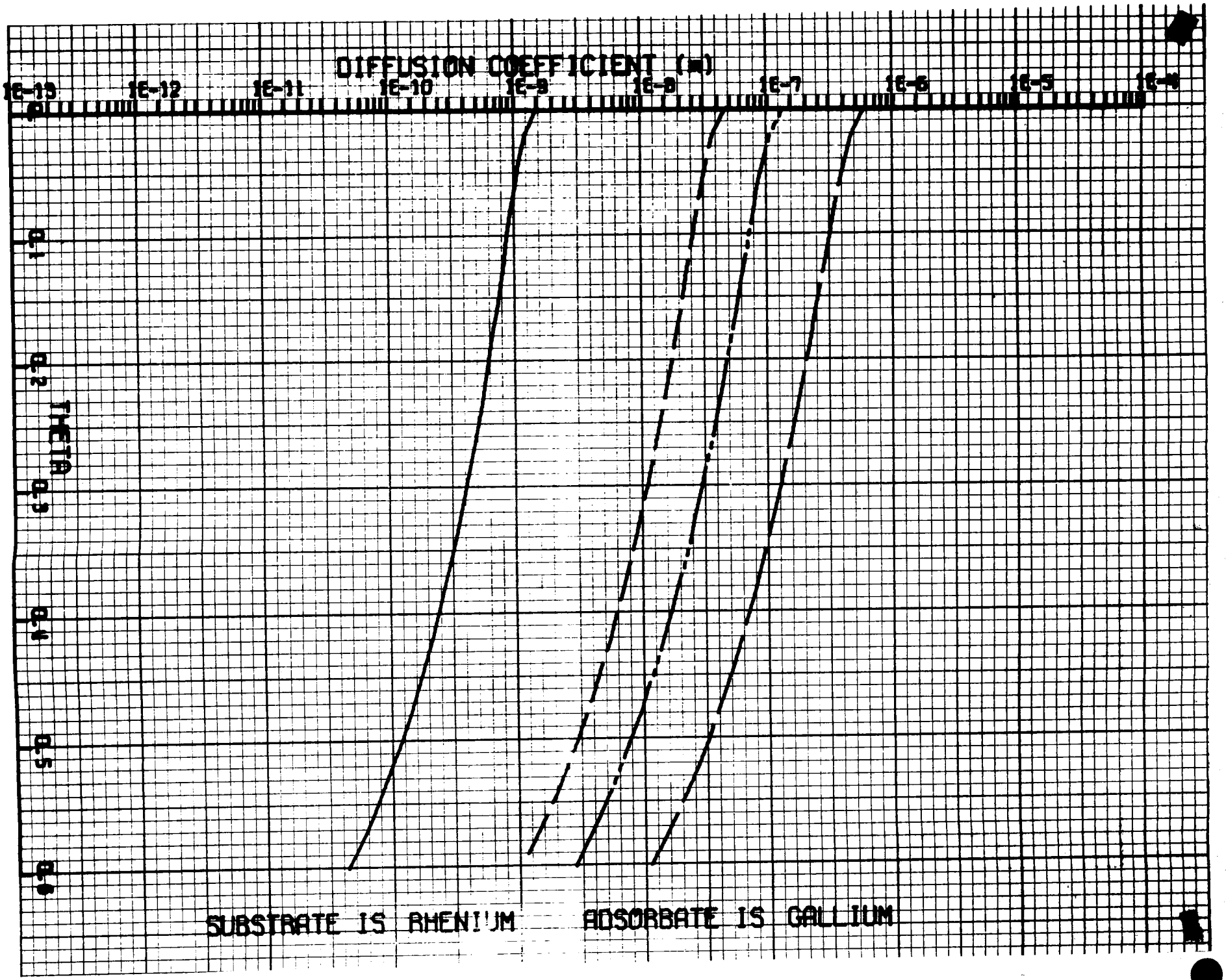
DIFFUSION COEFFICIENT (m)
1E-13
1E-12
1E-11
1E-10
1E-9
1E-8
1E-7
1E-6
1E-5
1E-4
THETA
0.1
0.2
0.3
0.4
0.5
0.6
SUBSTRATE IS RHEN!'JM
ADSORBATE IS GALLIUM

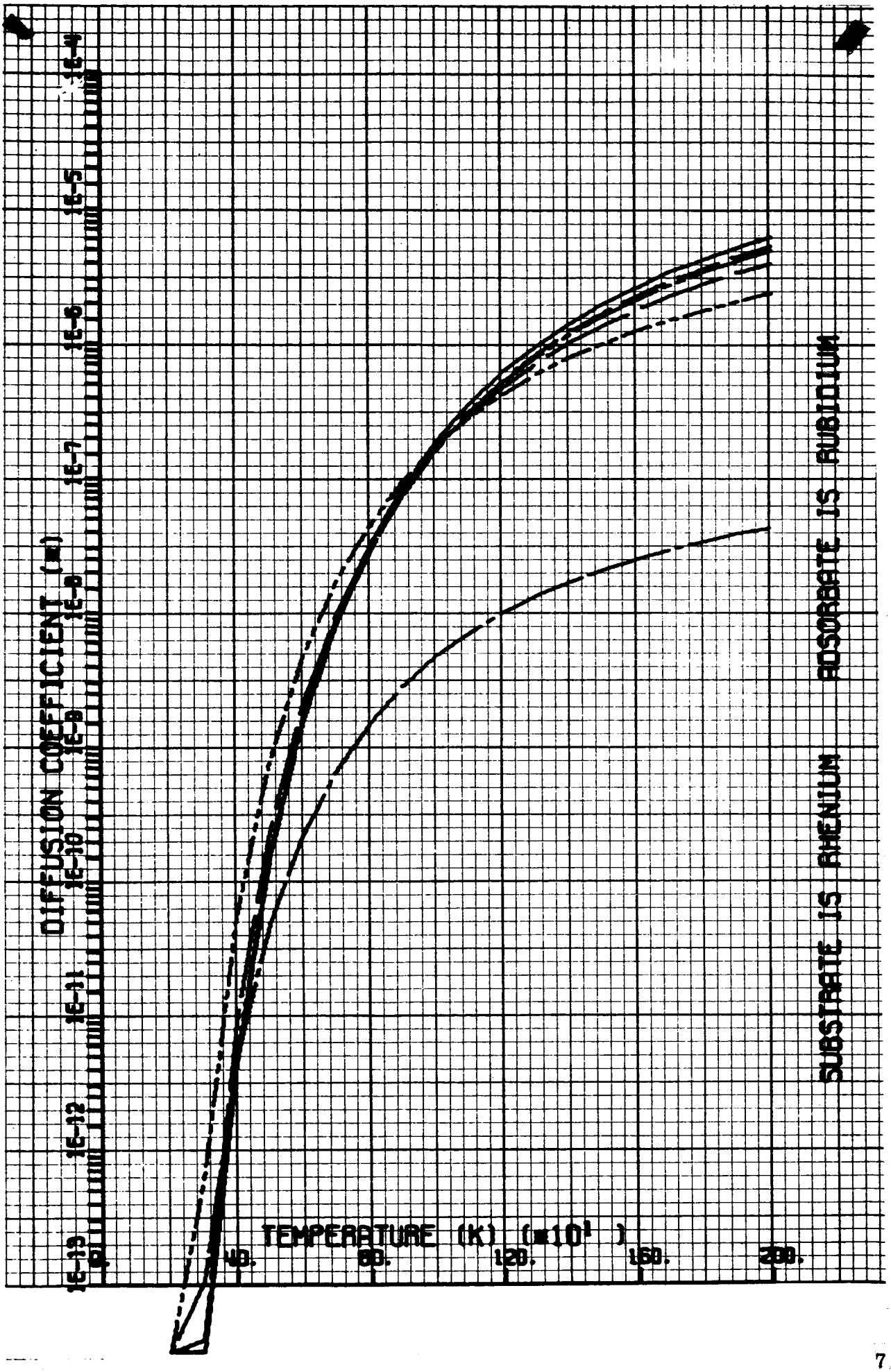
DIFFUSION COEFFICIENT (m²)
1E-4
1E-5
1E-6
1E-7
1E-8
1E-9
1E-10
1E-11
1E-12
1E-13
TEMPERATURE (K) (×10¹)
40.
80.
120.
160.
200.
SUBSTRATE IS RHENIUM ADSORBATE IS RUBIDIUM

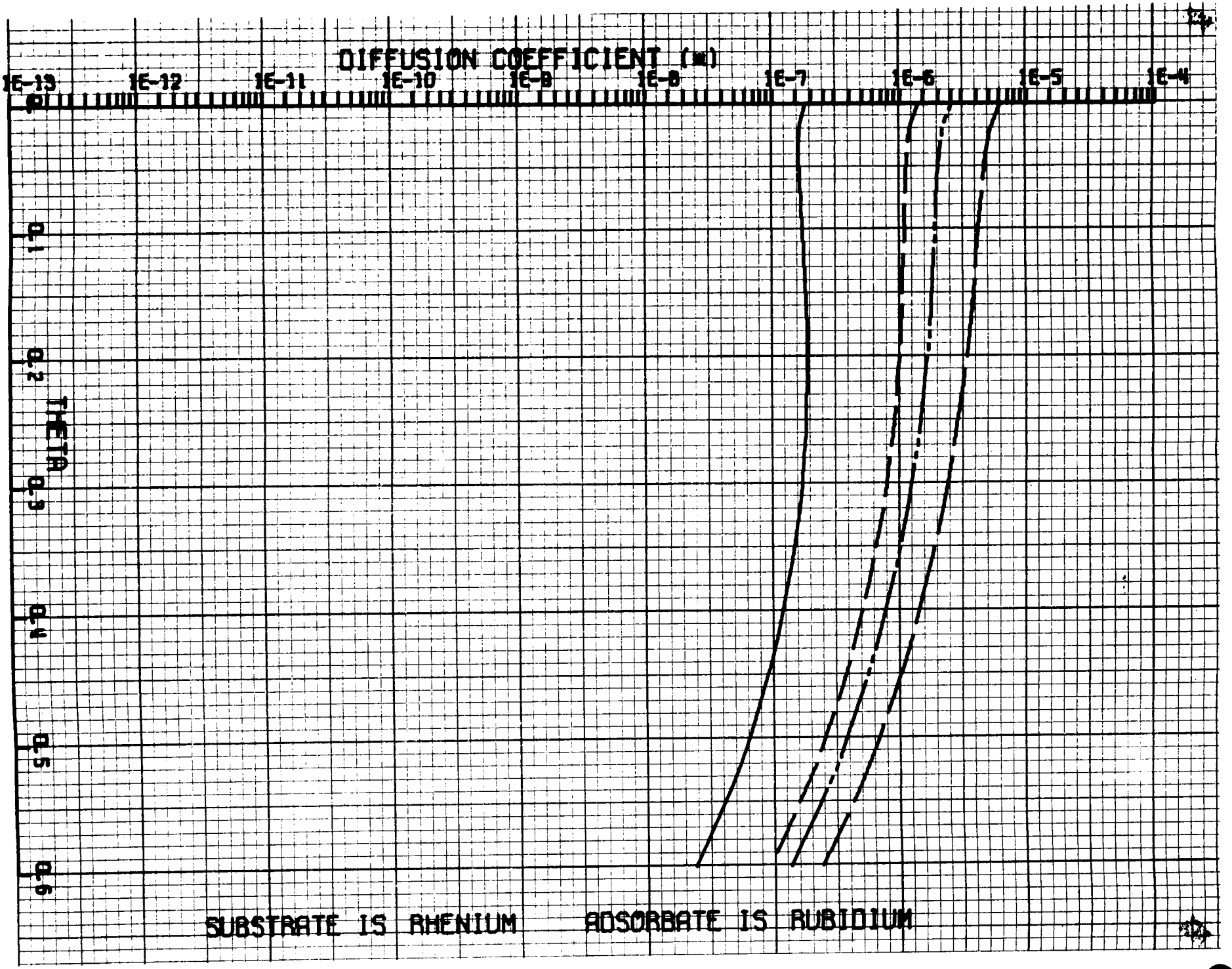
DIFFUSION COEFFICIENT (m)
1E-13
1E-12
1E-11
1E-10
1E-9
1E-8
1E-7
1E-6
1E-5
1E-4
THETA
0.1
0.2
0.3
0.4
0.5
0.6
SUBSTRATE IS RHENIUM
ADSORBATE IS RUBIDIUM

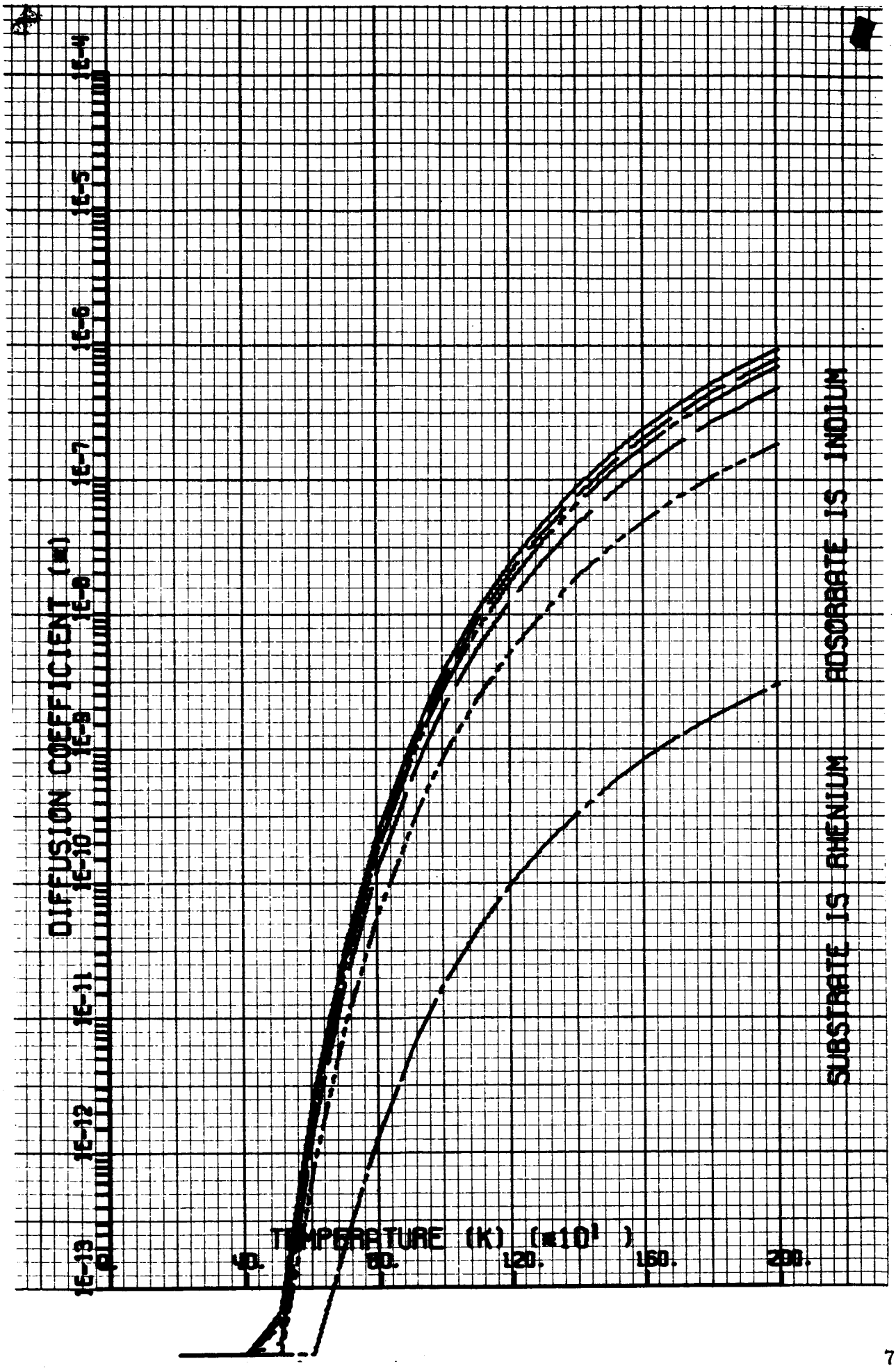
DIFFUSION COEFFICIENT (M)
1E-4
1E-5
1E-6
1E-7
1E-8
1E-9
1E-10
1E-11
1E-12
1E-13
TEMPERATURE (K) (*10¹)
40.
80.
120.
160.
200.
SUBSTRATE IS ARGENTUM ADSORBATE IS INDIUM

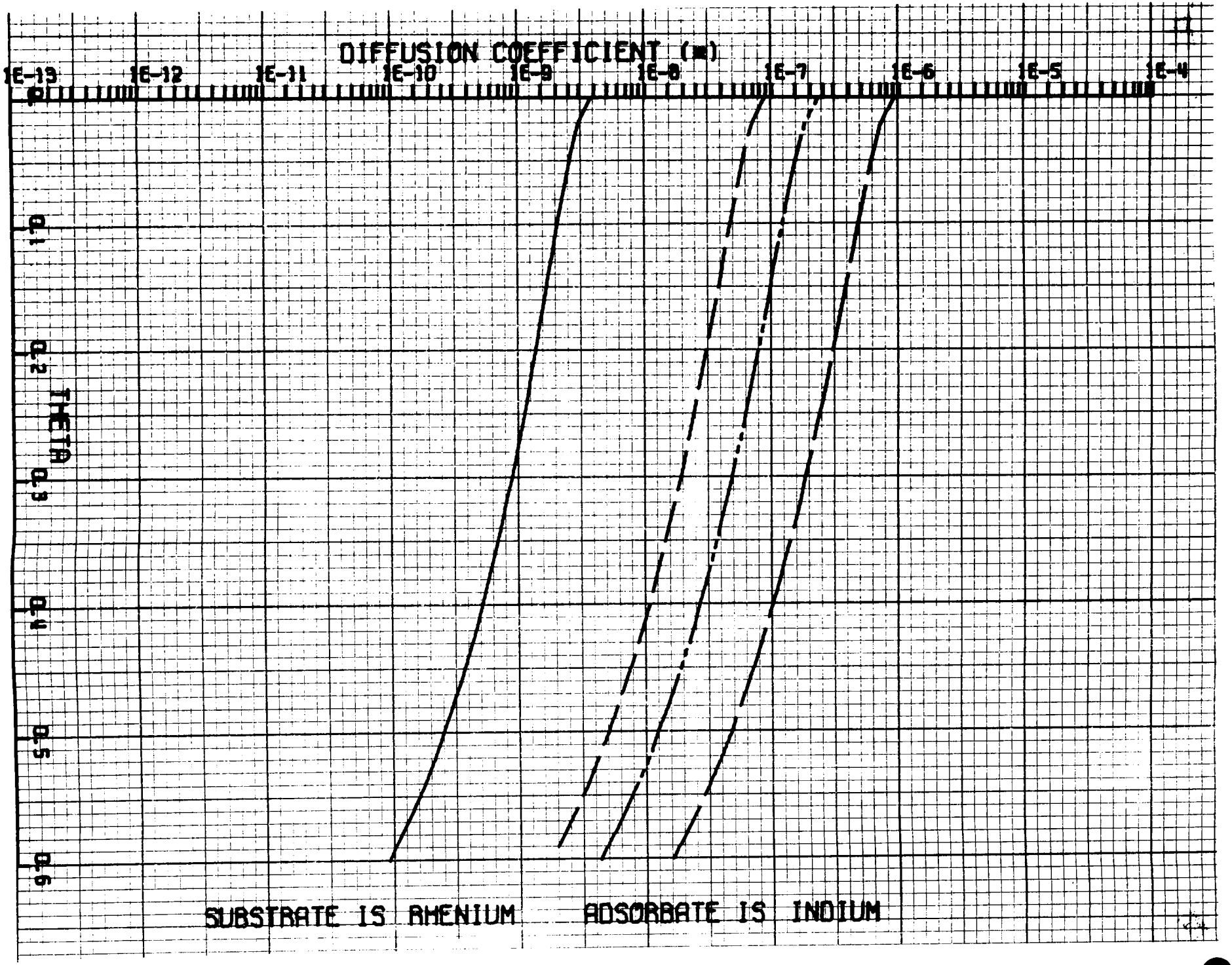
DIFFUSION COEFFICIENT (m)
1E-13
1E-12
1E-11
1E-10
1E-9
1E-8
1E-7
1E-6
1E-5
1E-4
THETA
0.1
0.2
0.3
0.4
0.5
0.6
SUBSTRATE IS RHENIUM
ADSORBATE IS INDIUM

DIFFUSION COEFFICIENT (m)
1E-4
1E-5
1E-6
1E-7
1E-8
1E-9
1E-10
1E-11
1E-12
1E-13
TEMPERATURE (K) (*10¹)
40.
80.
120.
160.
200.
SUBSTRATE IS ARRENIUM ADSORBATE IS TIN

DIFFUSION COEFFICIENT (M)
1E-4
1E-5
1E-6
1E-7
1E-8
1E-9
1E-10
1E-11
1E-12
1E-13
0
0.1
0.2
0.3
0.4
0.5
0.6
THETA
SUBSTRATE IS RHENIUM ADSORBATE IS TIN

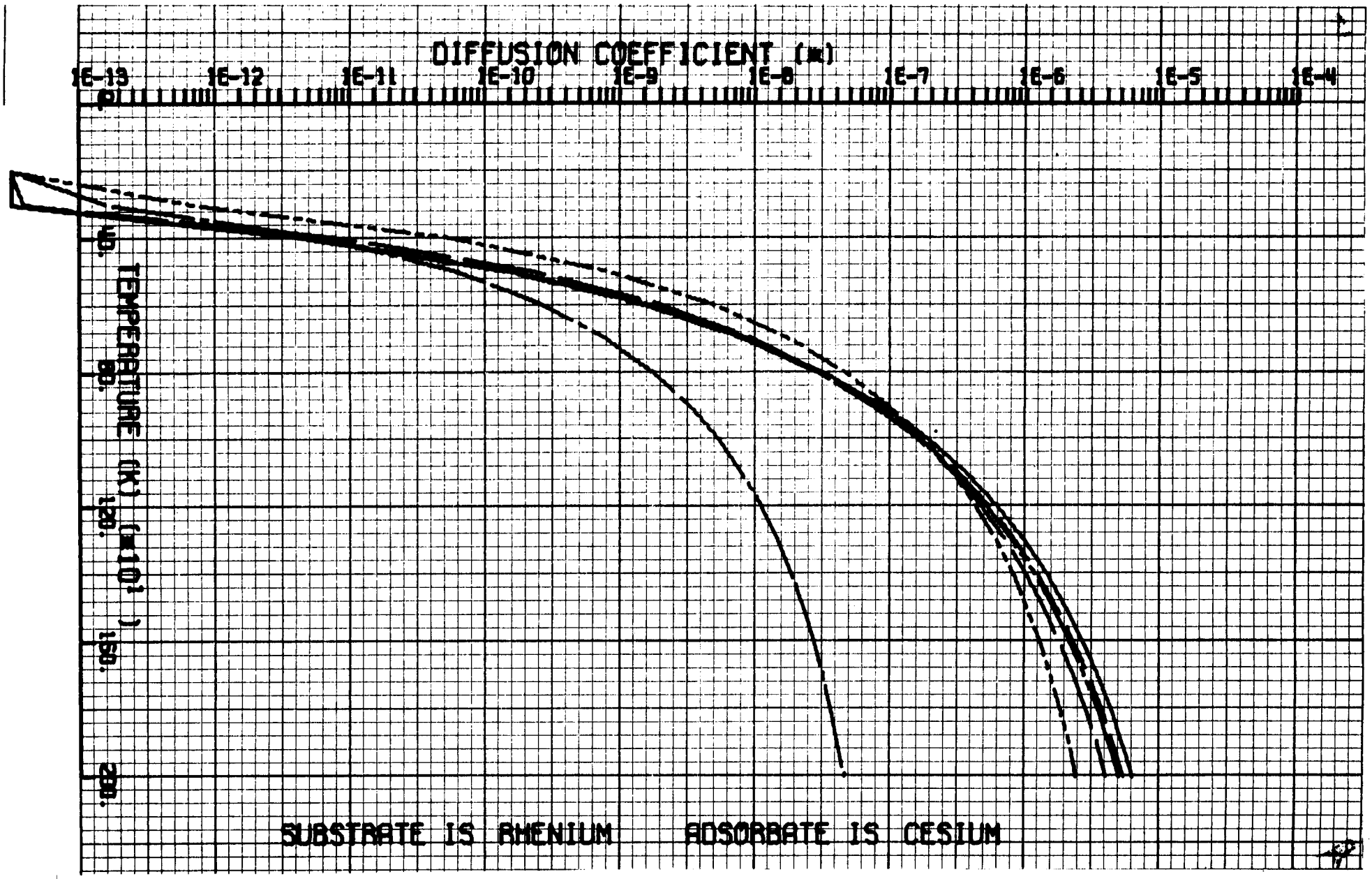
DIFFUSION COEFFICIENT (m)
1E-13
1E-12
1E-11
1E-10
1E-9
1E-8
1E-7
1E-6
1E-5
1E-4
TEMPERATURE (K) (x10)
180
150
120
90
60
SUBSTRATE IS RHENIUM
ADSORBATE IS CESIUM

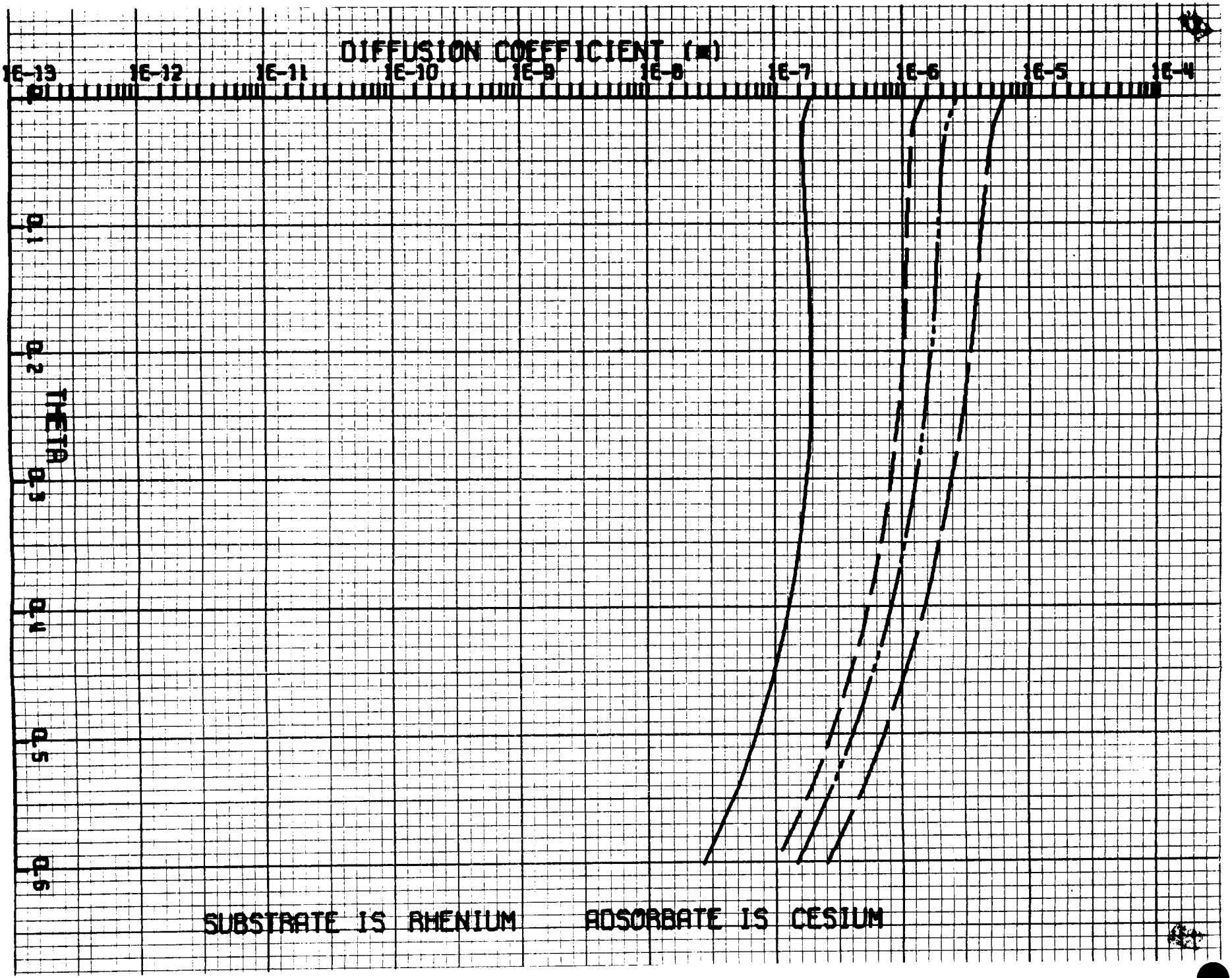
DIFFUSION COEFFICIENT (m)
1E-13
1E-12
1E-11
1E-10
1E-9
1E-8
1E-7
1E-6
1E-5
1E-4
TIME (s)
0.1
0.2
0.3
0.4
0.5
0.6
SUBSTRATE IS RHENIUM
ADSORBATE IS CESIUM

DIFFUSION COEFFICIENT (m)
1E-4
1E-5
1E-6
1E-7
1E-8
1E-9
1E-10
1E-11
1E-12
1E-13
TEMPERATURE (K) (*10¹)
40.
80.
120.
160.
200.
SUBSTRATE IS RHENIUM ADSORBATE IS BARIUM

DIFFUSION COEFFICIENT (cm²)
1E-4
1E-5
1E-6
1E-7
1E-8
1E-9
1E-10
1E-11
1E-12
1E-13
0
0.1
0.2
0.3
0.4
0.5
0.6
THETA
SUBSTRATE IS RHENIUM ADSORBATE IS BARIUM

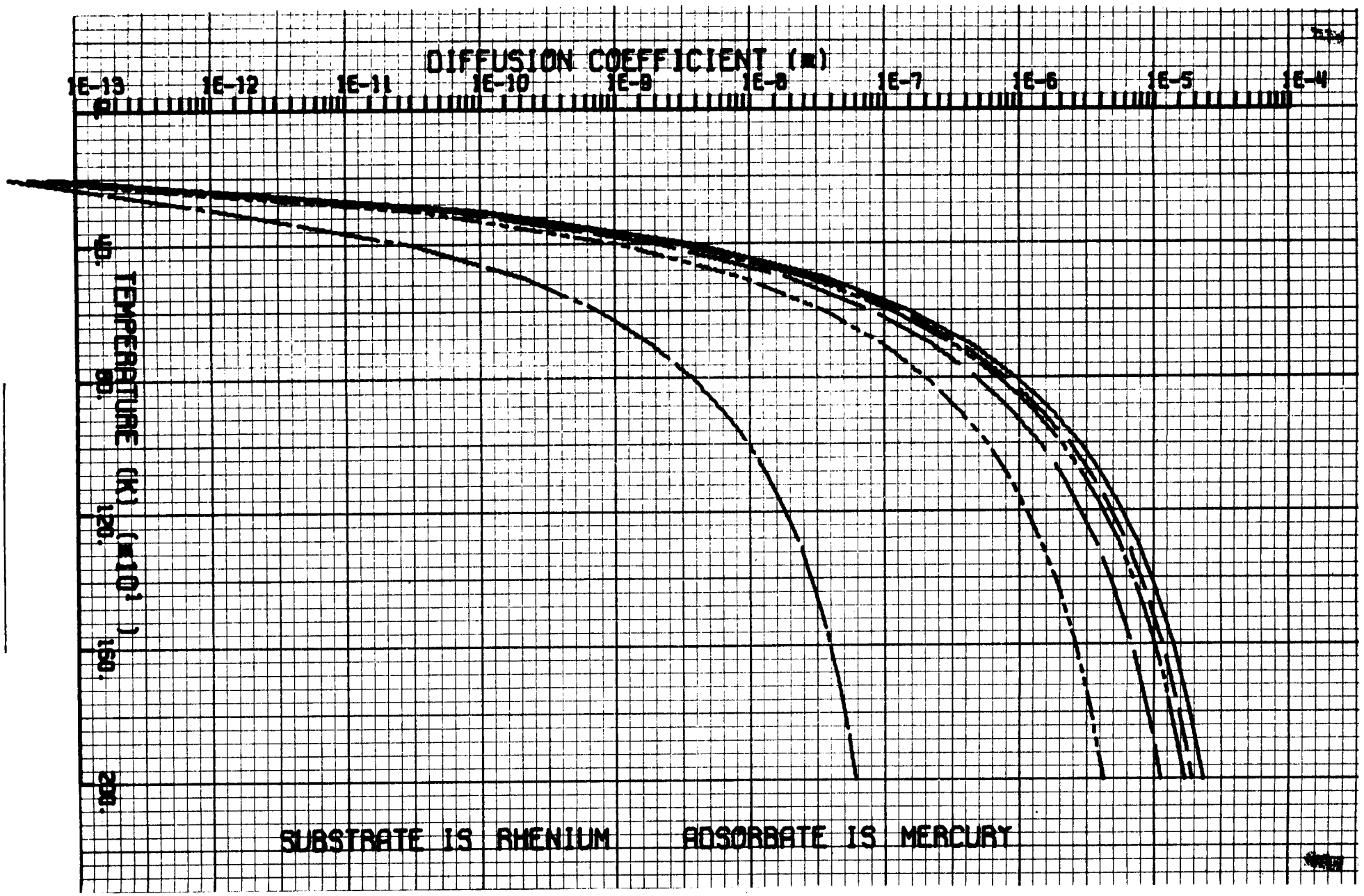
DIFFUSION COEFFICIENT (m)
1E-13
1E-12
1E-11
1E-10
1E-9
1E-8
1E-7
1E-6
1E-5
1E-4
TEMPERATURE (K) (m*10^-1)
200.
160.
120.
80.
SUBSTRATE IS RHENIUM
ADSORBATE IS MERCURY

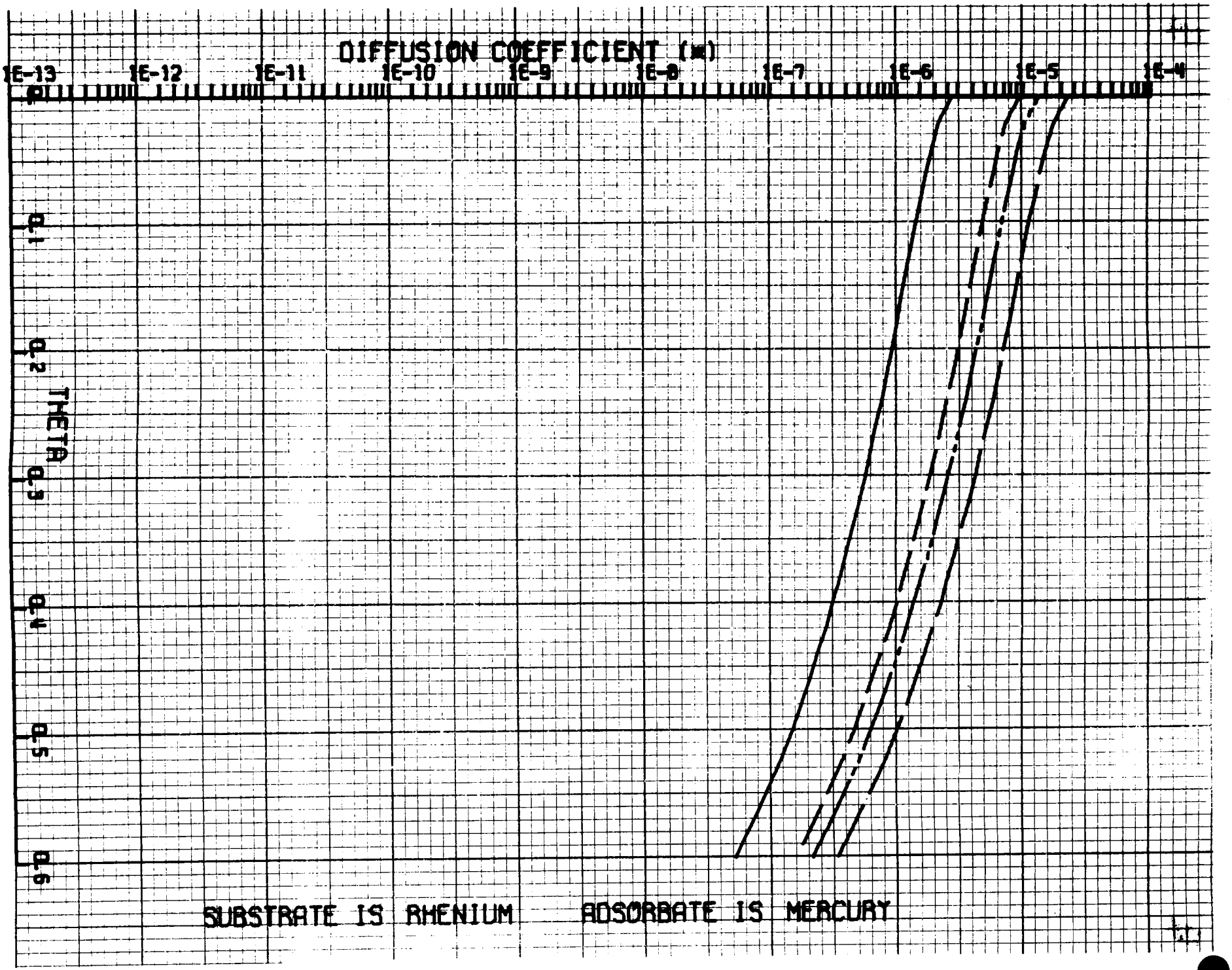
DIFFUSION COEFFICIENT (m)
1E-13
1E-12
1E-11
1E-10
1E-9
1E-8
1E-7
1E-6
1E-5
1E-4
THETA
θ1
θ2
θ3
θ4
θ5
θ6
SUBSTRATE IS RHENIUM
ADSORBATE IS MERCURY

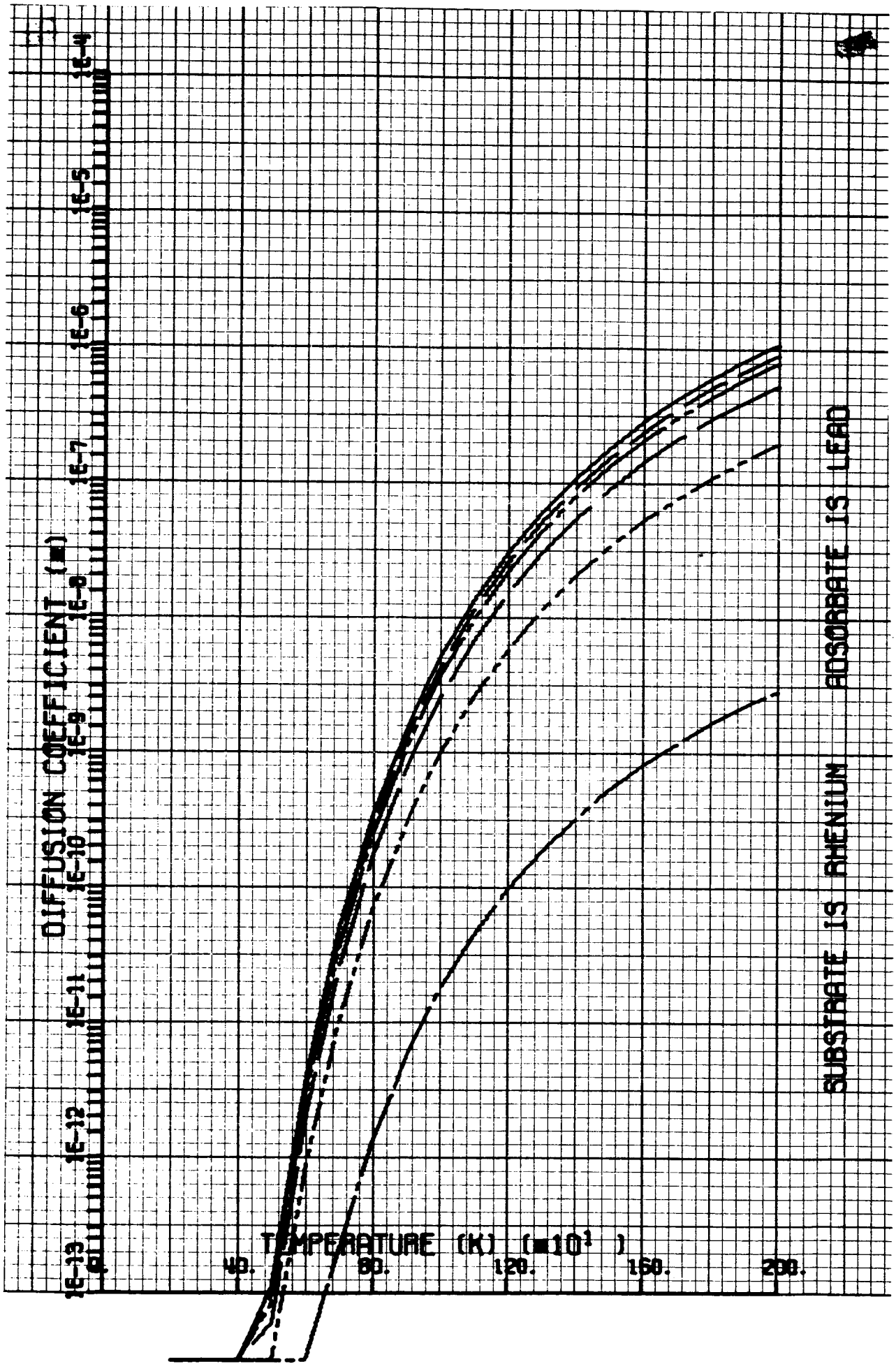
DIFFUSION COEFFICIENT (m)
1E-4
1E-5
1E-6
1E-7
1E-8
1E-9
1E-10
1E-11
1E-12
1E-13
TEMPERATURE (K) (*10^-1)
40.
80.
120.
160.
200.
SUBSTRATE IS RHENIUM ADSORBATE IS LEAD

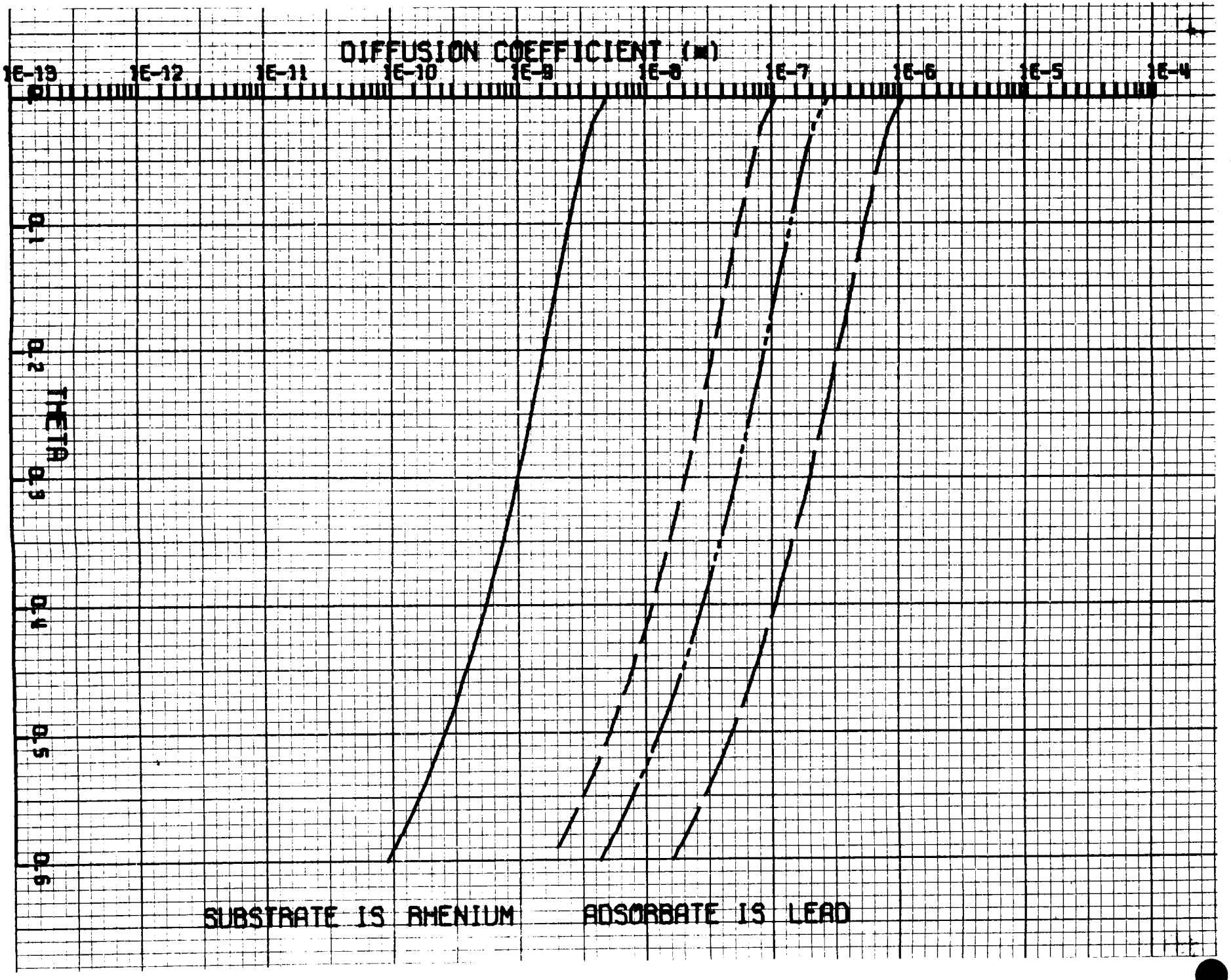
DIFFUSION COEFFICIENT (m)
1E-13
1E-12
1E-11
1E-10
1E-9
1E-8
1E-7
1E-6
1E-5
1E-4
THETA
0
0.1
0.2
0.3
0.4
0.5
0.6
SUBSTRATE IS RHENIUM
ADSORBATE IS LEAD

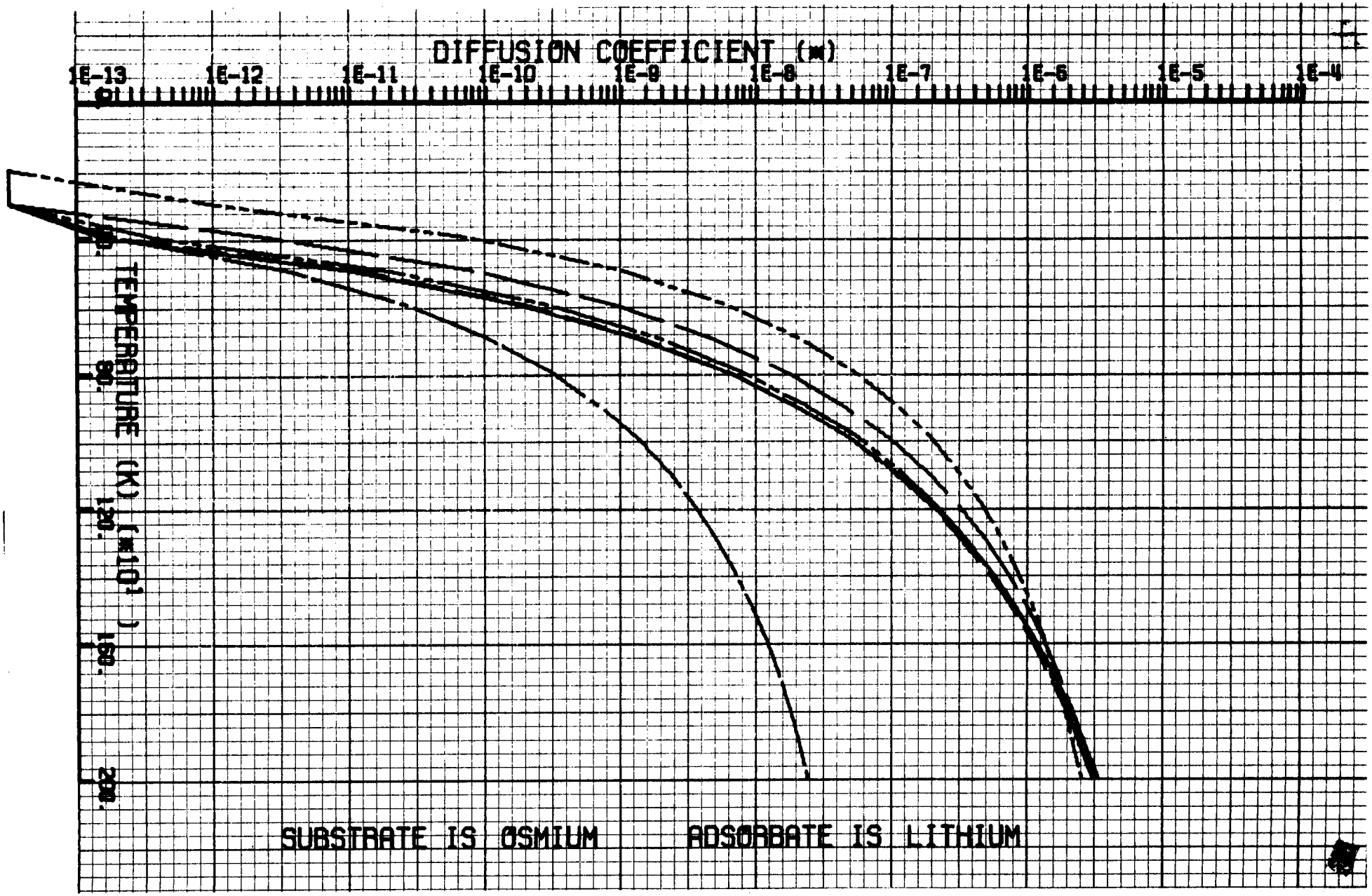
DIFFUSION COEFFICIENT (m)
1E-13
1E-12
1E-11
1E-10
1E-9
1E-8
1E-7
1E-6
1E-5
1E-4
TEMPERATURE (K) (m*10¹)
80.
120.
160.
200.
SUBSTRATE IS OSMIUM
ADSORBATE IS LITHIUM

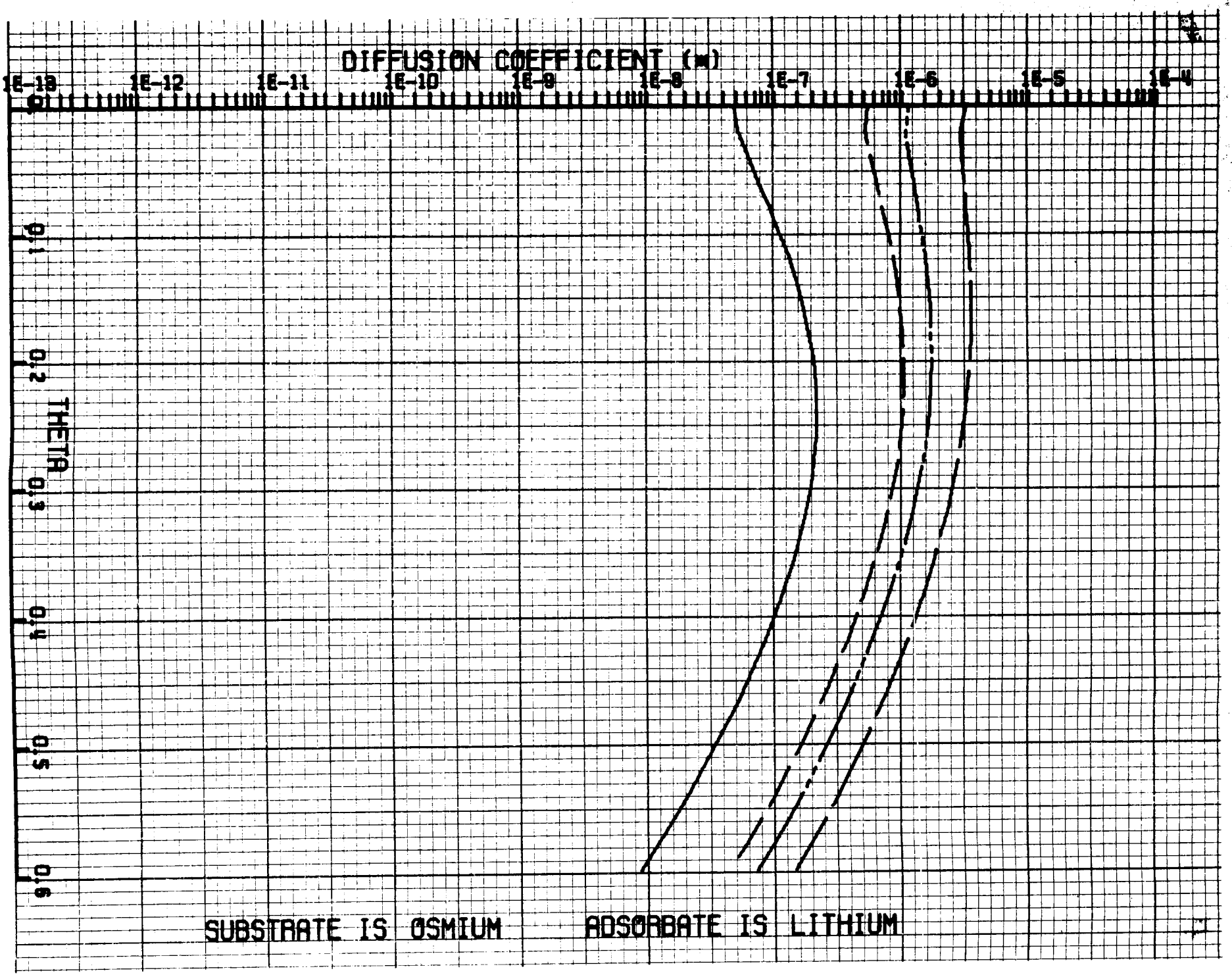
DIFFUSION COEFFICIENT (M)
1E-13
1E-12
1E-11
1E-10
1E-9
1E-8
1E-7
1E-6
1E-5
1E-4
THETA
0.1
0.2
0.3
0.4
0.5
0.6
SUBSTRATE IS OSMIUM
ADSORBATE IS LITHIUM

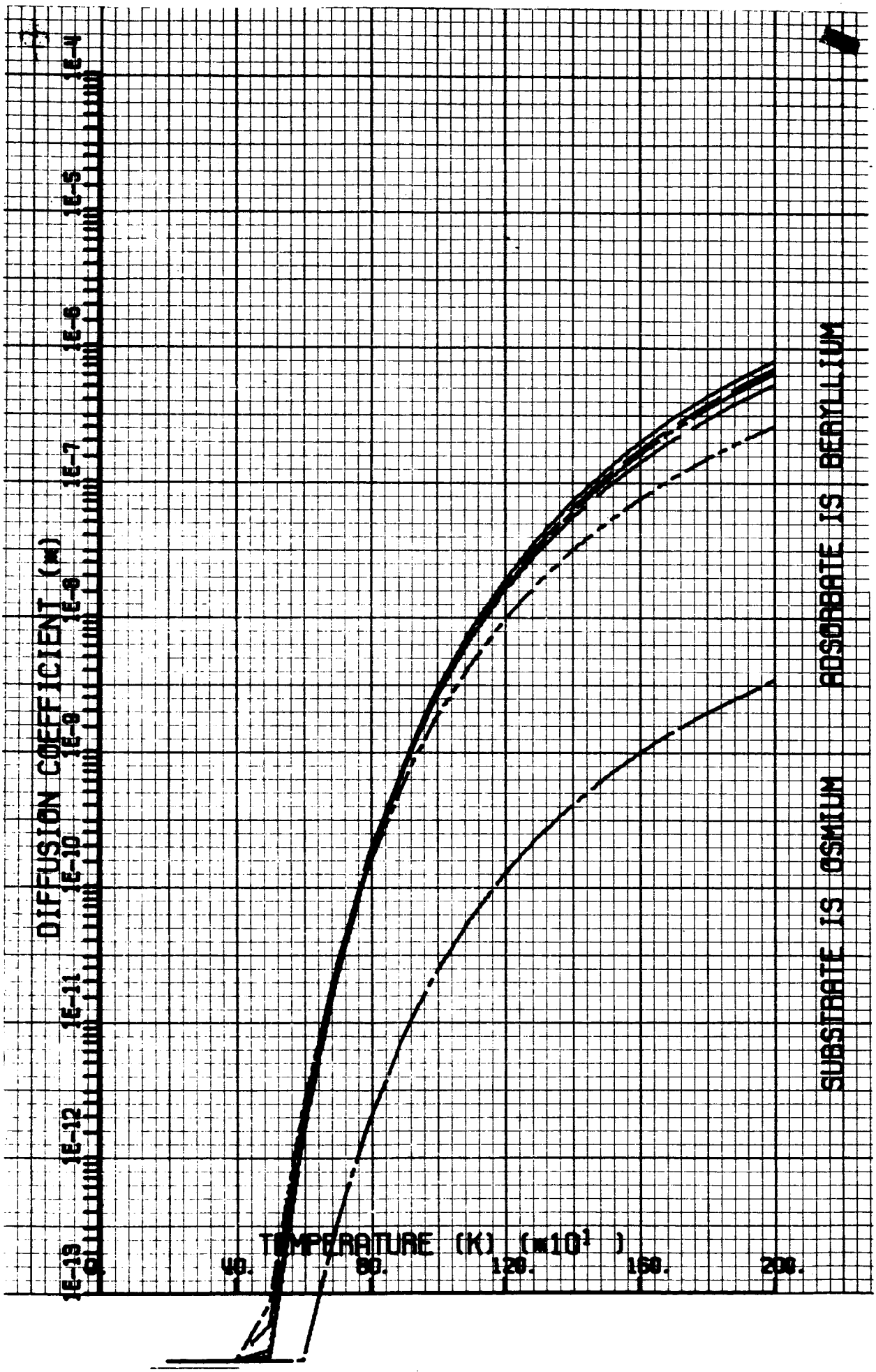
DIFFUSION COEFFICIENT (m)
1E-4
1E-5
1E-6
1E-7
1E-8
1E-9
1E-10
1E-11
1E-12
1E-13
TEMPERATURE (K) (*10¹)
40.
80.
120.
160.
200.
SUBSTRATE IS OSMIUM ADSORBATE IS BERYLLIUM

DIFFUSION COEFFICIENT (M)
1E-13
1E-12
1E-11
1E-10
1E-9
1E-8
1E-7
1E-6
1E-5
1E-4
0.1
0.2
0.3
0.4
0.5
0.6
THETA
SUBSTRATE IS OSMIUM
ADSORBATE IS BERYLLIUM

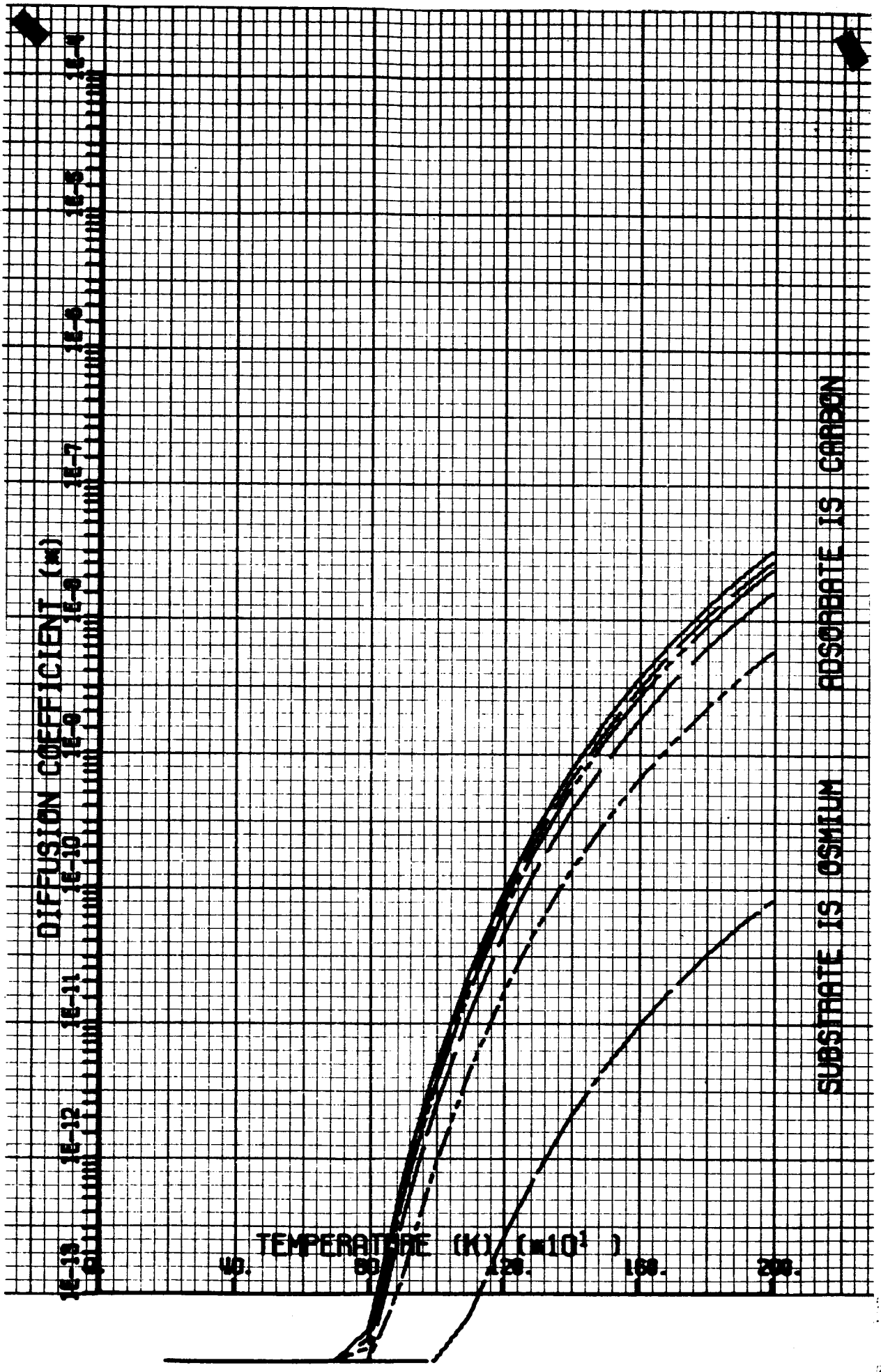
DIFFUSION COEFFICIENT (m²)
1E-4
1E-5
1E-6
1E-7
1E-8
1E-9
1E-10
1E-11
1E-12
1E-13
TEMPERATURE (K) (*10¹)
40.
80.
120.
160.
200.
SUBSTRATE IS OSMIUM ADSORBATE IS CARBON

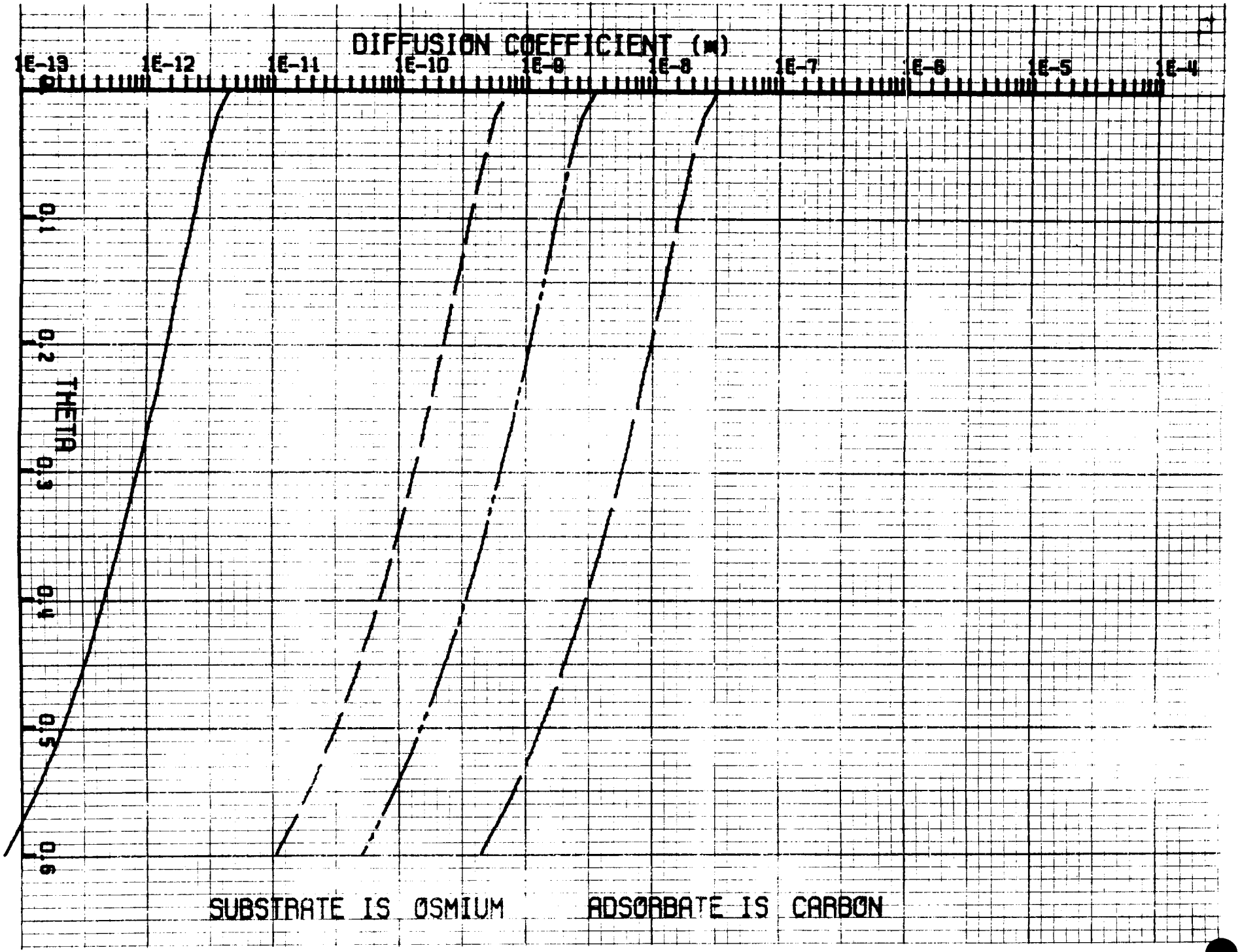
DIFFUSION COEFFICIENT (m)
1E-13
1E-12
1E-11
1E-10
1E-9
1E-8
1E-7
1E-6
1E-5
1E-4
THETA
0.1
0.2
0.3
0.4
0.5
0.6
SUBSTRATE IS OSMIUM
ADSORBATE IS CARBON

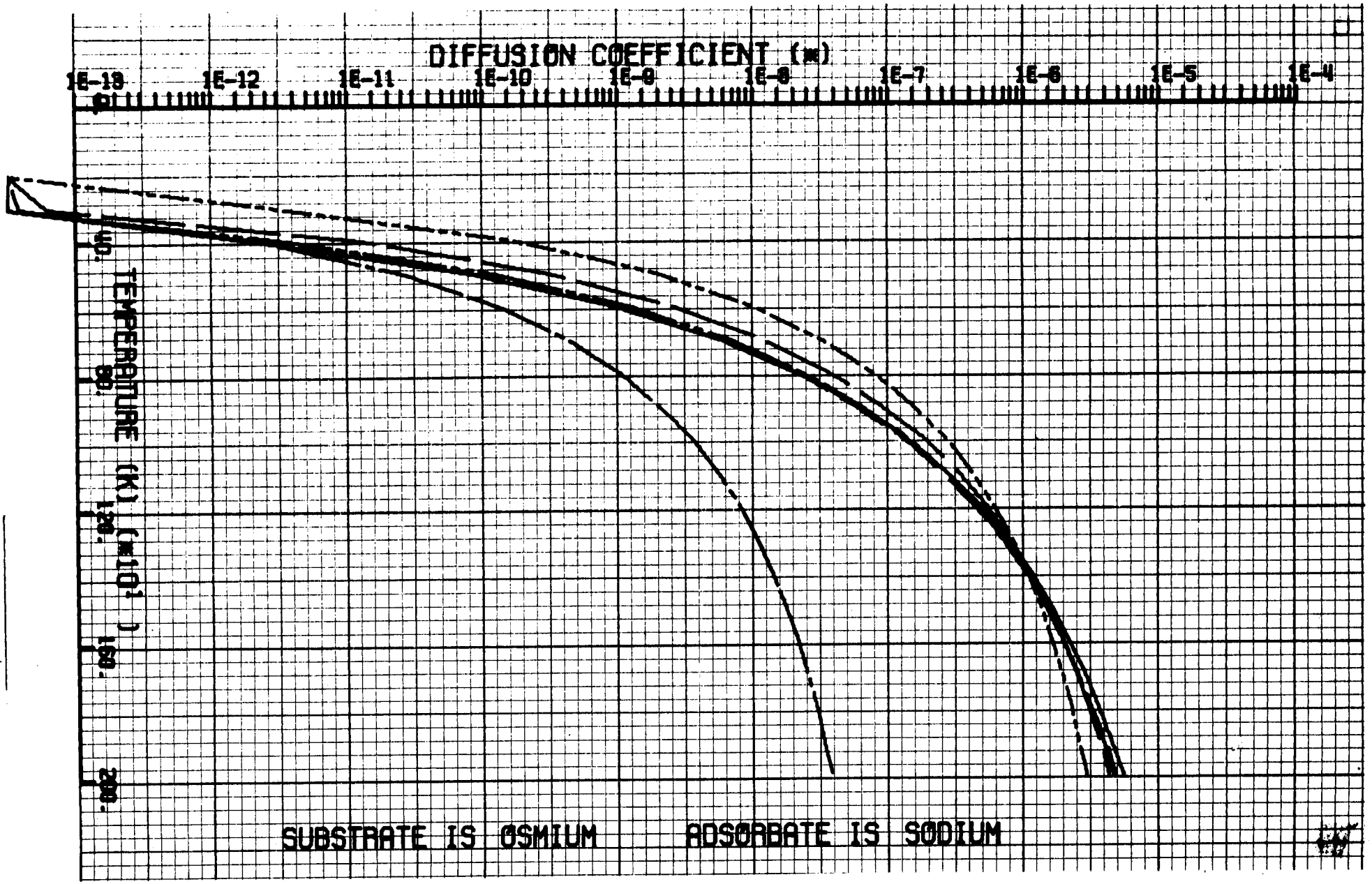
DIFFUSION COEFFICIENT (m)
1E-13
1E-12
1E-11
1E-10
1E-9
1E-8
1E-7
1E-6
1E-5
1E-4
TEMPERATURE (K) (m10)
SUBSTRATE IS OSMIUM
ADSORBATE IS SODIUM

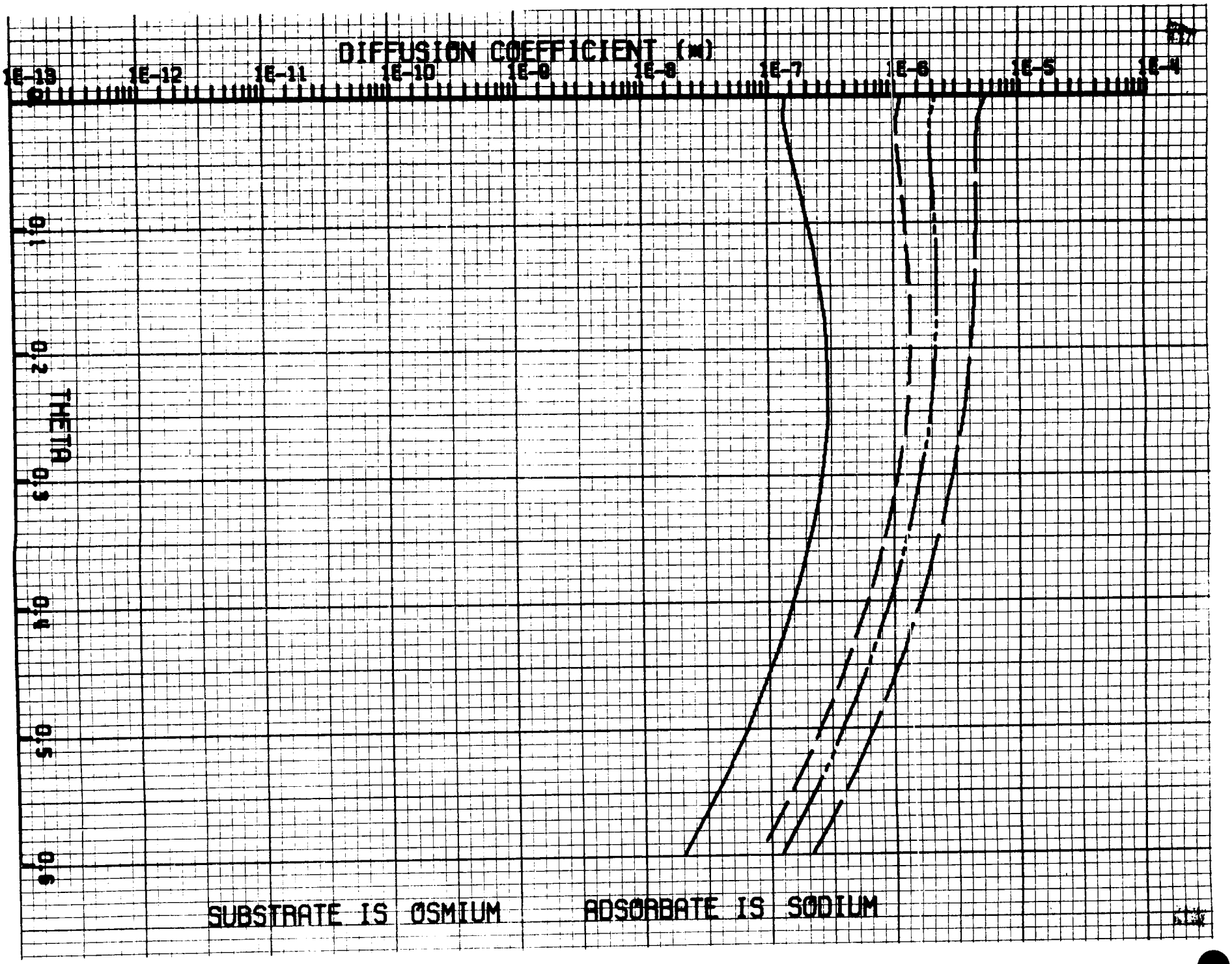
DIFFUSION COEFFICIENT (M)
1E-13
1E-12
1E-11
1E-10
1E-9
1E-8
1E-7
1E-6
1E-5
1E-4
THETA
0.1
0.2
0.3
0.4
0.5
0.6
SUBSTRATE IS OSMIUM
ADSORBATE IS SODIUM

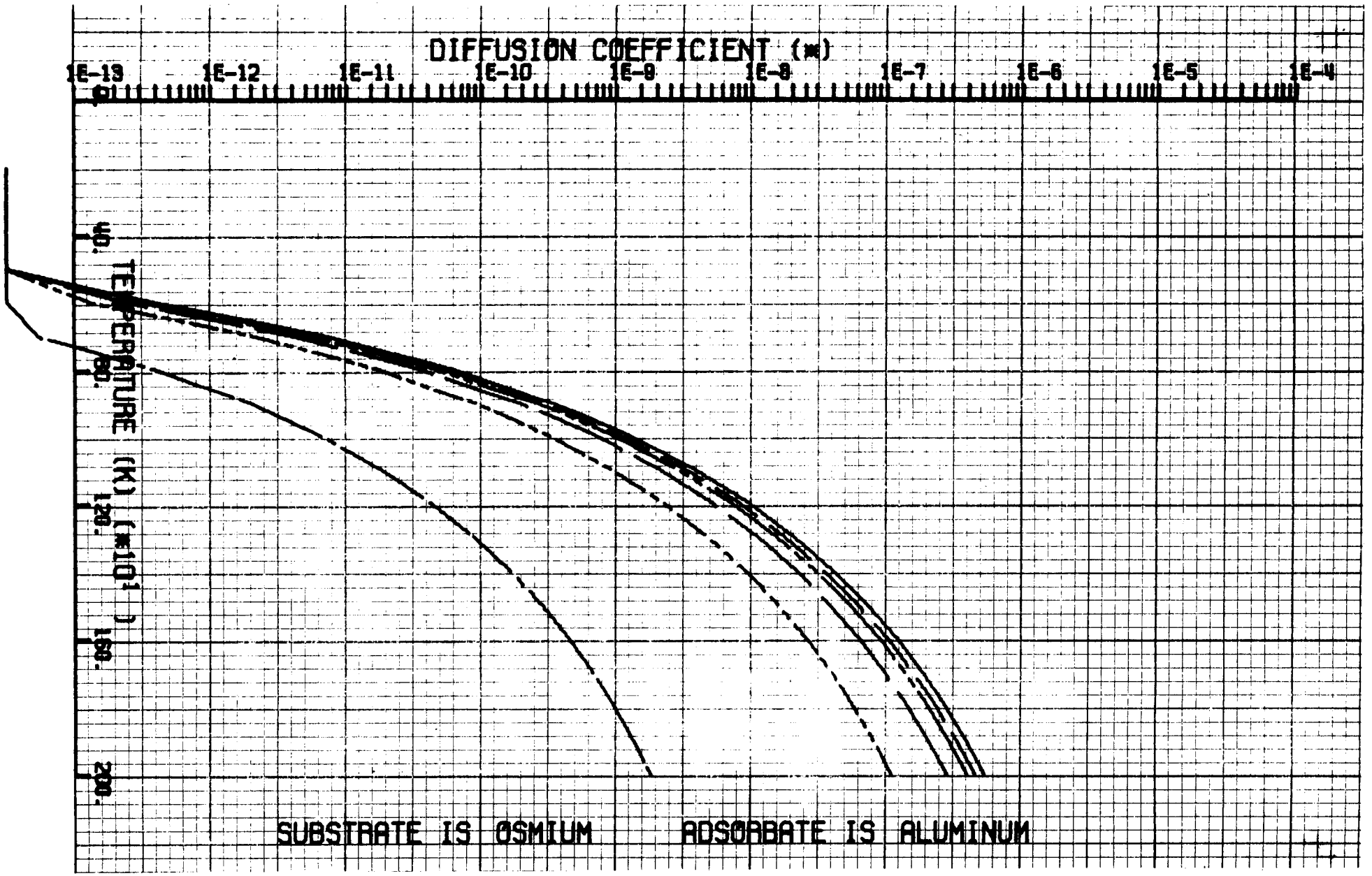
DIFFUSION COEFFICIENT (*)
1E-13
1E-12
1E-11
1E-10
1E-9
1E-8
1E-7
1E-6
1E-5
1E-4
TEMPERATURE (K) (*10^1)
200.
150.
120.
80.
40.
SUBSTRATE IS OSMIUM
ADSORBATE IS ALUMINUM

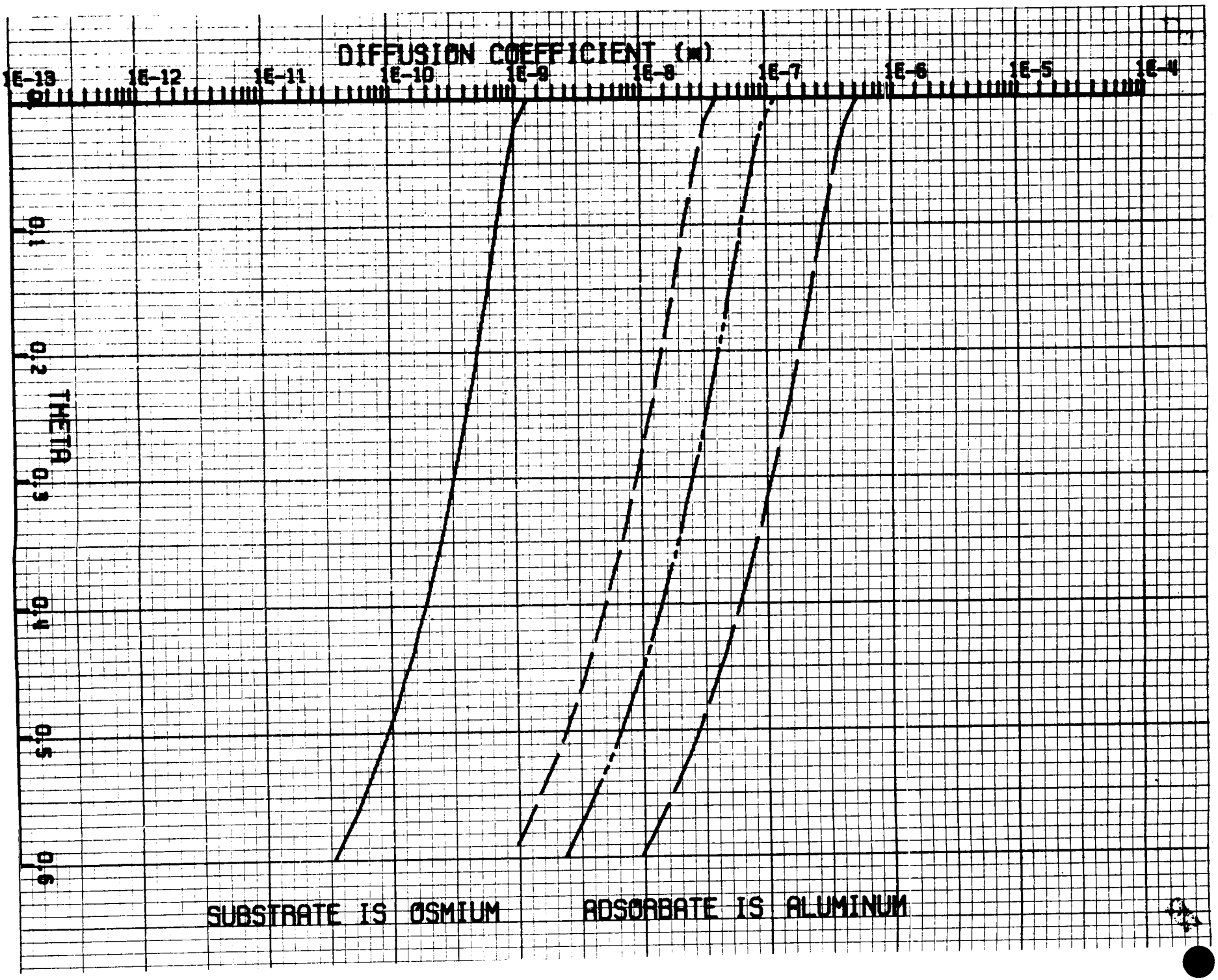
DIFFUSION COEFFICIENT (m)
1E-13
1E-12
1E-11
1E-10
1E-9
1E-8
1E-7
1E-6
1E-5
1E-4
THETA
0.1
0.2
0.3
0.4
0.5
0.6
SUBSTRATE IS OSMIUM
ADSORBATE IS ALUMINUM

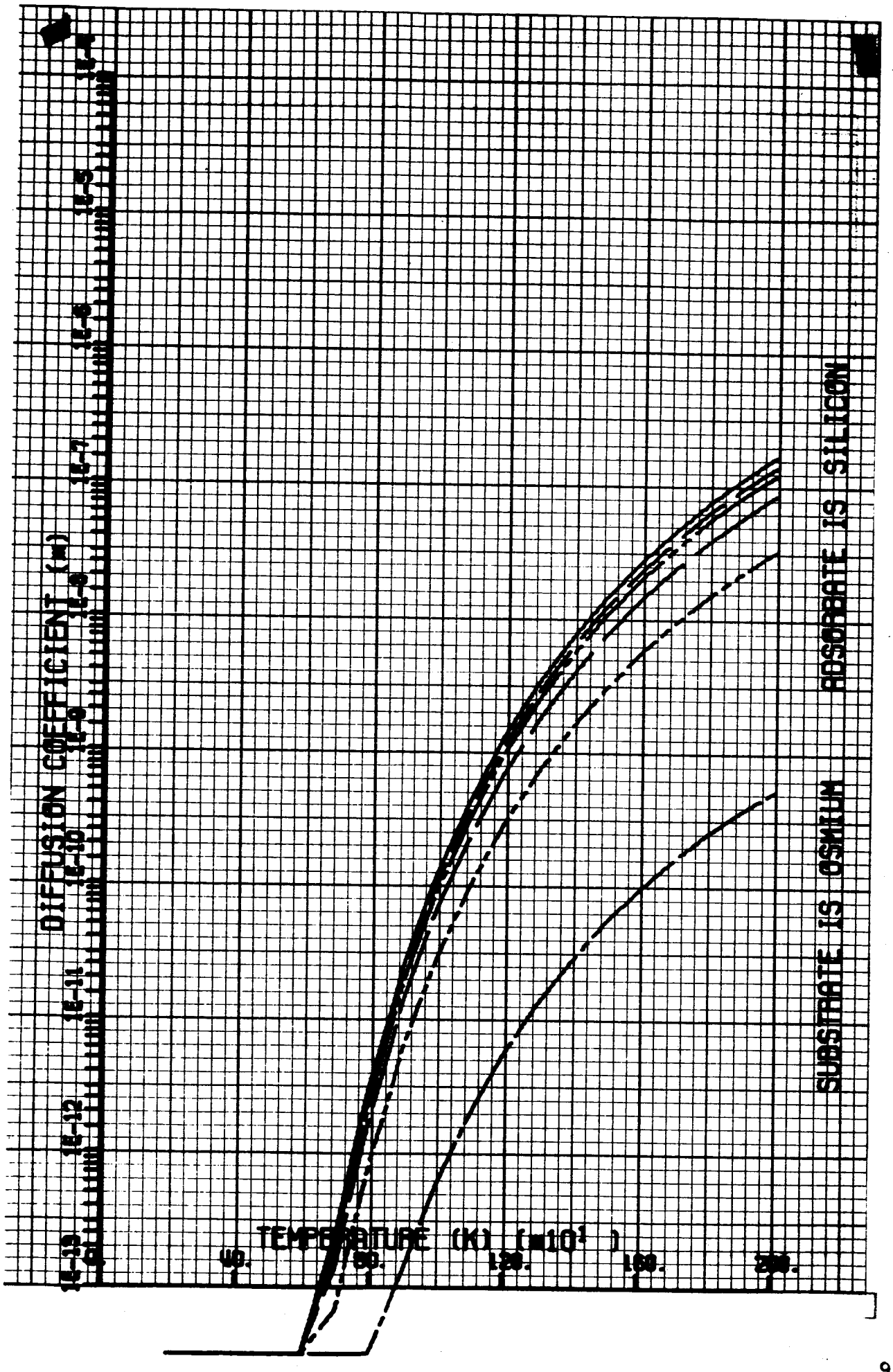
SUBSTRATE IS OSMIUM
ADSORBATE IS SILICON
DIFFUSION COEFFICIENT (m²)
1E-13
1E-12
1E-11
1E-10
1E-9
1E-8
1E-7
1E-6
1E-5
1E-4
40.
80.
120.
160.
200.
TEMPERATURE (K) (x10¹)

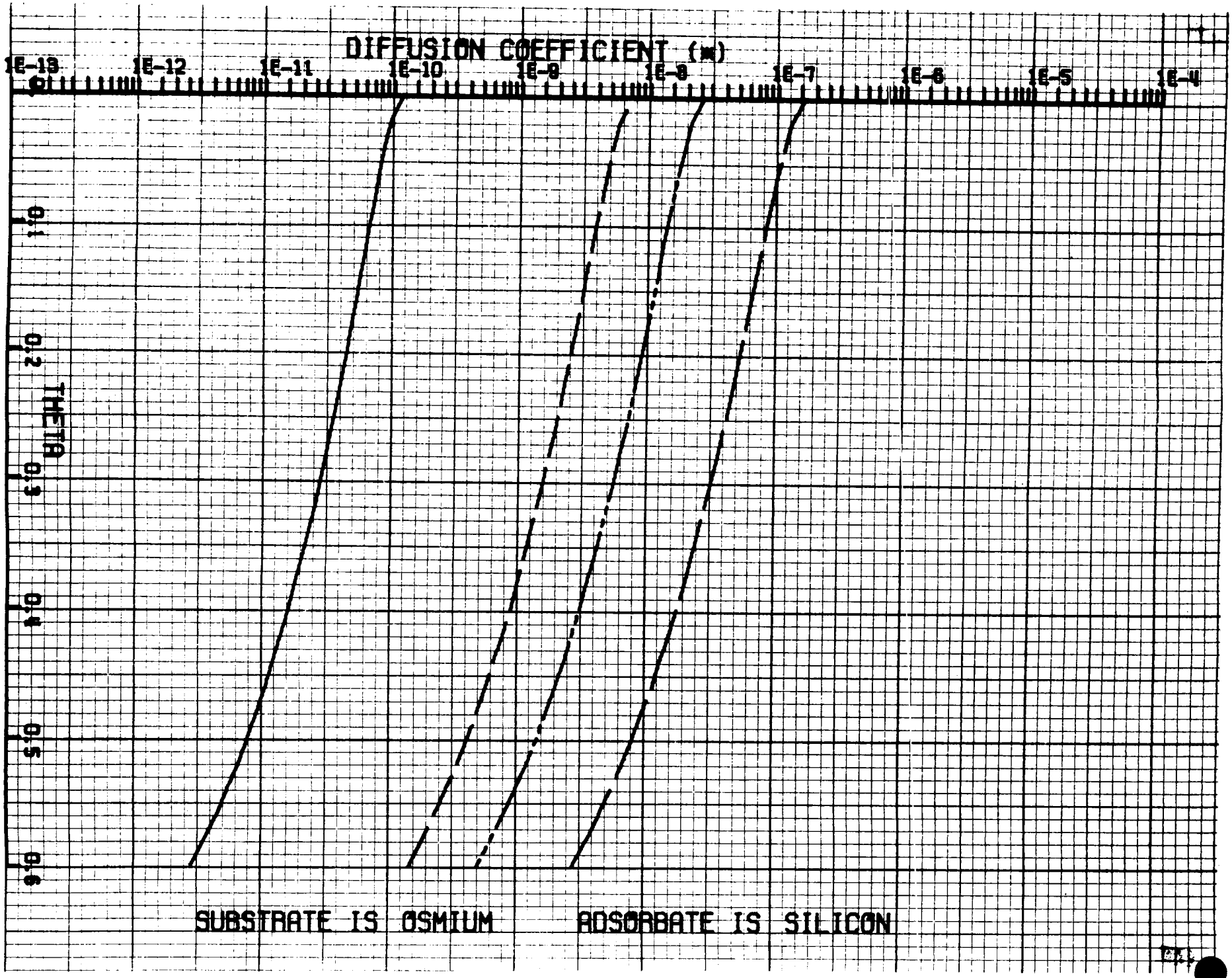
DIFFUSION COEFFICIENT (m)
1E-13
1E-12
1E-11
1E-10
1E-9
1E-8
1E-7
1E-6
1E-5
1E-4
THETA
.01
.02
.03
.04
.05
.06
SUBSTRATE IS OSMIUM
ADSORBATE IS SILICON

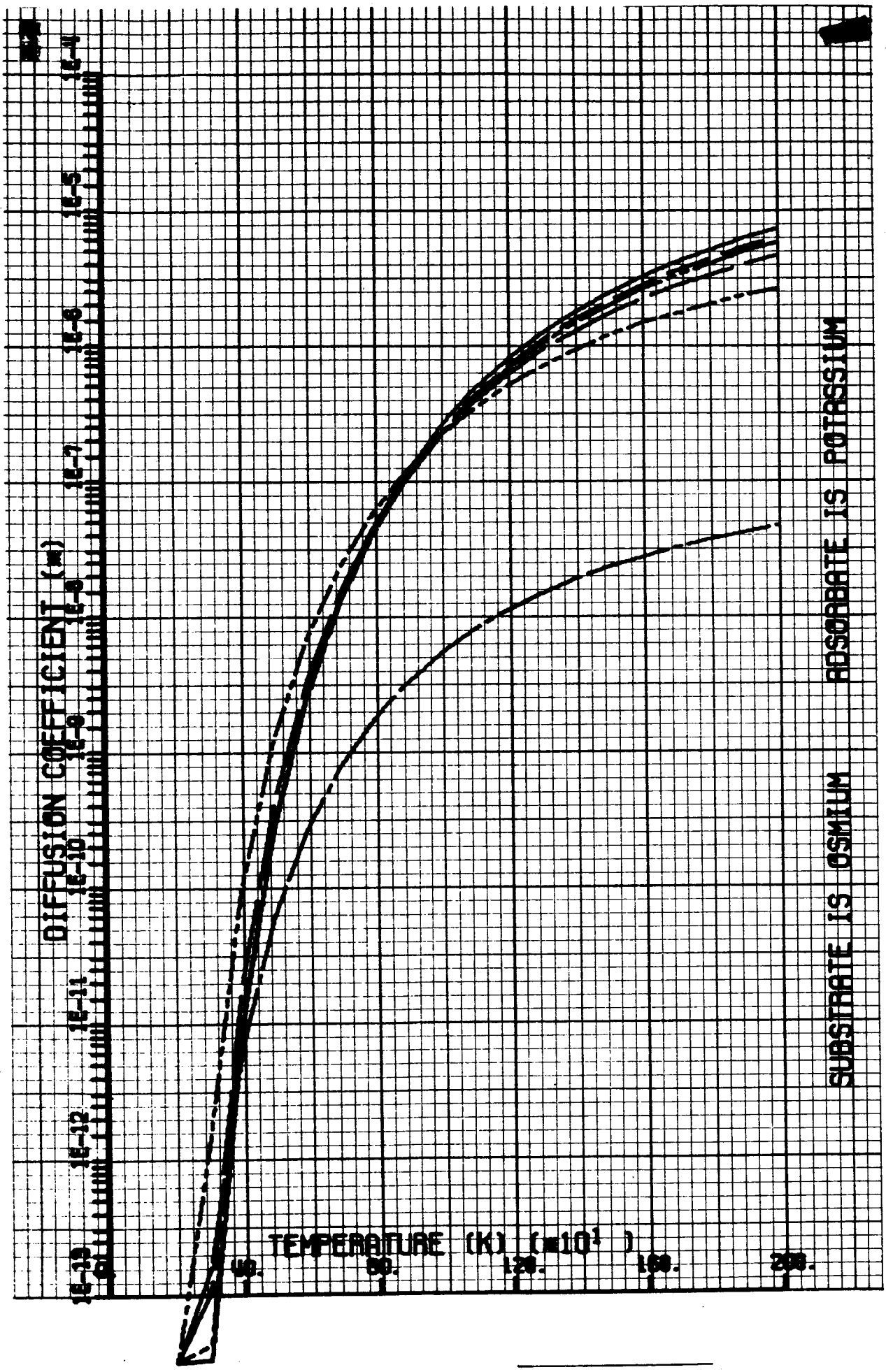
DIFFUSION COEFFICIENT (m)
1E-4
1E-5
1E-6
1E-7
1E-8
1E-9
1E-10
1E-11
1E-12
1E-13
TEMPERATURE (K) (*10¹)
40.
80.
120.
160.
200.
SUBSTRATE IS OSMIUM ADSORBATE IS POTASSIUM

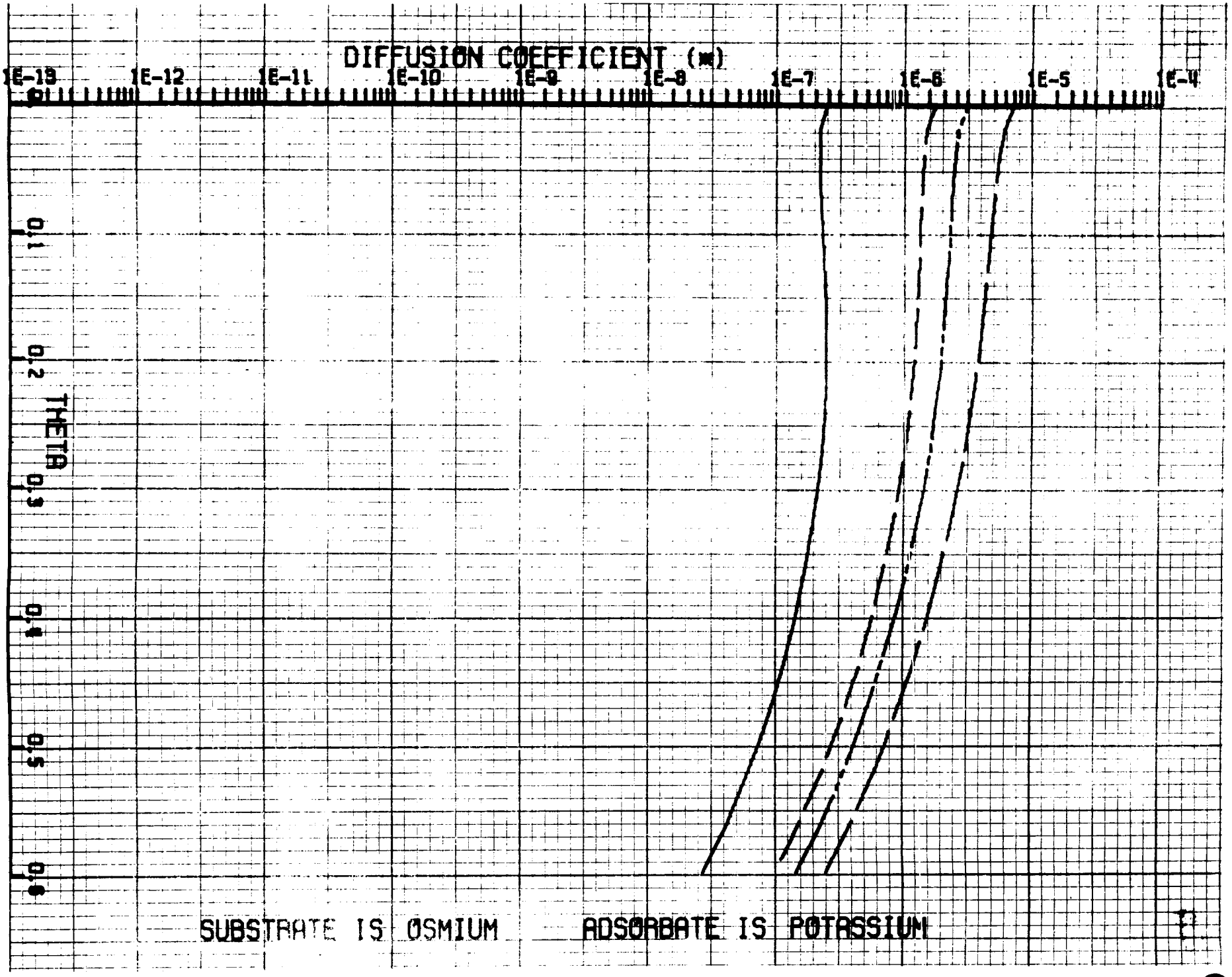
DIFFUSION COEFFICIENT (m)
1E-13
1E-12
1E-11
1E-10
1E-9
1E-8
1E-7
1E-6
1E-5
1E-4
THETA
0.1
0.2
0.3
0.4
0.5
0.6
SUBSTRATE IS OSMIUM
ADSORBATE IS POTASSIUM

DIFFUSION COEFFICIENT (m²)
1E-13
1E-12
1E-11
1E-10
1E-9
1E-8
1E-7
1E-6
1E-5
1E-4
TEMPERATURE /(K) (*10¹)
40.
80.
120.
160.
200.
SUBSTRATE IS OSMIUM
ADSORBATE IS TITANIUM

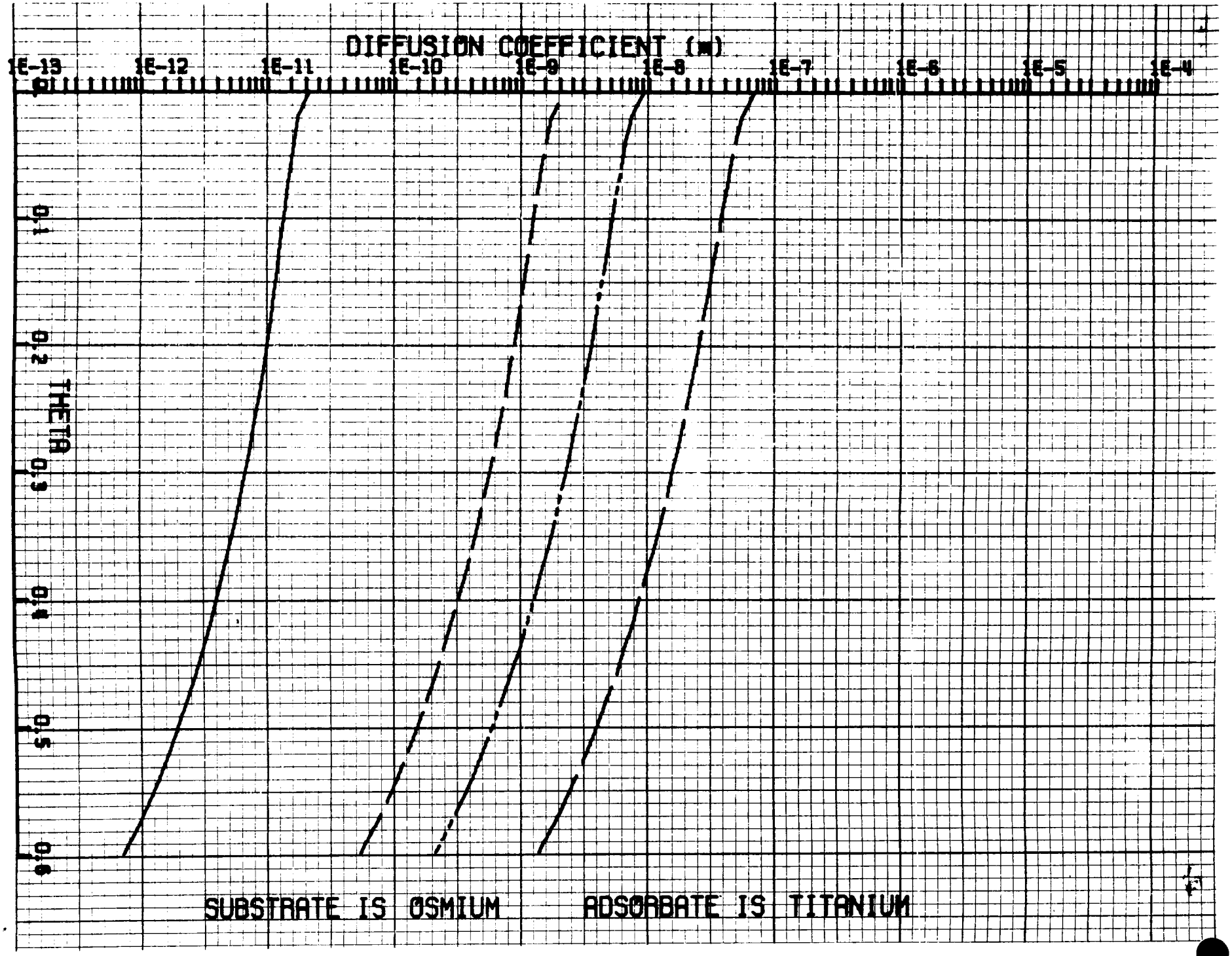
DIFFUSION COEFFICIENT (m)
1E-13
1E-12
1E-11
1E-10
1E-9
1E-8
1E-7
1E-6
1E-5
1E-4
THETA
0.1
0.2
0.3
0.4
0.5
0.6
SUBSTRATE IS OSMIUM
ADSORBATE IS TITANIUM

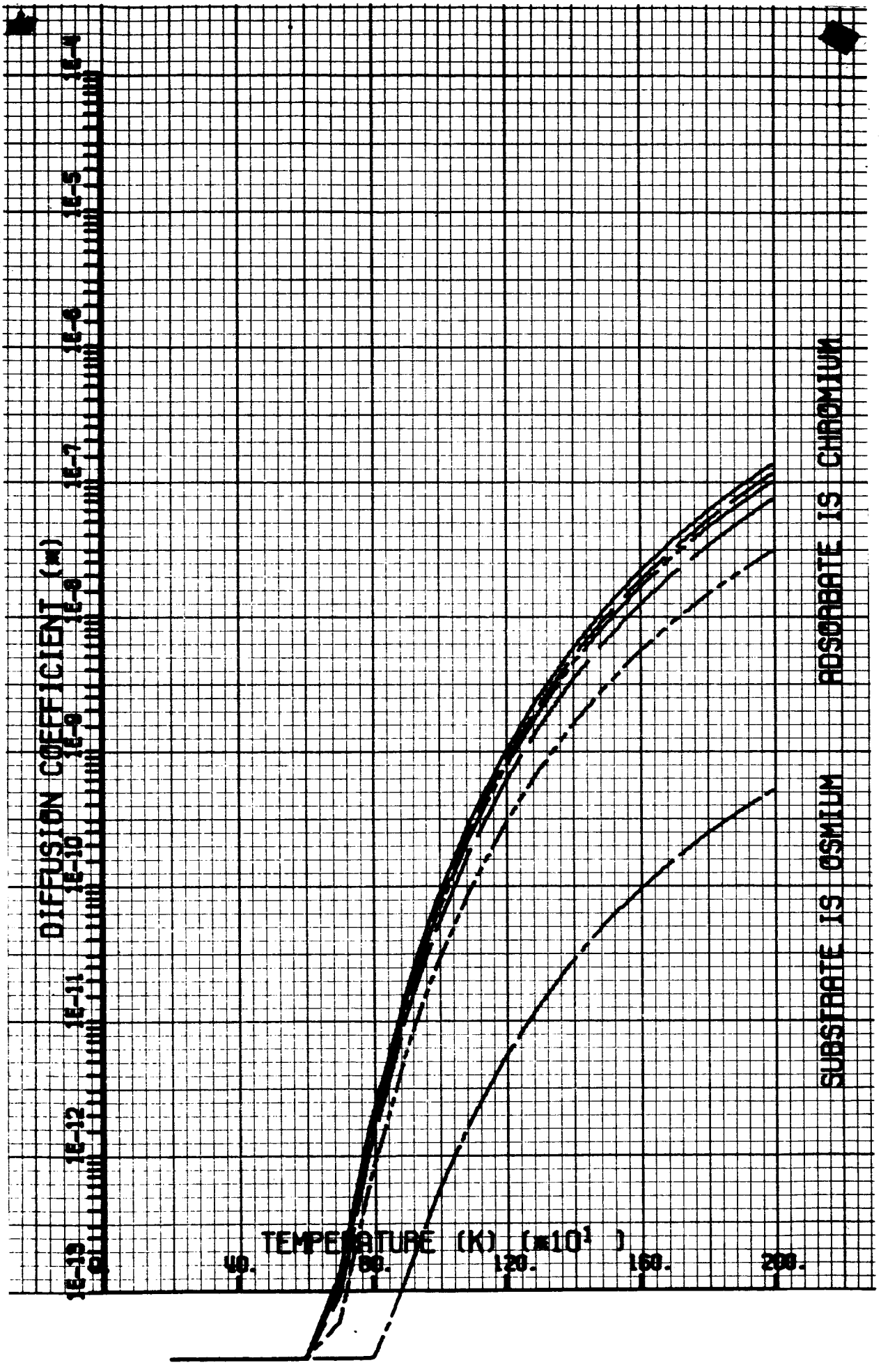
DIFFUSION COEFFICIENT (m)
1E-4
1E-5
1E-6
1E-7
1E-8
1E-9
1E-10
1E-11
1E-12
1E-13
40.
80.
120.
160.
200.
TEMPERATURE (K) (×10¹)
SUBSTRATE IS OSMIUM
ADSORBATE IS CHROMIUM

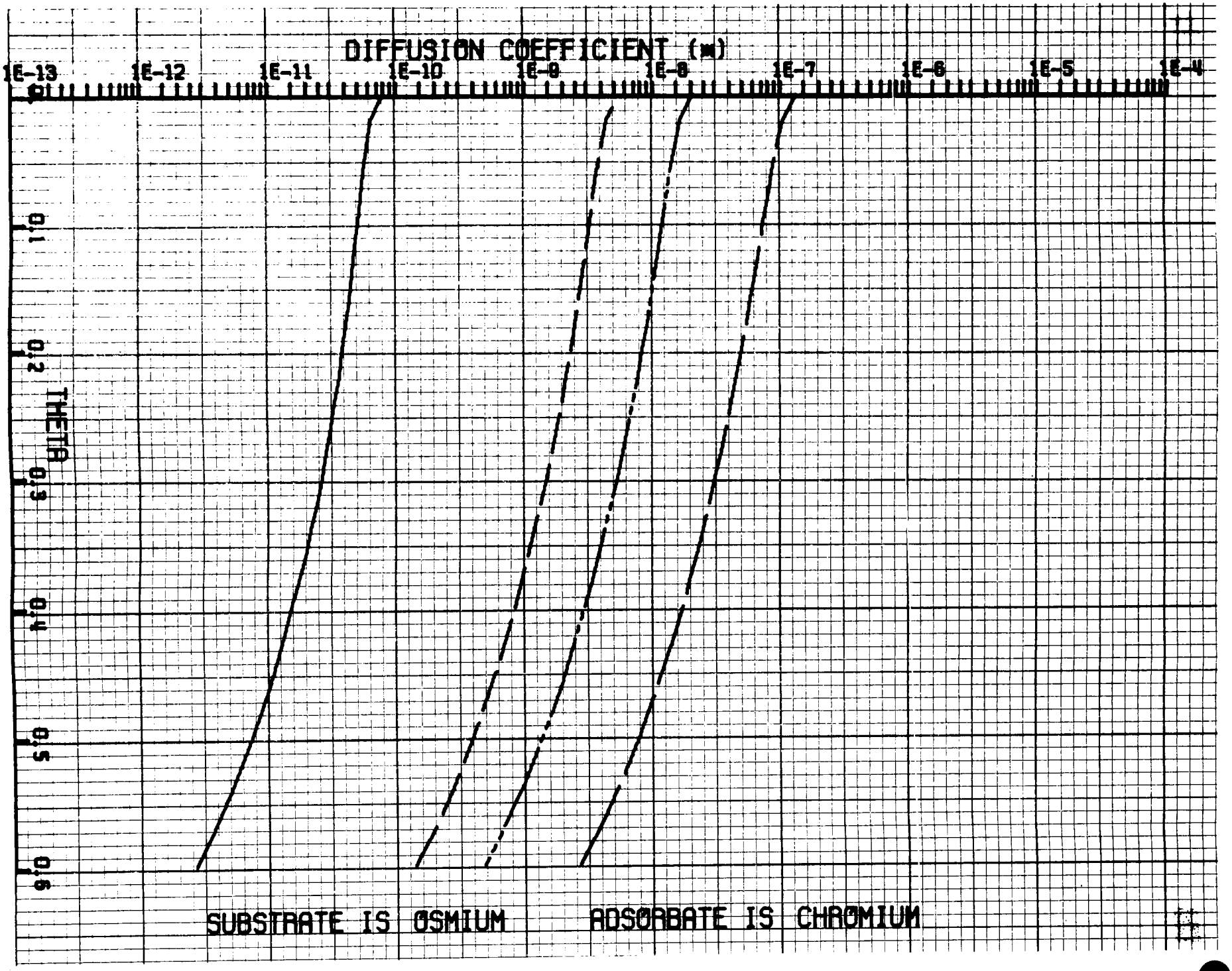
DIFFUSION COEFFICIENT (m)
1E-13
1E-12
1E-11
1E-10
1E-9
1E-8
1E-7
1E-6
1E-5
1E-4
THETA
0.1
0.2
0.3
0.4
0.5
0.6
SUBSTRATE IS OSMIUM
ADSORBATE IS CHROMIUM

DIFFUSION COEFFICIENT (m²)
1E-4
1E-5
1E-6
1E-7
1E-8
1E-9
1E-10
1E-11
1E-12
1E-13
TEMPERATURE (K) (×10¹)
40.
80.
120.
160.
200.
SUBSTRATE IS OSMIUM
ADSORBATE IS MANGANESE

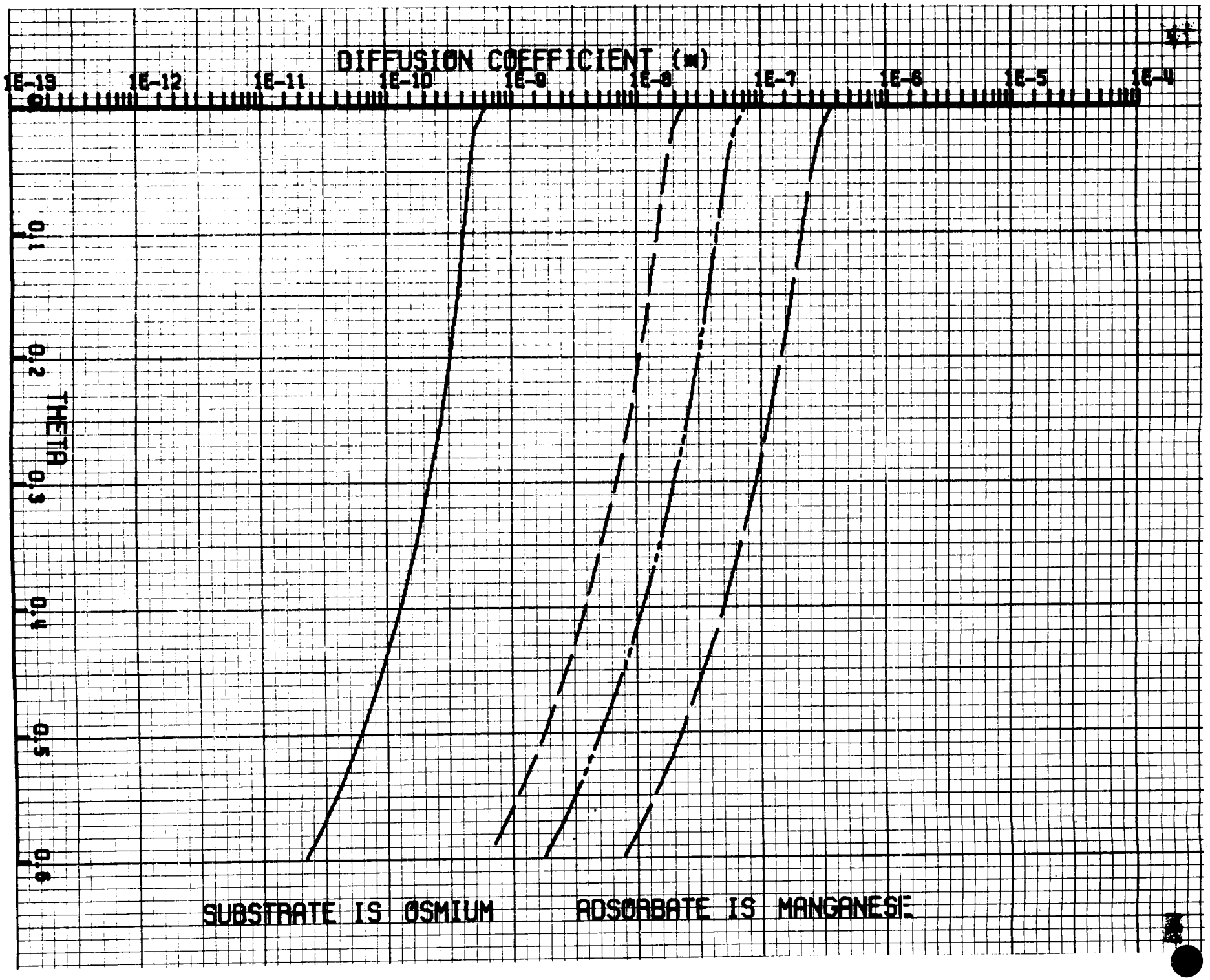
DIFFUSION COEFFICIENT (m)
1E-13
1E-12
1E-11
1E-10
1E-9
1E-8
1E-7
1E-6
1E-5
1E-4
THETA
0
0.1
0.2
0.3
0.4
0.5
0.6
SUBSTRATE IS OSMIUM
ADSORBATE IS MANGANESE

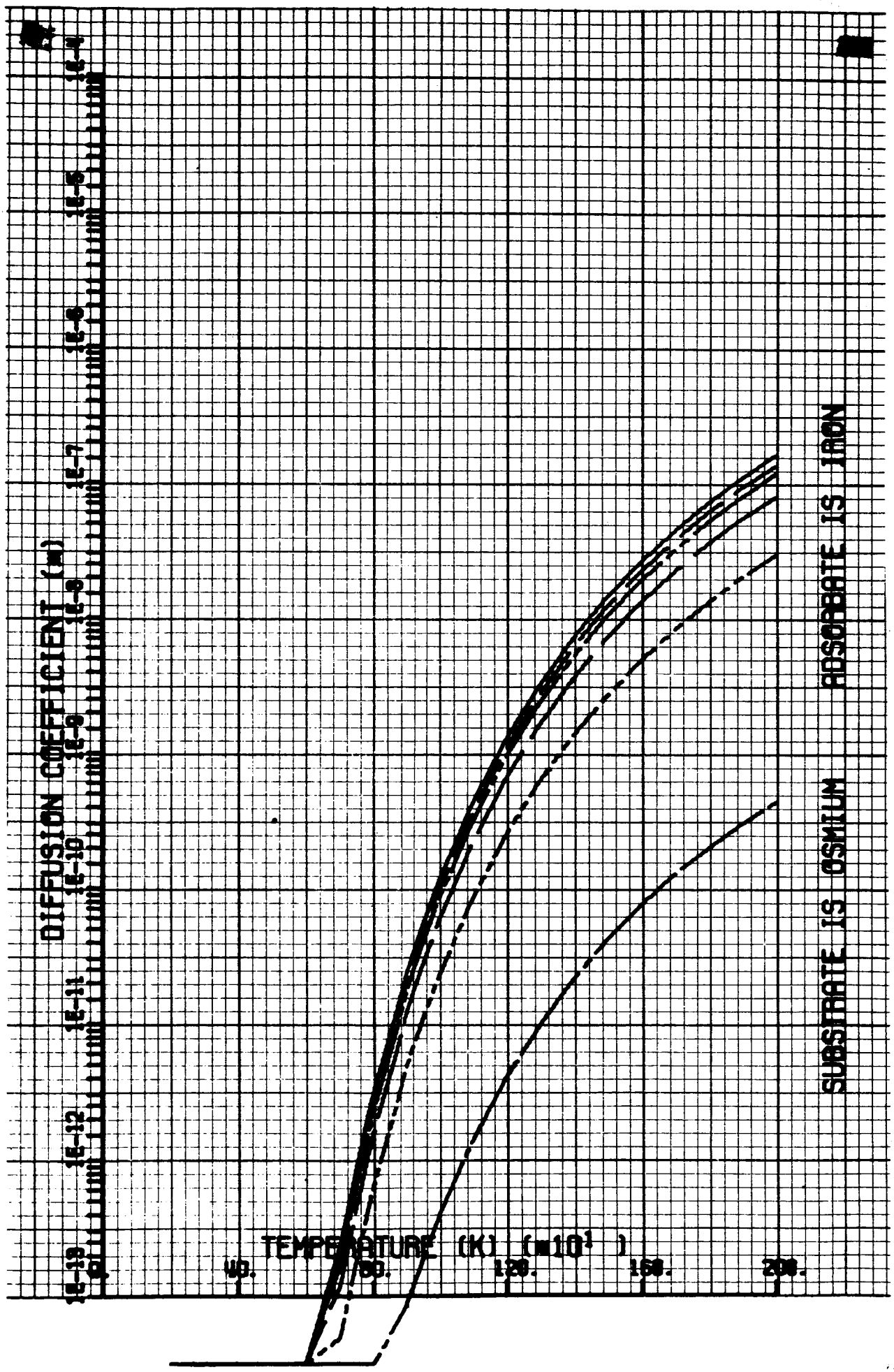
DIFFUSION COEFFICIENT (m)
1E-13
1E-12
1E-11
1E-10
1E-9
1E-8
1E-7
1E-6
1E-5
1E-4
TEMPERATURE (K) (*10¹)
40.
80.
120.
160.
200.
SUBSTRATE IS OSMIUM
ADSORBATE IS IRON

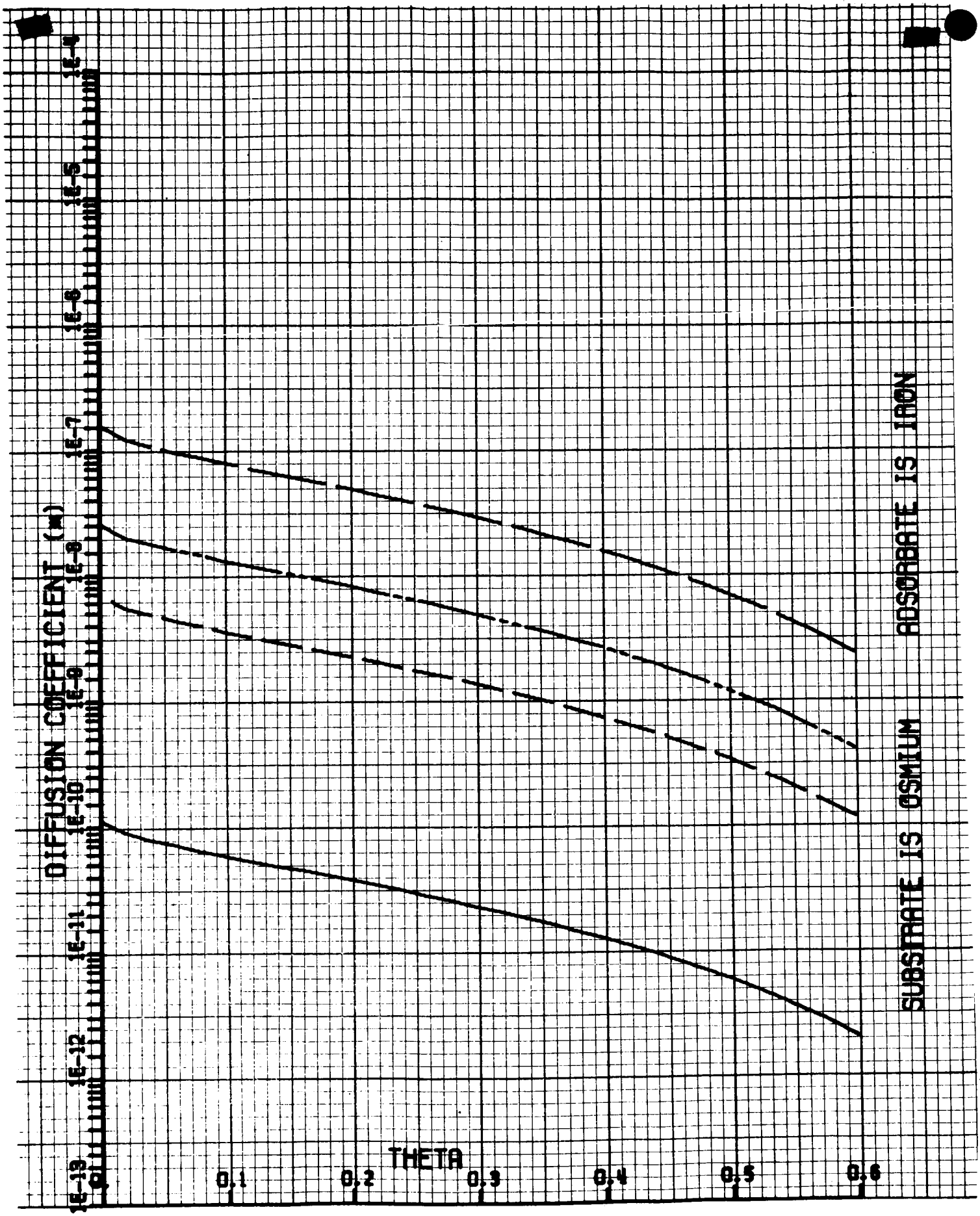
DIFFUSION COEFFICIENT (m²)
1E-7
1E-8
1E-5
1E-4
1E-9
1E-10
1E-11
1E-12
1E-13
THETA
0.1
0.2
0.3
0.4
0.5
0.6
SUBSTRATE IS OSMIUM ADSORBATE IS IRON

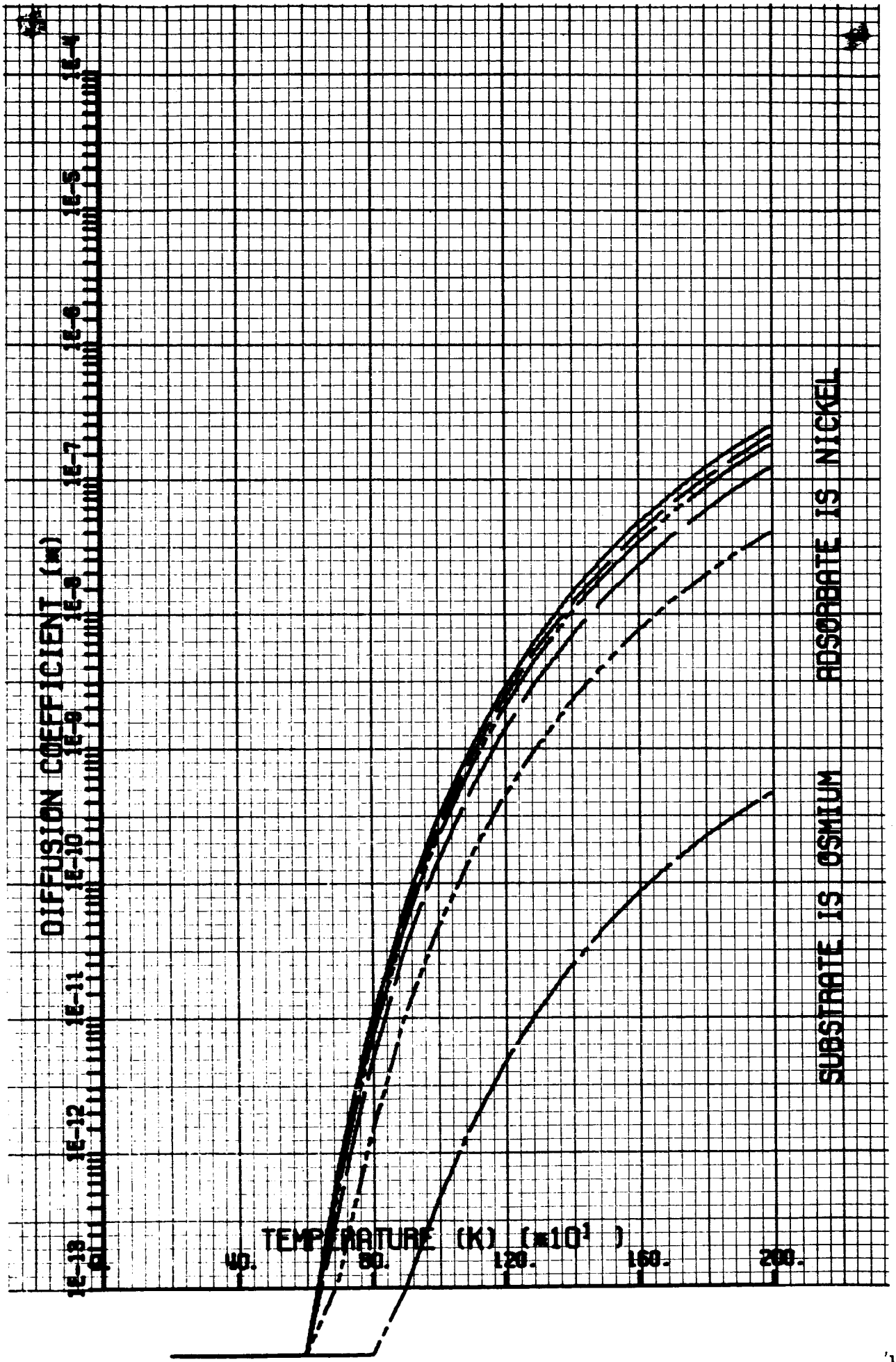
DIFFUSION COEFFICIENT (m)
1E-4
1E-5
1E-6
1E-7
1E-8
1E-9
1E-10
1E-11
1E-12
1E-13
TEMPERATURE (K) (x10¹)
40.
80.
120.
160.
200.
SUBSTRATE IS OSMIUM
ADSORBATE IS NICKEL

DIFFUSION COEFFICIENT (M²)
1E-4
1E-5
1E-6
1E-7
1E-8
1E-9
1E-10
1E-11
1E-12
1E-13
0
0.1
0.2
0.3
0.4
0.5
0.6
THETA
SUBSTRATE IS OSMIUM ADSORBATE IS NICKEL

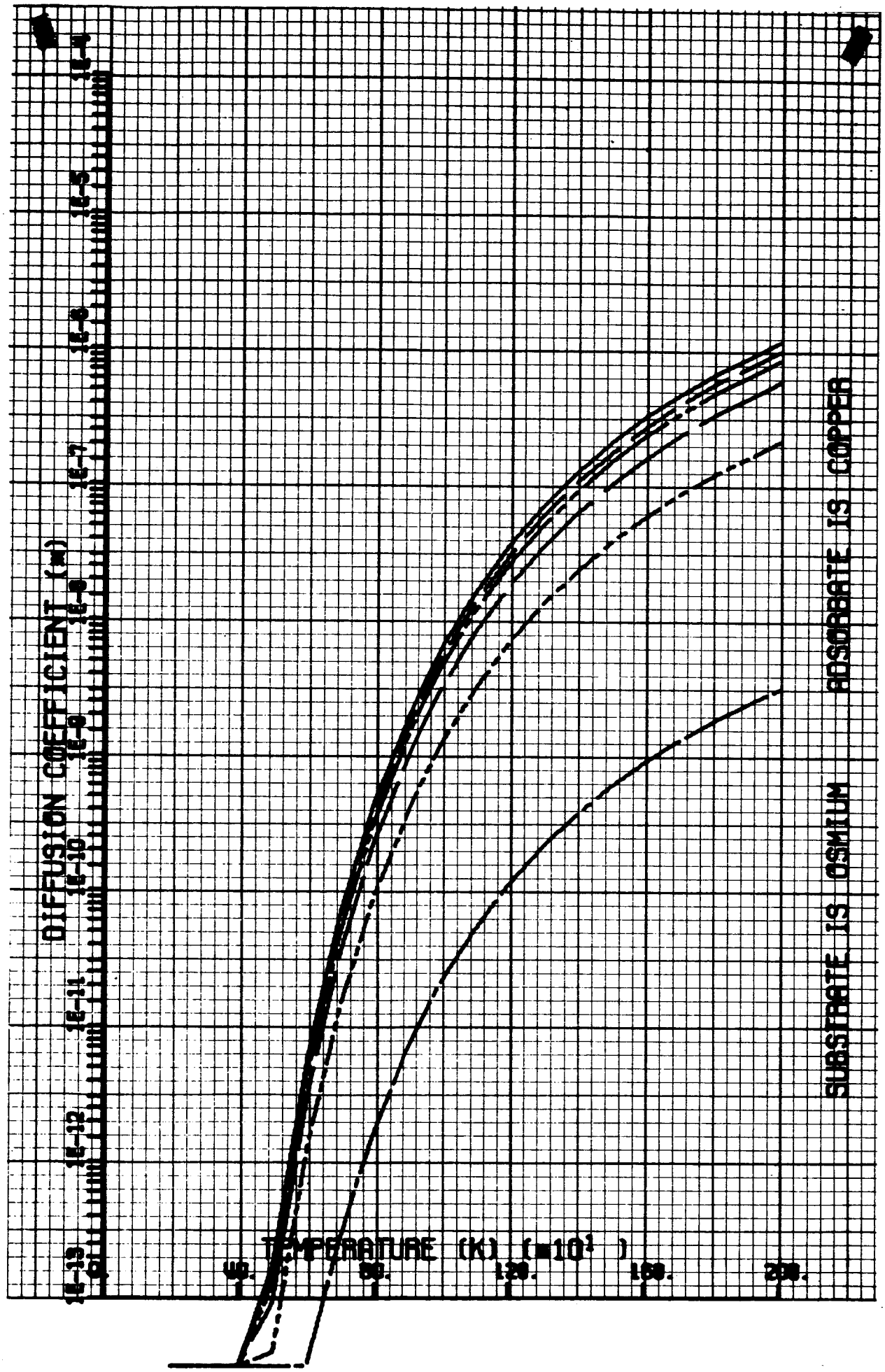
DIFFUSION COEFFICIENT (m²)
1E-13
1E-12
1E-11
1E-10
1E-9
1E-8
1E-7
1E-6
1E-5
1E-4
TEMPERATURE (K) (×10¹)
40.
80.
120.
160.
200.
SUBSTRATE IS OSMIUM ADSORBATE IS COPPER

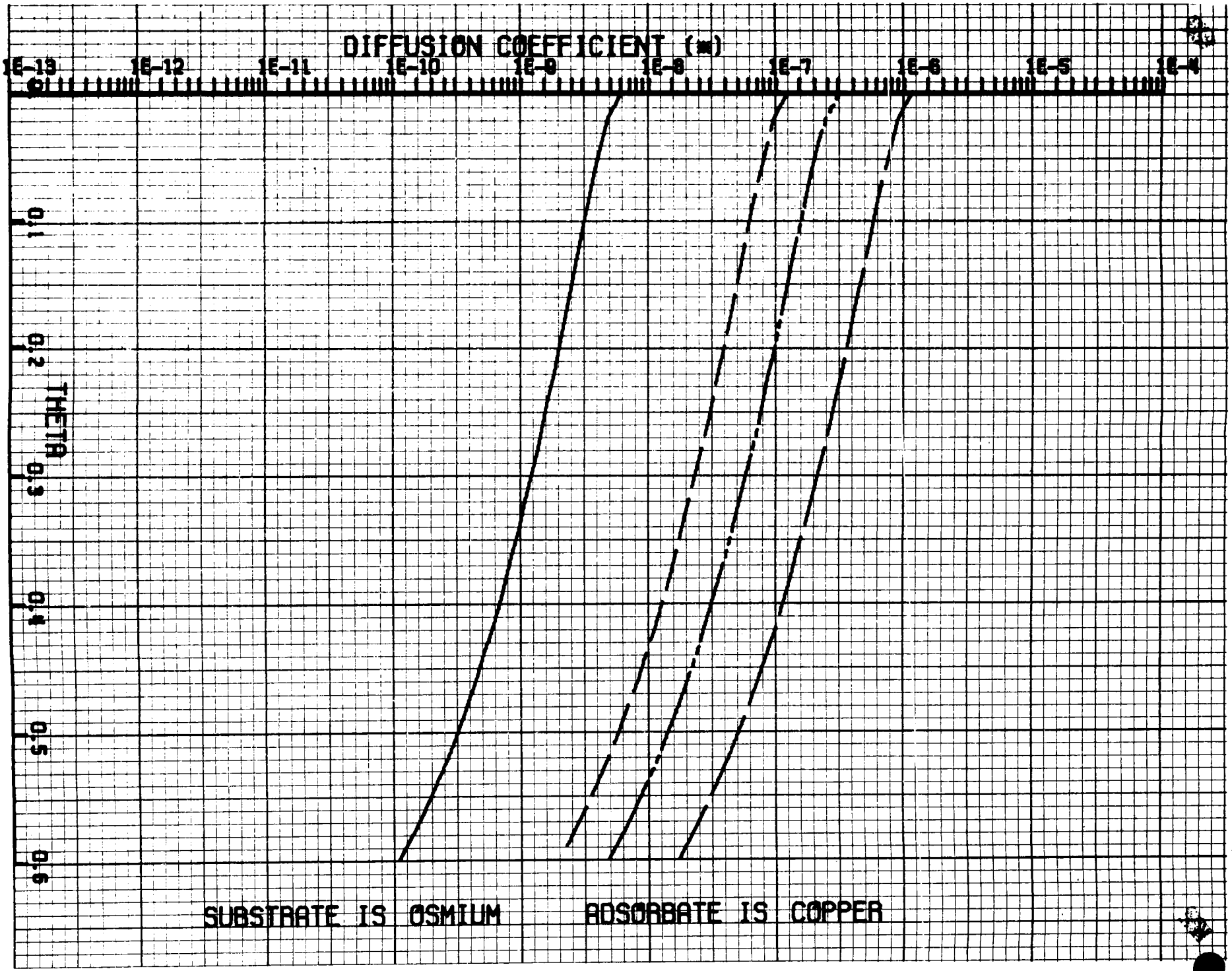
DIFFUSION COEFFICIENT (*)
1E-13
1E-12
1E-11
1E-10
1E-9
1E-8
1E-7
1E-6
1E-5
1E-4
THETA
0.0
0.1
0.2
0.3
0.4
0.5
0.6
SUBSTRATE IS OSMIUM
ADSORBATE IS COPPER

DIFFUSION COEFFICIENT (m)
1E-4
1E-5
1E-6
1E-7
1E-8
1E-9
1E-10
1E-11
1E-12
1E-13
TEMPERATURE (K) (*10¹)
40.
80.
120.
160.
200.
SUBSTRATE IS OSMIUM
ADSORBATE IS GALLIUM

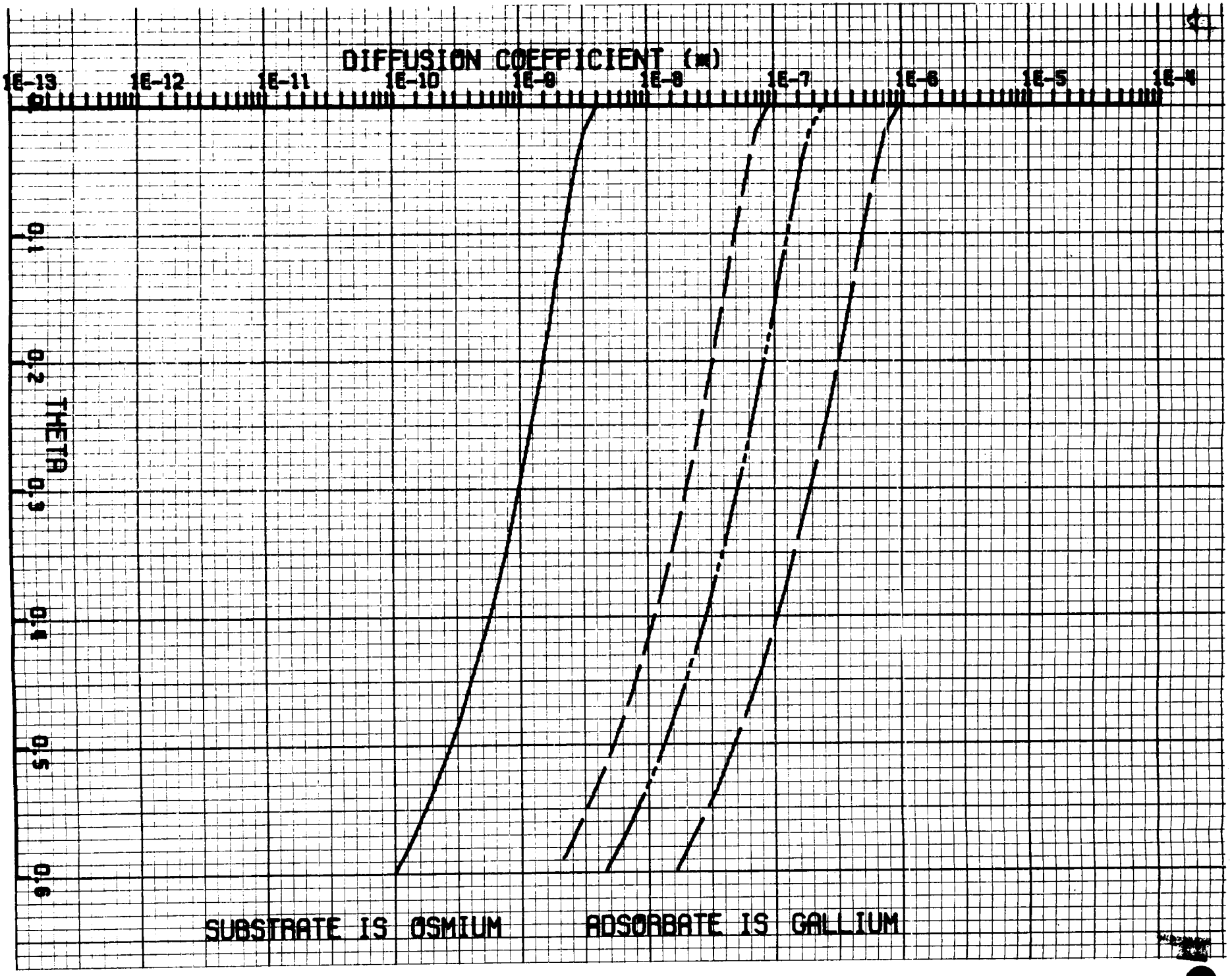
DIFFUSION COEFFICIENT (m)
1E-13
1E-12
1E-11
1E-10
1E-9
1E-8
1E-7
1E-6
1E-5
1E-4
THETA
0.0
0.1
0.2
0.3
0.4
0.5
0.6
SUBSTRATE IS OSMIUM
ADSORBATE IS GALLIUM

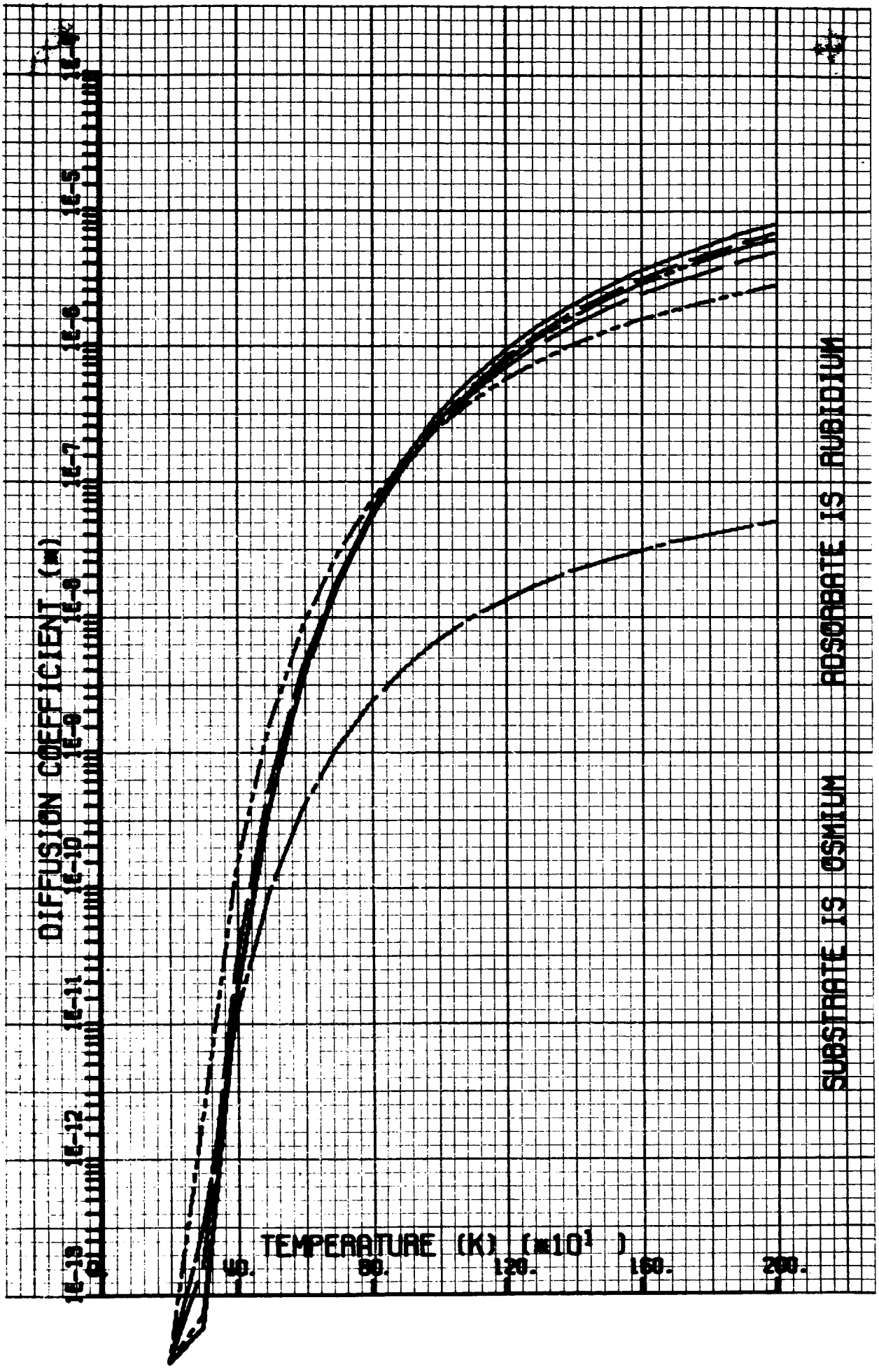
DIFFUSION COEFFICIENT (m)
1E-4
1E-5
1E-6
1E-7
1E-8
1E-9
1E-10
1E-11
1E-12
1E-13
TEMPERATURE (K) (*10¹)
40.
80.
120.
160.
200.
SUBSTRATE IS OSMIUM ADSORBATE IS RUBIDIUM

DIFFUSION COEFFICIENT (M)
1E-4
1E-5
1E-6
1E-7
1E-8
1E-9
1E-10
1E-11
1E-12
1E-13
0.1
0.2
0.3
0.4
0.5
0.6
THETA
SUBSTRATE IS OSMIUM ADSORBATE IS RUBIDIUM

DIFFUSION COEFFICIENT (m²)
1E-13
1E-12
1E-11
1E-10
1E-9
1E-8
1E-7
1E-6
1E-5
1E-4
TEMPERATURE (K) (×10¹)
40.
80.
120.
160.
200.
SUBSTRATE IS OSMIUM ADSORBATE IS INDIUM

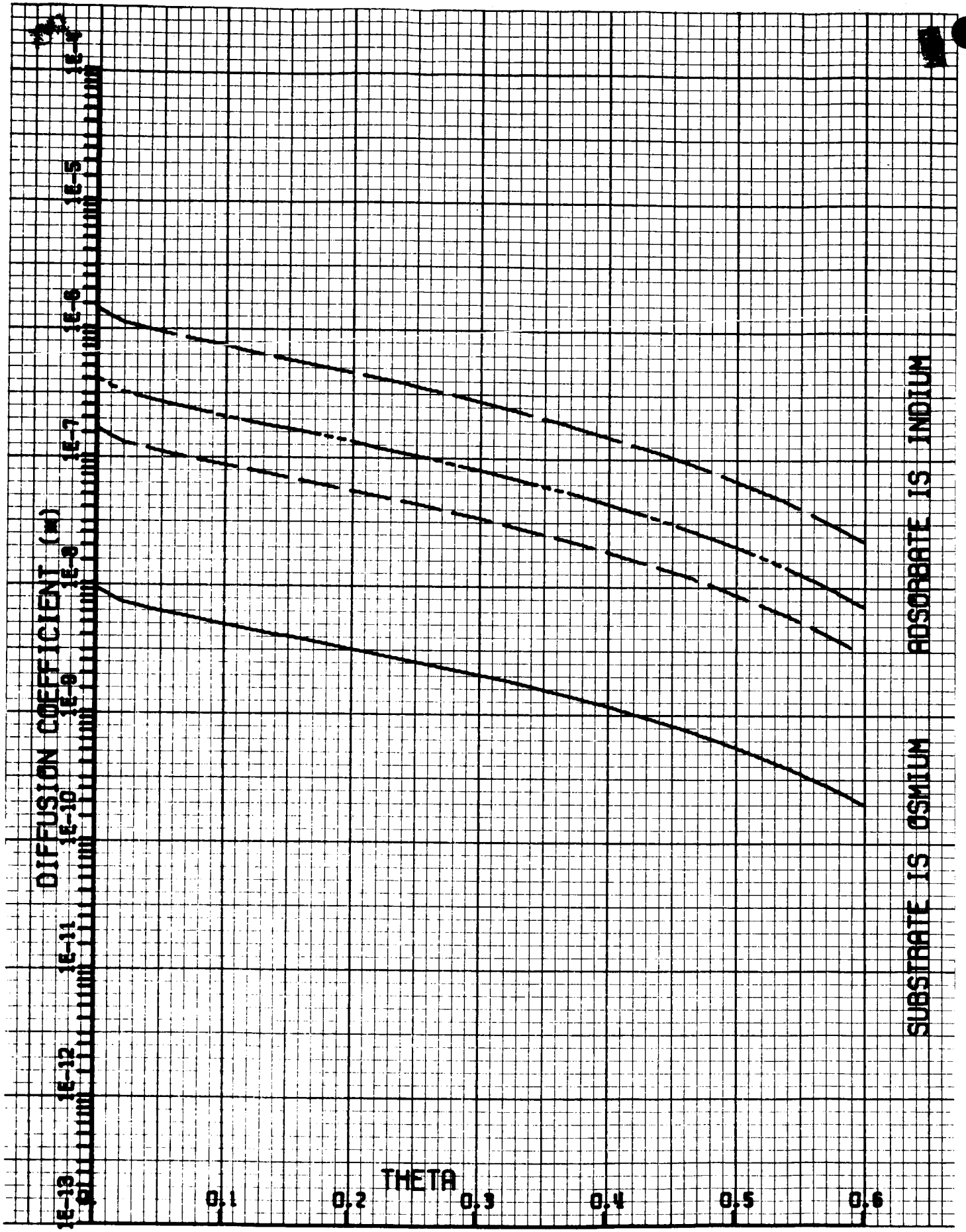
DIFFUSION COEFFICIENT (M)
1E-4
1E-5
1E-6
1E-7
1E-8
1E-9
1E-10
1E-11
1E-12
1E-13
THETA
0.1
0.2
0.3
0.4
0.5
0.6
SUBSTRATE IS OSMIUM ADSORBATE IS INDIUM

DIFFUSION COEFFICIENT (m)
1E-4
1E-5
1E-6
1E-7
1E-8
1E-9
1E-10
1E-11
1E-12
1E-13
TEMPERATURE (K) (*10¹)
40.
80.
120.
160.
200.
SUBSTRATE IS OSMIUM ADSORBATE IS TIN

DIFFUSION COEFFICIENT (m)
1E-13
1E-12
1E-11
1E-10
1E-9
1E-8
1E-7
1E-6
1E-5
1E-4
THETA
0.1
0.2
0.3
0.4
0.5
0.6
SUBSTRATE IS OSMIUM ADSORBATE IS TIN

DIFFUSION COEFFICIENT (m)
1E-13
1E-12
1E-11
1E-10
1E-9
1E-8
1E-7
1E-6
1E-5
1E-4
TEMPERATURE (K) (×10¹)
40.
80.
120.
160.
200.
SUBSTRATE IS OSMIUM
ADSORBATE IS CESIUM

DIFFUSION COEFFICIENT (m)
1E-4
1E-5
1E-6
1E-7
1E-8
1E-9
1E-10
1E-11
1E-12
1E-13
0
0.1
0.2
0.3
0.4
0.5
0.6
THETA
SUBSTRATE IS OSMIUM
ADSORBATE IS CESIUM

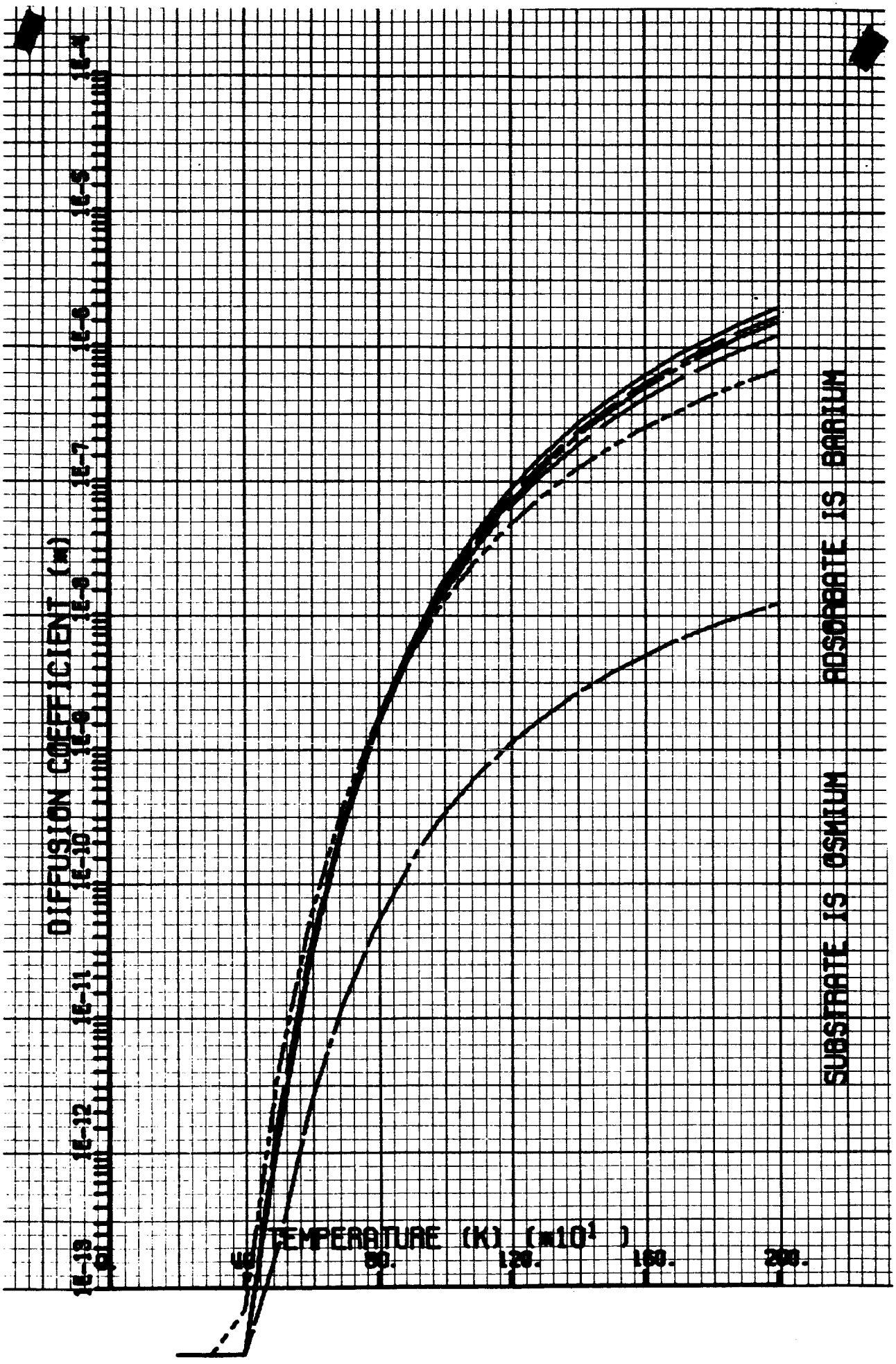
DIFFUSION COEFFICIENT (m)
1E-4
1E-5
1E-6
1E-7
1E-8
1E-9
1E-10
1E-11
1E-12
1E-13
TEMPERATURE (K) (*10¹)
80.
120.
160.
200.
SUBSTRATE IS OSMIUM ADSORBATE IS BARIUM

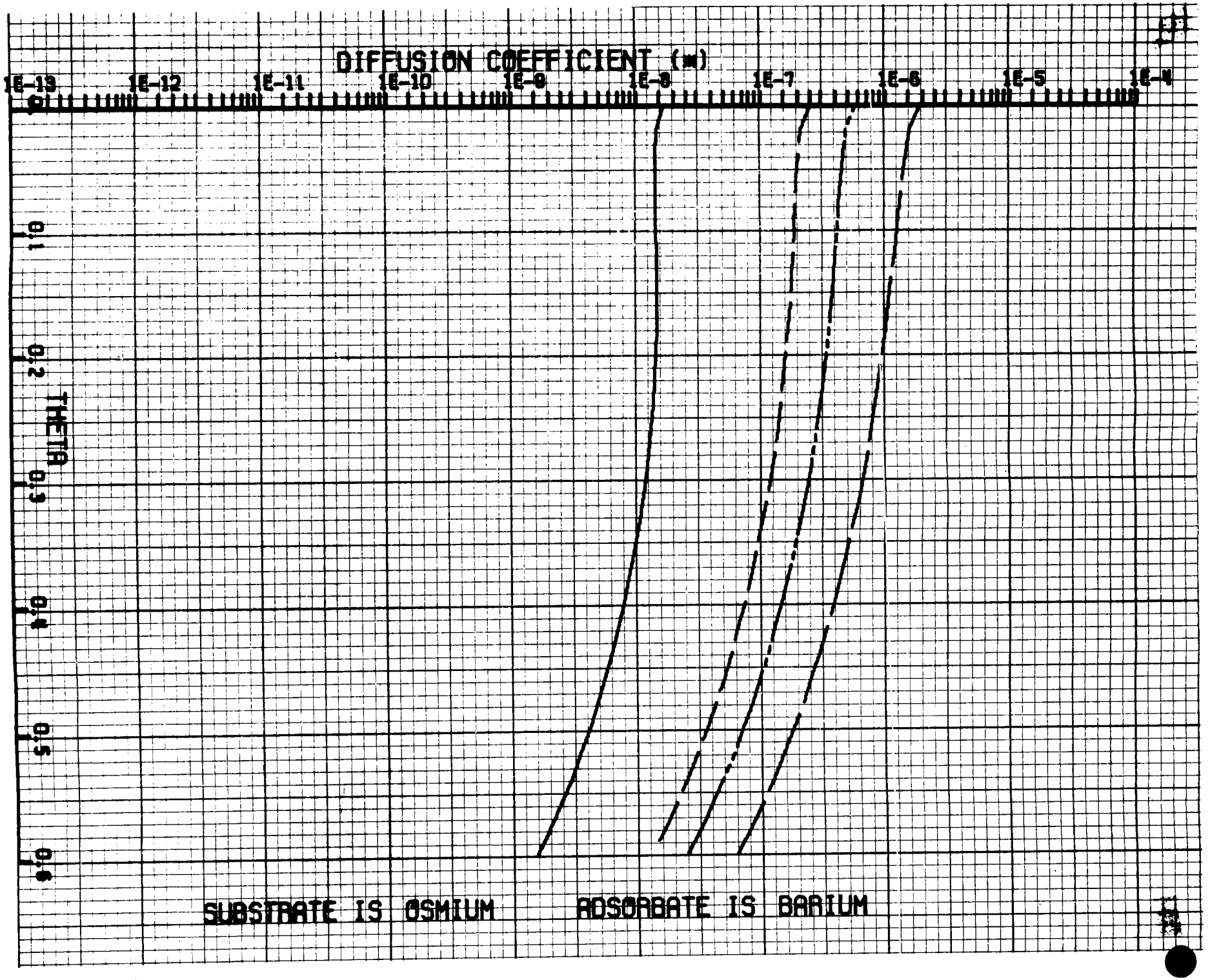
DIFFUSION COEFFICIENT (*)
1E-13
1E-12
1E-11
1E-10
1E-9
1E-8
1E-7
1E-6
1E-5
1E-4
0
0.1
0.2
0.3
0.4
0.5
0.6
THETA
SUBSTRATE IS OSMIUM
ADSORBATE IS BARIUM

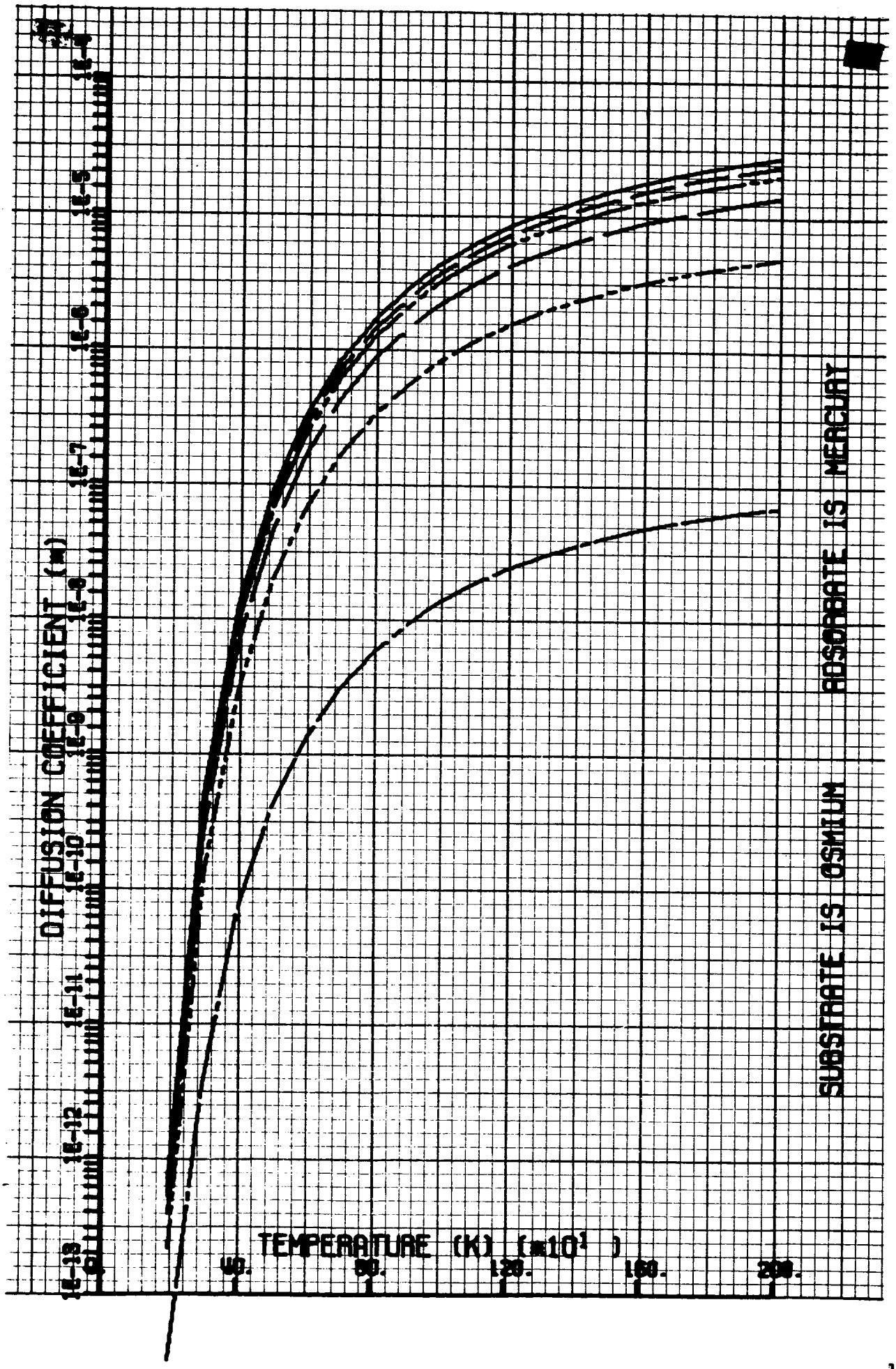
DIFFUSION COEFFICIENT (m²)
1E-4
1E-5
1E-6
1E-7
1E-8
1E-9
1E-10
1E-11
1E-12
1E-13
TEMPERATURE (K) (×10¹)
40.
80.
120.
160.
200.
SUBSTRATE IS OSMIUM
ADSORBATE IS MERCURY

DIFFUSION COEFFICIENT (m)
1E-4
1E-5
1E-6
1E-7
1E-8
1E-9
1E-10
1E-11
1E-12
1E-13
THETA
0.1
0.2
0.3
0.4
0.5
0.6
SUBSTRATE IS OSMIUM ADSORBATE IS MERCURY

DIFFUSION COEFFICIENT (m)
1E-13
1E-12
1E-11
1E-10
1E-9
1E-8
1E-7
1E-6
1E-5
1E-4
TEMPERATURE (K) (*10^1)
40.
80.
120.
160.
200.
SUBSTRATE IS OSMIUM
ADSORBATE IS LEAD

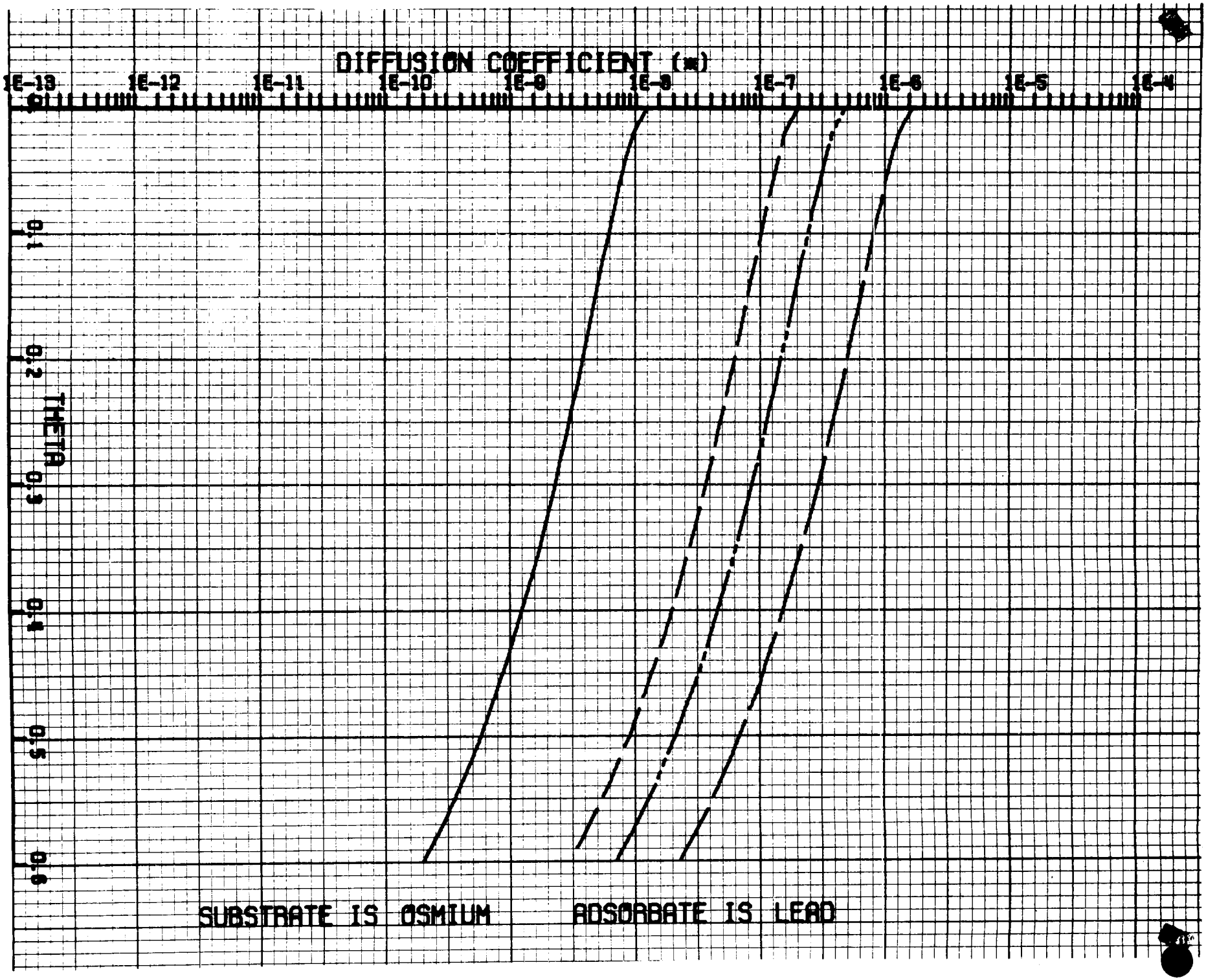
DIFFUSION COEFFICIENT (m)
1E-13
1E-12
1E-11
1E-10
1E-9
1E-8
1E-7
1E-6
1E-5
1E-4
THETA
0.1
0.2
0.3
0.4
0.5
0.6
SUBSTRATE IS OSMIUM
ADSORBATE IS LEAD

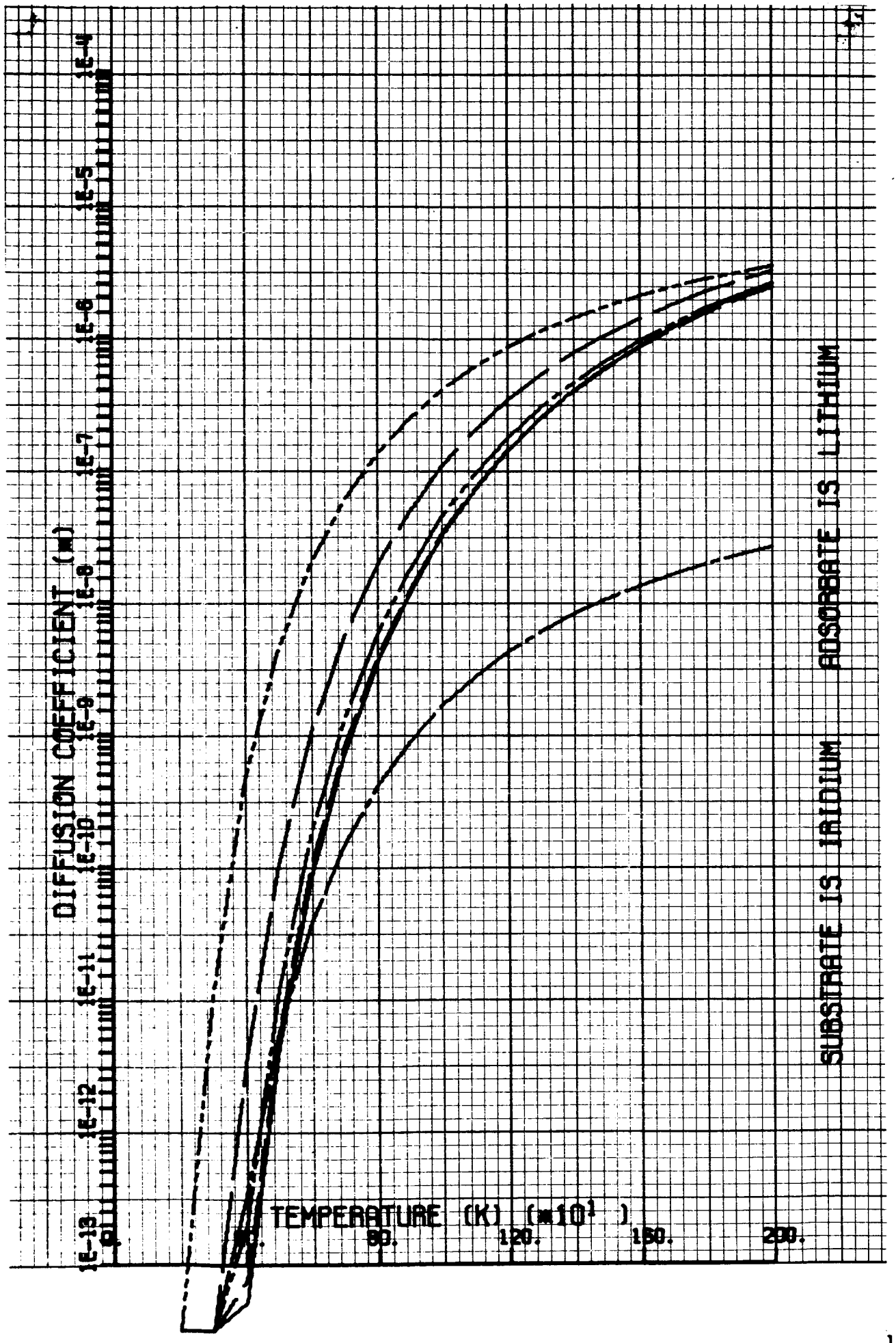
DIFFUSION COEFFICIENT (m²)
1E-4
1E-5
1E-6
1E-7
1E-8
1E-9
1E-10
1E-11
1E-12
1E-13
TEMPERATURE (K) (*10¹)
80.
120.
150.
200.
SUBSTRATE IS IRIDIUM ADSORBATE IS LITHIUM

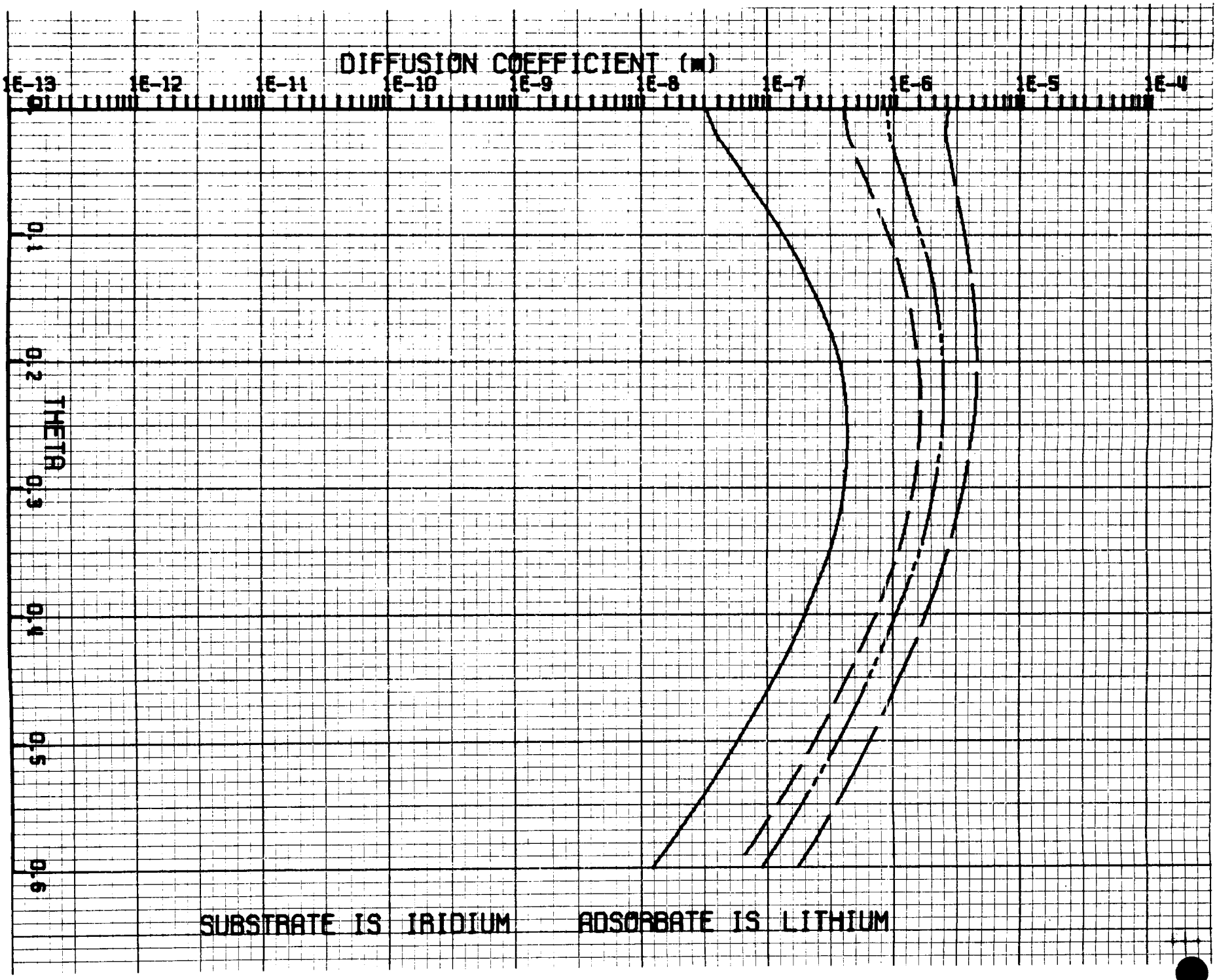
DIFFUSION COEFFICIENT (m)
1E-13
1E-12
1E-11
1E-10
1E-9
1E-8
1E-7
1E-6
1E-5
1E-4
THETA
0.1
0.2
0.3
0.4
0.5
0.6
SUBSTRATE IS IRIDIUM
ADSORBATE IS LITHIUM

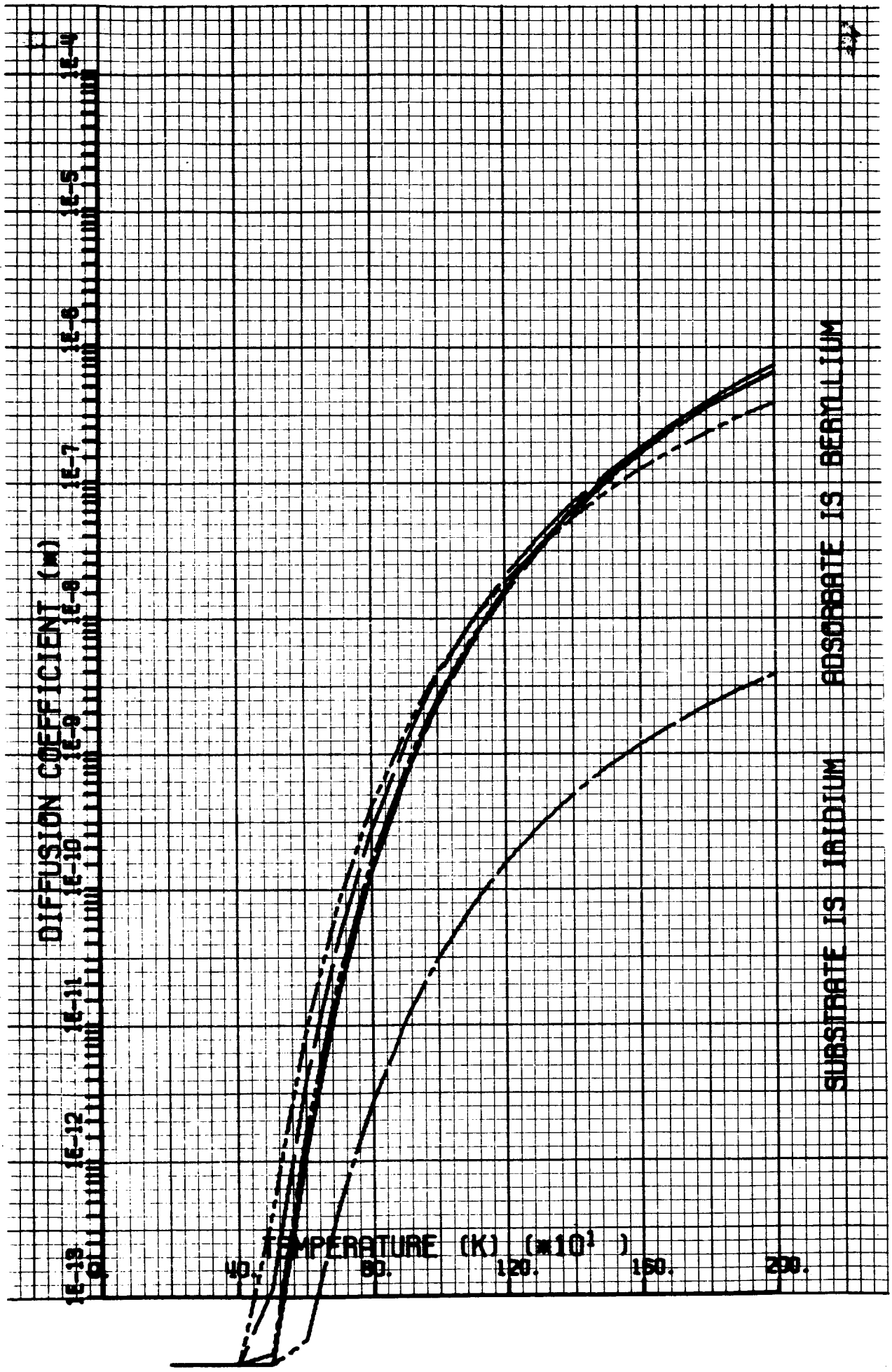
DIFFUSION COEFFICIENT (m²)
1E-4
1E-5
1E-6
1E-7
1E-8
1E-9
1E-10
1E-11
1E-12
1E-13
TEMPERATURE (K) (x10¹)
40.
80.
120.
160.
200.
SUBSTRATE IS IRIDIUM ADSORBATE IS BERYLLIUM

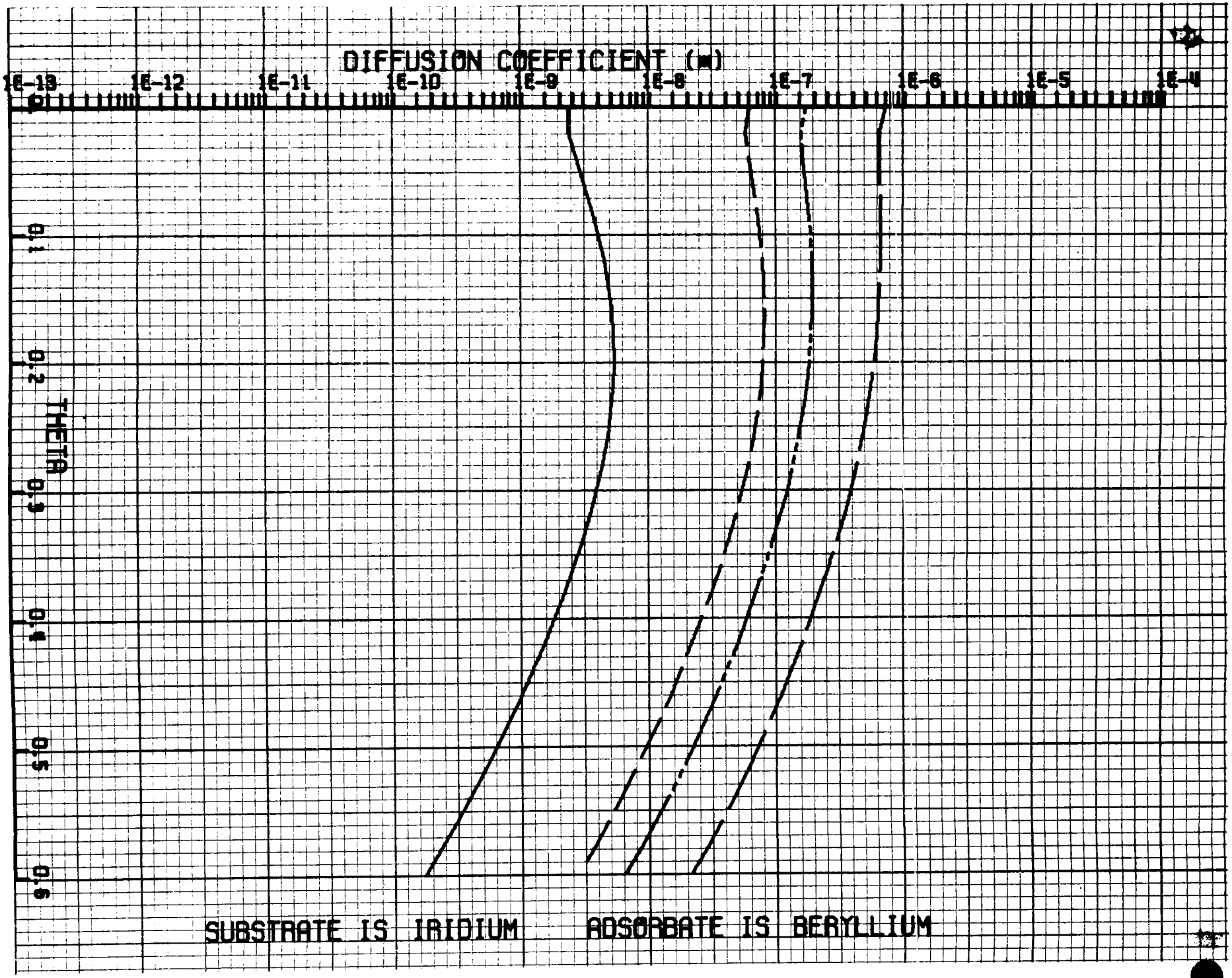
DIFFUSION COEFFICIENT (m)
1E-13
1E-12
1E-11
1E-10
1E-9
1E-8
1E-7
1E-6
1E-5
1E-4
0
0.1
0.2
0.3
0.4
0.5
0.6
THETA
SUBSTRATE IS IRIDIUM
ADSORBATE IS BERYLLIUM

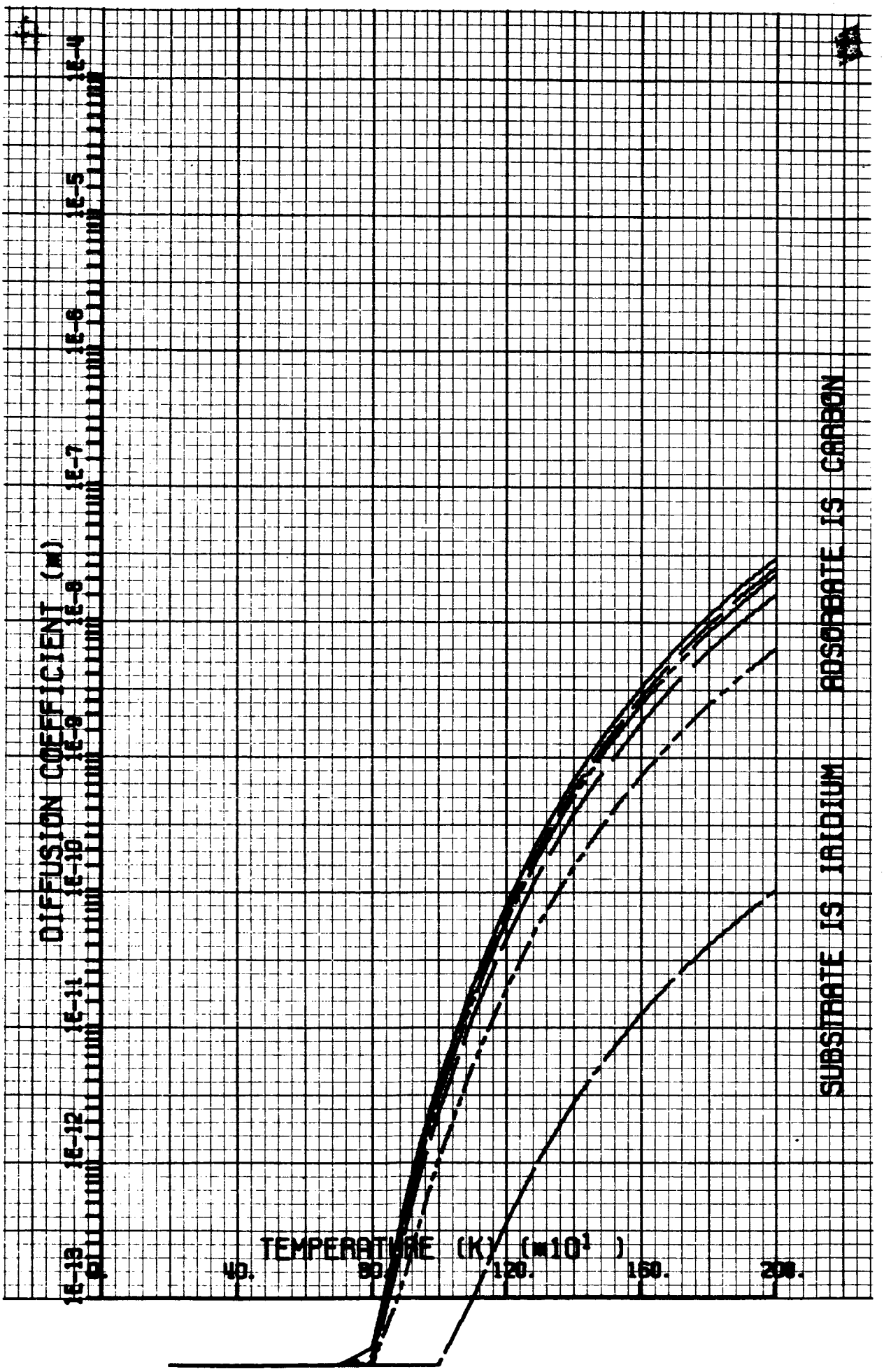
DIFFUSION COEFFICIENT (m²)
1E-4
1E-5
1E-6
1E-7
1E-8
1E-9
1E-10
1E-11
1E-12
1E-13
TEMPERATURE (K) (*10¹)
40.
80.
120.
160.
200.
SUBSTRATE IS IRIDIUM ADSORBATE IS CARBON

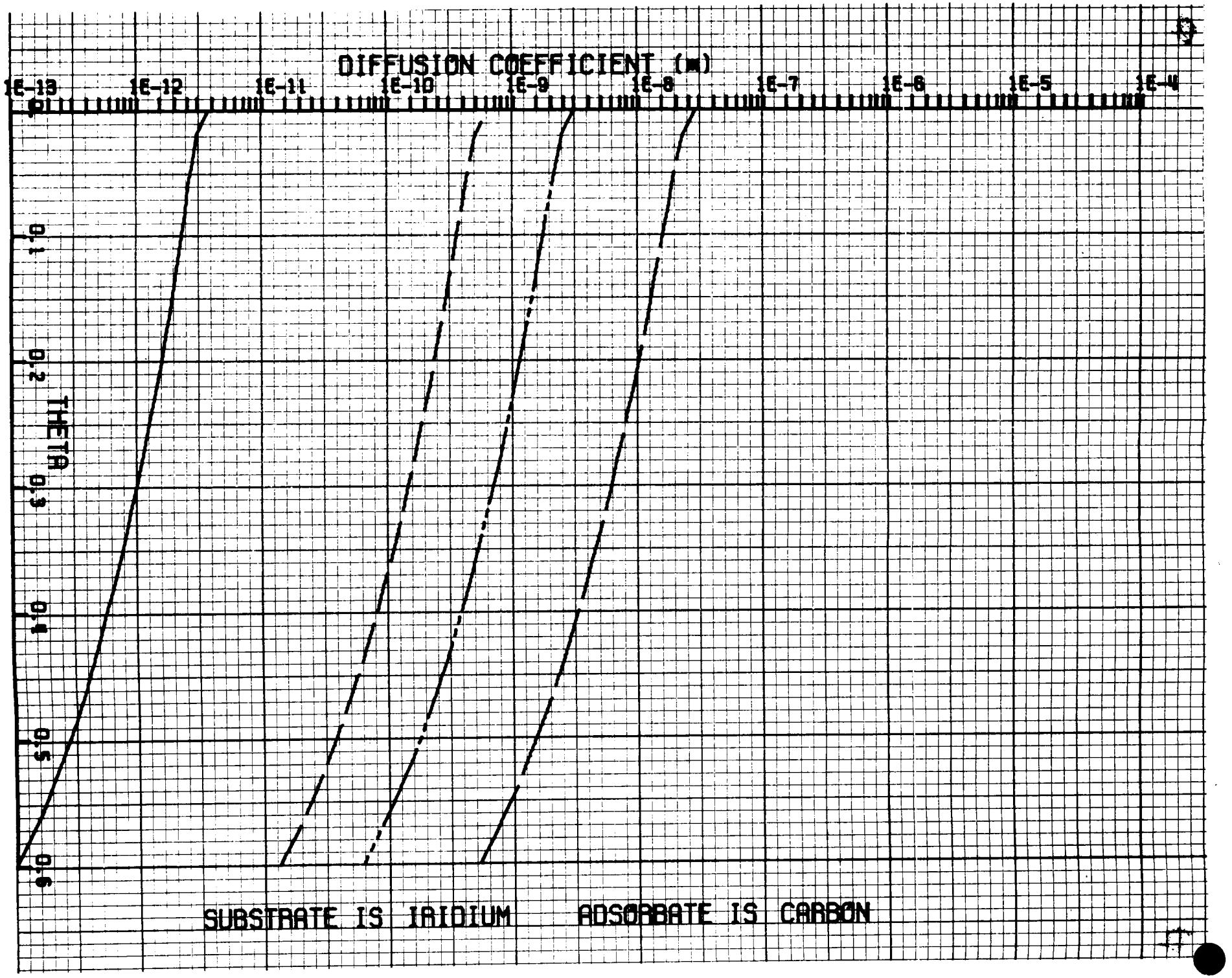
DIFFUSION COEFFICIENT (m)
1E-13
1E-12
1E-11
1E-10
1E-9
1E-8
1E-7
1E-6
1E-5
1E-4
THETA
0.1
0.2
0.3
0.4
0.5
0.6
SUBSTRATE IS IRIDIUM
ADSORBATE IS CARBON

DIFFUSION COEFFICIENT (■)
1E-4
1E-5
1E-6
1E-7
1E-8
1E-9
1E-10
1E-11
1E-12
1E-13
TEMPERATURE (K) (×10¹)
40.
80.
120.
160.
200.
SUBSTRATE IS IRIDIUM ADSORBATE IS SODIUM

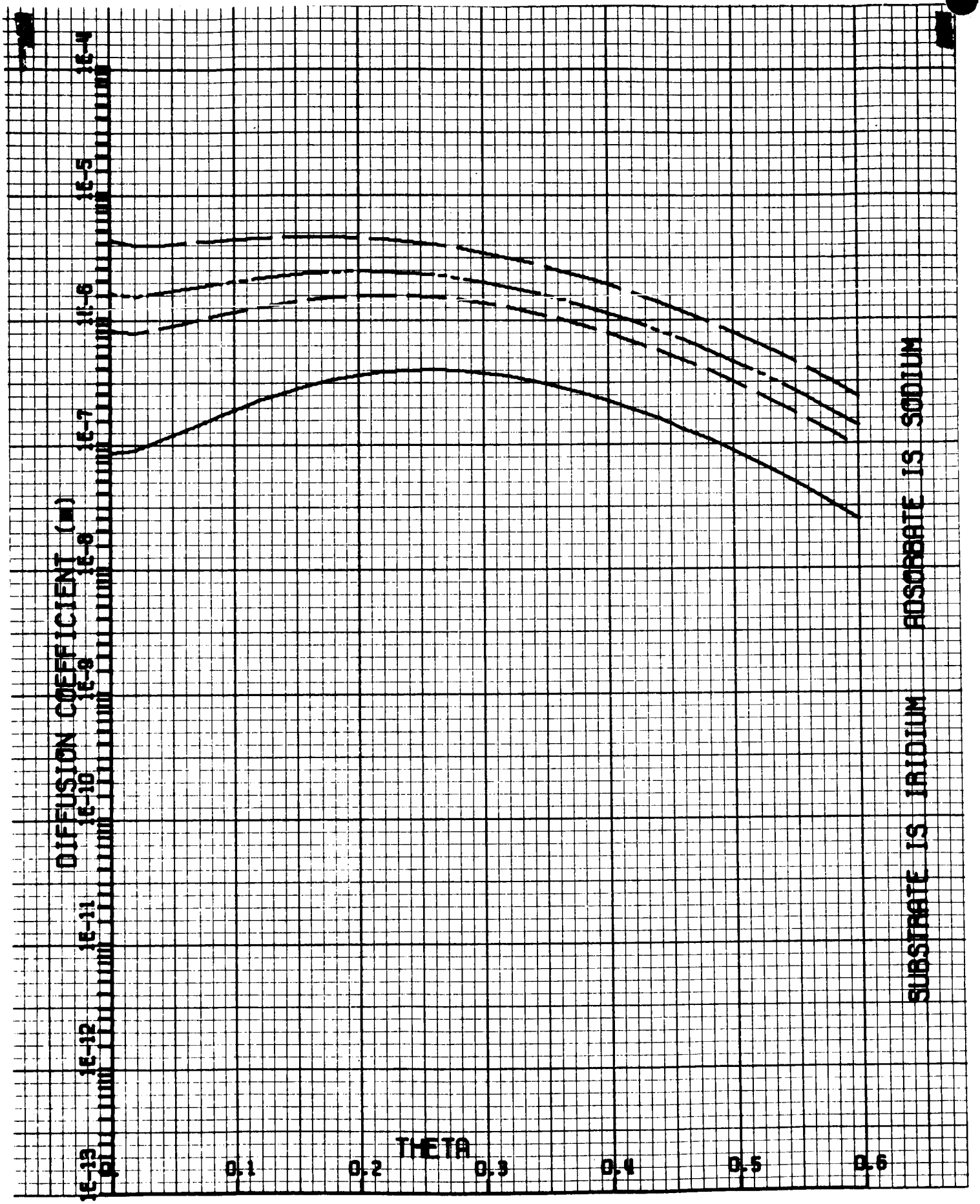
DIFFUSION COEFFICIENT (cm)
1E-4
1E-5
1E-6
1E-7
1E-8
1E-9
1E-10
1E-11
1E-12
1E-13
THETA
0.1
0.2
0.3
0.4
0.5
0.6
SUBSTRATE IS IRIDIUM ADSORBATE IS SODIUM

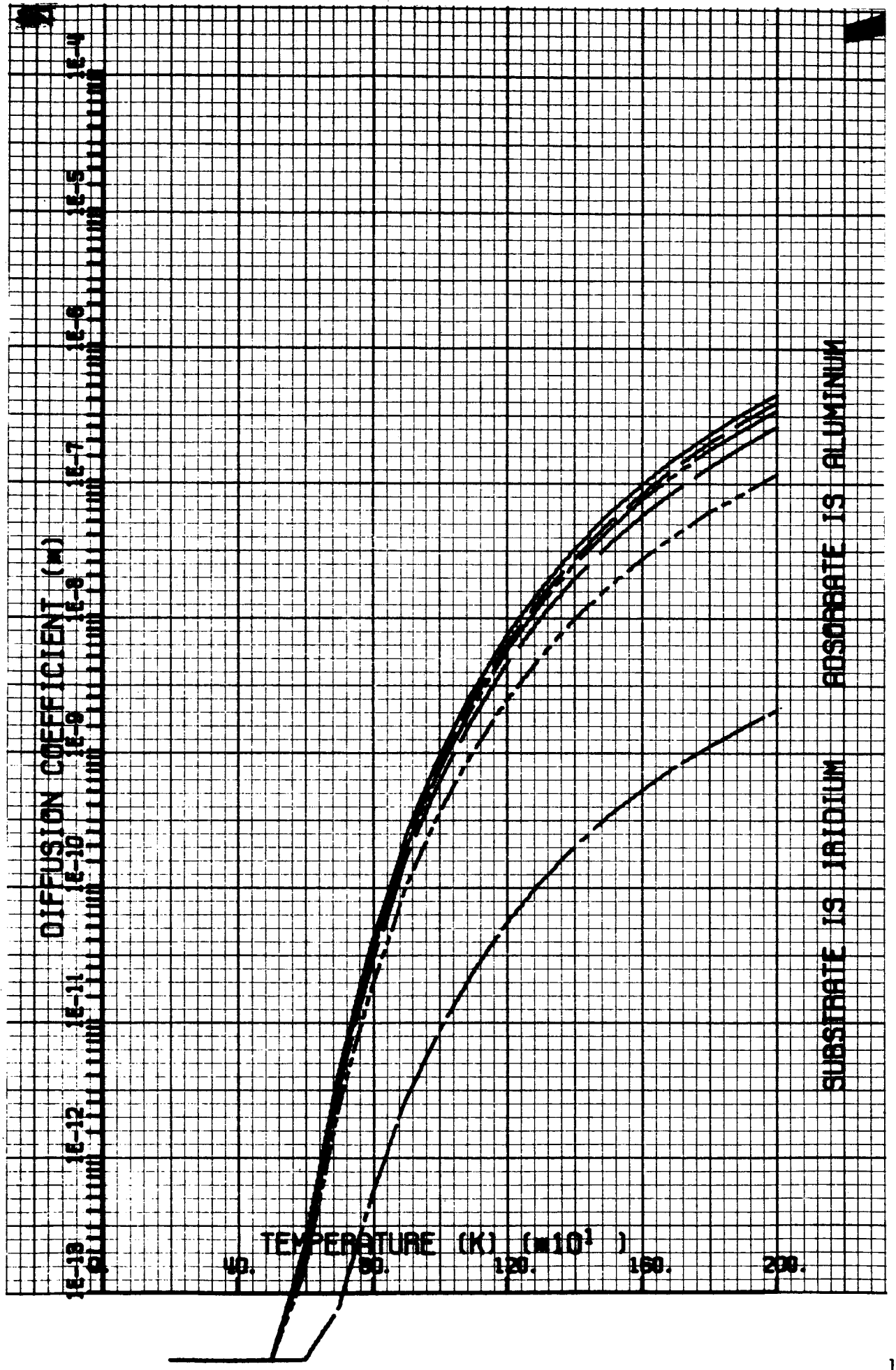
DIFFUSION COEFFICIENT (m)
1E-4
1E-5
1E-6
1E-7
1E-8
1E-9
1E-10
1E-11
1E-12
1E-13
TEMPERATURE (K) (*10¹)
40.
80.
120.
160.
200.
SUBSTRATE IS IRIDIUM
ADSORBATE IS ALUMINUM

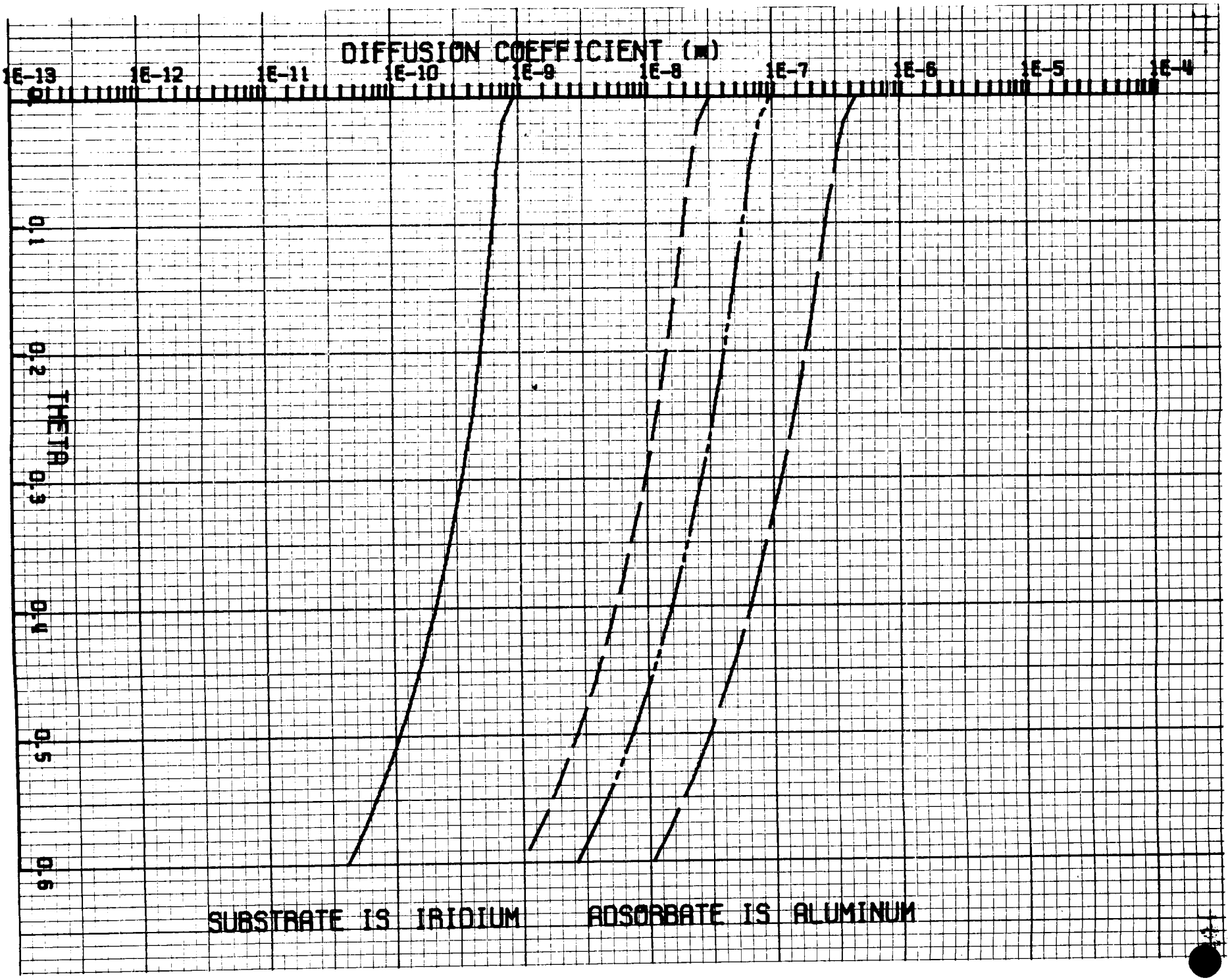
DIFFUSION COEFFICIENT (m)
1E-13
1E-12
1E-11
1E-10
1E-9
1E-8
1E-7
1E-6
1E-5
1E-4
0
0.1
0.2
0.3
0.4
0.5
0.6
THETA
SUBSTRATE IS IRIDIUM
ADSORBATE IS ALUMINUM

DIFFUSION COEFFICIENT (M)
1E-4
1E-5
1E-6
1E-7
1E-8
1E-9
1E-10
1E-11
1E-12
1E-13
TEMPERATURE (K) (*10^1)
40.
80.
120.
160.
200.
SUBSTRATE IS IRIDIUM ADSORBATE IS SILICON

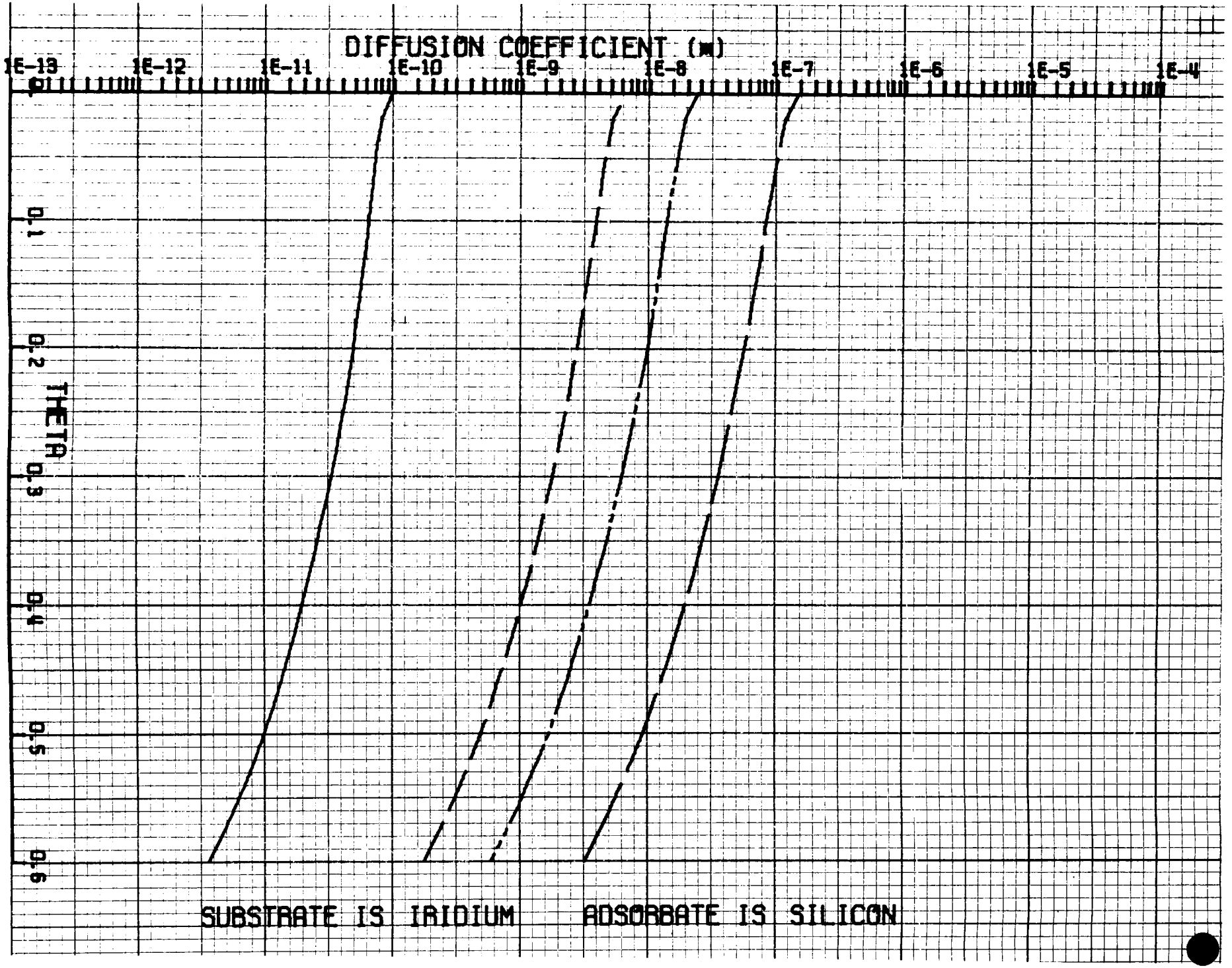
DIFFUSION COEFFICIENT (m)
1E-13
1E-12
1E-11
1E-10
1E-9
1E-8
1E-7
1E-6
1E-5
1E-4
THETA
0.1
0.2
0.3
0.4
0.5
0.6
SUBSTRATE IS IRIDIUM
ADSORBATE IS SILICON

DIFFUSION COEFFICIENT (m²)
1E-4
1E-5
1E-6
1E-7
1E-8
1E-9
1E-10
1E-11
1E-12
1E-13
TEMPERATURE (K) (×10¹)
40.
80.
120.
160.
200.
SUBSTRATE IS IRIDIUM ADSORBATE IS POTASSIUM

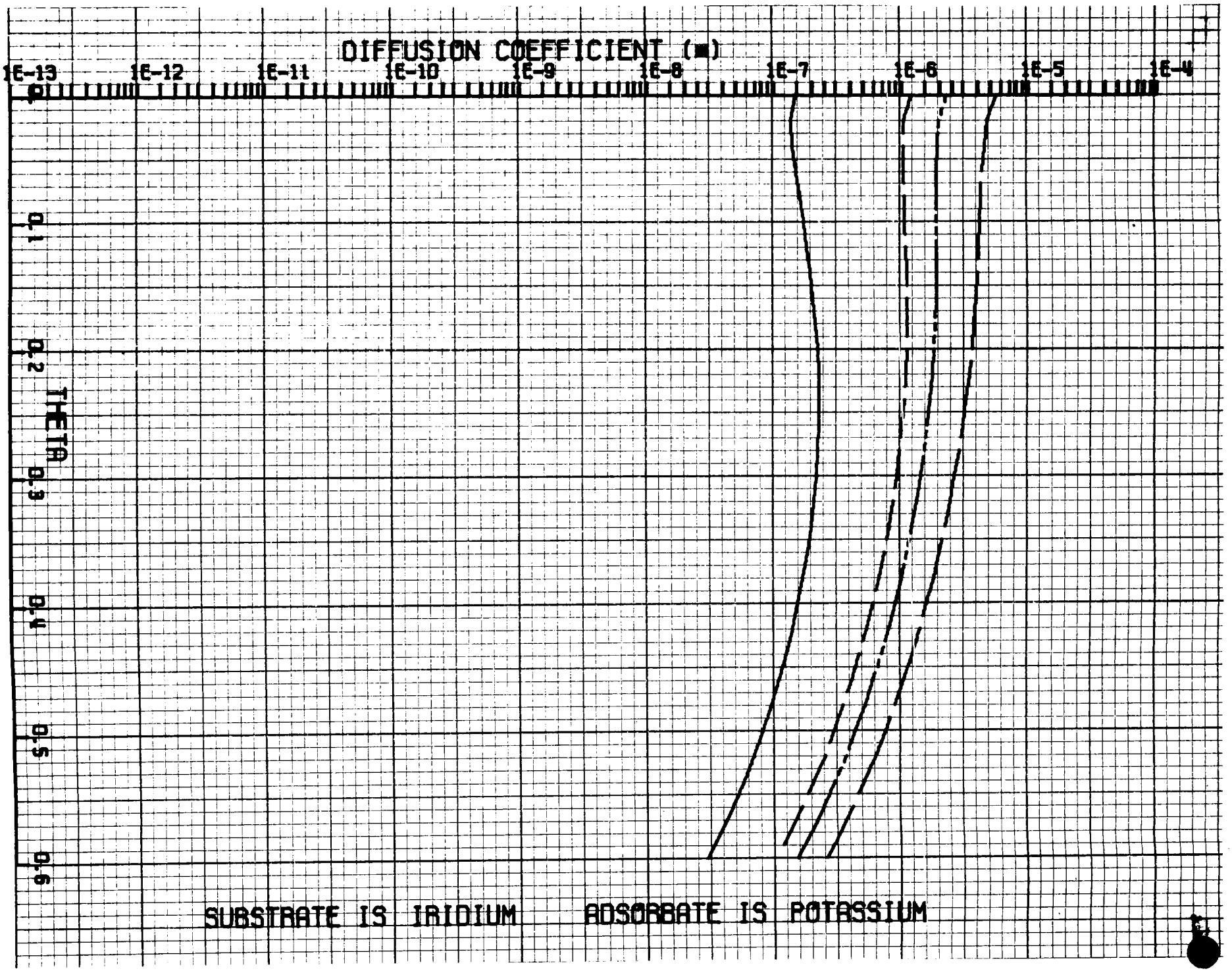
DIFFUSION COEFFICIENT (m)
1E-13
1E-12
1E-11
1E-10
1E-9
1E-8
1E-7
1E-6
1E-5
1E-4
0
0.1
0.2
0.3
0.4
0.5
0.6
THETA
SUBSTRATE IS IRIDIUM
ADSORBATE IS POTASSIUM

DIFFUSION COEFFICIENT (m²)
1E-13
1E-12
1E-11
1E-10
1E-9
1E-8
1E-7
1E-6
1E-5
1E-4
TEMPERATURE (K) (*10¹)
40.
80.
120.
160.
200.
SUBSTRATE IS IRIDIUM
ADSORBATE IS TITANIUM

SUBSTRATE IS IRIDIUM ADSORBATE IS TITANIUM
DIFFUSION COEFFICIENT (M²)
1E-4
1E-5
1E-6
1E-7
1E-8
1E-9
1E-10
1E-11
1E-12
1E-13
THETA
0.1
0.2
0.3
0.4
0.5
0.6

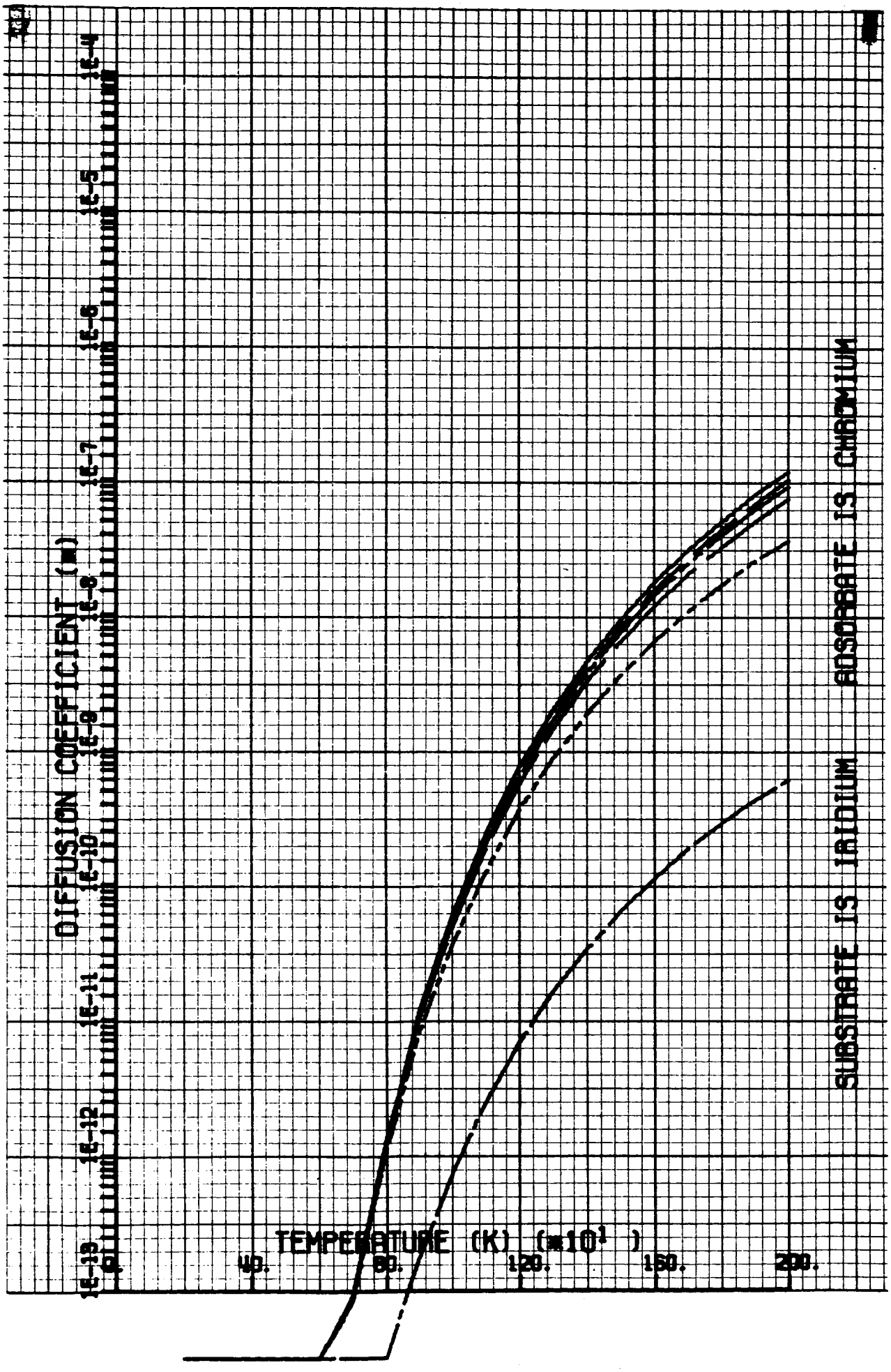
DIFFUSION COEFFICIENT (cm)
1E-4
1E-5
1E-6
1E-7
1E-8
1E-9
1E-10
1E-11
1E-12
1E-13
0.
40.
80.
120.
160.
200.
TEMPERATURE (K) (*10¹)
SUBSTRATE IS IRIDIUM ADSORBATE IS CHROMIUM

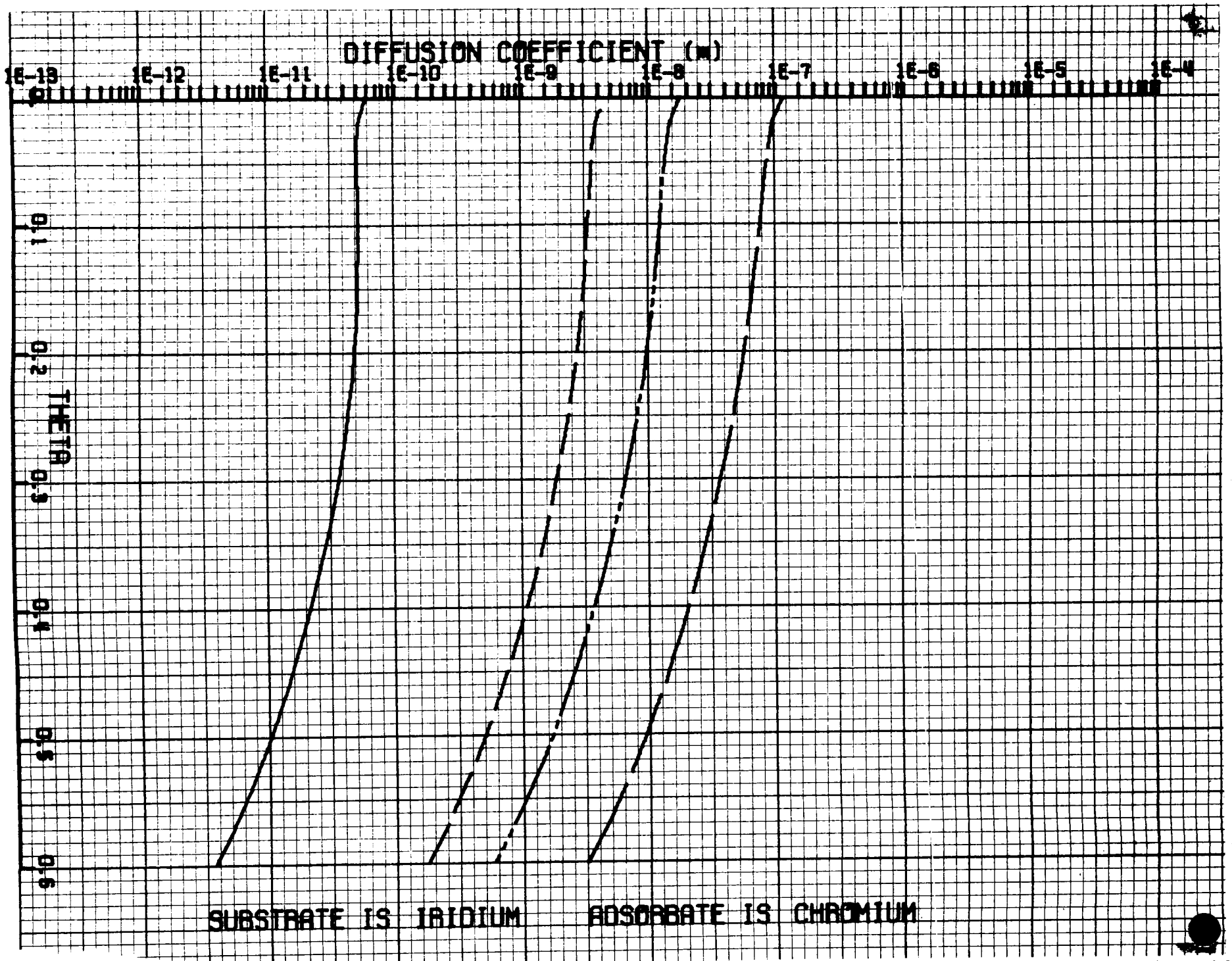
DIFFUSION COEFFICIENT (M)
1E-13
1E-12
1E-11
1E-10
1E-9
1E-8
1E-7
1E-6
1E-5
1E-4
THETA
0.1
0.2
0.3
0.4
0.5
0.6
SUBSTRATE IS IRIDIUM ADSORBATE IS CHROMIUM

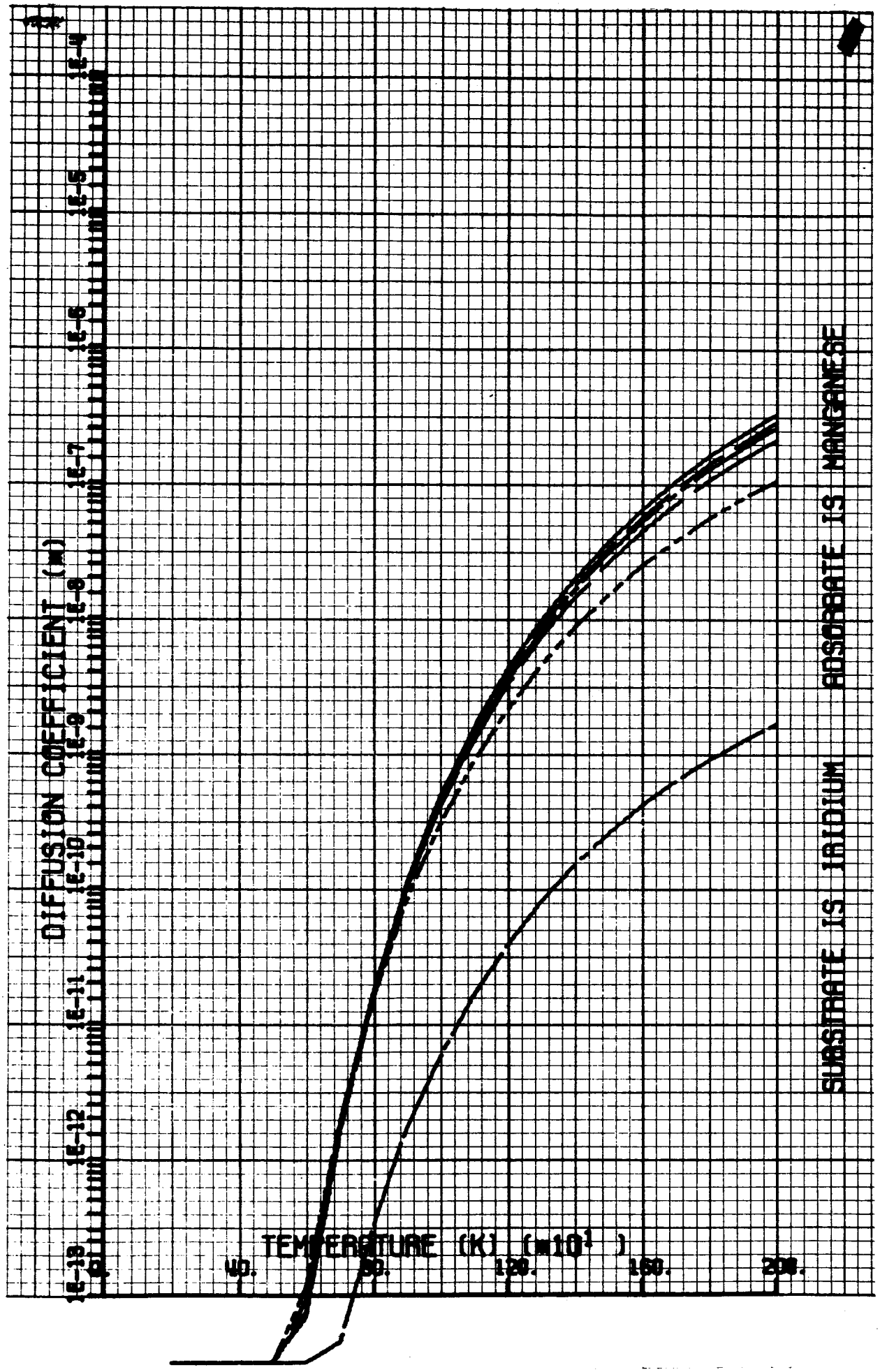
DIFFUSION COEFFICIENT (m)
1E-4
1E-5
1E-6
1E-7
1E-8
1E-9
1E-10
1E-11
1E-12
1E-13
40.
80.
120.
160.
200.
TEMPERATURE (K) (*10¹)
SUBSTRATE IS IRIDIUM ADSORBATE IS MANGANESE

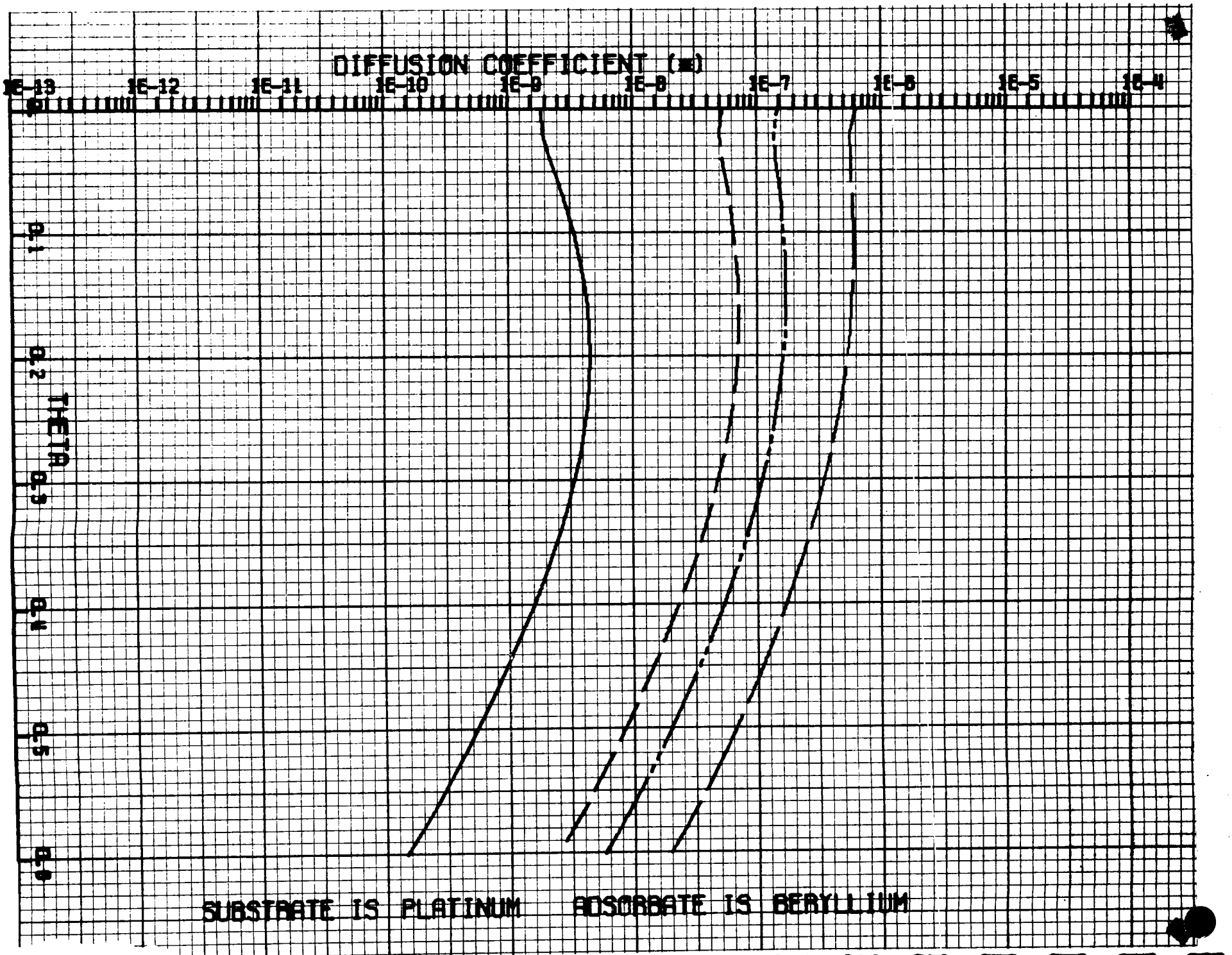
DIFFUSION COEFFICIENT (m)
1E-13
1E-12
1E-11
1E-10
1E-9
1E-8
1E-7
1E-6
1E-5
1E-4
THETA
θ1
θ2
θ3
θ4
θ5
θ6
SUBSTRATE IS PLATINUM ADSORBATE IS BERYLLIUM

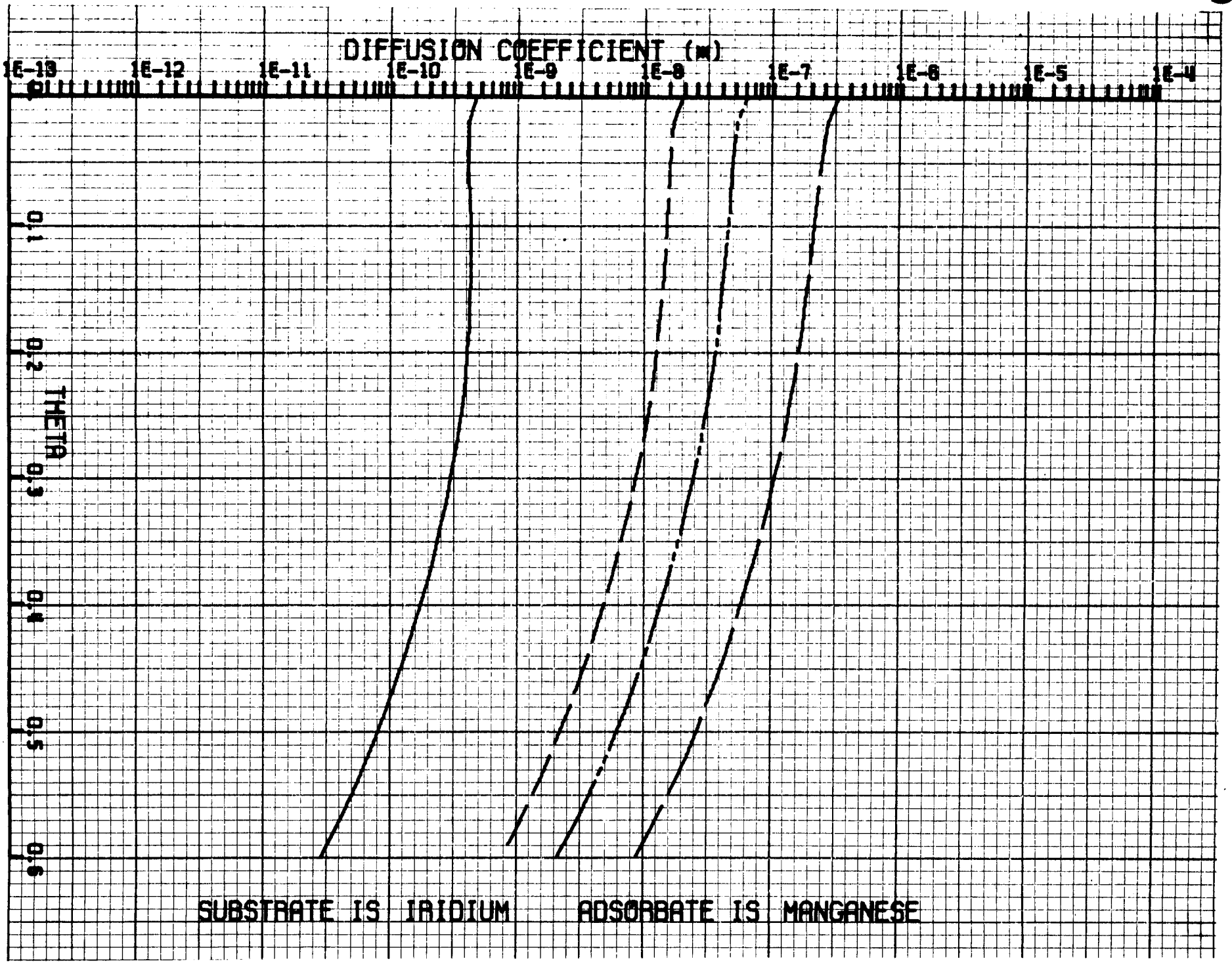
DIFFUSION COEFFICIENT (m)
1E-13
1E-12
1E-11
1E-10
1E-9
1E-8
1E-7
1E-6
1E-5
1E-4
THETA
0.1
0.2
0.3
0.4
0.5
0.6
SUBSTRATE IS IRIDIUM
ADSORBATE IS MANGANESE

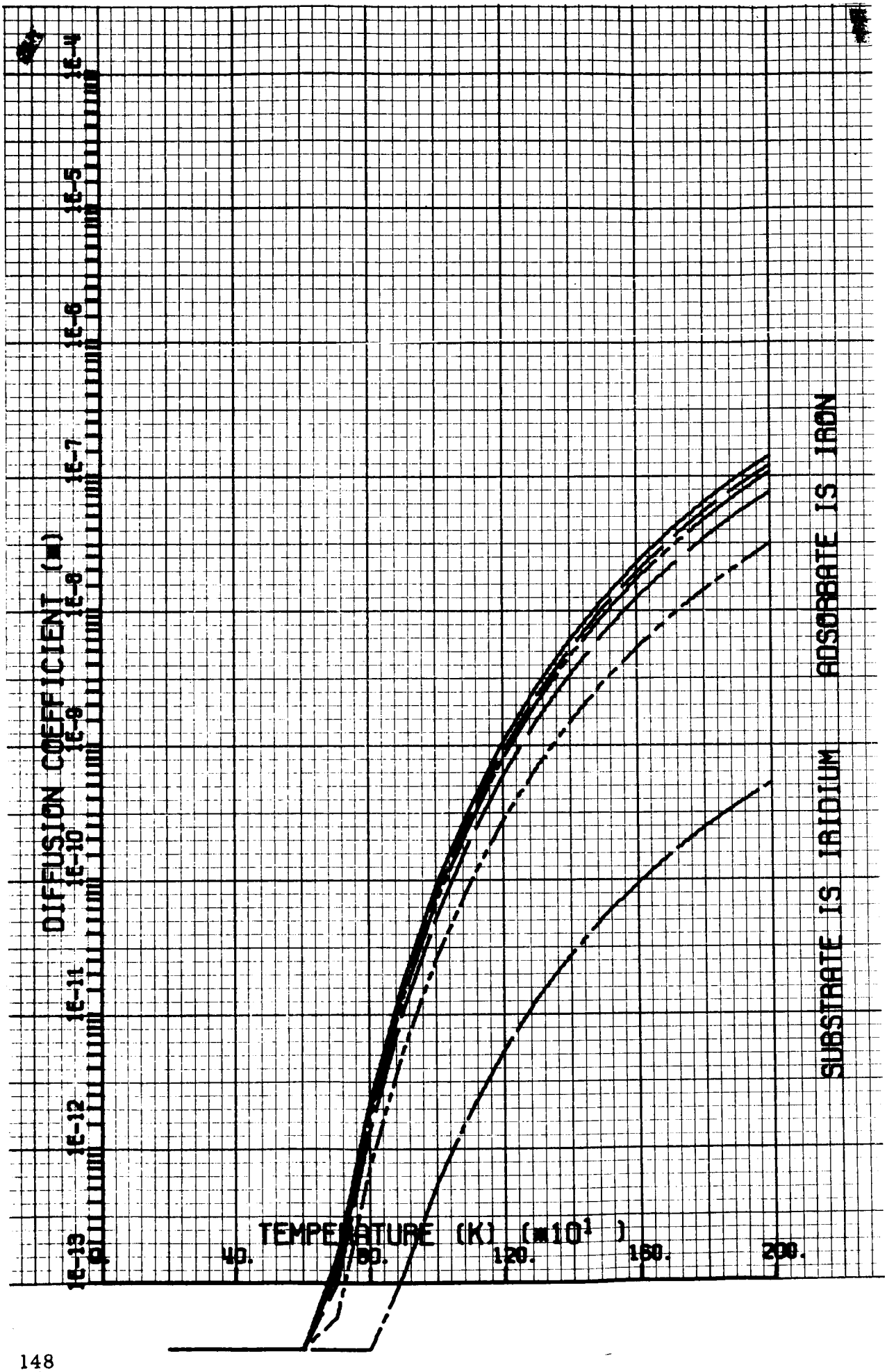
DIFFUSION COEFFICIENT (M²)
1E-4
1E-5
1E-6
1E-7
1E-8
1E-9
1E-10
1E-11
1E-12
1E-13
0.
40.
80.
120.
160.
200.
TEMPERATURE (K) (*10¹)
SUBSTRATE IS IRIDIUM ADSORBATE IS IRON

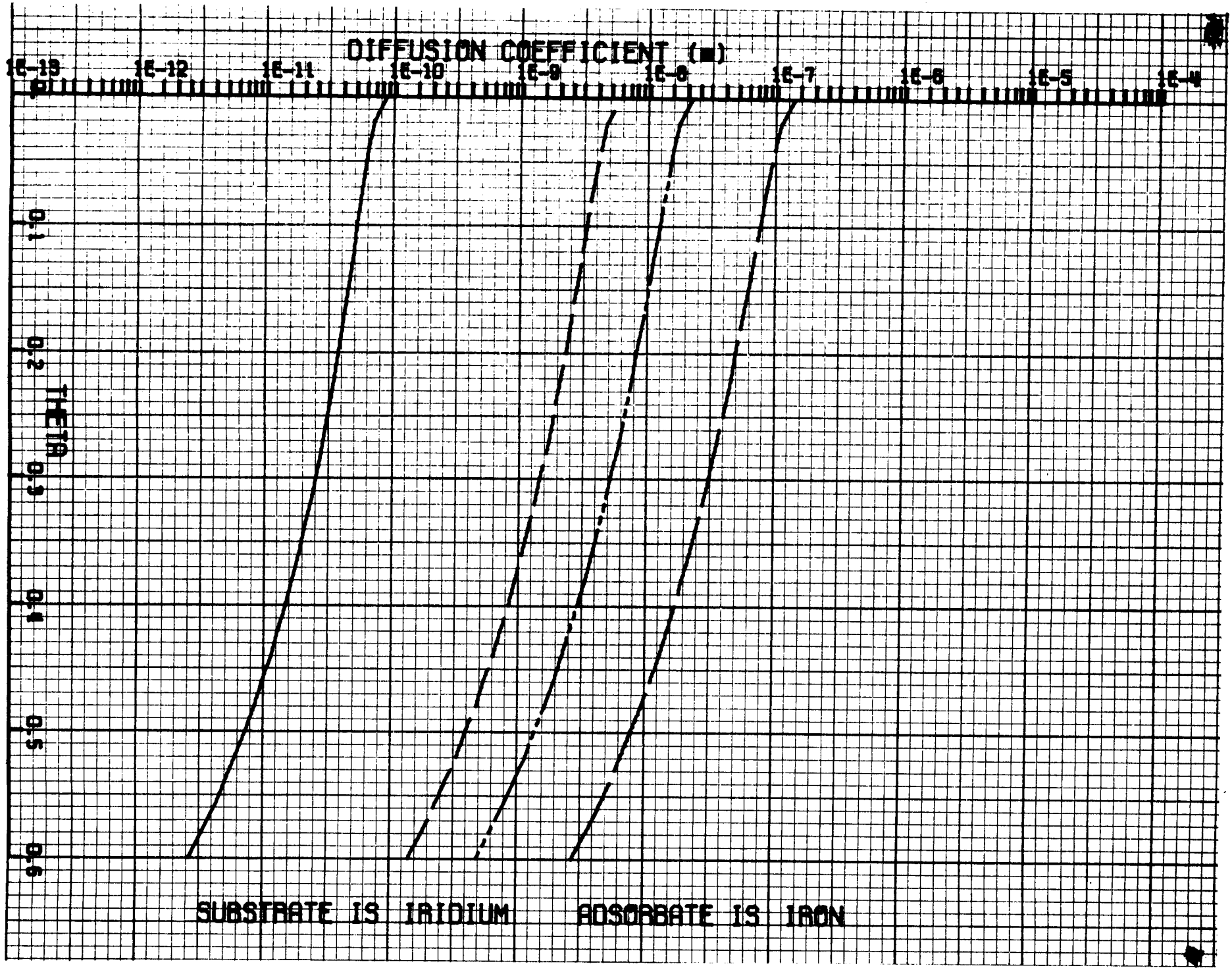
DIFFUSION COEFFICIENT (m)
1E-13
1E-12
1E-11
1E-10
1E-9
1E-8
1E-7
1E-6
1E-5
1E-4
THETA
0.1
0.2
0.3
0.4
0.5
0.6
SUBSTRATE IS IRIDIUM
ADSORBATE IS IRON

DIFFUSION COEFFICIENT (M)
1E-4
1E-5
1E-6
1E-7
1E-8
1E-9
1E-10
1E-11
1E-12
1E-13
40.
80.
120.
160.
200.
TEMPERATURE (K) (*10¹)
SUBSTRATE IS IRIDIUM ADSORBATE IS NICKEL

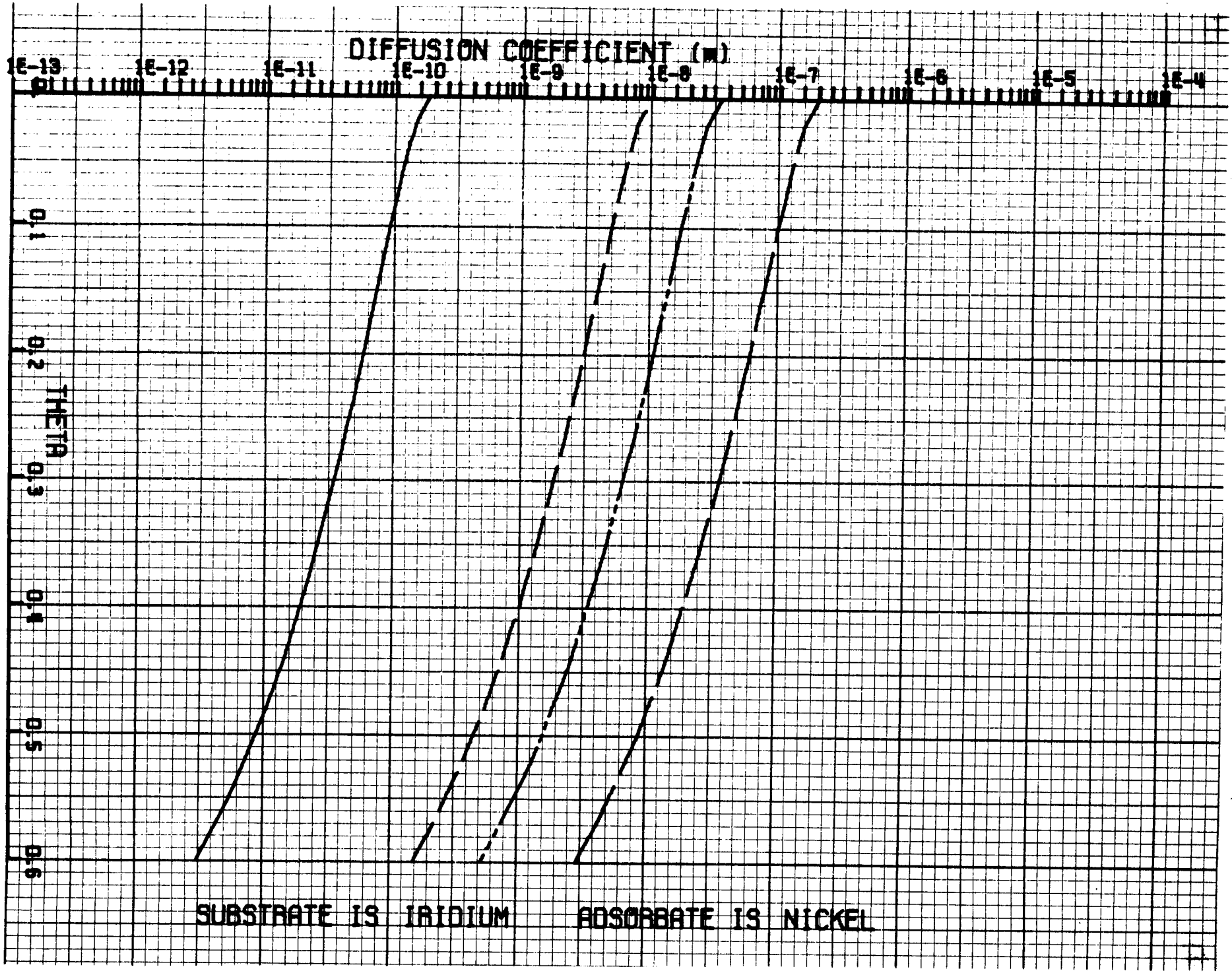
DIFFUSION COEFFICIENT (m)
1E-13
1E-12
1E-11
1E-10
1E-9
1E-8
1E-7
1E-6
1E-5
1E-4
THETA
0.1
0.2
0.3
0.4
0.5
0.6
SUBSTRATE IS IRIDIUM
ADSORBATE IS NICKEL

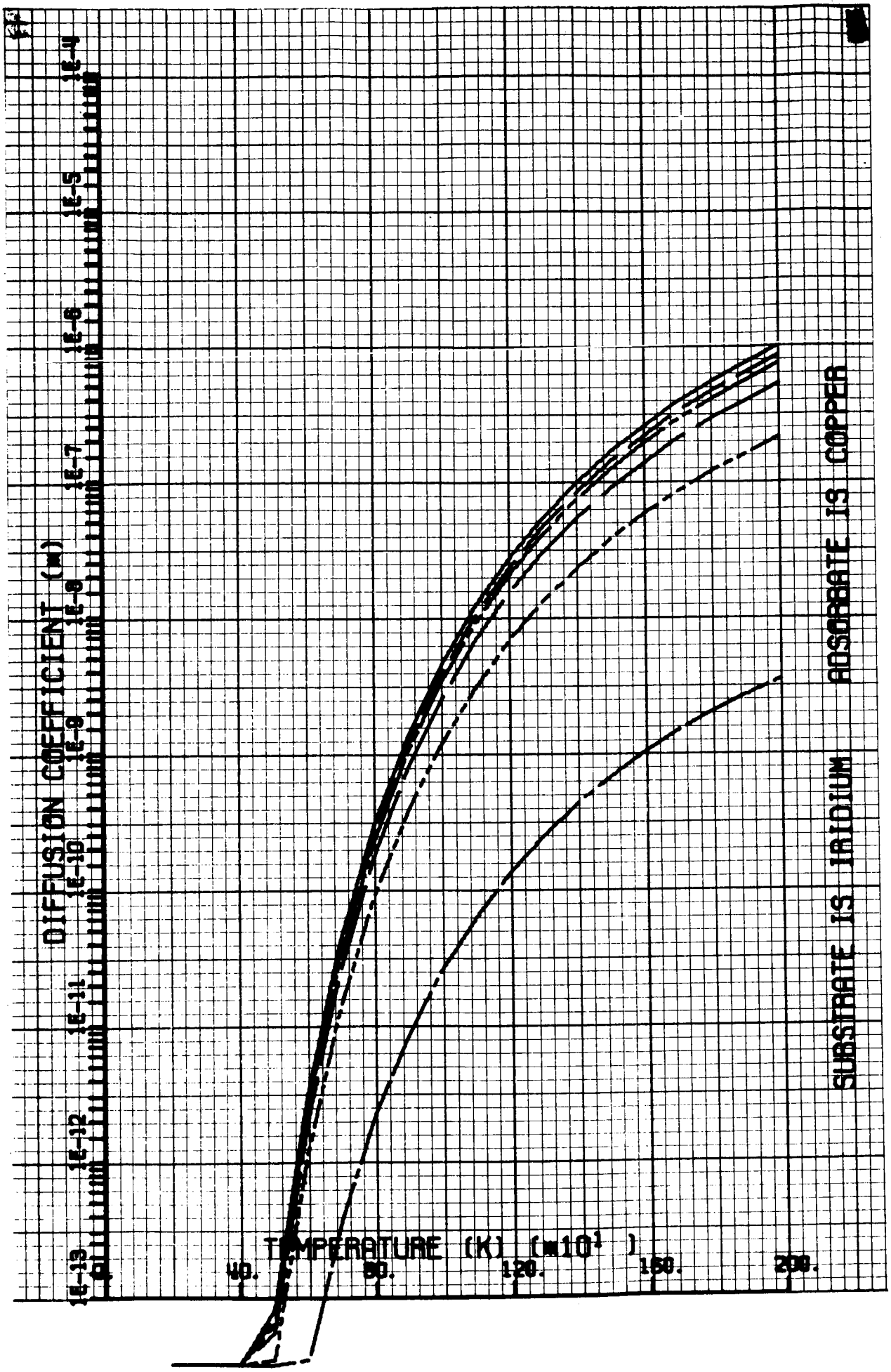
DIFFUSION COEFFICIENT (M²)
1E-4
1E-5
1E-6
1E-7
1E-8
1E-9
1E-10
1E-11
1E-12
1E-13
TEMPERATURE (K) (*10¹)
40.
80.
120.
160.
200.
SUBSTRATE IS IRIDIUM ADSORBATE IS COPPER

DIFFUSION COEFFICIENT (cm²)
1E-13
1E-12
1E-11
1E-10
1E-9
1E-8
1E-7
1E-6
1E-5
1E-4
0.1
0.2
0.3
0.4
0.5
0.6
THETA
SUBSTRATE IS IRIDIUM ADSORBATE IS COPPER

DIFFUSION COEFFICIENT (M)
1E-4
1E-5
1E-6
1E-7
1E-8
1E-9
1E-10
1E-11
1E-12
1E-13
TEMPERATURE (K) (*10¹)
40.
80.
120.
160.
200.
SUBSTRATE IS IRIDIUM ADSORBATE IS GALLIUM

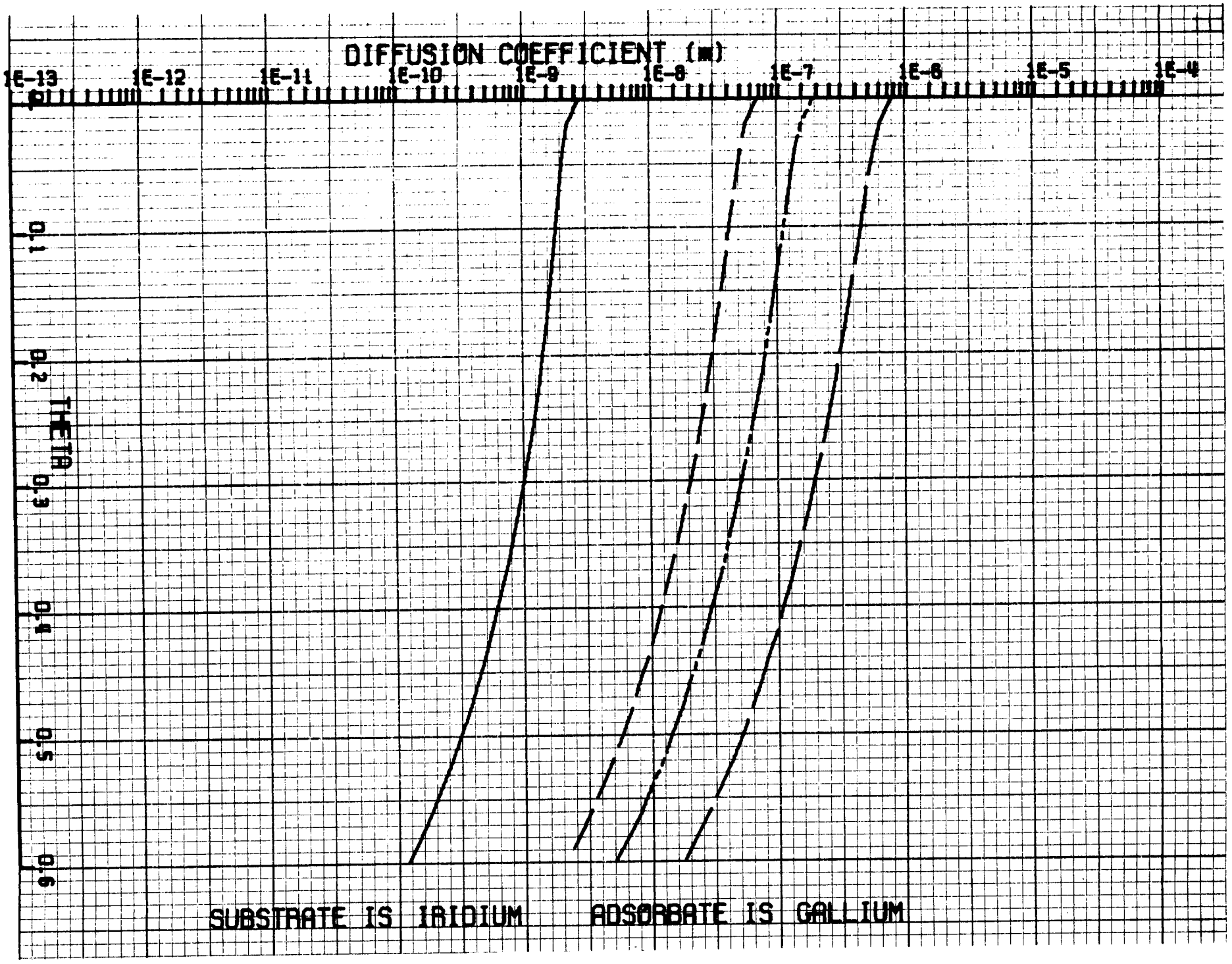
DIFFUSION COEFFICIENT (m)
1E-13
1E-12
1E-11
1E-10
1E-9
1E-8
1E-7
1E-6
1E-5
1E-4
THETA
0.1
0.2
0.3
0.4
0.5
0.6
SUBSTRATE IS IRIDIUM ADSORBATE IS GALLIUM

DIFFUSION COEFFICIENT (m)
1E-4
1E-5
1E-6
1E-7
1E-8
1E-9
1E-10
1E-11
1E-12
1E-13
TEMPERATURE (K) (*10¹)
40.
80.
120.
160.
200.
SUBSTRATE IS IRIDIUM ADSORBATE IS RUBIDIUM

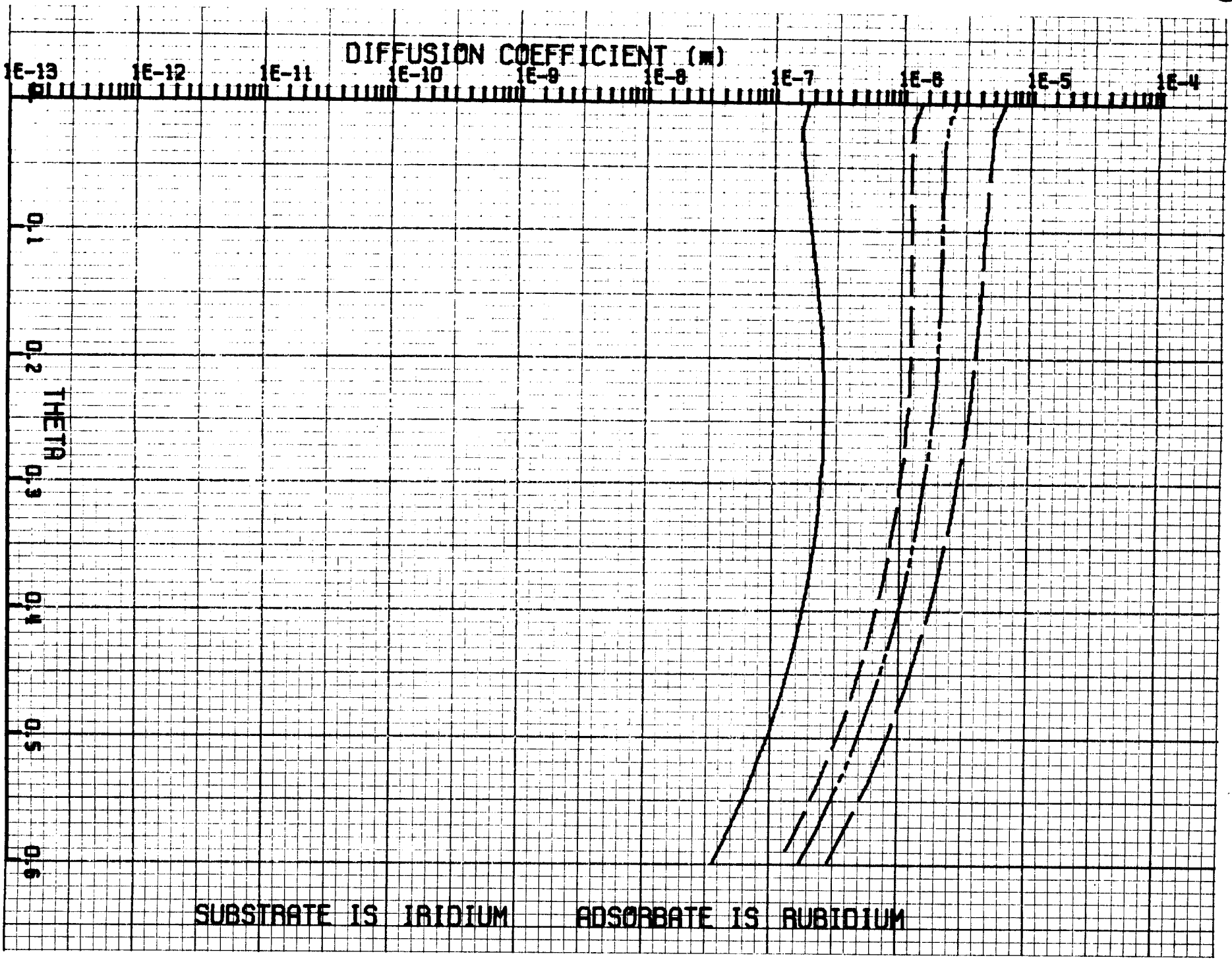
DIFFUSION COEFFICIENT (m)
1E-13
1E-12
1E-11
1E-10
1E-9
1E-8
1E-7
1E-6
1E-5
1E-4
THETA
0.1
0.2
0.3
0.4
0.5
0.6
SUBSTRATE IS IRIDIUM
ADSORBATE IS RUBIDIUM

DIFFUSION COEFFICIENT (m)
1E-4
1E-5
1E-6
1E-7
1E-8
1E-9
1E-10
1E-11
1E-12
1E-13
40.
80.
120.
160.
200.
TEMPERATURE (K) (*10¹)
SUBSTRATE IS IRIDIUM ADSORBATE IS INDIUM

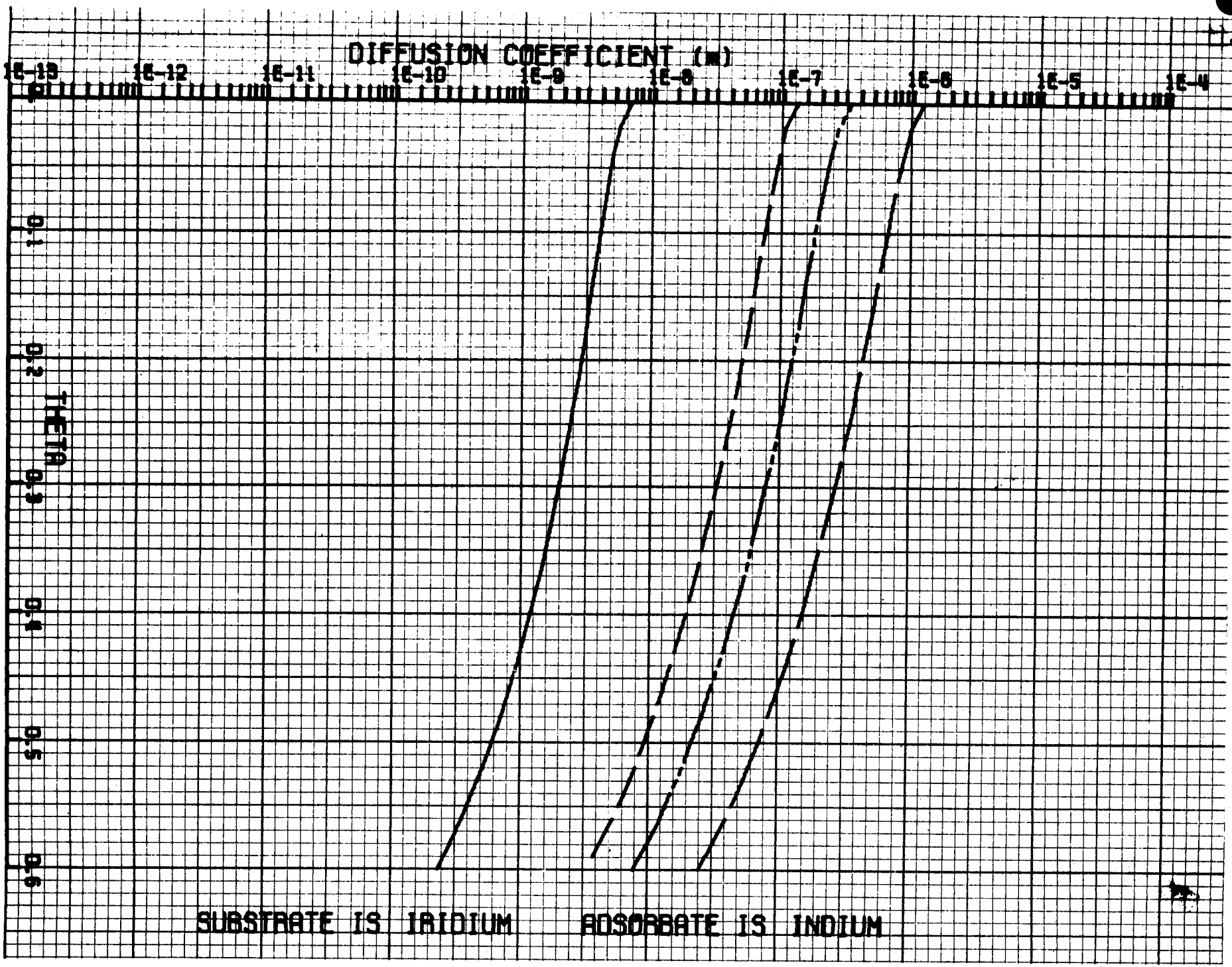
DIFFUSION COEFFICIENT (m)
1E-13
1E-12
1E-11
1E-10
1E-9
1E-8
1E-7
1E-6
1E-5
1E-4
TIME (s)
1.0
2.0
3.0
4.0
5.0
6.0
SUBSTRATE IS IRIDIUM
ADSORBATE IS INDIUM

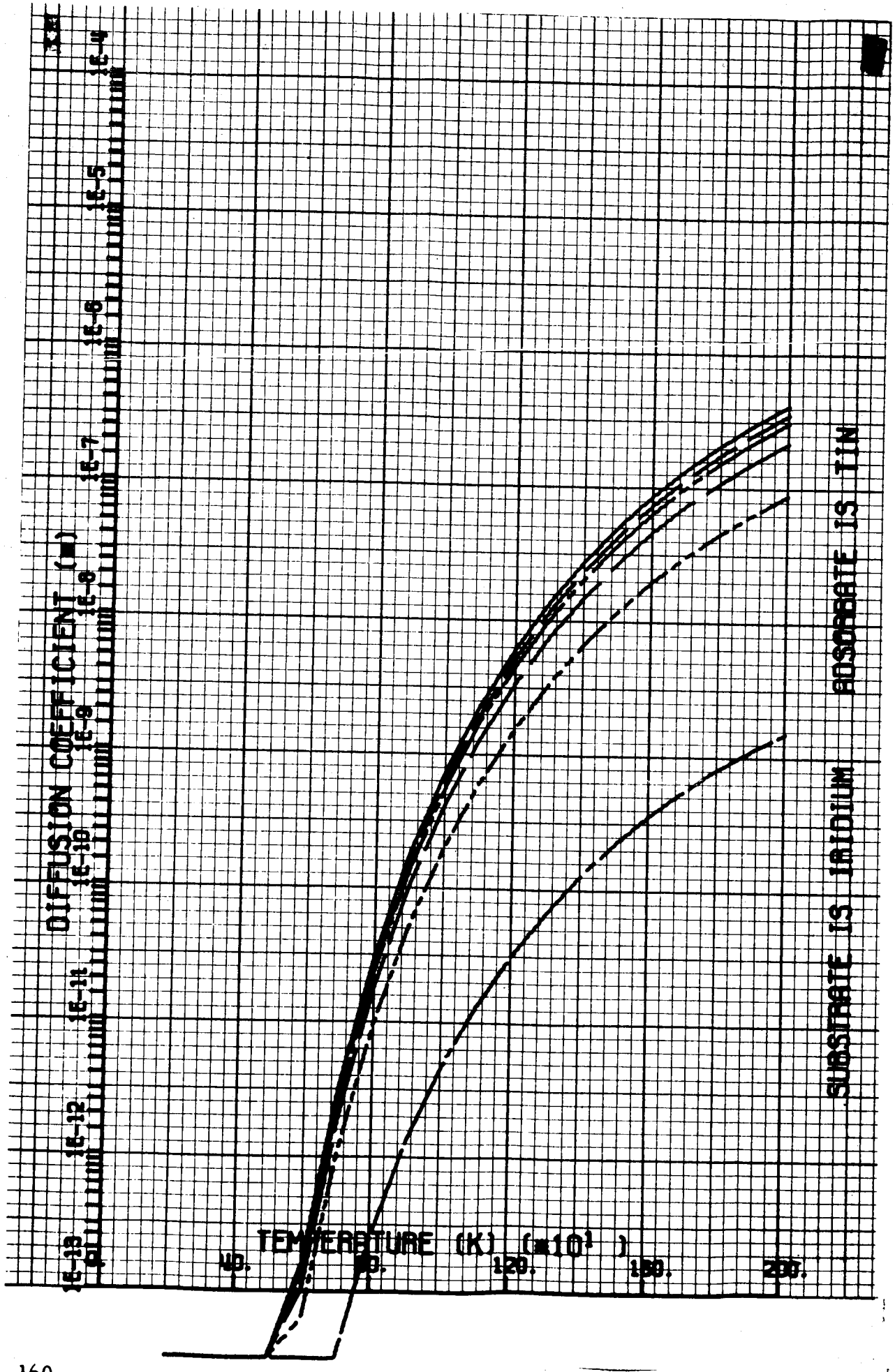
DIFFUSION COEFFICIENT (m²)
1E-4
1E-5
1E-6
1E-7
1E-8
1E-9
1E-10
1E-11
1E-12
1E-13
TEMPERATURE (K) (*10²)
40.
80.
120.
160.
200.
SUBSTRATE IS IRIDIUM
ADSORBATE IS TIN

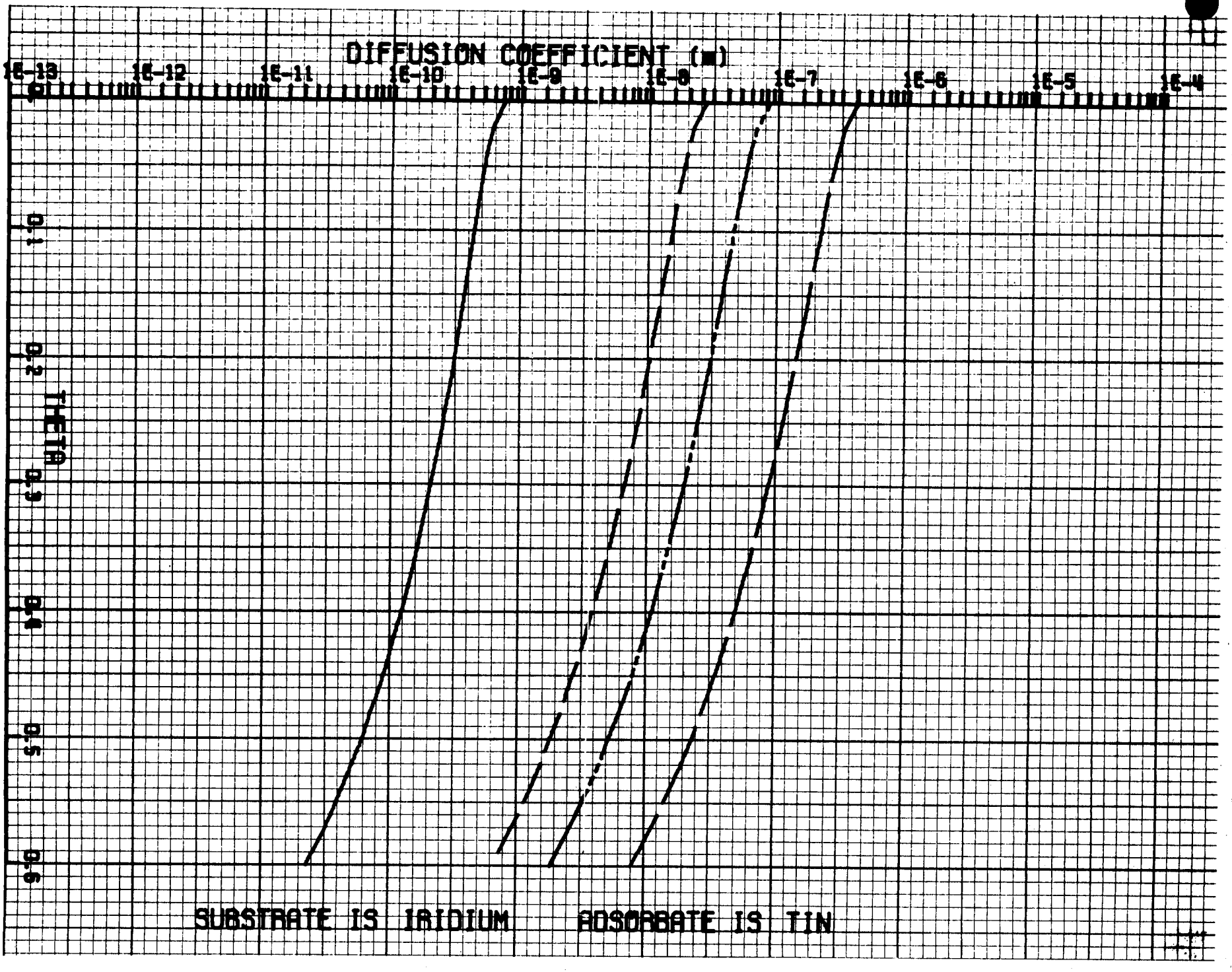
DIFFUSION COEFFICIENT (m)
1E-13
1E-12
1E-11
1E-10
1E-9
1E-8
1E-7
1E-6
1E-5
1E-4
THETA
0.1
0.2
0.3
0.4
0.5
0.6
SUBSTRATE IS IRIDIUM
ADSORBATE IS TIN

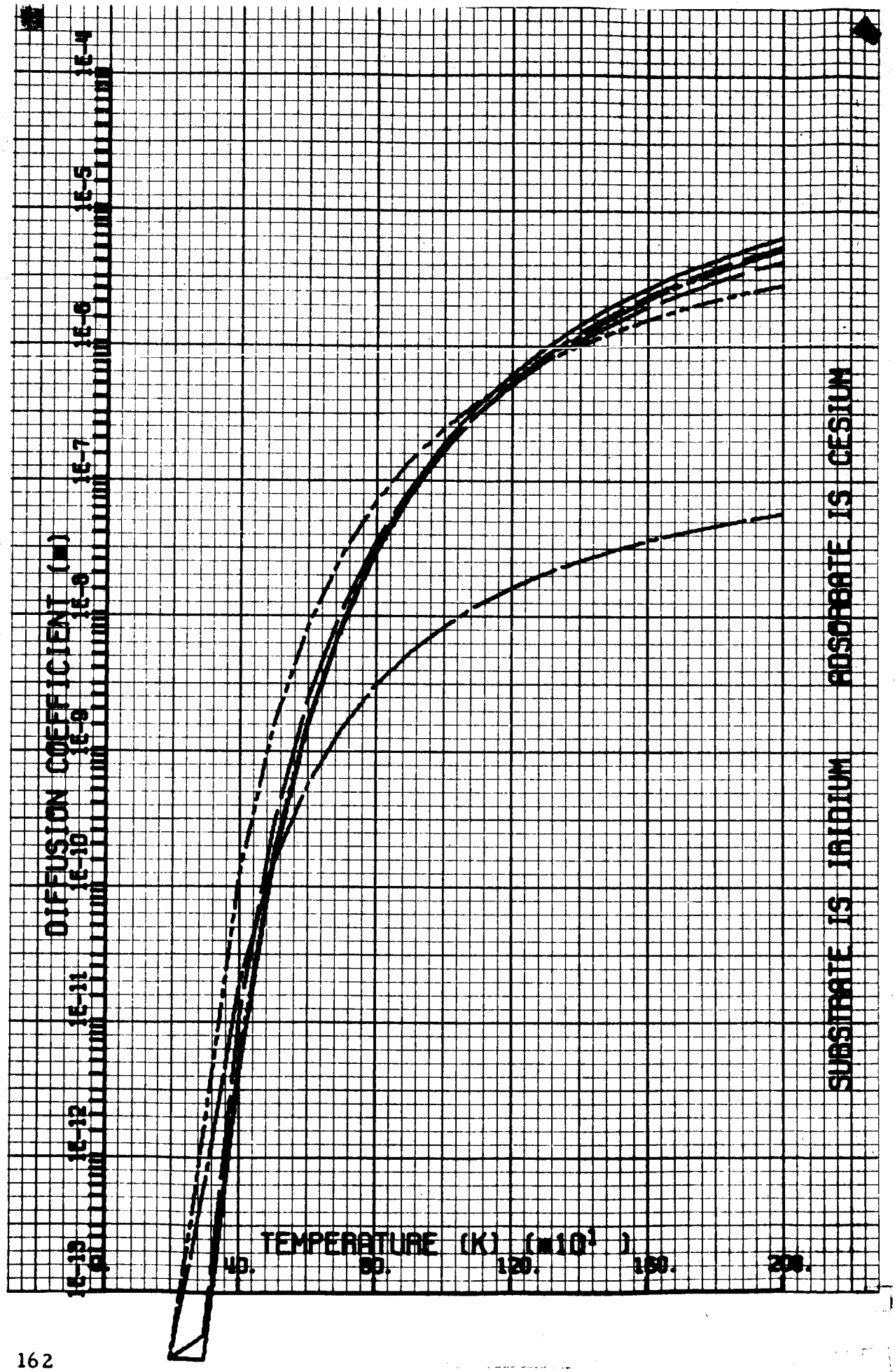
DIFFUSION COEFFICIENT (m)
1E-4
1E-5
1E-6
1E-7
1E-8
1E-9
1E-10
1E-11
1E-12
1E-13
TEMPERATURE (K) (*10¹)
40.
80.
120.
160.
200.
SUBSTRATE IS IRIDIUM ADSORBATE IS CESIUM

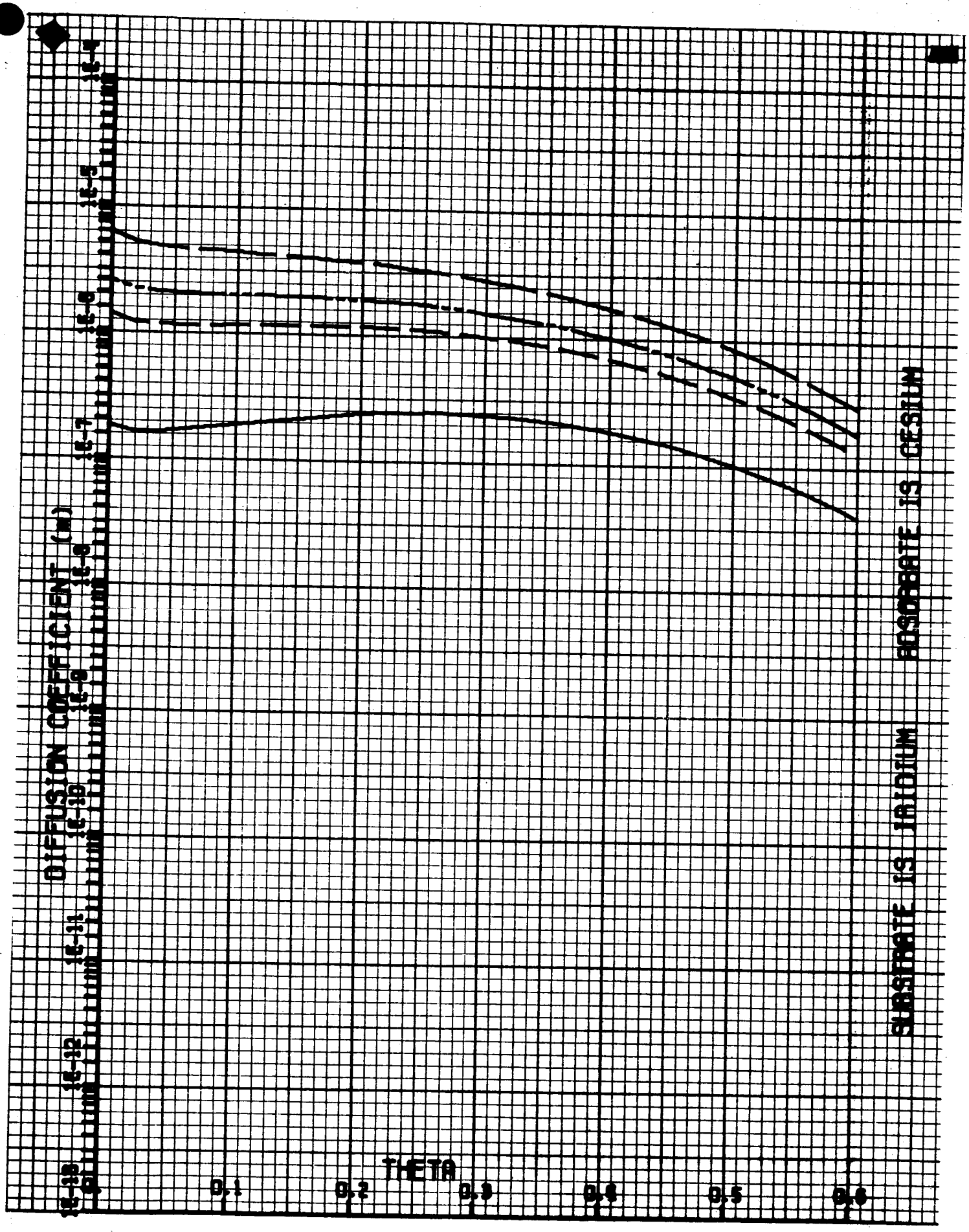
DIFFUSION COEFFICIENT (M)
1E-13
1E-12
1E-11
1E-10
1E-9
1E-8
1E-7
1E-6
1E-5
1E-4
THETA
0.1
0.2
0.3
0.4
0.5
0.6
SUBSTRATE IS IRIDIUM
ADSORBATE IS CESIUM

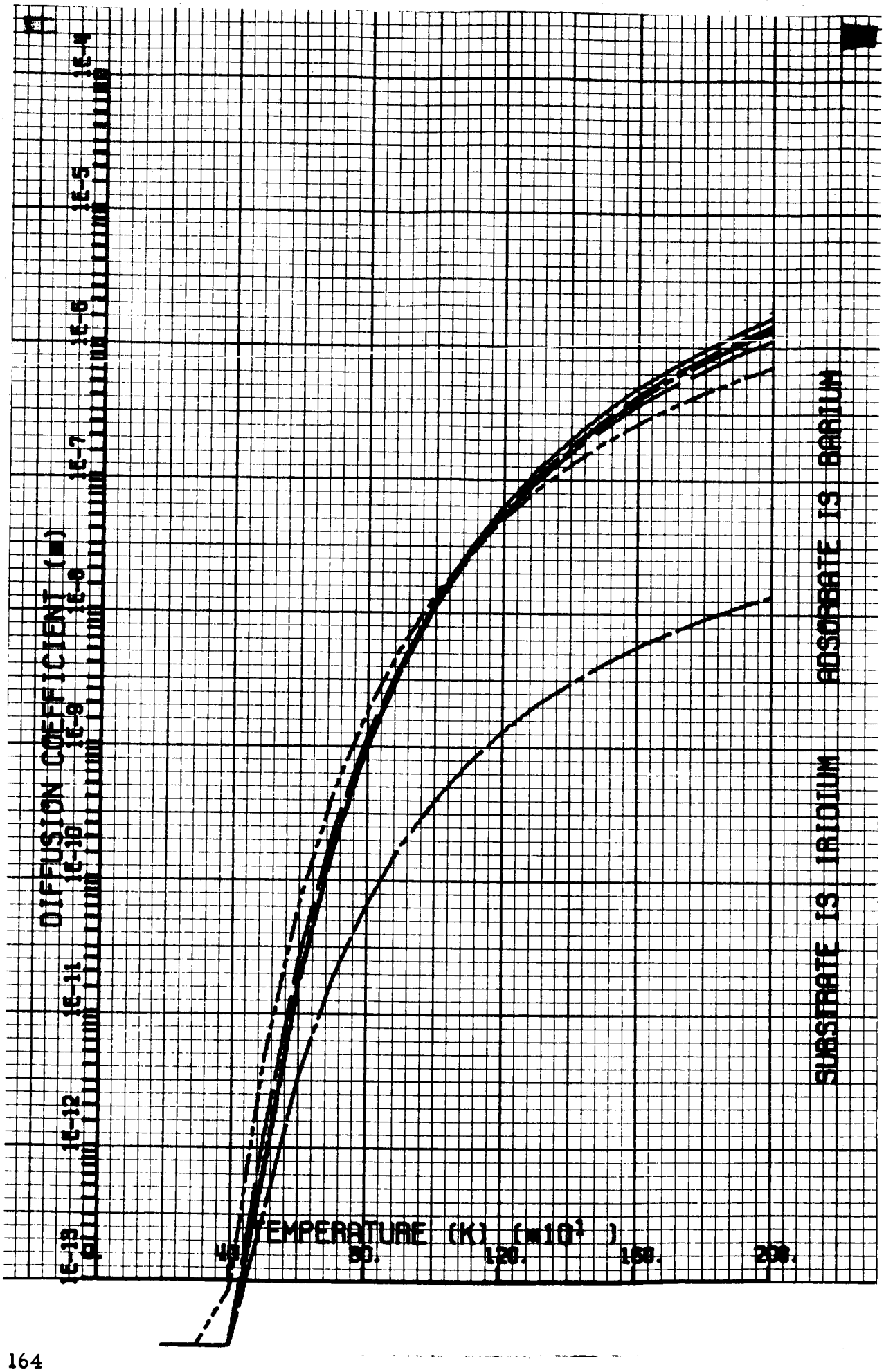
DIFFUSION COEFFICIENT (■)
1E-4
1E-5
1E-6
1E-7
1E-8
1E-9
1E-10
1E-11
1E-12
1E-13
TEMPERATURE (K) (×10¹)
40.
80.
120.
160.
200.
SUBSTRATE IS IRIDIUM ADSORBATE IS BARIUM

DIFFUSION COEFFICIENT (cm²)
1E-13
1E-12
1E-11
1E-10
1E-9
1E-8
1E-7
1E-6
1E-5
1E-4
0
0.1
0.2
0.3
0.4
0.5
0.6
THETA
SUBSTRATE IS IRIDIUM
ADSORBATE IS BARIUM

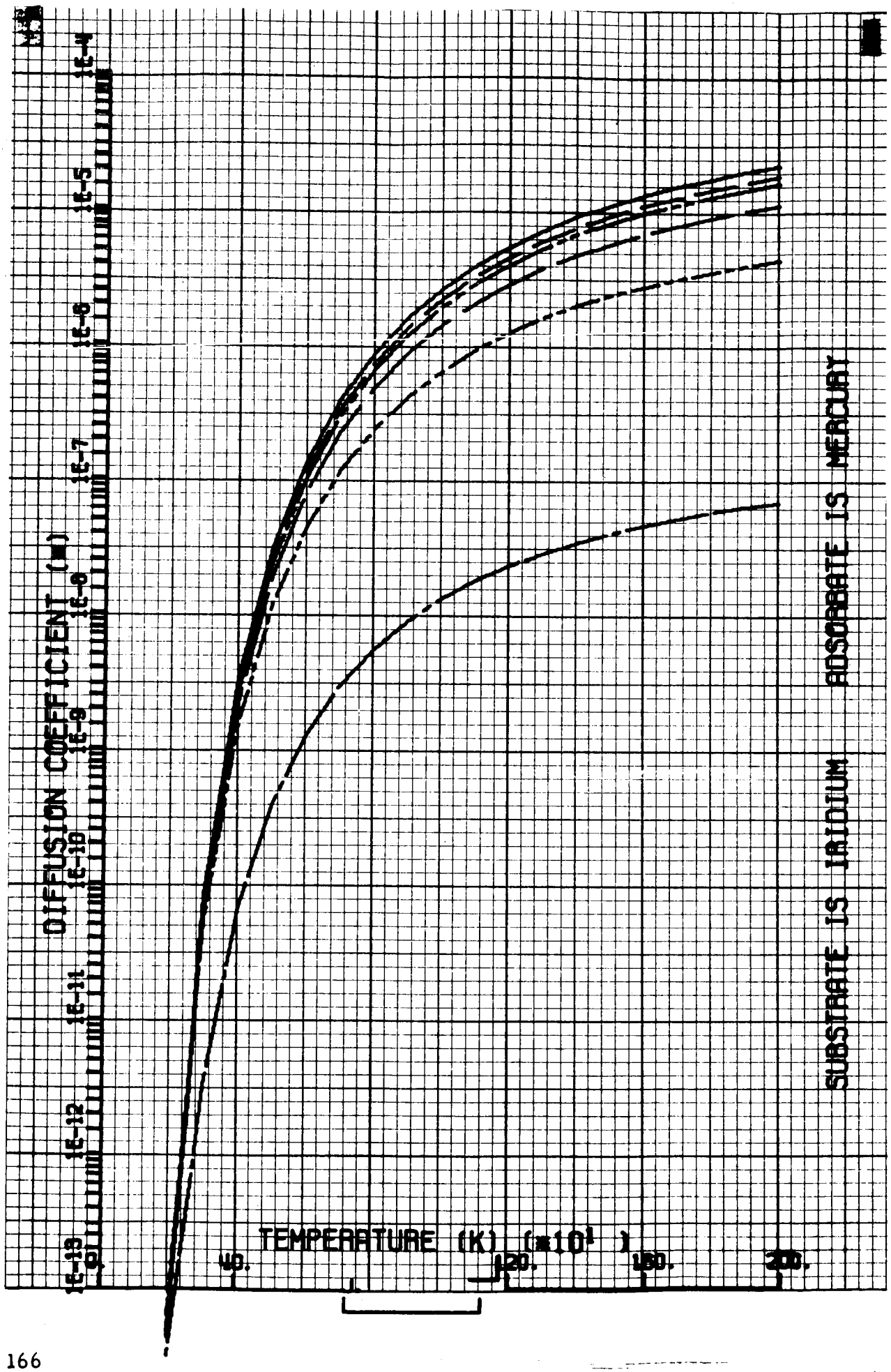
DIFFUSION COEFFICIENT (cm²)
1E-4
1E-5
1E-6
1E-7
1E-8
1E-9
1E-10
1E-11
1E-12
1E-13
TEMPERATURE (K) (×10¹)
40.
120.
160.
200.
SUBSTRATE IS IRIDIUM ADSORBATE IS MERCURY

DIFFUSION COEFFICIENT (M)
1E-13
1E-12
1E-11
1E-10
1E-9
1E-8
1E-7
1E-6
1E-5
1E-4
THETA
0.1
0.2
0.3
0.4
0.5
0.6
SUBSTRATE IS IRIDIUM
ADSORBATE IS MERCURY

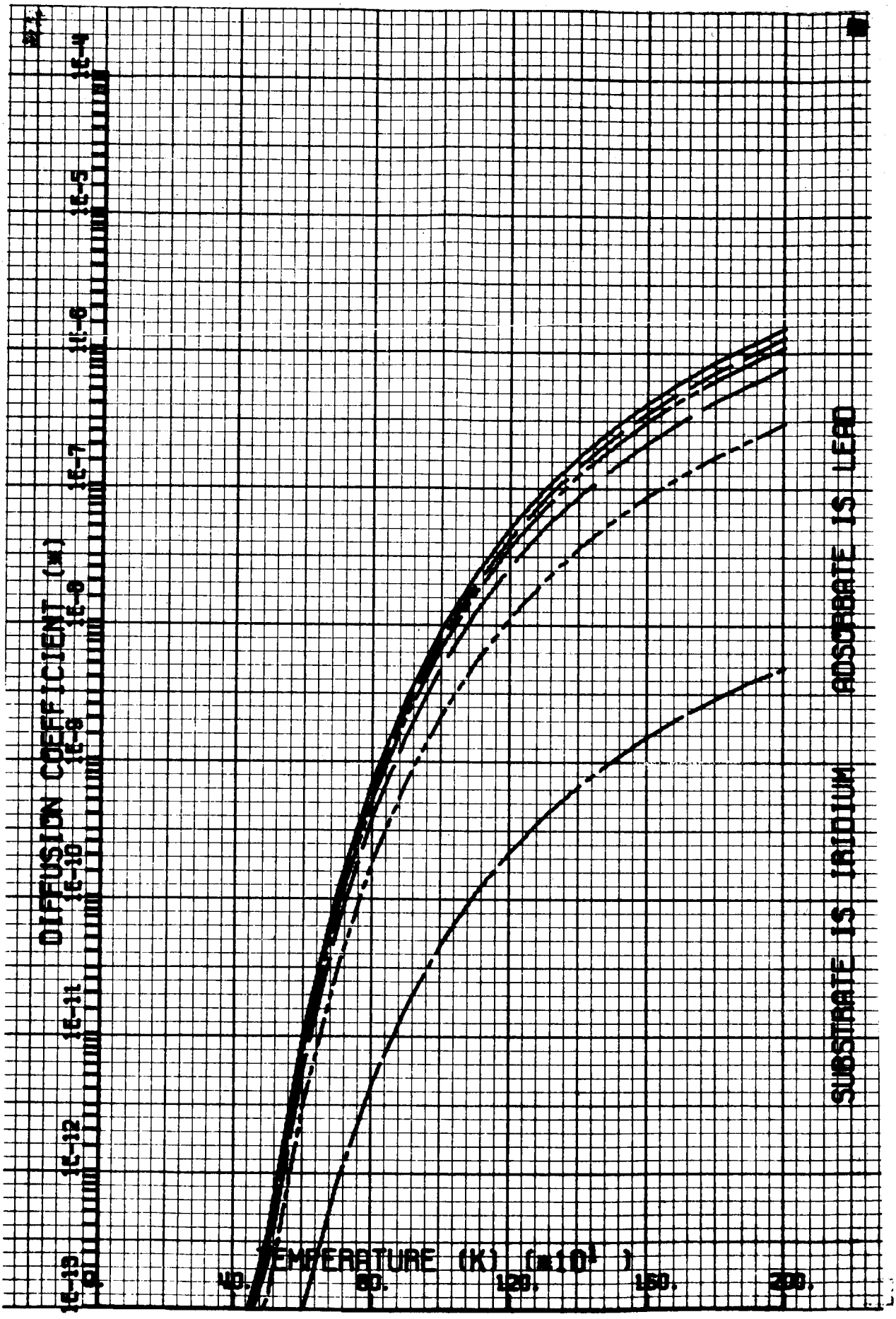
DIFFUSION COEFFICIENT (M)
1E-4
1E-5
1E-6
1E-7
1E-8
1E-9
1E-10
1E-11
1E-12
1E-13
TEMPERATURE (K) (*10¹)
40.
80.
120.
150.
200.
SUBSTRATE IS IRIDIUM ADSORBATE IS LEAD

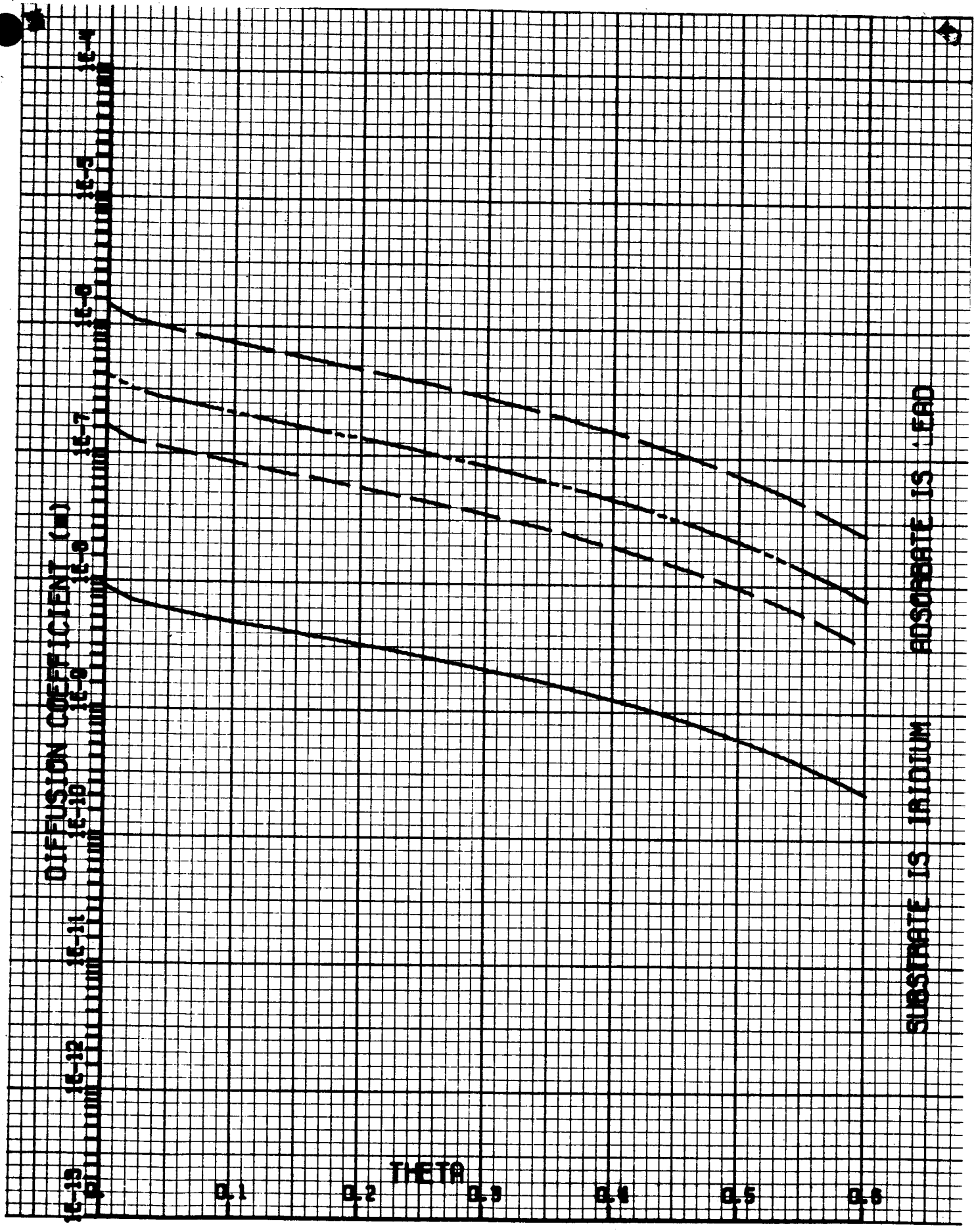
DIFFUSION COEFFICIENT (M)
1E-4
1E-5
1E-6
1E-7
1E-8
1E-9
1E-10
1E-11
1E-12
1E-13
0.1
0.2
0.3
0.4
0.5
0.6
THETA
SUBSTRATE IS IRIDIUM ADSORBATE IS LEAD

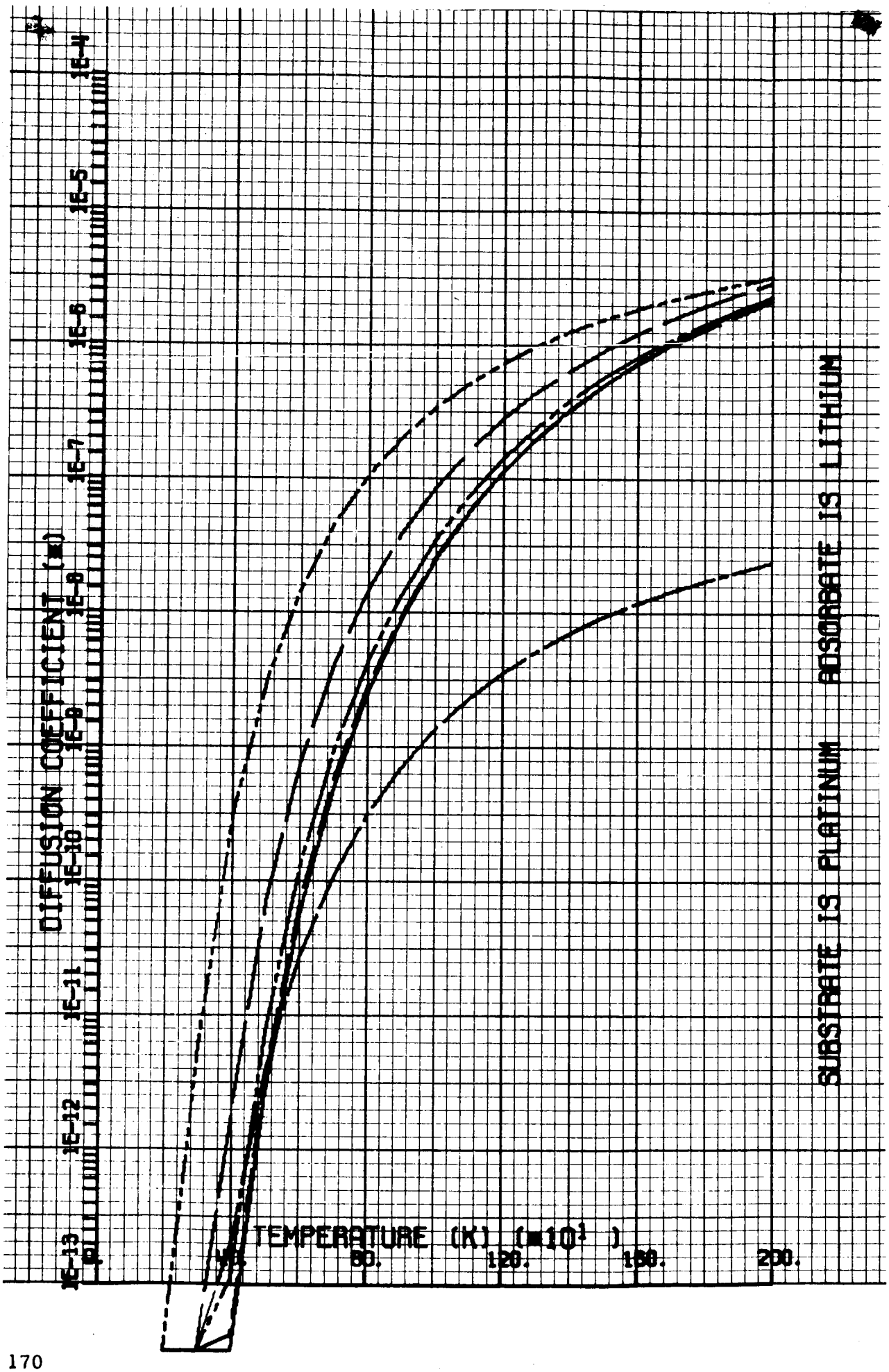
DIFFUSION COEFFICIENT (M²)
1E-4
1E-5
1E-6
1E-7
1E-8
1E-9
1E-10
1E-11
1E-12
1E-13
0.
40.
80.
120.
160.
200.
TEMPERATURE (K) (*10¹)
SUBSTRATE IS PLATINUM ADSORBATE IS LITHIUM

SUBSTRATE IS PLATINUM ADSORBATE IS LITHIUM
DIFFUSION COEFFICIENT (M)
1E-3
1E-4
1E-5
1E-6
1E-7
1E-8
1E-9
1E-10
1E-11
1E-12
1E-13
0.1
0.2
THETA
0.3
0.5
0.6

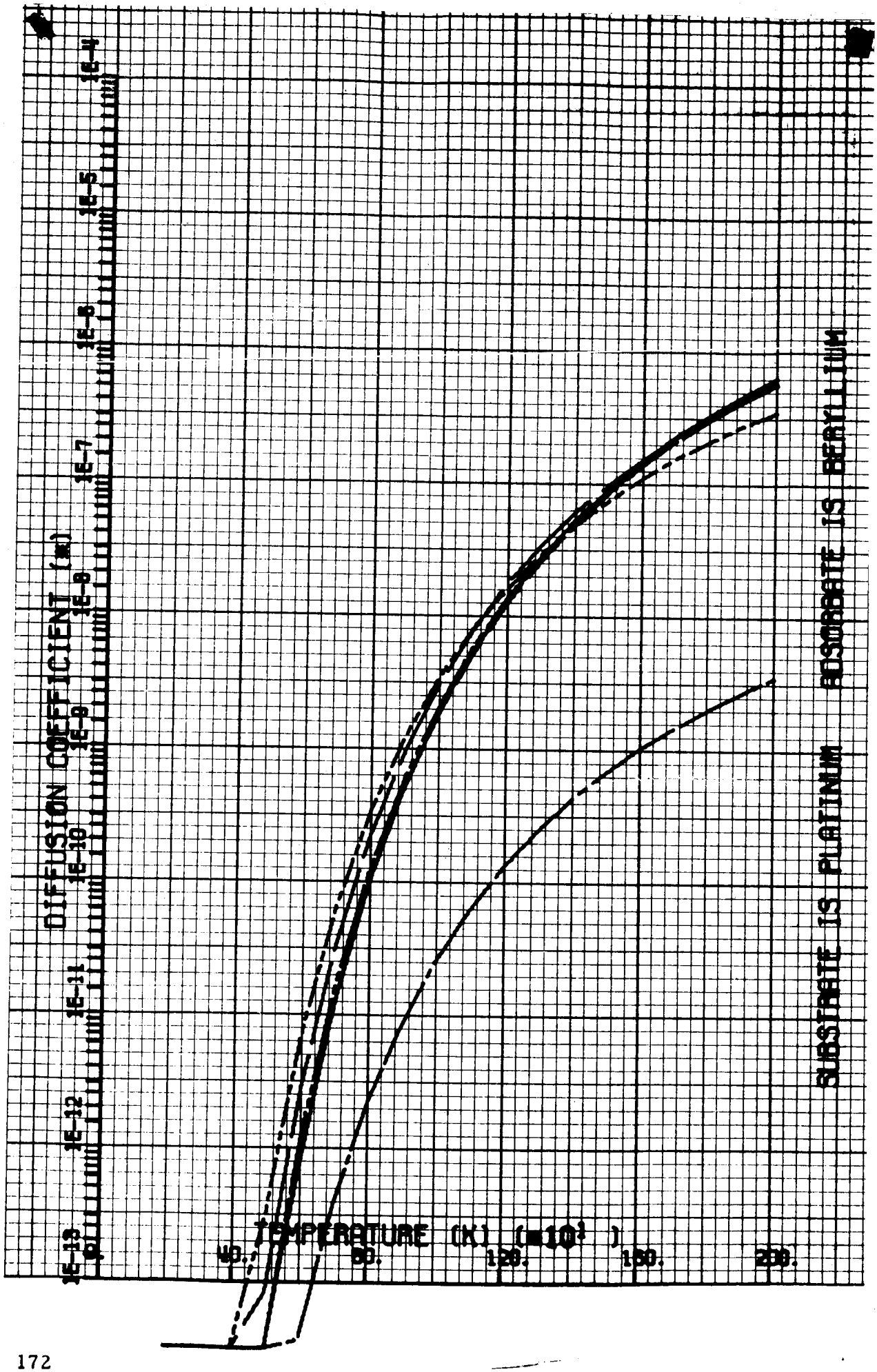
DIFFUSION COEFFICIENT (cm²)
1E-4
1E-5
1E-6
1E-7
1E-8
1E-9
1E-10
1E-11
1E-12
1E-13
TEMPERATURE (K) (=10³)
40.
80.
120.
160.
200.
SUBSTRATE IS PLATINUM ADSORBATE IS BERYLLIUM

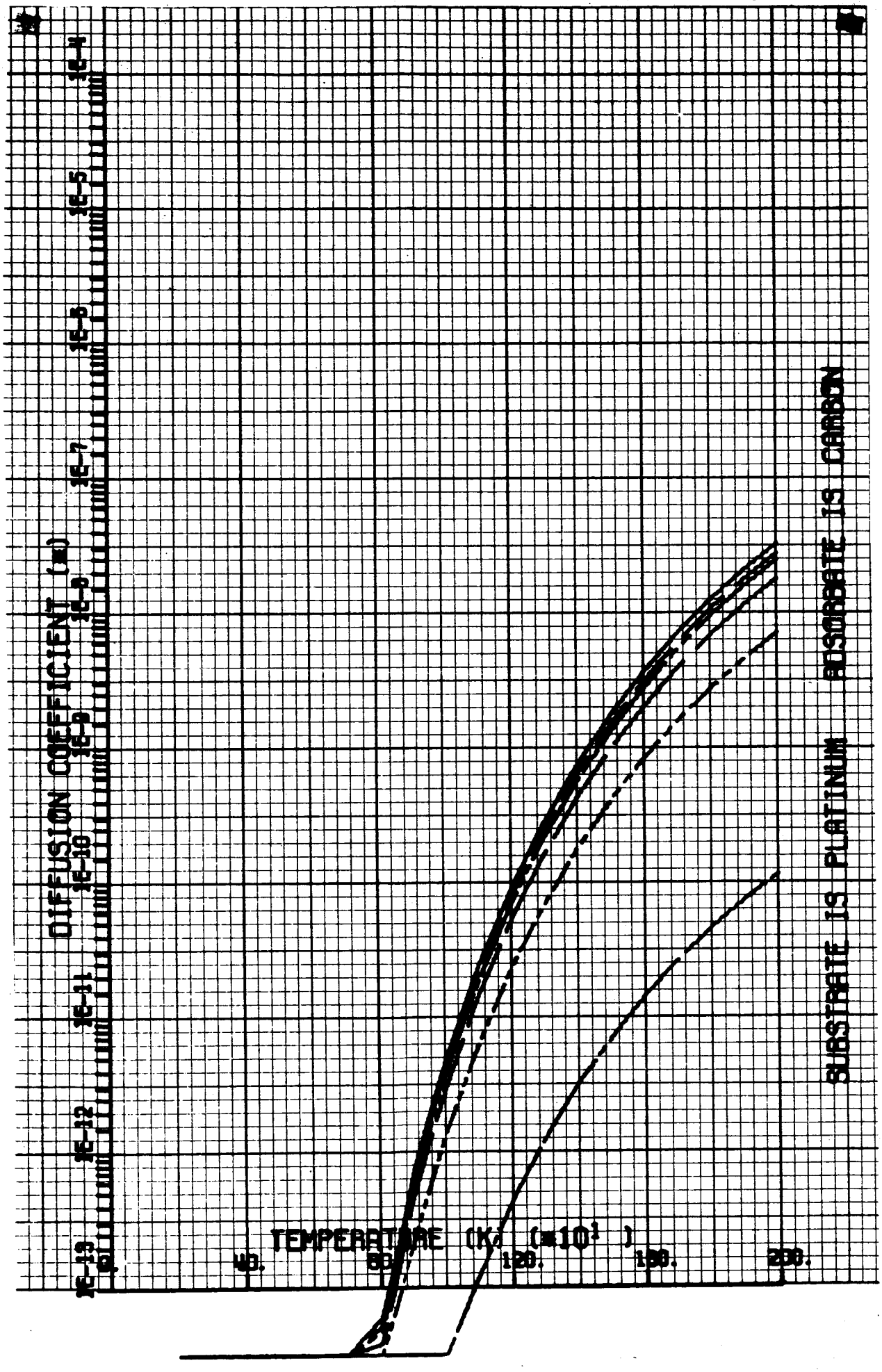
DIFFUSION COEFFICIENT (m²)
1E-4
1E-5
1E-6
1E-7
1E-8
1E-9
1E-10
1E-11
1E-12
1E-13
TEMPERATURE (K) (×10³)
40.
80.
120.
160.
200.
SUBSTRATE IS PLATINUM ADSORBATE IS CARBON

DIFFUSION COEFFICIENT (M2)
1E-4
1E-5
1E-6
1E-7
1E-8
1E-9
1E-10
1E-11
1E-12
1E-13
0
0.1
0.2
THETA
0.3
0.4
0.5
0.6
SUBSTRATE IS PLATINUM ADSORBATE IS CARBON

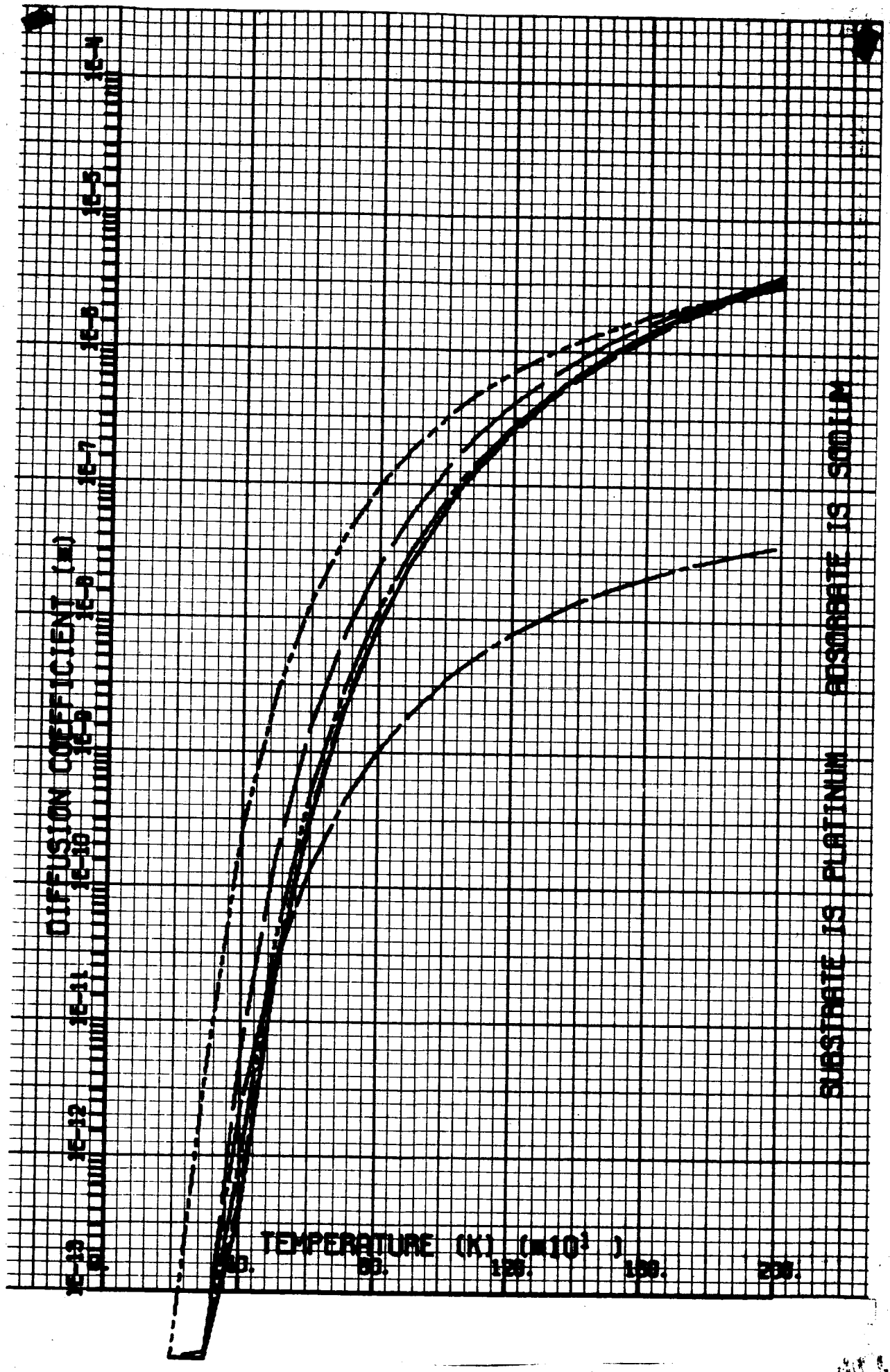
DIFFUSION COEFFICIENT (m²)
1E-7
1E-5
1E-3
1E-8
1E-7
1E-6
1E-9
1E-10
1E-11
1E-12
1E-13
TEMPERATURE (K) (×10²)
50.
100.
150.
200.
SUBSTRATE IS PLATINUM ADSORBATE IS SODIUM

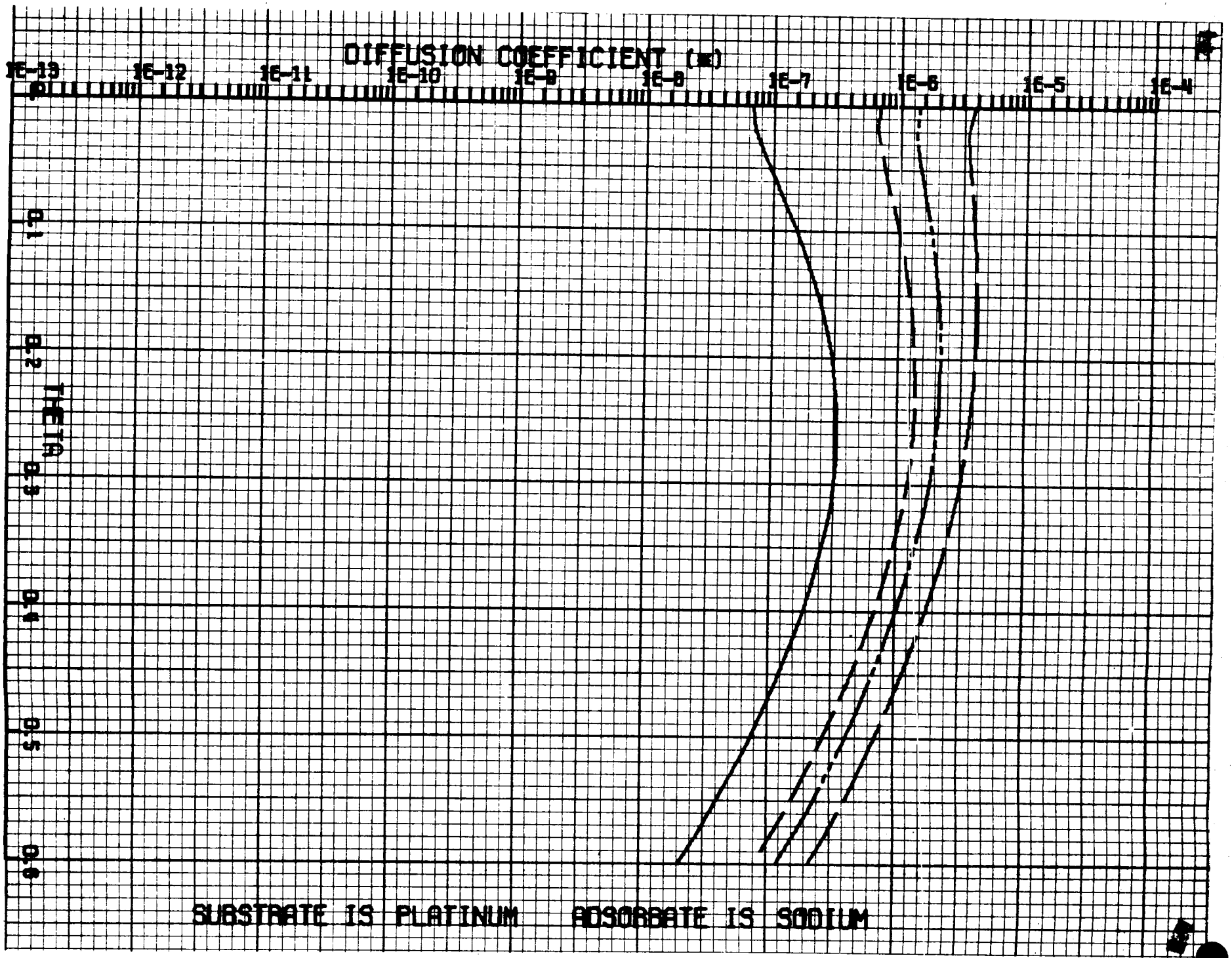
DIFFUSION COEFFICIENT (m)
1E-13
1E-12
1E-11
1E-10
1E-9
1E-8
1E-7
1E-6
1E-5
1E-4
0
0.1
0.2
0.3
0.4
0.5
0.6
THETA
SUBSTRATE IS PLATINUM ADSORBATE IS SODIUM

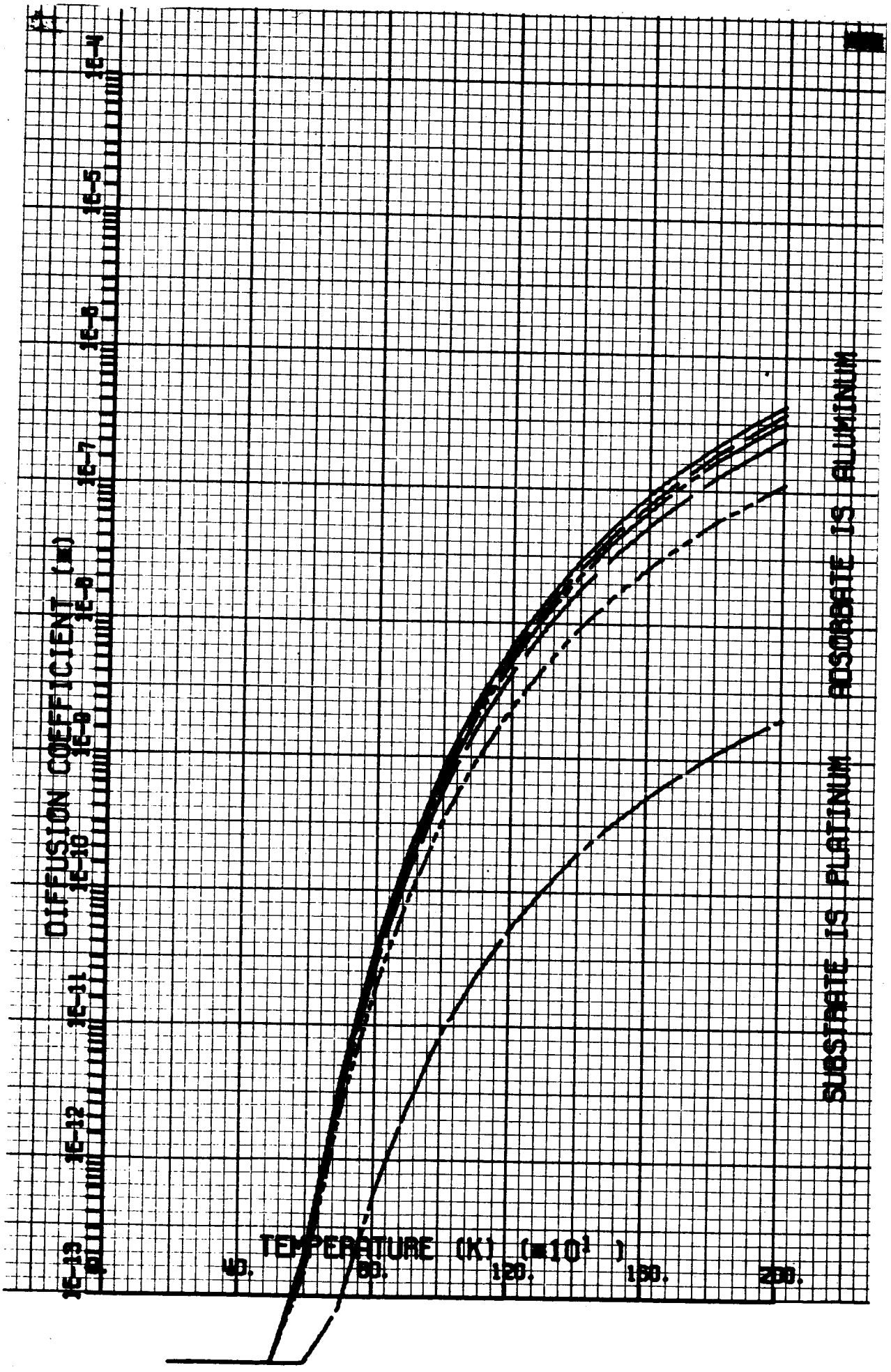
DIFFUSION COEFFICIENT (M²)
1E-4
1E-5
1E-6
1E-7
1E-8
1E-9
1E-10
1E-11
1E-12
1E-13
TEMPERATURE (K) (*10¹)
40.
80.
120.
160.
200.
SUBSTRATE IS PLATINUM ADSORBATE IS ALUMINUM

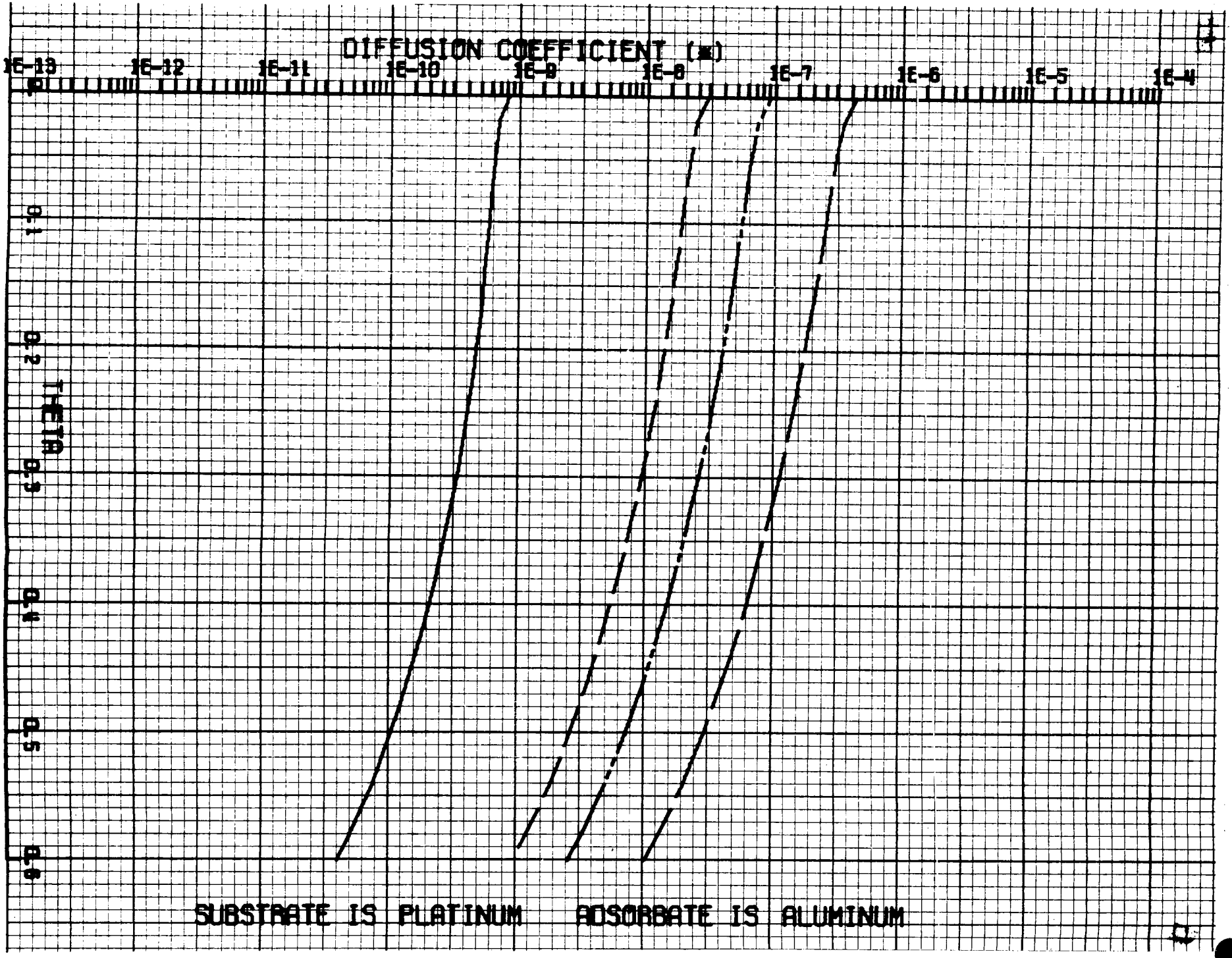
DIFFUSION COEFFICIENT (m)
1E-13
1E-12
1E-11
1E-10
1E-9
1E-8
1E-7
1E-6
1E-5
1E-4
0.1
0.2
0.3
0.4
0.5
0.6
THETA
SUBSTRATE IS PLATINUM ADSORBATE IS ALUMINUM

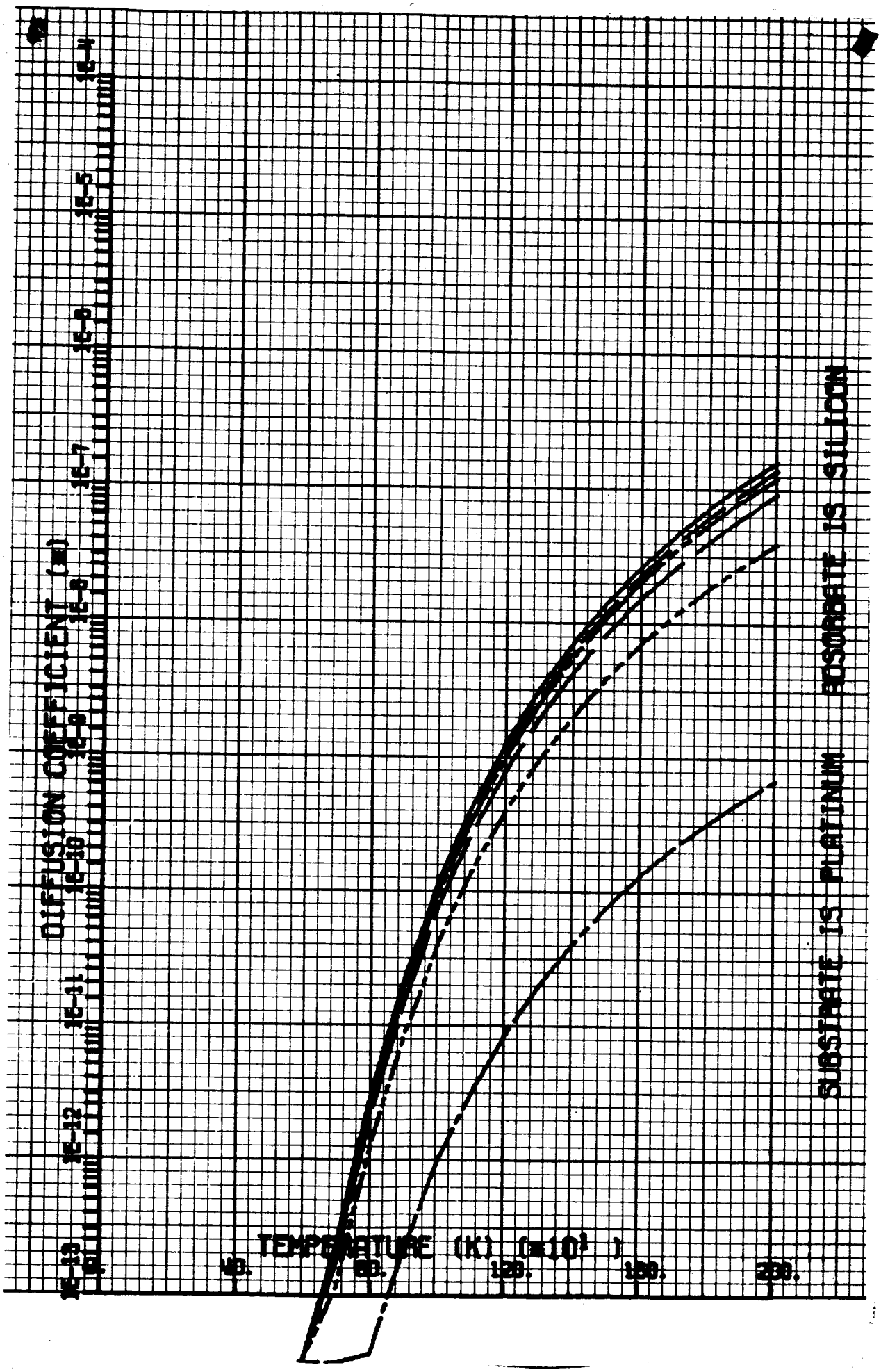
DIFFUSION COEFFICIENT (m²)
1E-13
1E-12
1E-11
1E-10
1E-9
1E-8
1E-7
1E-6
1E-5
1E-4
TEMPERATURE (K) (×10¹)
40.
80.
120.
160.
200.
SUBSTRATE IS PLATINUM ADSORBATE IS SILICON

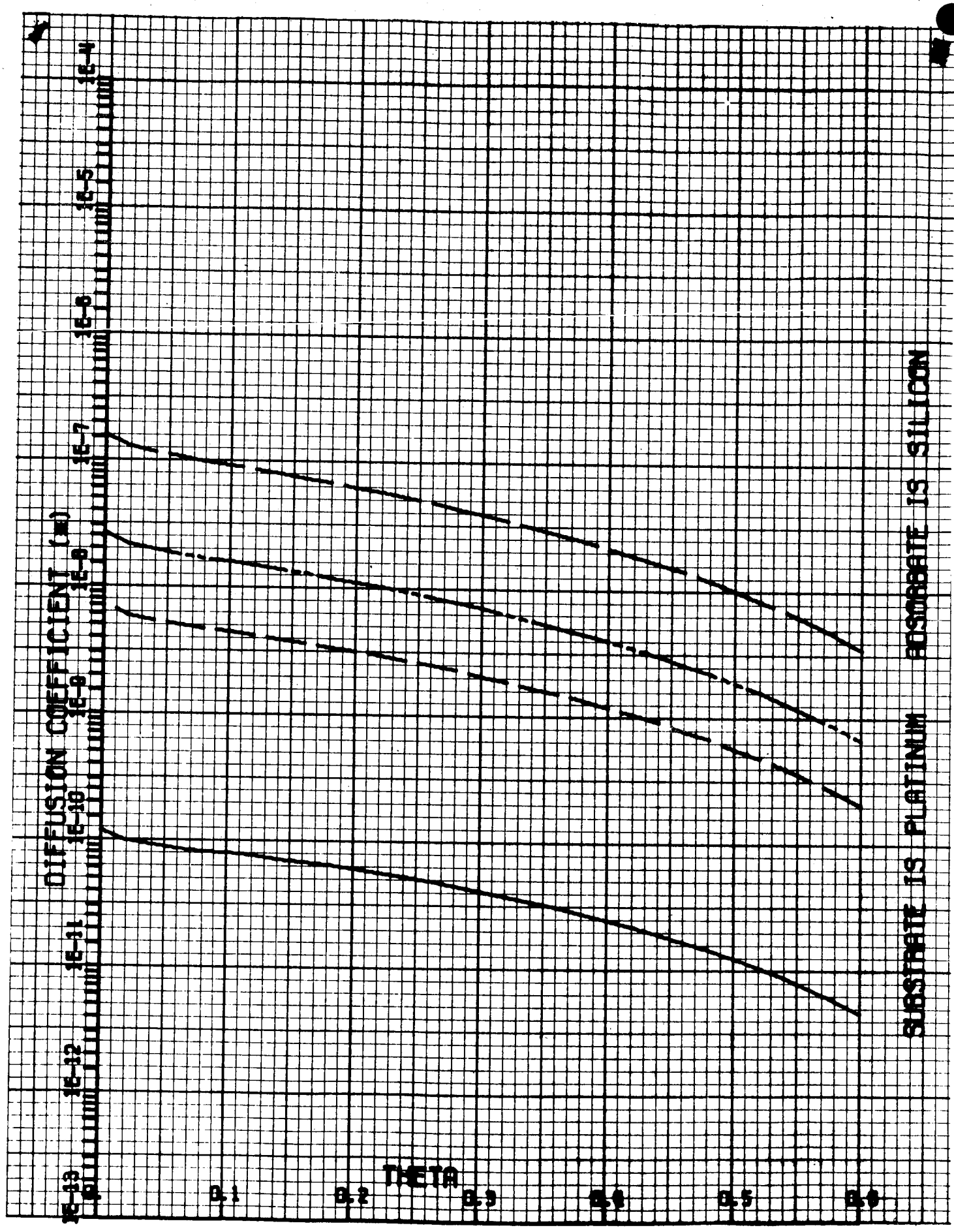
DIFFUSION COEFFICIENT (cm²)
1E-4
1E-5
1E-6
1E-7
1E-8
1E-9
1E-10
1E-11
1E-12
1E-13
0.1
0.2
0.3
0.4
0.5
0.6
THETA
SUBSTRATE IS PLATINUM ADSORBATE IS SILICON

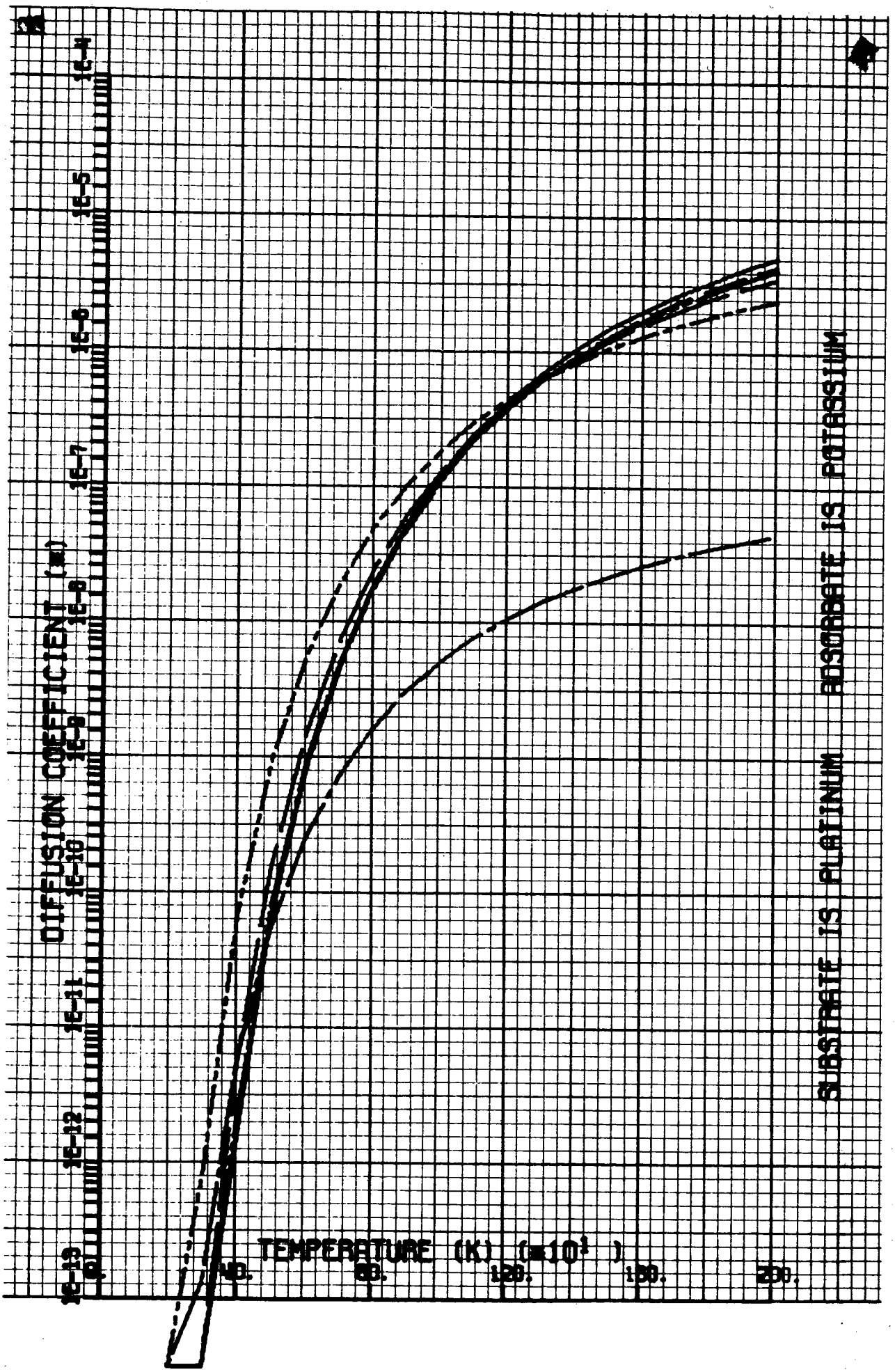
DIFFUSION COEFFICIENT (M²)
1E-4
1E-5
1E-6
1E-7
1E-8
1E-9
1E-10
1E-11
1E-12
1E-13
TEMPERATURE (K) (×10¹)
40.
80.
120.
160.
200.
SUBSTRATE IS PLATINUM - ADSORBATE IS POTASSIUM

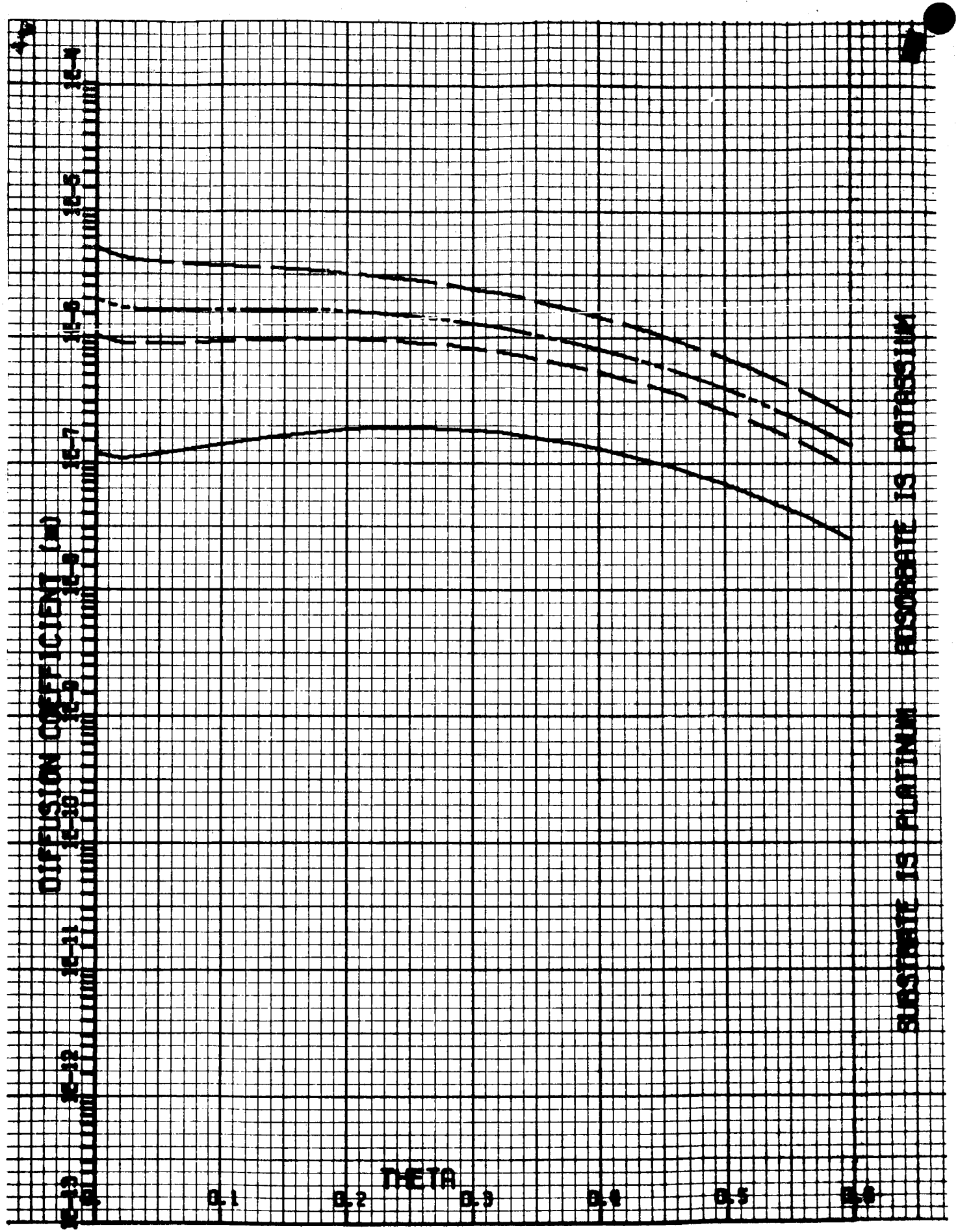
SUBSTRATE IS PLATINUM ADSORBATE IS POTASSIUM
DIFFUSION COEFFICIENT (M2)
1E-4
1E-5
1E-6
1E-7
1E-8
1E-9
1E-10
1E-11
1E-12
1E-13
0.1
0.2
0.3
0.4
0.5
0.6
THETA

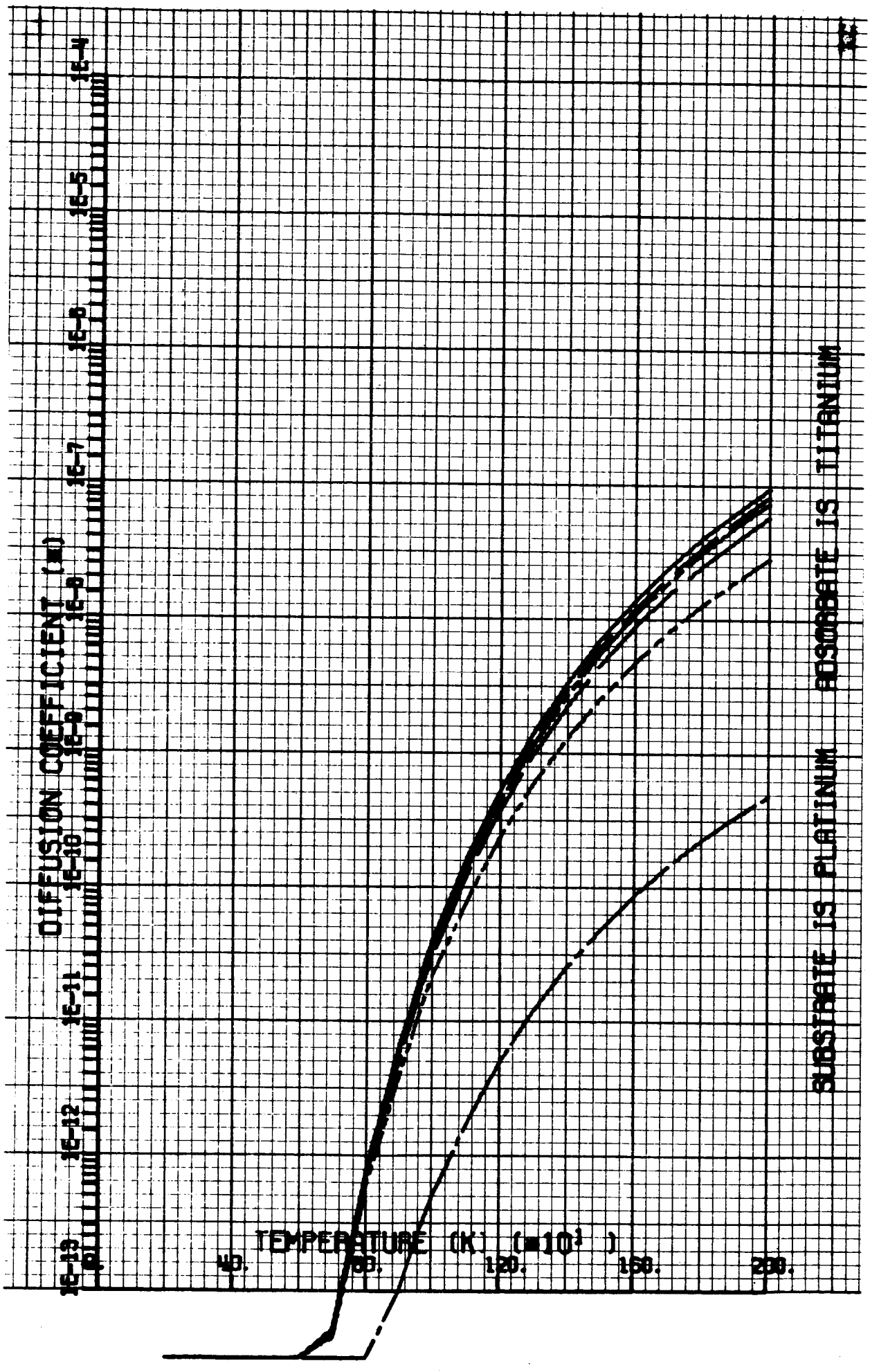
DIFFUSION COEFFICIENT (cm²)
1E-4
1E-5
1E-6
1E-7
1E-8
1E-9
1E-10
1E-11
1E-12
1E-13
TEMPERATURE (K) (×10¹)
40.
80.
120.
160.
200.
SUBSTRATE IS PLATINUM ADSORBATE IS TITANIUM

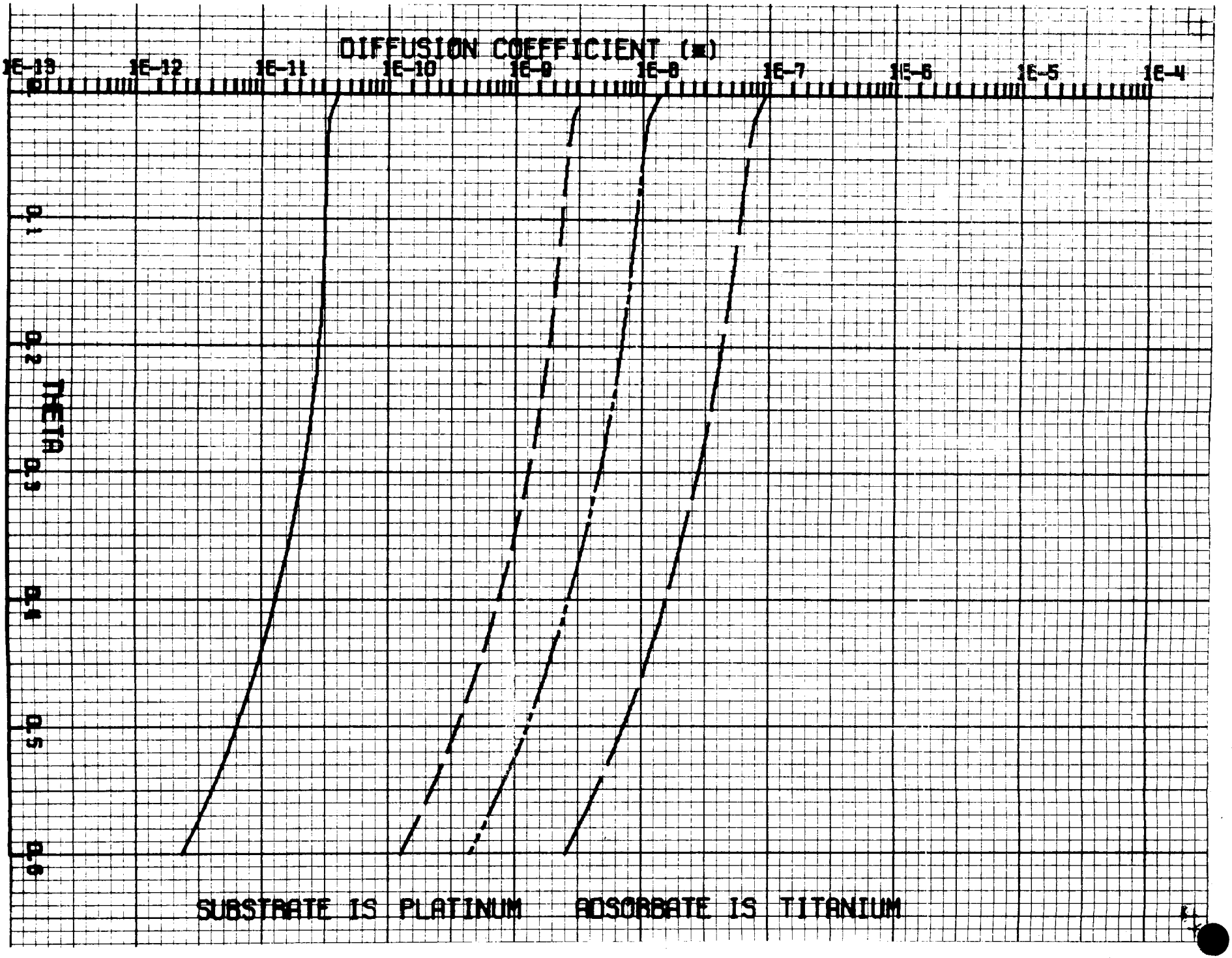
DIFFUSION COEFFICIENT (m)
1E-13
1E-12
1E-11
1E-10
1E-9
1E-8
1E-7
1E-6
1E-5
1E-4
THETA
0.1
0.2
0.3
0.4
0.5
0.6
SUBSTRATE IS PLATINUM ADSORBATE IS TITANIUM

DIFFUSION COEFFICIENT (m²)
1E-4
1E-5
1E-6
1E-7
1E-8
1E-9
1E-10
1E-11
1E-12
1E-13
TEMPERATURE (K) (×10³)
40.
80.
120.
160.
200.
SUBSTRATE IS PLATINUM ADSORBATE IS CHROMIUM

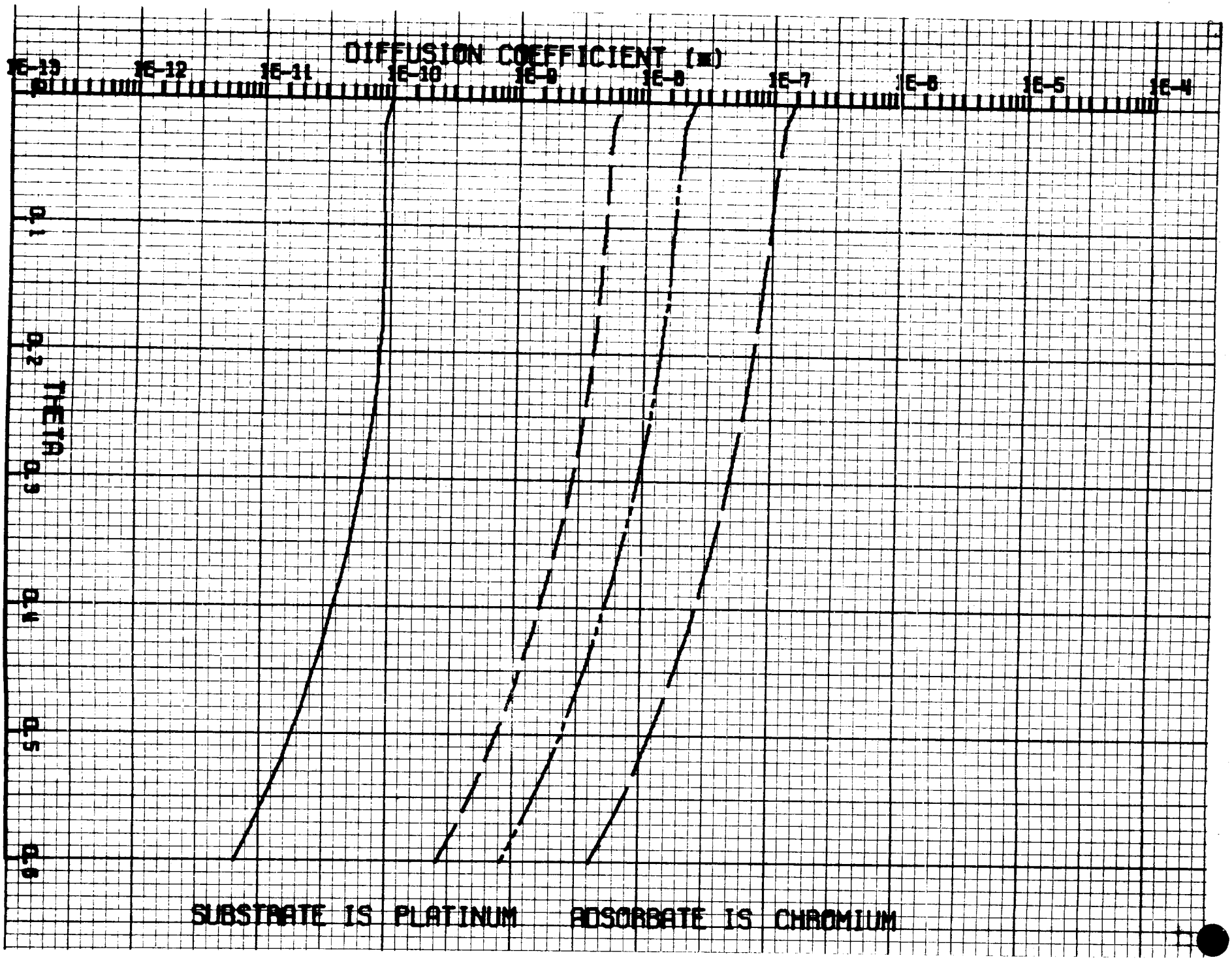
DIFFUSION COEFFICIENT (m)
1E-13
1E-12
1E-11
1E-10
1E-9
1E-8
1E-7
1E-6
1E-5
1E-4
THETA
0.1
0.2
0.3
0.4
0.5
0.6
SUBSTRATE IS PLATINUM ADSORBATE IS CHROMIUM

DIFFUSION COEFFICIENT (m²)
1E-4
1E-5
1E-6
1E-7
1E-8
1E-9
1E-10
1E-11
1E-12
1E-13
TEMPERATURE (K) (×10²)
40.
80.
120.
160.
200.
SUBSTRATE IS PLATINUM ADSORBATE IS MANGANESE

DIFFUSION COEFFICIENT (cm)
1E-4
1E-5
1E-6
1E-7
1E-8
1E-9
1E-10
1E-11
1E-12
1E-13
0.1
0.2
0.3
0.4
0.5
0.6
THETA
SUBSTRATE IS PLATINUM ADSORBATE IS MANGANESE

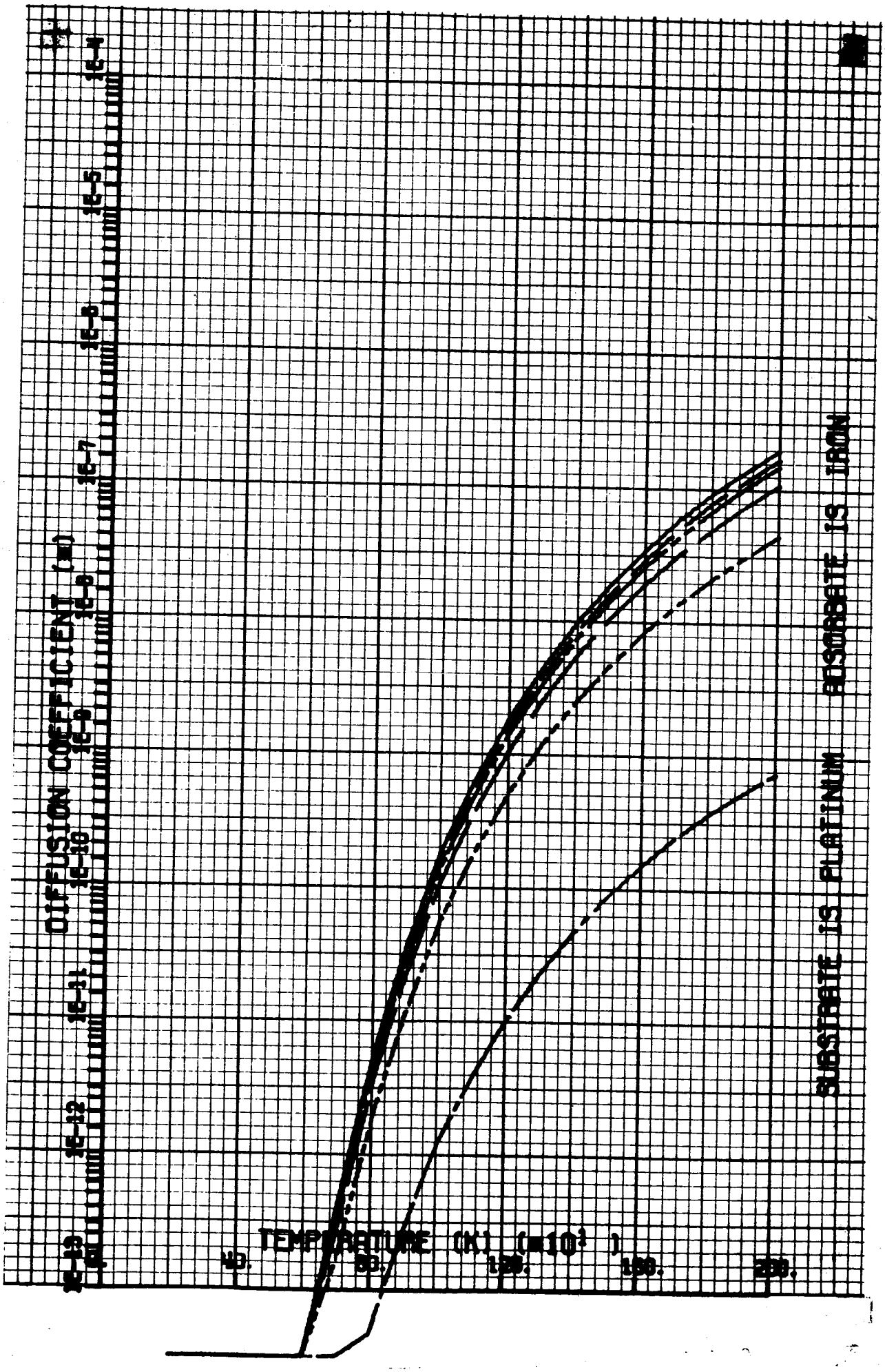
DIFFUSION COEFFICIENT (m)
1E-4
1E-5
1E-6
1E-7
1E-8
1E-9
1E-10
1E-11
1E-12
1E-13
TEMPERATURE (K) (×10²)
50.
100.
150.
200.
SUBSTRATE IS PLATINUM ADSORBATE IS IRON

DIFFUSION COEFFICIENT (cm²)
1E-4
1E-5
1E-6
1E-7
1E-8
1E-9
1E-10
1E-11
1E-12
1E-13
0.1
0.2
0.3
0.4
0.5
0.6
THETA
SUBSTRATE IS PLATINUM ADSORBATE IS IRON

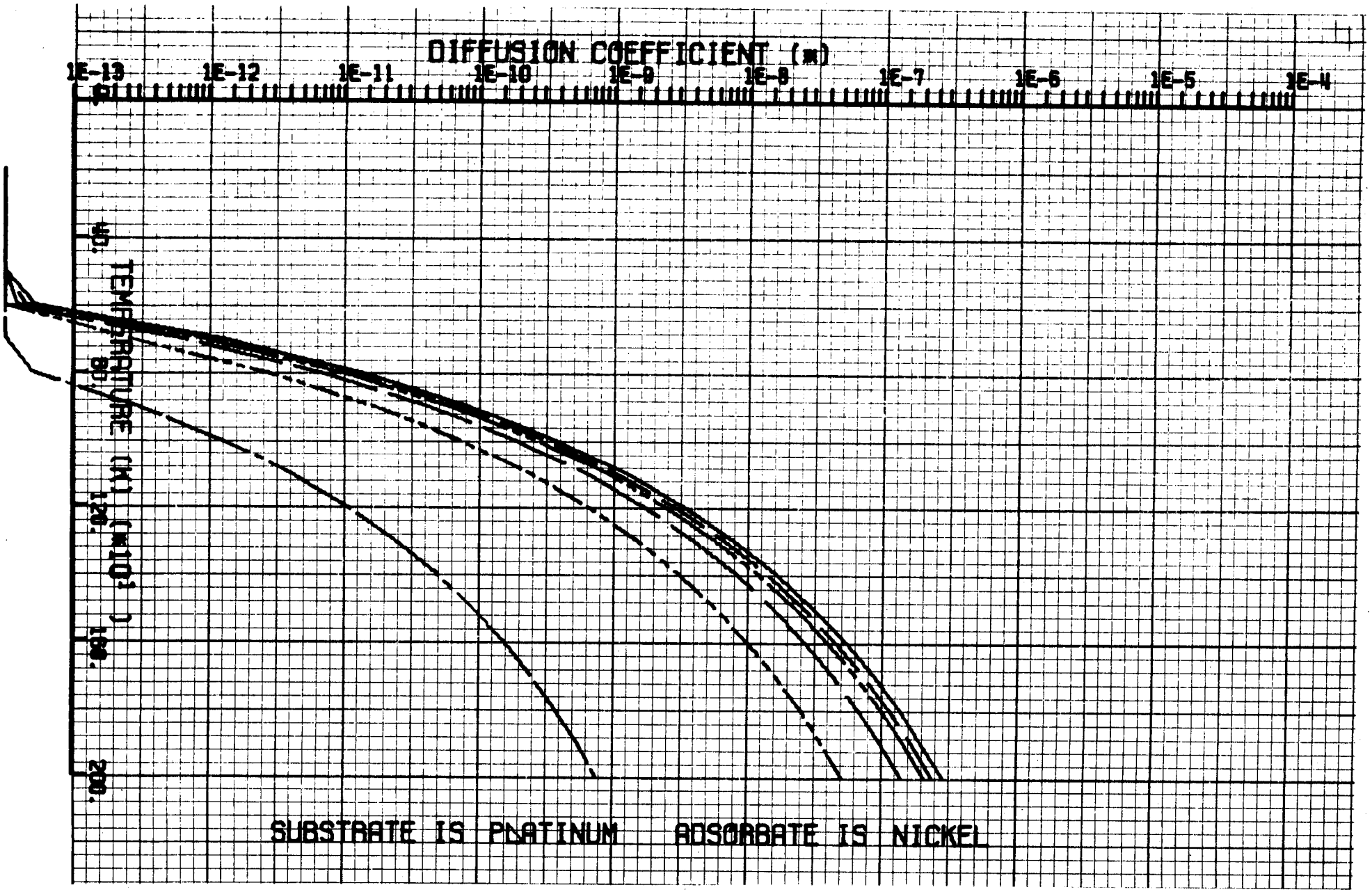
DIFFUSION COEFFICIENT (m)
1E-13
1E-12
1E-11
1E-10
1E-9
1E-8
1E-7
1E-6
1E-5
1E-4
TEMPERATURE (K) (x10.)
80.
120.
160.
200.
SUBSTRATE IS PLATINUM ADSORBATE IS NICKEL

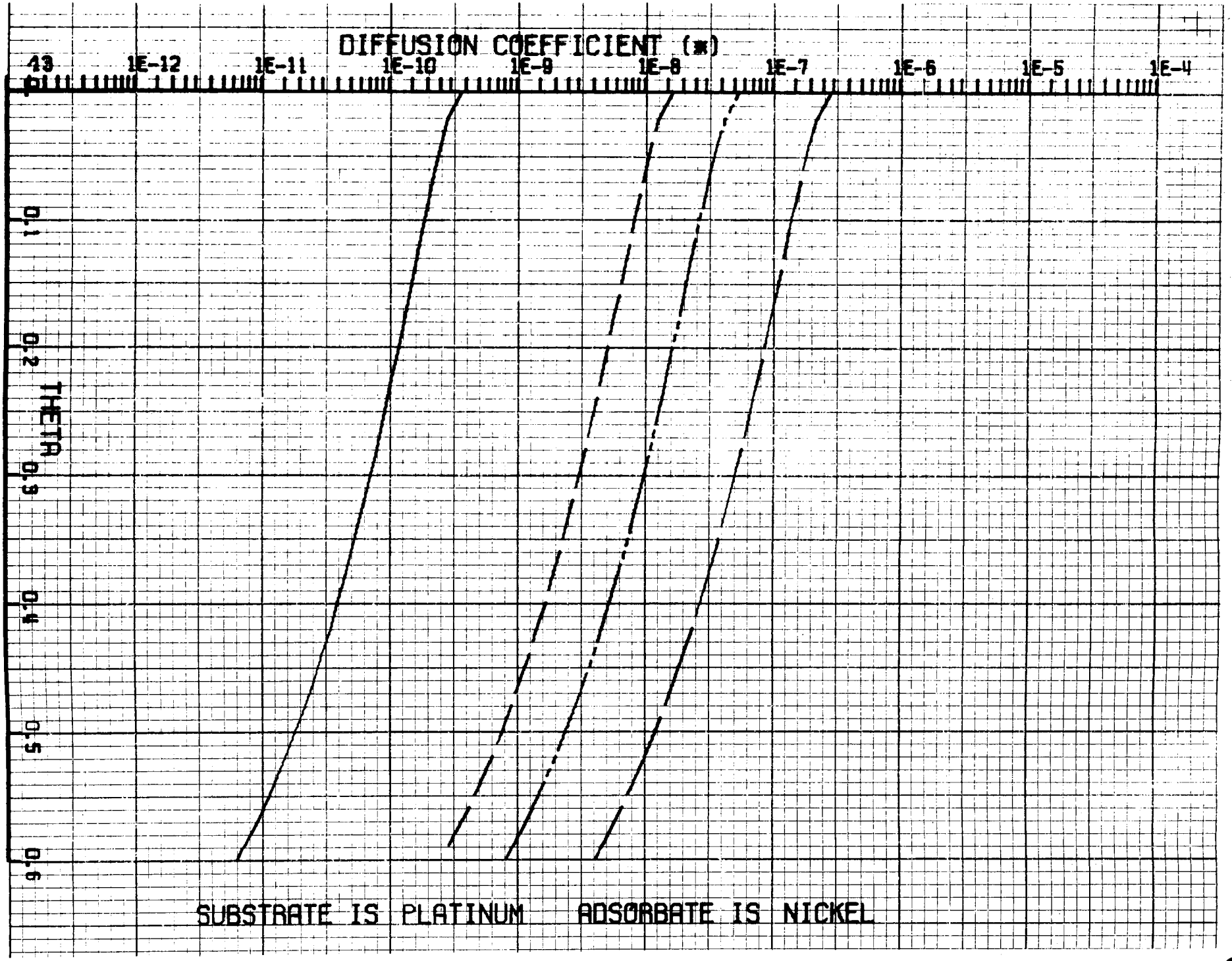
DIFFUSION COEFFICIENT (*)
43
1E-12
1E-11
1E-10
1E-9
1E-8
1E-7
1E-6
1E-5
1E-4
THETA
0.1
0.2
0.3
0.4
0.5
0.6
SUBSTRATE IS PLATINUM ADSORBATE IS NICKEL

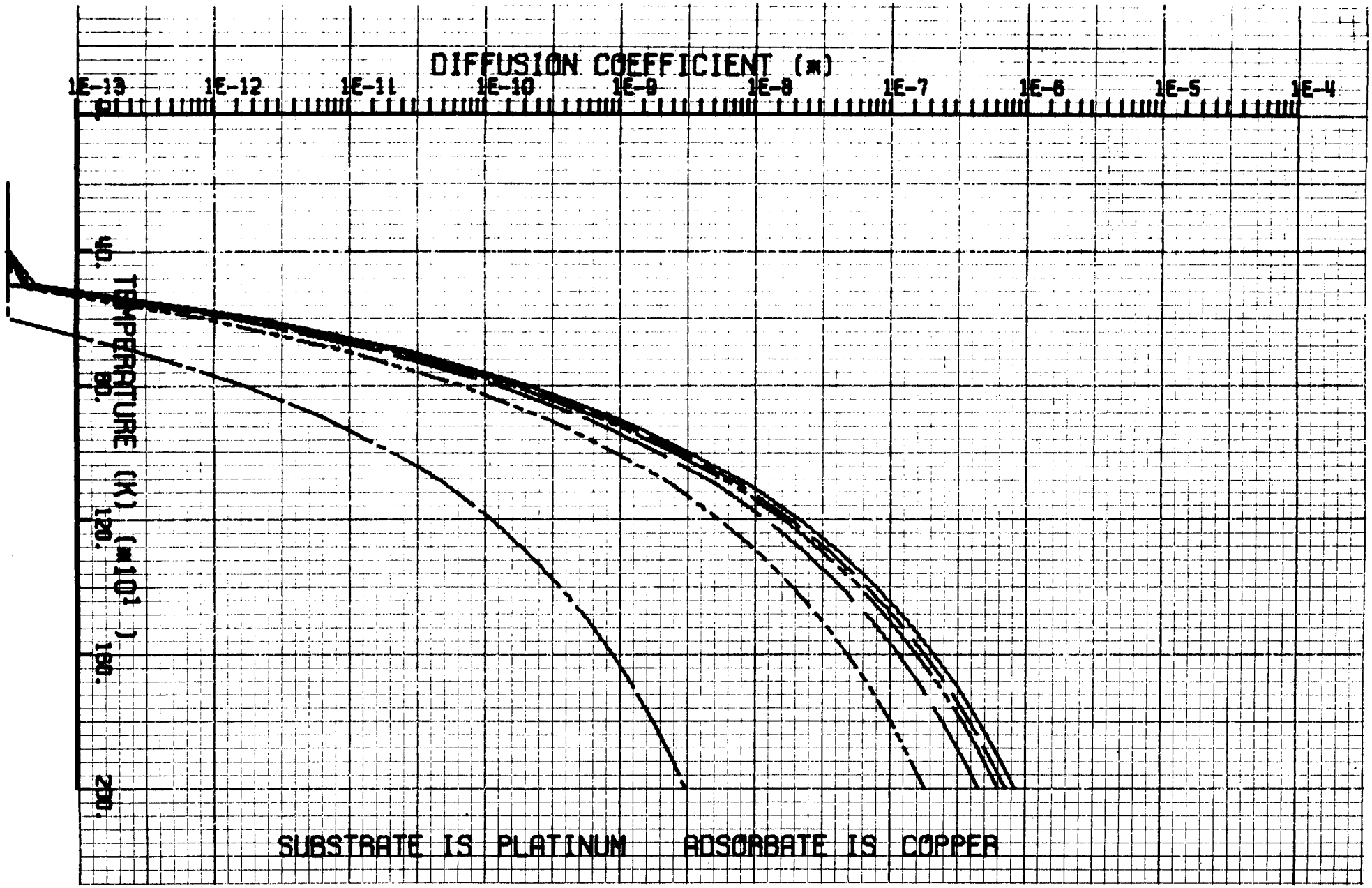
DIFFUSION COEFFICIENT (m)
1E-13
1E-12
1E-11
1E-10
1E-9
1E-8
1E-7
1E-6
1E-5
1E-4
TEMPERATURE (K) (m*10³)
40.
80.
120.
160.
200.
SUBSTRATE IS PLATINUM ADSORBATE IS COPPER

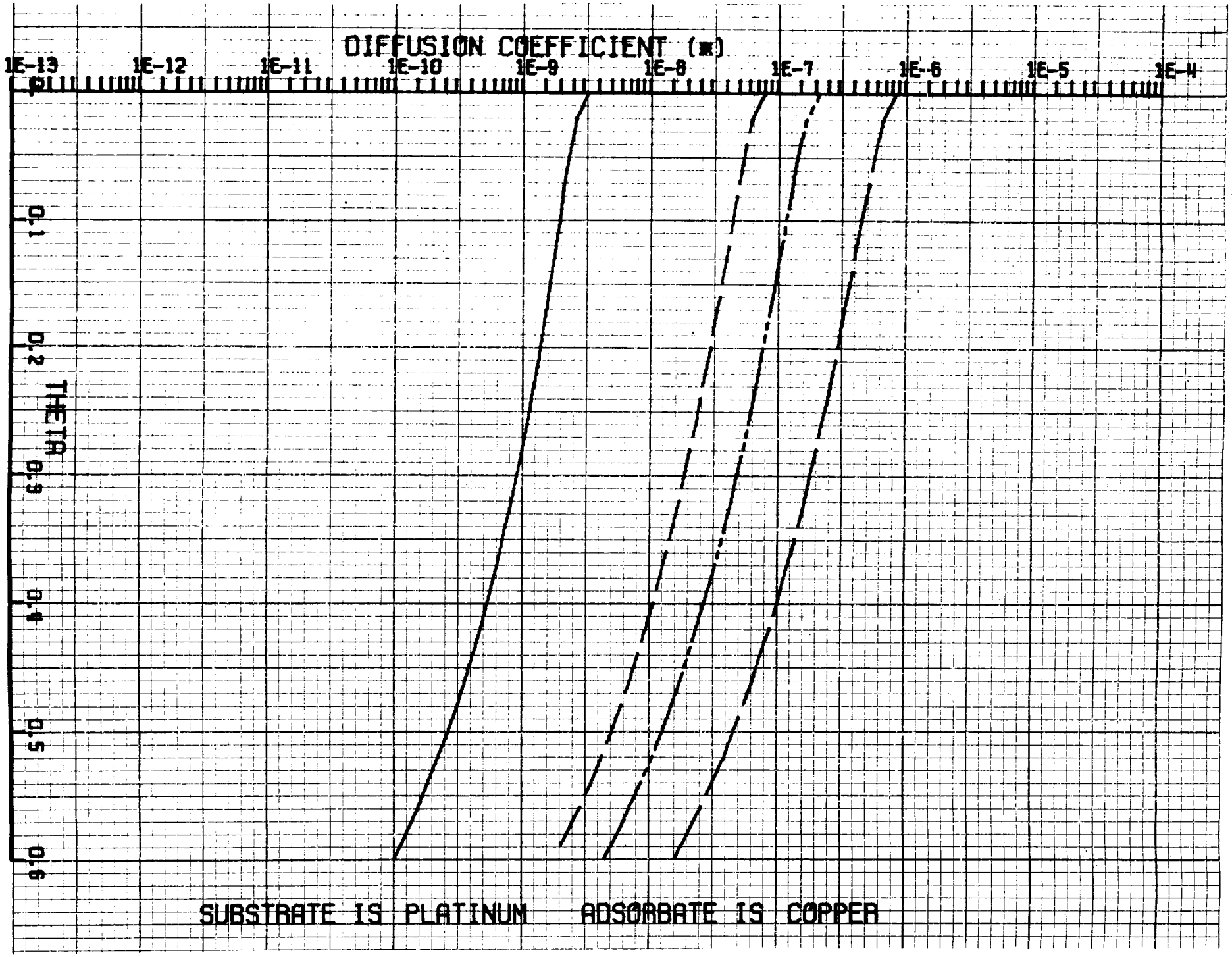
DIFFUSION COEFFICIENT (m)
1E-13
1E-12
1E-11
1E-10
1E-9
1E-8
1E-7
1E-6
1E-5
1E-4
THETA
0.1
0.2
0.3
0.4
0.5
0.6
SUBSTRATE IS PLATINUM ADSORBATE IS COPPER

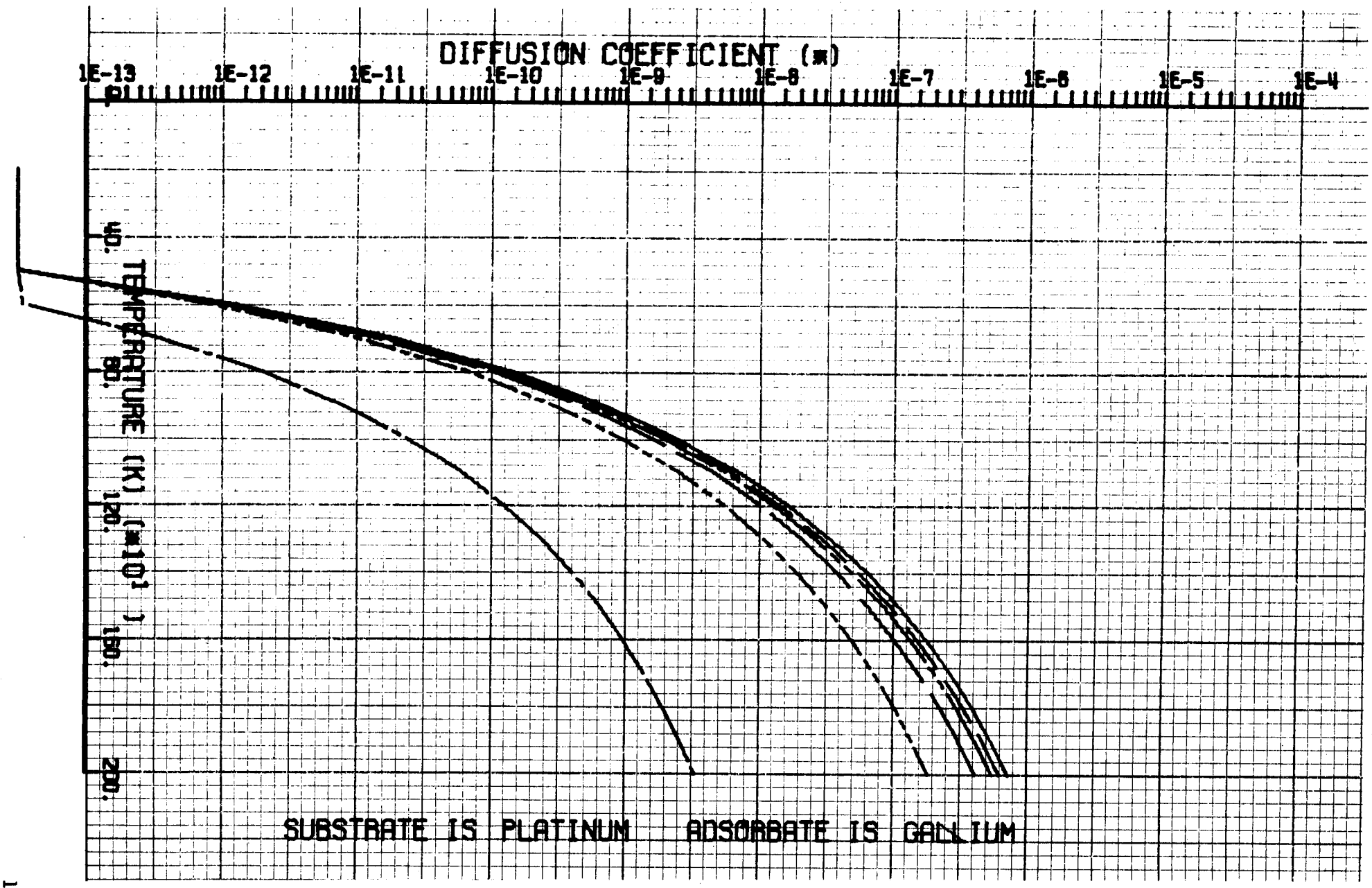
DIFFUSION COEFFICIENT (m)
1E-13
1E-12
1E-11
1E-10
1E-9
1E-8
1E-7
1E-6
1E-5
1E-4
TEMPERATURE (K) (*10¹)
40.
80.
120.
160.
200.
SUBSTRATE IS PLATINUM ADSORBATE IS GALLIUM

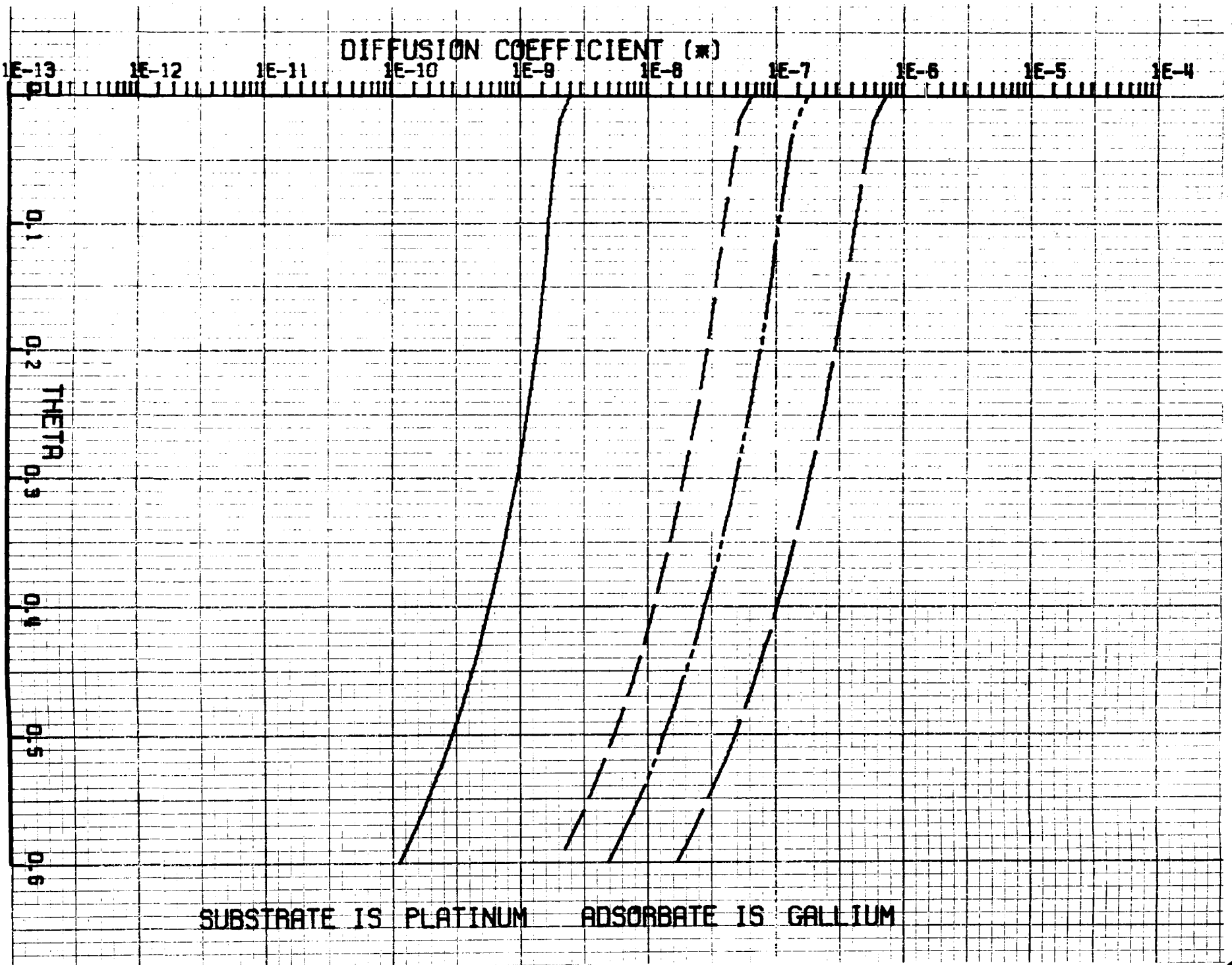
DIFFUSION COEFFICIENT (*)
1E-13
1E-12
1E-11
1E-10
1E-9
1E-8
1E-7
1E-6
1E-5
1E-4
THETA
0.1
0.2
0.3
0.4
0.5
0.6
SUBSTRATE IS PLATINUM ADSORBATE IS GALLIUM

DIFFUSION COEFFICIENT (*)
1E-13
1E-12
1E-11
1E-10
1E-9
1E-8
1E-7
1E-6
1E-5
1E-4
TEMPERATURE (K) (*10^1)
40.
80.
120.
160.
200.
SUBSTRATE IS PLATINUM ADSORBATE IS RUBIDIUM

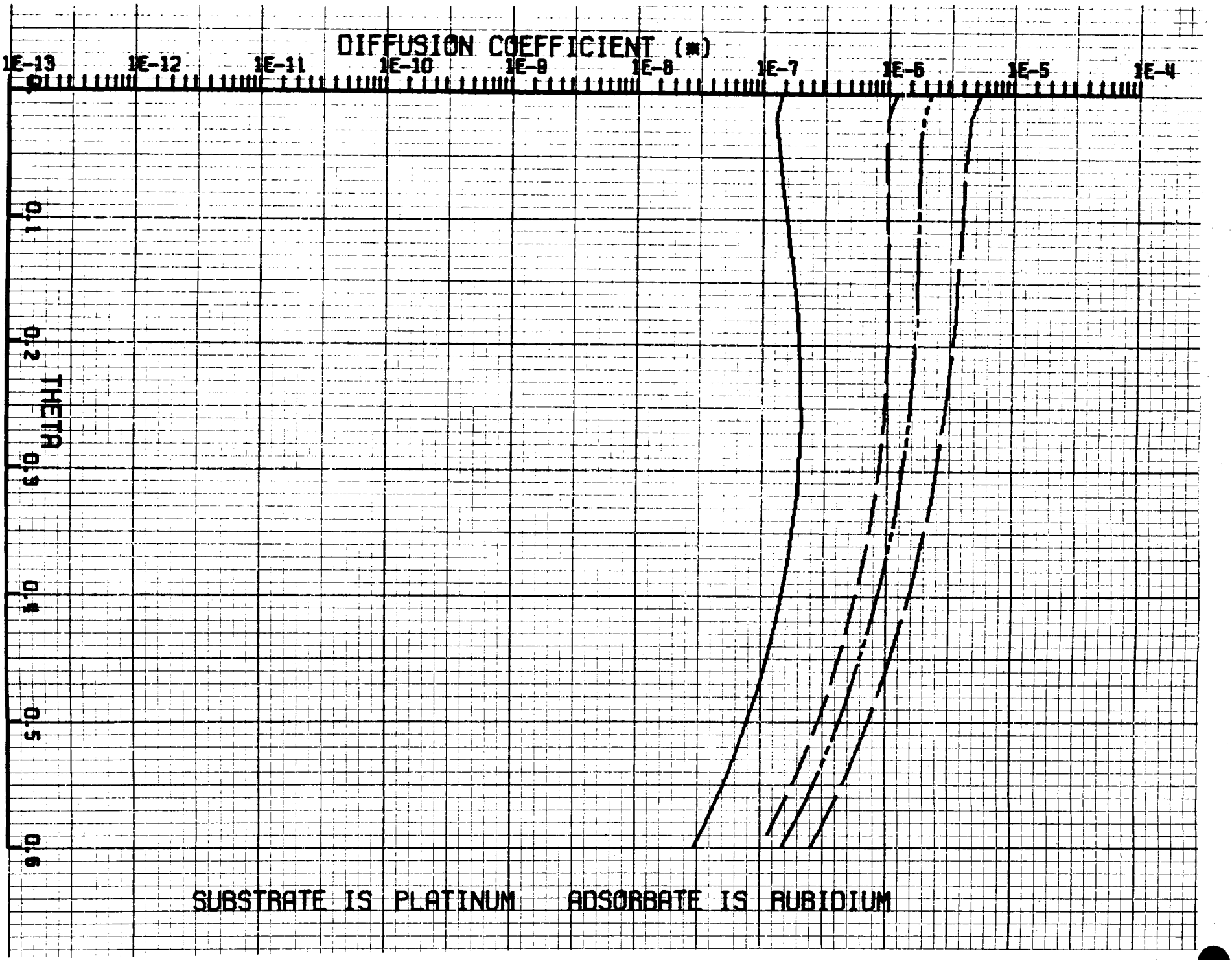
DIFFUSION COEFFICIENT (*)
1E-13
1E-12
1E-11
1E-10
1E-9
1E-8
1E-7
1E-6
1E-5
1E-4
0
0.1
0.2
0.3
0.4
0.5
0.6
THETA
SUBSTRATE IS PLATINUM ADSORBATE IS RUBIDIUM

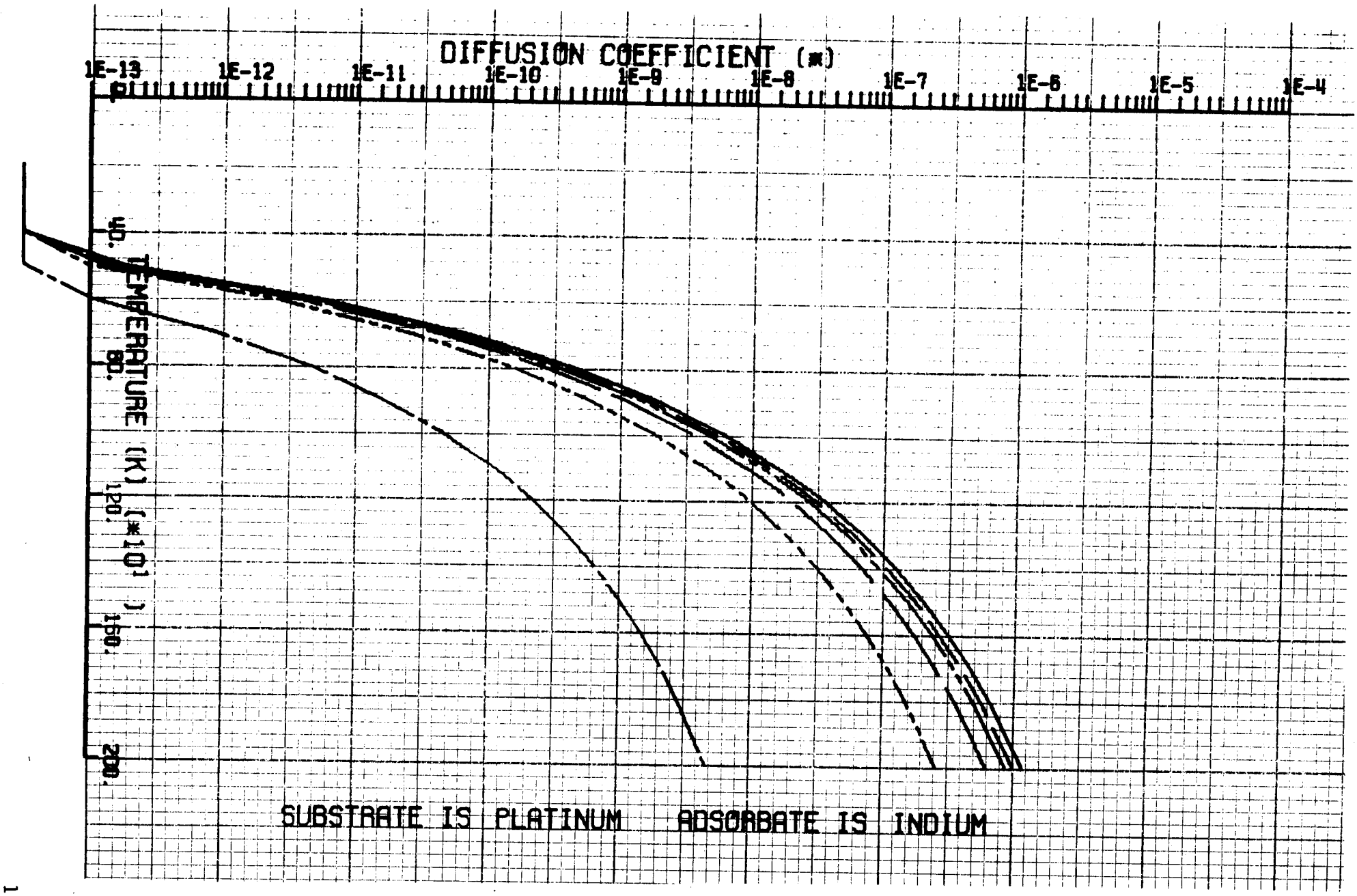
DIFFUSION COEFFICIENT (*)
1E-13
1E-12
1E-11
1E-10
1E-9
1E-8
1E-7
1E-6
1E-5
1E-4
TEMPERATURE (K) (*10)
40.
80.
120.
160.
200.
SUBSTRATE IS PLATINUM ADSORBATE IS INDIUM

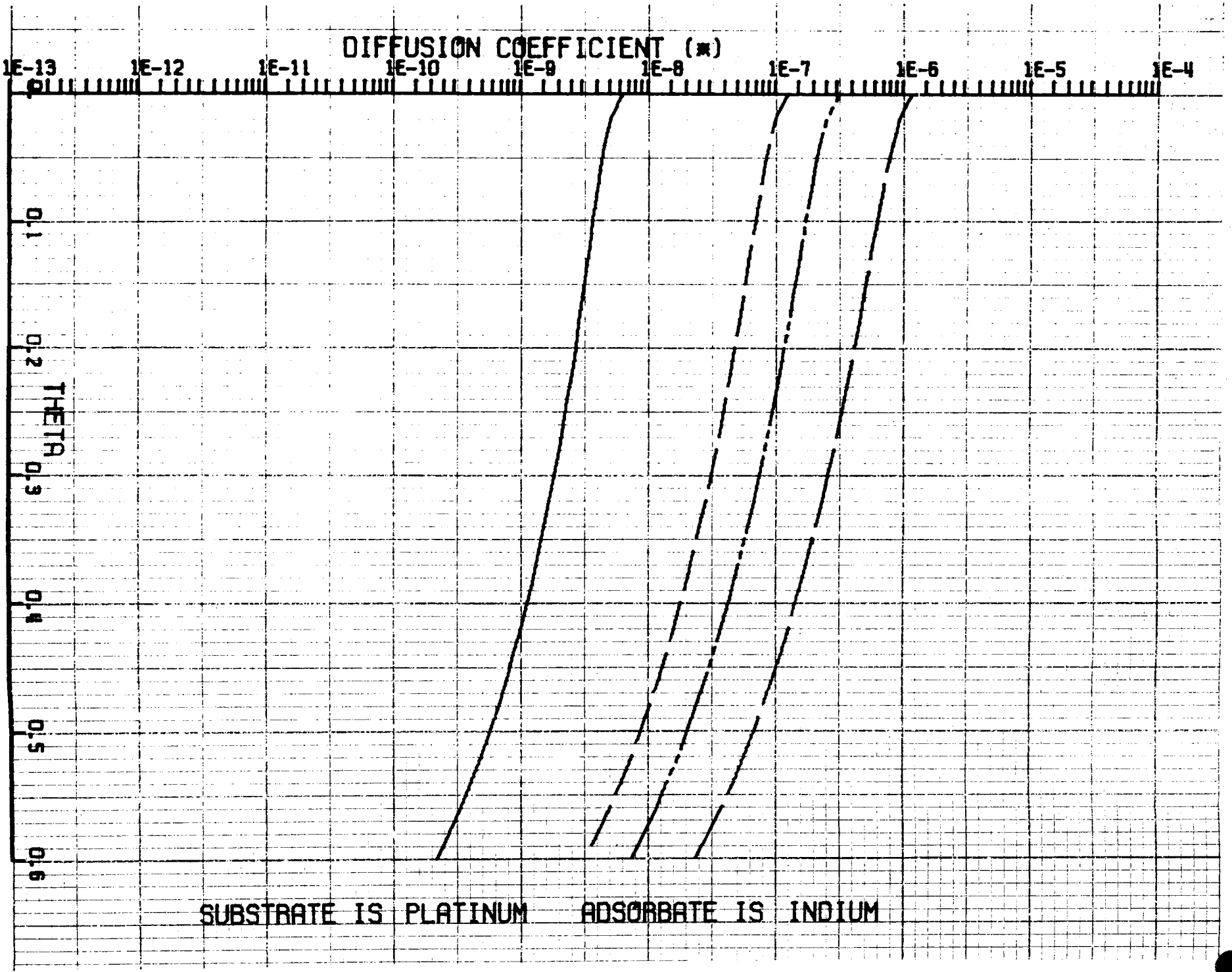
DIFFUSION COEFFICIENT (*)
1E-13
1E-12
1E-11
1E-10
1E-9
1E-8
1E-7
1E-6
1E-5
1E-4
0
0.1
0.2
0.3
0.4
0.5
0.6
THETA
SUBSTRATE IS PLATINUM ADSORBATE IS INDIUM

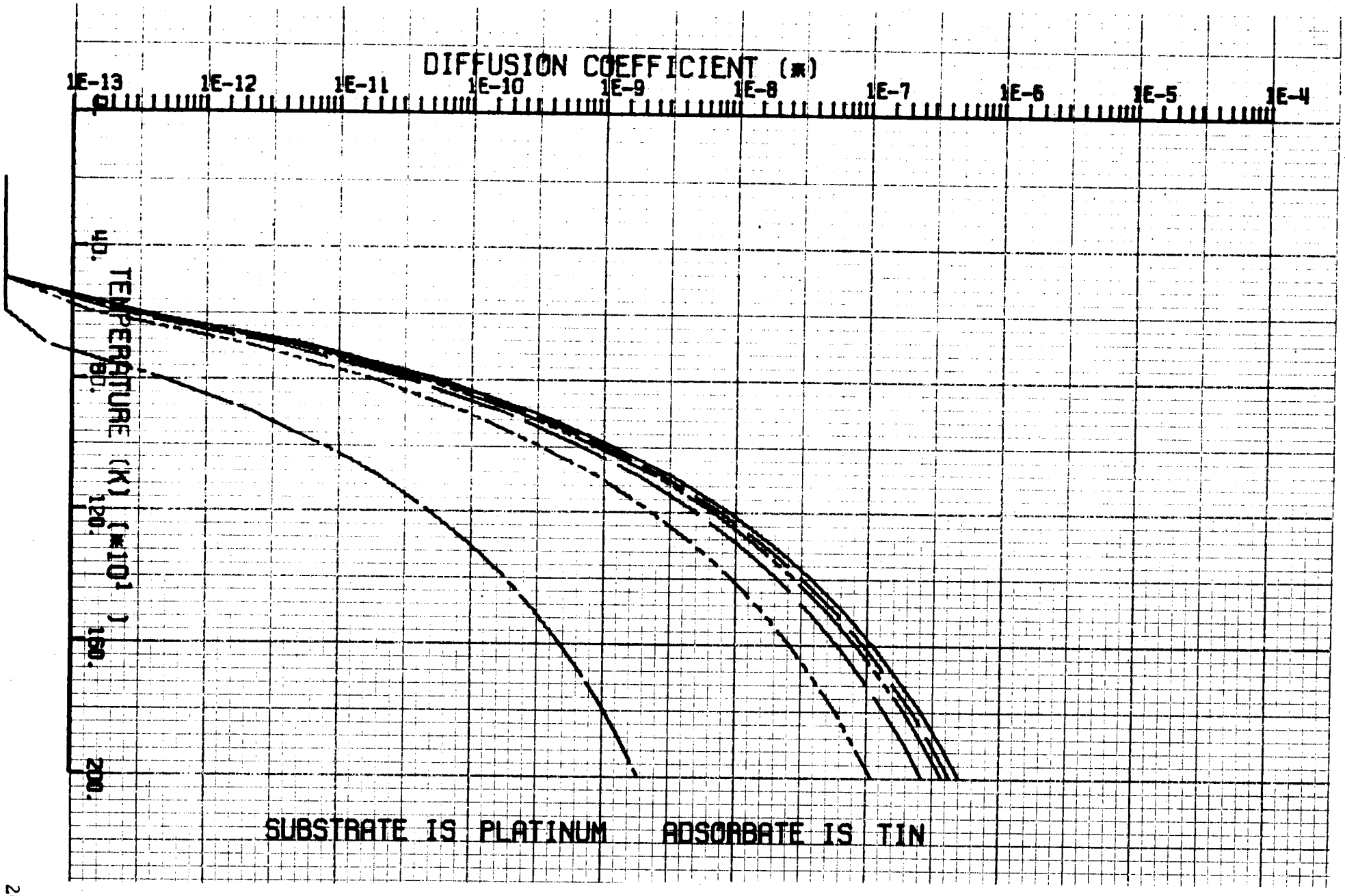
DIFFUSION COEFFICIENT (*)
1E-13
1E-12
1E-11
1E-10
1E-9
1E-8
1E-7
1E-6
1E-5
1E-4
TEMPERATURE (K) [*10]
40.
80.
120.
160.
200.
SUBSTRATE IS PLATINUM ADSORBATE IS TIN

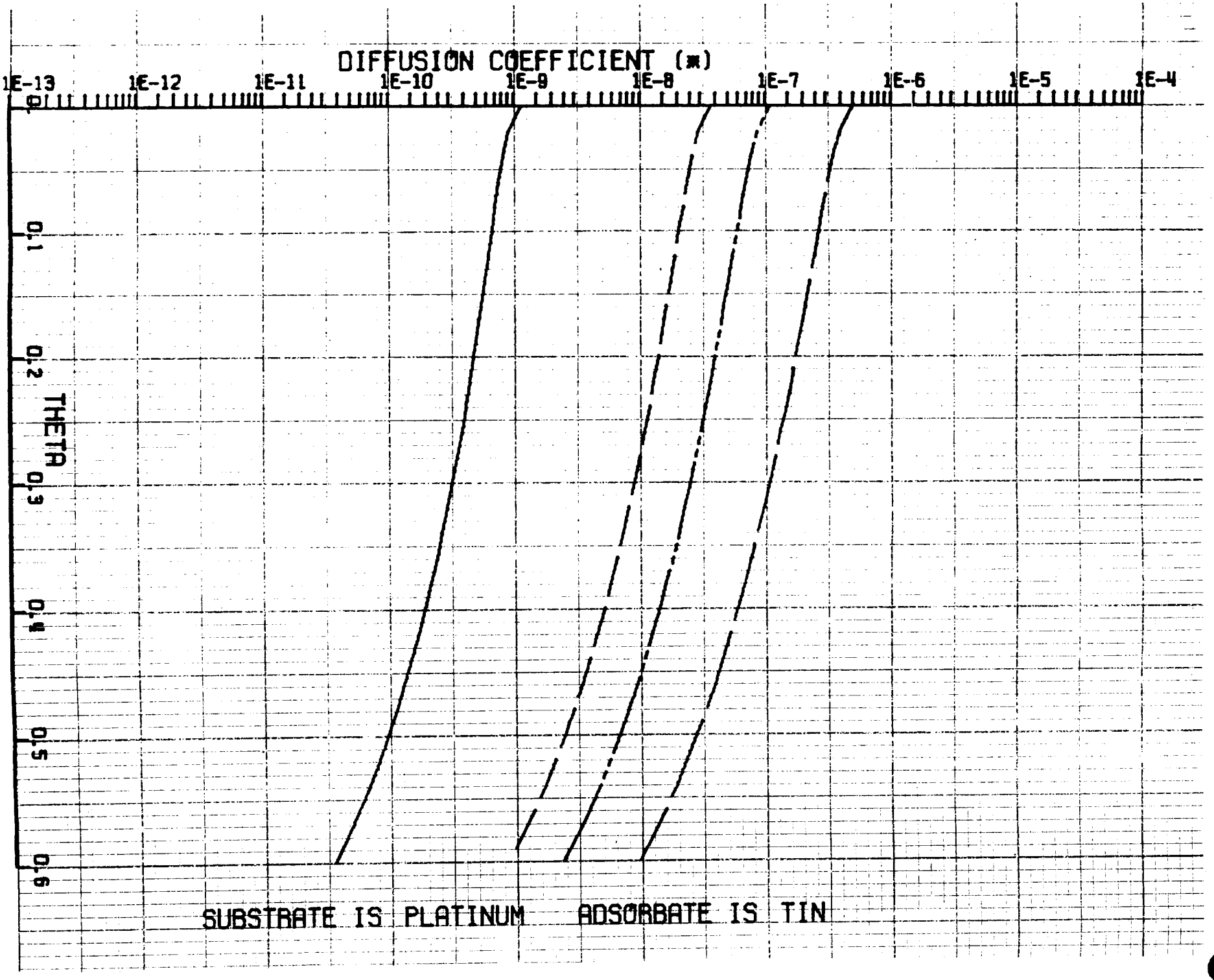
DIFFUSION COEFFICIENT (*)
1E-13
1E-12
1E-11
1E-10
1E-9
1E-8
1E-7
1E-6
1E-5
1E-4
THETA
0
0.1
0.2
0.3
0.4
0.5
0.6
SUBSTRATE IS PLATINUM ADSORBATE IS TIN

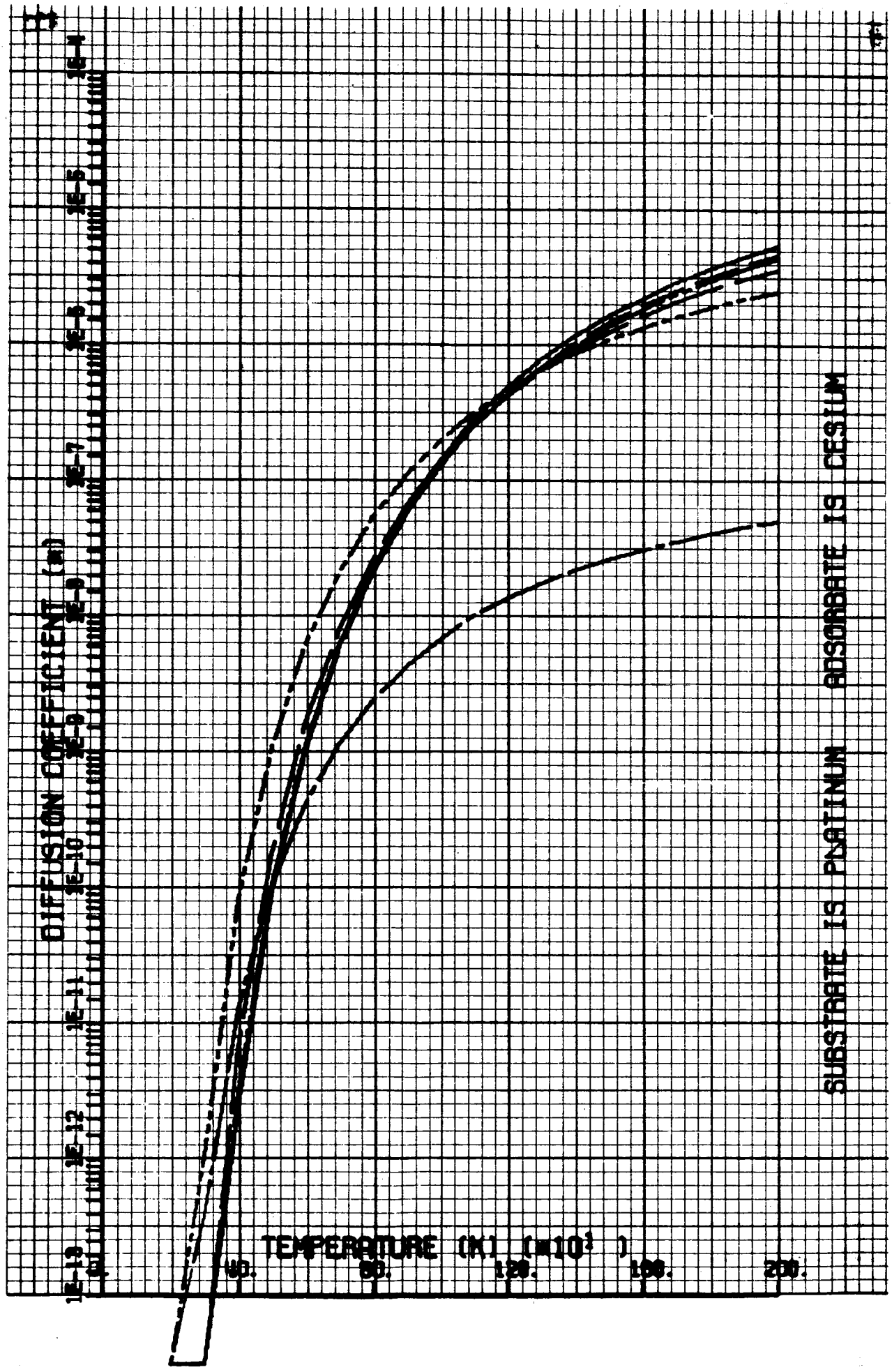
DIFFUSION COEFFICIENT (m²)
1E-13
1E-12
1E-11
1E-10
1E-9
1E-8
1E-7
1E-6
1E-5
1E-4
TEMPERATURE (K) (*10³)
40.
60.
120.
160.
200.
SUBSTRATE IS PLATINUM ADSORBATE IS CESIUM

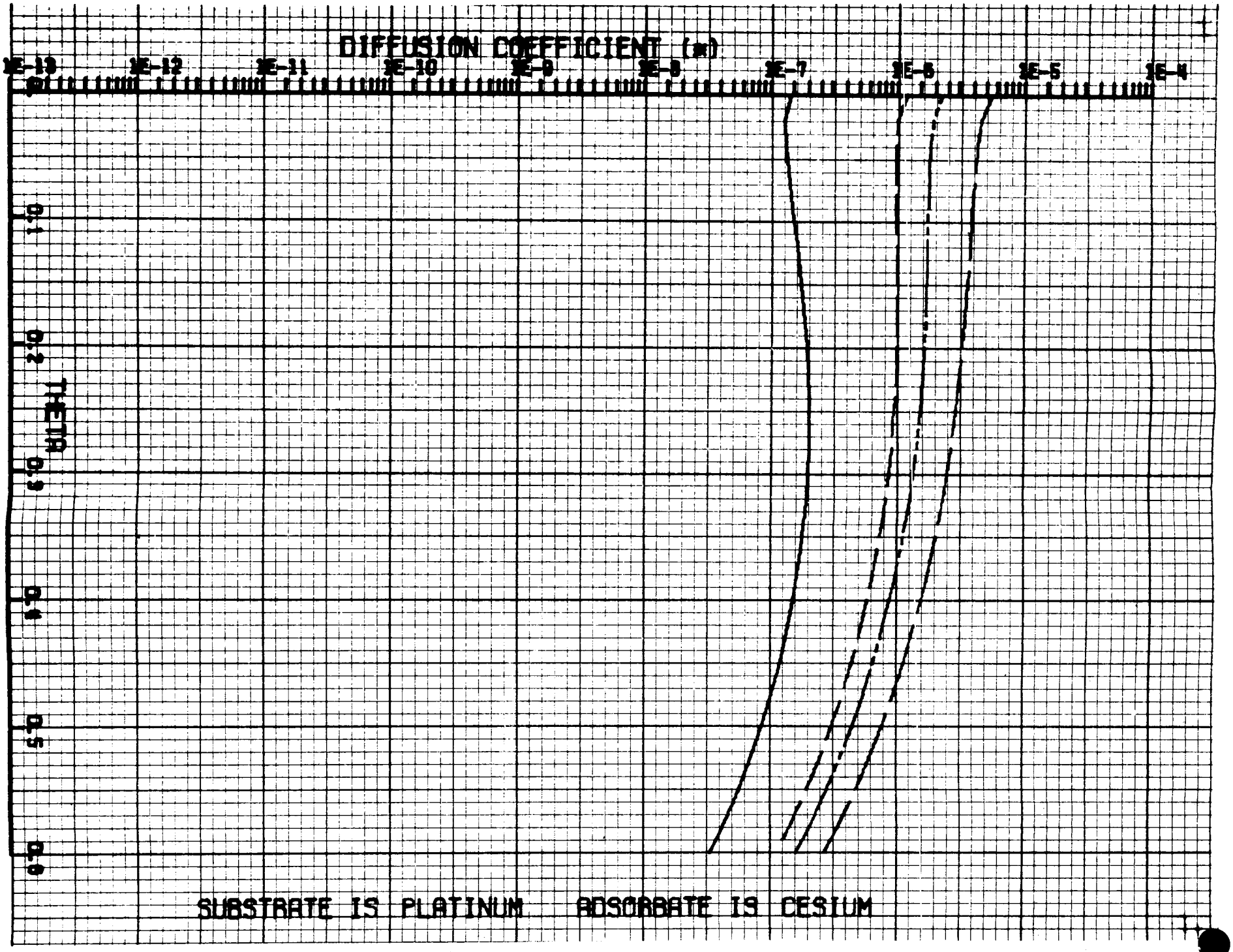
DIFFUSION COEFFICIENT (m)
1E-13
1E-12
1E-11
1E-10
1E-9
1E-8
1E-7
1E-6
1E-5
1E-4
THETA
0.1
0.2
0.3
0.4
0.5
0.6
SUBSTRATE IS PLATINUM ADSORBATE IS CESIUM

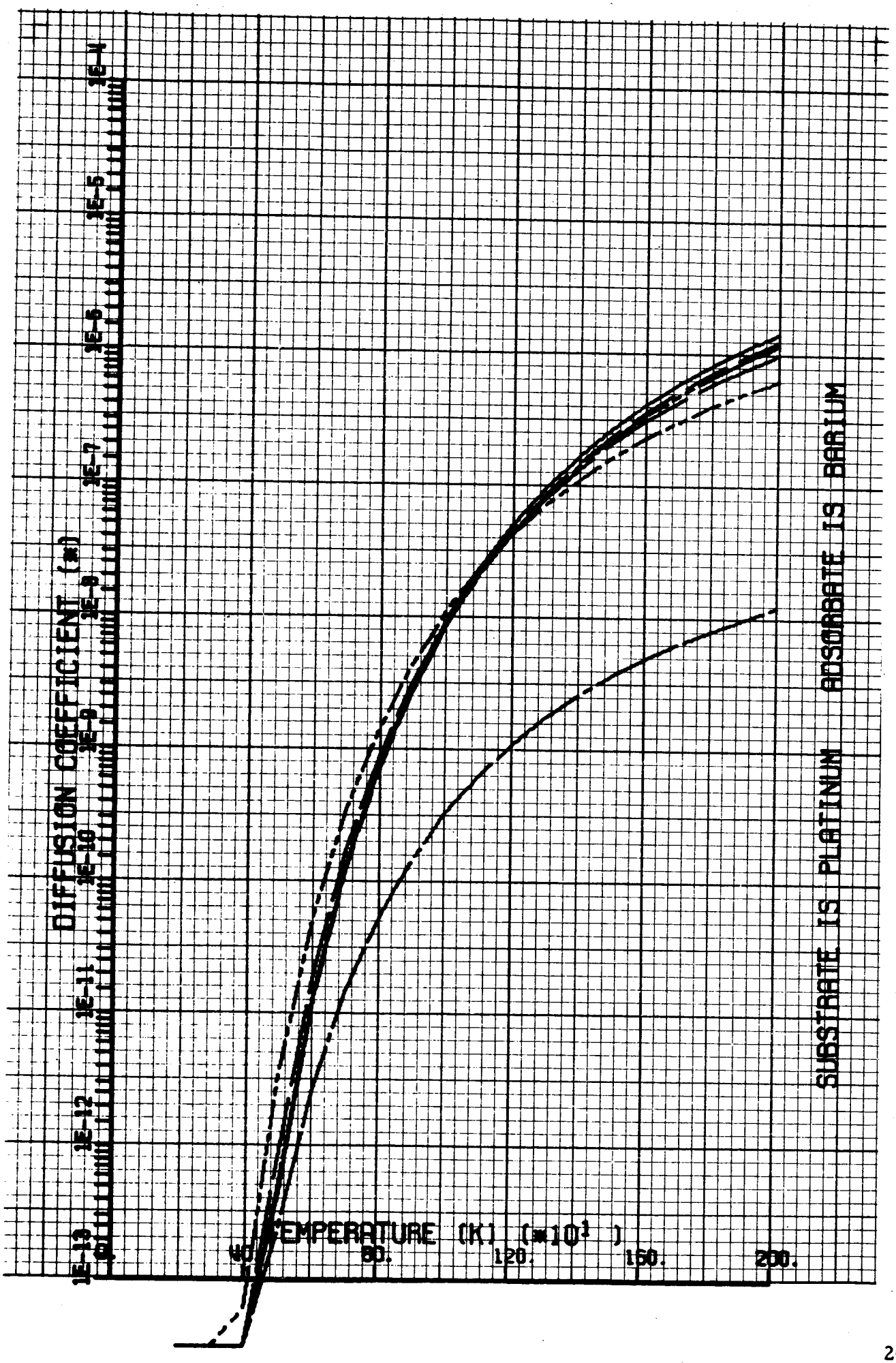
DIFFUSION COEFFICIENT (m²)
1E-13
1E-12
1E-11
1E-10
1E-9
1E-8
1E-7
1E-6
1E-5
1E-4
TEMPERATURE (K) (×10¹)
40.
80.
120.
160.
200.
SUBSTRATE IS PLATINUM ADSORBATE IS BARIUM

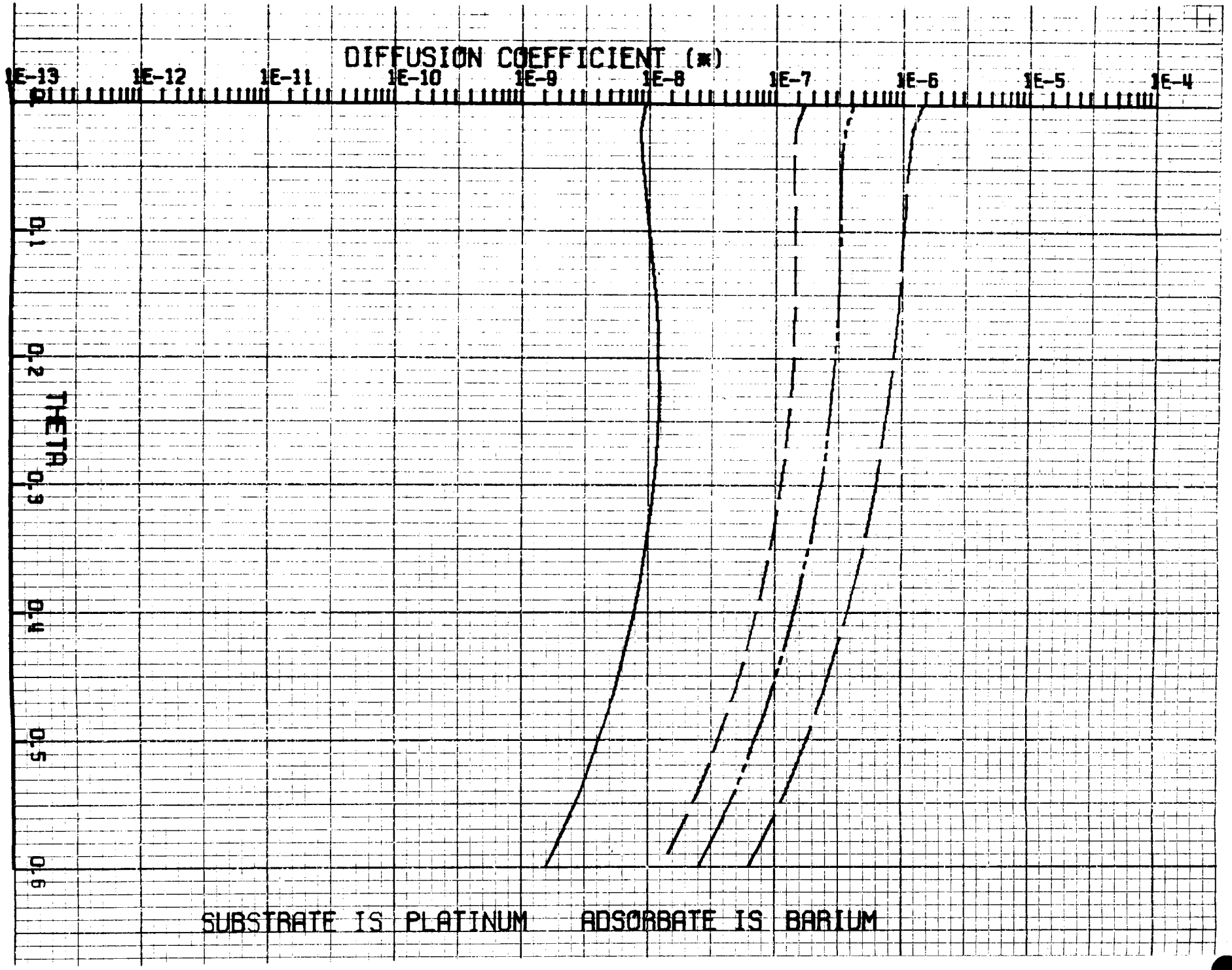
DIFFUSION COEFFICIENT (*)
1E-13
1E-12
1E-11
1E-10
1E-9
1E-8
1E-7
1E-6
1E-5
1E-4
THETA
0.1
0.2
0.3
0.4
0.5
0.6
SUBSTRATE IS PLATINUM ADSORBATE IS BARIUM

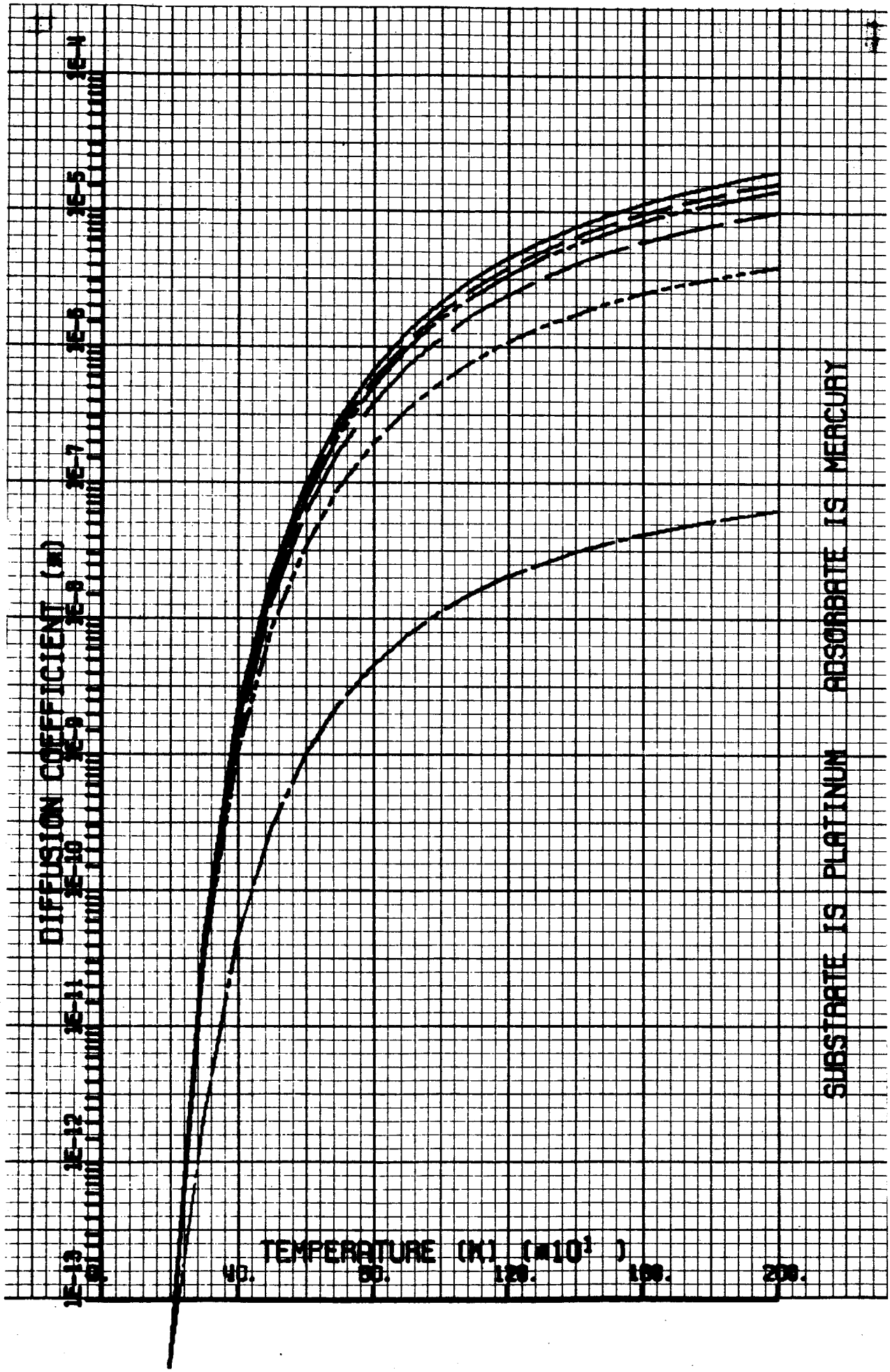
DIFFUSION COEFFICIENT (m)
1E-4
1E-5
1E-6
1E-7
1E-8
1E-9
1E-10
1E-11
1E-12
1E-13
TEMPERATURE (K) (×10⁻¹)
40.
80.
120.
160.
200.
SUBSTRATE IS PLATINUM ADSORBATE IS MERCURY

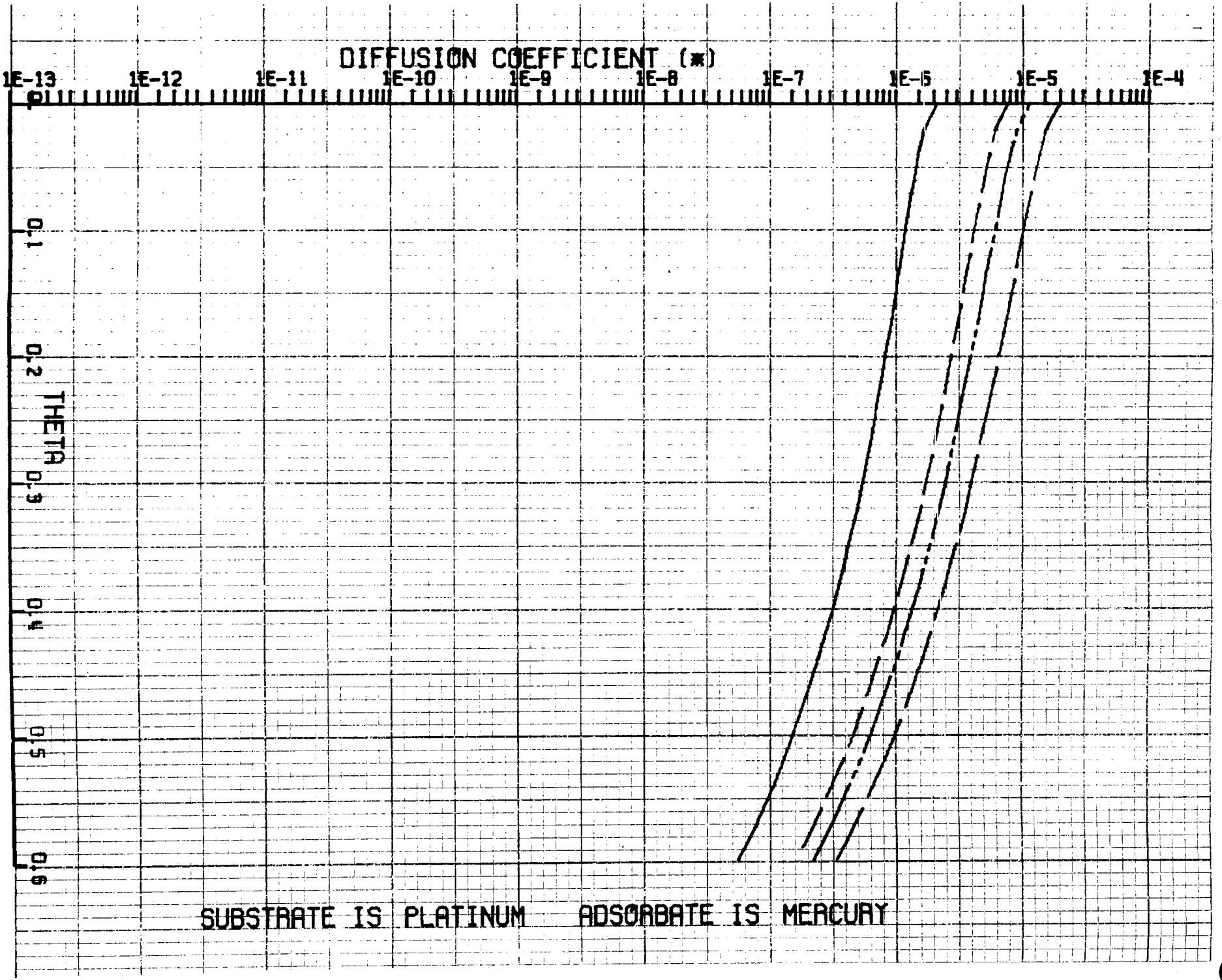
DIFFUSION COEFFICIENT (*)
1E-13
1E-12
1E-11
1E-10
1E-9
1E-8
1E-7
1E-6
1E-5
1E-4
0
0.1
0.2
0.3
0.4
0.5
0.6
THETA
SUBSTRATE IS PLATINUM ADSORBATE IS MERCURY

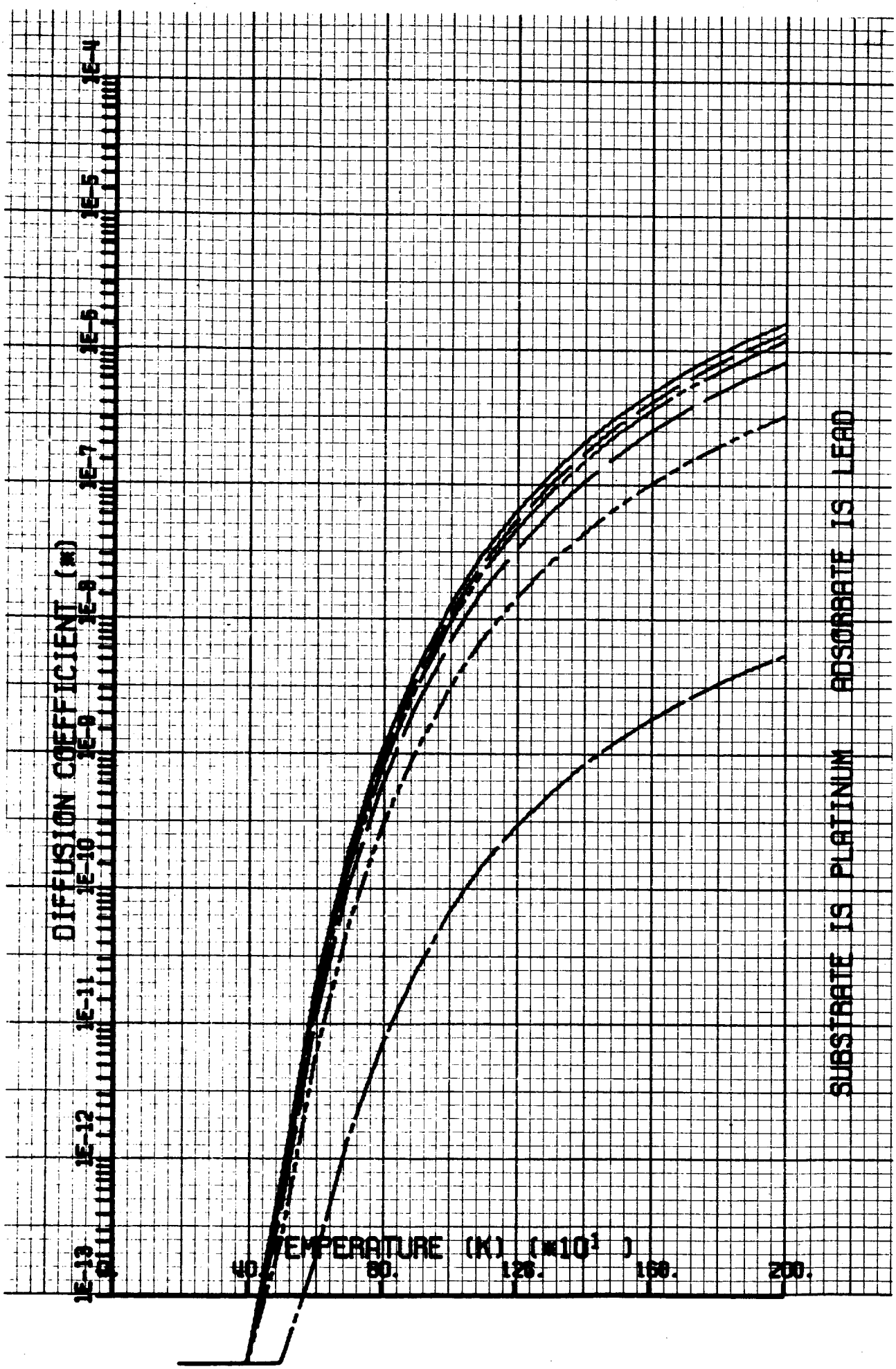
DIFFUSION COEFFICIENT (m)
1E-4
1E-5
1E-6
1E-7
1E-8
1E-9
1E-10
1E-11
1E-12
1E-13
TEMPERATURE (K) (*10^1)
40.
80.
120.
160.
200.
SUBSTRATE IS PLATINUM ADSORBATE IS LEAD

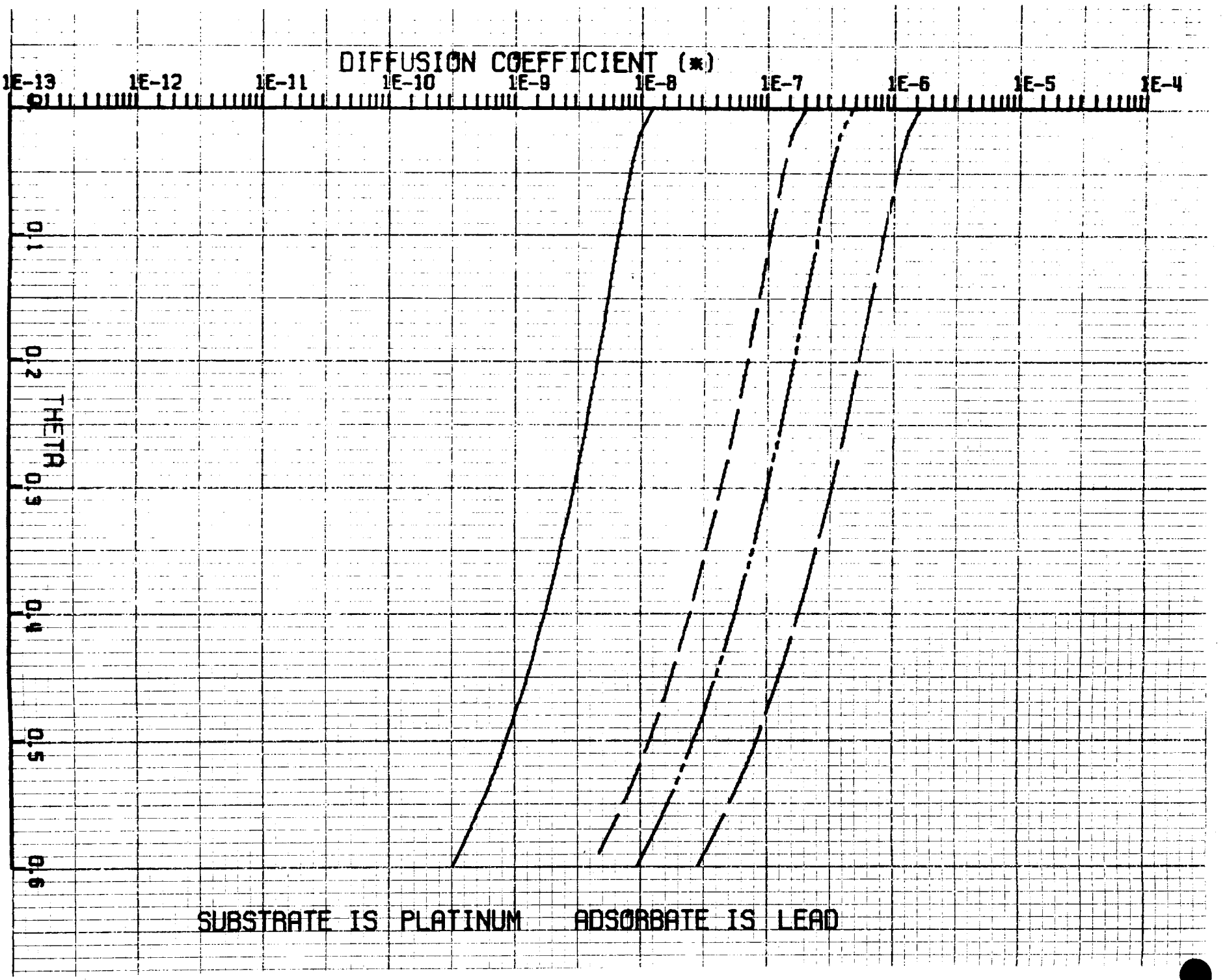
DIFFUSION COEFFICIENT (*)
1E-13
1E-12
1E-11
1E-10
1E-9
1E-8
1E-7
1E-6
1E-5
1E-4
0
0.1
0.2
0.3
0.4
0.5
0.6
THETA
SUBSTRATE IS PLATINUM ADSORBATE IS LEAD

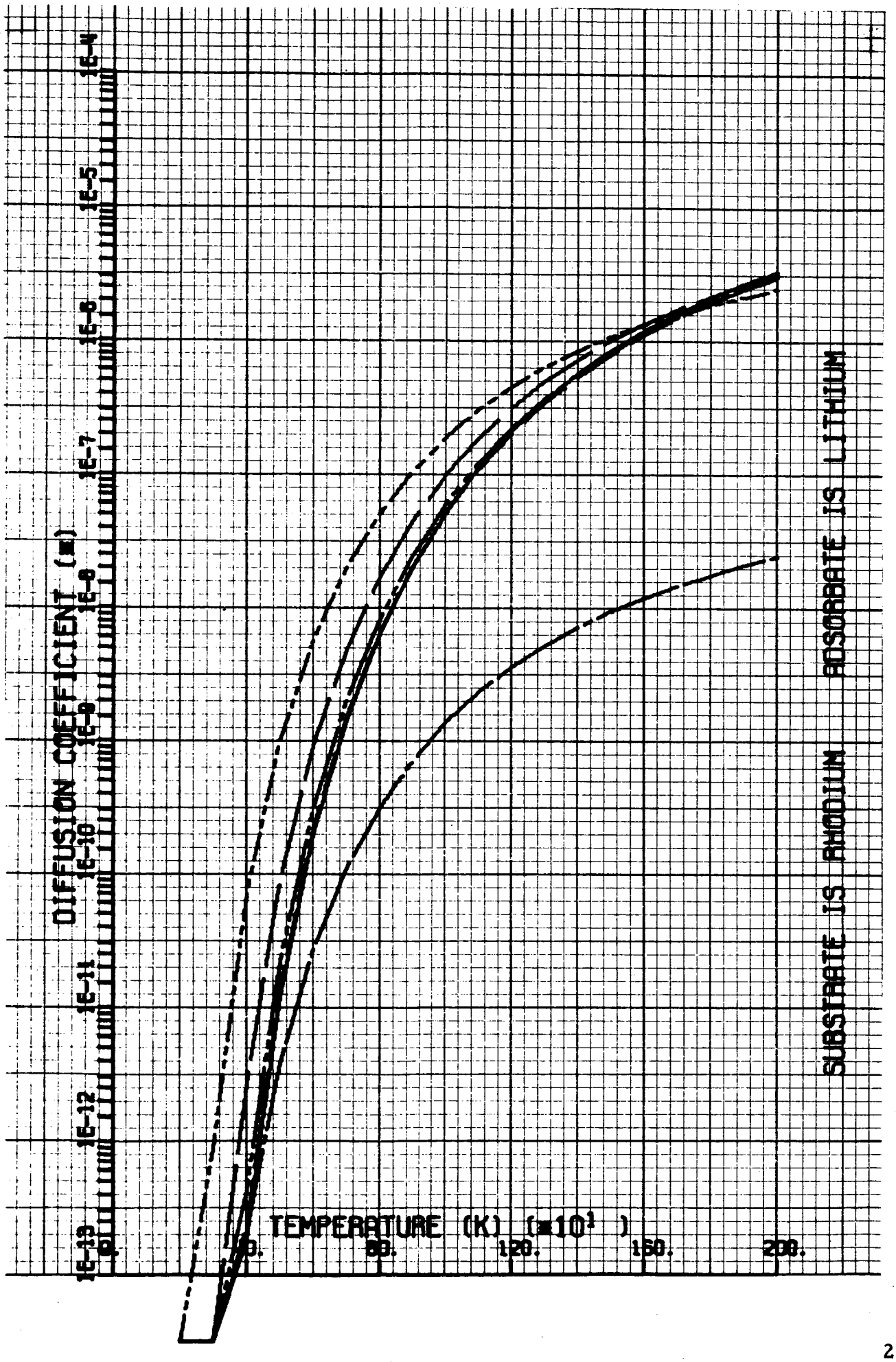
DIFFUSION COEFFICIENT (cm²)
1E-4
1E-5
1E-6
1E-7
1E-8
1E-9
1E-10
1E-11
1E-12
1E-13
TEMPERATURE (K) (x10¹)
90.
120.
150.
200.
SUBSTRATE IS RHODIUM ADSORBATE IS LITHIUM

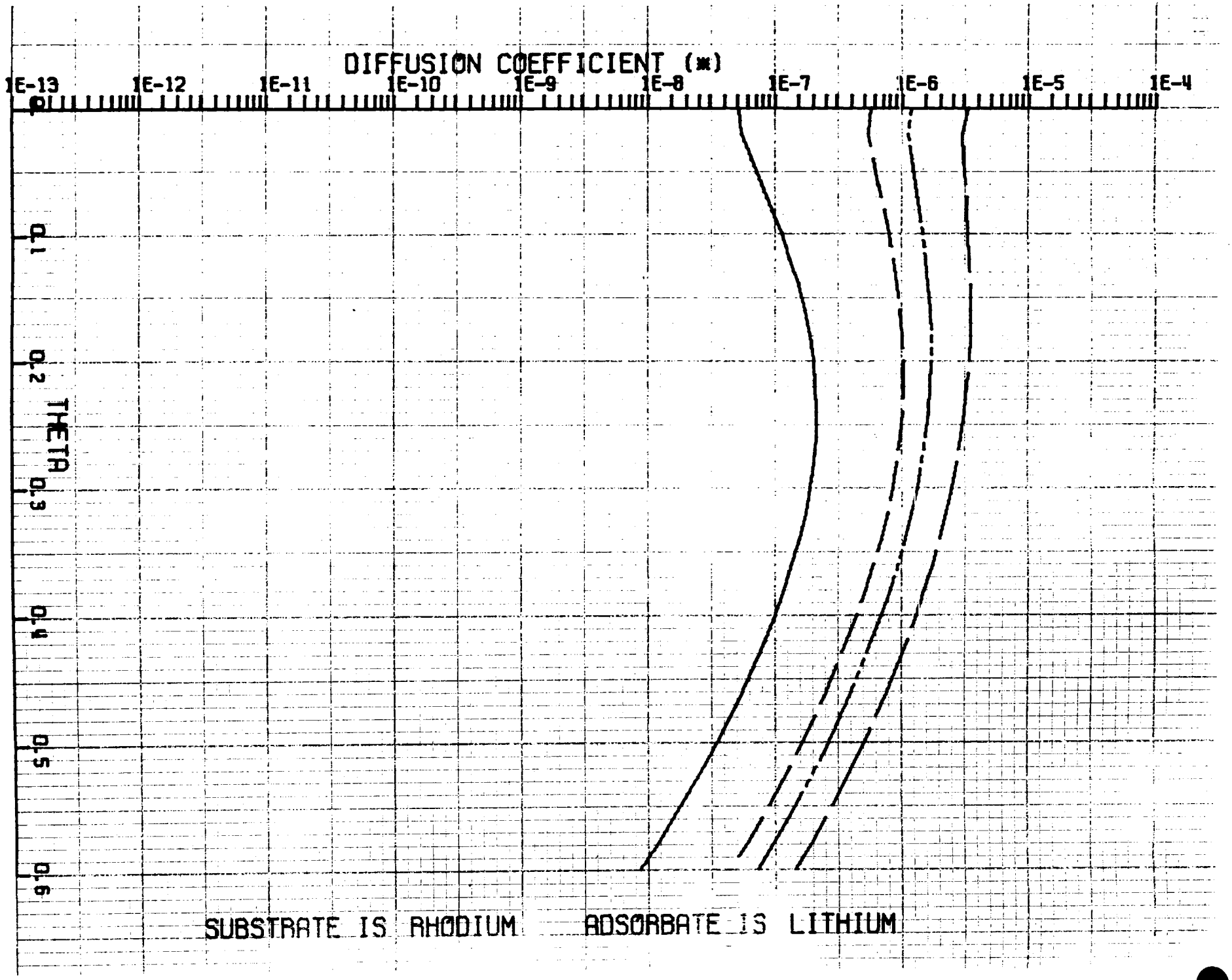
DIFFUSION COEFFICIENT (*)
1E-13
1E-12
1E-11
1E-10
1E-9
1E-8
1E-7
1E-6
1E-5
1E-4
THETA
0
0.1
0.2
0.3
0.4
0.5
0.6
SUBSTRATE IS RHODIUM ADSORBATE IS LITHIUM

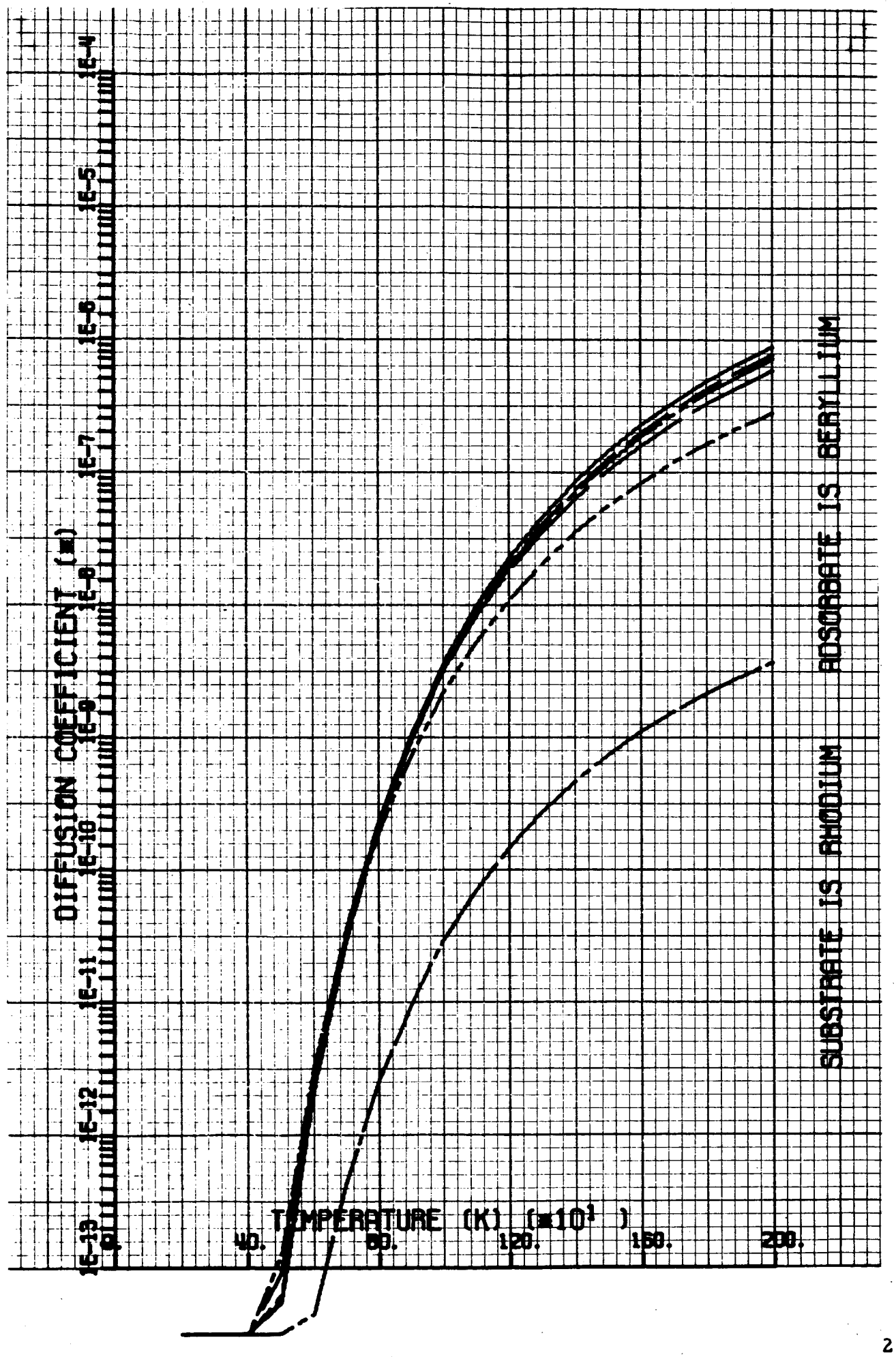
DIFFUSION COEFFICIENT (M²)
1E-4
1E-5
1E-6
1E-7
1E-8
1E-9
1E-10
1E-11
1E-12
1E-13
TEMPERATURE (K) (×10¹)
40.
80.
120.
160.
200.
SUBSTRATE IS RHODIUM ADSORBATE IS BERYLLIUM

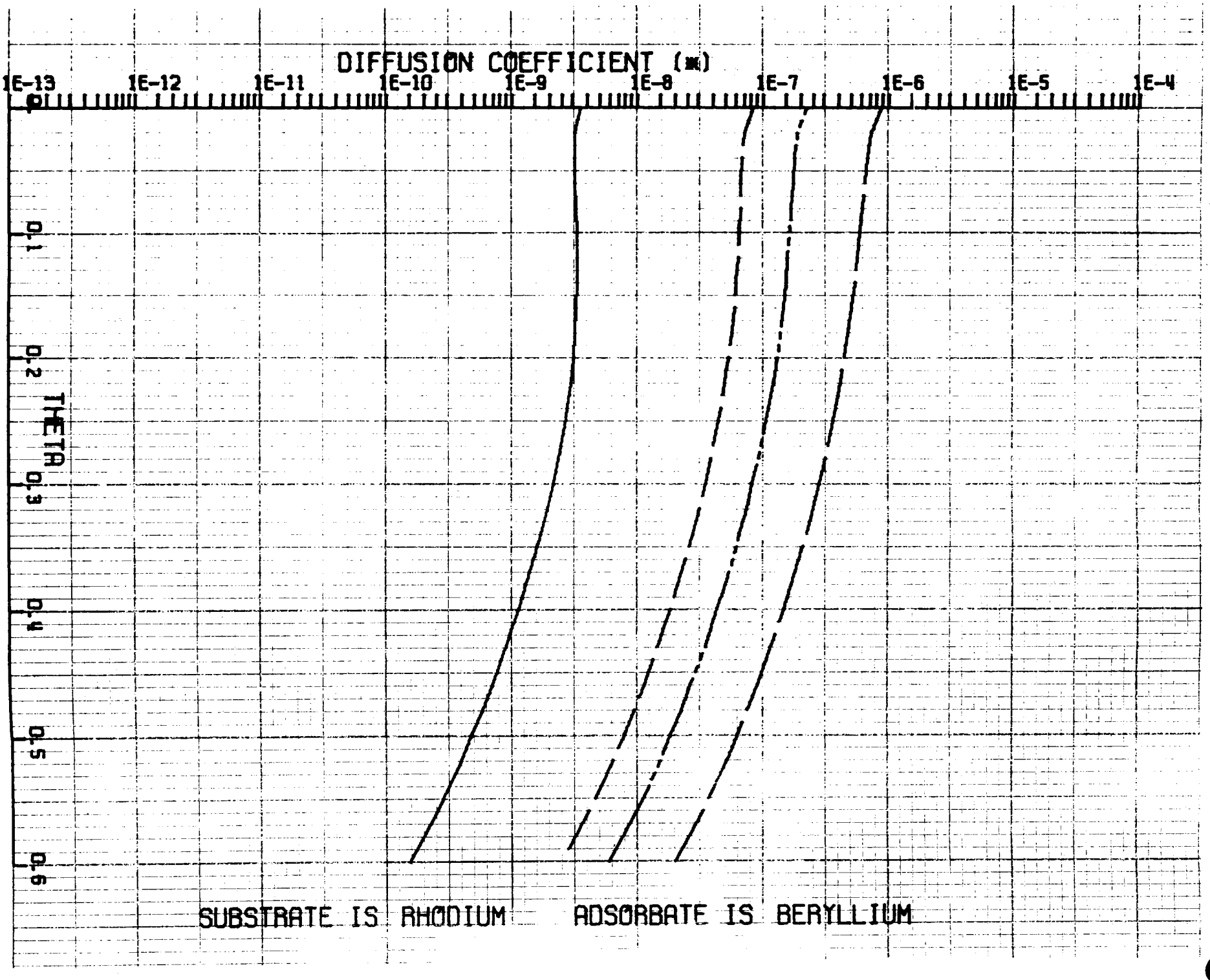
DIFFUSION COEFFICIENT (*)
1E-13
1E-12
1E-11
1E-10
1E-9
1E-8
1E-7
1E-6
1E-5
1E-4
0
0.1
0.2
0.3
0.4
0.5
0.6
THETA
SUBSTRATE IS RHODIUM
ADSORBATE IS BERYLLIUM

DIFFUSION COEFFICIENT (M²)
1E-13
1E-12
1E-11
1E-10
1E-9
1E-8
1E-7
1E-6
1E-5
1E-4
TEMPERATURE (K) (×10¹)
40.
120.
160.
200.
SUBSTRATE IS RHODIUM ADSORBATE IS CARBON

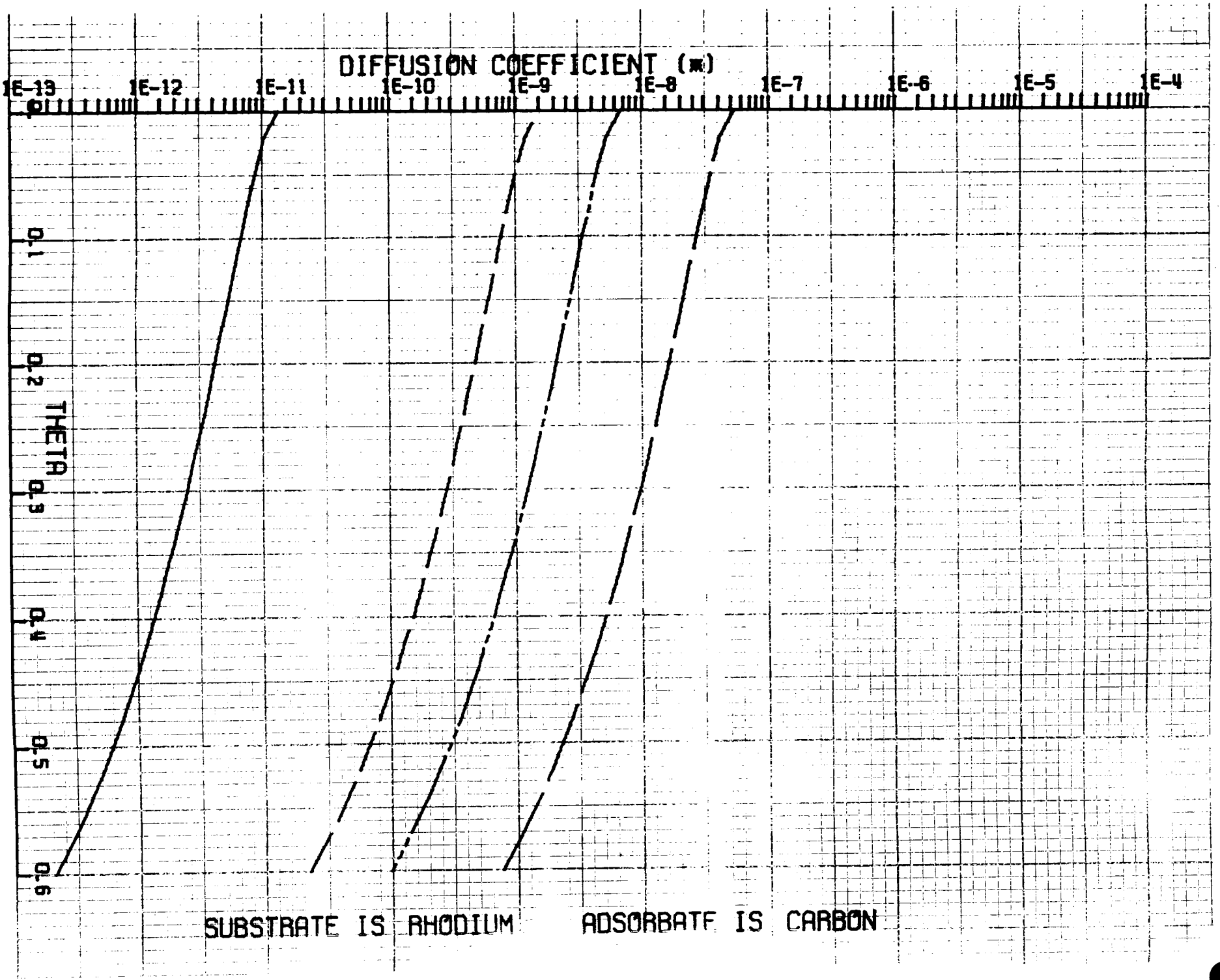
DIFFUSION COEFFICIENT (*)
1E-13
1E-12
1E-11
1E-10
1E-9
1E-8
1E-7
1E-6
1E-5
1E-4
THETA
0.1
0.2
0.3
0.4
0.5
0.6
SUBSTRATE IS RHODIUM
ADSORBATE IS CARBON

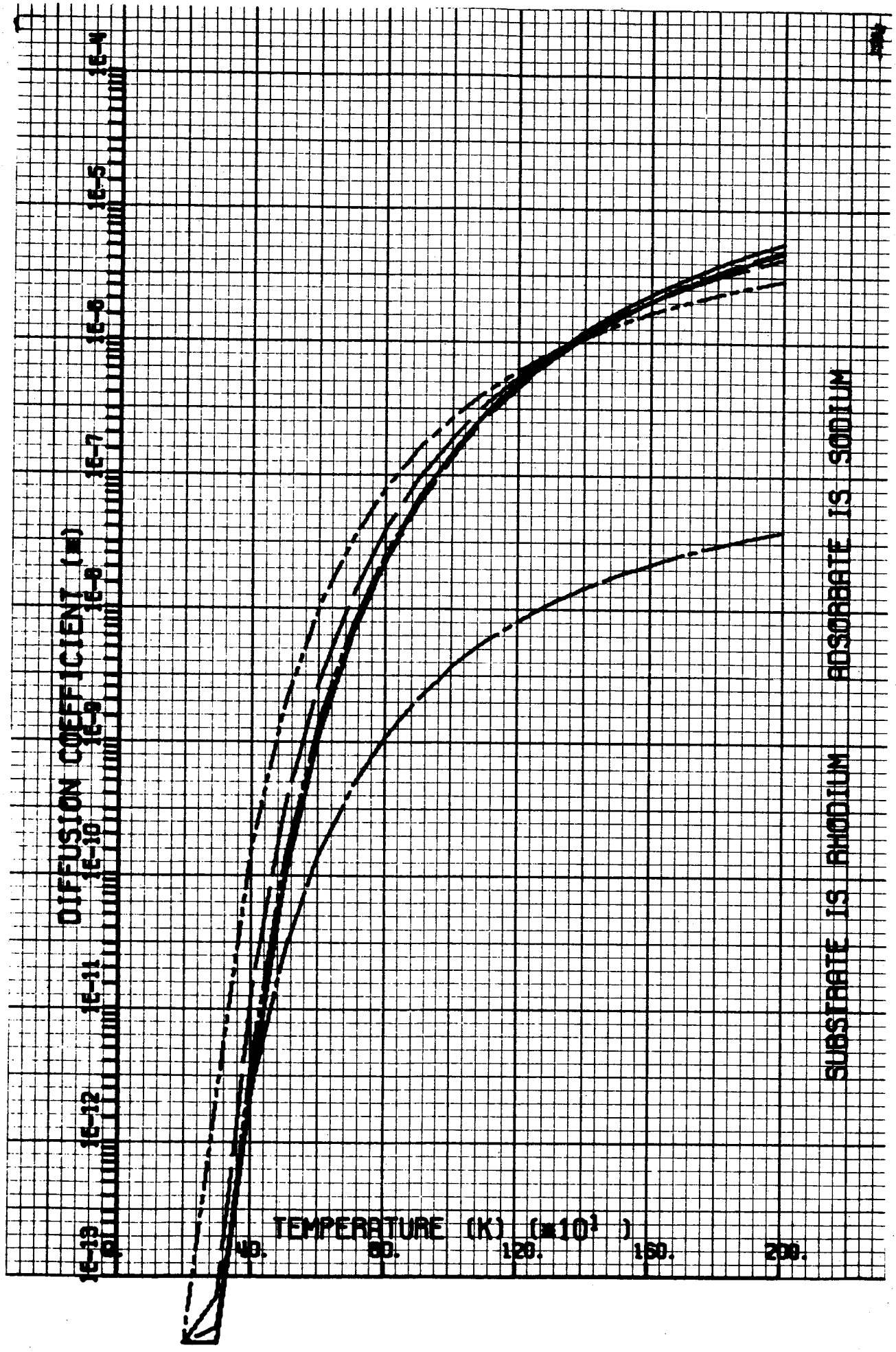
SUBSTRATE IS RHODIUM ADSORBATE IS SODIUM
DIFFUSION COEFFICIENT (M²)
1E-4
1E-5
1E-6
1E-7
1E-8
1E-9
1E-10
1E-11
1E-12
1E-13
TEMPERATURE (K) (×10¹)
40.
80.
120.
160.
200.

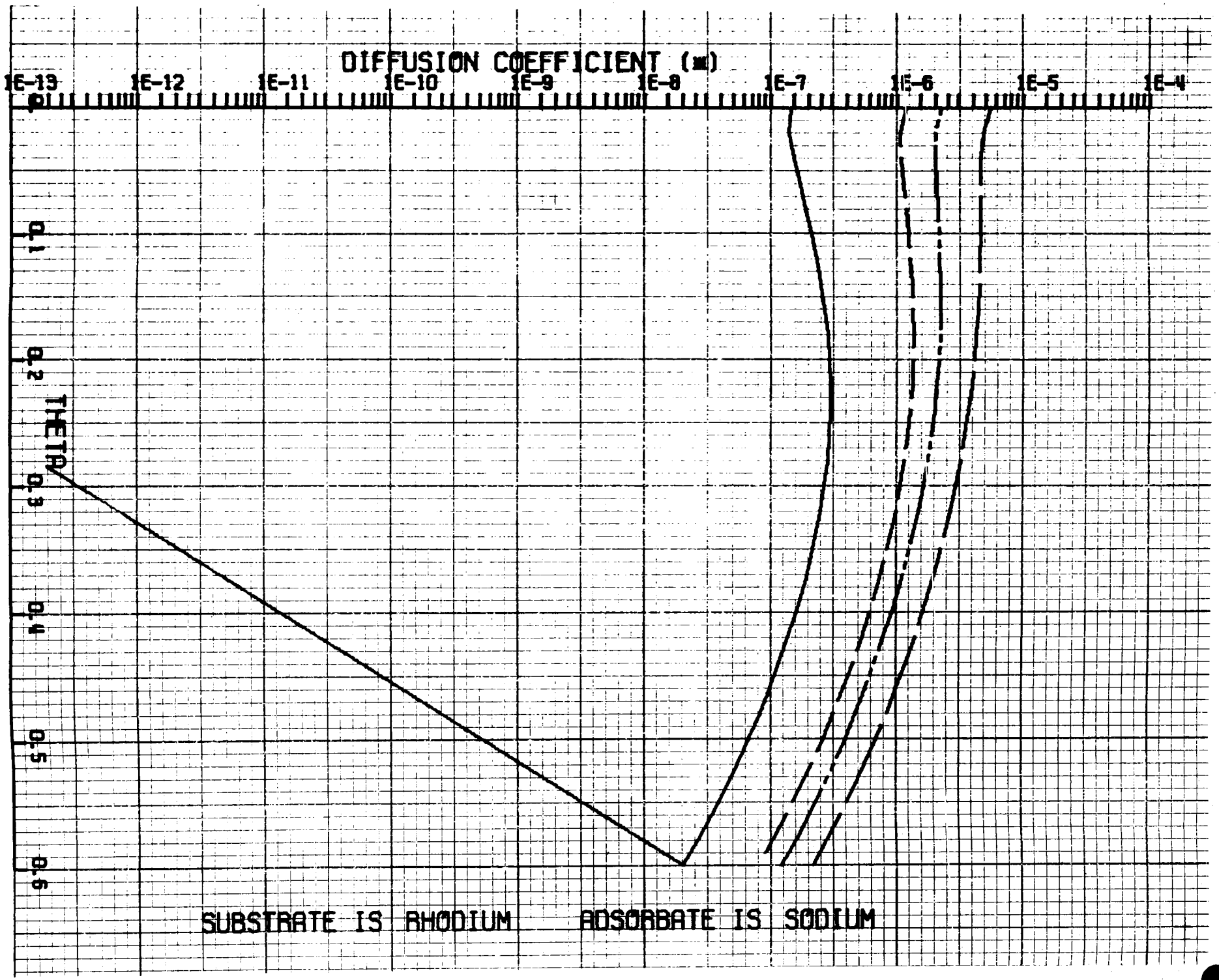
DIFFUSION COEFFICIENT (m)
1E-13
1E-12
1E-11
1E-10
1E-9
1E-8
1E-7
1E-6
1E-5
1E-4
THETA
0.1
0.2
0.3
0.4
0.5
0.6
SUBSTRATE IS RHODIUM ADSORBATE IS SODIUM

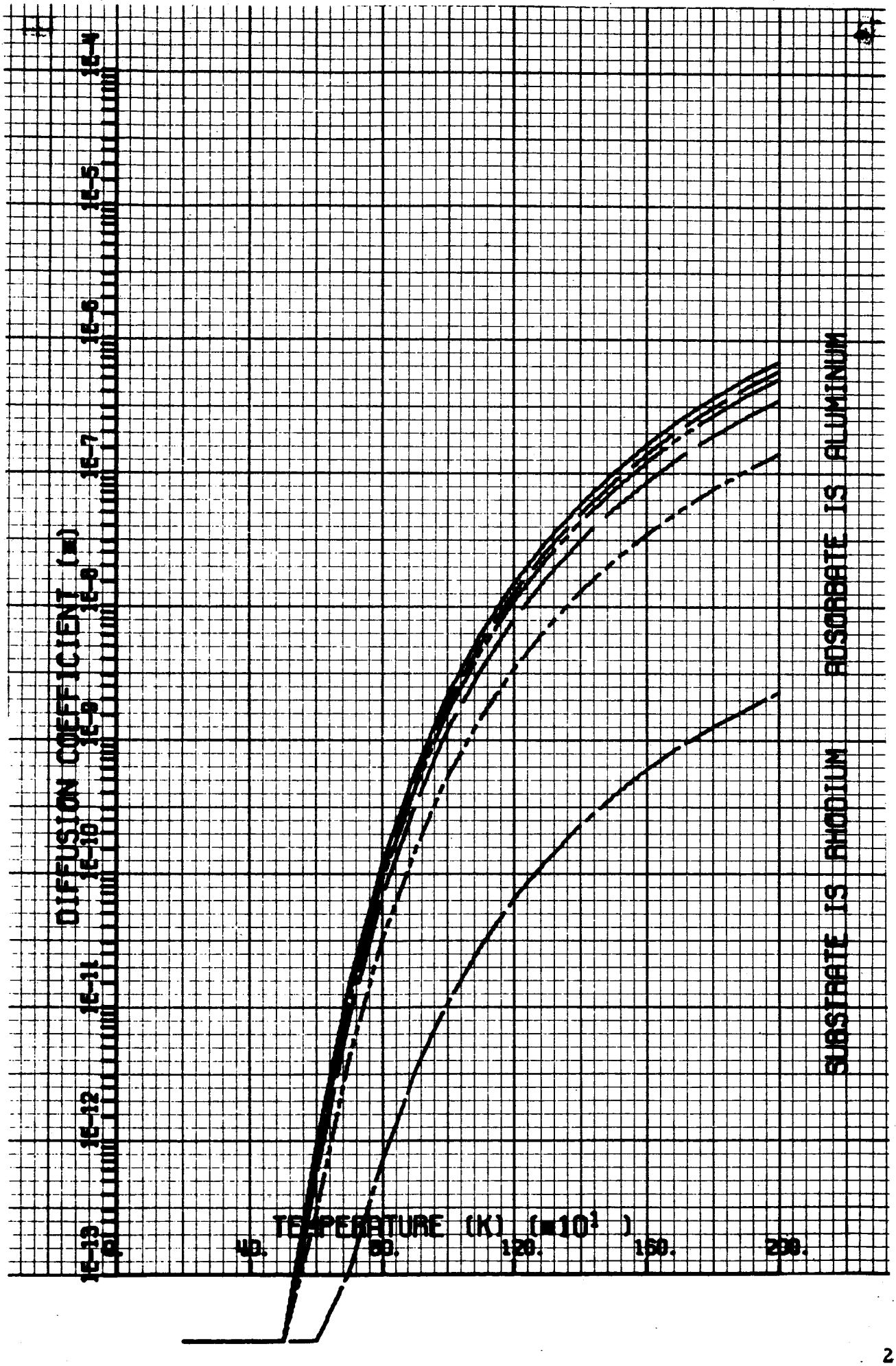
DIFFUSION COEFFICIENT (M²)
1E-4
1E-5
1E-6
1E-7
1E-8
1E-9
1E-10
1E-11
1E-12
1E-13
TEMPERATURE (K) (*10¹)
40.
80.
120.
160.
200.
SUBSTRATE IS RHODIUM ADSORBATE IS ALUMINUM

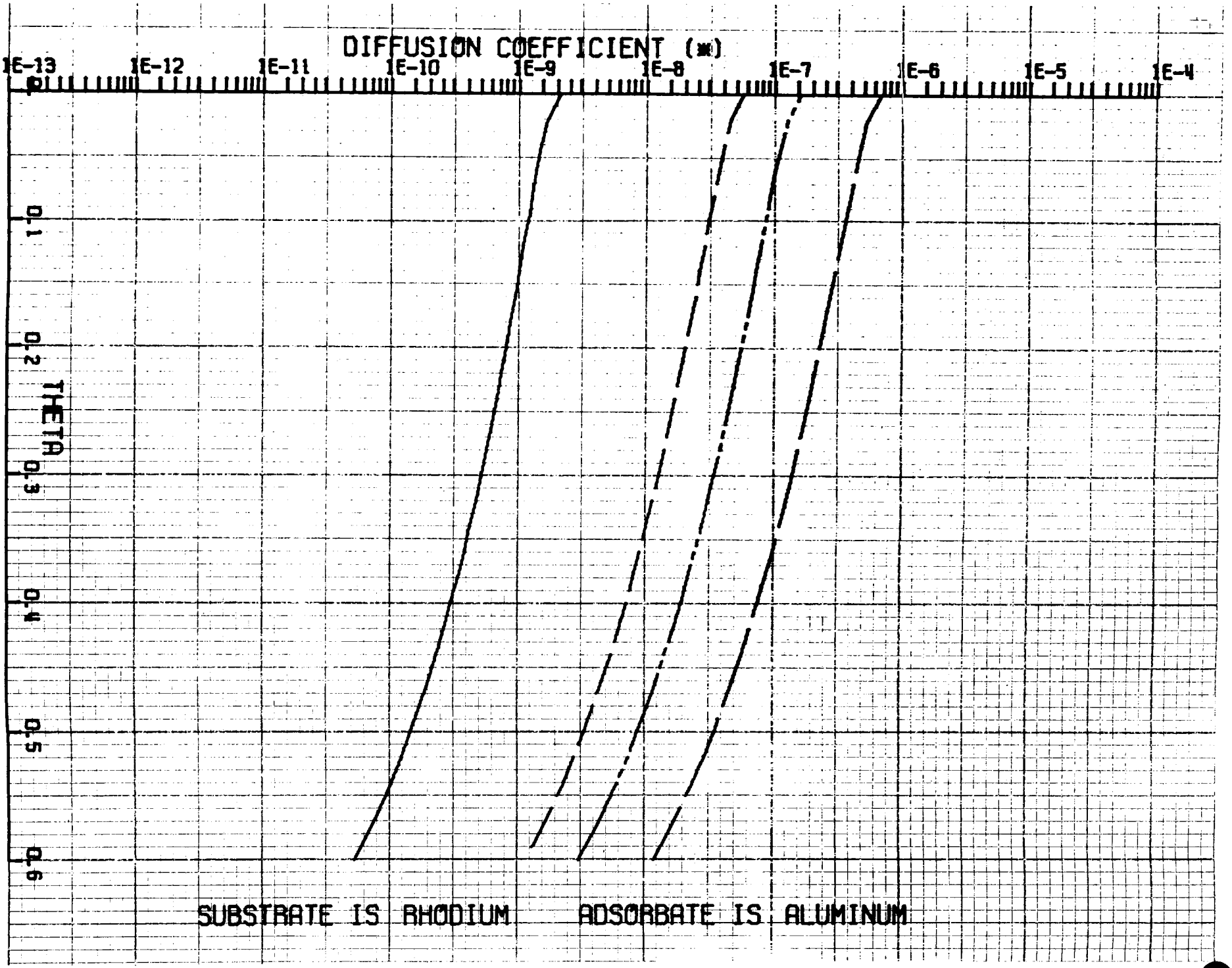
DIFFUSION COEFFICIENT (*)
1E-13
1E-12
1E-11
1E-10
1E-9
1E-8
1E-7
1E-6
1E-5
1E-4
0
0.1
0.2
0.3
0.4
0.5
0.6
THETA
SUBSTRATE IS RHODIUM ADSORBATE IS ALUMINUM

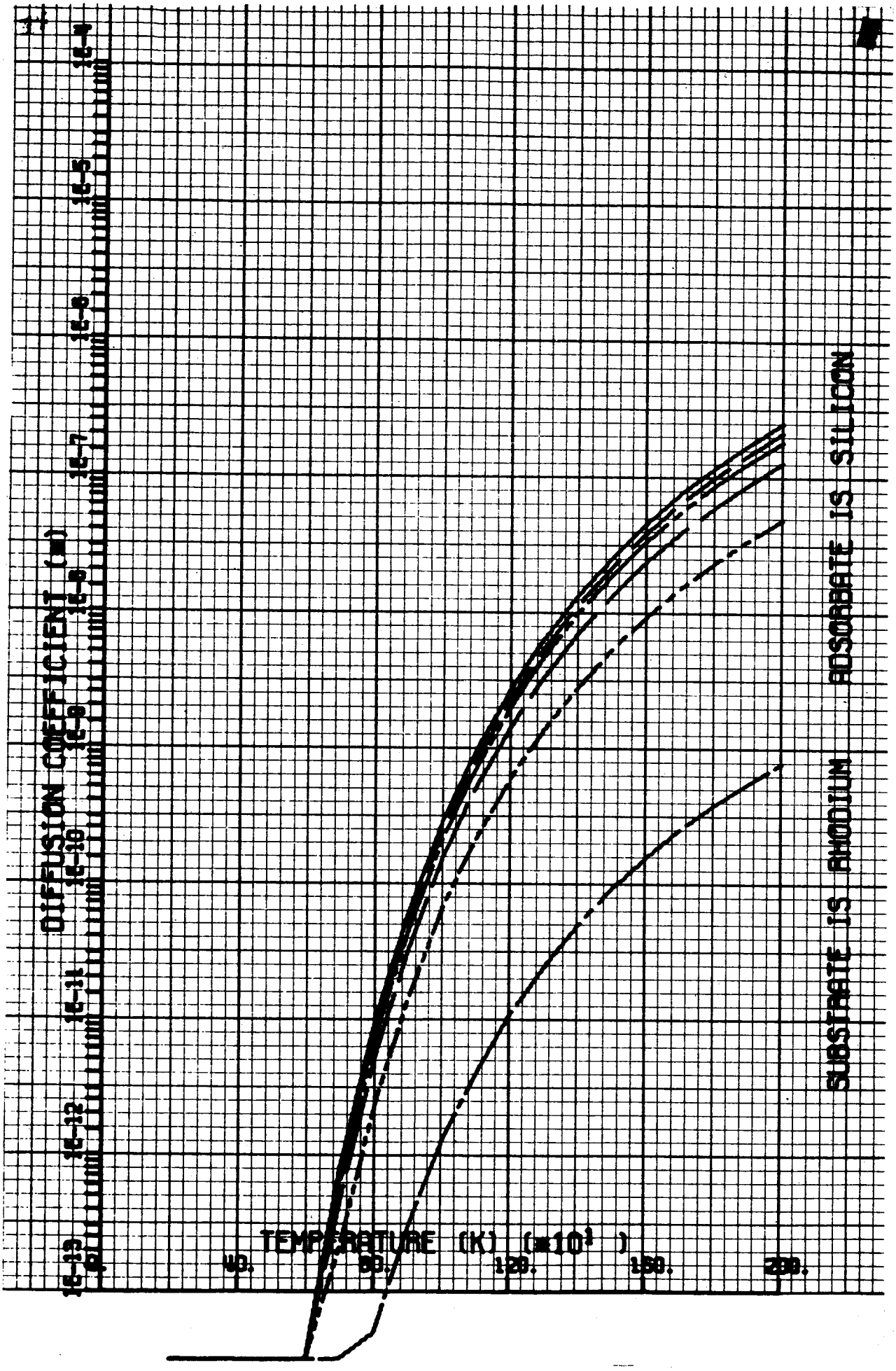
DIFFUSION COEFFICIENT (cm²)
10⁻⁴
10⁻⁵
10⁻⁶
10⁻⁷
10⁻⁸
10⁻⁹
10⁻¹⁰
10⁻¹¹
10⁻¹²
10⁻¹³
TEMPERATURE (K) (×10³)
40.
80.
120.
160.
200.
SUBSTRATE IS RHODIUM ADSORBATE IS SILICON

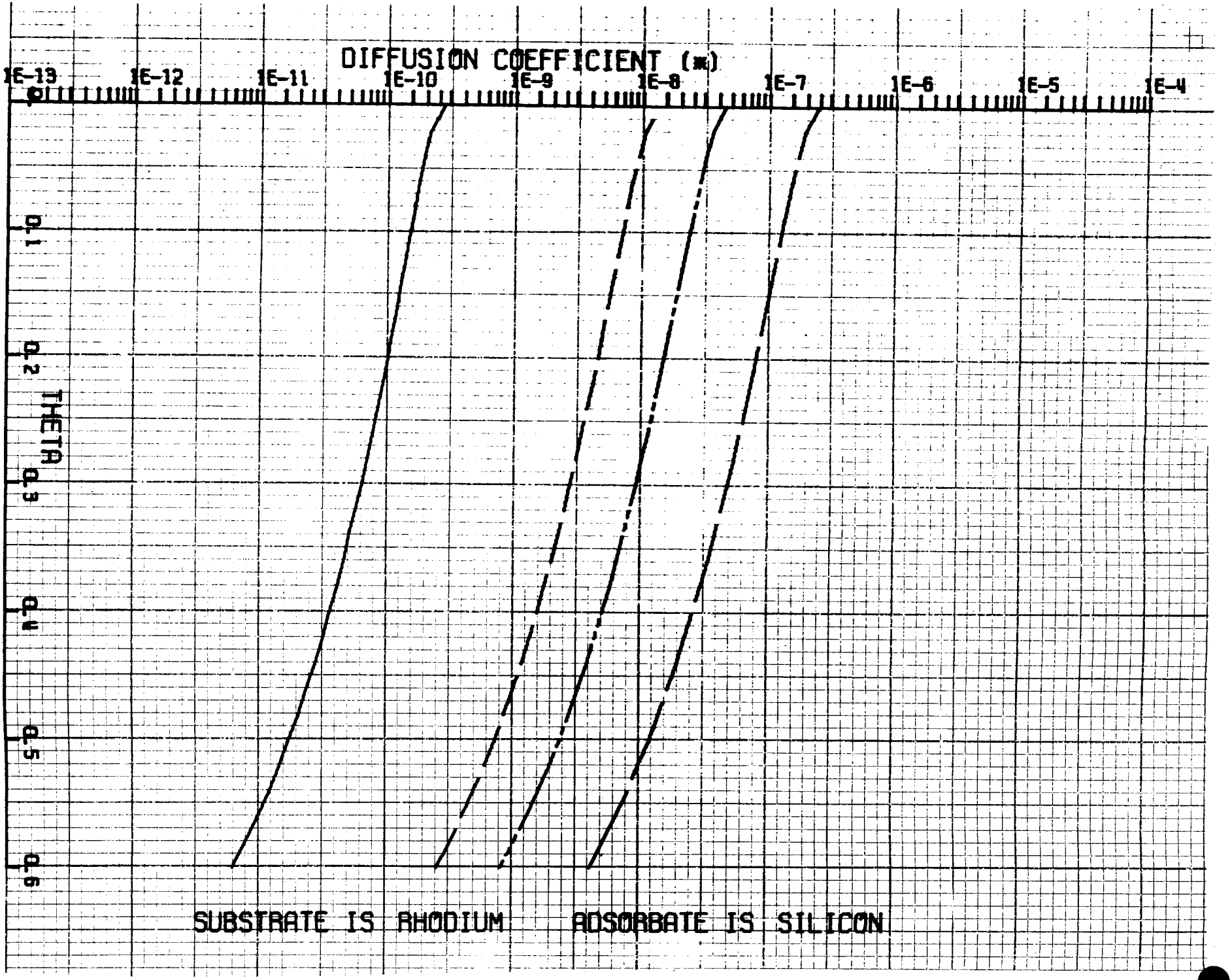
DIFFUSION COEFFICIENT (*)
1E-13
1E-12
1E-11
1E-10
1E-9
1E-8
1E-7
1E-6
1E-5
1E-4
0.1
0.2
0.3
0.4
0.5
0.6
THETA
SUBSTRATE IS RHODIUM
ADSORBATE IS SILICON

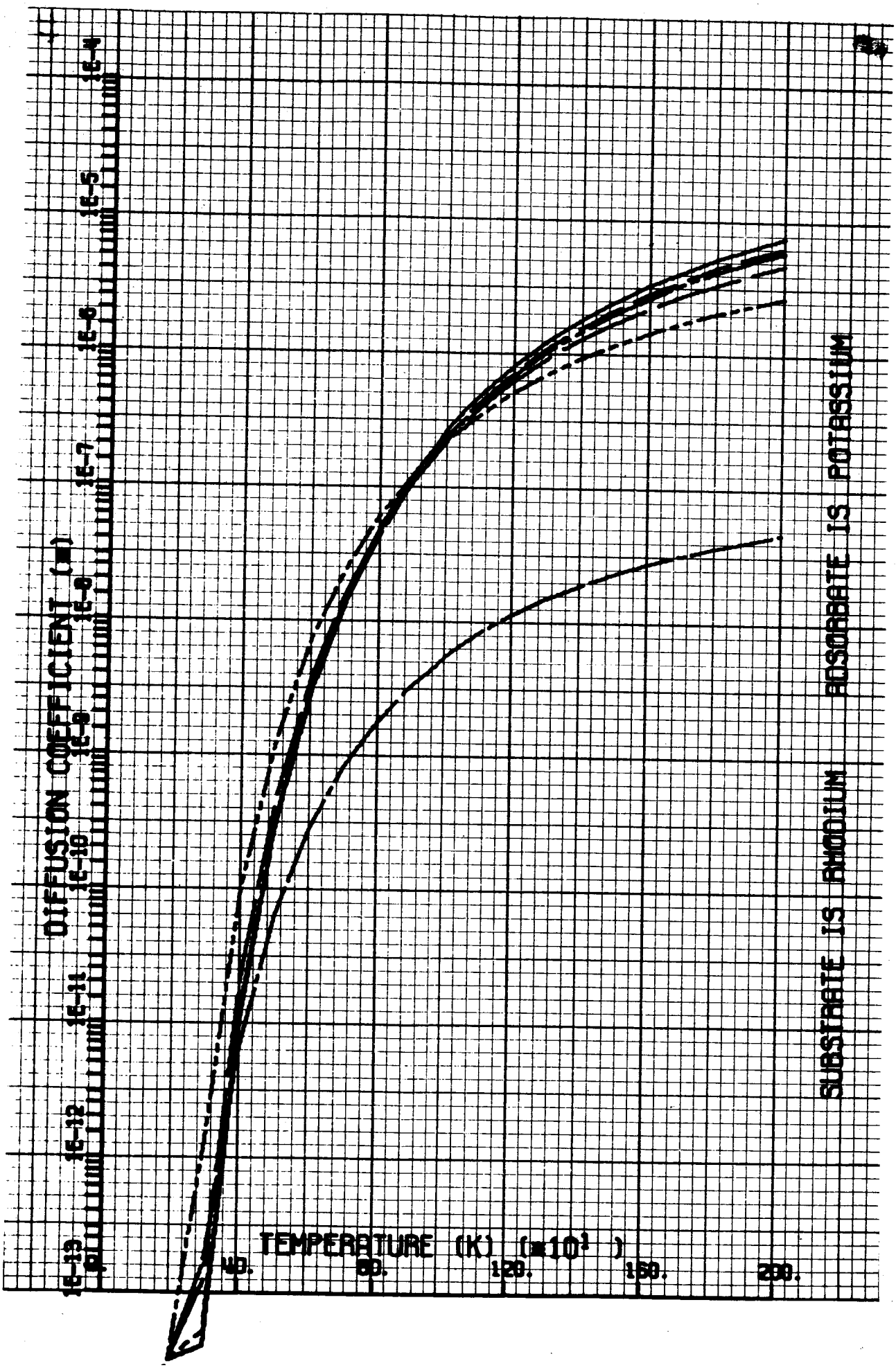
DIFFUSION COEFFICIENT (cm²)
1E-13
1E-12
1E-11
1E-10
1E-9
1E-8
1E-7
1E-6
1E-5
1E-4
TEMPERATURE (K) (x10¹)
40.
80.
120.
160.
200.
SUBSTRATE IS RHODIUM ADSORBATE IS POTASSIUM

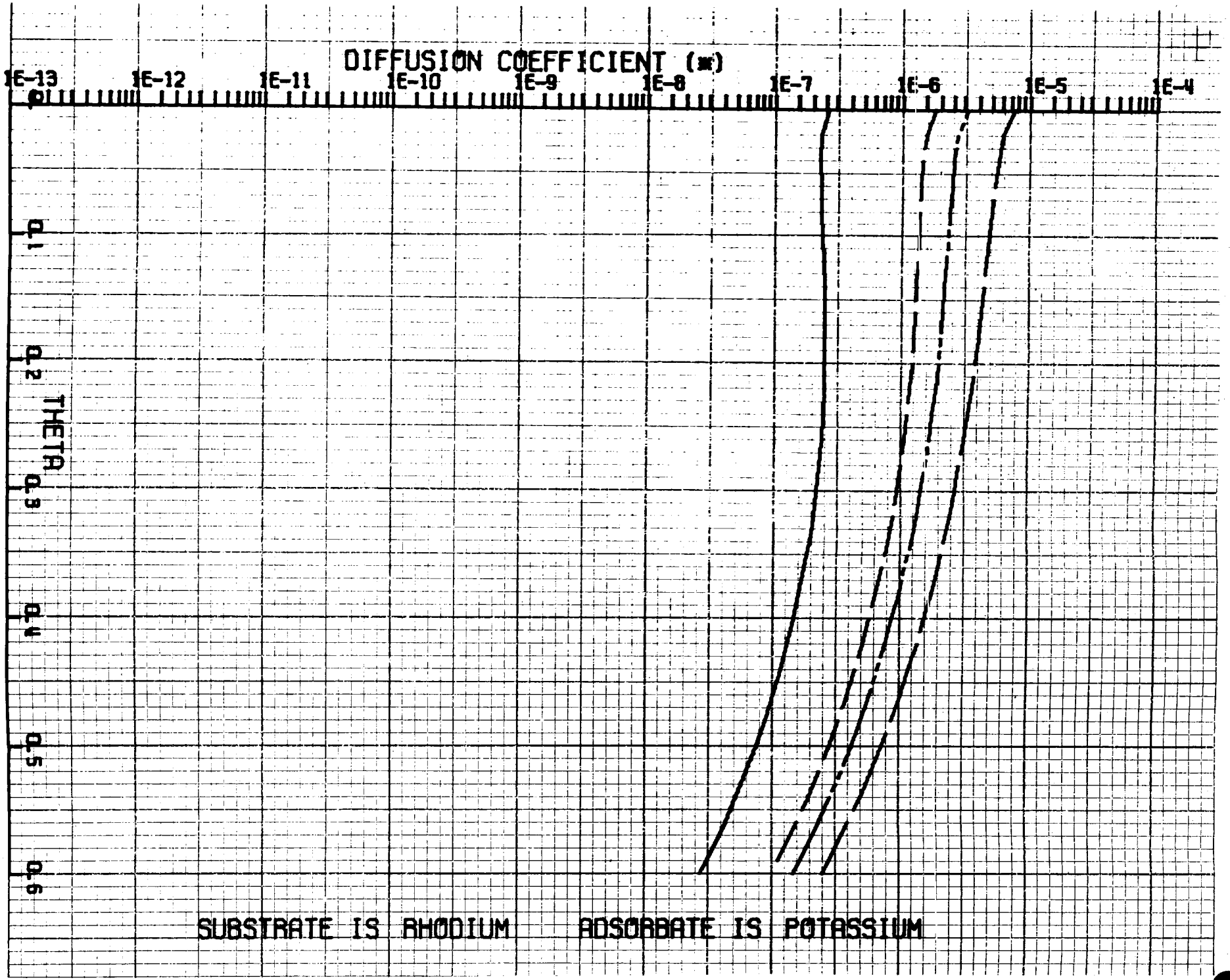
DIFFUSION COEFFICIENT (*)
1E-13
1E-12
1E-11
1E-10
1E-9
1E-8
1E-7
1E-6
1E-5
1E-4
THETA
0.1
0.2
0.3
0.4
0.5
0.6
SUBSTRATE IS RHODIUM
ADSORBATE IS POTASSIUM

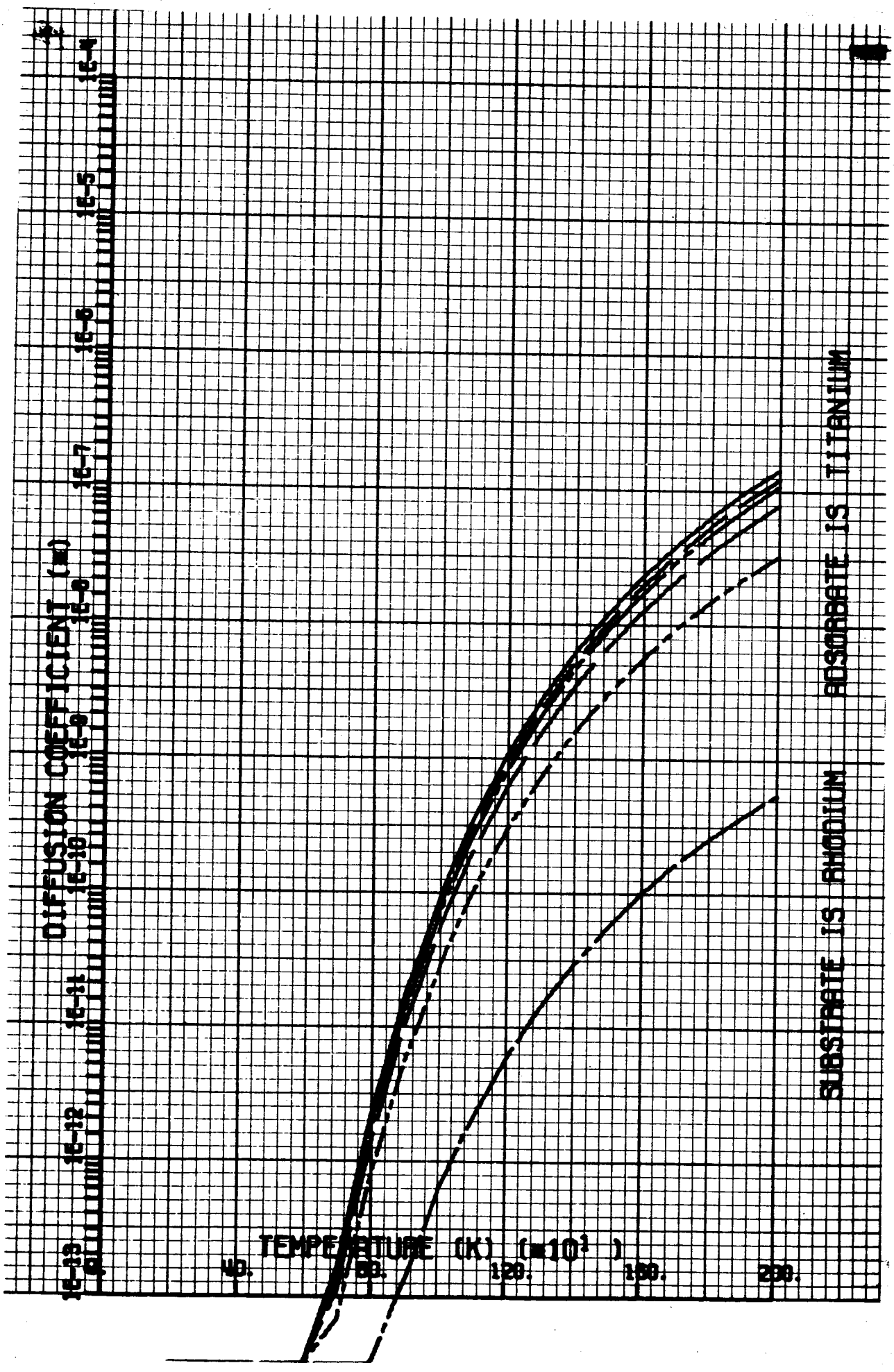
DIFFUSION COEFFICIENT (M²)
1E-4
1E-5
1E-6
1E-7
1E-8
1E-9
1E-10
1E-11
1E-12
1E-13
TEMPERATURE (K) (×10¹)
80.
120.
160.
200.
SUBSTRATE IS RHODIUM ADSORBATE IS TITANIUM

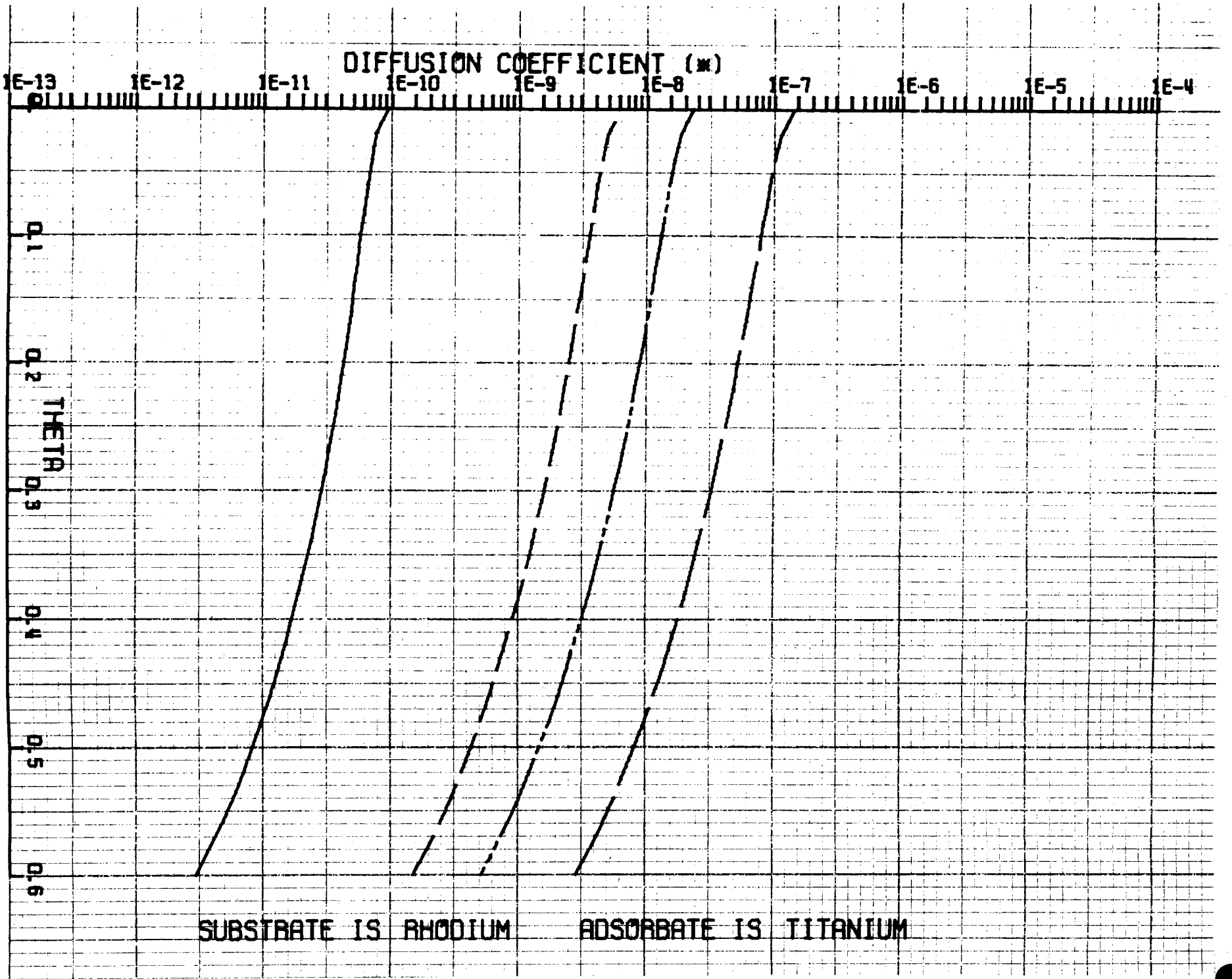
DIFFUSION COEFFICIENT (*)
1E-13
1E-12
1E-11
1E-10
1E-9
1E-8
1E-7
1E-6
1E-5
1E-4
THETA
0.1
0.2
0.3
0.4
0.5
0.6
SUBSTRATE IS RHODIUM
ADSORBATE IS TITANIUM

DIFFUSION COEFFICIENT (m²)
1E-4
1E-5
1E-6
1E-7
1E-8
1E-9
1E-10
1E-11
1E-12
1E-13
TEMPERATURE (K) (×10²)
40.
80.
120.
160.
200.
SUBSTRATE IS RHODIUM ADSORBATE IS CHROMIUM

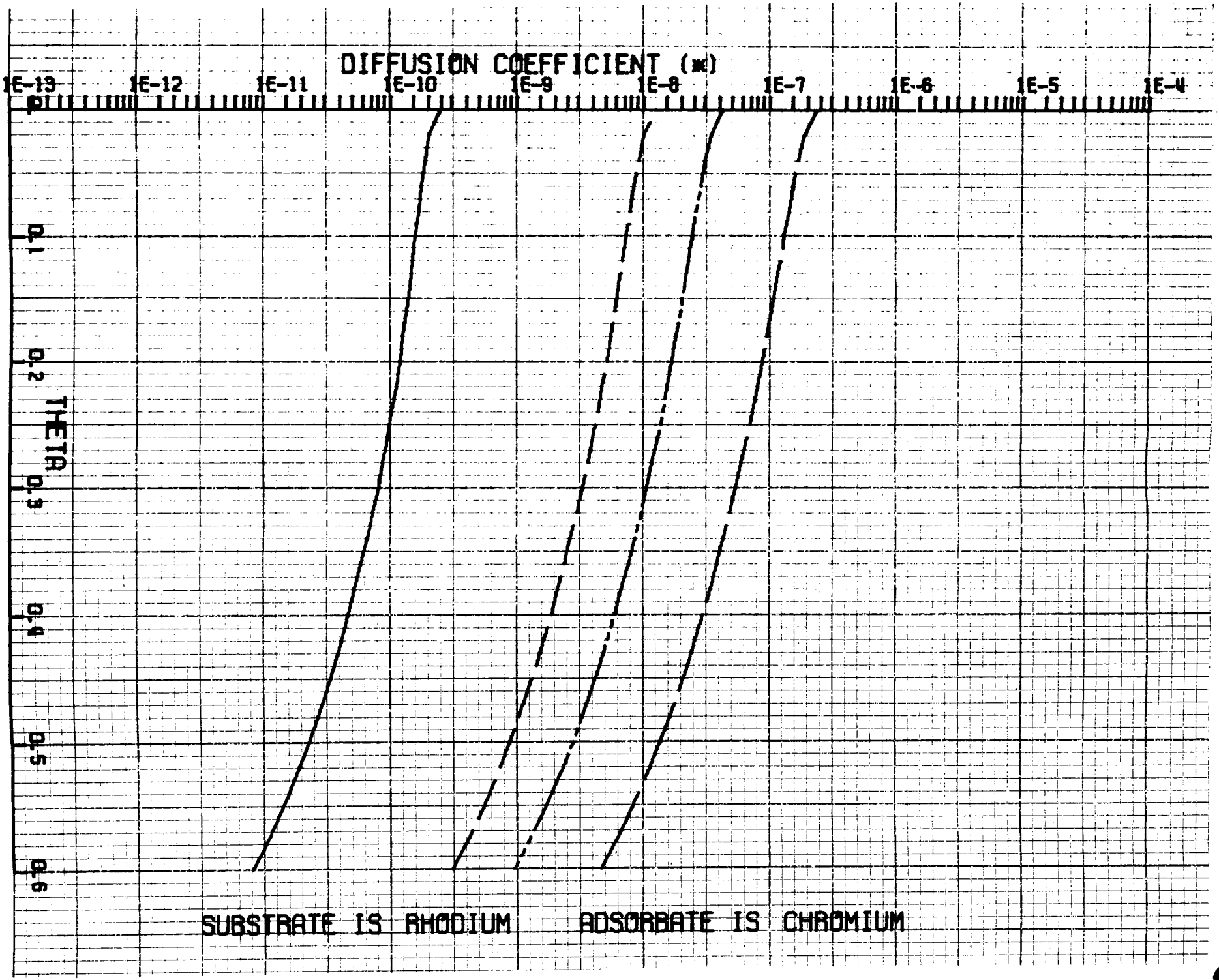
DIFFUSION COEFFICIENT (m)
1E-13
1E-12
1E-11
1E-10
1E-9
1E-8
1E-7
1E-6
1E-5
1E-4
THETA
0.1
0.2
0.3
0.4
0.5
0.6
SUBSTRATE IS RHODIUM
ADSORBATE IS CHROMIUM

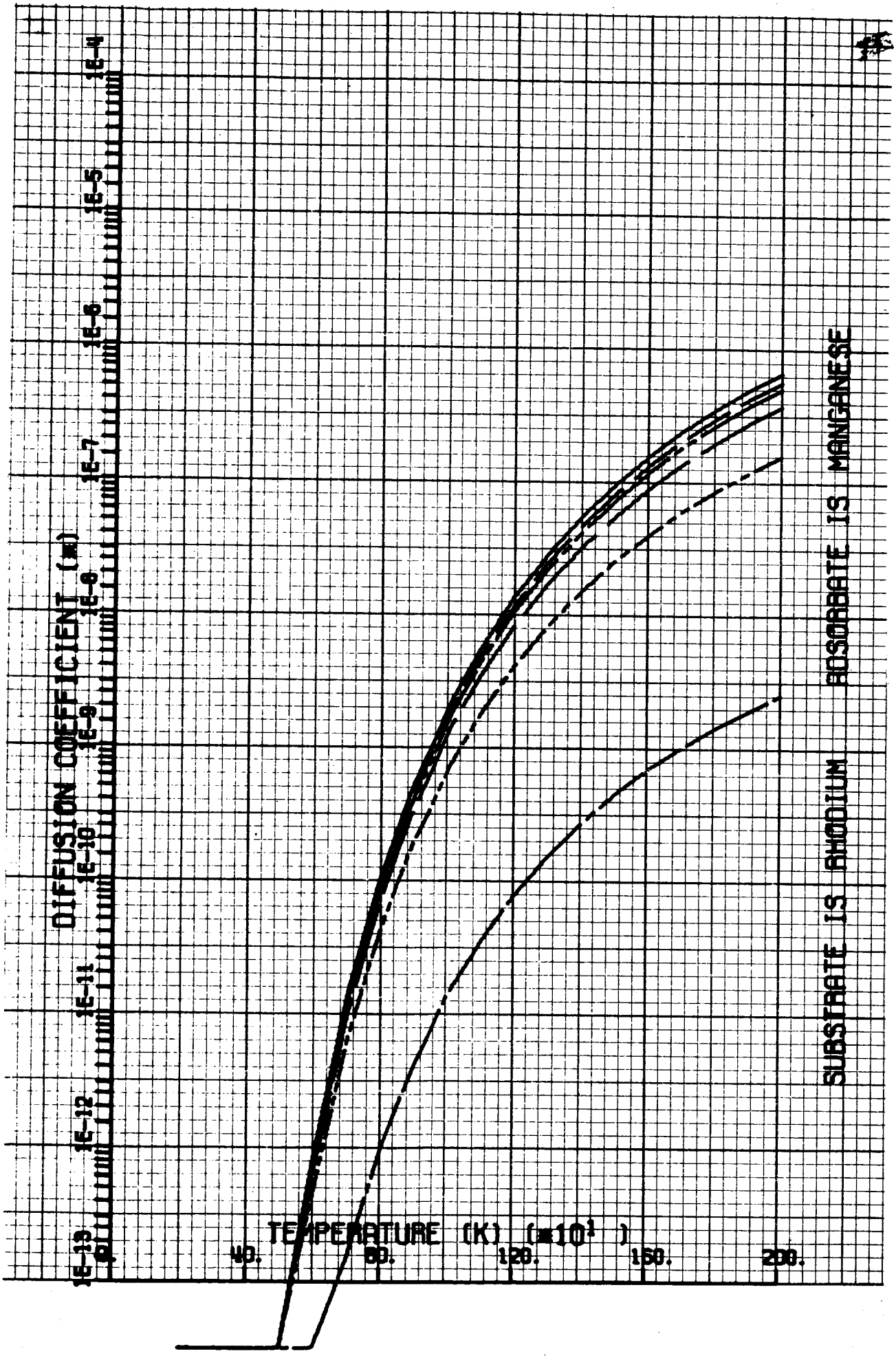
DIFFUSION COEFFICIENT (m)
1E-4
1E-5
1E-6
1E-7
1E-8
1E-9
1E-10
1E-11
1E-12
1E-13
TEMPERATURE (K) (×10¹)
40.
80.
120.
160.
200.
SUBSTRATE IS RHODIUM ADSORBATE IS MANGANESE

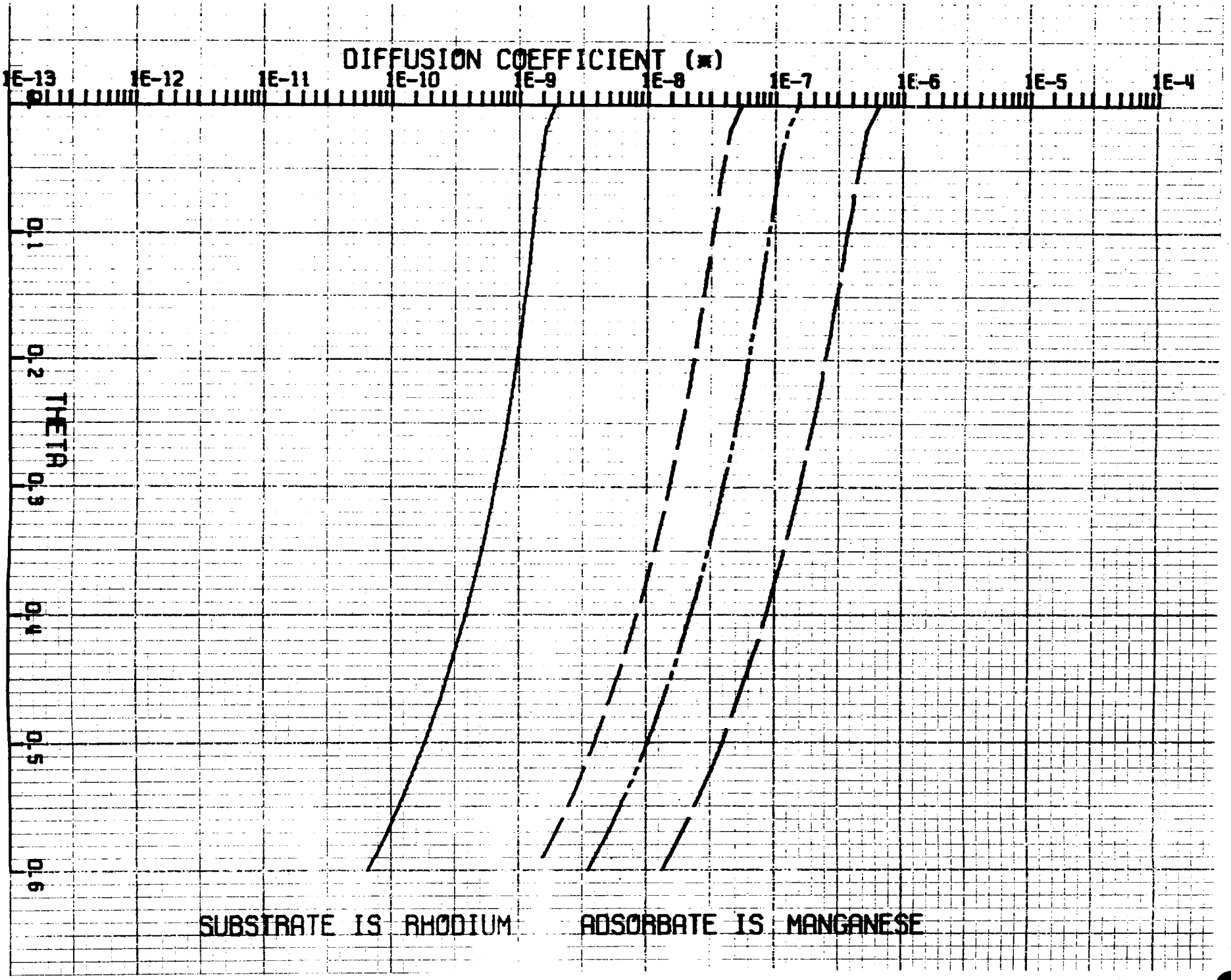
DIFFUSION COEFFICIENT (*)
1E-13
1E-12
1E-11
1E-10
1E-9
1E-8
1E-7
1E-6
1E-5
1E-4
0
0.1
0.2
0.3
0.4
0.5
0.6
THETA
SUBSTRATE IS RHODIUM
ADSORBATE IS MANGANESE

DIFFUSION COEFFICIENT (cm²)
1E-4
1E-5
1E-6
1E-7
1E-8
1E-9
1E-10
1E-11
1E-12
1E-13
TEMPERATURE (K) (×10¹)
40.
80.
120.
150.
200.
SUBSTRATE IS RHODIUM ADSORBATE IS IRON

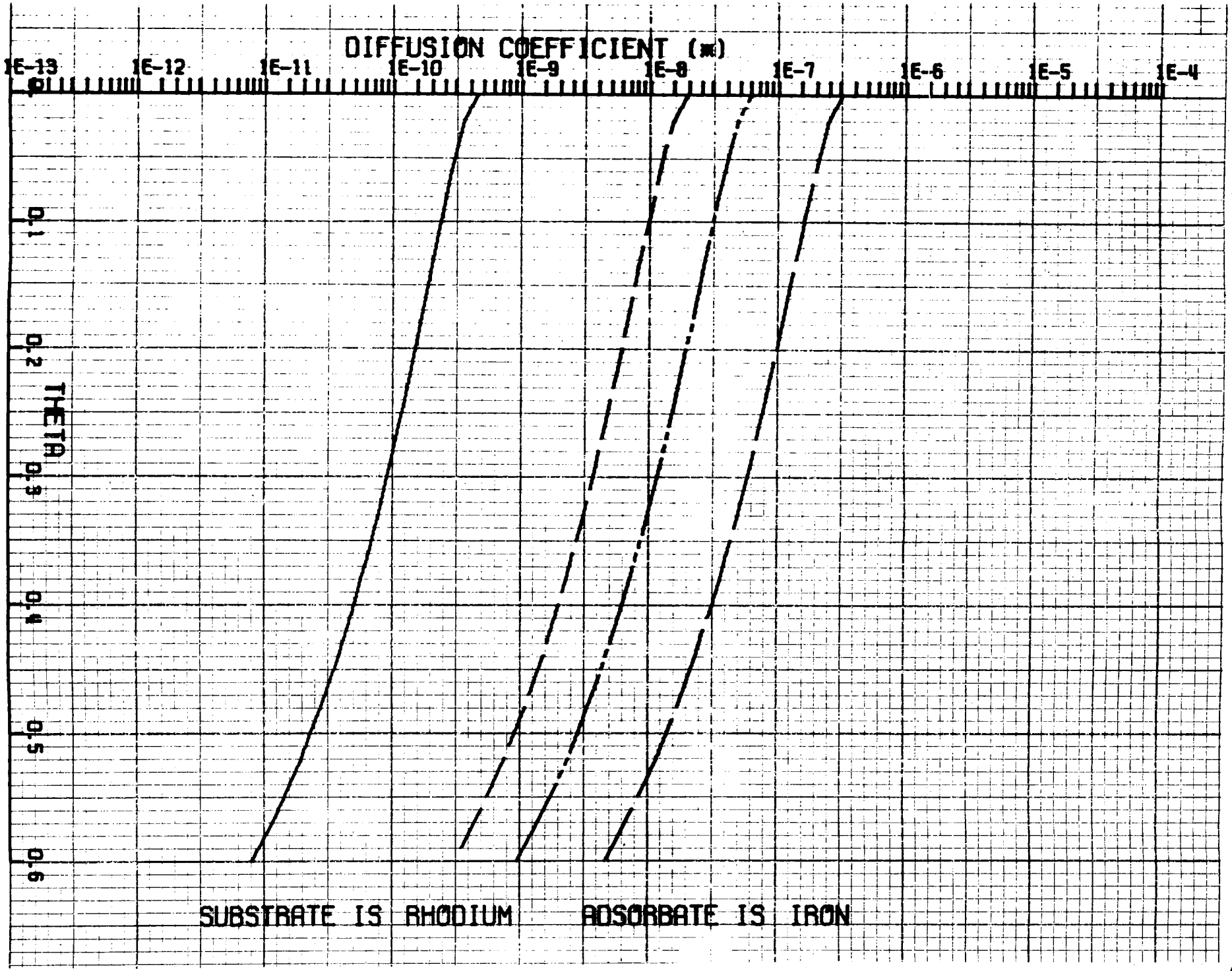
DIFFUSION COEFFICIENT (m)
1E-13
1E-12
1E-11
1E-10
1E-9
1E-8
1E-7
1E-6
1E-5
1E-4
THETA
0.1
0.2
0.3
0.4
0.5
0.6
SUBSTRATE IS RHODIUM ADSORBATE IS IRON

D
DIFFUSION COEFFICIENT (m²)
1E-4
1E-5
1E-6
1E-7
1E-8
1E-9
1E-10
1E-11
1E-12
1E-13
0.
40.
80.
120.
160.
200.
TEMPERATURE (K) (×10¹)
SUBSTRATE IS RHODIUM ADSORBATE IS NICKEL

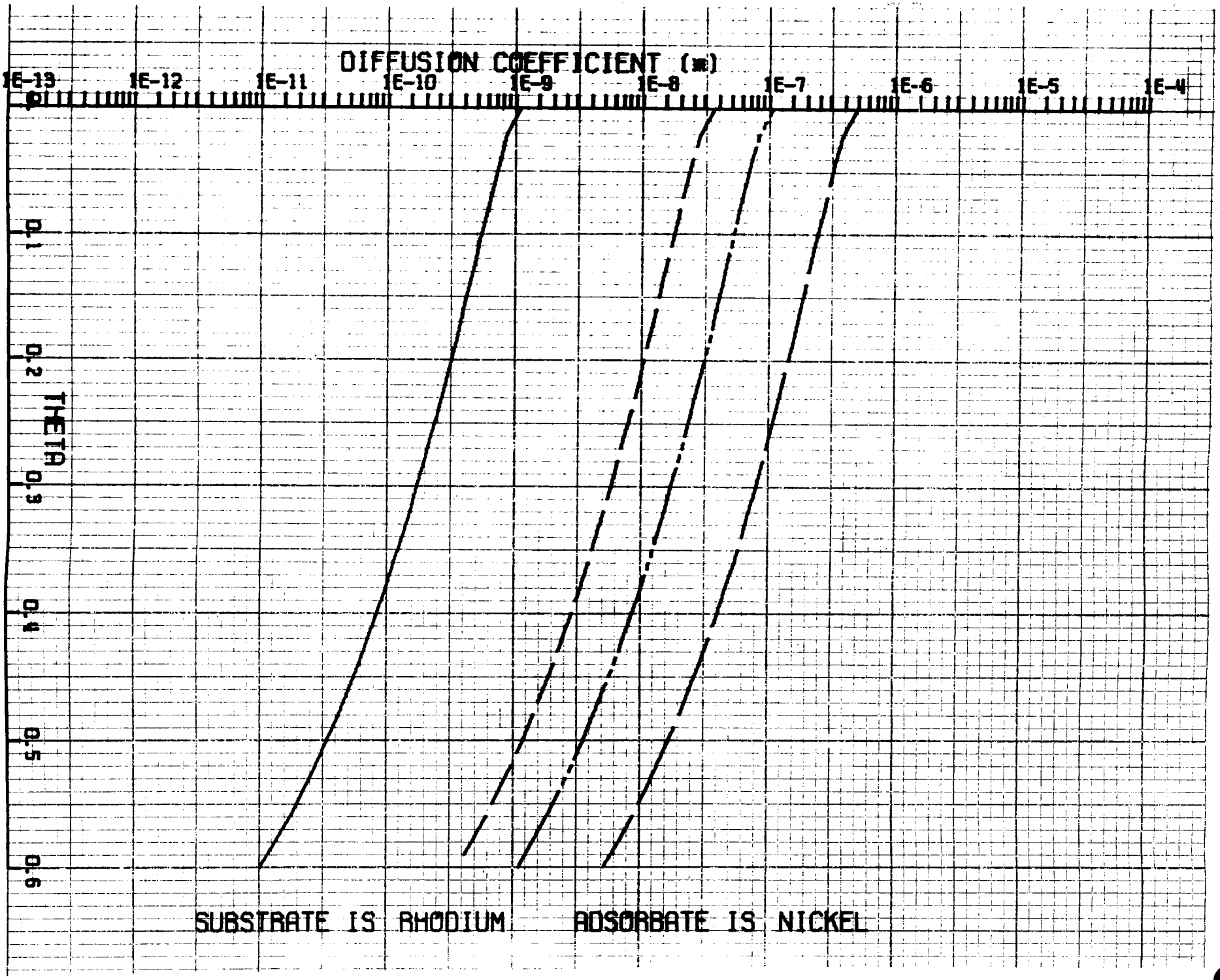
DIFFUSION COEFFICIENT (m)
1E-13
1E-12
1E-11
1E-10
1E-9
1E-8
1E-7
1E-6
1E-5
1E-4
THETA
0
0.1
0.2
0.3
0.4
0.5
0.6
SUBSTRATE IS RHODIUM
ADSORBATE IS NICKEL

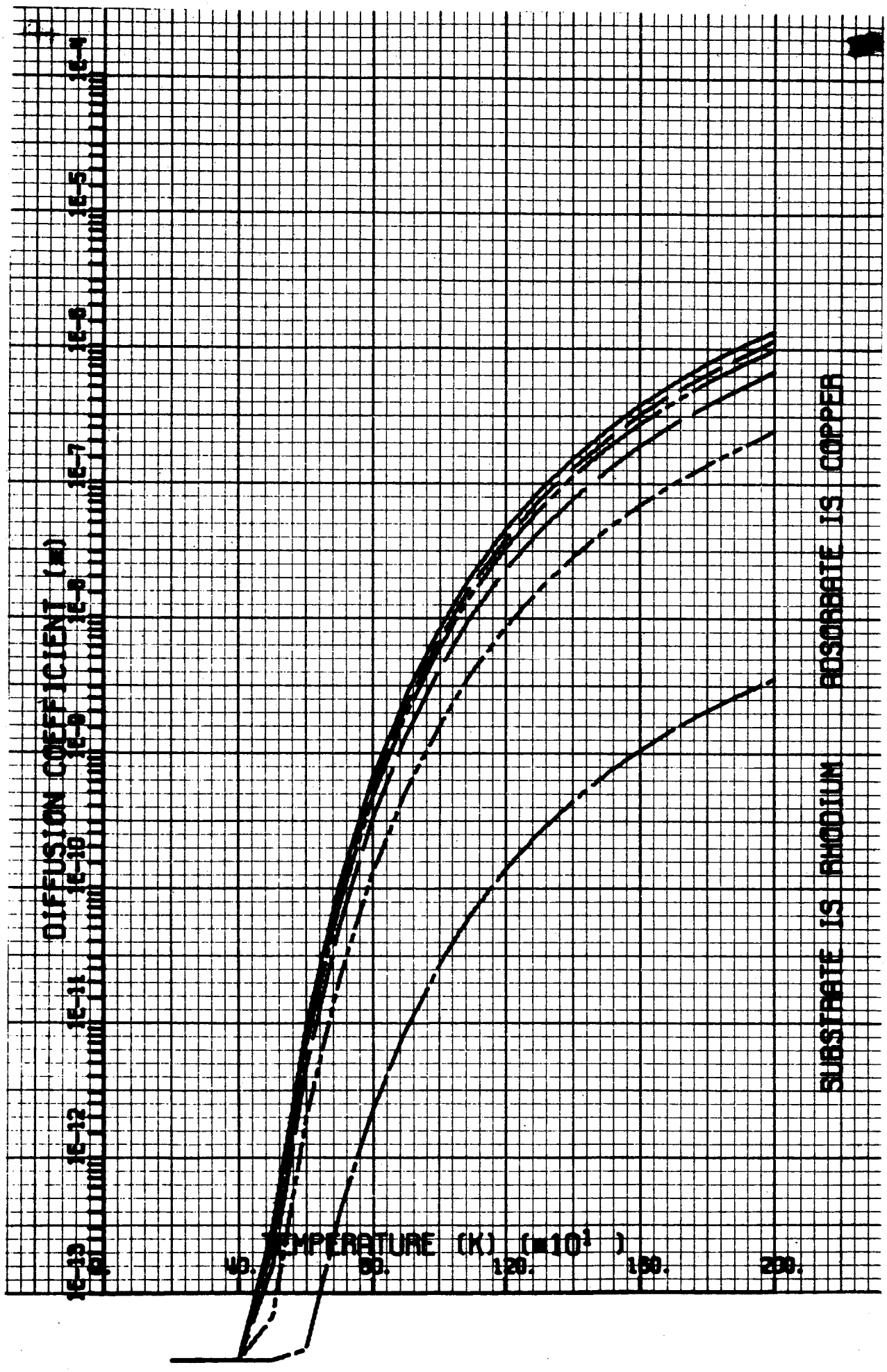
DIFFUSION COEFFICIENT (M)
1E-4
1E-5
1E-6
1E-7
1E-8
1E-9
1E-10
1E-11
1E-12
1E-13
TEMPERATURE (K) (=10²)
40.
80.
120.
160.
200.
SUBSTRATE IS RHODIUM ADSORBATE IS COPPER

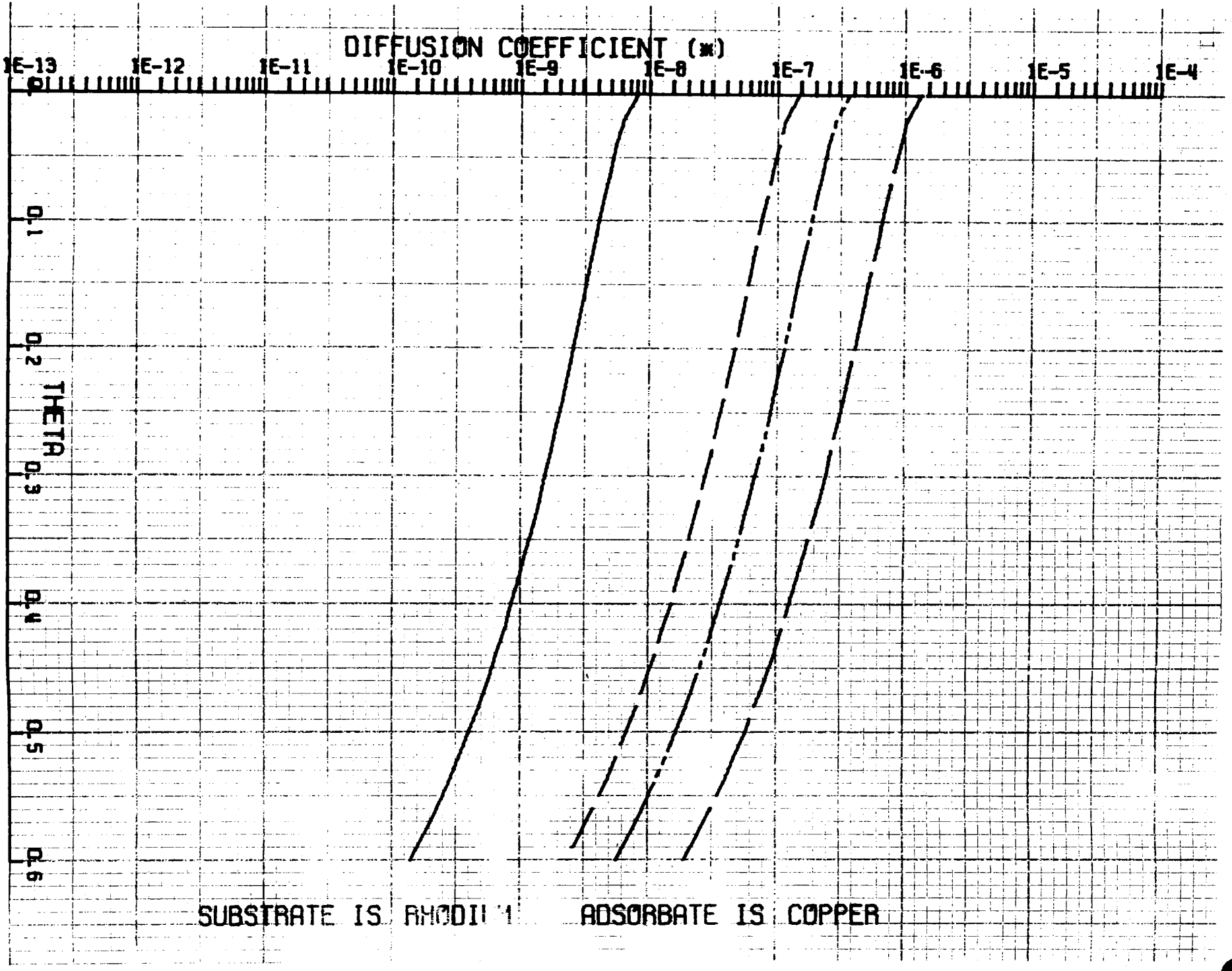
DIFFUSION COEFFICIENT (*)
1E-13
1E-12
1E-11
1E-10
1E-9
1E-8
1E-7
1E-6
1E-5
1E-4
THETA
0.1
0.2
0.3
0.4
0.5
0.6
SUBSTRATE IS RHODIUM
ADSORBATE IS COPPER

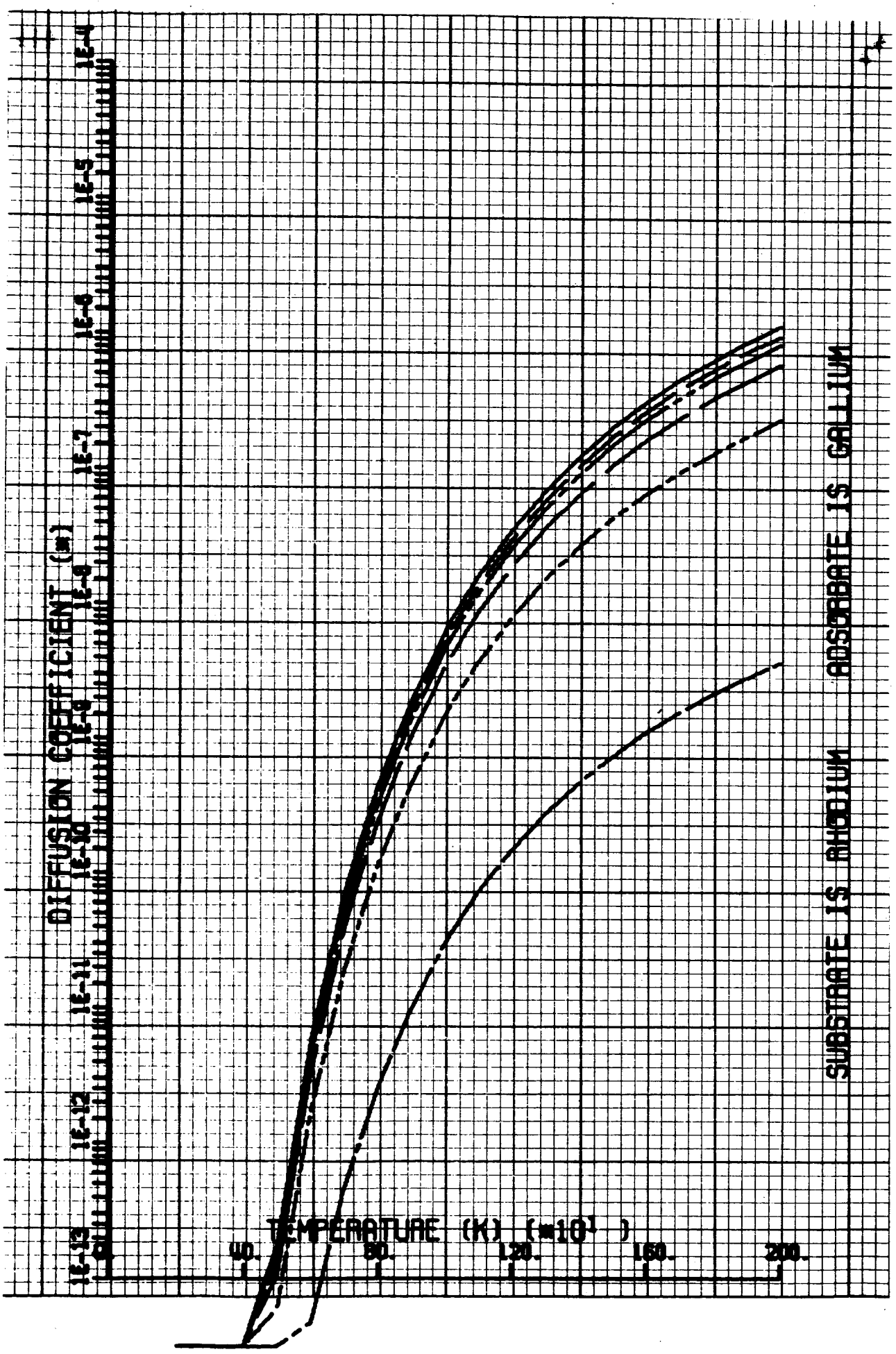
DIFFUSION COEFFICIENT (m²)
1E-13
1E-12
1E-11
1E-10
1E-9
1E-8
1E-7
1E-6
1E-5
1E-4
TEMPERATURE (K) (*10¹)
40.
80.
120.
160.
200.
SUBSTRATE IS RHODIUM ADSORBATE IS GALLIUM

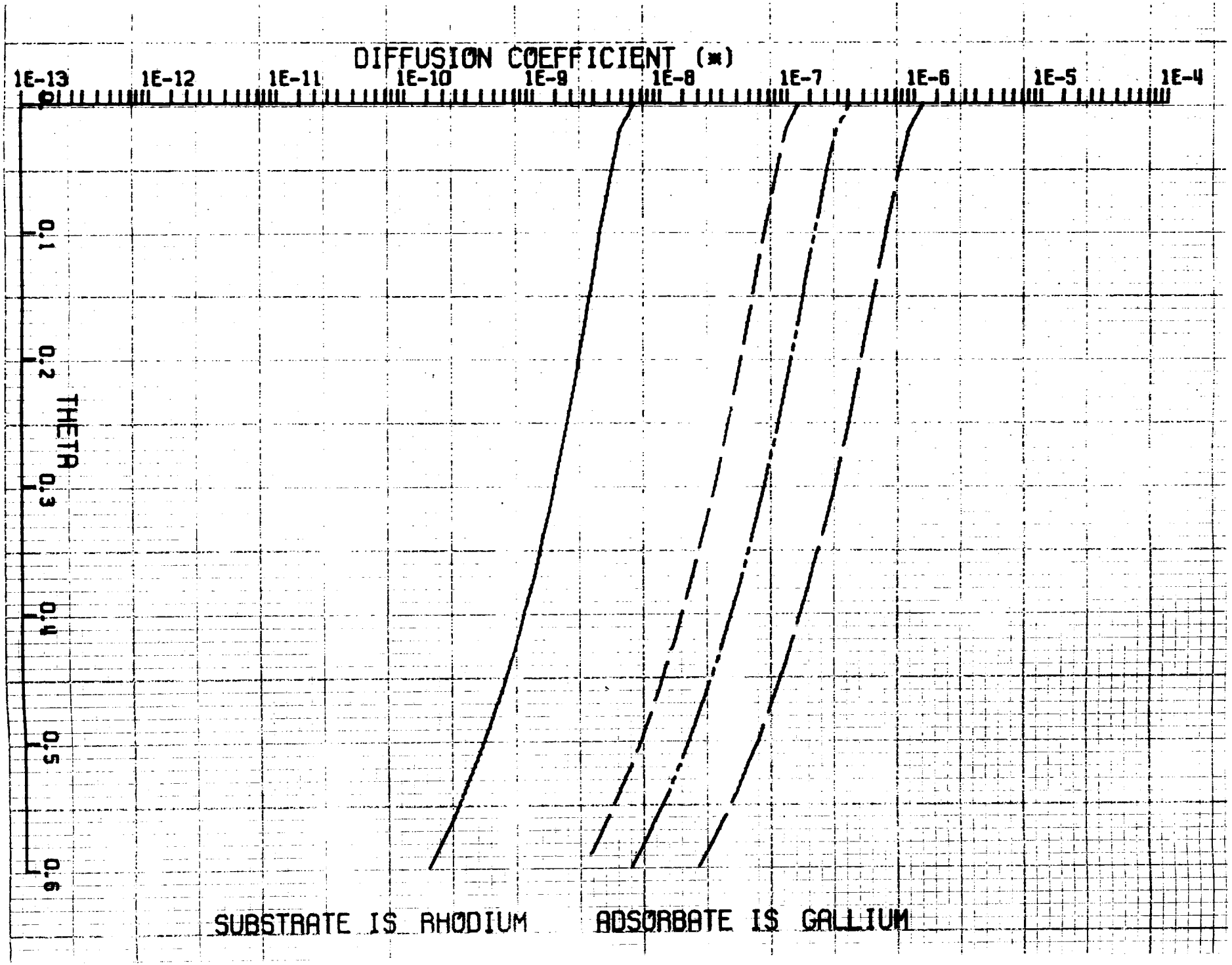
DIFFUSION COEFFICIENT (*)
1E-13
1E-12
1E-11
1E-10
1E-9
1E-8
1E-7
1E-6
1E-5
1E-4
THETA
0.1
0.2
0.3
0.4
0.5
0.6
SUBSTRATE IS RHODIUM
ADSORBATE IS GALLIUM

SUBSTRATE IS RHODIUM ADSORBATE IS RUBIDIUM
DIFFUSION COEFFICIENT (m²)
1E-4
1E-5
1E-6
1E-7
1E-8
1E-9
1E-10
1E-11
1E-12
1E-13
TEMPERATURE (K) (*10¹)
40.
80.
120.
160.
200.

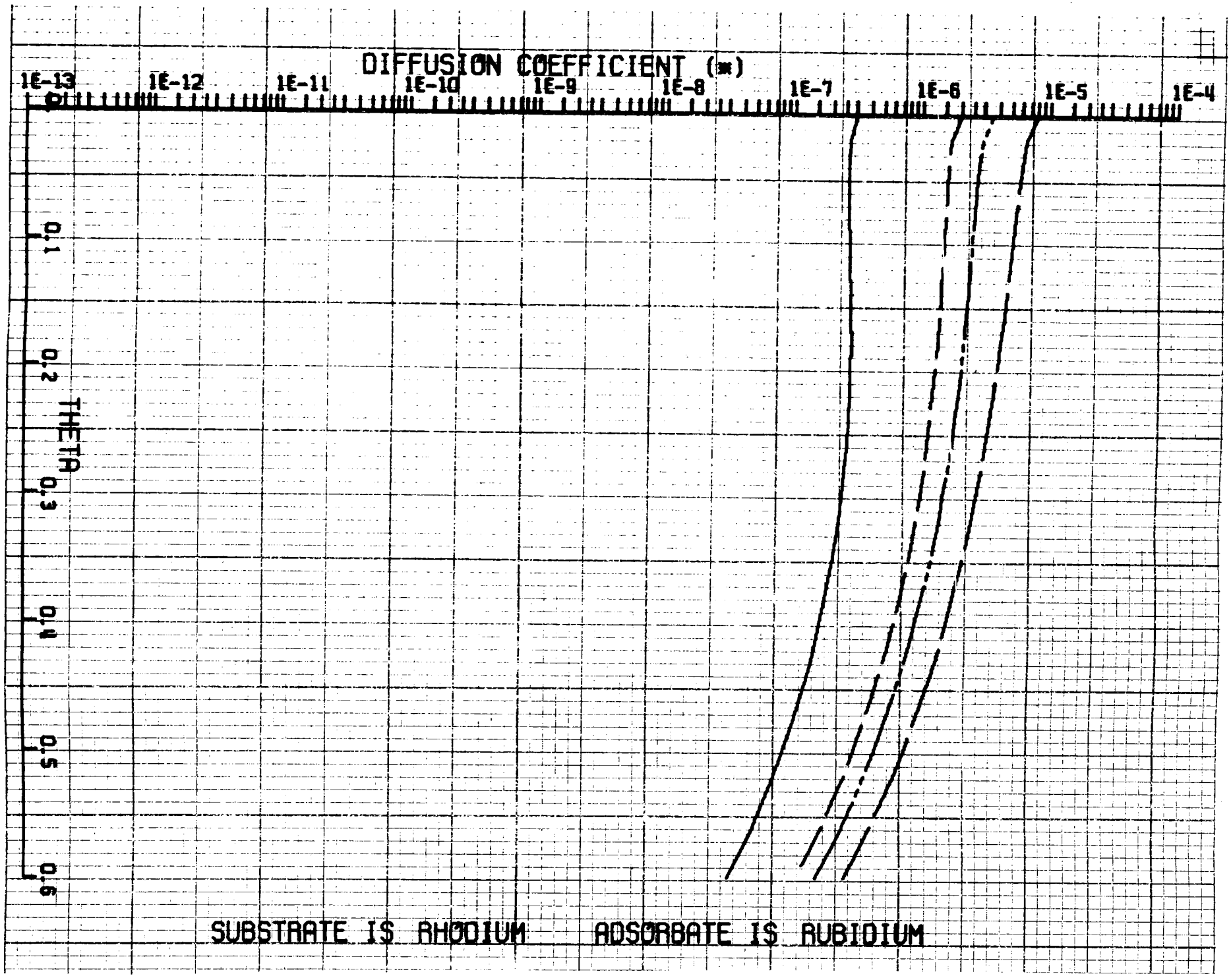
DIFFUSION COEFFICIENT (*)
1E-13
1E-12
1E-11
1E-10
1E-9
1E-8
1E-7
1E-6
1E-5
1E-4
THETA
0.1
0.2
0.3
0.4
0.5
0.6
SUBSTRATE IS RHODIUM ADSORBATE IS RUBIDIUM

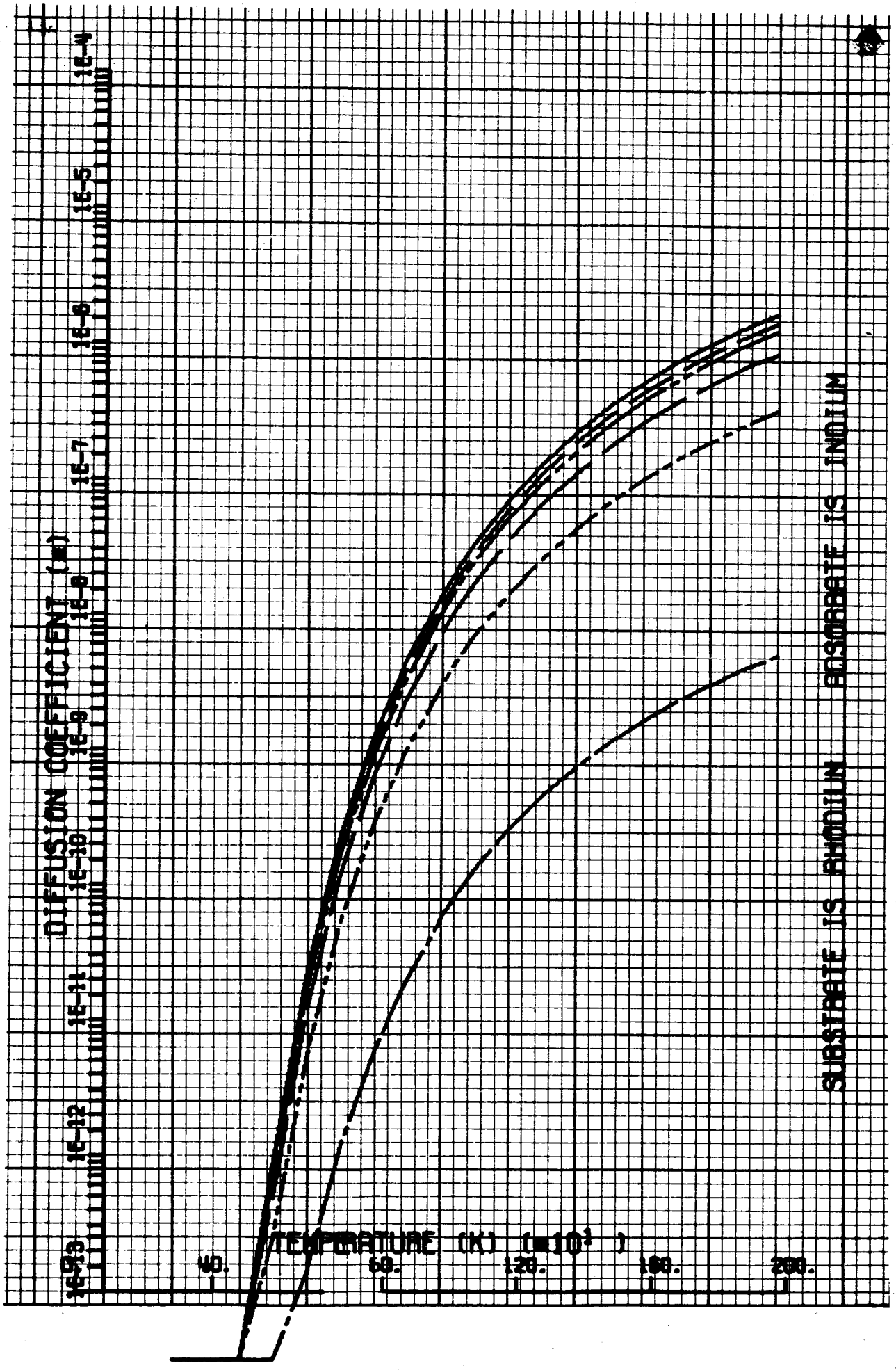
DIFFUSION COEFFICIENT (m²)
1E-4
1E-5
1E-6
1E-7
1E-8
1E-9
1E-10
1E-11
1E-12
1E-13
TEMPERATURE (K) (*10¹)
40.
60.
120.
160.
200.
SUBSTRATE IS RHODIUM ADSORBATE IS INDIUM

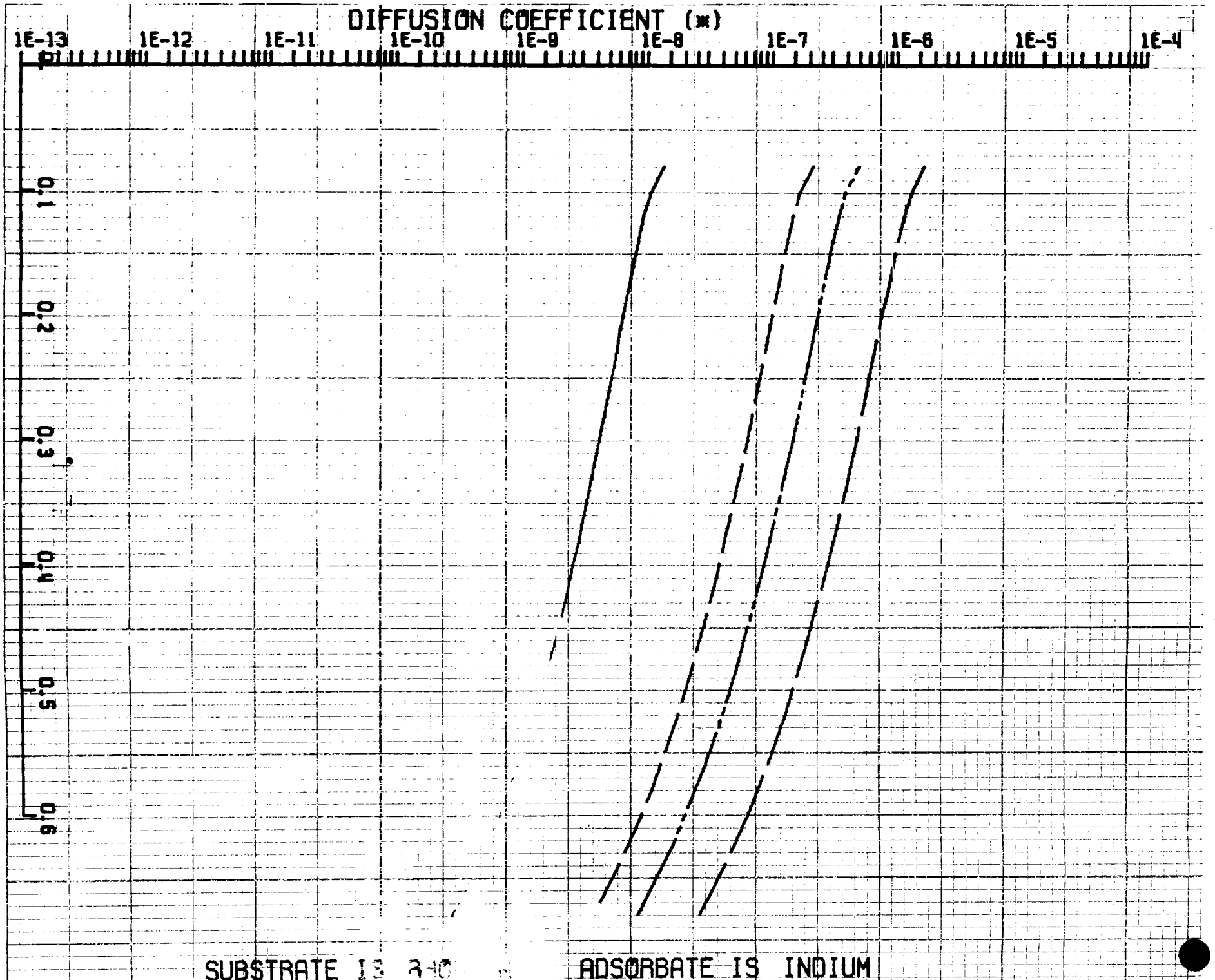
DIFFUSION COEFFICIENT (*)
1E-13
1E-12
1E-11
1E-10
1E-9
1E-8
1E-7
1E-6
1E-5
1E-4
0.1
0.2
0.3
0.4
0.5
0.6
SUBSTRATE IS
ADSORBATE IS INDIUM

DIFFUSION COEFFICIENT (m²)
1E-4
1E-5
1E-6
1E-7
1E-8
1E-9
1E-10
1E-11
1E-12
1E-13
0.
40.
80.
120.
160.
200.
TEMPERATURE (K) (×10¹)
SUBSTRATE IS RHODIUM ADSORBATE IS TIN

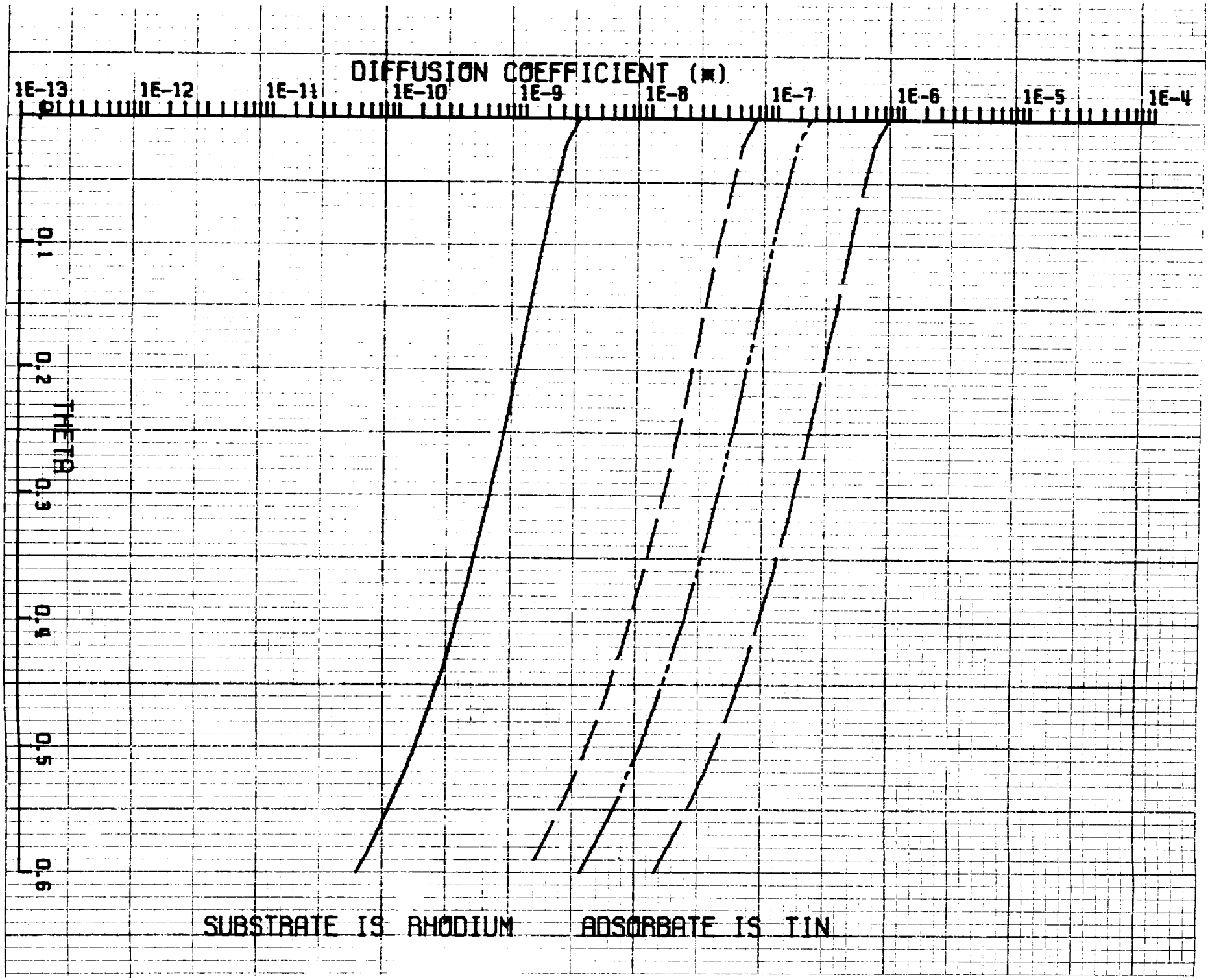
DIFFUSION COEFFICIENT (*)
1E-13
1E-12
1E-11
1E-10
1E-9
1E-8
1E-7
1E-6
1E-5
1E-4
0
0.1
0.2
0.3
0.4
0.5
0.6
THETA
SUBSTRATE IS RHODIUM
ADSORBATE IS TIN

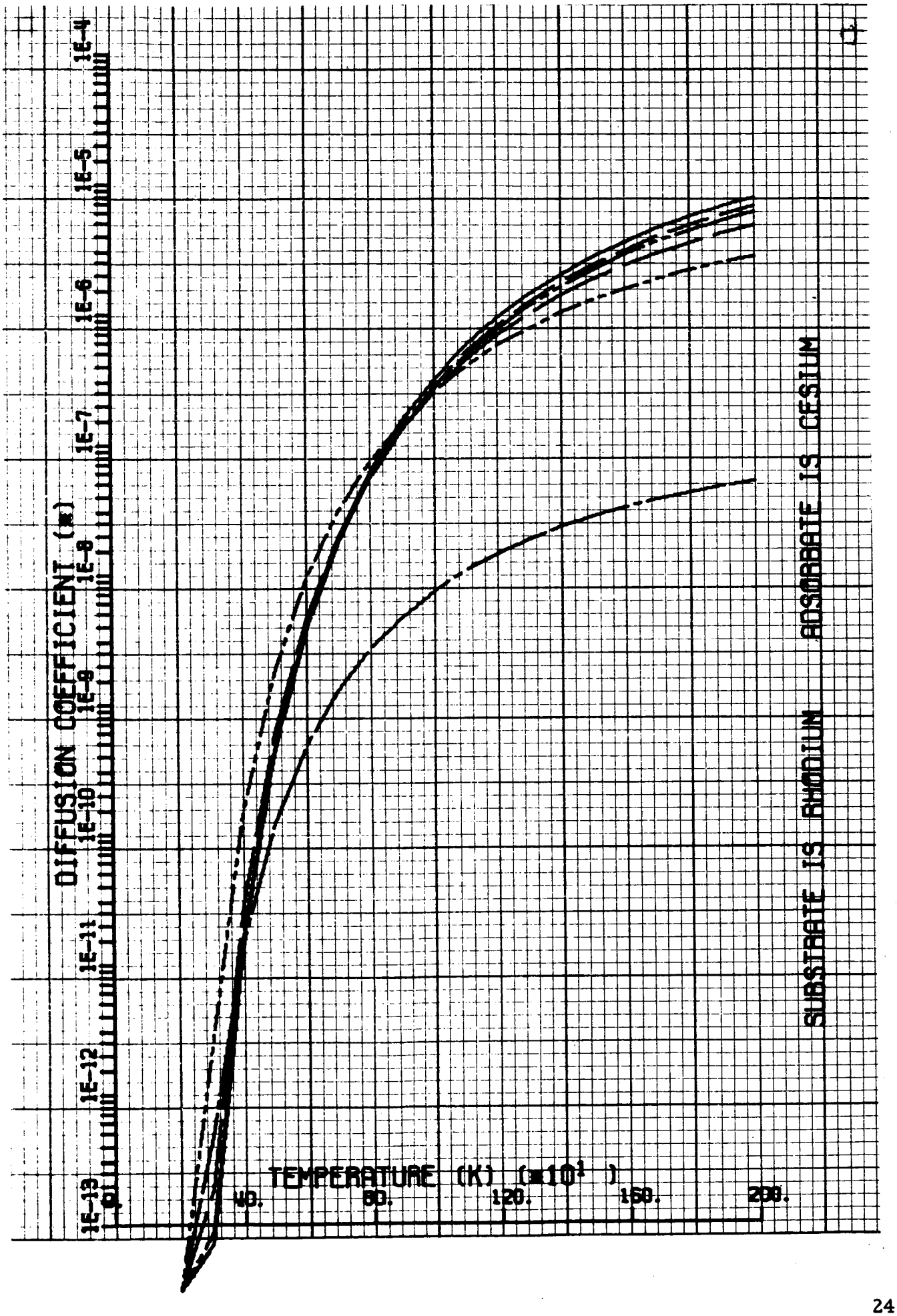
DIFFUSION COEFFICIENT (m)
1E-4
1E-5
1E-6
1E-7
1E-8
1E-9
1E-10
1E-11
1E-12
1E-13
TEMPERATURE (K) (×10¹)
40.
80.
120.
160.
200.
SUBSTRATE IS RHODIUM ADSORBATE IS CESIUM

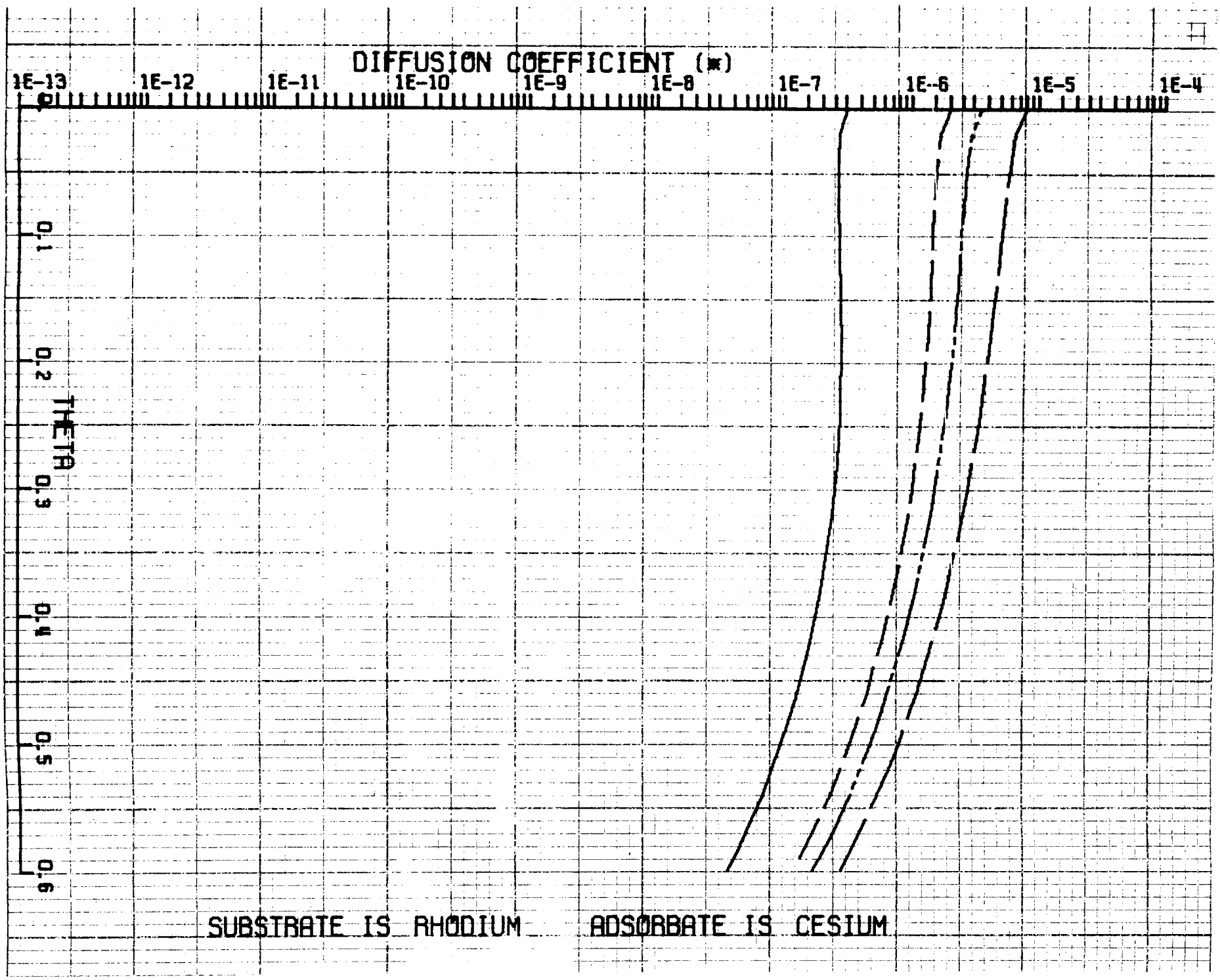
DIFFUSION COEFFICIENT (*)
1E-13
1E-12
1E-11
1E-10
1E-9
1E-8
1E-7
1E-6
1E-5
1E-4
0
0.1
0.2
0.3
0.4
0.5
0.6
THETA
SUBSTRATE IS RHODIUM
ADSORBATE IS CESIUM

DIFFUSION COEFFICIENT (m²)
1E-4
1E-5
1E-6
1E-7
1E-8
1E-9
1E-10
1E-11
1E-12
1E-13
TEMPERATURE (K) (×10¹)
40.
80.
120.
160.
200.
SUBSTRATE IS RHODIUM ADSORBATE IS BARIUM

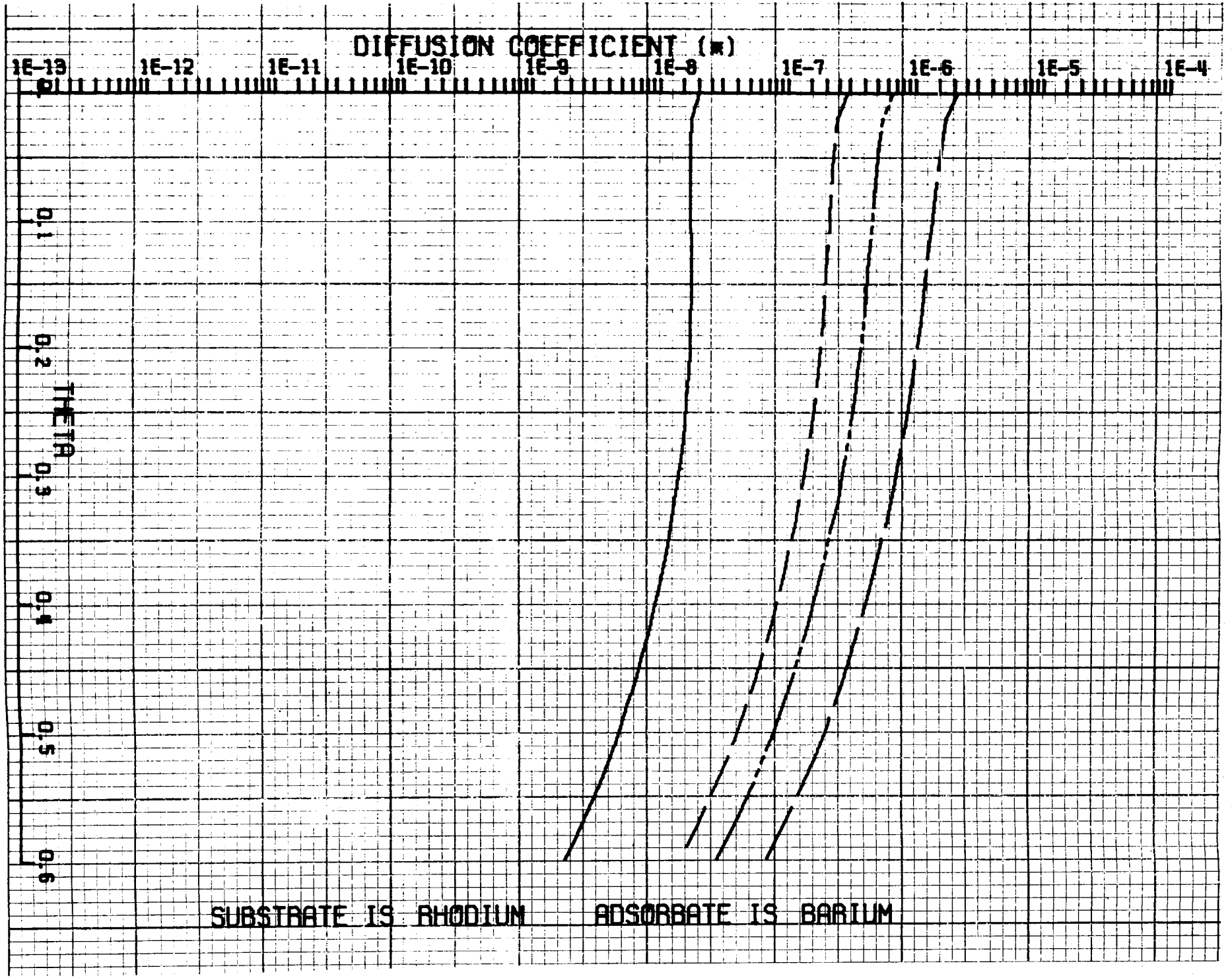
DIFFUSION COEFFICIENT (m)
1E-13
1E-12
1E-11
1E-10
1E-9
1E-8
1E-7
1E-6
1E-5
1E-4
THETA
0.1
0.2
0.3
0.4
0.5
0.6
SUBSTRATE IS RHODIUM
ADSORBATE IS BARIUM

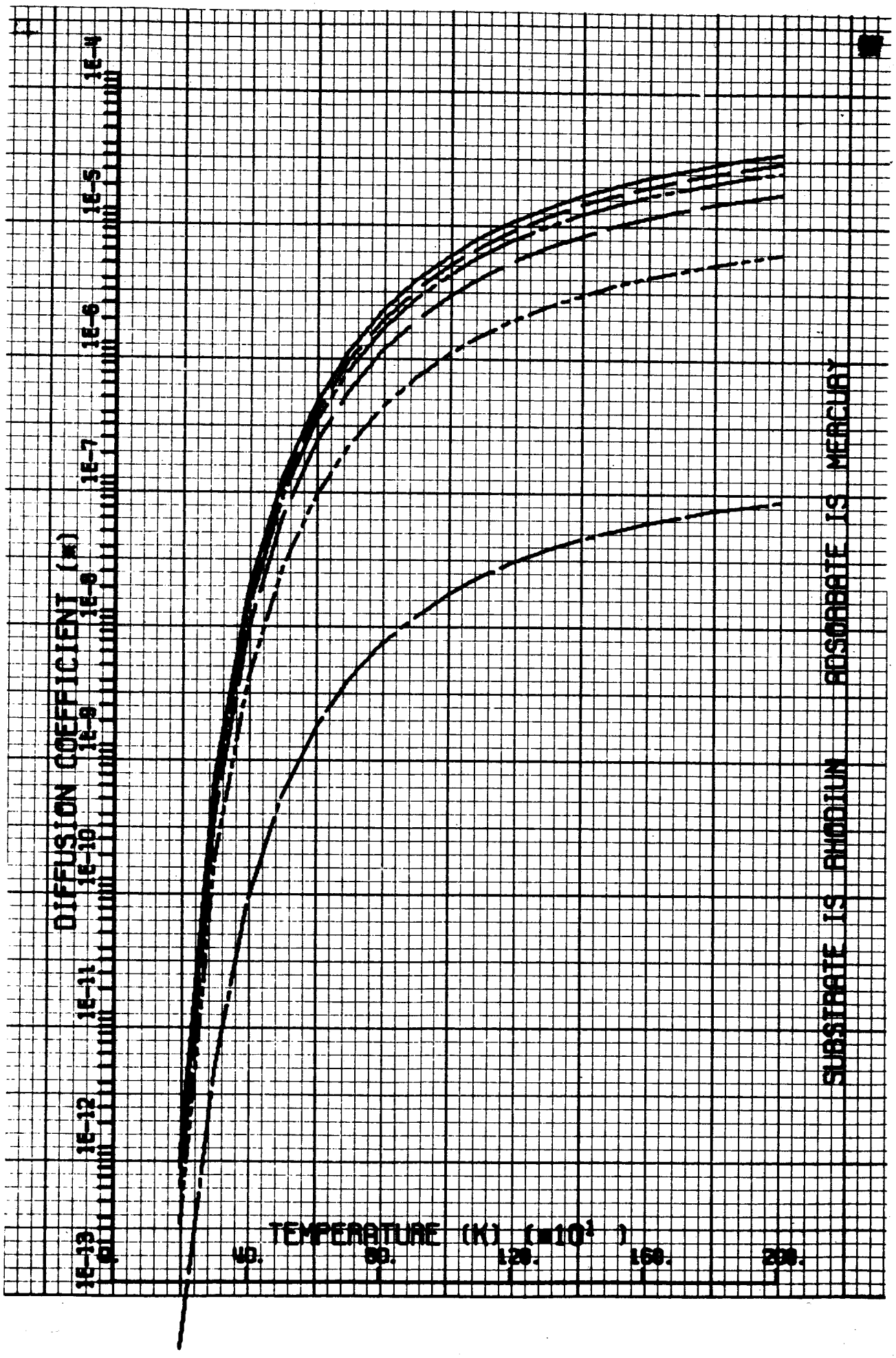
DIFFUSION COEFFICIENT (m²)
1E-4
1E-5
1E-6
1E-7
1E-8
1E-9
1E-10
1E-11
1E-12
1E-13
TEMPERATURE (K) (=10¹)
40.
80.
120.
160.
200.
SUBSTRATE IS RHODIUM ADSORBATE IS MERCURY

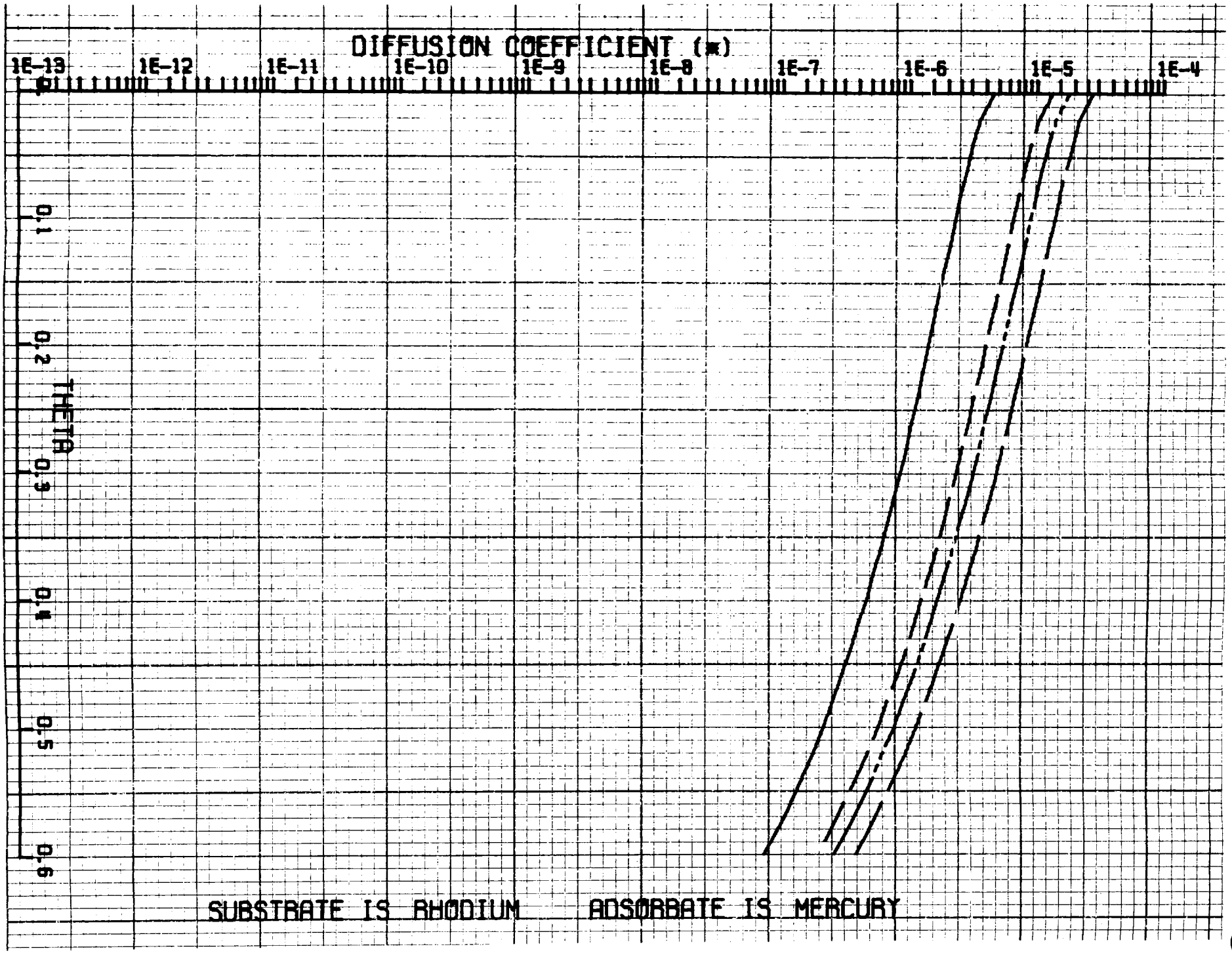
DIFFUSION COEFFICIENT (*)
1E-13
1E-12
1E-11
1E-10
1E-9
1E-8
1E-7
1E-6
1E-5
1E-4
THETA
0.1
0.2
0.3
0.4
0.5
0.6
SUBSTRATE IS RHODIUM
ADSORBATE IS MERCURY

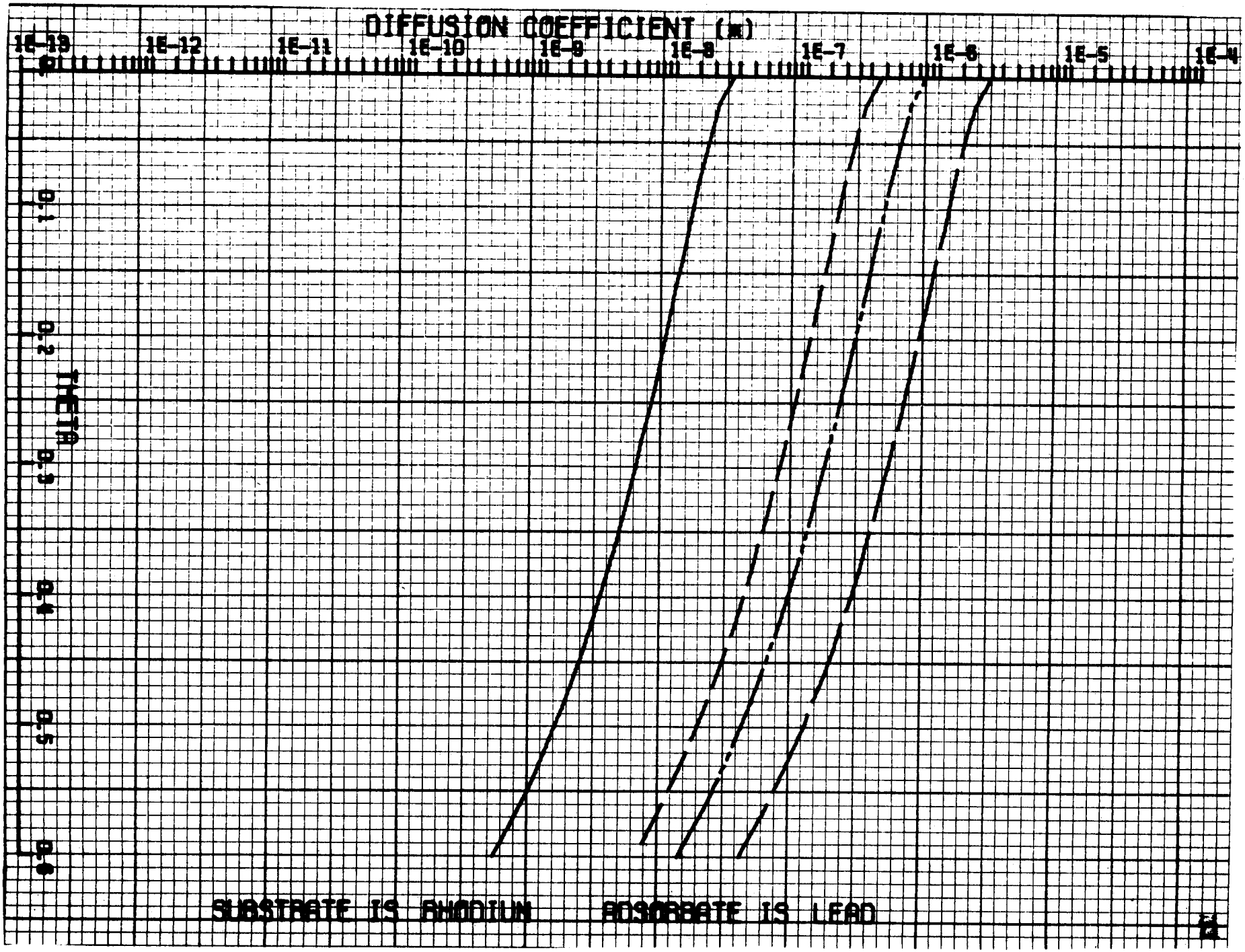
DIFFUSION COEFFICIENT (m)
1E-13
1E-12
1E-11
1E-10
1E-9
1E-8
1E-7
1E-6
1E-5
1E-4
0.1
0.2
0.3
0.4
0.5
0.6
SUBSTRATE IS RHODIUM
SUBSTRATE IS LEAD

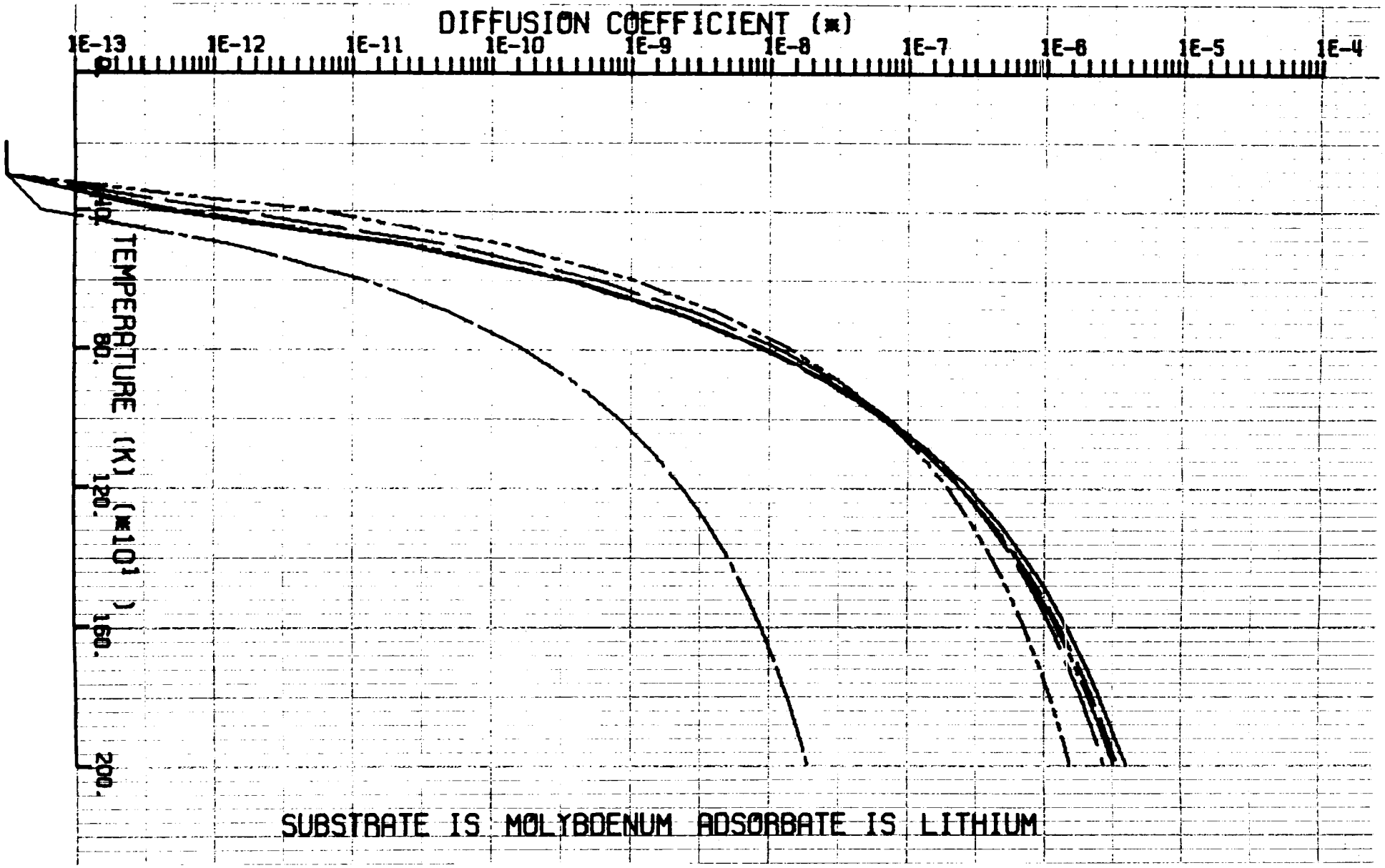
DIFFUSION COEFFICIENT (*)
1E-13
1E-12
1E-11
1E-10
1E-9
1E-8
1E-7
1E-6
1E-5
1E-4
TEMPERATURE (K) (*10^1)
80.
120.
160.
200.
SUBSTRATE IS MOLYBDENUM ADSORBATE IS LITHIUM

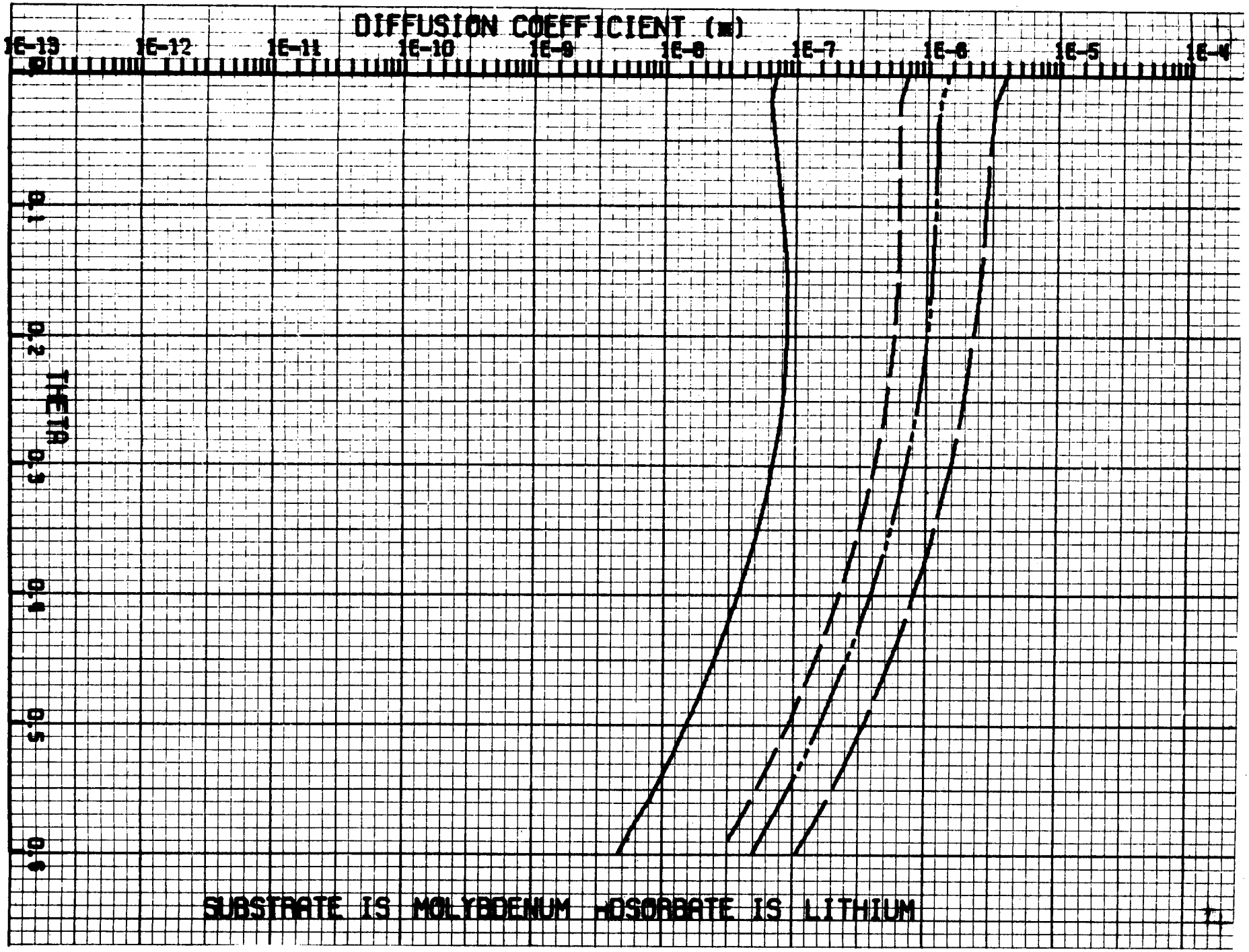
DIFFUSION COEFFICIENT (m)
1E-13
1E-12
1E-11
1E-10
1E-9
1E-8
1E-7
1E-6
1E-5
1E-4
THETA
0.1
0.2
0.3
0.4
0.5
0.6
SUBSTRATE IS MOLYBDENUM ADSORBATE IS LITHIUM

DIFFUSION COEFFICIENT (M)
1E-4
1E-5
1E-6
1E-7
1E-8
1E-9
1E-10
1E-11
1E-12
1E-13
TEMPERATURE (K) (*10¹)
40.
80.
120.
160.
200.
SUBSTRATE IS MOLYBDENUM ADSORBATE IS BERYLLIUM

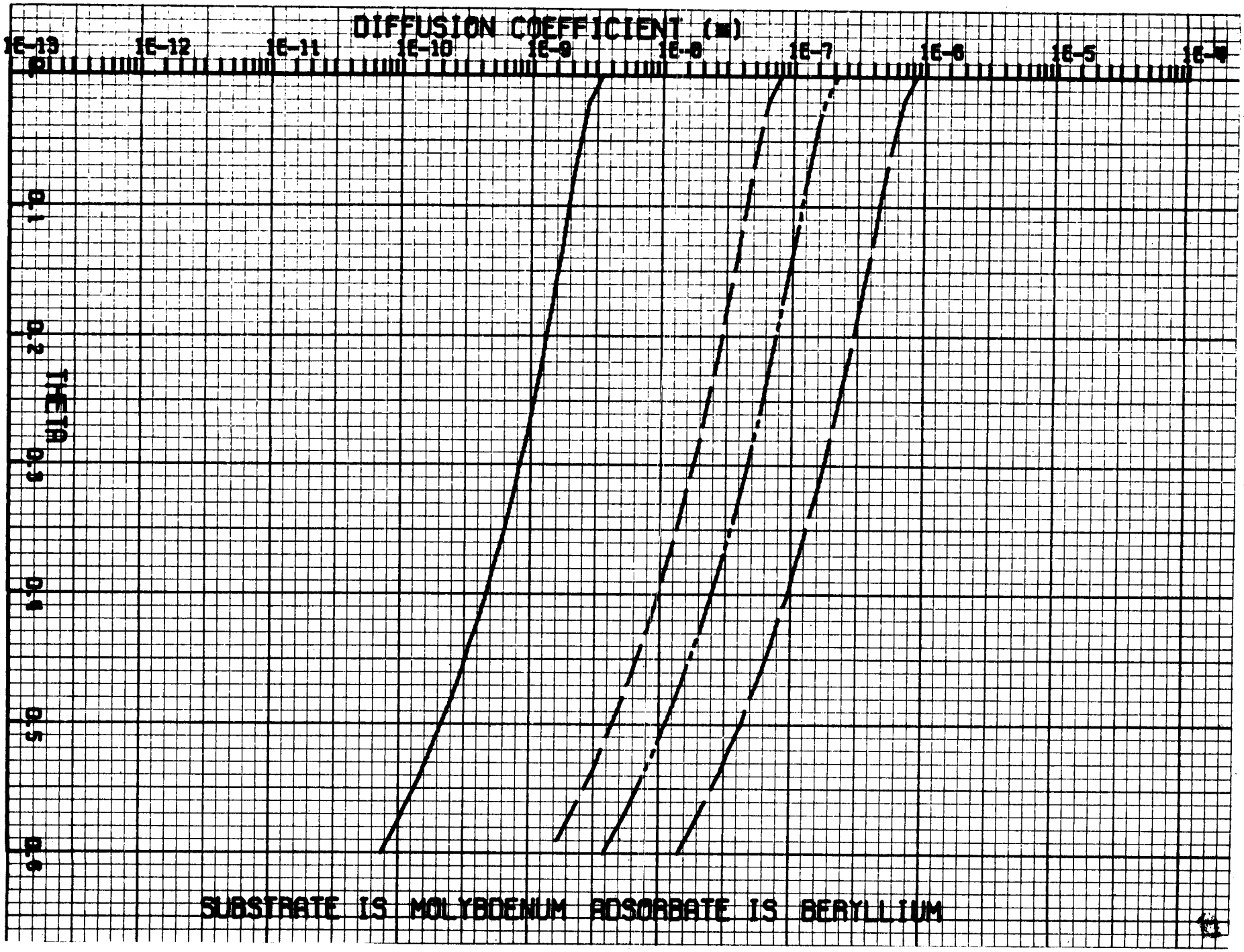
DIFFUSION COEFFICIENT (m)
1E-13
1E-12
1E-11
1E-10
1E-9
1E-8
1E-7
1E-6
1E-5
1E-4
THETA
0.1
0.2
0.3
0.4
0.5
0.6
SUBSTRATE IS MOLYBDENUM ADSORBATE IS BERYLLIUM

DIFFUSION COEFFICIENT (*)
1E-4
1E-5
1E-6
1E-7
1E-8
1E-9
1E-10
1E-11
1E-12
1E-13
TEMPERATURE (K) (*10¹)
40.
120.
160.
200.
SUBSTRATE IS MOLYBDENUM ADSORBATE IS CARBON

DIFFUSION COEFFICIENT (m)
1E-13
1E-12
1E-11
1E-10
1E-9
1E-8
1E-7
1E-6
1E-5
1E-4
0.1
0.2
0.3
0.4
0.5
0.6
THETA
SUBSTRATE IS MOLYBDENUM ADSORBATE IS CARBON

DIFFUSION COEFFICIENT (*)
1E-4
1E-5
1E-6
1E-7
1E-8
1E-9
1E-10
1E-11
1E-12
1E-13
TEMPERATURE (K) (*10¹)
40.
80.
120.
160.
200.
SUBSTRATE IS MOLYBDENUM ADSORBATE IS SODIUM

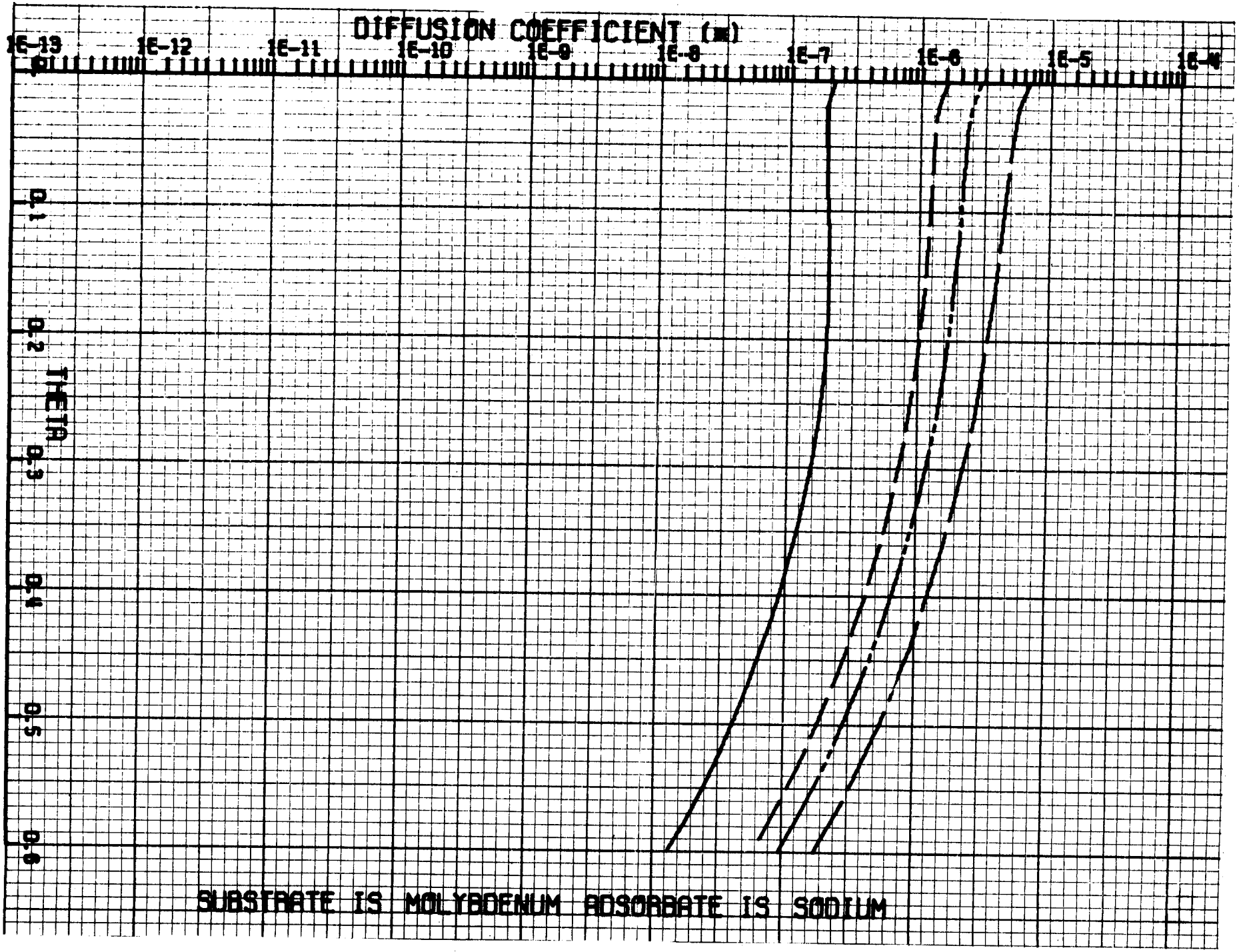
DIFFUSION COEFFICIENT (cm)
1E-13
1E-12
1E-11
1E-10
1E-9
1E-8
1E-7
1E-6
1E-5
1E-4
THETA
0.1
0.2
0.3
0.4
0.5
0.6
SUBSTRATE IS MOLYBDENUM ADSORBATE IS SODIUM

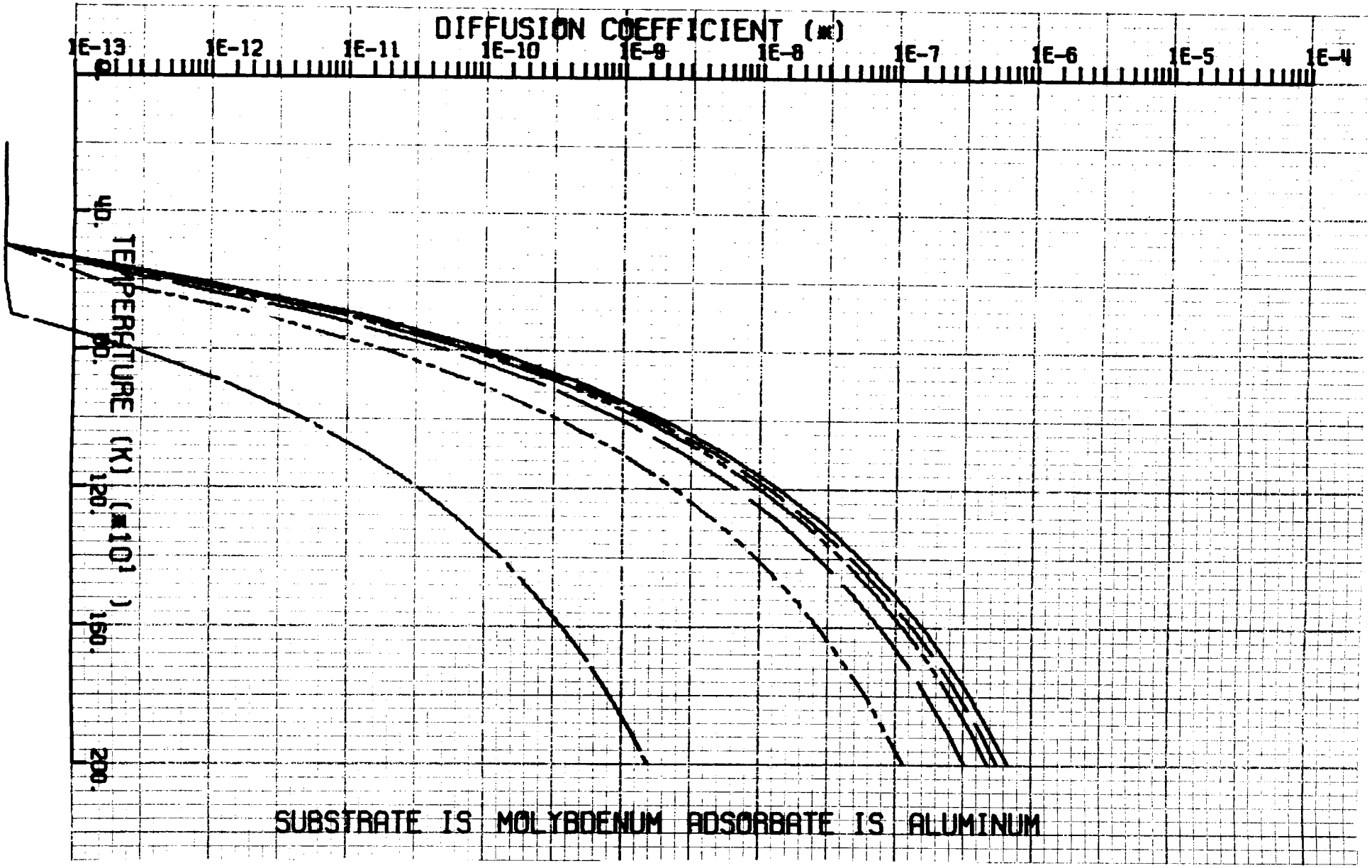
DIFFUSION COEFFICIENT (*)
1E-13
1E-12
1E-11
1E-10
1E-9
1E-8
1E-7
1E-6
1E-5
1E-4
TEMPERATURE (K) (*10¹)
40.
80.
120.
160.
200.
SUBSTRATE IS MOLYBDENUM ADSORBATE IS ALUMINUM

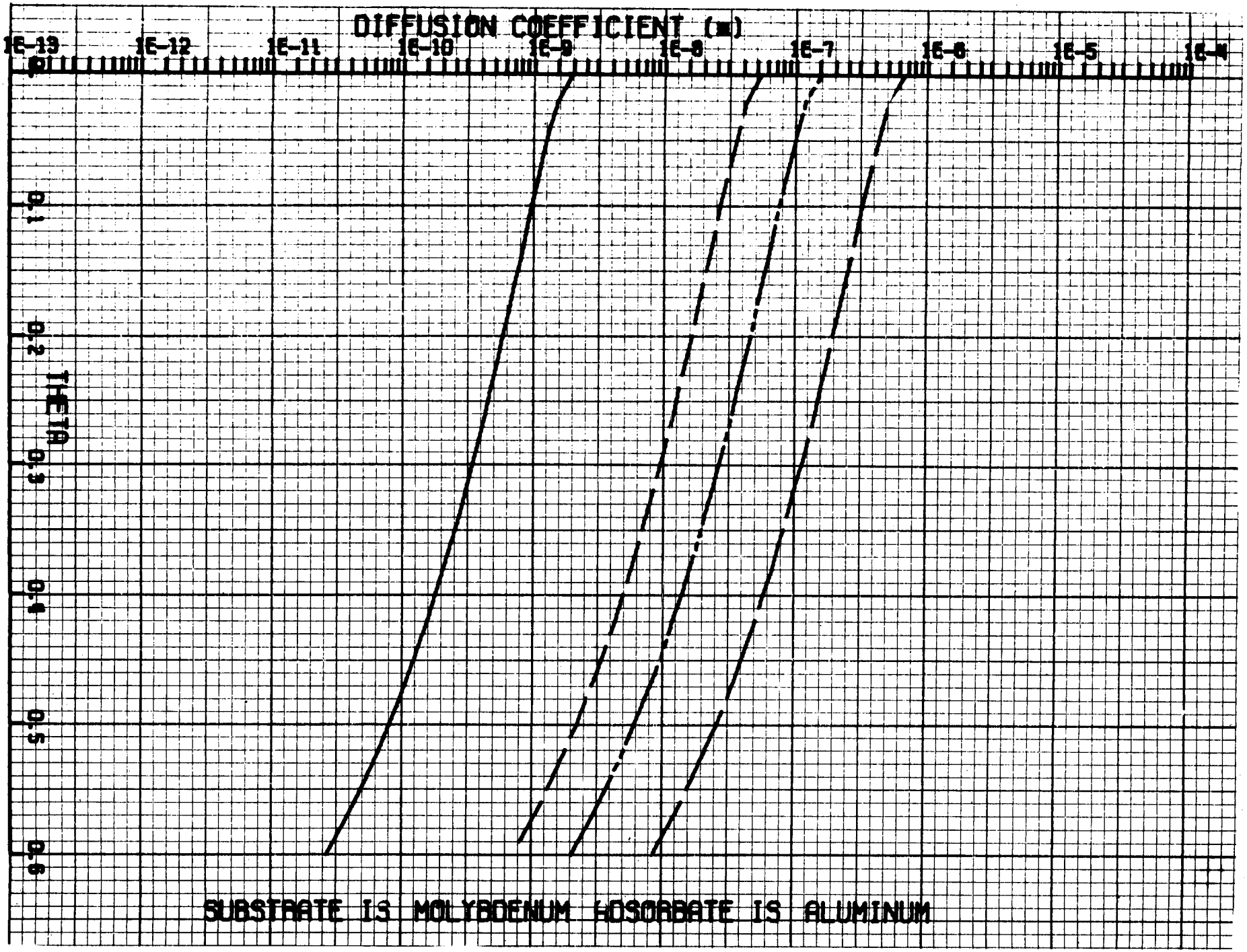
DIFFUSION COEFFICIENT (m)
1E-13
1E-12
1E-11
1E-10
1E-9
1E-8
1E-7
1E-6
1E-5
1E-4
THETA
0.1
0.2
0.3
0.4
0.5
0.6
SUBSTRATE IS MOLYBDENUM ADSORBATE IS ALUMINUM

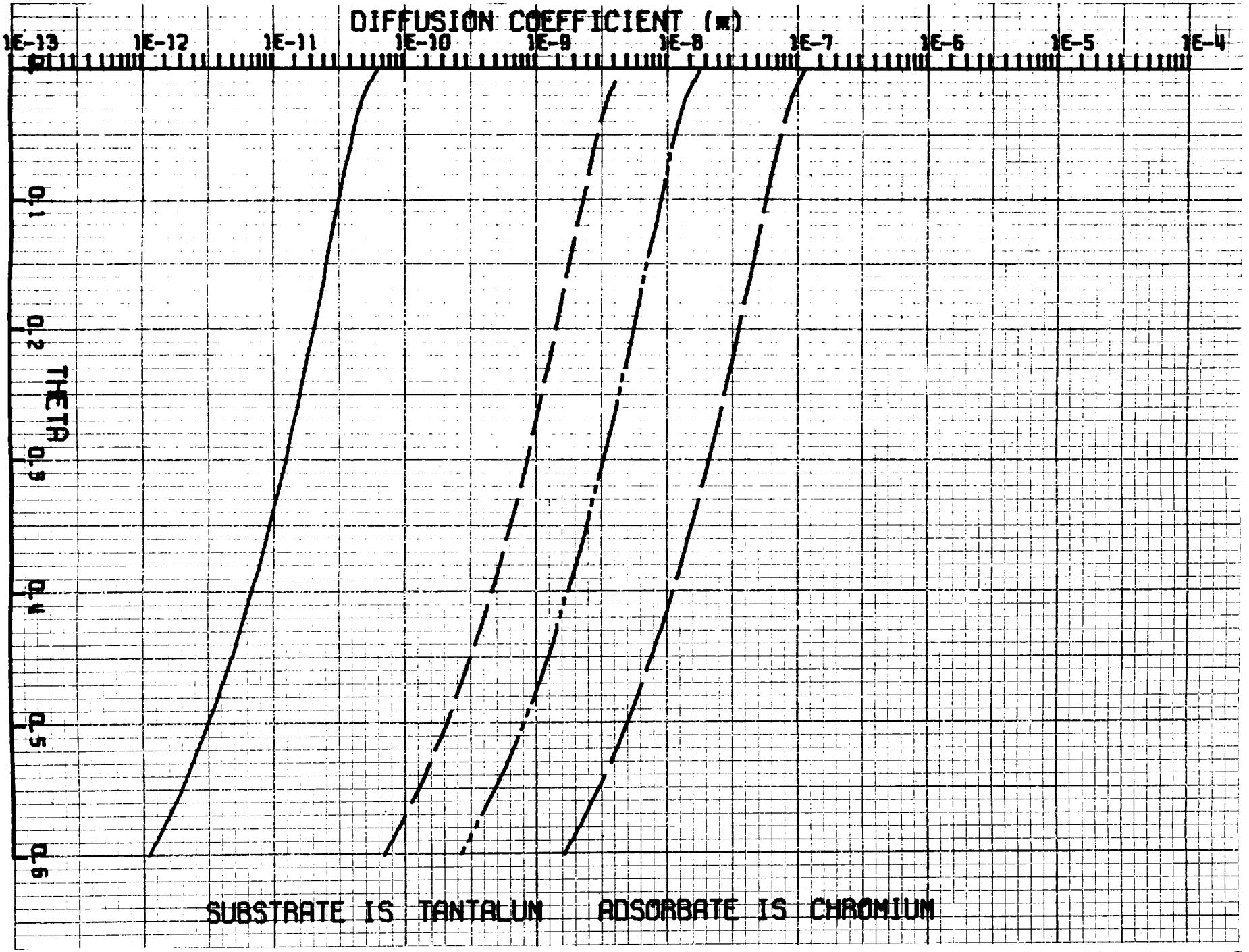
DIFFUSION COEFFICIENT (m)
1E-13
1E-12
1E-11
1E-10
1E-9
1E-8
1E-7
1E-6
1E-5
1E-4
0.1
0.2
THETA
0.3
0.4
0.5
0.6
SUBSTRATE IS TANTALUN ADSORBATE IS CHROMIUM

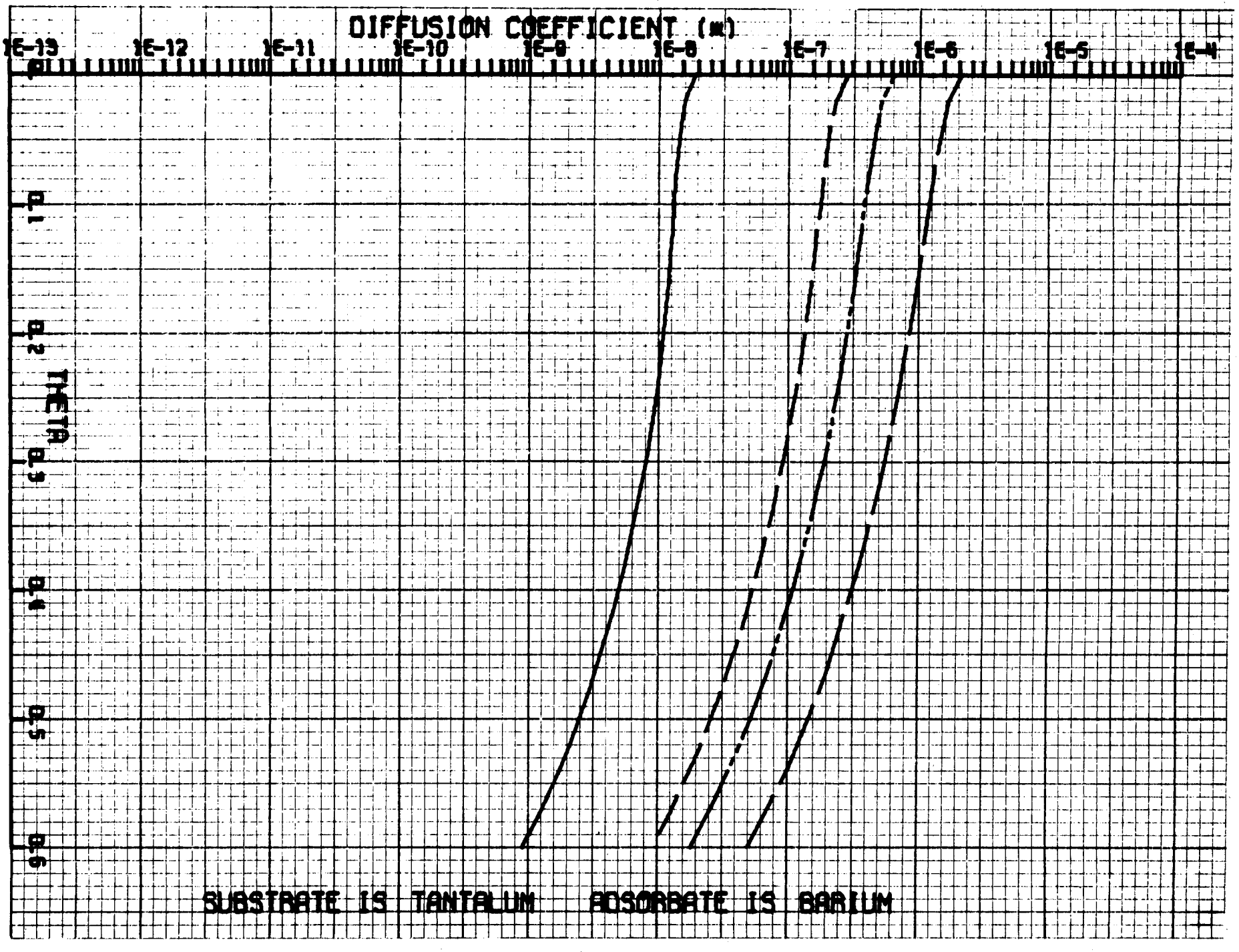
DIFFUSION COEFFICIENT (α)
1E-13
1E-12
1E-11
1E-10
1E-9
1E-8
1E-7
1E-6
1E-5
1E-4
0
0.1
0.2
0.3
0.4
0.5
0.6
THETA
SUBSTRATE IS TANTALUM ADSORBATE IS BARIUM

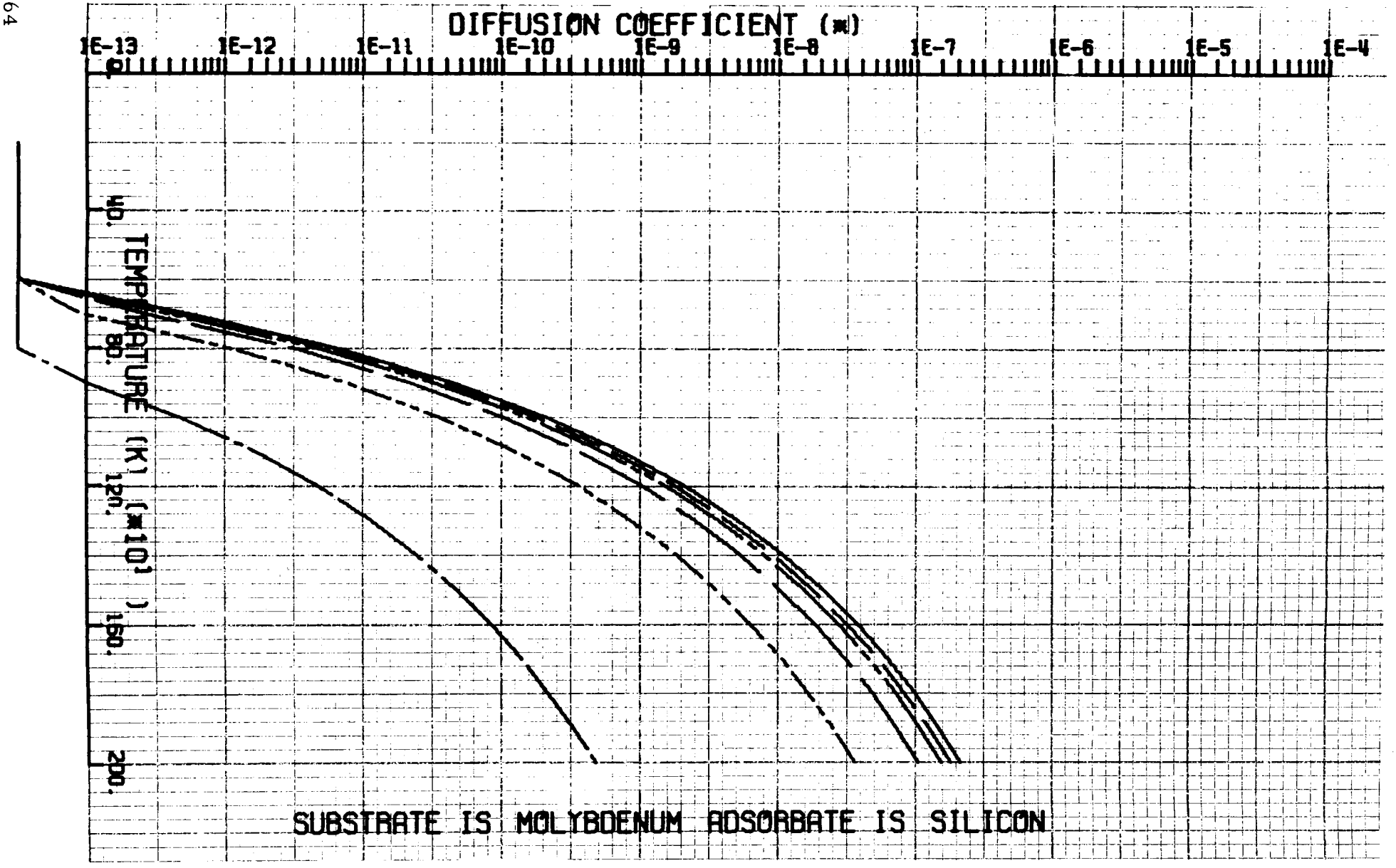
DIFFUSION COEFFICIENT (*)
1E-13
1E-12
1E-11
1E-10
1E-9
1E-8
1E-7
1E-6
1E-5
1E-4
TEMPERATURE (K) (*10¹)
40.
80.
120.
160.
200.
SUBSTRATE IS MOLYBDENUM ADSORBATE IS SILICON

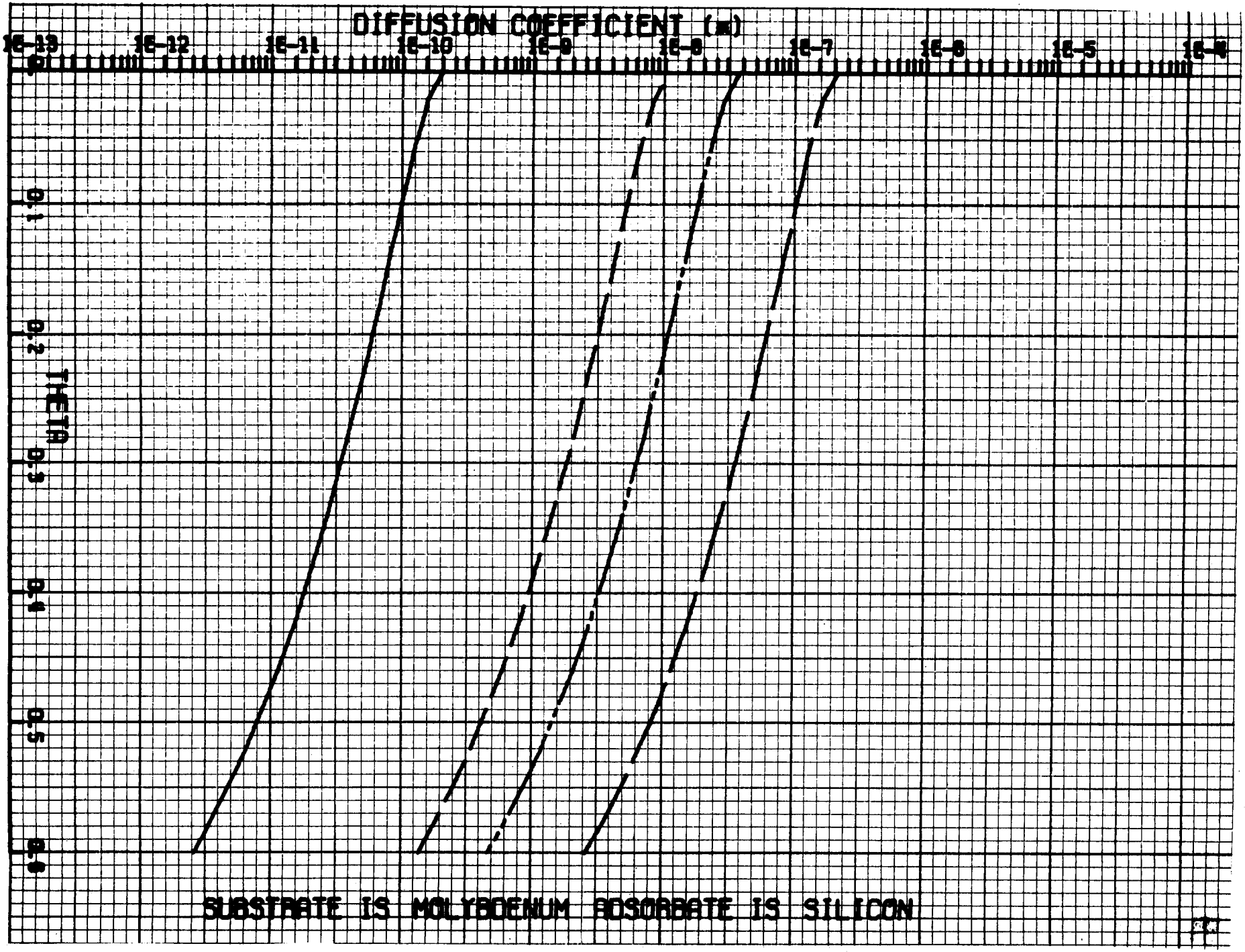
DIFFUSION COEFFICIENT (m)
1E-13
1E-12
1E-11
1E-10
1E-9
1E-8
1E-7
1E-6
1E-5
1E-4
THETA
0.1
0.2
0.3
0.4
0.5
0.6
SUBSTRATE IS MOLYBDENUM ADSORBATE IS SILICON

DIFFUSION COEFFICIENT (m)
1E-4
1E-5
1E-6
1E-7
1E-8
1E-9
1E-10
1E-11
1E-12
1E-13
TEMPERATURE (K) (×10¹)
40.
80.
120.
160.
200.
SUBSTRATE IS MOLYBDENUM ADSORBATE IS POTASSIUM

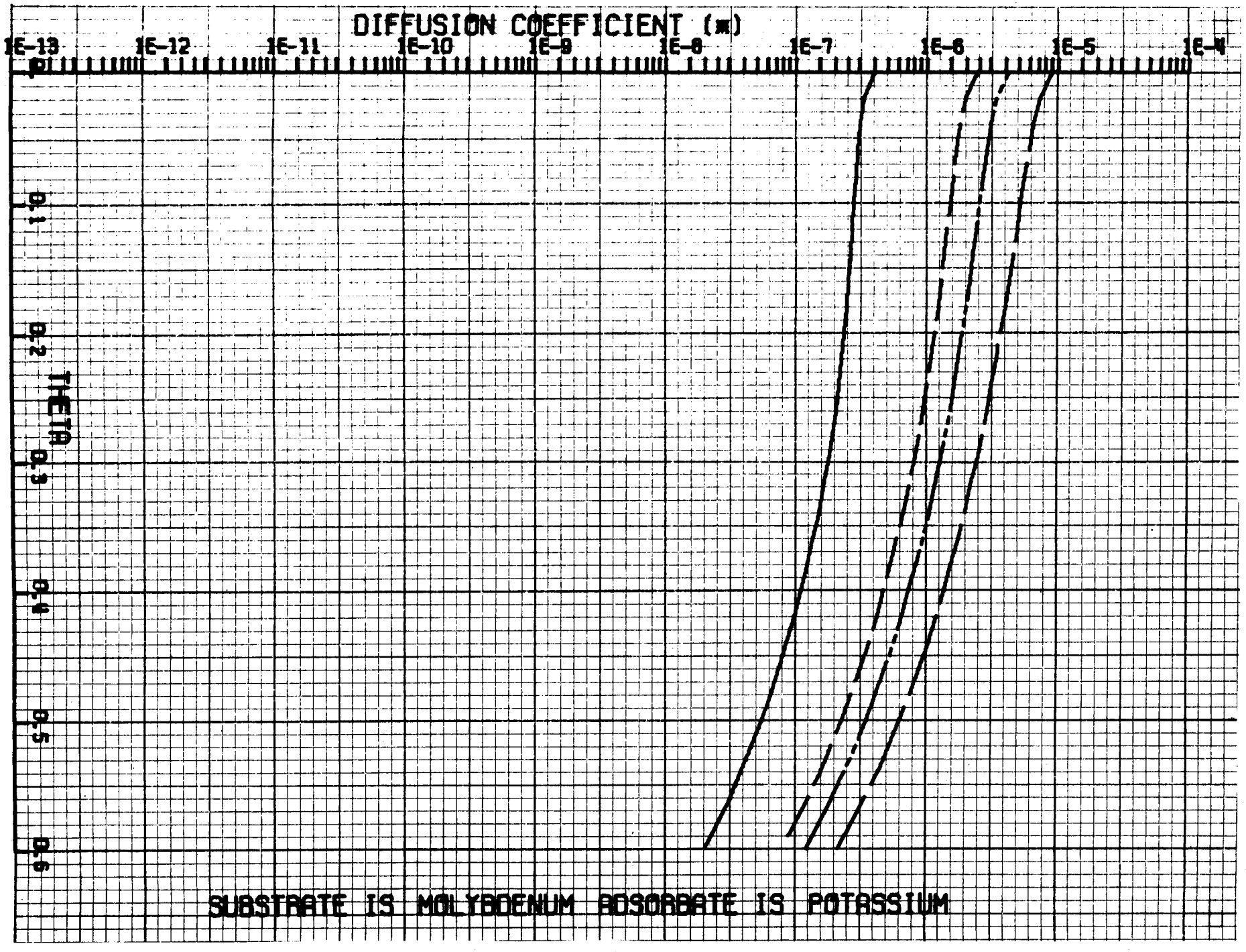
DIFFUSION COEFFICIENT (m)
1E-13
1E-12
1E-11
1E-10
1E-9
1E-8
1E-7
1E-6
1E-5
1E-4
THETA
0.1
0.2
0.3
0.4
0.5
0.6
SUBSTRATE IS MOLYBDENUM ADSORBATE IS POTASSIUM

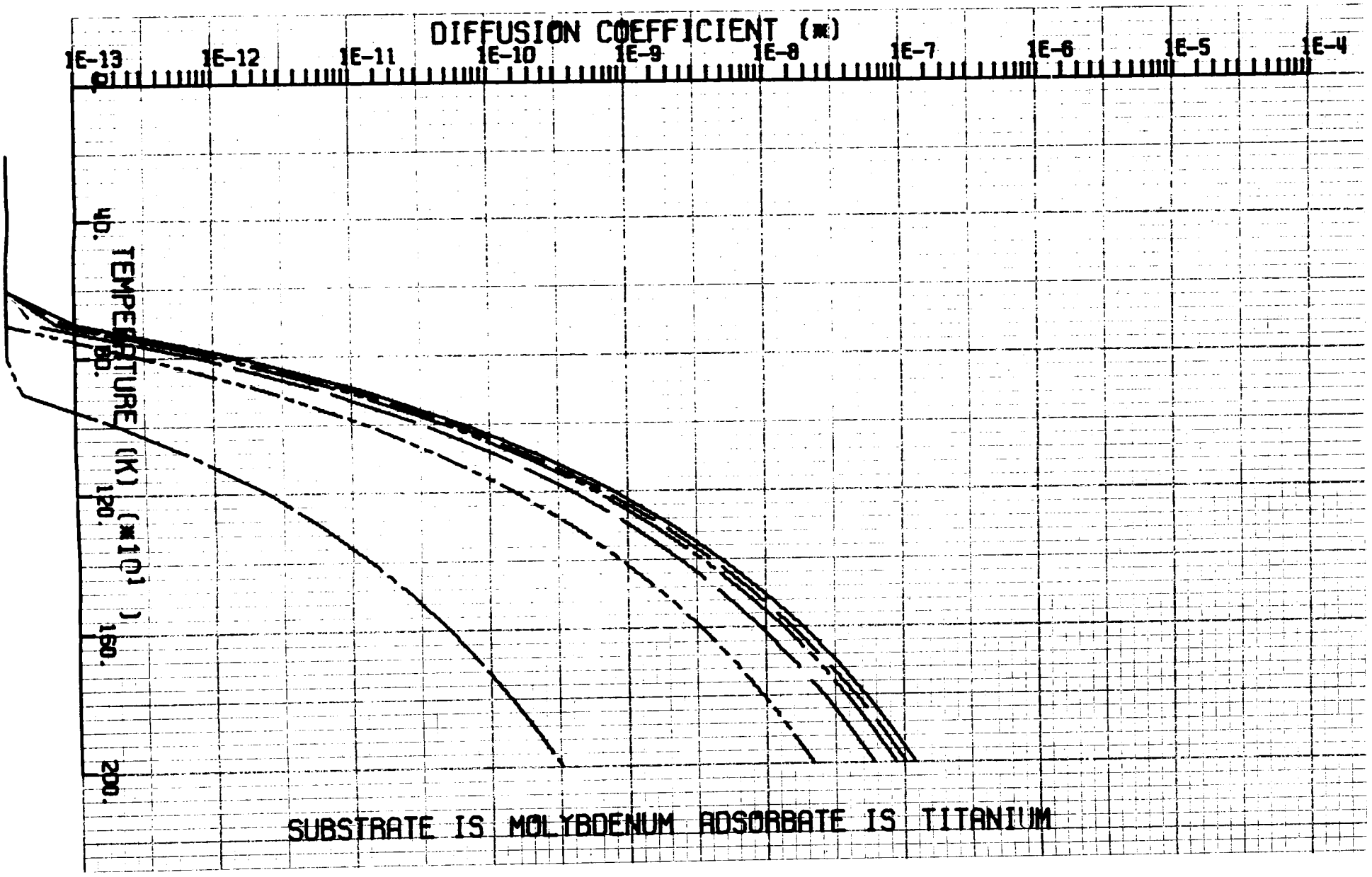
DIFFUSION COEFFICIENT (*)
1E-13
1E-12
1E-11
1E-10
1E-9
1E-8
1E-7
1E-6
1E-5
1E-4
TEMPERATURE (K) (*10^1)
40.
80.
120.
160.
200.
SUBSTRATE IS MOLYBDENUM ADSORBATE IS TITANIUM

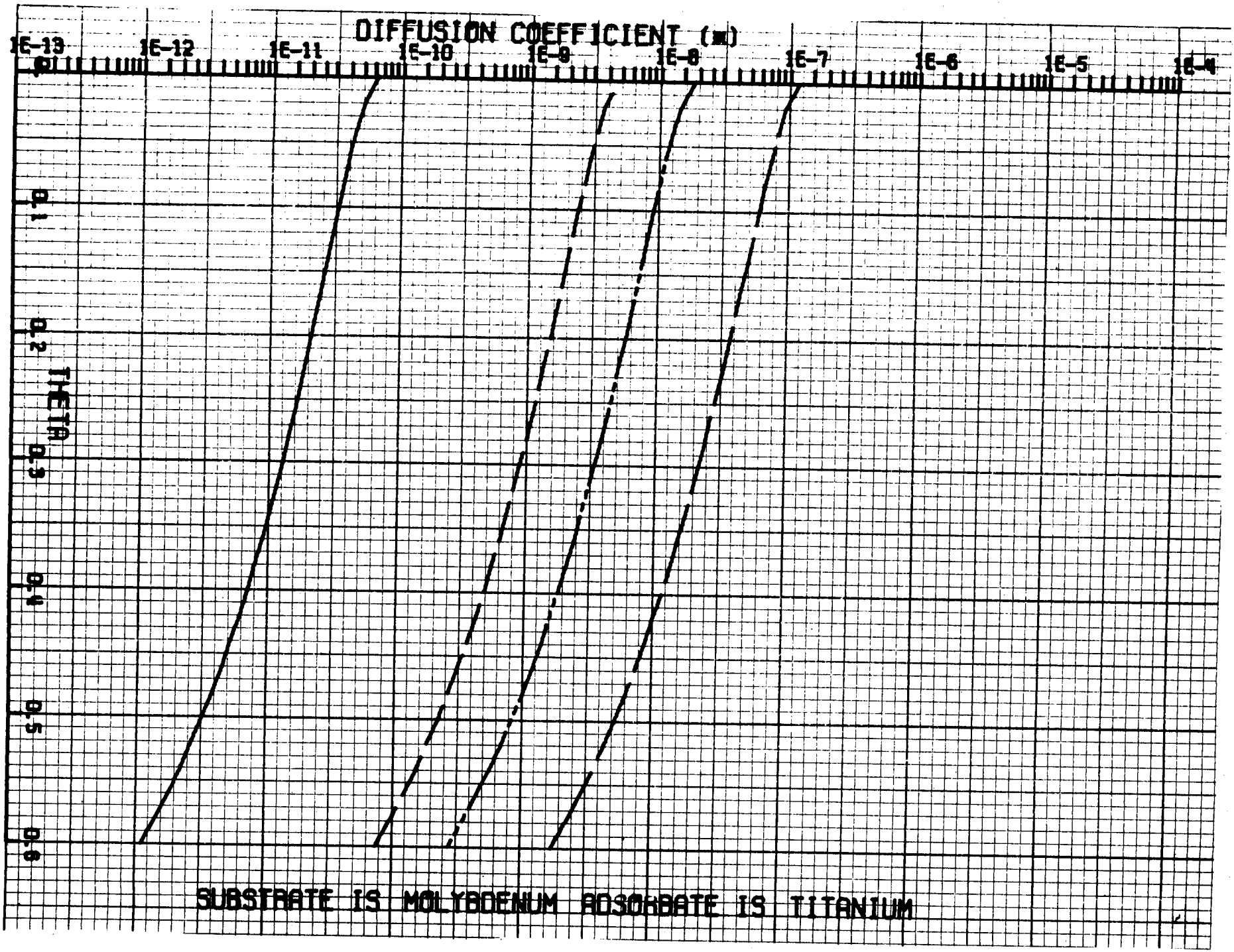
DIFFUSION COEFFICIENT (m)
1E-13
1E-12
1E-11
1E-10
1E-9
1E-8
1E-7
1E-6
1E-5
1E-4
THETA
0.1
0.2
0.3
0.4
0.5
0.6
SUBSTRATE IS MOLYBDENUM ADSORBATE IS TITANIUM

DIFFUSION COEFFICIENT (m²)
1E-4
1E-5
1E-6
1E-7
1E-8
1E-9
1E-10
1E-11
1E-12
1E-13
TEMPERATURE (K) (×10¹)
40.
80.
120.
160.
200.
SUBSTRATE IS MOLYBDENUM ADSORBATE IS CHROMIUM

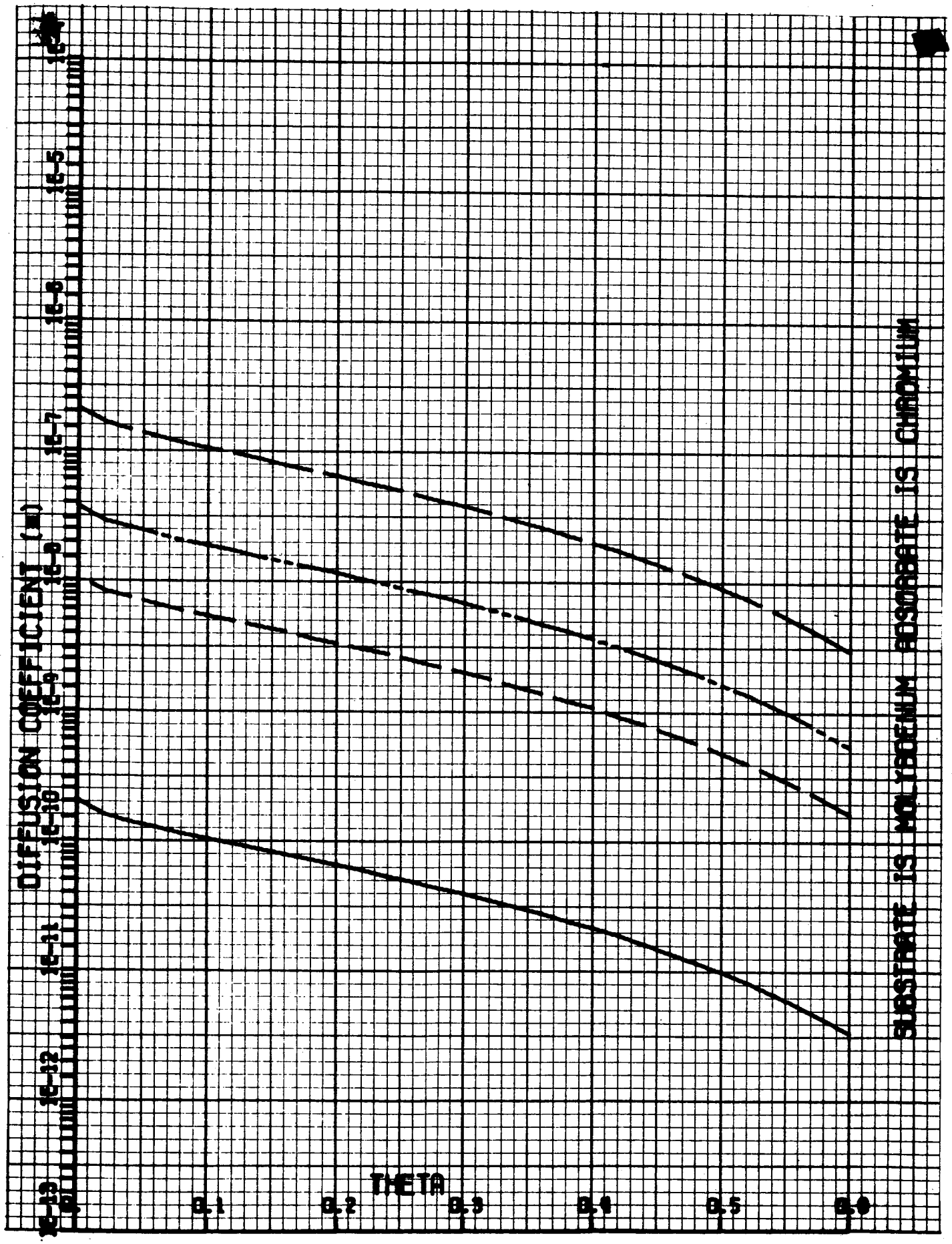
DIFFUSION COEFFICIENT (M)
1E-5
1E-6
1E-7
1E-8
1E-9
1E-10
1E-11
1E-12
1E-13
0.1
0.2
0.3
0.4
0.5
0.6
THETA
SUBSTRATE IS MOLYBDENUM ASSUMING IS CHROMIUM

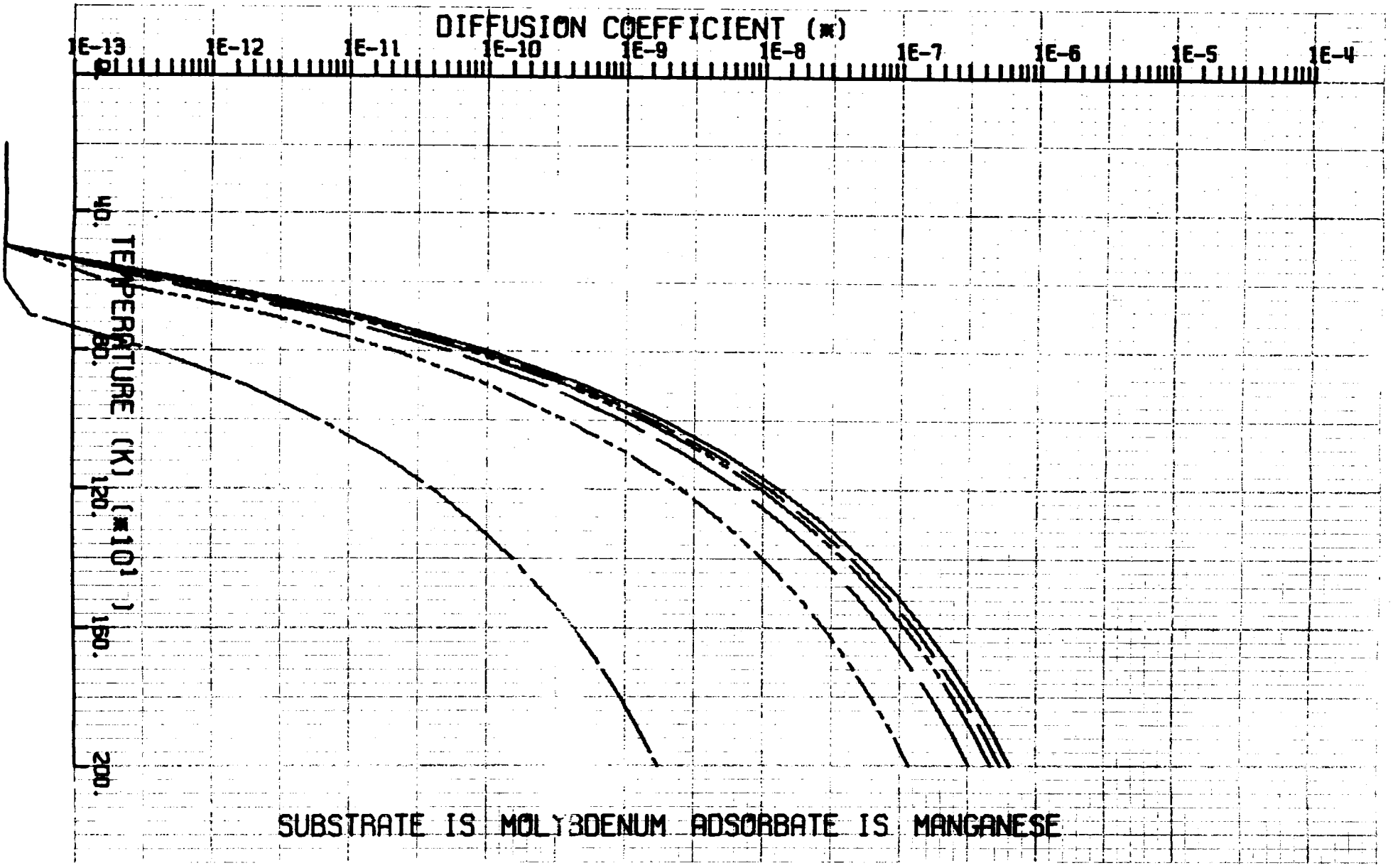
DIFFUSION COEFFICIENT (*)
1E-13
1E-12
1E-11
1E-10
1E-9
1E-8
1E-7
1E-6
1E-5
1E-4
40.
80.
120.
160.
200.
TEMPERATURE (K) (*10¹)
SUBSTRATE IS MOLYBDENUM ADSORBATE IS MANGANESE

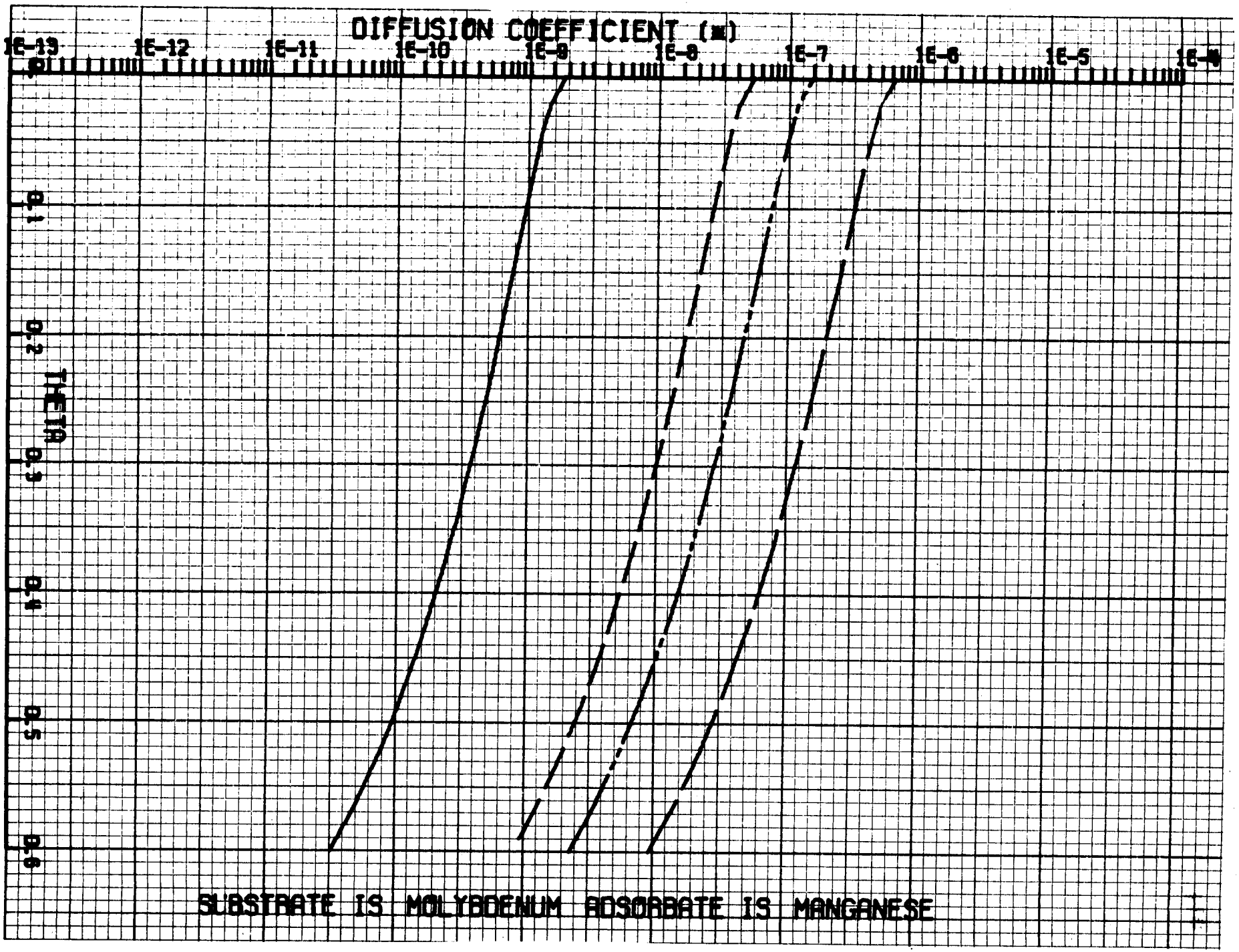
DIFFUSION COEFFICIENT (m)
1E-13
1E-12
1E-11
1E-10
1E-9
1E-8
1E-7
1E-6
1E-5
1E-4
THETA
0.1
0.2
0.3
0.4
0.5
0.6
SUBSTRATE IS MOLYBDENUM ADSORBATE IS MANGANESE

DIFFUSION COEFFICIENT (*)
1E-4
1E-5
1E-6
1E-7
1E-8
1E-9
1E-10
1E-11
1E-12
1E-13
TEMPERATURE (K) (*10¹)
40.
80.
120.
160.
200.
SUBSTRATE IS MOLYBDENUM ADSORBATE IS IRON

DIFFUSION COEFFICIENT (D)
1E-4
1E-5
1E-6
1E-7
1E-8
1E-9
1E-10
1E-11
1E-12
1E-13
0
0.1
0.2
0.3
0.4
0.5
0.6
THETA
SUBSTRATE IS MOLYBDENUM ADSORBATE IS IRON

DIFFUSION COEFFICIENT (*)
1E-4
1E-5
1E-6
1E-7
1E-8
1E-9
1E-10
1E-11
1E-12
1E-13
TEMPERATURE (K) (*10¹)
40.
80.
120.
160.
200.
SUBSTRATE IS MOLYBDENUM ADSORBATE IS NICKEL

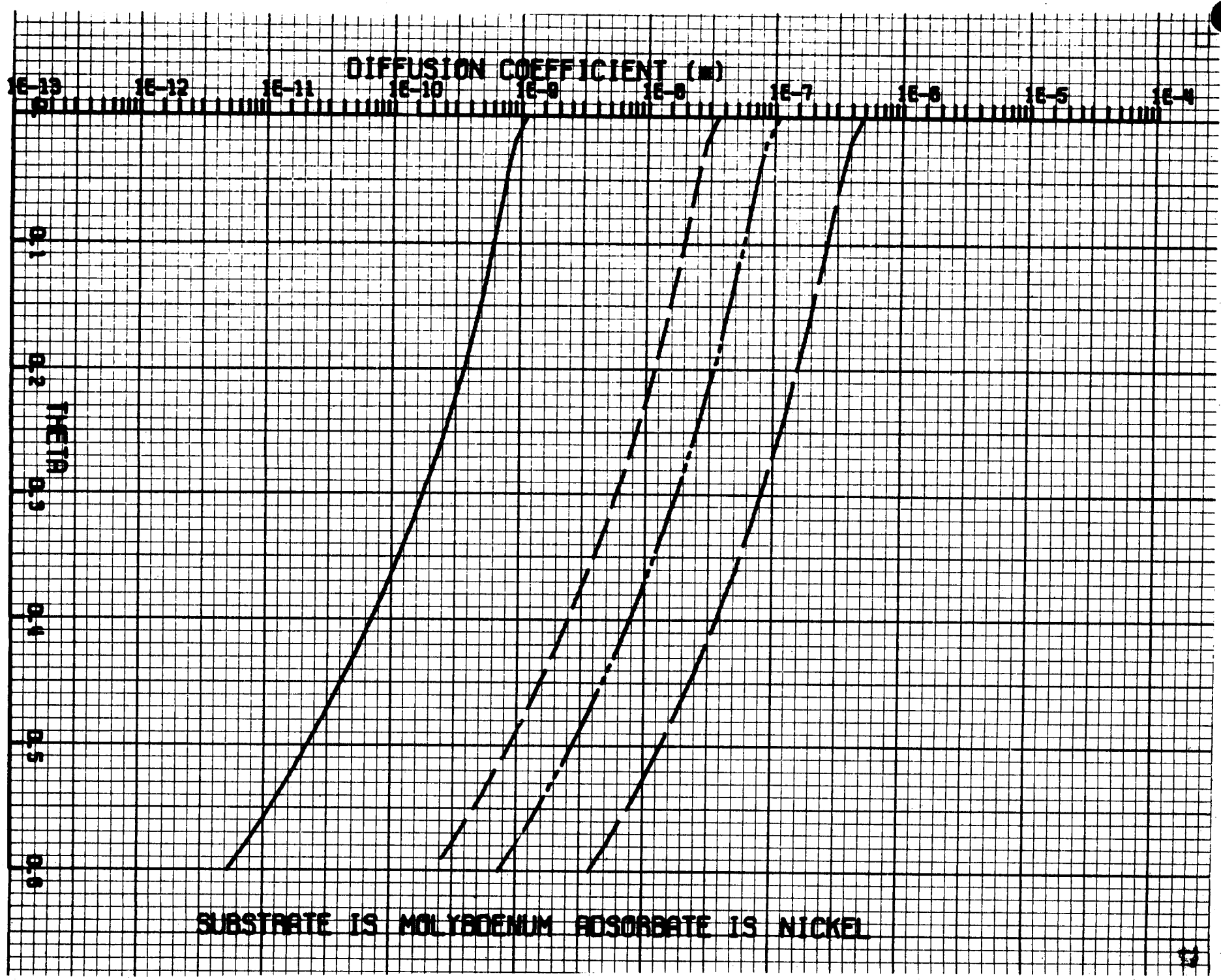
DIFFUSION COEFFICIENT (m)
1E-13
1E-12
1E-11
1E-10
1E-9
1E-8
1E-7
1E-6
1E-5
1E-4
FIELD
-9.1
-9.2
-9.3
-9.4
-9.5
-9.6
SUBSTRATE IS MOLYBDENUM ADSORBATE IS NICKEL

DIFFUSION COEFFICIENT (*)
1E-4
1E-5
1E-6
1E-7
1E-8
1E-9
1E-10
1E-11
1E-12
1E-13
TEMPERATURE (K) (*10¹)
40.
80.
120.
160.
200.
SUBSTRATE IS MOLYBDENUM ADSORBATE IS COPPER

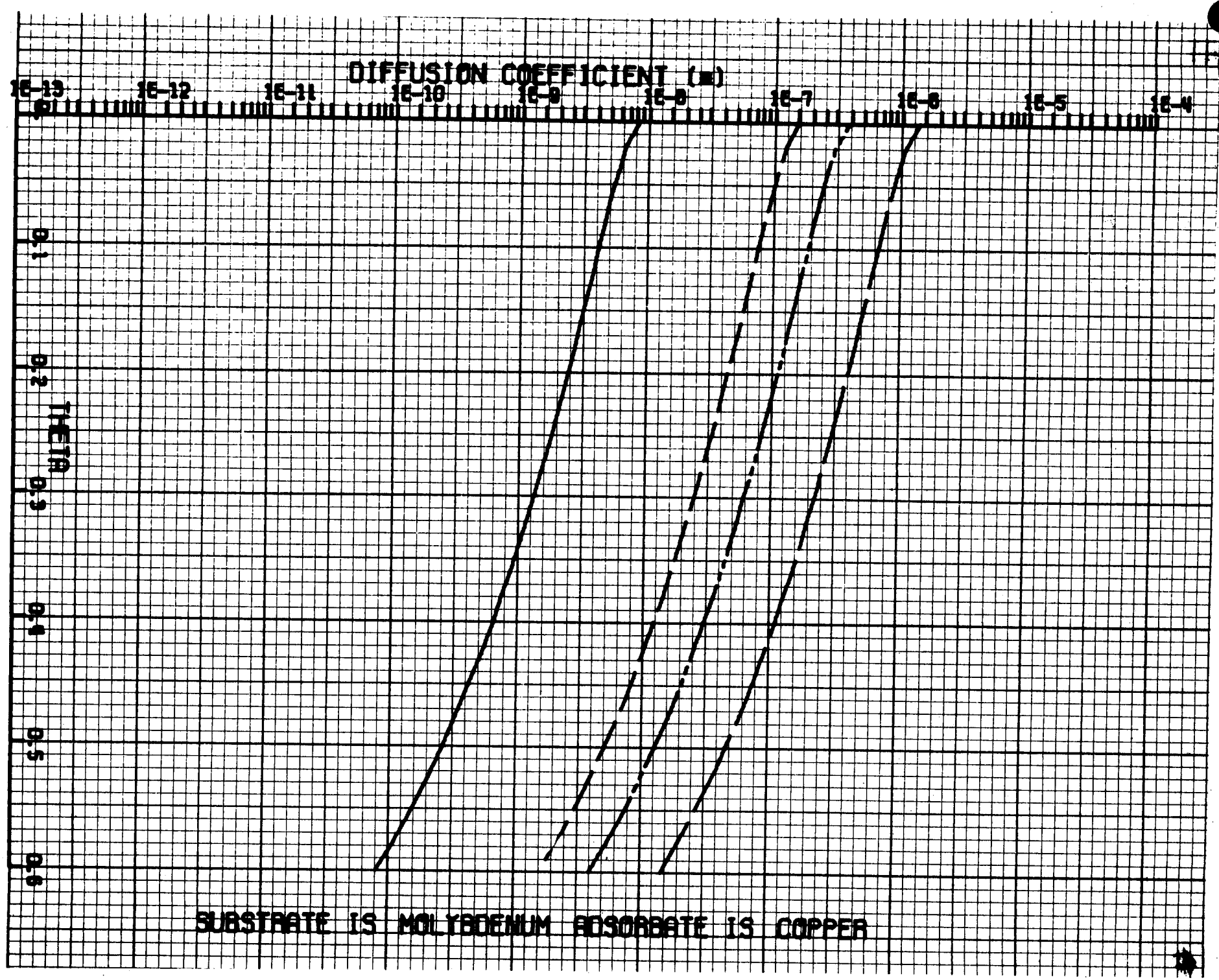
DIFFUSION COEFFICIENT (m)
1E-13
1E-12
1E-11
1E-10
1E-9
1E-8
1E-7
1E-6
1E-5
1E-4
THETA
0.1
0.2
0.3
0.4
0.5
0.6
SUBSTRATE IS MOLYBDENUM ADSORBATE IS COPPER

DIFFUSION COEFFICIENT (m)
1E-4
1E-5
1E-6
1E-7
1E-8
1E-9
1E-10
1E-11
1E-12
1E-13
TEMPERATURE (K) (*10^1)
40.
80.
120.
160.
200.
SUBSTRATE IS MOLYBDENUM ADSORBATE IS GALLIUM

DIFFUSION COEFFICIENT (cm)
1E-4
1E-5
1E-6
1E-7
1E-8
1E-9
1E-10
1E-11
1E-12
1E-13
0
0.1
0.2
0.3
0.4
0.5
0.6
THETA
SUBSTRATE IS MOLYBDENUM ADSORBATE IS GALLIUM

DIFFUSION COEFFICIENT (m²)
1E-4
1E-5
1E-6
1E-7
1E-8
1E-9
1E-10
1E-11
1E-12
1E-13
TEMPERATURE (K) (×10¹)
40.
80.
120.
160.
200.
SUBSTRATE IS MOLYBDENUM ADSORBATE IS RUBIDIUM

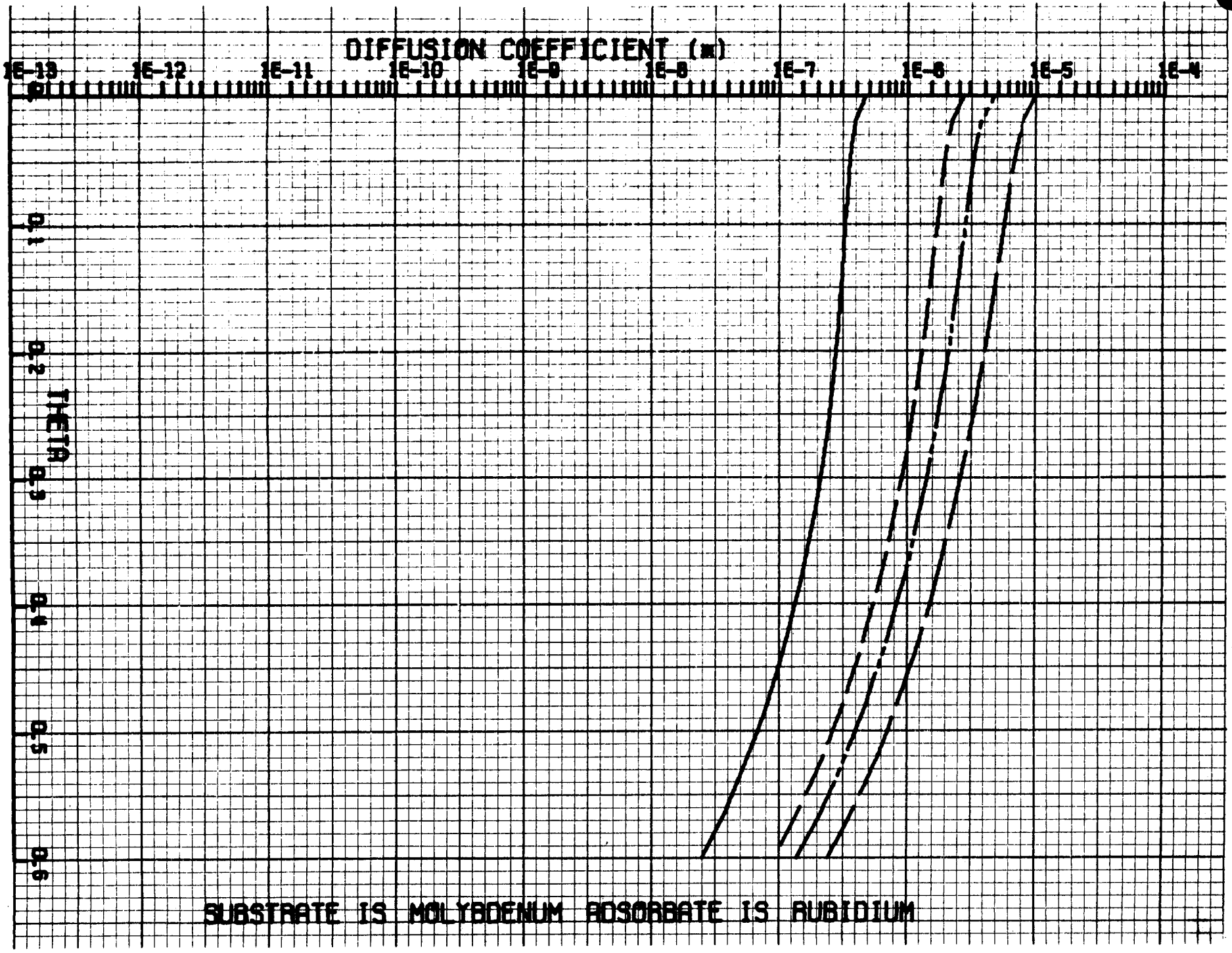
DIFFUSION COEFFICIENT (m)
1E-13
1E-12
1E-11
1E-10
1E-9
1E-8
1E-7
1E-6
1E-5
1E-4
THETA
0.1
0.2
0.3
0.4
0.5
0.6
SUBSTRATE IS MOLYBDENUM ADSORBATE IS RUBIDIUM

DIFFUSION COEFFICIENT (m²)
1E-4
1E-5
1E-6
1E-7
1E-8
1E-9
1E-10
1E-11
1E-12
1E-13
TEMPERATURE (K) (×10¹)
40.
80.
120.
160.
200.
SUBSTRATE IS MOLYBDENUM ADSORBATE IS INDIUM

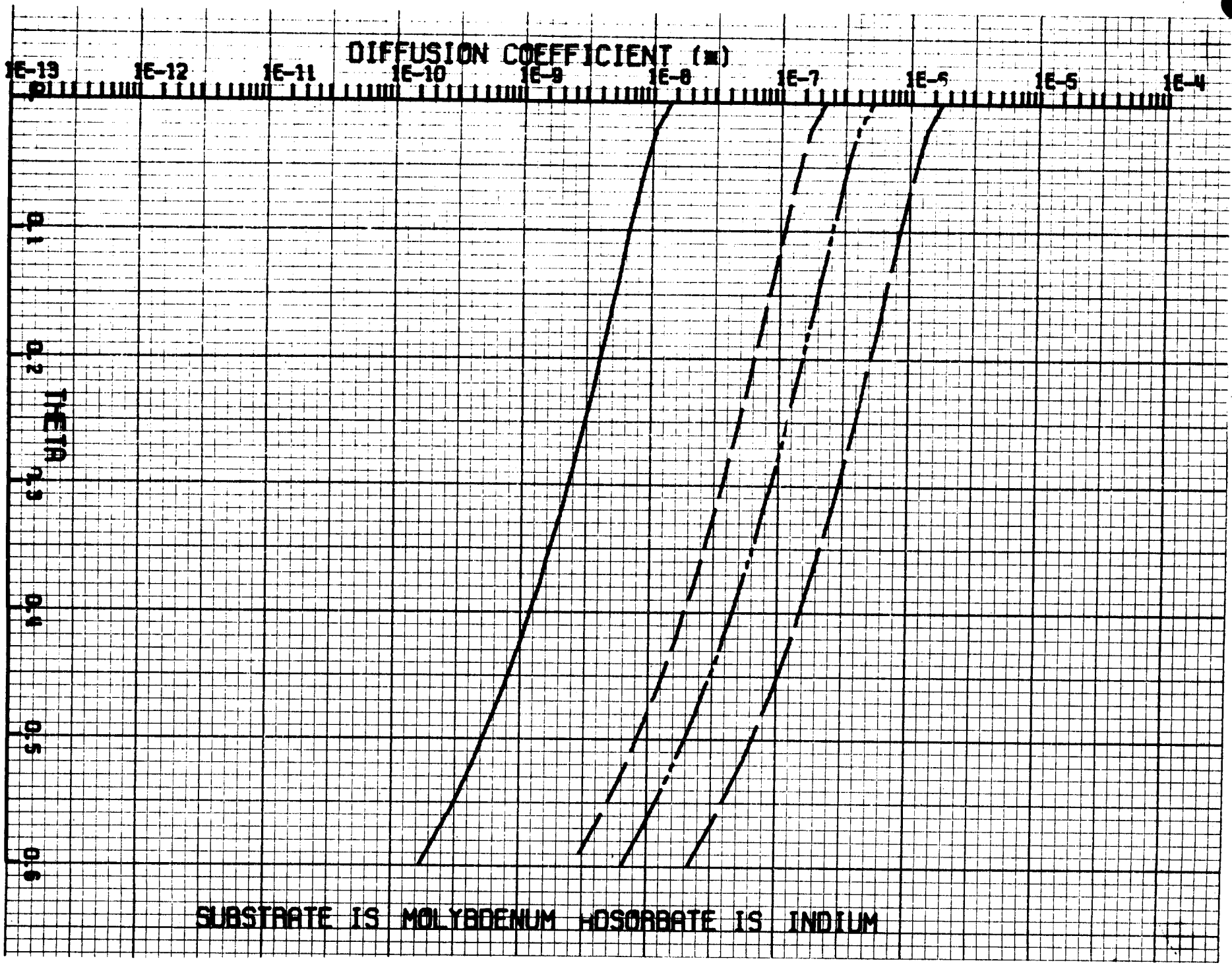
DIFFUSION COEFFICIENT (m)
1E-13
1E-12
1E-11
1E-10
1E-9
1E-8
1E-7
1E-6
1E-5
1E-4
THETA
0.1
0.2
0.3
0.4
0.5
0.6
SUBSTRATE IS MOLYBDENUM ADSORBATE IS INDIUM

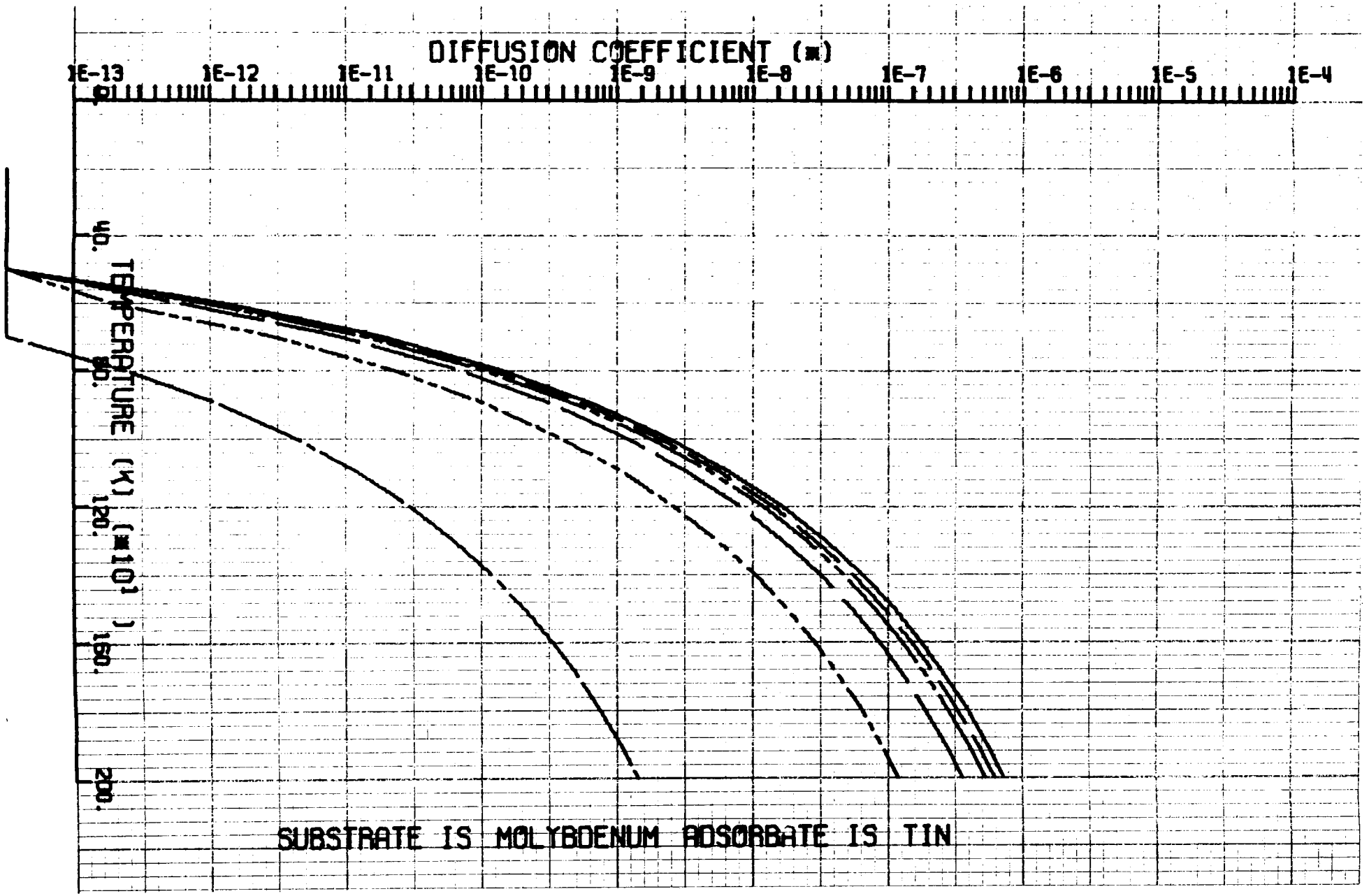
DIFFUSION COEFFICIENT (m)
1E-13
1E-12
1E-11
1E-10
1E-9
1E-8
1E-7
1E-6
1E-5
1E-4
TEMPERATURE (K) (*10^1)
40.
80.
120.
160.
200.
SUBSTRATE IS MOLYBDENUM ADSORBATE IS TIN

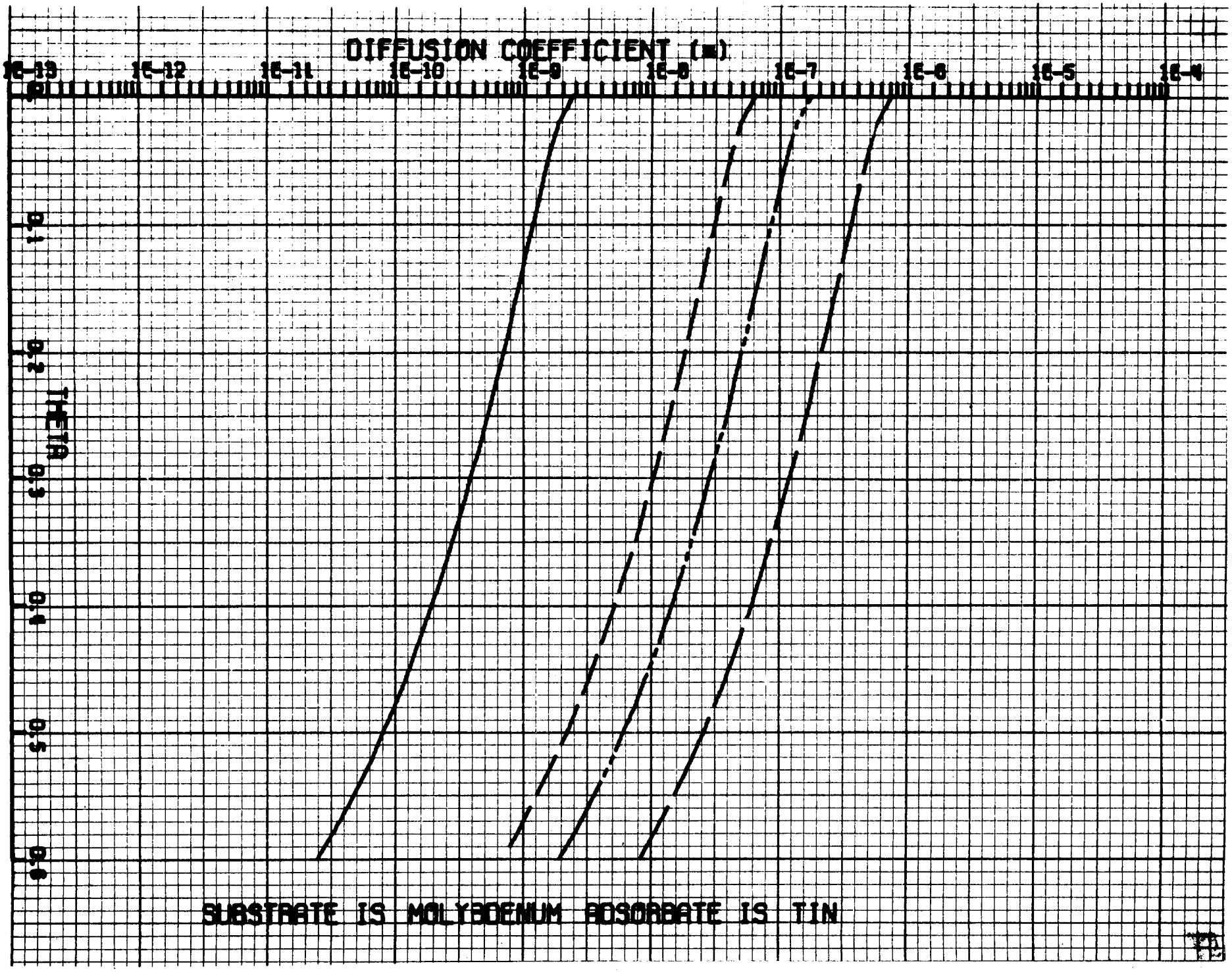
DIFFUSION COEFFICIENT (m)
1E-13
1E-12
1E-11
1E-10
1E-9
1E-8
1E-7
1E-6
1E-5
1E-4
THETA
0.1
0.2
0.3
0.4
0.5
0.6
SUBSTRATE IS MOLYBDENUM ADSORBATE IS TIN

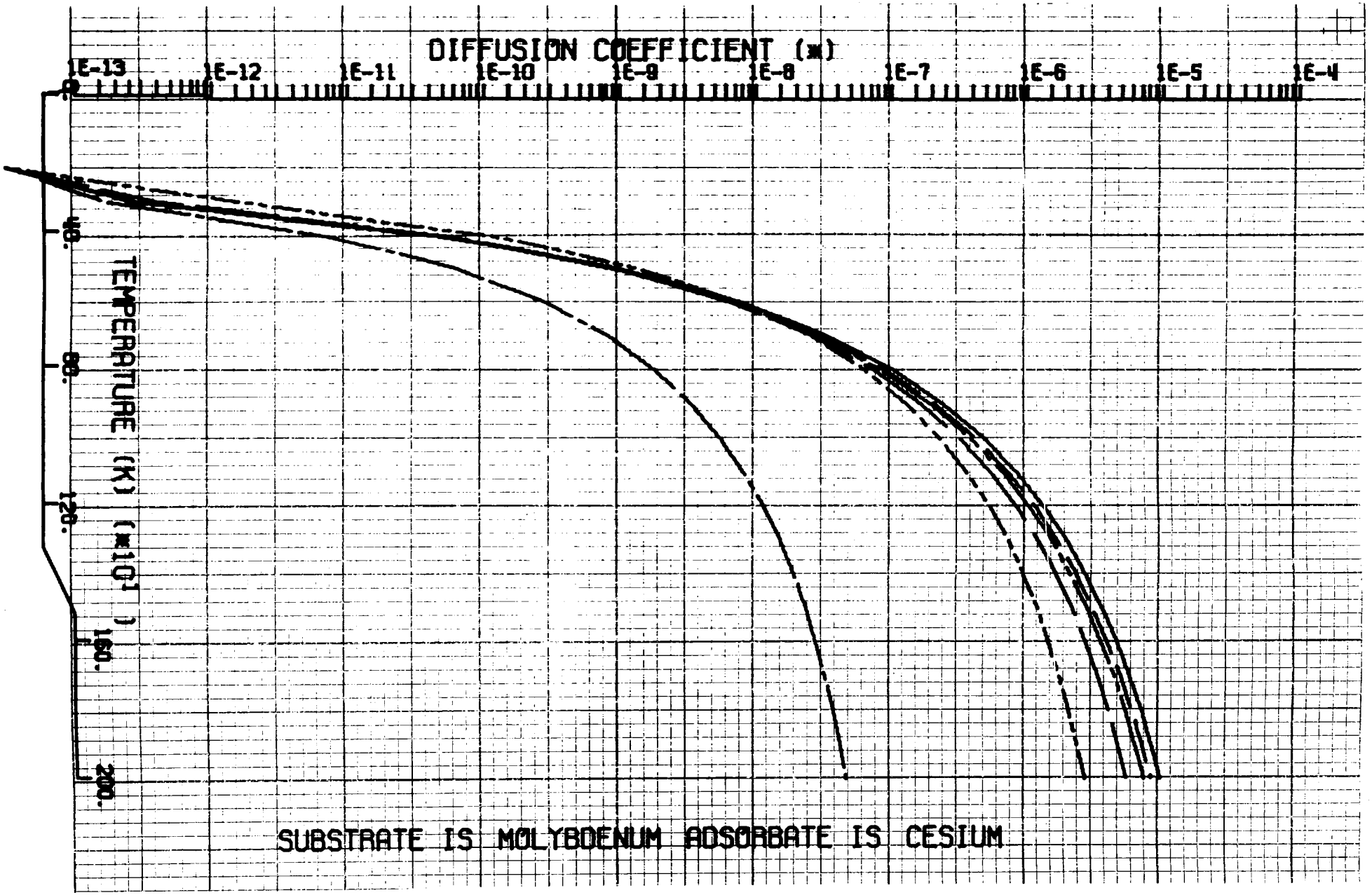
DIFFUSION COEFFICIENT (m)
1E-13
1E-12
1E-11
1E-10
1E-9
1E-8
1E-7
1E-6
1E-5
1E-4
TEMPERATURE (K) (*10^1)
40.
80.
120.
160.
200.
SUBSTRATE IS MOLYBDENUM ADSORBATE IS CESIUM

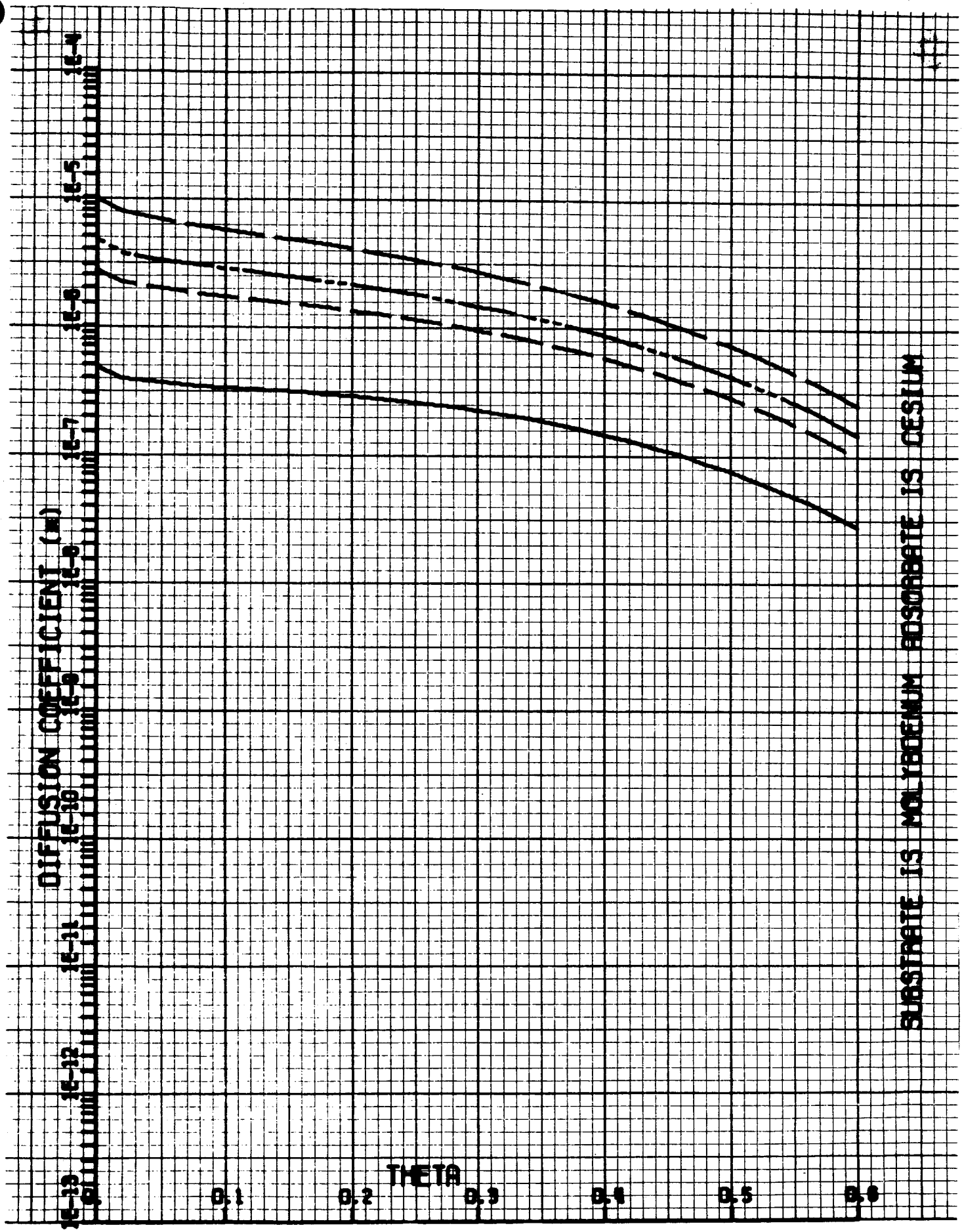
DIFFUSION COEFFICIENT (m)
1E-4
1E-5
1E-6
1E-7
1E-8
1E-9
1E-10
1E-11
1E-12
1E-13
0.1
0.2
0.3
0.4
0.5
0.6
THETA
SUBSTRATE IS MOLYBDENUM ADSORBATE IS CESIUM

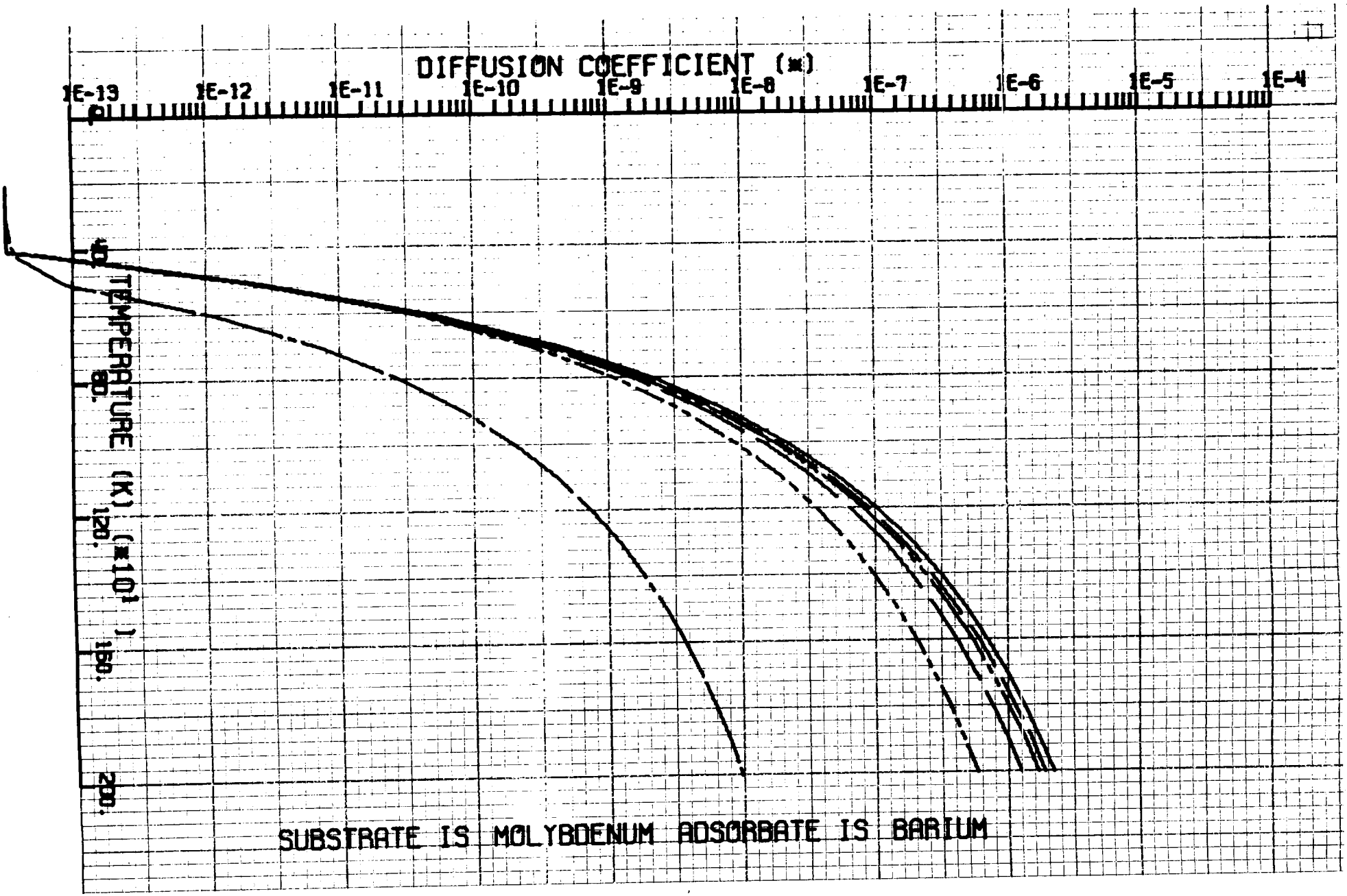
DIFFUSION COEFFICIENT (*)
1E-13
1E-12
1E-11
1E-10
1E-9
1E-8
1E-7
1E-6
1E-5
1E-4
TEMPERATURE (K) (*10¹)
80.
120.
160.
200.
SUBSTRATE IS MOLYBDENUM ADSORBATE IS BARIUM

DIFFUSION COEFFICIENT (M)
1E-4
1E-5
1E-6
1E-7
1E-8
1E-9
1E-10
1E-11
1E-12
1E-13
0.1
0.2
0.3
0.4
0.5
0.6
THETA
SUBSTRATE IS MOLYBDENUM ADSORBATE IS BARIUM

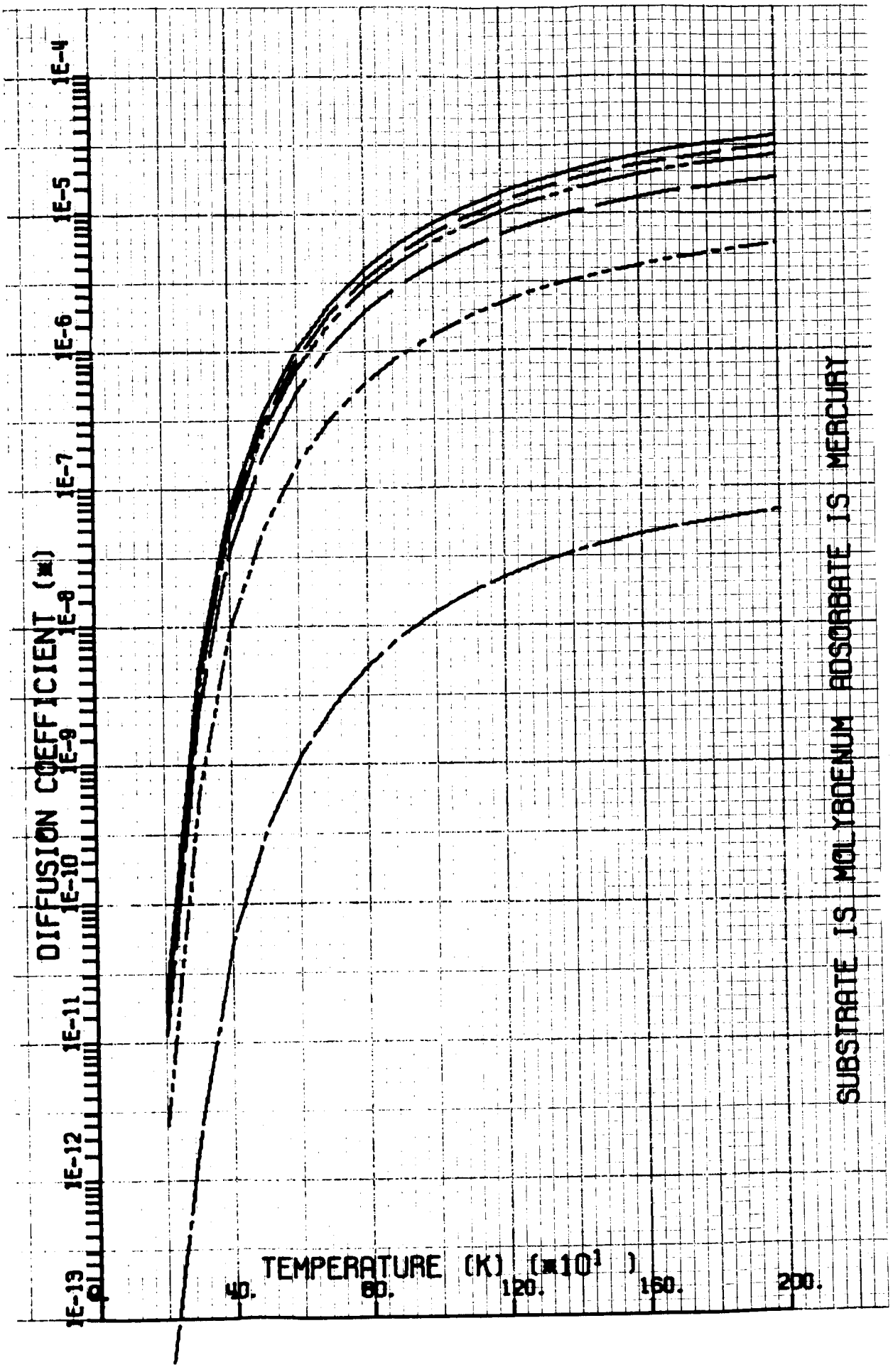
DIFFUSION COEFFICIENT (M)
1E-4
1E-5
1E-6
1E-7
1E-8
1E-9
1E-10
1E-11
1E-12
1E-13
TEMPERATURE (K) (*10^1)
40.
80.
120.
160.
200.
SUBSTRATE IS MOLYBDENUM ADSORBATE IS MERCURY

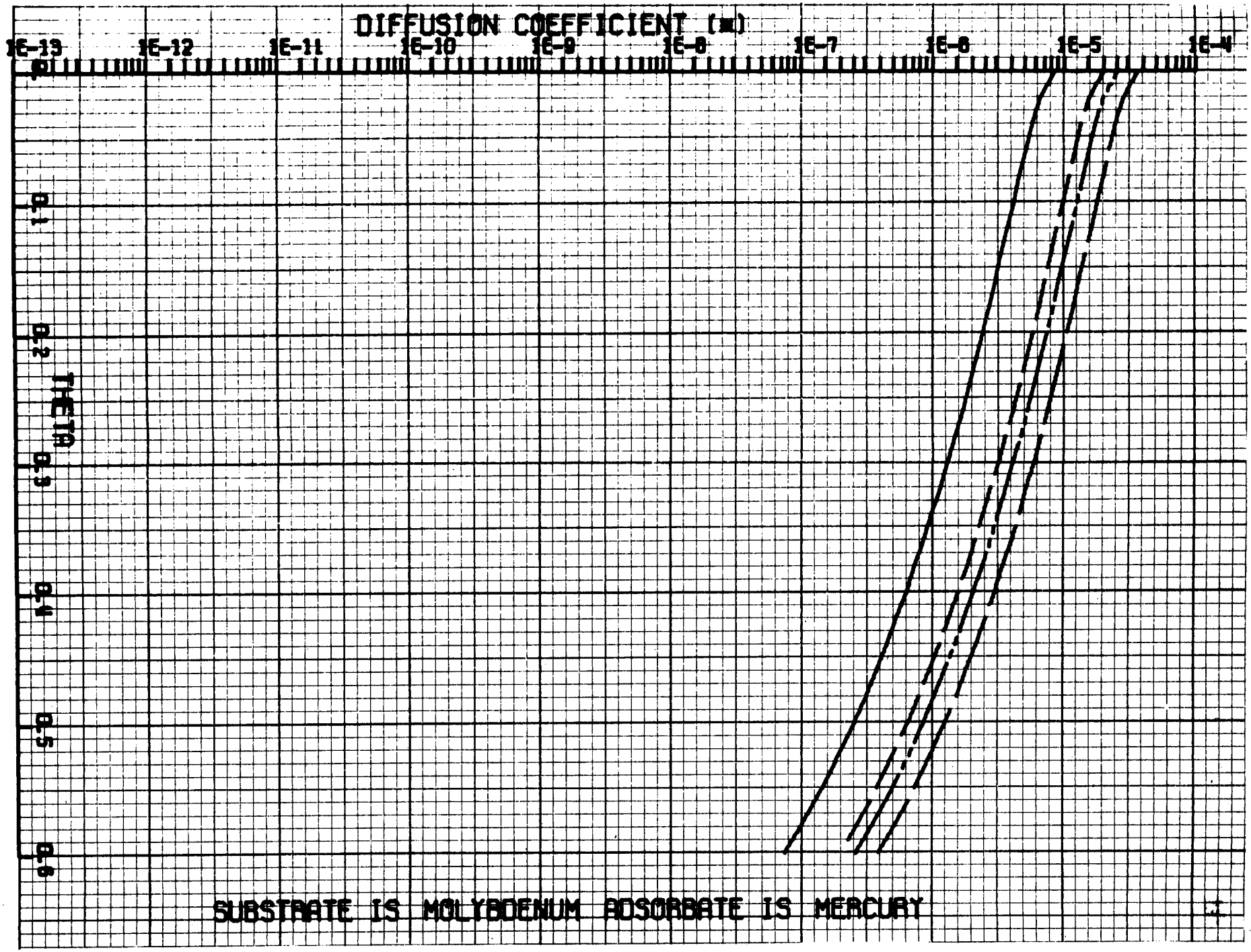
DIFFUSION COEFFICIENT (m)
1E-13
1E-12
1E-11
1E-10
1E-9
1E-8
1E-7
1E-6
1E-5
1E-4
0.1
0.2
0.3
0.4
0.5
0.6
YIELD
SUBSTRATE IS MOLYBDENUM ADSORBATE IS MERCURY

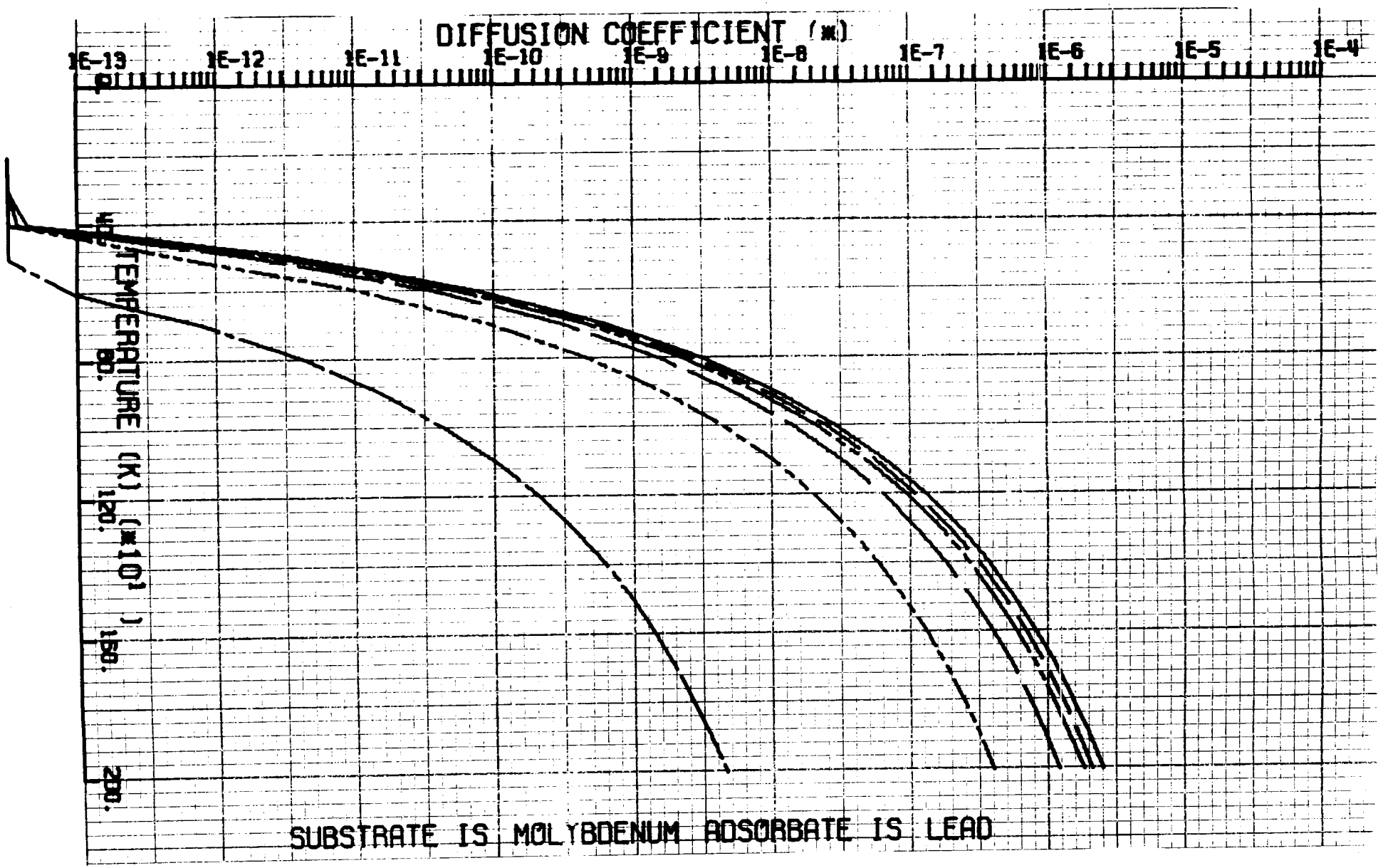
DIFFUSION COEFFICIENT (*)
1E-13
1E-12
1E-11
1E-10
1E-9
1E-8
1E-7
1E-6
1E-5
1E-4
TEMPERATURE (K) (*10¹)
40.
80.
120.
160.
200.
SUBSTRATE IS MOLYBDENUM ADSORBATE IS LEAD

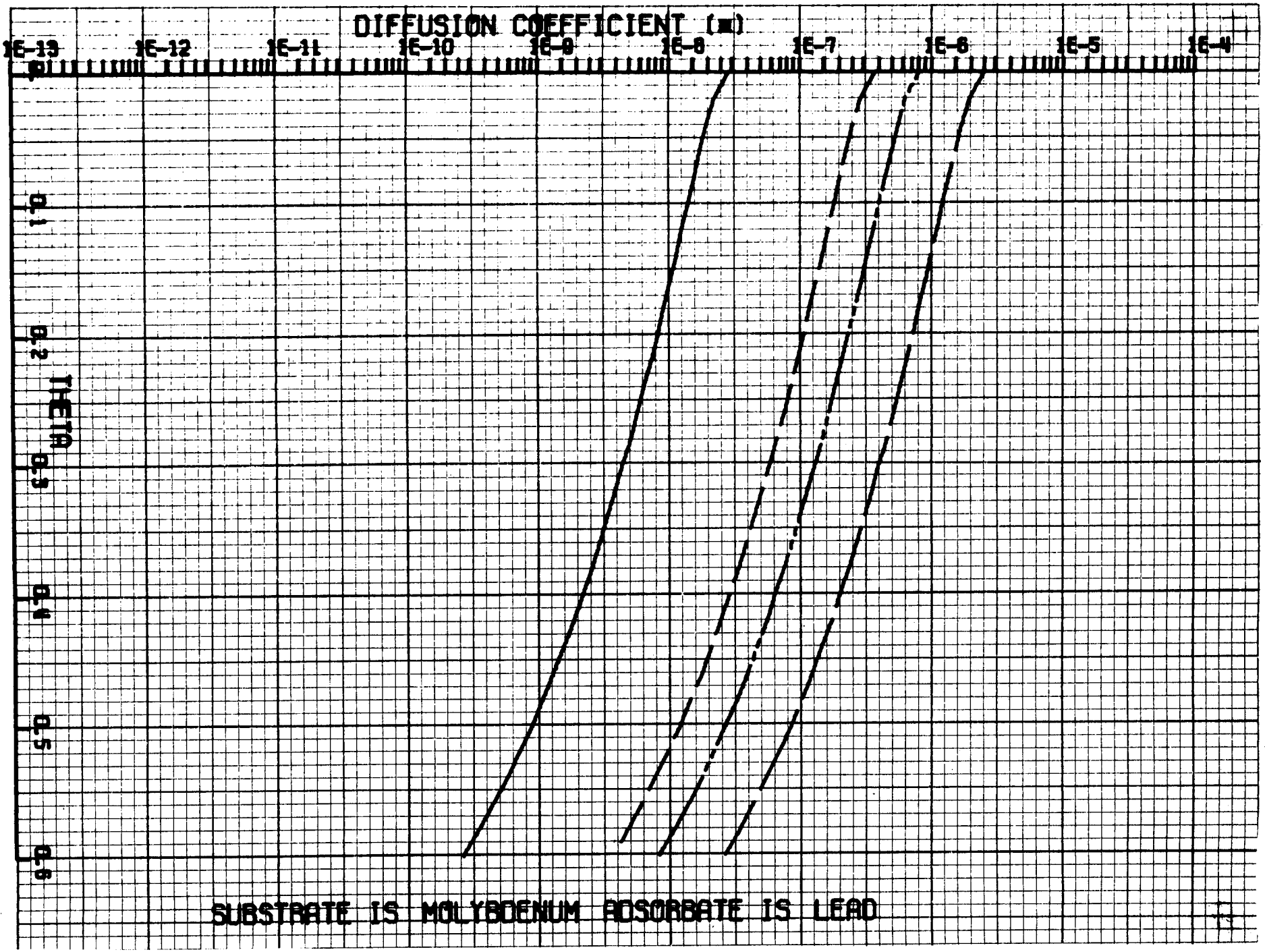
DIFFUSION COEFFICIENT (m)
1E-13
1E-12
1E-11
1E-10
1E-9
1E-8
1E-7
1E-6
1E-5
1E-4
THETA
0.1
0.2
0.3
0.4
0.5
0.6
SUBSTRATE IS MOLYBDENUM ADSORBATE IS LEAD

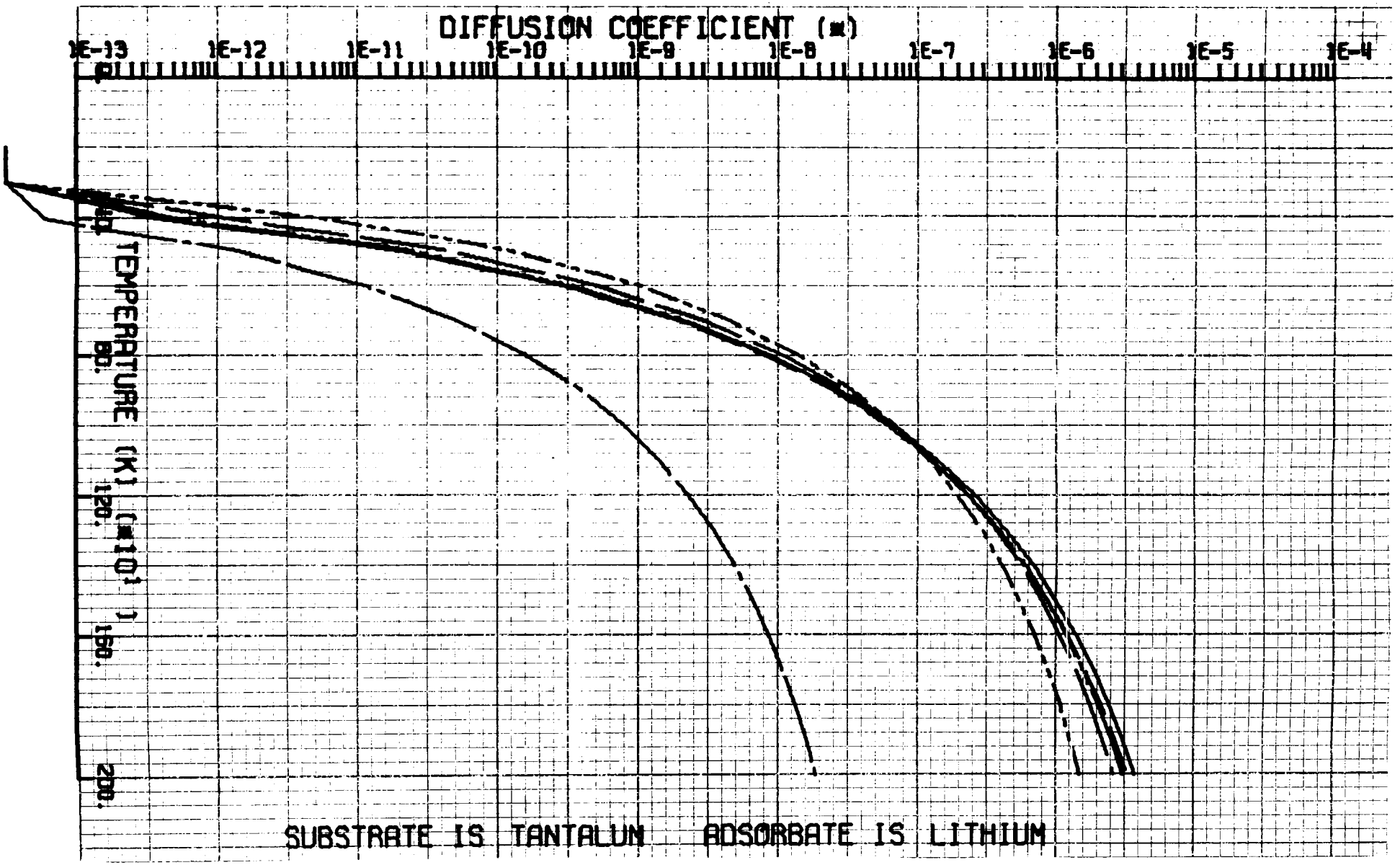
DIFFUSION COEFFICIENT (α)
1E-13
1E-12
1E-11
1E-10
1E-9
1E-8
1E-7
1E-6
1E-5
1E-4
TEMPERATURE (K) (α*10³)
80.
120.
160.
200.
SUBSTRATE IS TANTALUM ADSORBATE IS LITHIUM

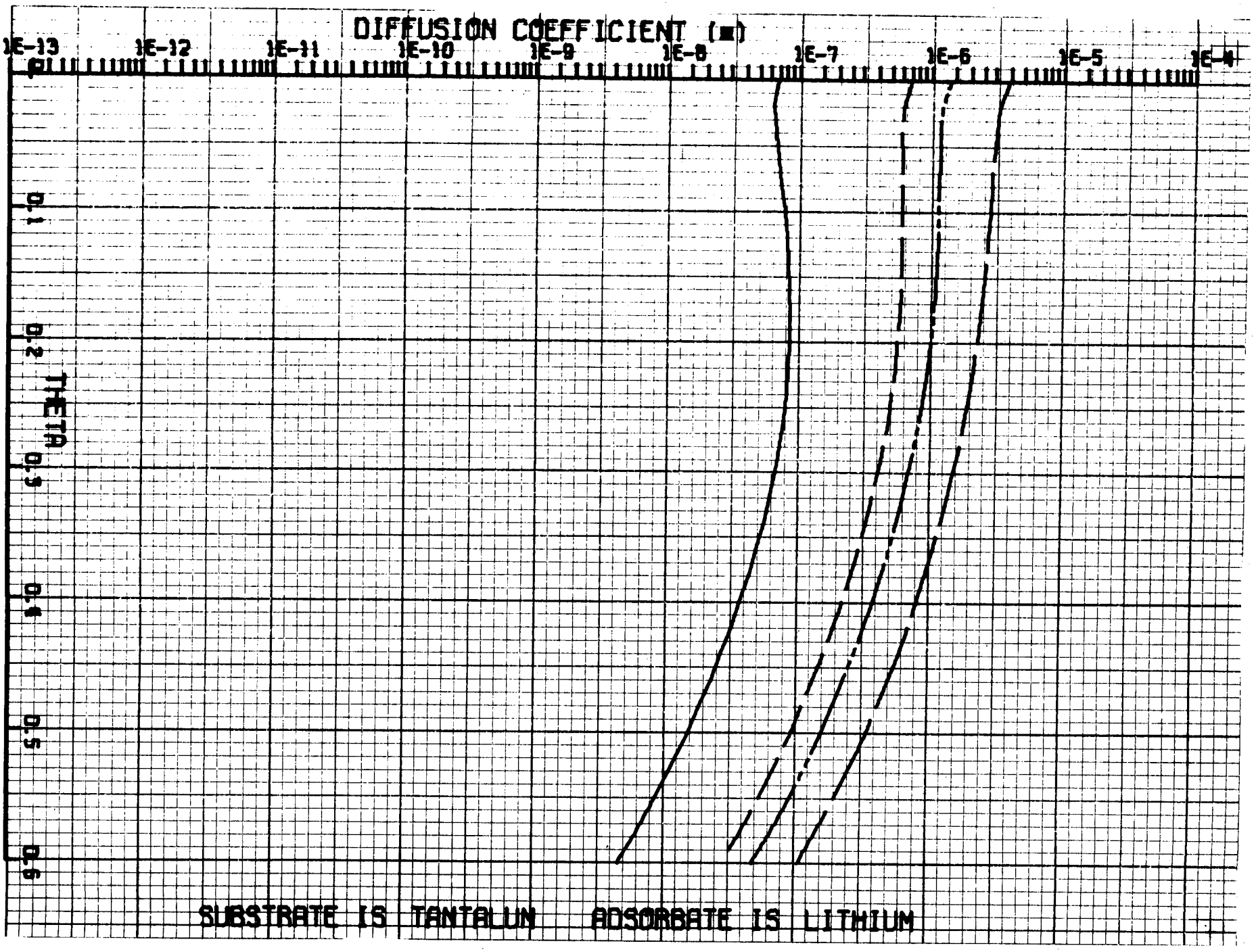
DIFFUSION COEFFICIENT (m)
1E-13
1E-12
1E-11
1E-10
1E-9
1E-8
1E-7
1E-6
1E-5
1E-4
THETA
0.1
0.2
0.3
0.4
0.5
0.6
SUBSTRATE IS TANTALUM ADSORBATE IS LITHIUM

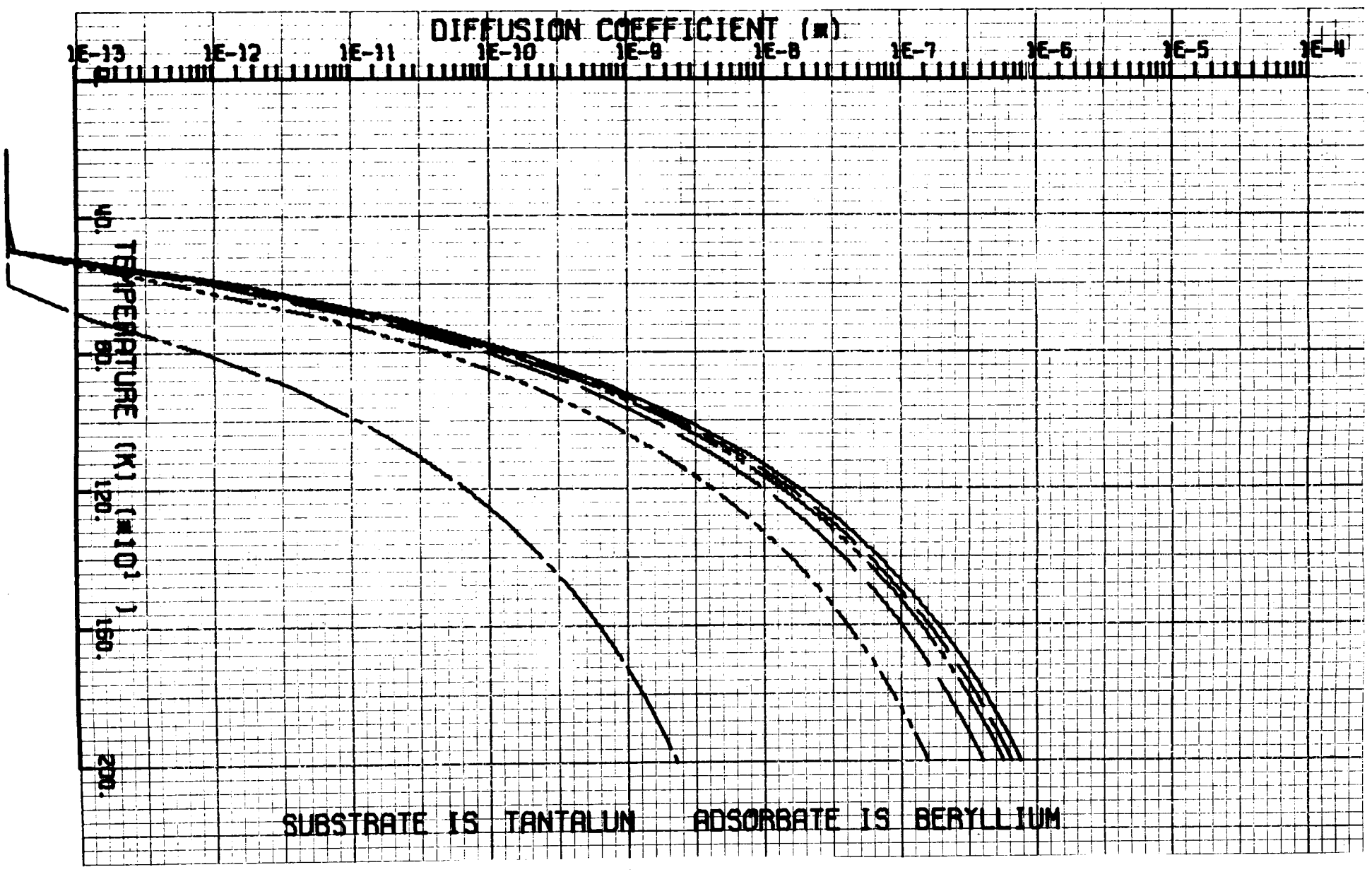
DIFFUSION COEFFICIENT (m)
1E-13
1E-12
1E-11
1E-10
1E-9
1E-8
1E-7
1E-6
1E-5
1E-4
TEMPERATURE (K) (*10)
40.
80.
120.
160.
200.
SUBSTRATE IS TANTALUM ADSORBATE IS BERYLLIUM

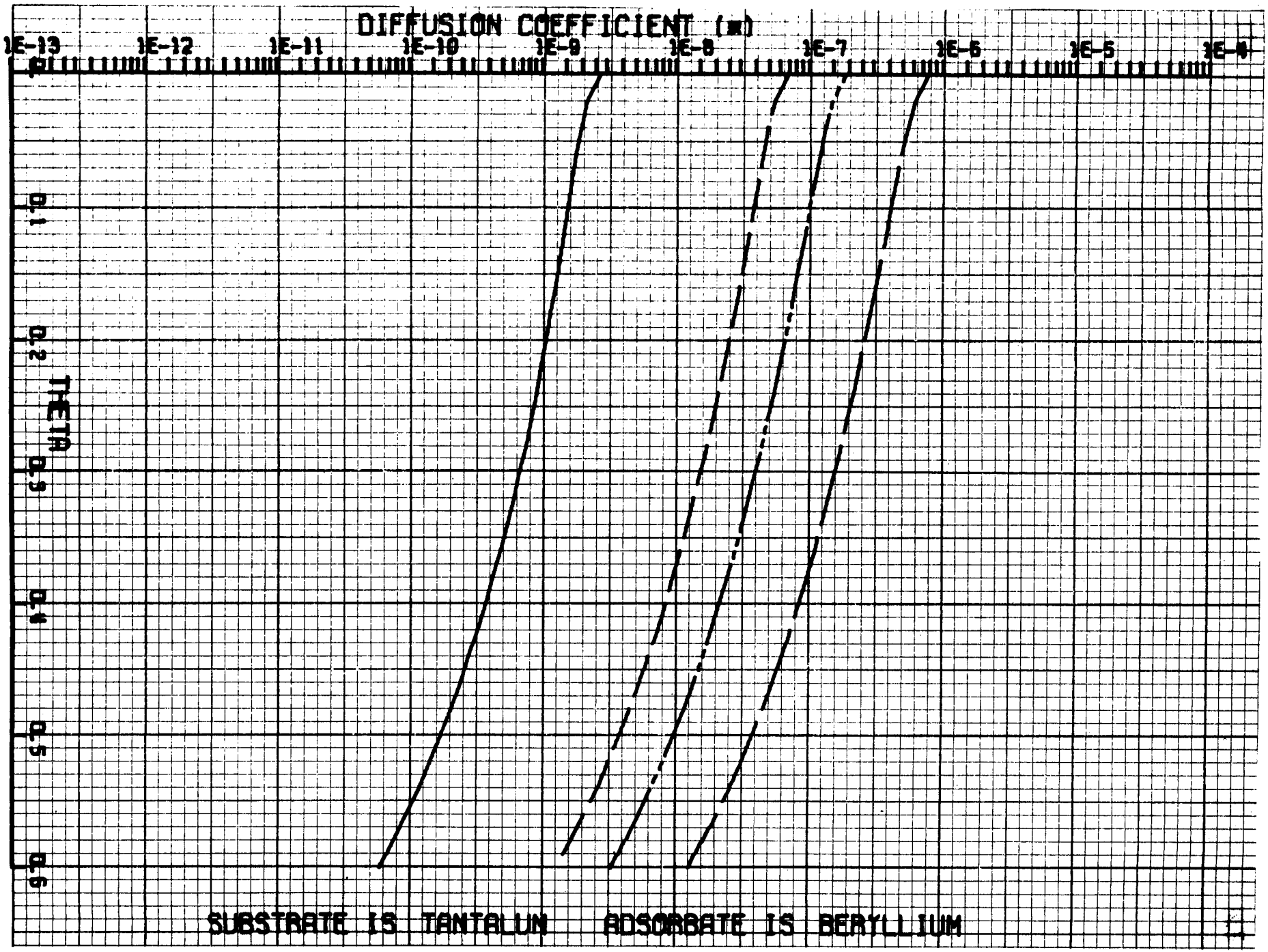
DIFFUSION COEFFICIENT (m)
1E-13
1E-12
1E-11
1E-10
1E-9
1E-8
1E-7
1E-6
1E-5
1E-4
THETA
0.1
0.2
0.3
0.4
0.5
0.6
SUBSTRATE IS TANTALUM ADSORBATE IS BERYLLIUM

DIFFUSION COEFFICIENT (cm²)
1E-4
1E-5
1E-6
1E-7
1E-8
1E-9
1E-10
1E-11
1E-12
1E-13
TEMPERATURE (K) (×10¹)
40.
80.
120.
160.
200.
SUBSTRATE IS TANTALUM ADSORBATE IS CARBON

SUBSTRATE IS TANTALUM ADSORBATE IS CARBON
DIFFUSION COEFFICIENT (M²)
1E-4
1E-5
1E-6
1E-7
1E-8
1E-9
1E-10
1E-11
1E-12
1E-13
THETA
0.1
0.2
0.3
0.4
0.5
0.6

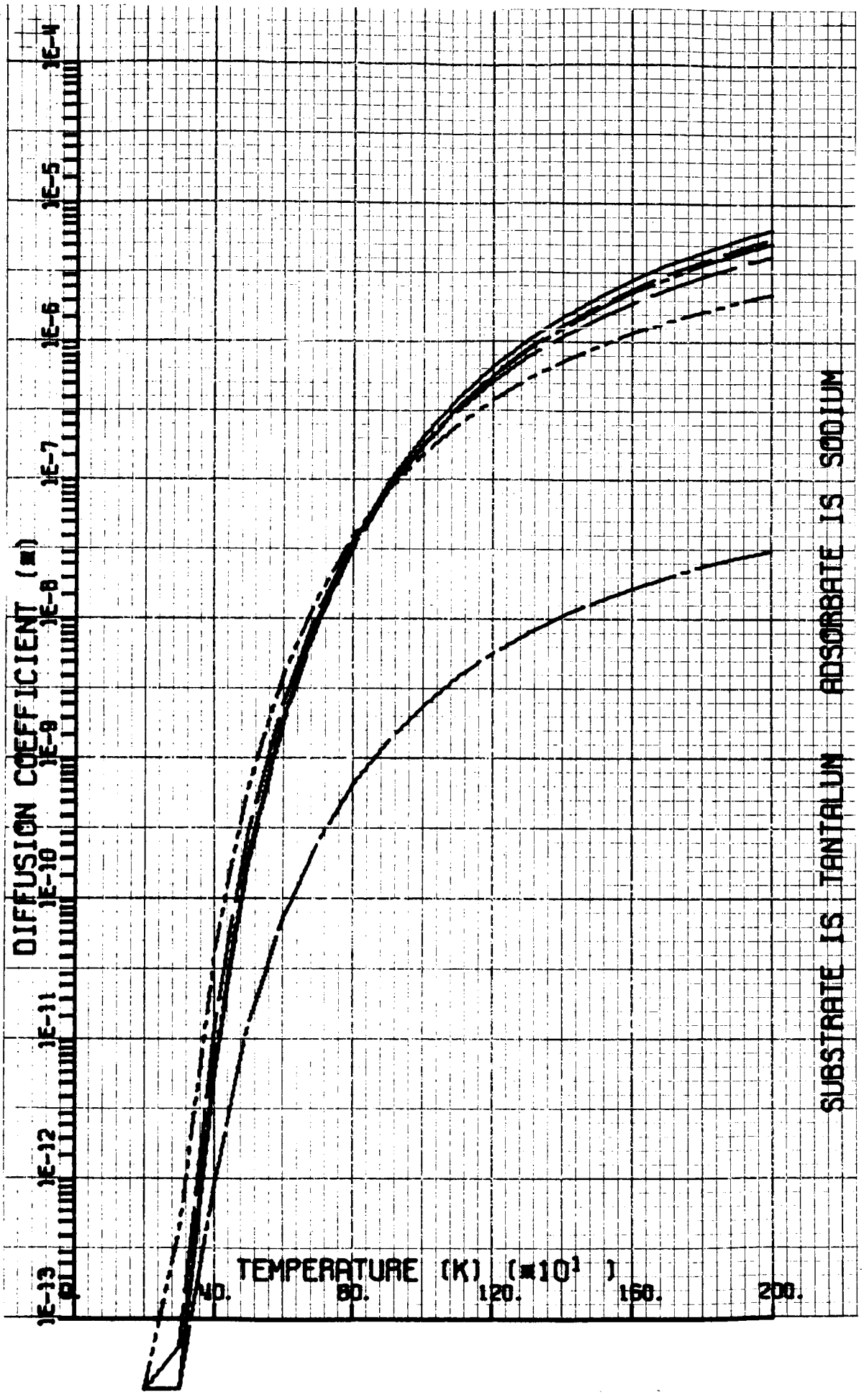
DIFFUSION COEFFICIENT (■)
1E-4
1E-5
1E-6
1E-7
1E-8
1E-9
1E-10
1E-11
1E-12
1E-13
TEMPERATURE (K) (×10¹)
40.
80.
120.
160.
200.
SUBSTRATE IS TANTALUM ADSORBATE IS SODIUM

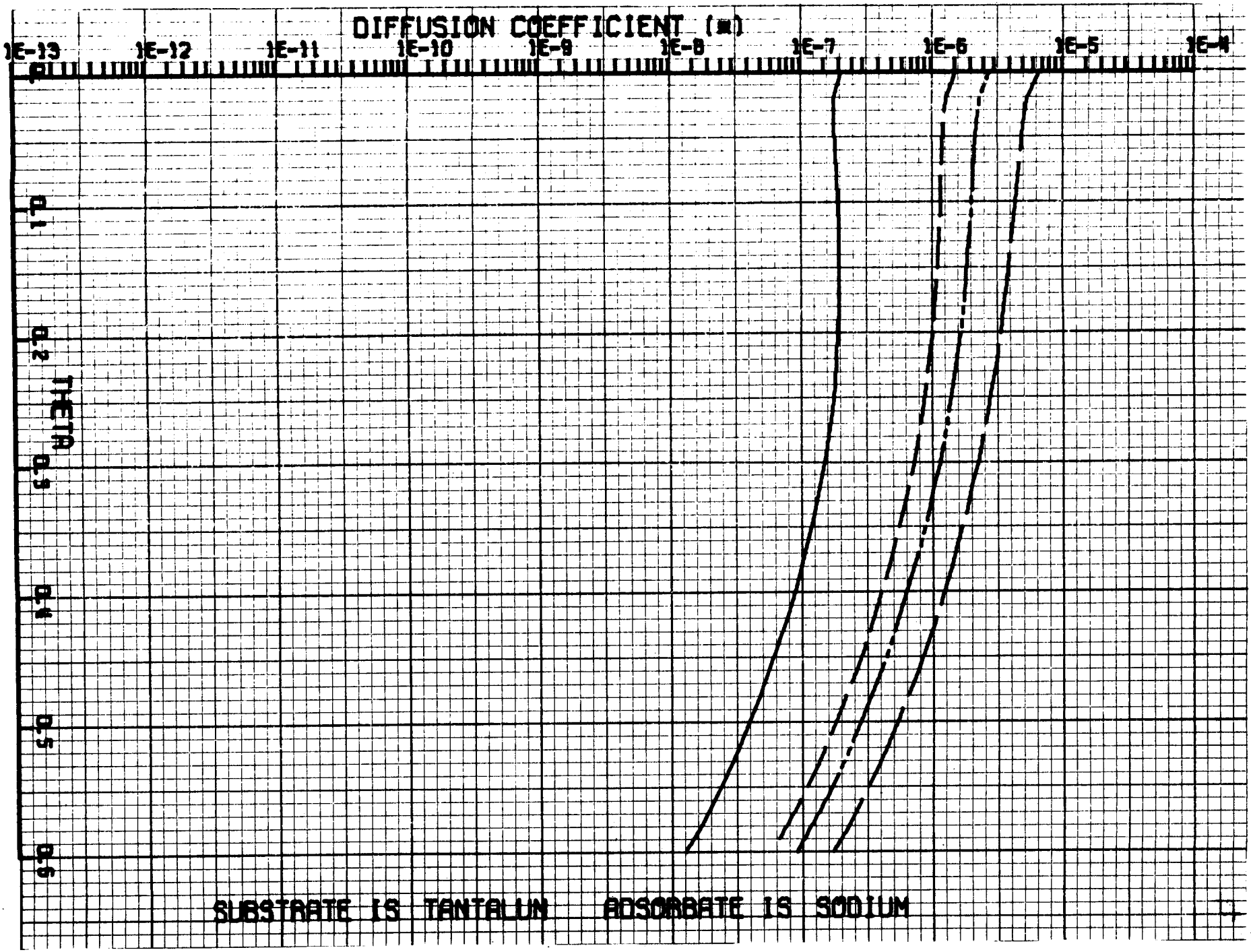
DIFFUSION COEFFICIENT (m)
1E-13
1E-12
1E-11
1E-10
1E-9
1E-8
1E-7
1E-6
1E-5
1E-4
THETA
0.1
0.2
0.3
0.4
0.5
0.6
SUBSTRATE IS TANTALUM ADSORBATE IS SODIUM

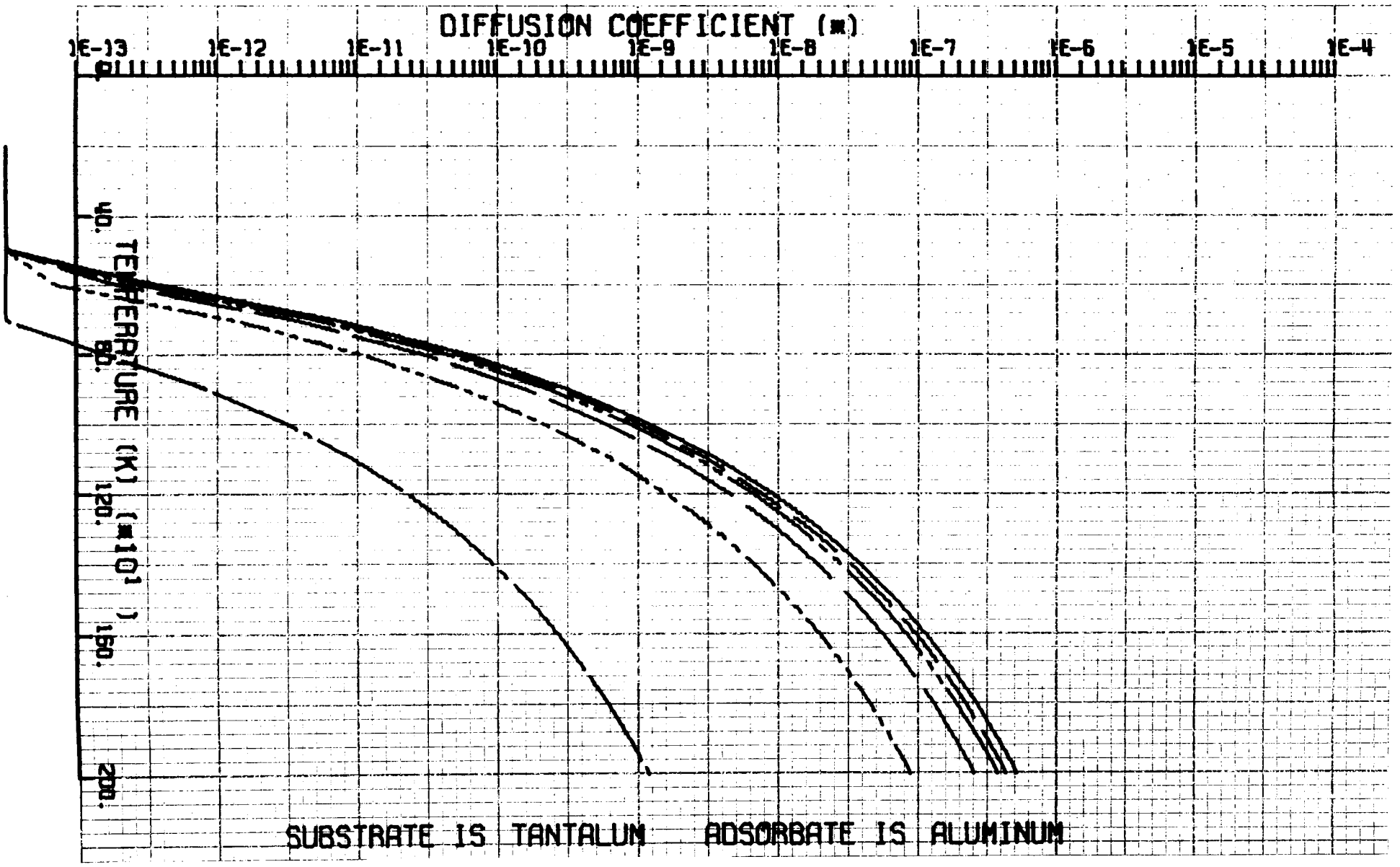
DIFFUSION COEFFICIENT (m)
1E-13
1E-12
1E-11
1E-10
1E-9
1E-8
1E-7
1E-6
1E-5
1E-4
TEMPERATURE (K) (*10¹)
40.
80.
120.
160.
200.
SUBSTRATE IS TANTALUM ADSORBATE IS ALUMINUM

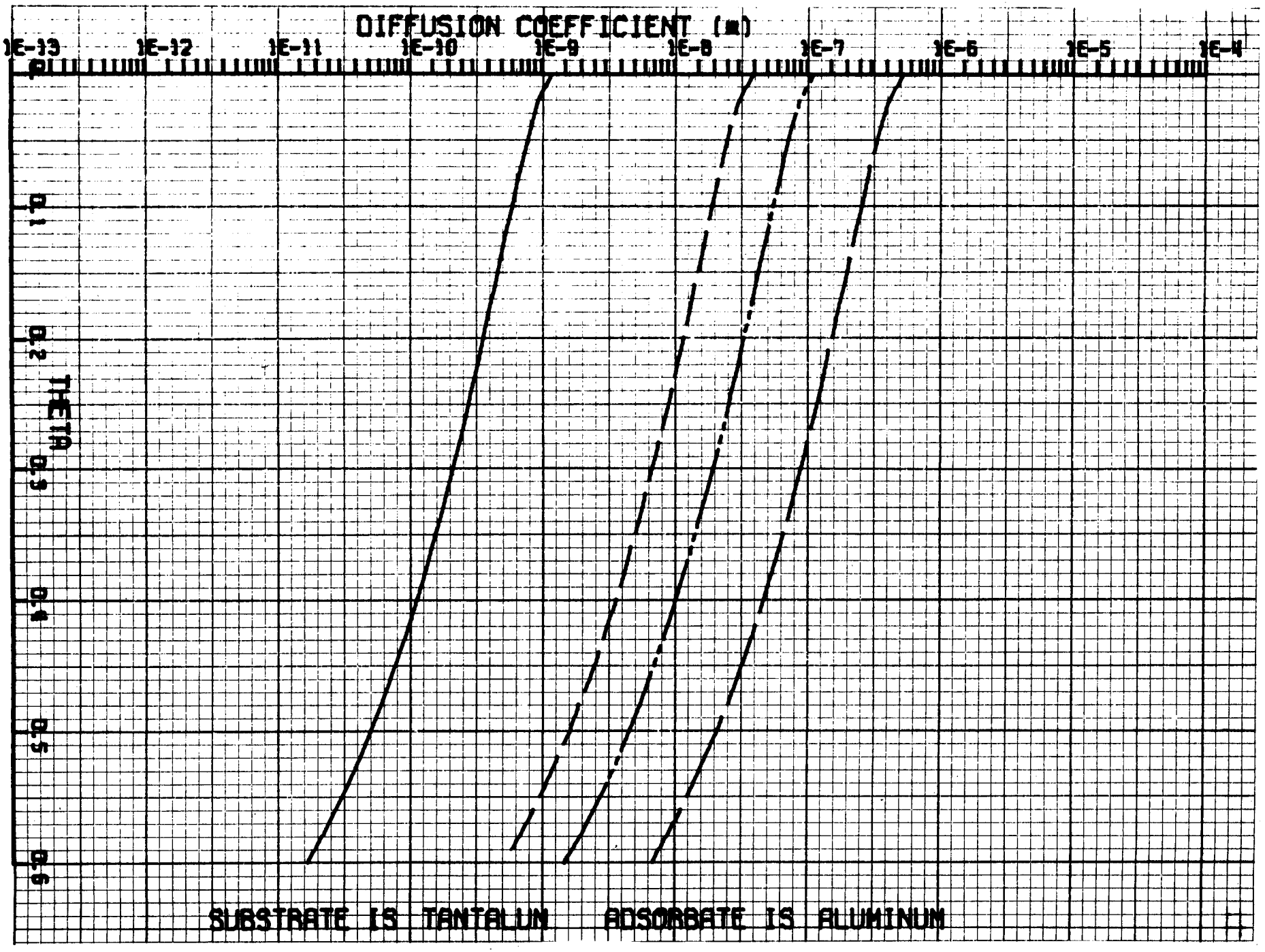
DIFFUSION COEFFICIENT (m)
1E-13
1E-12
1E-11
1E-10
1E-9
1E-8
1E-7
1E-6
1E-5
1E-4
THETA
0.1
0.2
0.3
0.4
0.5
0.6
SUBSTRATE IS TANTALUM ADSORBATE IS ALUMINUM

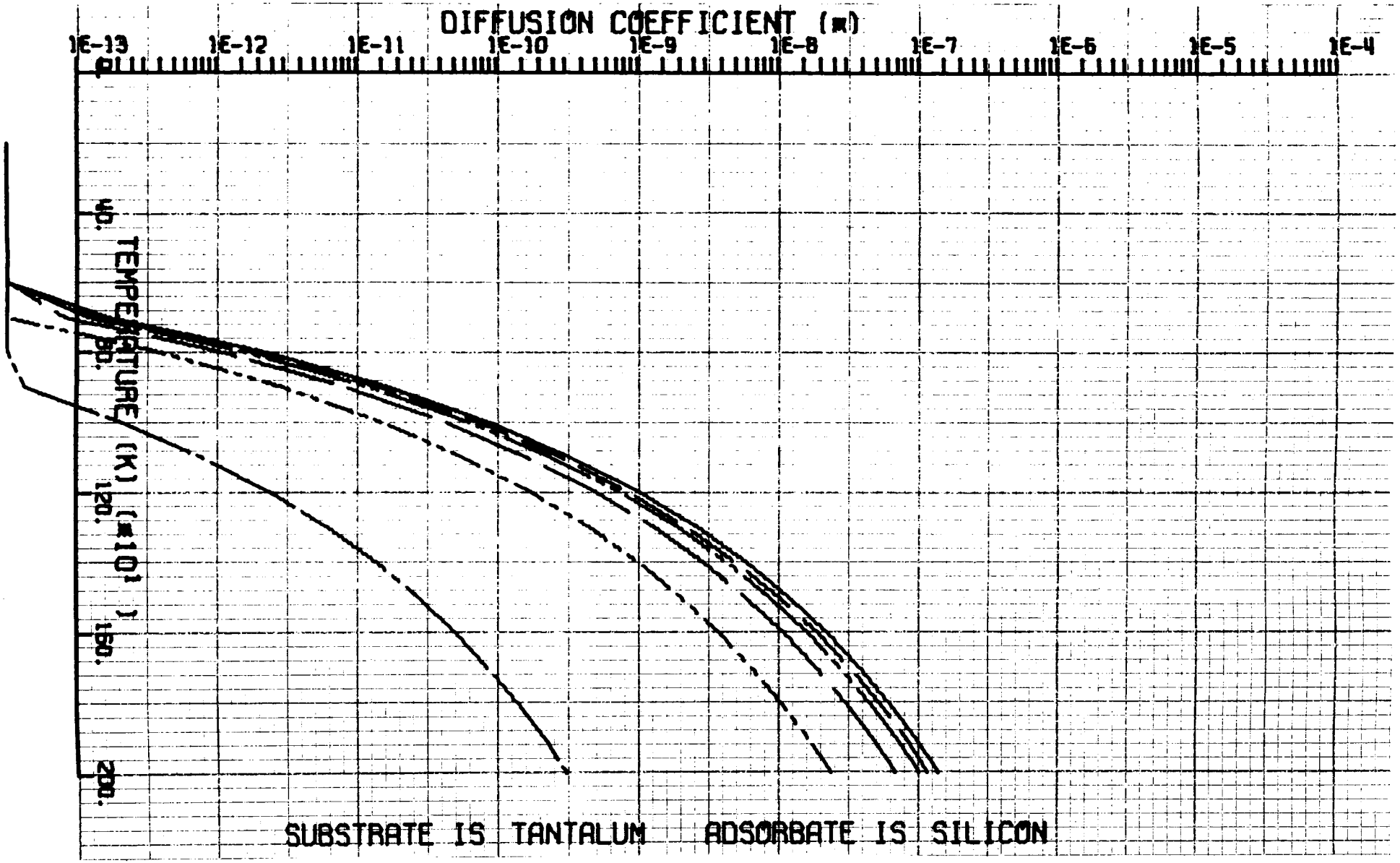
DIFFUSION COEFFICIENT (m)
1E-13
1E-12
1E-11
1E-10
1E-9
1E-8
1E-7
1E-6
1E-5
1E-4
TEMPERATURE (K) [*10^1]
40.
80.
120.
160.
200.
SUBSTRATE IS TANTALUM ADSORBATE IS SILICON

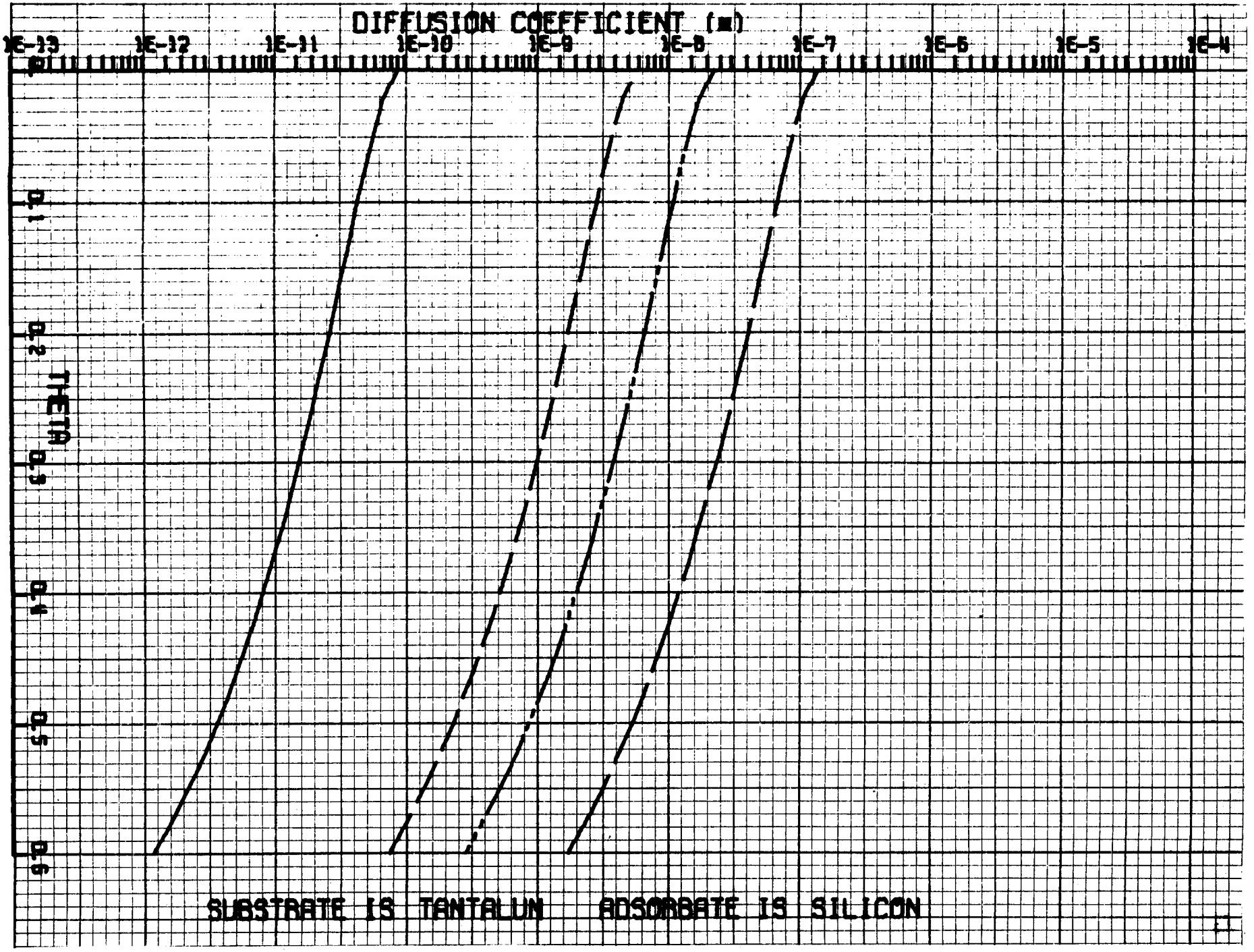
DIFFUSION COEFFICIENT (m)
1E-13
1E-12
1E-11
1E-10
1E-9
1E-8
1E-7
1E-6
1E-5
1E-4
THETA
0.1
0.2
0.3
0.4
0.5
0.6
SUBSTRATE IS TANTALUM ADSORBATE IS SILICON

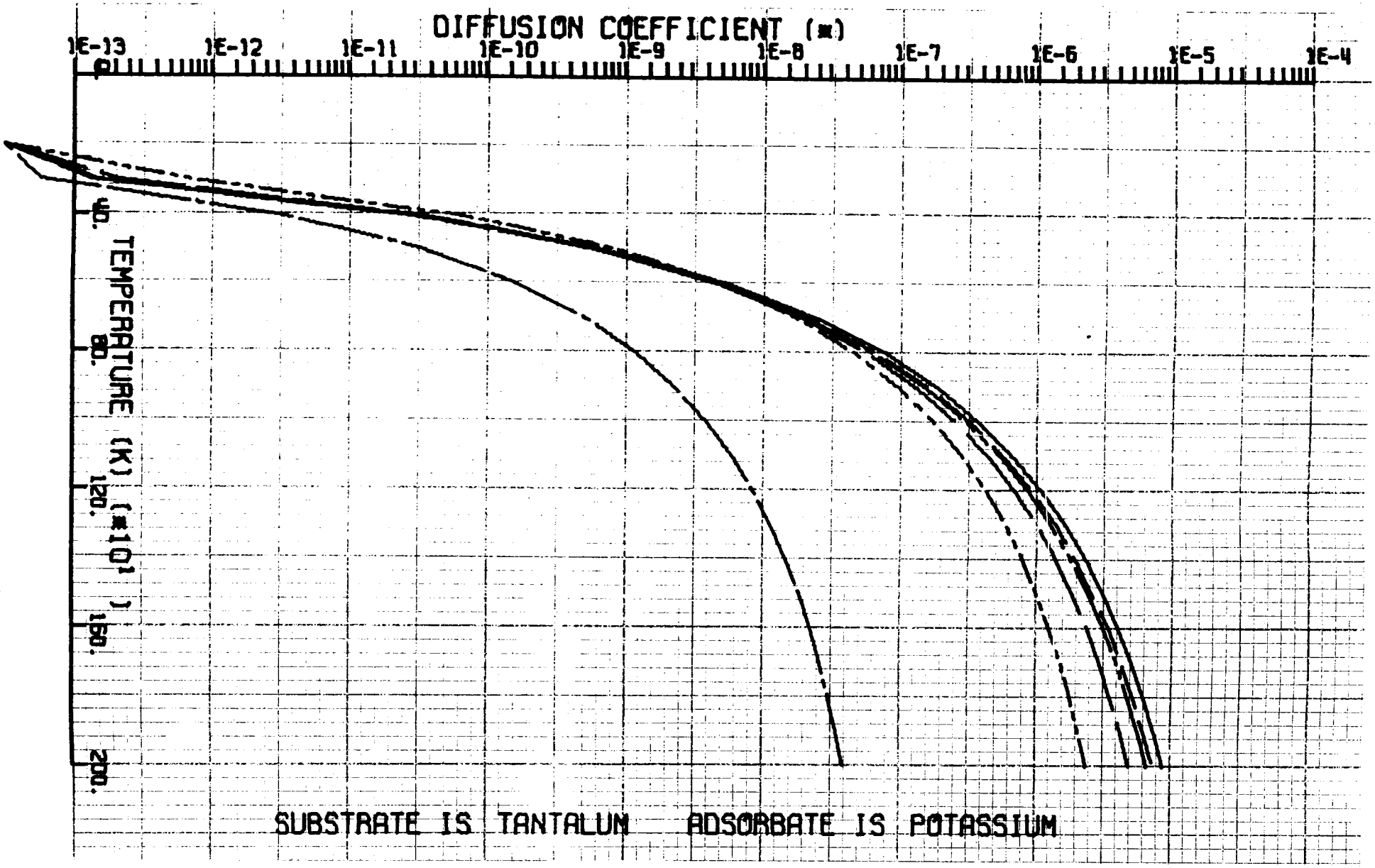
DIFFUSION COEFFICIENT (m)
1E-13
1E-12
1E-11
1E-10
1E-9
1E-8
1E-7
1E-6
1E-5
1E-4
TEMPERATURE (K) (*10^1)
40.
80.
120.
160.
200.
SUBSTRATE IS TANTALUM ADSORBATE IS POTASSIUM

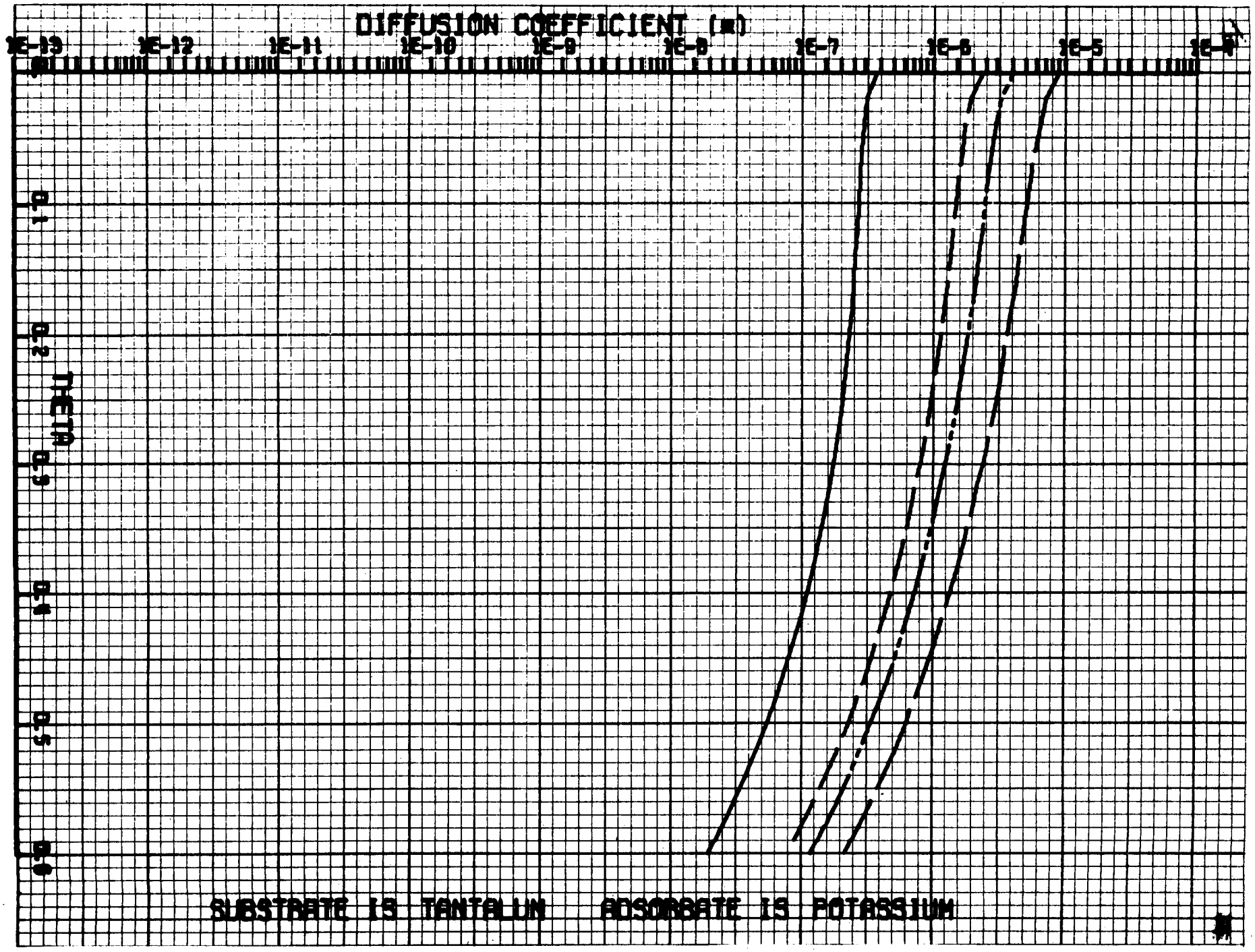
DIFFUSION COEFFICIENT (m)
1E-13
1E-12
1E-11
1E-10
1E-9
1E-8
1E-7
1E-6
1E-5
1E-4
THETA
0.1
0.2
0.3
0.4
0.5
0.6
SUBSTRATE IS TANTALUM ADSORBATE IS POTASSIUM

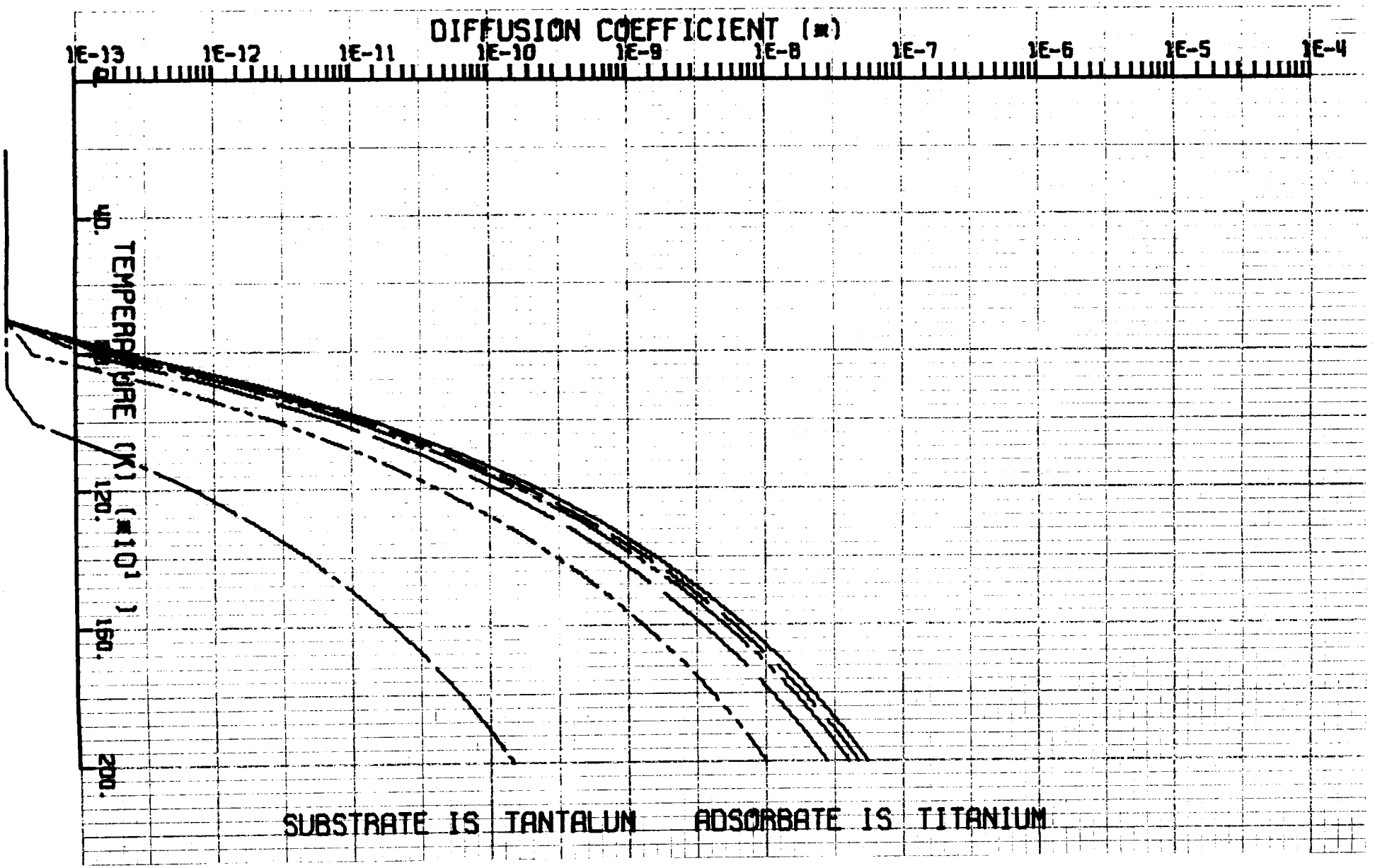
DIFFUSION COEFFICIENT (*)
1E-13
1E-12
1E-11
1E-10
1E-9
1E-8
1E-7
1E-6
1E-5
1E-4
TEMPERATURE (K) (*10¹)
40.
120.
160.
200.
SUBSTRATE IS TANTALUM ADSORBATE IS TITANIUM

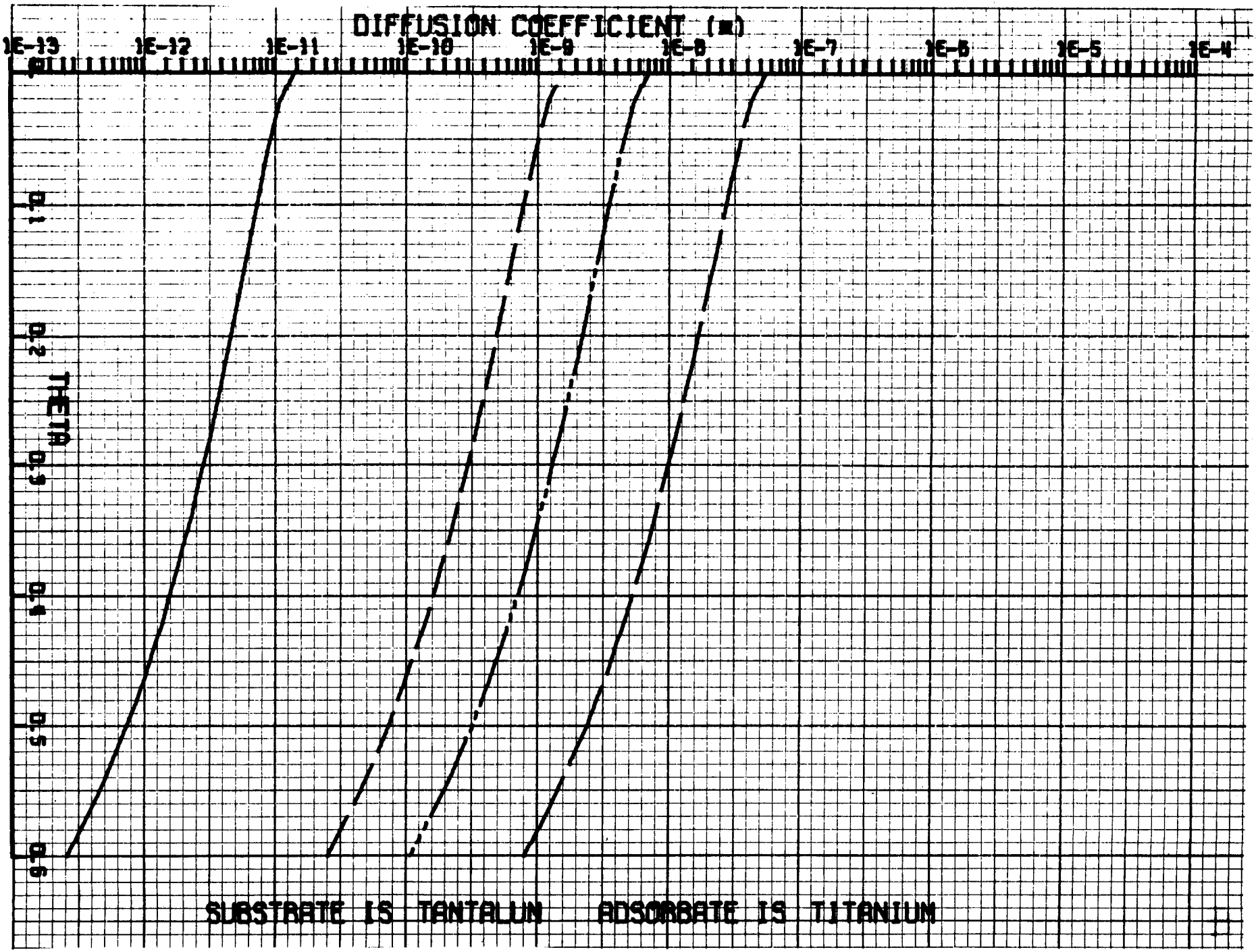
DIFFUSION COEFFICIENT (m)
1E-13
1E-12
1E-11
1E-10
1E-9
1E-8
1E-7
1E-6
1E-5
1E-4
0.1
0.2
0.3
0.4
0.5
0.6
THETA
SUBSTRATE IS TANTALUM ADSORBATE IS TITANIUM

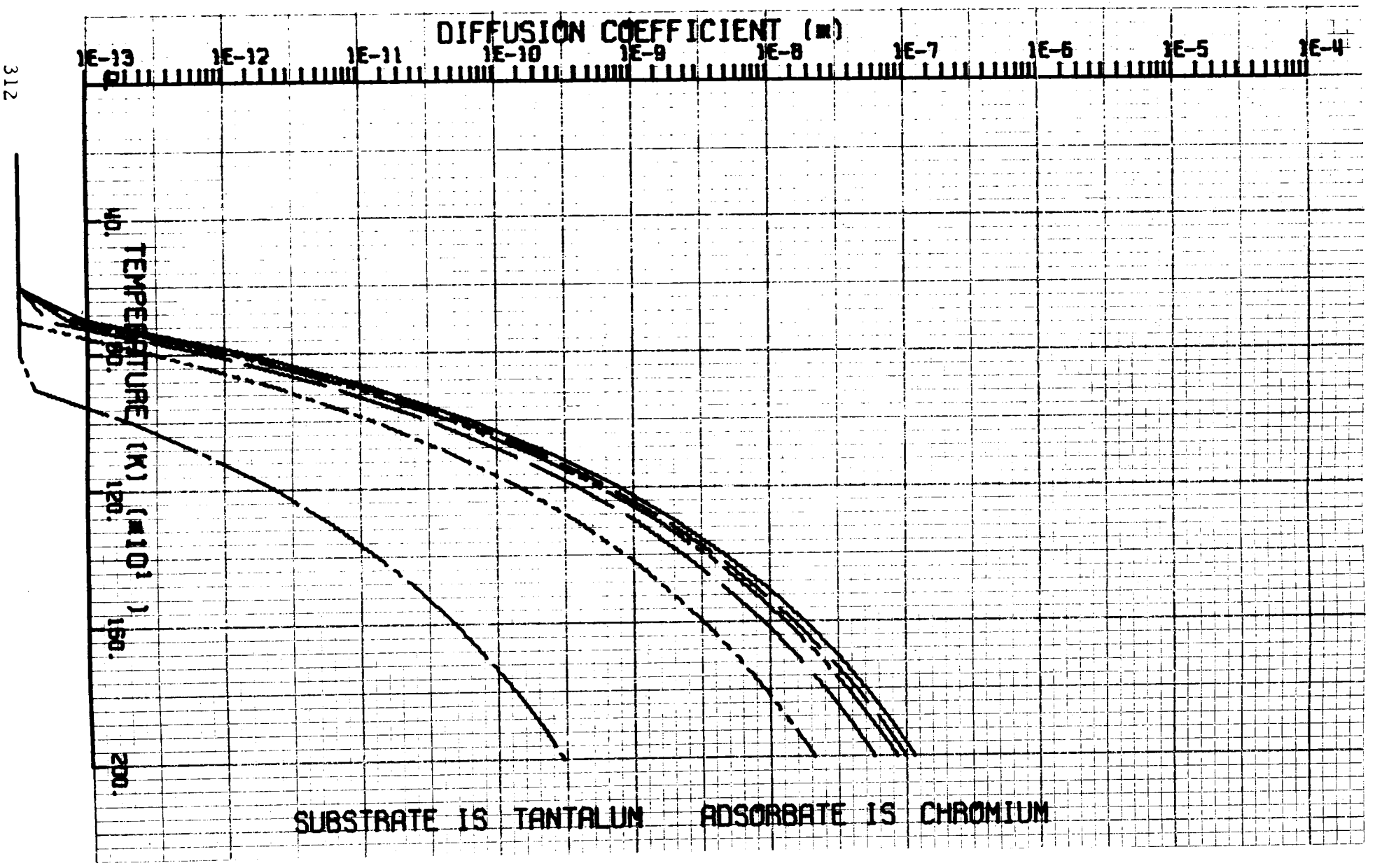
DIFFUSION COEFFICIENT (m)
1E-13
1E-12
1E-11
1E-10
1E-9
1E-8
1E-7
1E-6
1E-5
1E-4
TEMPERATURE (K) (=10³)
40.
80.
120.
160.
200.
SUBSTRATE IS TANTALUM ADSORBATE IS CHROMIUM

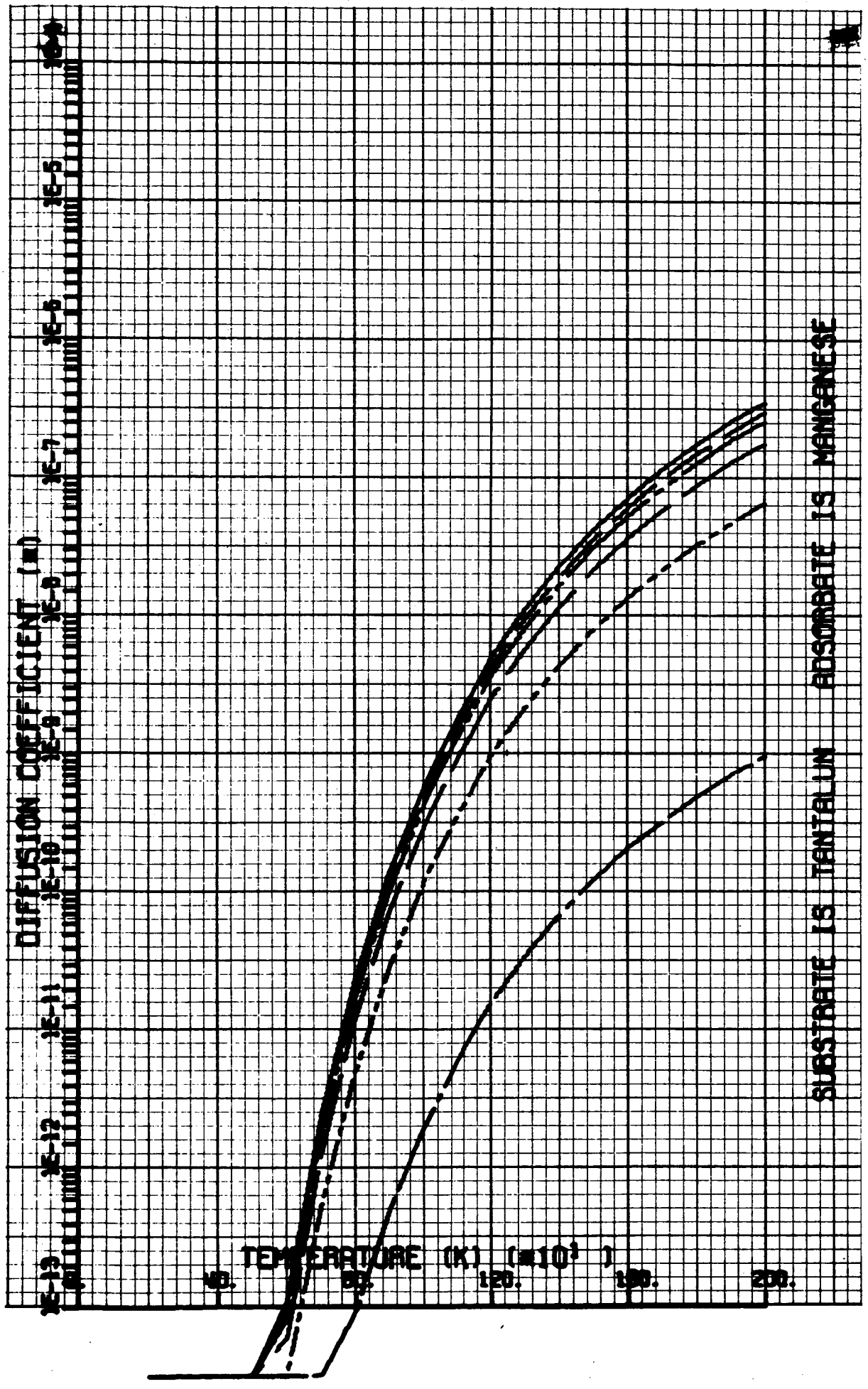
DIFFUSION COEFFICIENT (M)
1E-4
1E-5
1E-6
1E-7
1E-8
1E-9
1E-10
1E-11
1E-12
1E-13
TEMPERATURE (K) (*10³)
40.
80.
120.
160.
200.
SUBSTRATE IS TANTALUM ABSORBATE IS MANGANESE

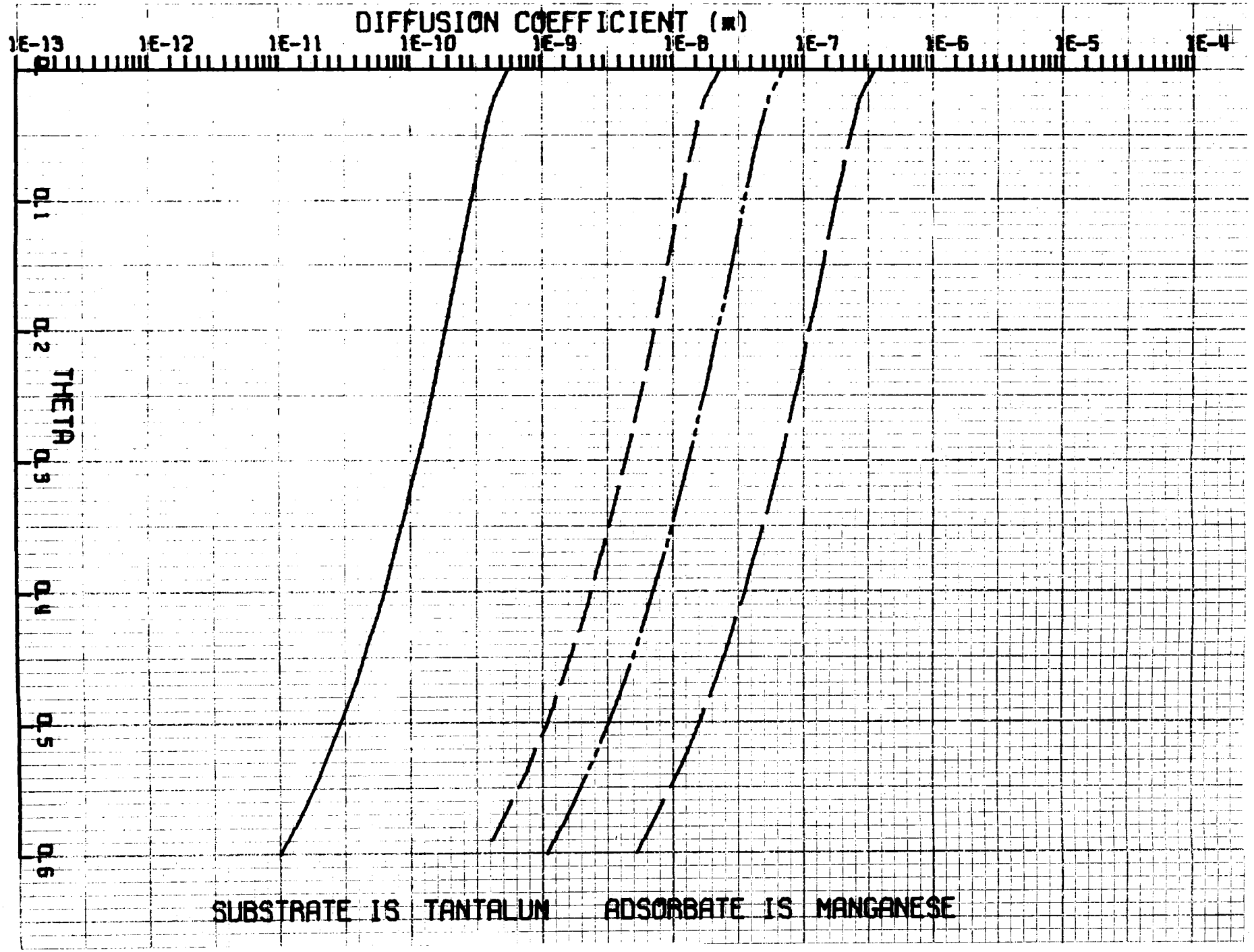
DIFFUSION COEFFICIENT (m)
1E-13
1E-12
1E-11
1E-10
1E-9
1E-8
1E-7
1E-6
1E-5
1E-4
0
0.1
0.2
0.3
0.4
0.5
0.6
THETA
SUBSTRATE IS TANTALUM ADSORBATE IS MANGANESE

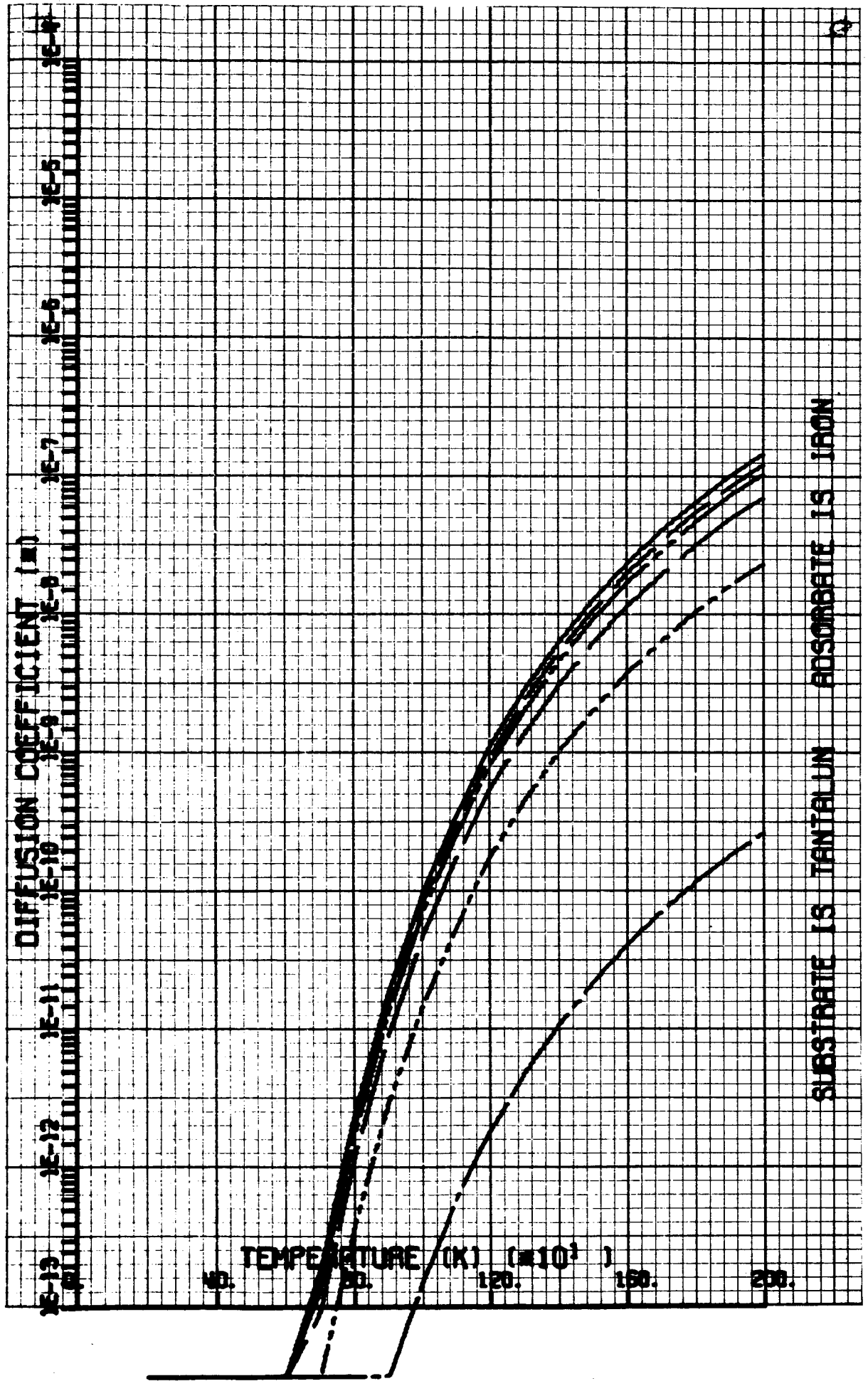
DIFFUSION COEFFICIENT (m²)
1E-4
1E-5
1E-6
1E-7
1E-8
1E-9
1E-10
1E-11
1E-12
1E-13
TEMPERATURE (K) (×10³)
40.
80.
120.
160.
200.
SUBSTRATE IS TANTALUM ADSORBATE IS IRON

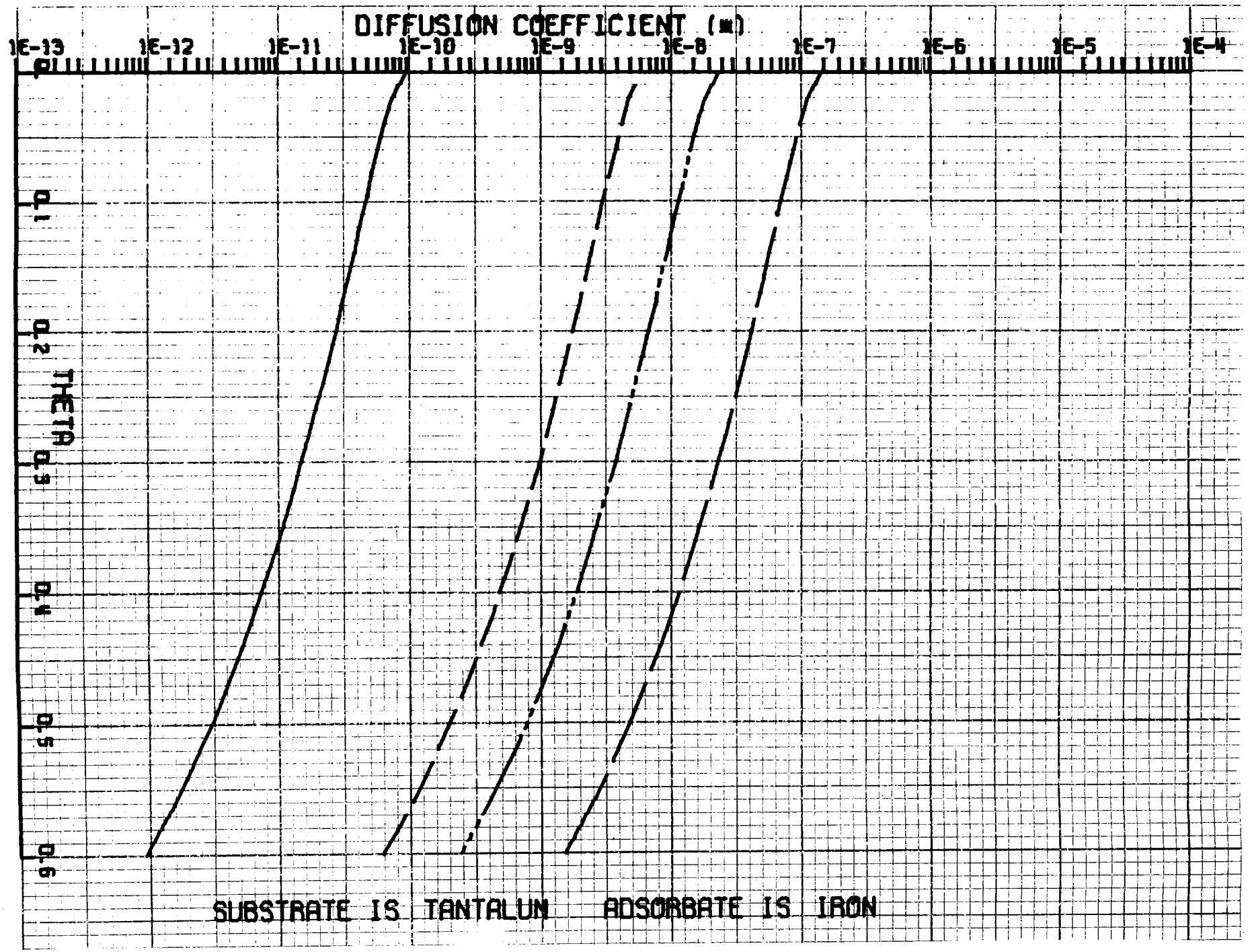
DIFFUSION COEFFICIENT (m)
1E-13
1E-12
1E-11
1E-10
1E-9
1E-8
1E-7
1E-6
1E-5
1E-4
THETA
0.1
0.2
0.3
0.4
0.5
0.6
SUBSTRATE IS TANTALUN ADSORBATE IS IRON

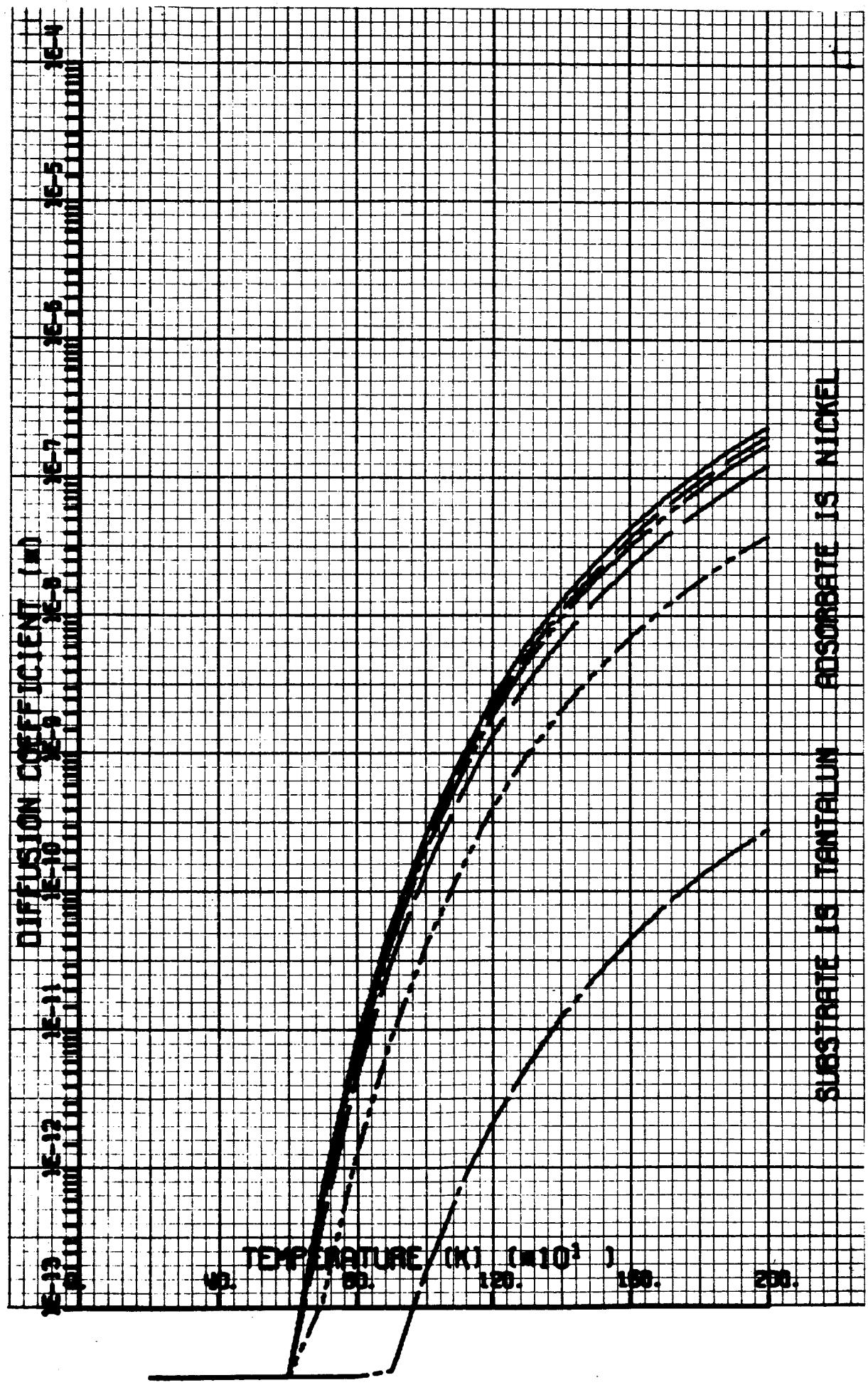
DIFFUSION COEFFICIENT (m)
1E-4
1E-5
1E-6
1E-7
1E-8
1E-9
1E-10
1E-11
1E-12
1E-13
TEMPERATURE (K) (*10¹)
40.
80.
120.
160.
200.
SUBSTRATE IS TANTALUM ADSORBATE IS NICKEL

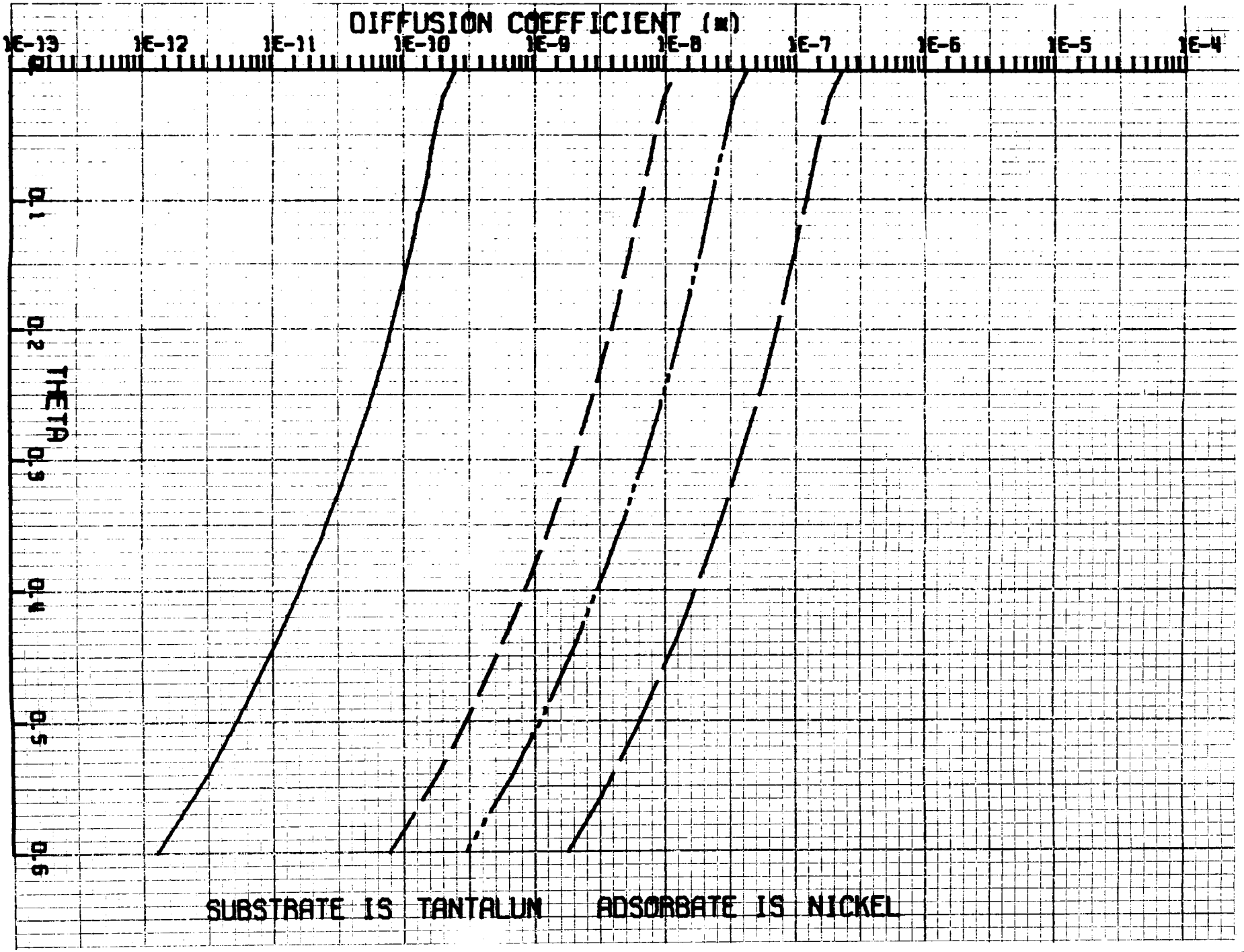
DIFFUSION COEFFICIENT (m)
1E-13
1E-12
1E-11
1E-10
1E-9
1E-8
1E-7
1E-6
1E-5
1E-4
0
0.1
0.2
THETA
0.3
0.4
0.5
0.6
SUBSTRATE IS TANTALUM ADSORBATE IS NICKEL

DIFFUSION COEFFICIENT (m)
1E-4
1E-5
1E-6
1E-7
1E-8
1E-9
1E-10
1E-11
1E-12
1E-13
TEMPERATURE (K) (*10¹)
40.
80.
120.
160.
200.
SUBSTRATE IS TANTALUM ADSORBATE IS COPPER

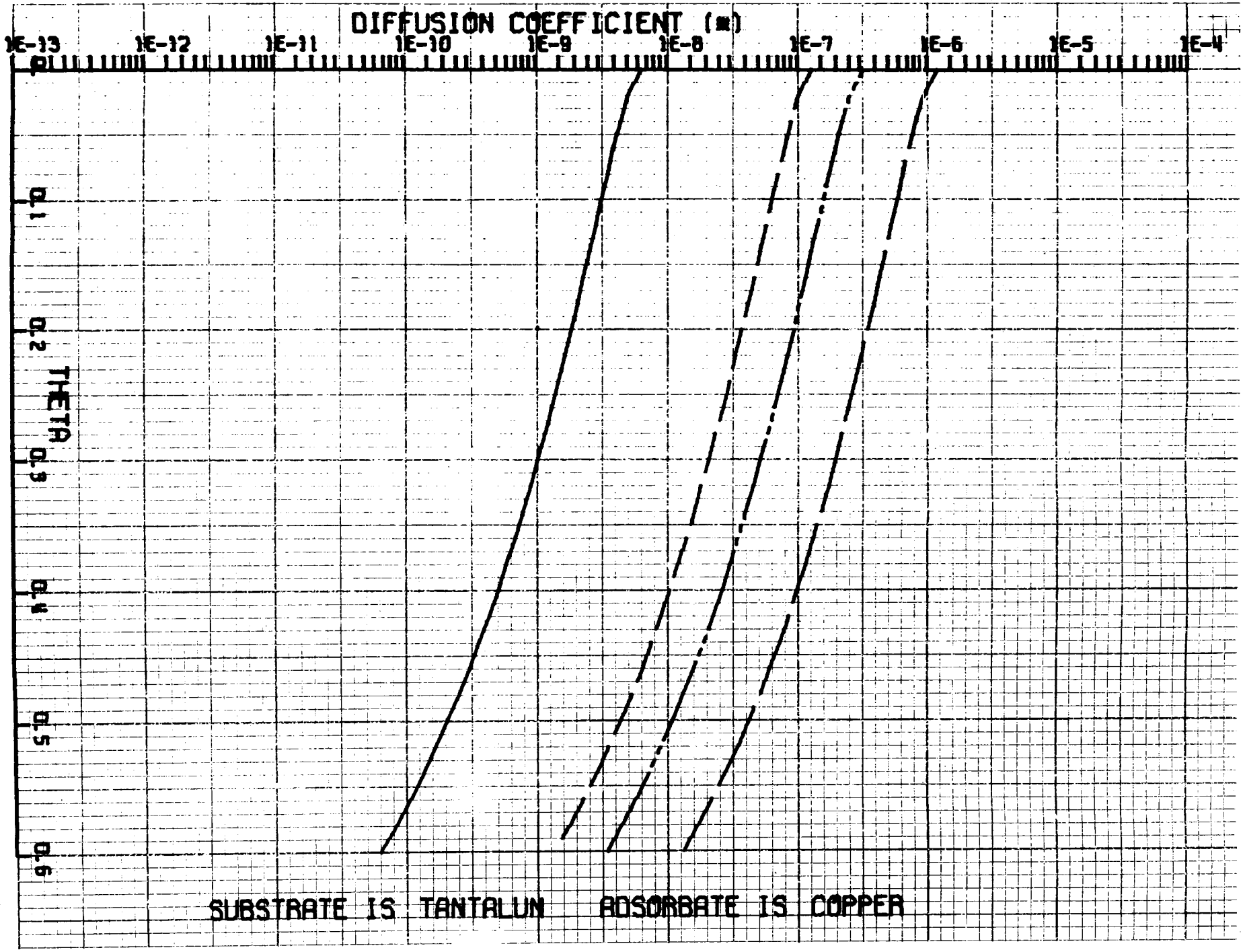
DIFFUSION COEFFICIENT (cm²)
1E-13
1E-12
1E-11
1E-10
1E-9
1E-8
1E-7
1E-6
1E-5
1E-4
0
0.1
0.2
0.3
0.4
0.5
0.6
THETA
SUBSTRATE IS TANTALUM ADSORBATE IS COPPER

DIFFUSION COEFFICIENT (cm²)
1E-4
1E-5
1E-6
1E-7
1E-8
1E-9
1E-10
1E-11
1E-12
1E-13
TEMPERATURE (K) (×10³)
40.
80.
120.
160.
200.
SUBSTRATE IS TANTALUM ADSORBATE IS GALLIUM

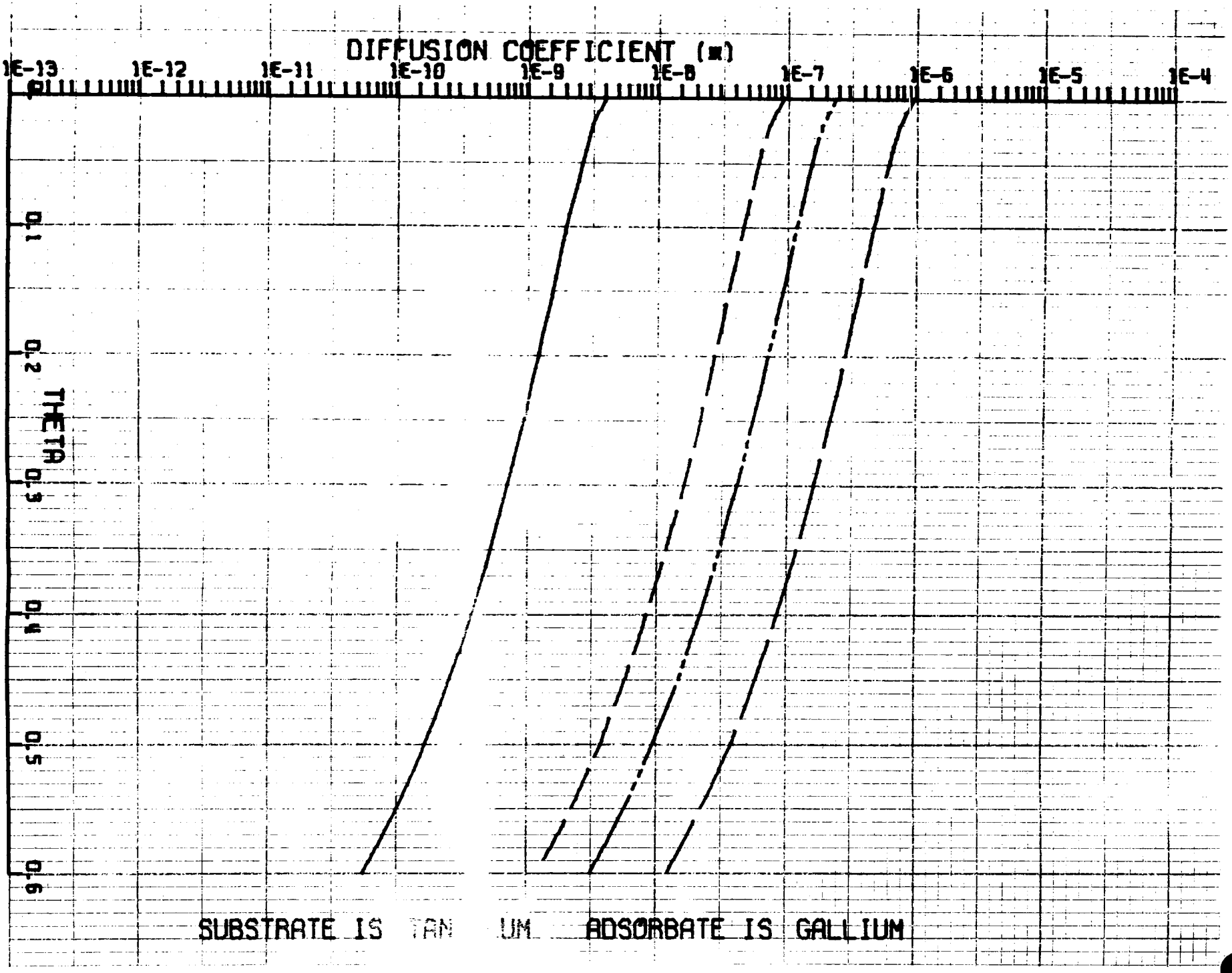
DIFFUSION COEFFICIENT (m)
1E-13
1E-12
1E-11
1E-10
1E-9
1E-8
1E-7
1E-6
1E-5
1E-4
THETA
0.1
0.2
0.3
0.4
0.5
0.6
SUBSTRATE IS TAN UM ADSORBATE IS GALLIUM

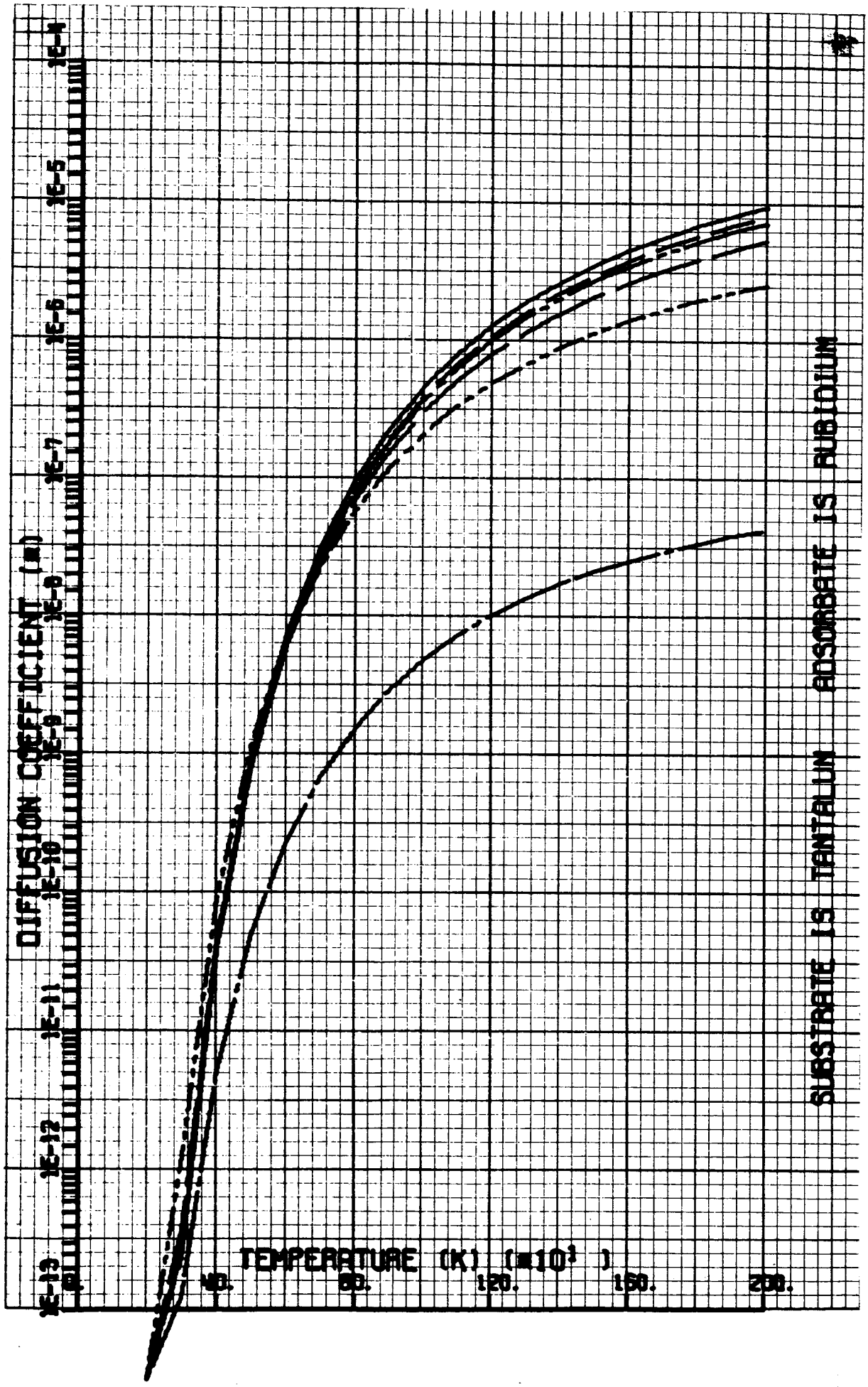
DIFFUSION COEFFICIENT (m²)
1E-4
1E-5
1E-6
1E-7
1E-8
1E-9
1E-10
1E-11
1E-12
1E-13
TEMPERATURE (K) (×10³)
40.
80.
120.
160.
200.
SUBSTRATE IS TANTALUM ADSORBATE IS RUBIDIUM

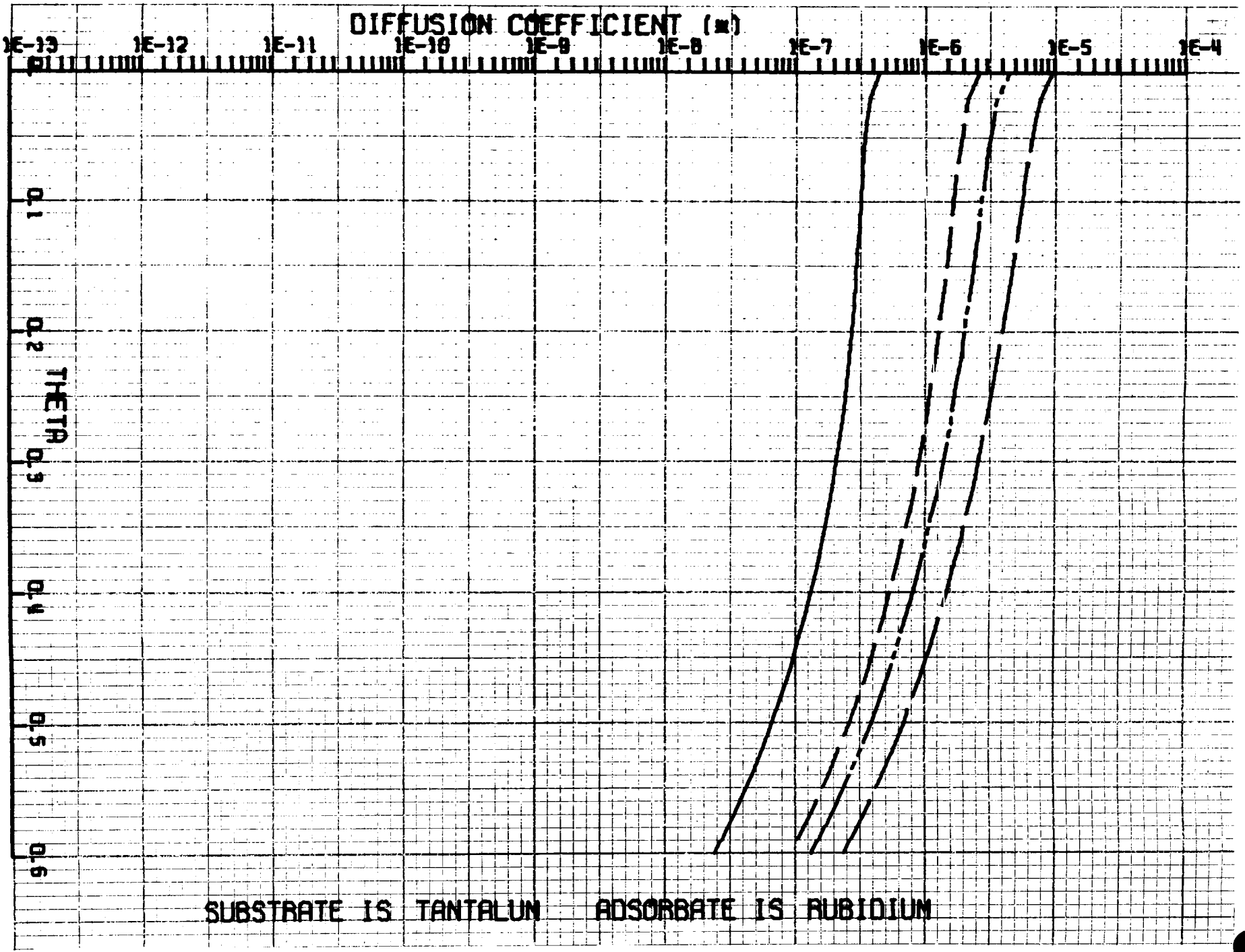
DIFFUSION COEFFICIENT (m)
1E-13
1E-12
1E-11
1E-10
1E-9
1E-8
1E-7
1E-6
1E-5
1E-4
THETA
0.1
0.2
0.3
0.4
0.5
0.6
SUBSTRATE IS TANTALUN ADSORBATE IS RUBIDIUM

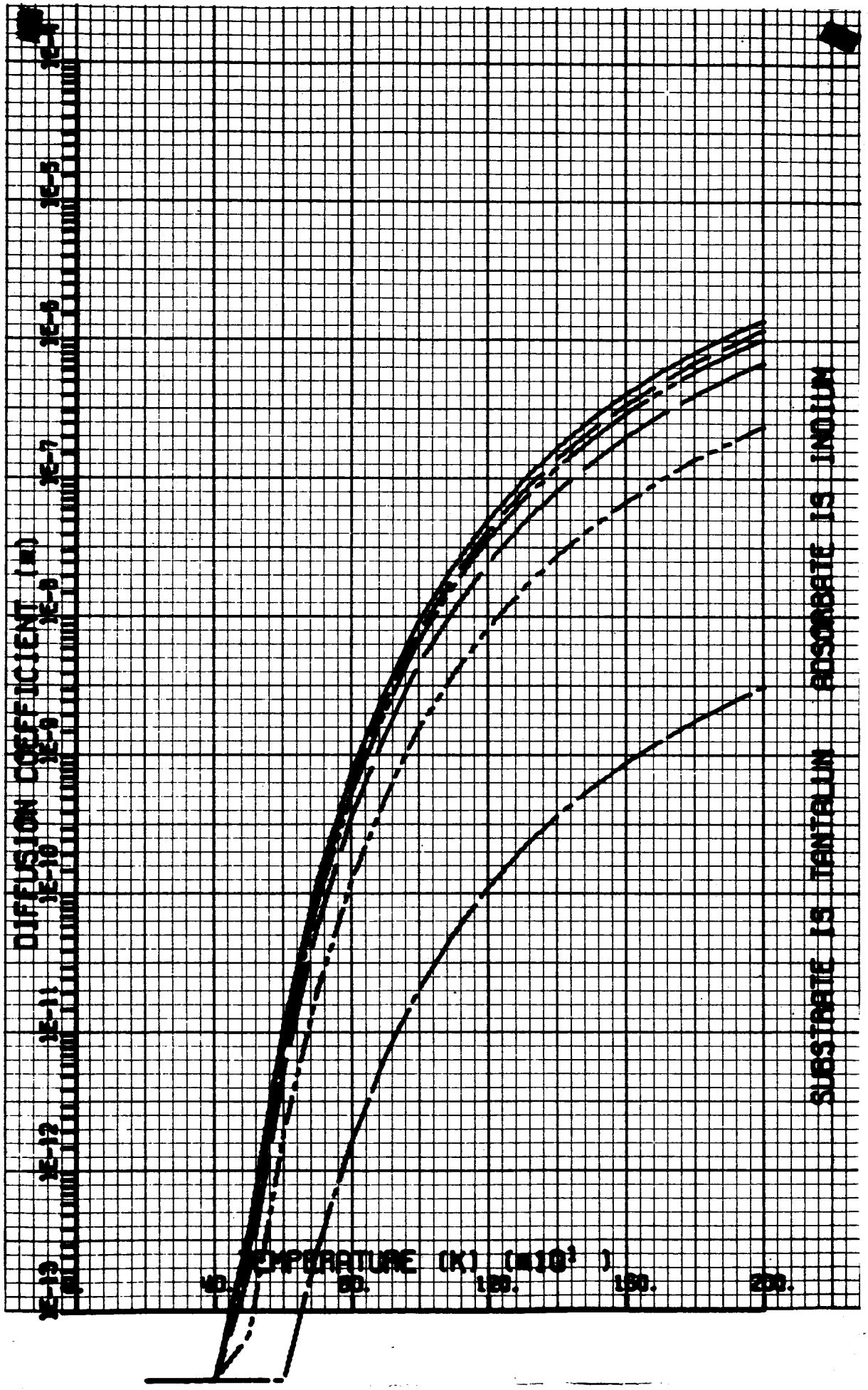
DIFFUSION COEFFICIENT (M)
1E-3
1E-4
1E-5
1E-6
1E-7
1E-8
1E-9
1E-10
1E-11
1E-12
1E-13
TEMPERATURE (K) (*10³)
0.
50.
100.
150.
200.
SUBSTRATE IS TANTALUM ADSORBATE IS INDIUM

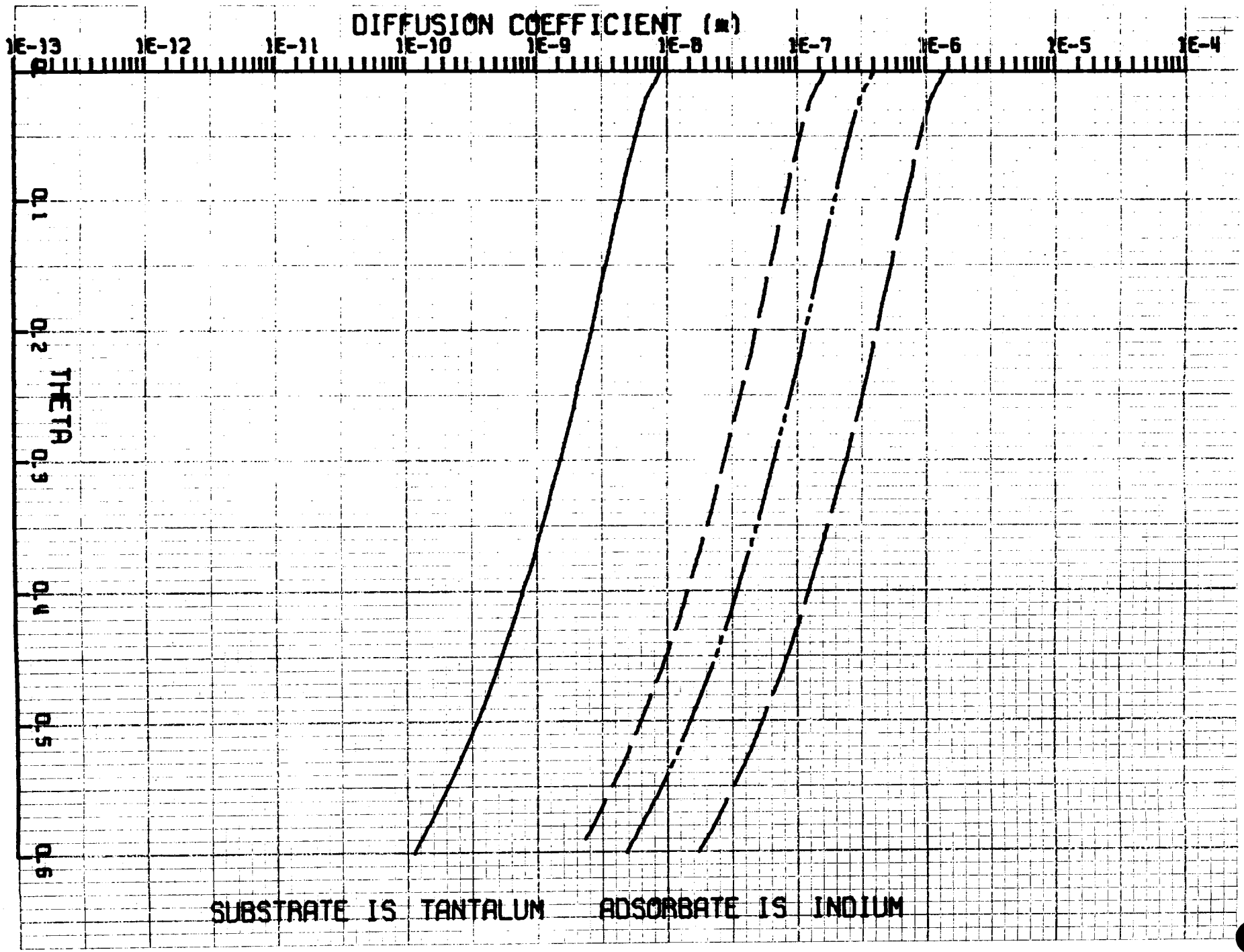
DIFFUSION COEFFICIENT (m)
1E-13
1E-12
1E-11
1E-10
1E-9
1E-8
1E-7
1E-6
1E-5
1E-4
THETA
0.1
0.2
0.3
0.4
0.5
0.6
SUBSTRATE IS TANTALUM ADSORBATE IS INDIUM

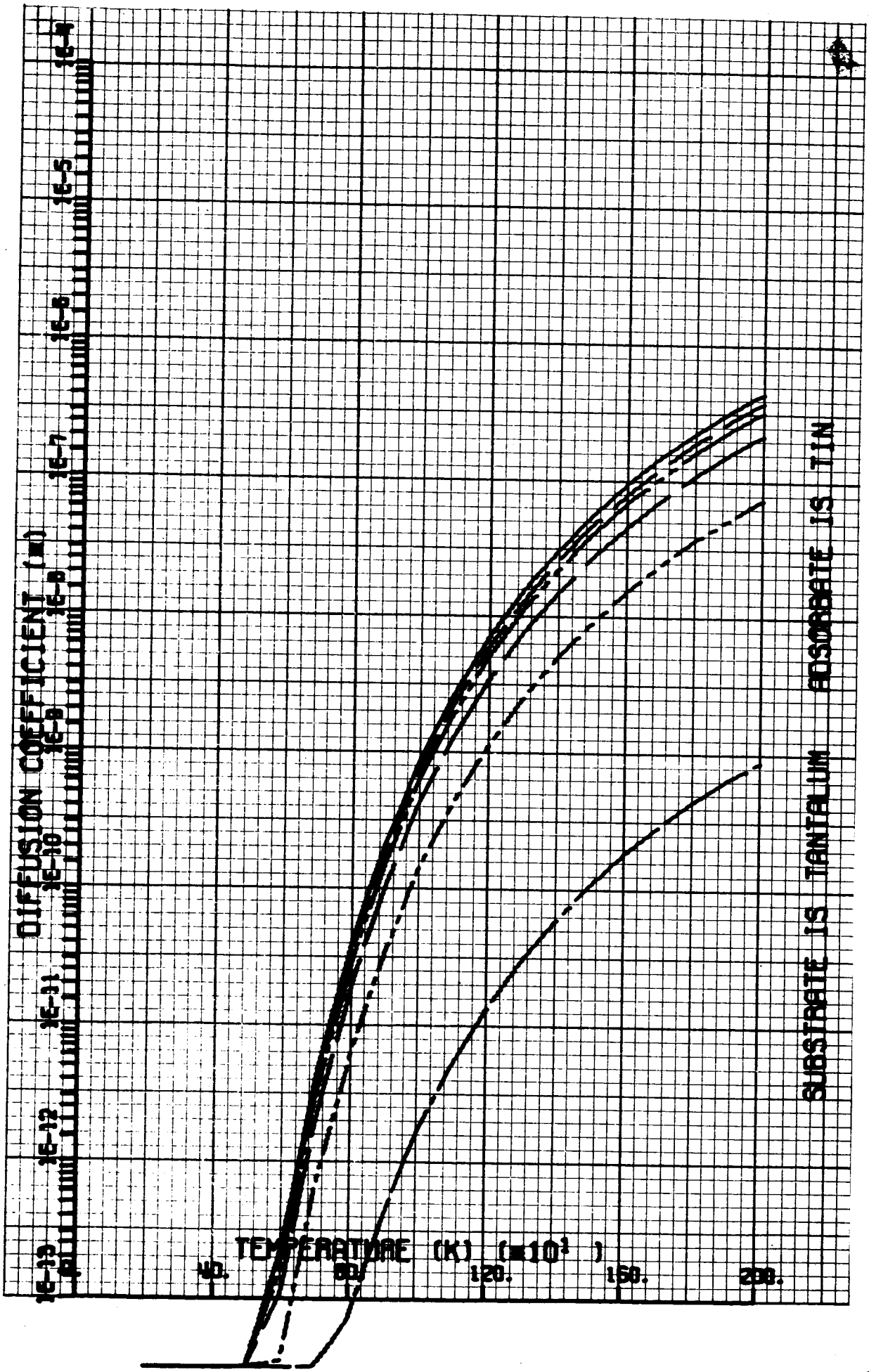
DIFFUSION COEFFICIENT (M²)
1E-4
1E-5
1E-6
1E-7
1E-8
1E-9
1E-10
1E-11
1E-12
1E-13
TEMPERATURE (K) (×10¹)
40.
80.
120.
160.
200.
SUBSTRATE IS TANTALUM ADSORBATE IS TIN

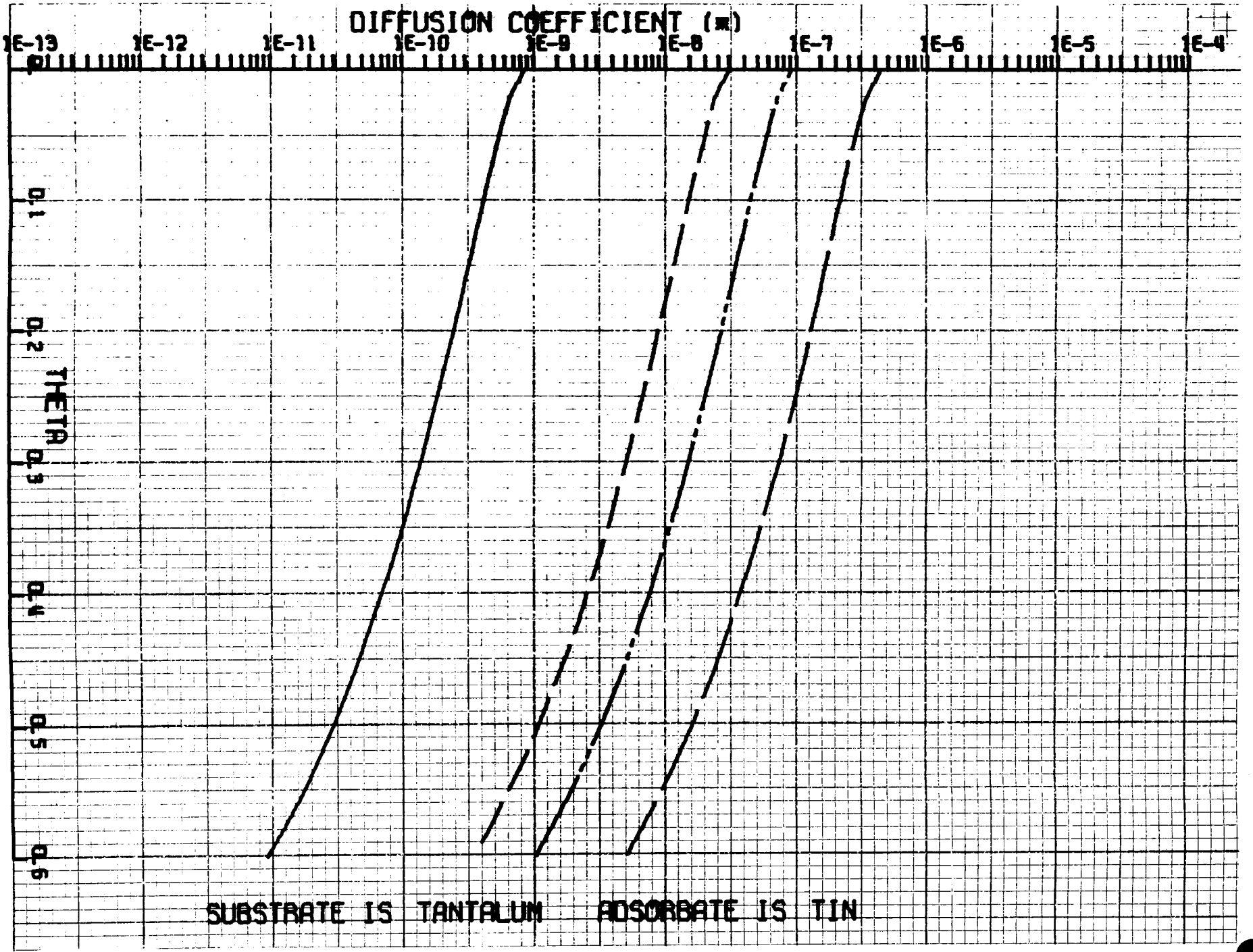
DIFFUSION COEFFICIENT (m)
1E-13
1E-12
1E-11
1E-10
1E-9
1E-8
1E-7
1E-6
1E-5
1E-4
0
0.1
0.2
0.3
0.4
0.5
0.6
THETA
SUBSTRATE IS TANTALUM ADSORBATE IS TIN

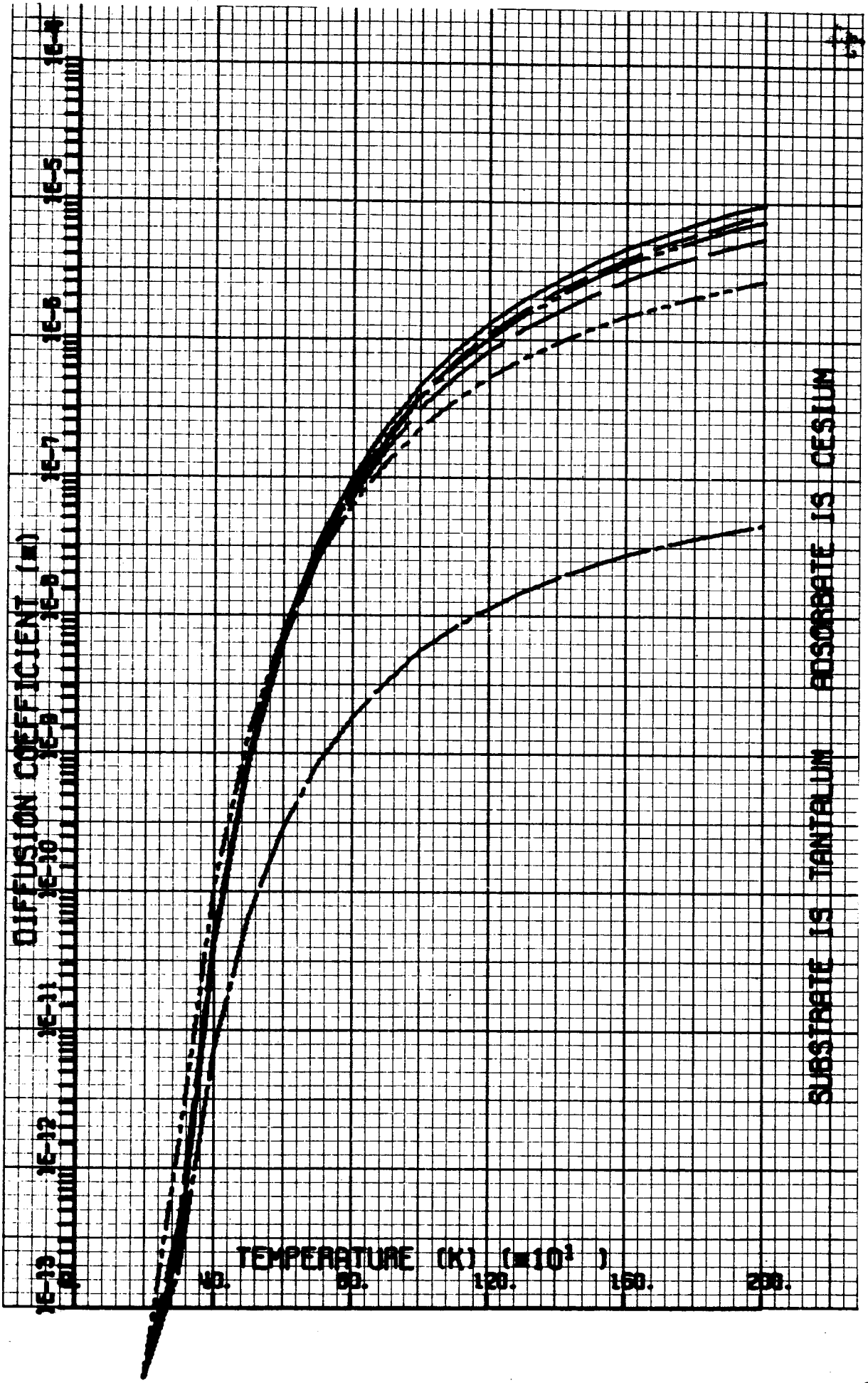
DIFFUSION COEFFICIENT (cm²)
1E-4
1E-5
1E-6
1E-7
1E-8
1E-9
1E-10
1E-11
1E-12
1E-13
TEMPERATURE (K) (×10¹)
40.
80.
120.
160.
200.
SUBSTRATE IS TANTALUM ADSORBATE IS CESIUM

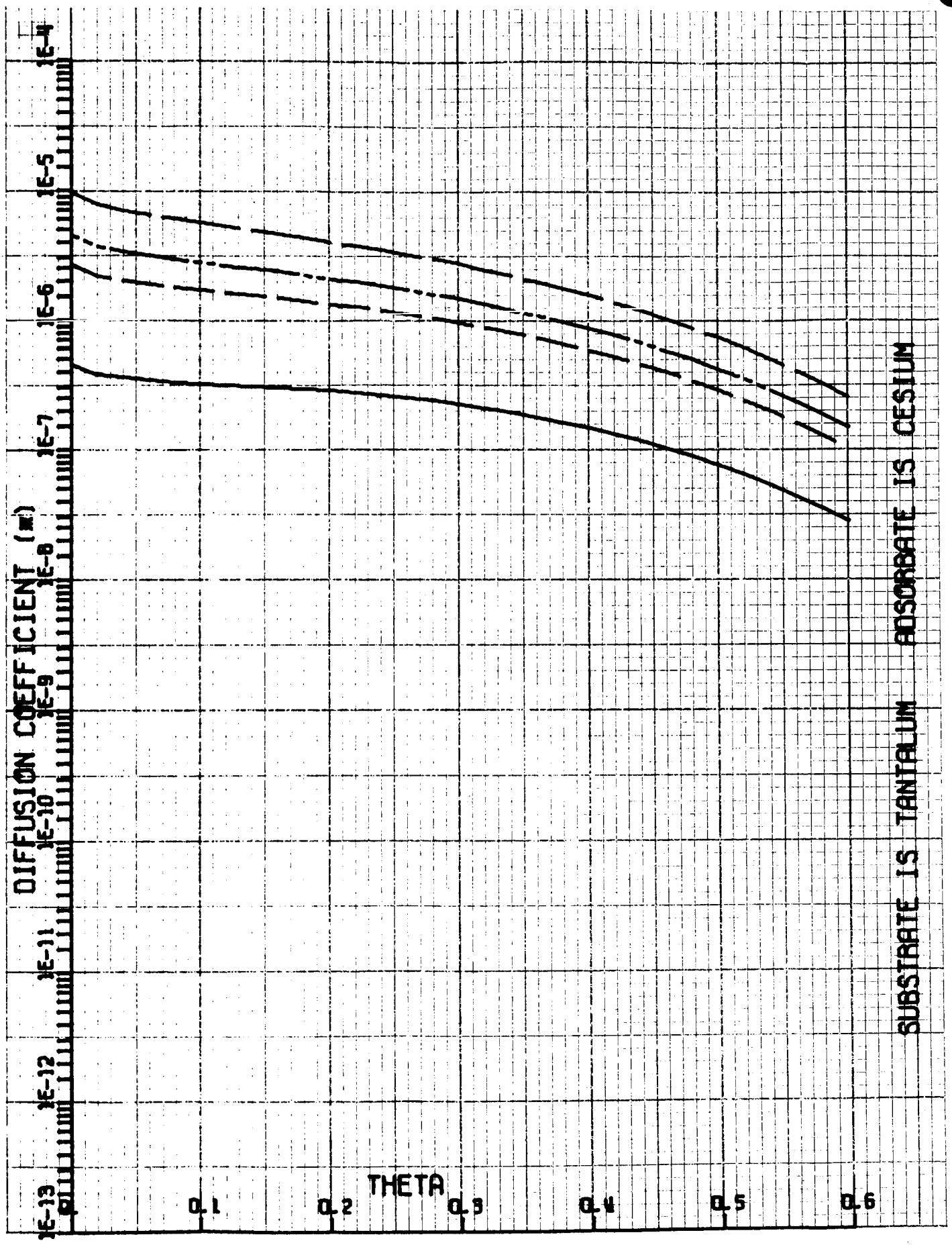
DIFFUSION COEFFICIENT (m)
1E-4
1E-5
1E-6
1E-7
1E-8
1E-9
1E-10
1E-11
1E-12
1E-13
0.1
0.2
0.3
0.4
0.5
0.6
THETA
SUBSTRATE IS TANTALUM ADSORBATE IS CESIUM

DIFFUSION COEFFICIENT (m²)
1E-4
1E-5
1E-6
1E-7
1E-8
1E-9
1E-10
1E-11
1E-12
1E-13
TEMPERATURE (K) (×10³)
40.
80.
120.
160.
200.
SUBSTRATE IS TANTALUM ADSORBATE IS BARIUM

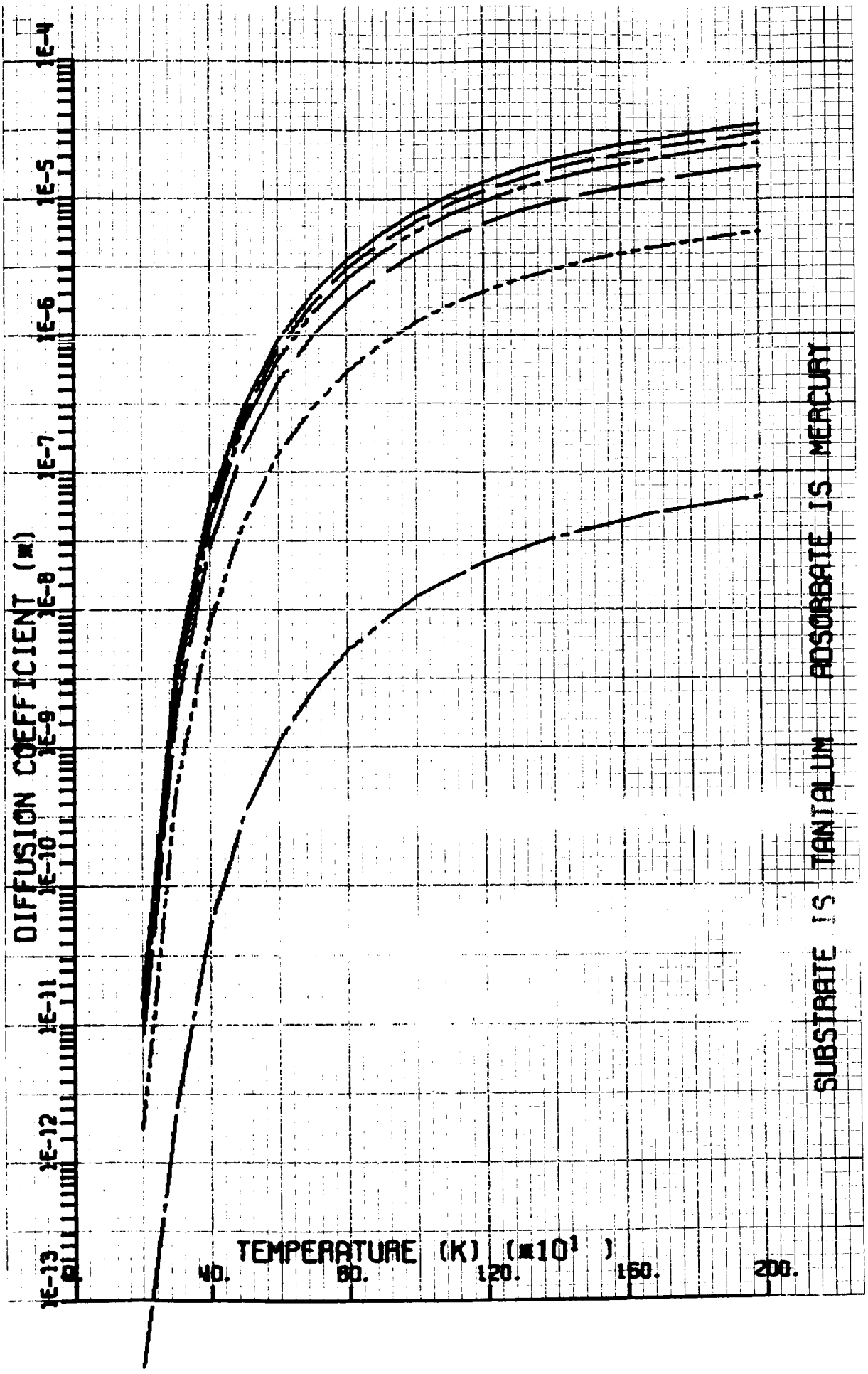
DIFFUSION COEFFICIENT (M)
1E-4
1E-5
1E-6
1E-7
1E-8
1E-9
1E-10
1E-11
1E-12
1E-13
TEMPERATURE (K) (*10^1)
40.
80.
120.
160.
200.
SUBSTRATE IS TANTALUM ADSORBATE IS MERCURY

DIFFUSION COEFFICIENT (M)
1E-7
1E-8
1E-9
1E-10
1E-11
1E-12
1E-13
THETA
0.1
0.2
0.3
0.4
0.5
0.6
SUBSTRATE IS TANTALUM ADSORBATE IS MERCURY

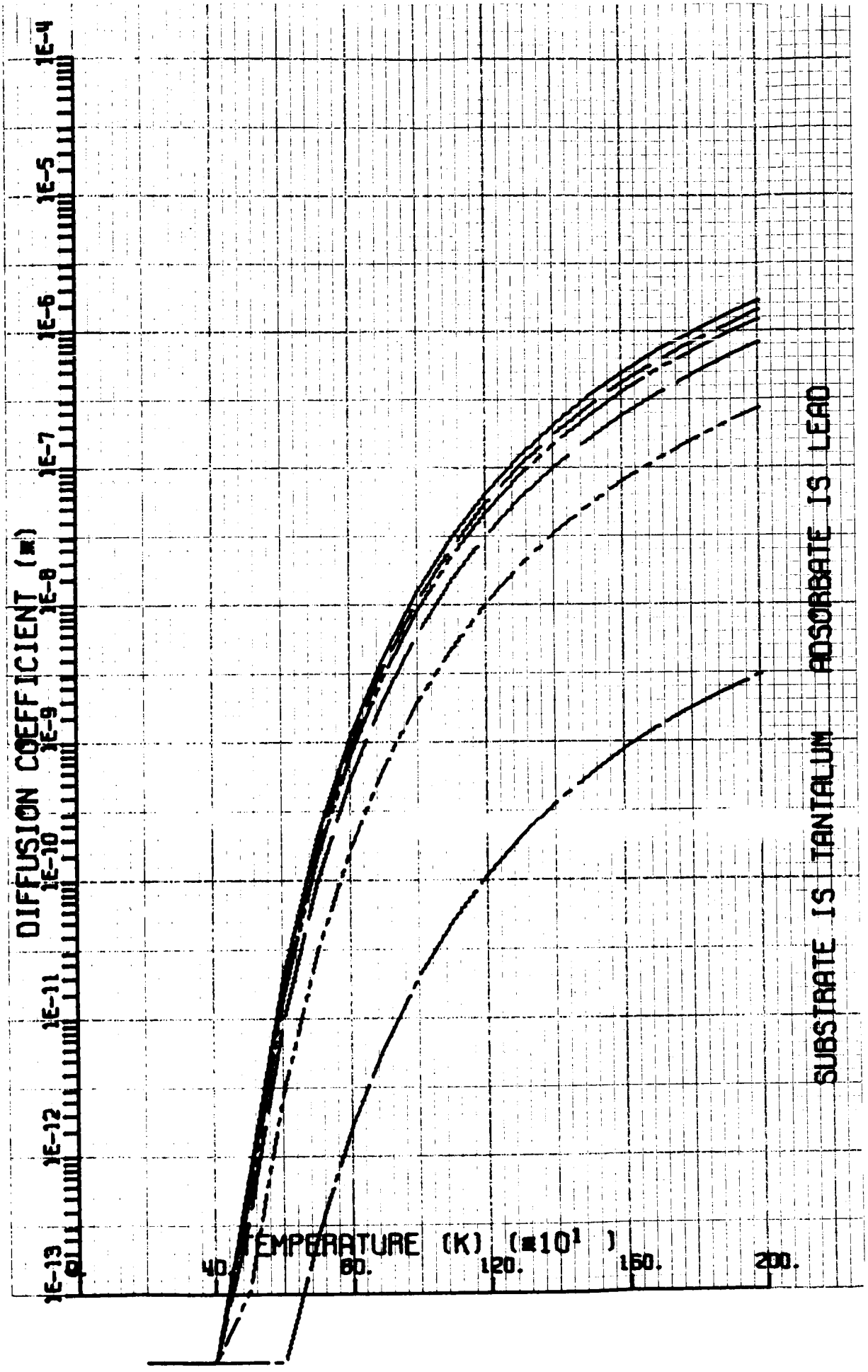
DIFFUSION COEFFICIENT (■)
1E-4
1E-5
1E-6
1E-7
1E-8
1E-9
1E-10
1E-11
1E-12
1E-13
TEMPERATURE (K) (■10¹)
40.
80.
120.
160.
200.
SUBSTRATE IS TANTALUM ADSORBATE IS LEAD

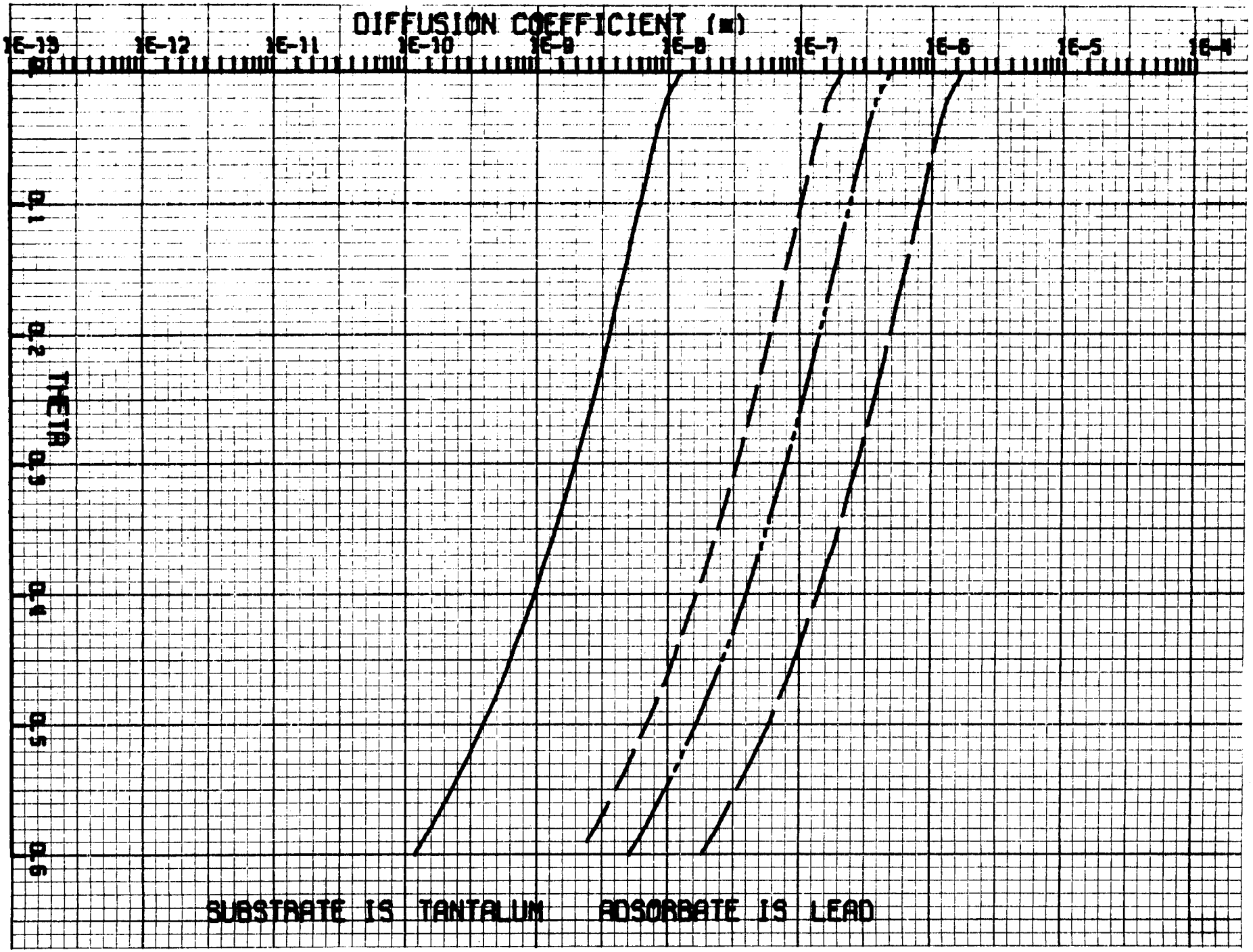
DIFFUSION COEFFICIENT (m)
1E-13
1E-12
1E-11
1E-10
1E-9
1E-8
1E-7
1E-6
1E-5
1E-4
THETA
0.1
0.2
0.3
0.4
0.5
0.6
SUBSTRATE IS TANTALUM ADSORBATE IS LEAD

DIFFUSION COEFFICIENT (m²)
1E-4
1E-5
1E-6
1E-7
1E-8
1E-9
1E-10
1E-11
1E-12
1E-13
TEMPERATURE (K) (×10¹)
40.
80.
120.
160.
200.
SUBSTRATE IS NICKEL ADSORBATE IS LITHIUM

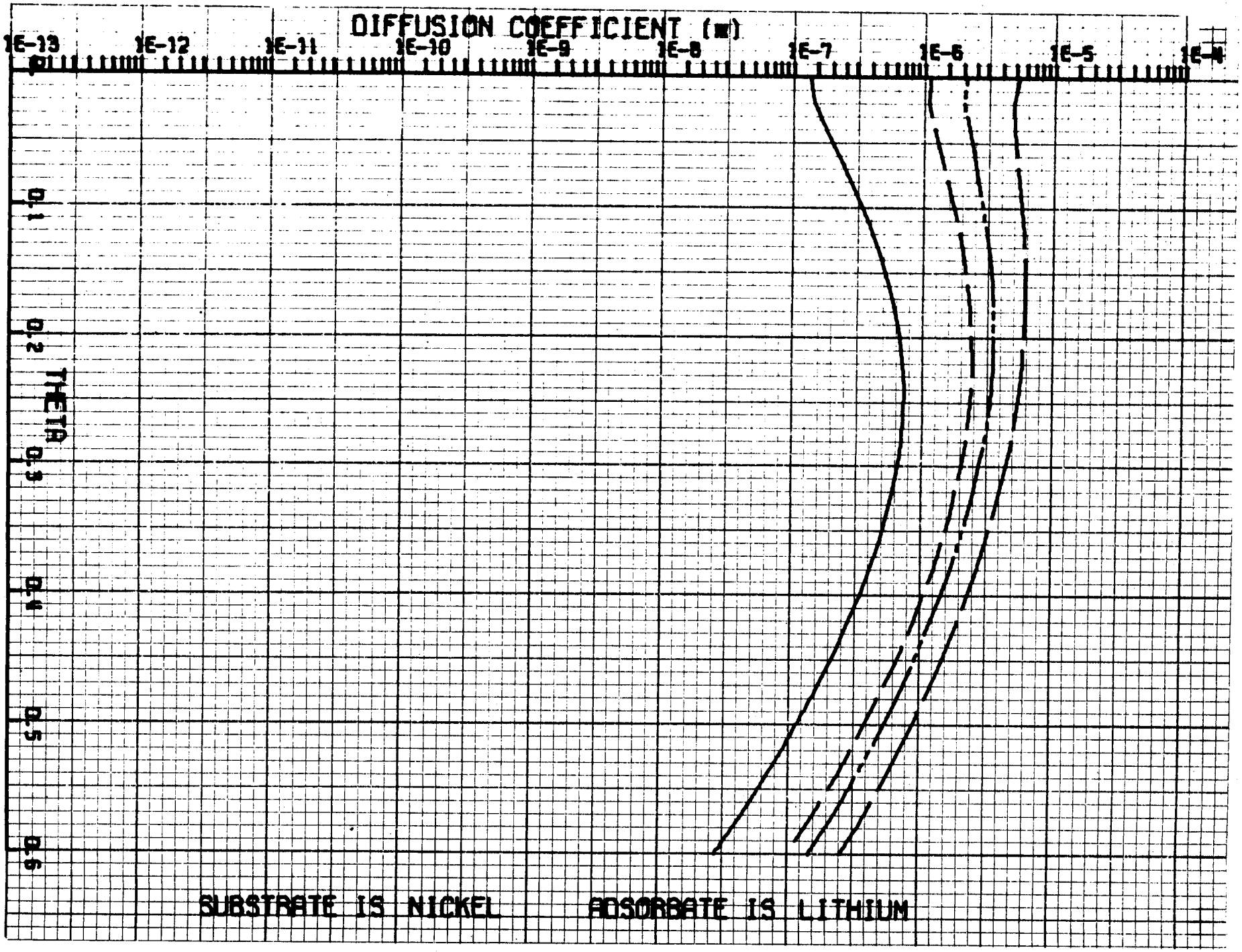
DIFFUSION COEFFICIENT (m)
1E-13
1E-12
1E-11
1E-10
1E-9
1E-8
1E-7
1E-6
1E-5
1E-4
0.1
0.2
THETA
0.3
0.4
0.5
0.6
SUBSTRATE IS NICKEL
ADSORBATE IS LITHIUM

DIFFUSION COEFFICIENT (cm²)
1E-4
1E-5
1E-6
1E-7
1E-8
1E-9
1E-10
1E-11
1E-12
1E-13
TEMPERATURE (K) (=10¹)
40.
80.
120.
160.
200.
SUBSTRATE IS NICKEL ADSORBATE IS BERYLLIUM

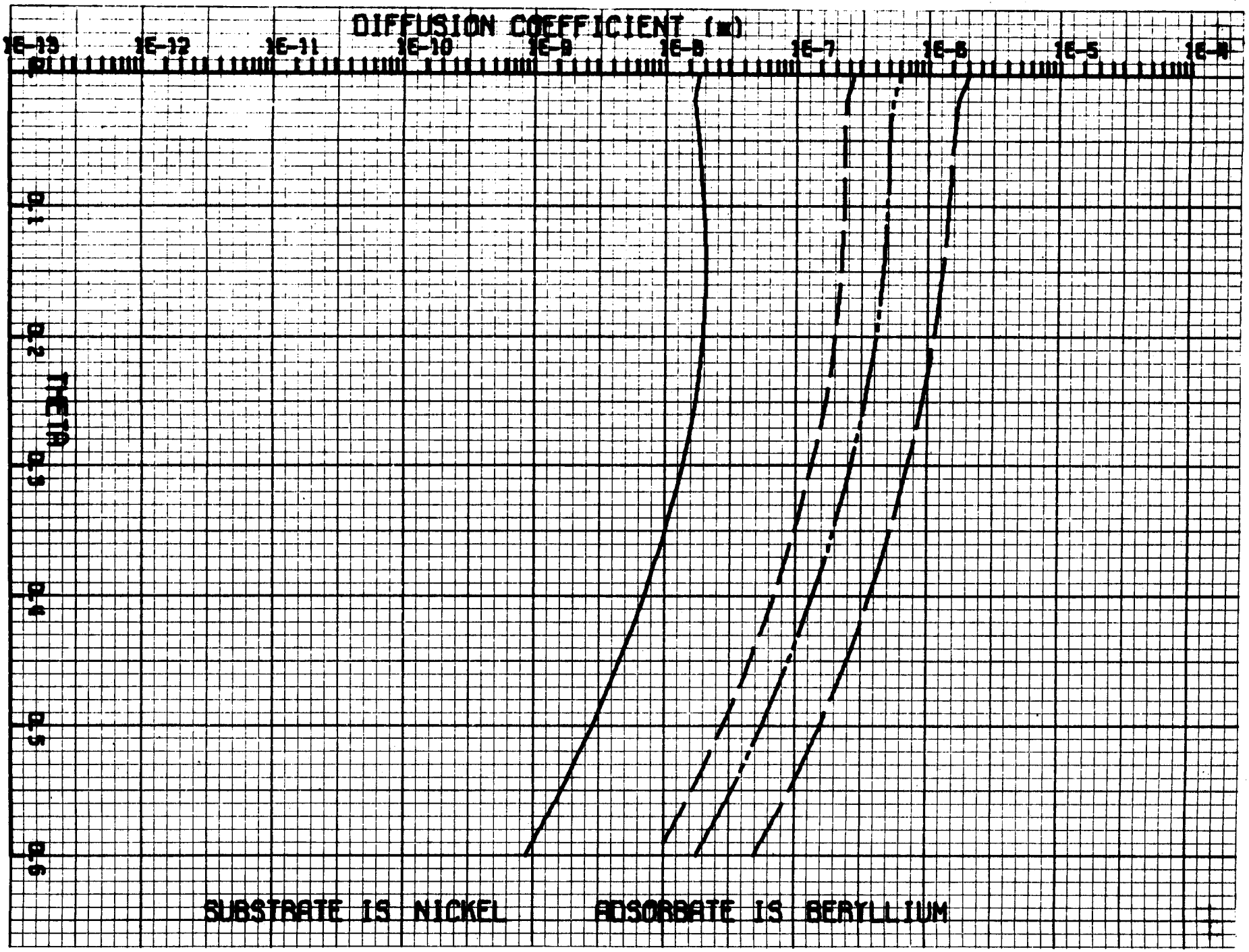
DIFFUSION COEFFICIENT (m)
1E-13
1E-12
1E-11
1E-10
1E-9
1E-8
1E-7
1E-6
1E-5
1E-4
0.1
0.2
0.3
0.4
0.5
0.6
INCH
SUBSTRATE IS NICKEL
ADSORBATE IS BERYLLIUM

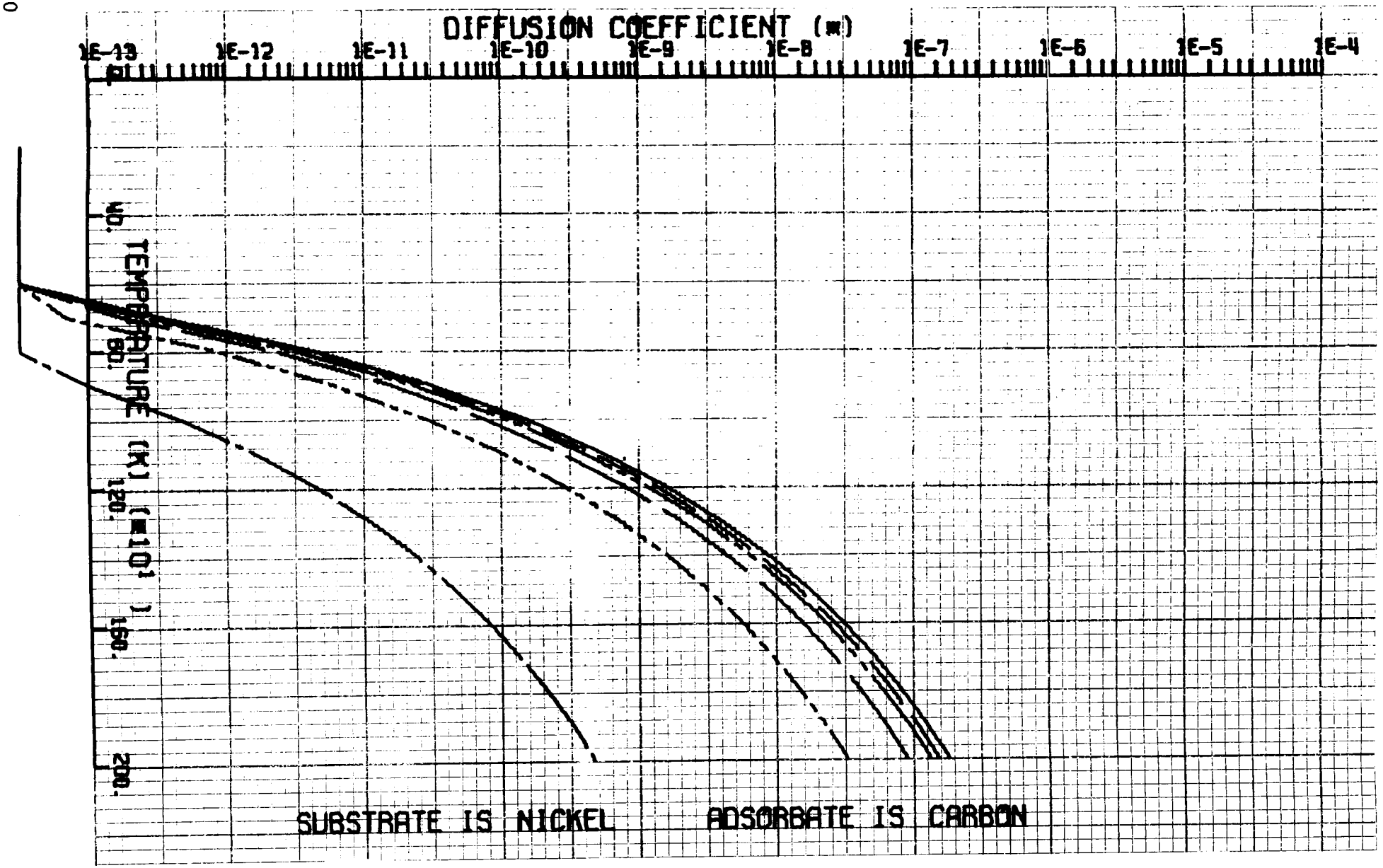
DIFFUSION COEFFICIENT (m)
1E-13
1E-12
1E-11
1E-10
1E-9
1E-8
1E-7
1E-6
1E-5
1E-4
40.
TEMPERATURE (K) (m=10⁻¹)
80.
120.
160.
200.
SUBSTRATE IS NICKEL
ADSORBATE IS CARBON

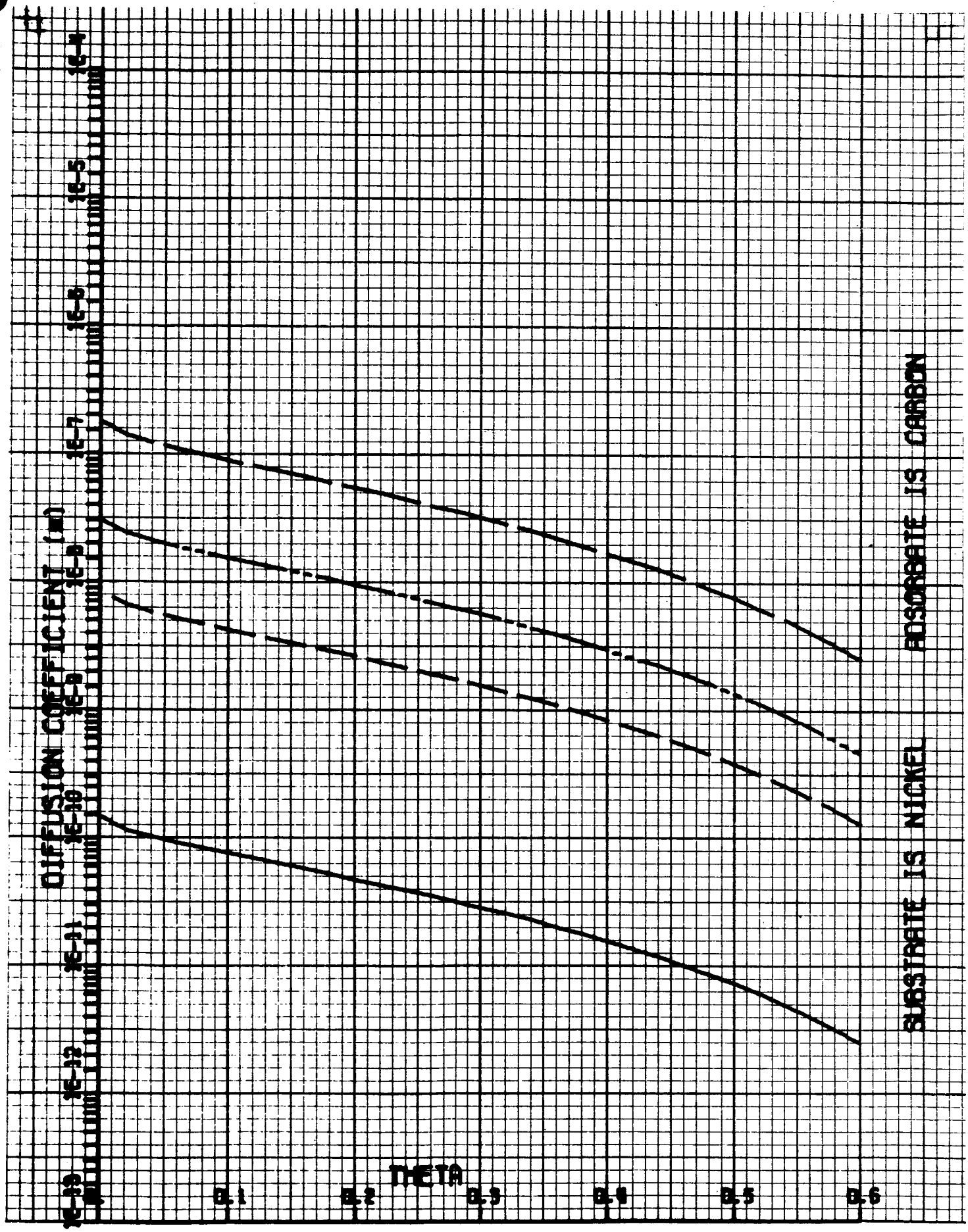
DIFFUSION COEFFICIENT (M)
1E-4
1E-5
1E-6
1E-7
1E-8
1E-9
1E-10
1E-11
1E-12
1E-13
0.1
0.2
0.3
0.4
0.5
0.6
THETA
SUBSTRATE IS NICKEL
ADSORBATE IS CARBON

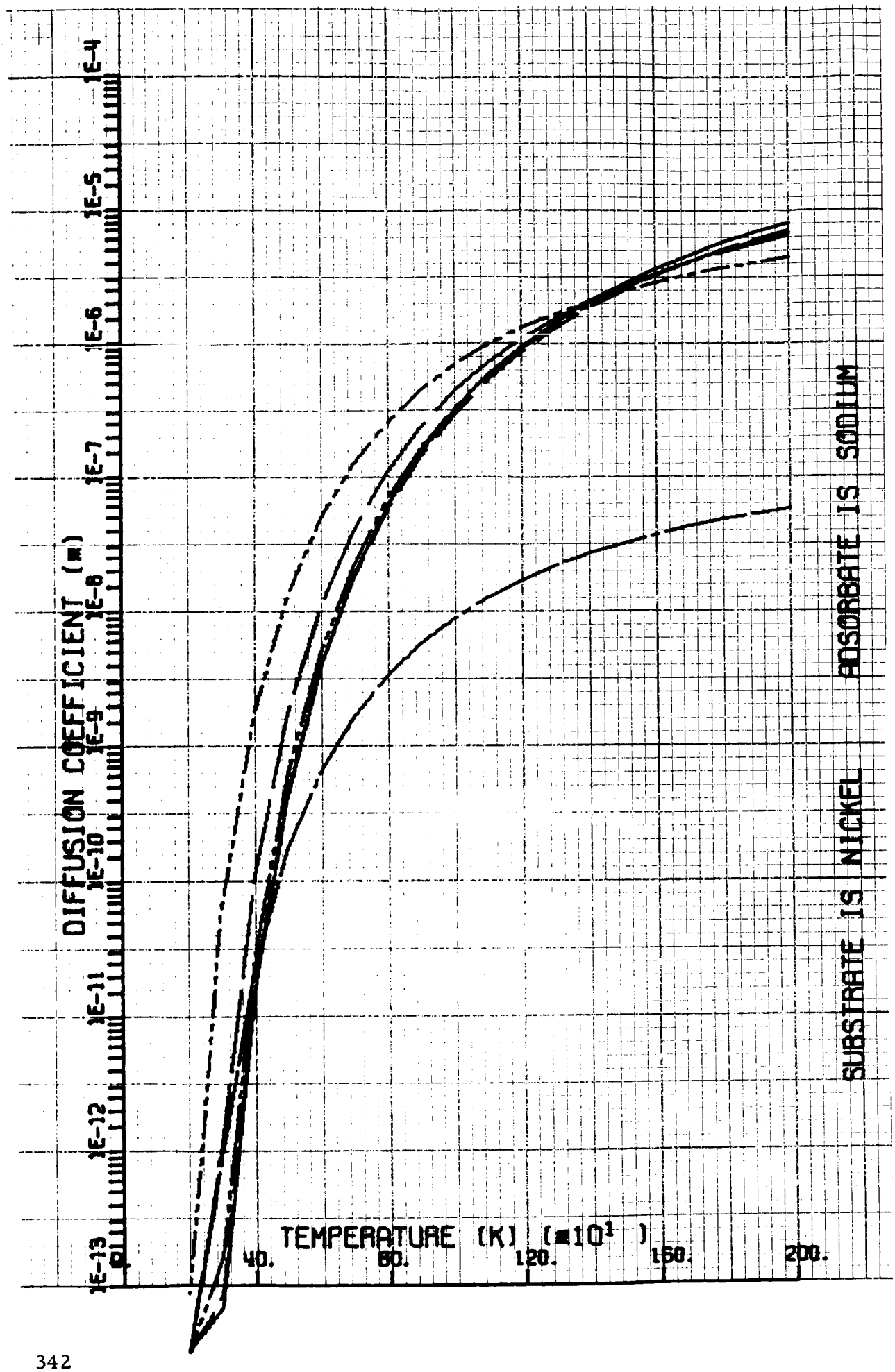
DIFFUSION COEFFICIENT (■)
1E-4
1E-5
1E-6
1E-7
1E-8
1E-9
1E-10
1E-11
1E-12
1E-13
TEMPERATURE (K) (■10¹)
40.
80.
120.
160.
200.
SUBSTRATE IS NICKEL
ADSORBATE IS SODIUM

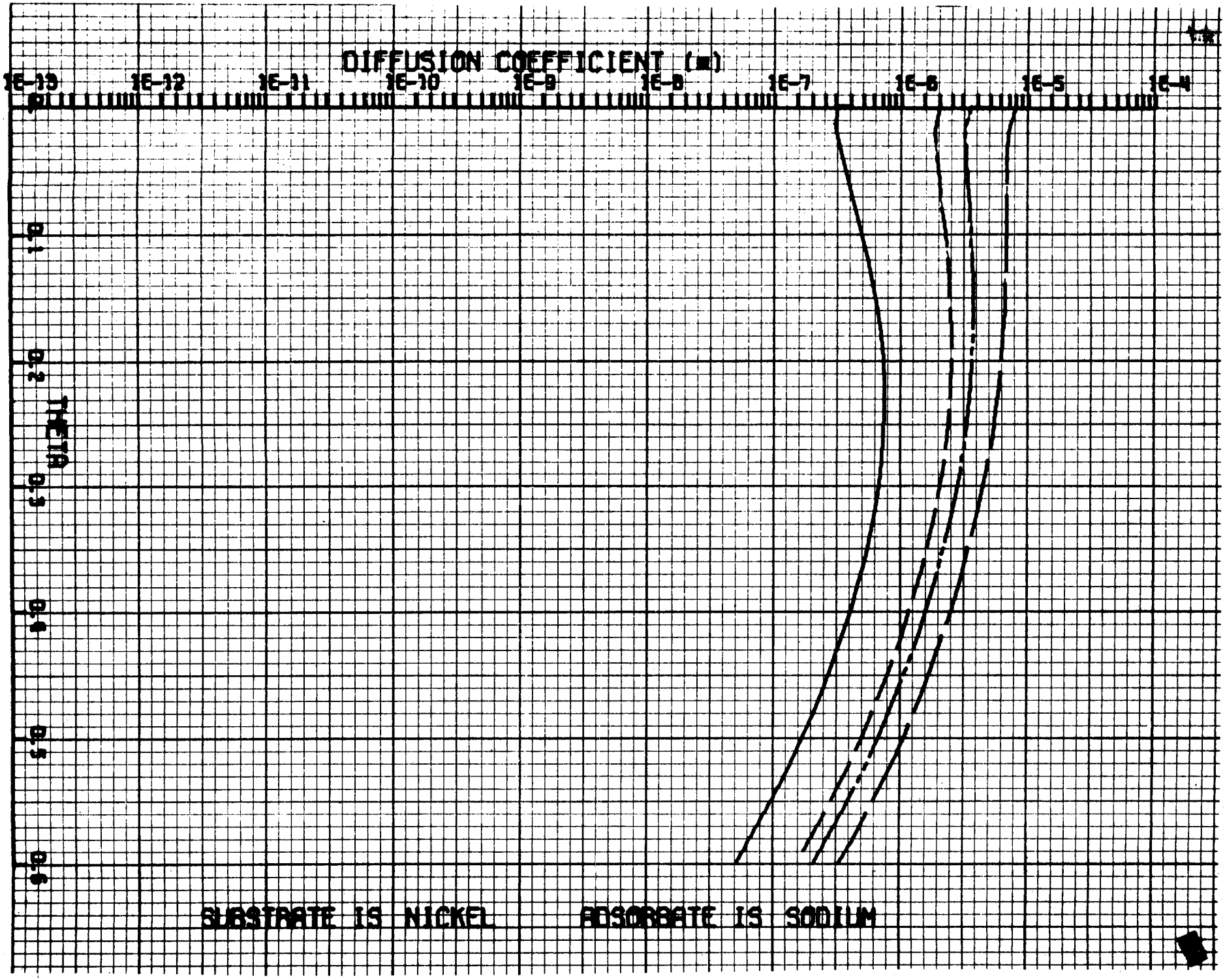
DIFFUSION COEFFICIENT (m)
1E-13
1E-12
1E-11
1E-10
1E-9
1E-8
1E-7
1E-6
1E-5
1E-4
THETA
0.1
0.2
0.3
0.4
0.5
0.6
SUBSTRATE IS NICKEL
ADSORBATE IS SODIUM

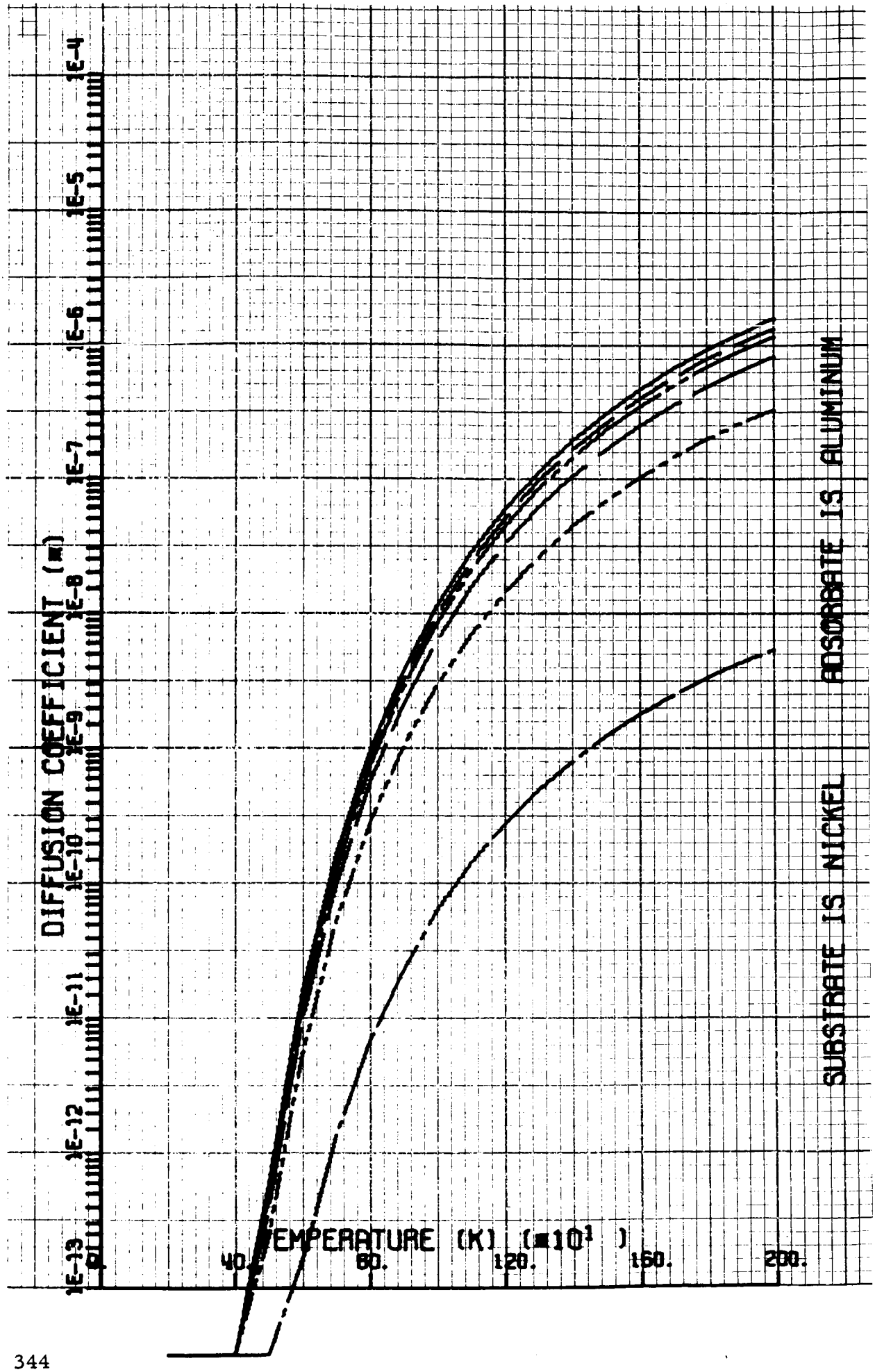
DIFFUSION COEFFICIENT (m)
1E-4
1E-5
1E-6
1E-7
1E-8
1E-9
1E-10
1E-11
1E-12
1E-13
TEMPERATURE (K) (×10¹)
40.
80.
120.
160.
200.
SUBSTRATE IS NICKEL ADSORBATE IS ALUMINUM

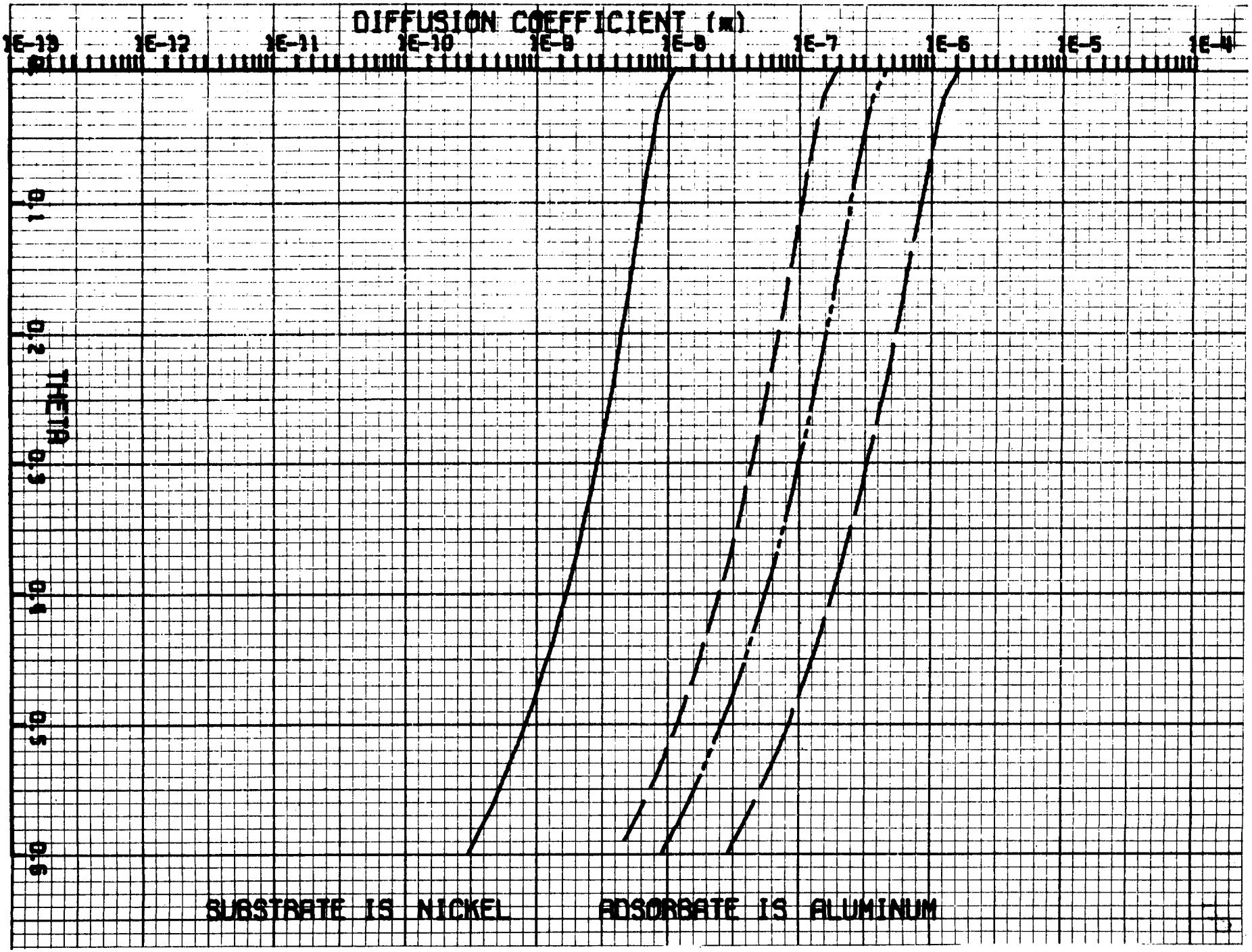
DIFFUSION COEFFICIENT (m)
1E-13
1E-12
1E-11
1E-10
1E-9
1E-8
1E-7
1E-6
1E-5
1E-4
0.1
0.2
THETA
0.3
0.4
0.5
0.6
SUBSTRATE IS NICKEL
ADSORBATE IS ALUMINUM

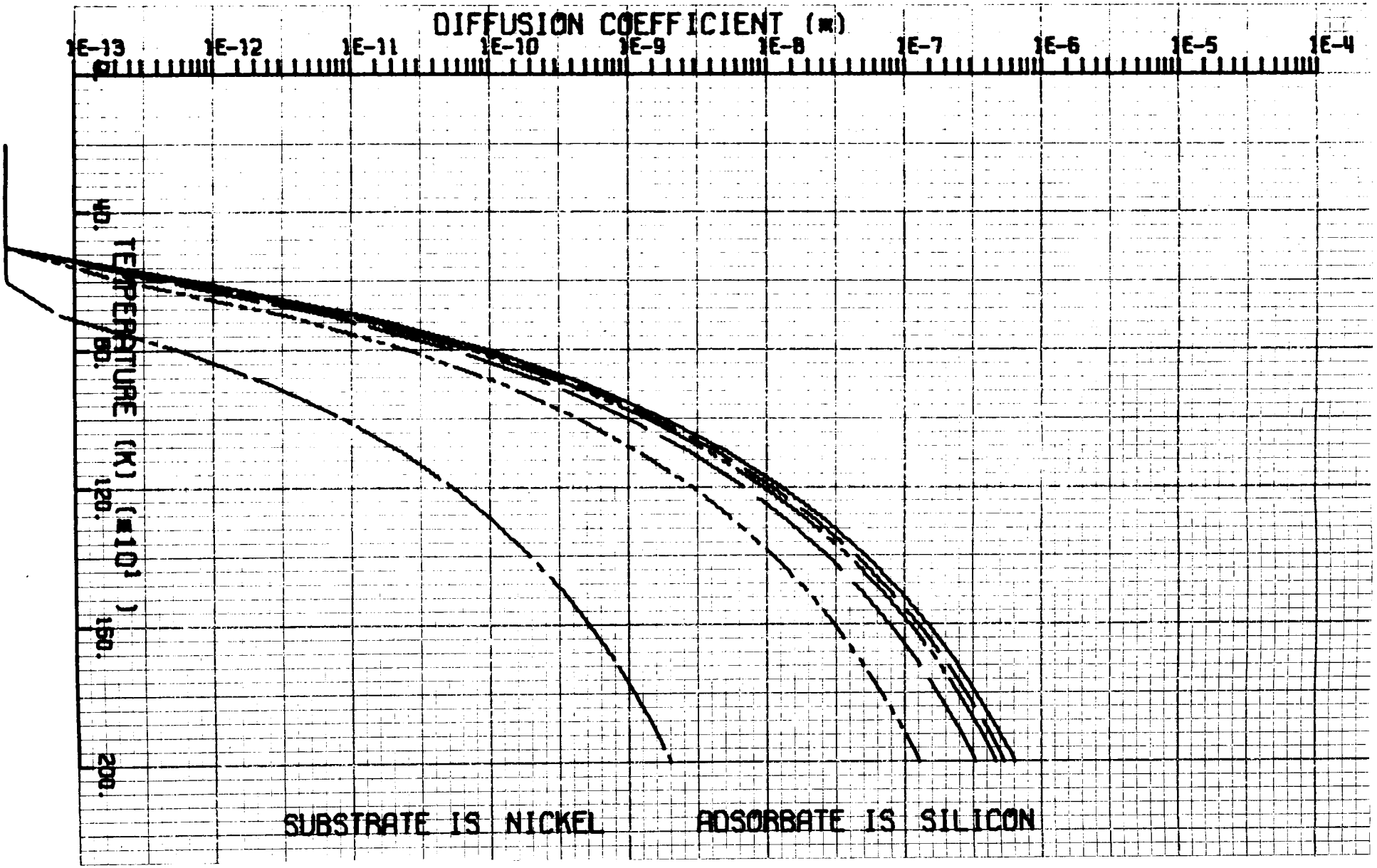
DIFFUSION COEFFICIENT (*)
1E-13
1E-12
1E-11
1E-10
1E-9
1E-8
1E-7
1E-6
1E-5
1E-4
TEMPERATURE (K) (*10^1)
40.
80.
120.
160.
200.
SUBSTRATE IS NICKEL
ADSORBATE IS SILICON

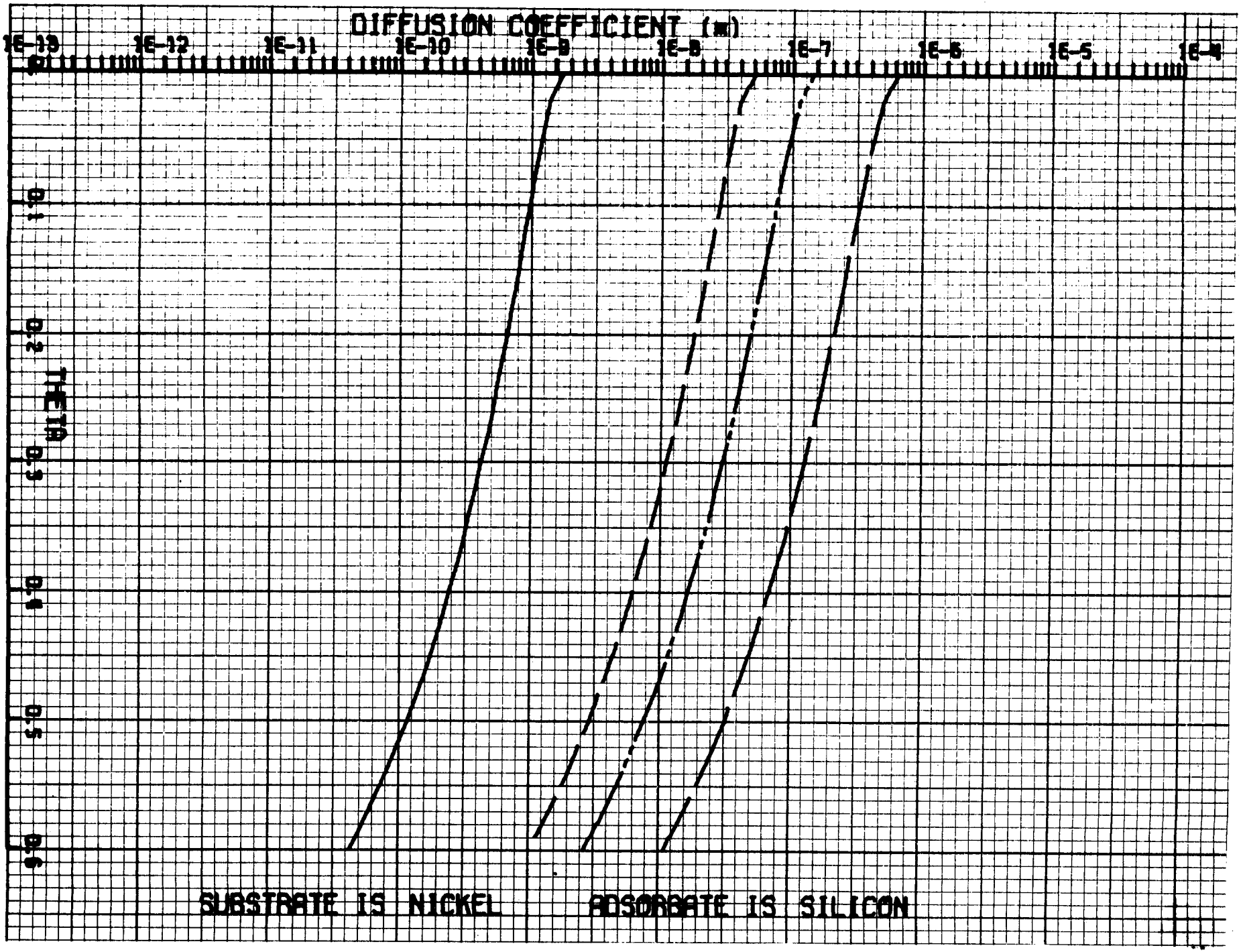
DIFFUSION COEFFICIENT (m)
1E-13
1E-12
1E-11
1E-10
1E-9
1E-8
1E-7
1E-6
1E-5
1E-4
THETA
0.1
0.2
0.3
0.4
0.5
0.6
SUBSTRATE IS NICKEL
ADSORBATE IS SILICON

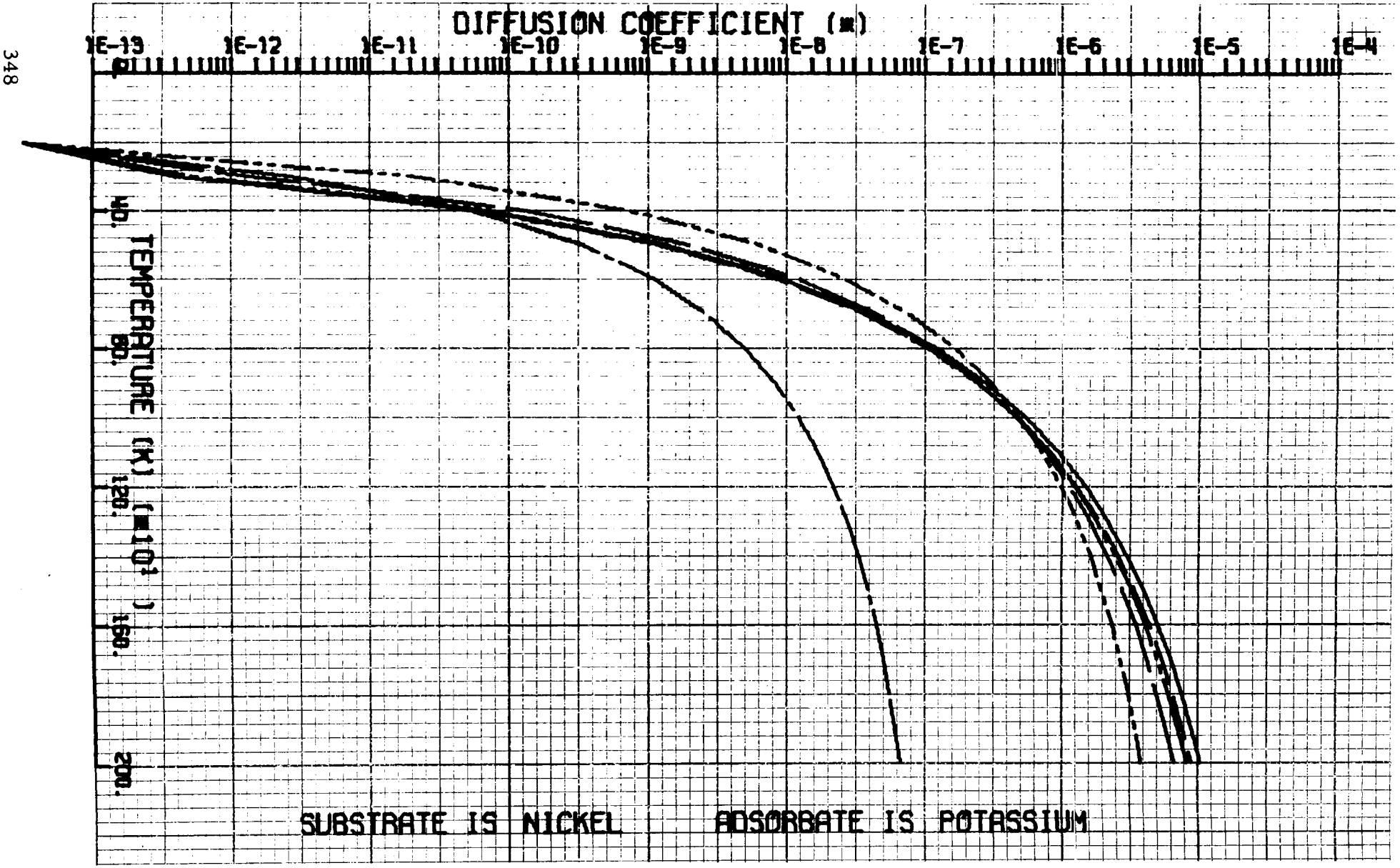
DIFFUSION COEFFICIENT (m)
1E-13
1E-12
1E-11
1E-10
1E-9
1E-8
1E-7
1E-6
1E-5
1E-4
40.
TEMPERATURE (K)
80.
120.
160.
200.
SUBSTRATE IS NICKEL
ADSORBATE IS POTASSIUM

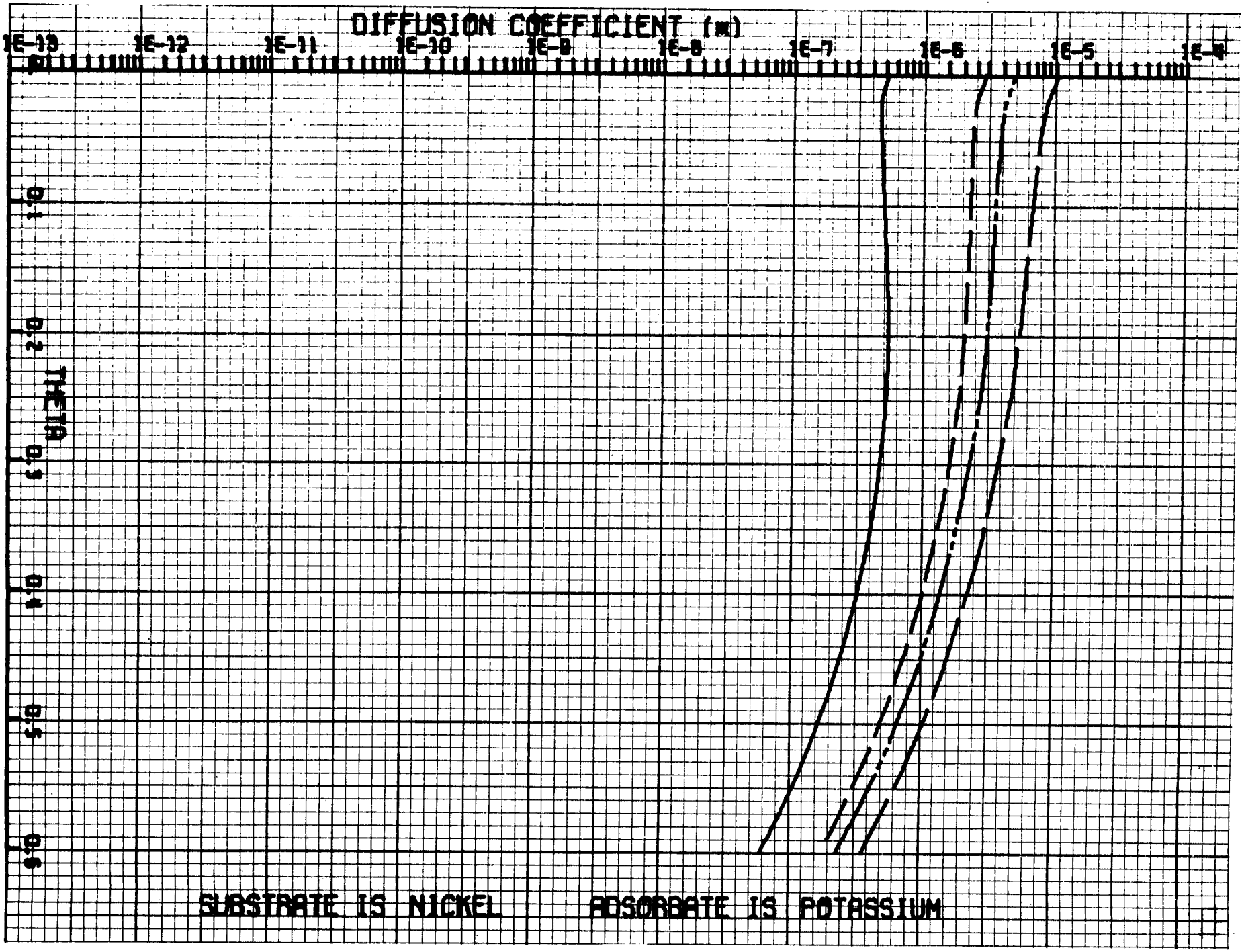
DIFFUSION COEFFICIENT (m)
1E-13
1E-12
1E-11
1E-10
1E-9
1E-8
1E-7
1E-6
1E-5
1E-4
THETA
0.1
0.2
0.3
0.4
0.5
0.6
SUBSTRATE IS NICKEL
ADSORBATE IS POTASSIUM

DIFFUSION COEFFICIENT (m²)
1E-4
1E-5
1E-6
1E-7
1E-8
1E-9
1E-10
1E-11
1E-12
1E-13
TEMPERATURE (K) (=10¹)
40.
80.
120.
160.
200.
SUBSTRATE IS NICKEL ADSORBATE IS TITANIUM

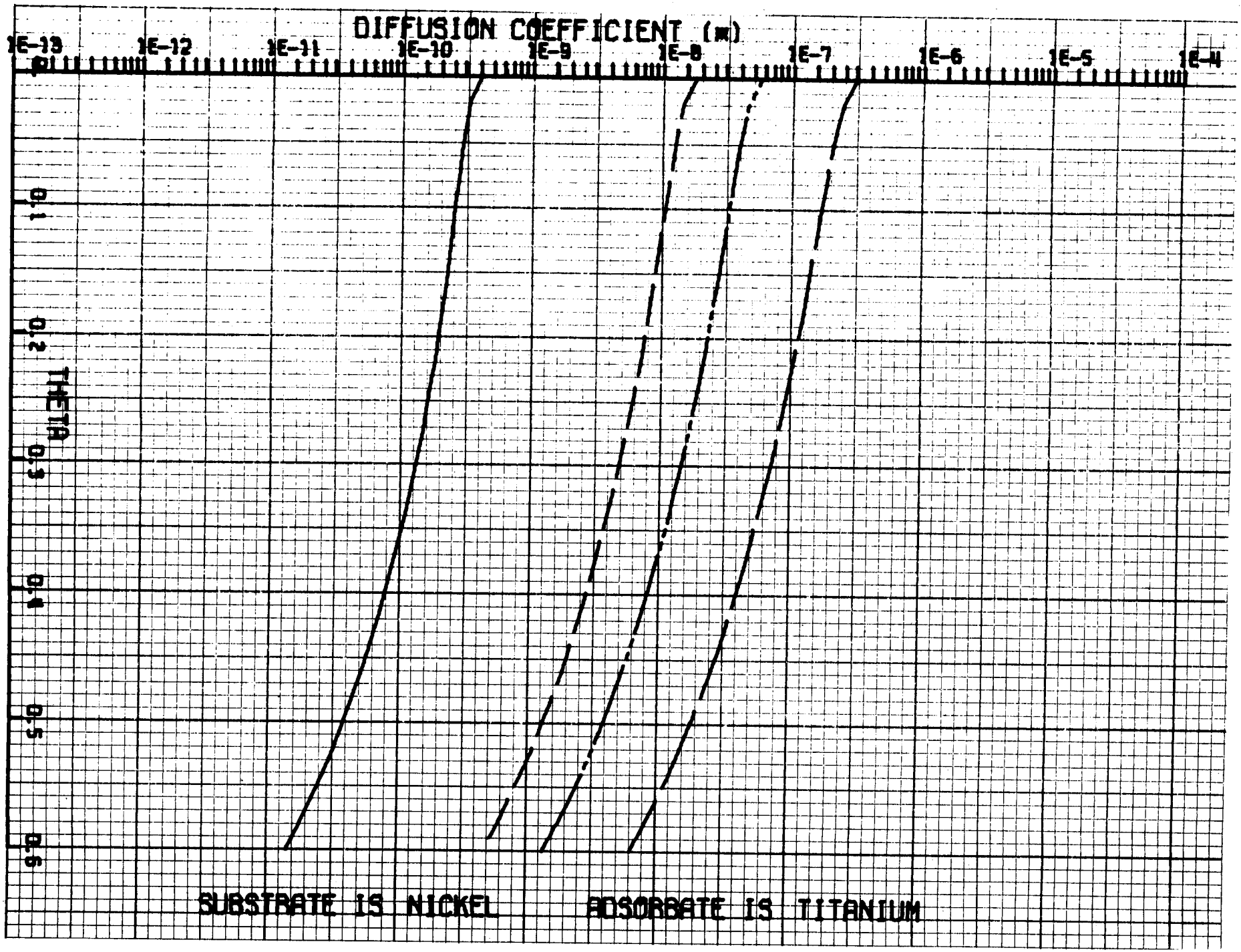
DIFFUSION COEFFICIENT (m)
1E-13
1E-12
1E-11
1E-10
1E-9
1E-8
1E-7
1E-6
1E-5
1E-4
0.1
0.2
0.3
0.4
0.5
0.6
THETA
SUBSTRATE IS NICKEL
ADSORBATE IS TITANIUM

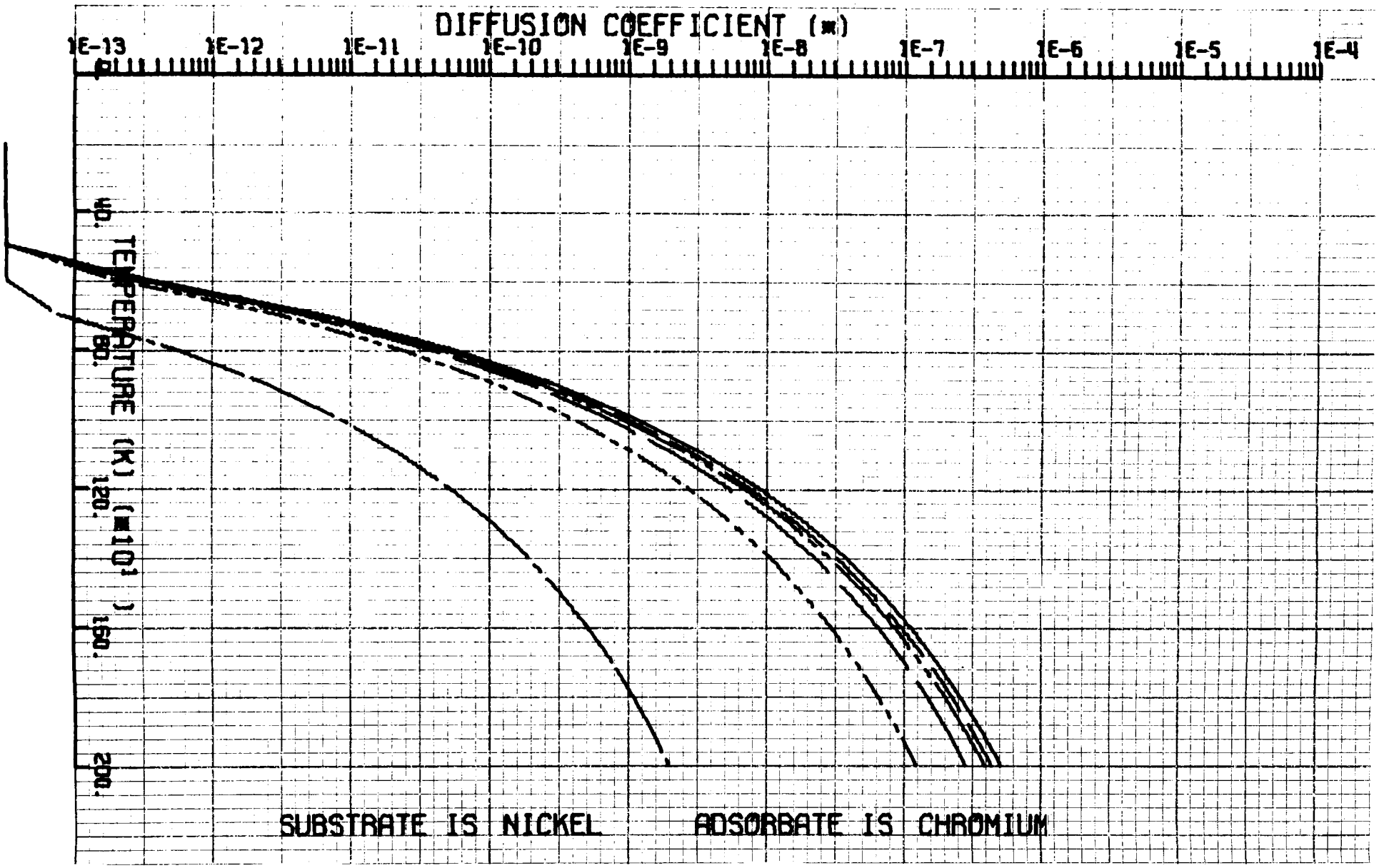
DIFFUSION COEFFICIENT (*)
1E-13
1E-12
1E-11
1E-10
1E-9
1E-8
1E-7
1E-6
1E-5
1E-4
TEMPERATURE (K) (*10¹)
40.
80.
120.
160.
200.
SUBSTRATE IS NICKEL
ADSORBATE IS CHROMIUM

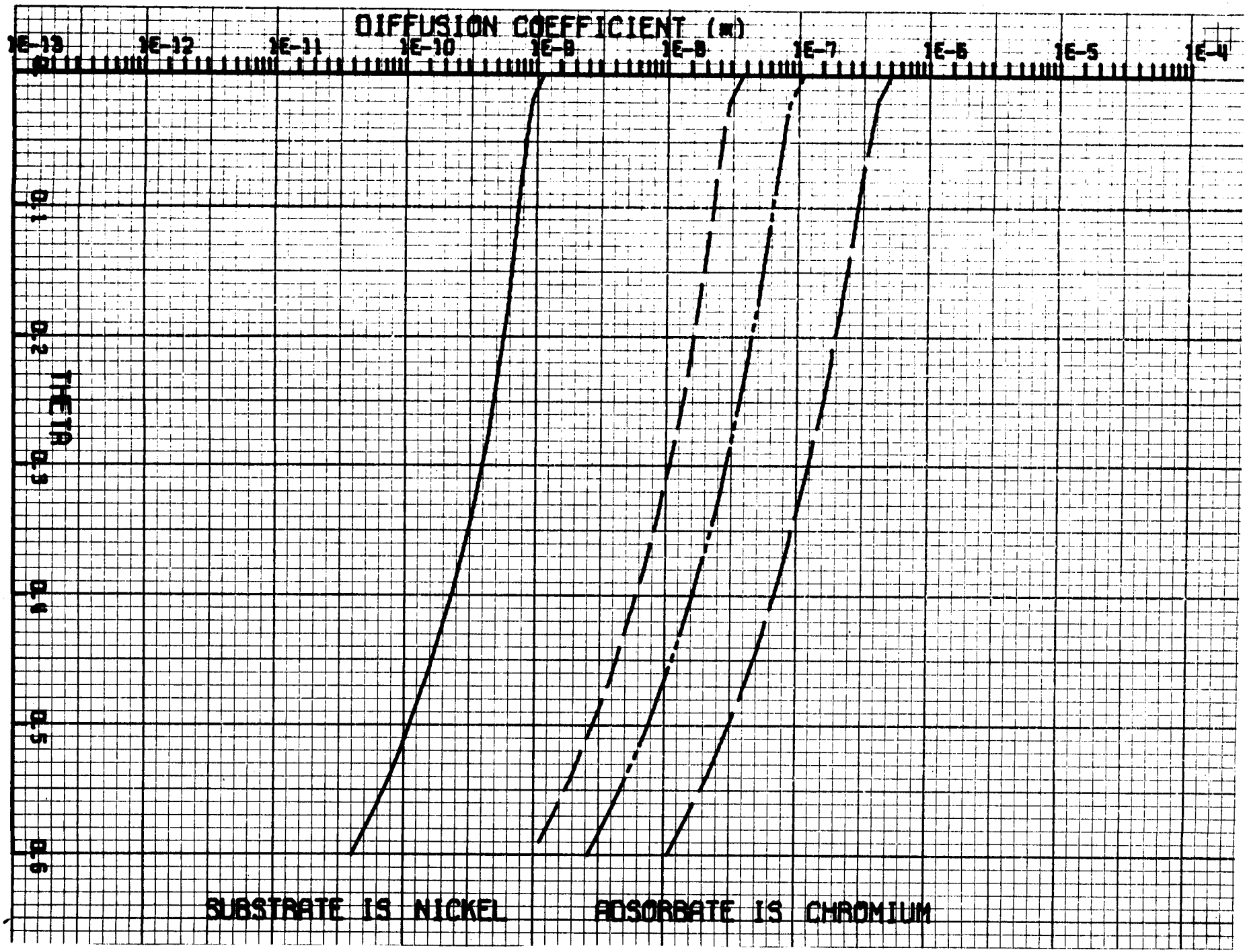
DIFFUSION COEFFICIENT (m)
1E-13
1E-12
1E-11
1E-10
1E-9
1E-8
1E-7
1E-6
1E-5
1E-4
THETA
0.1
0.2
0.3
0.4
0.5
0.6
SUBSTRATE IS NICKEL
ADSORBATE IS CHROMIUM

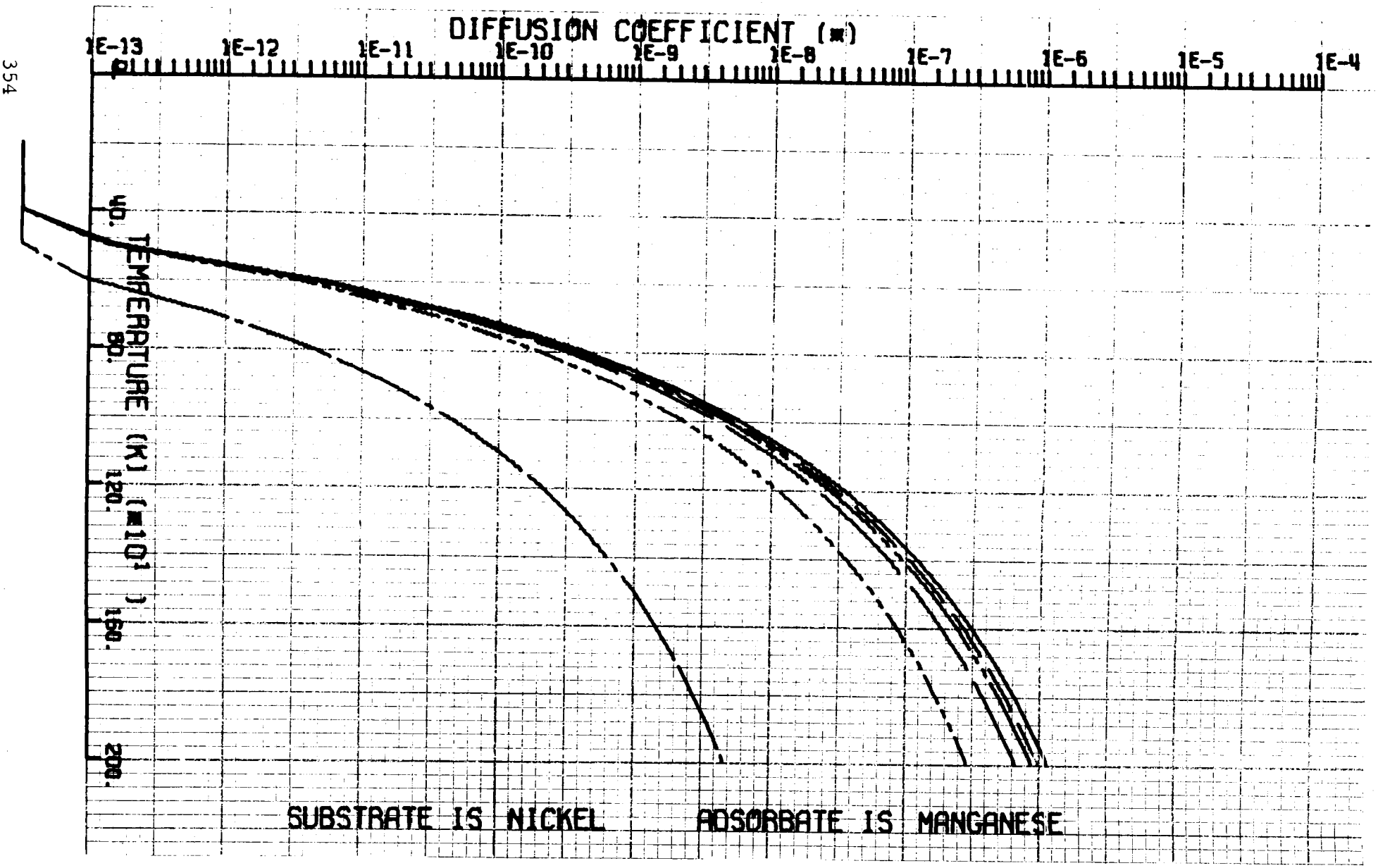
DIFFUSION COEFFICIENT (m)
1E-13
1E-12
1E-11
1E-10
1E-9
1E-8
1E-7
1E-6
1E-5
1E-4
TEMPERATURE (K) (m10¹)
40.
80.
120.
160.
200.
SUBSTRATE IS NICKEL
ADSORBATE IS MANGANESE

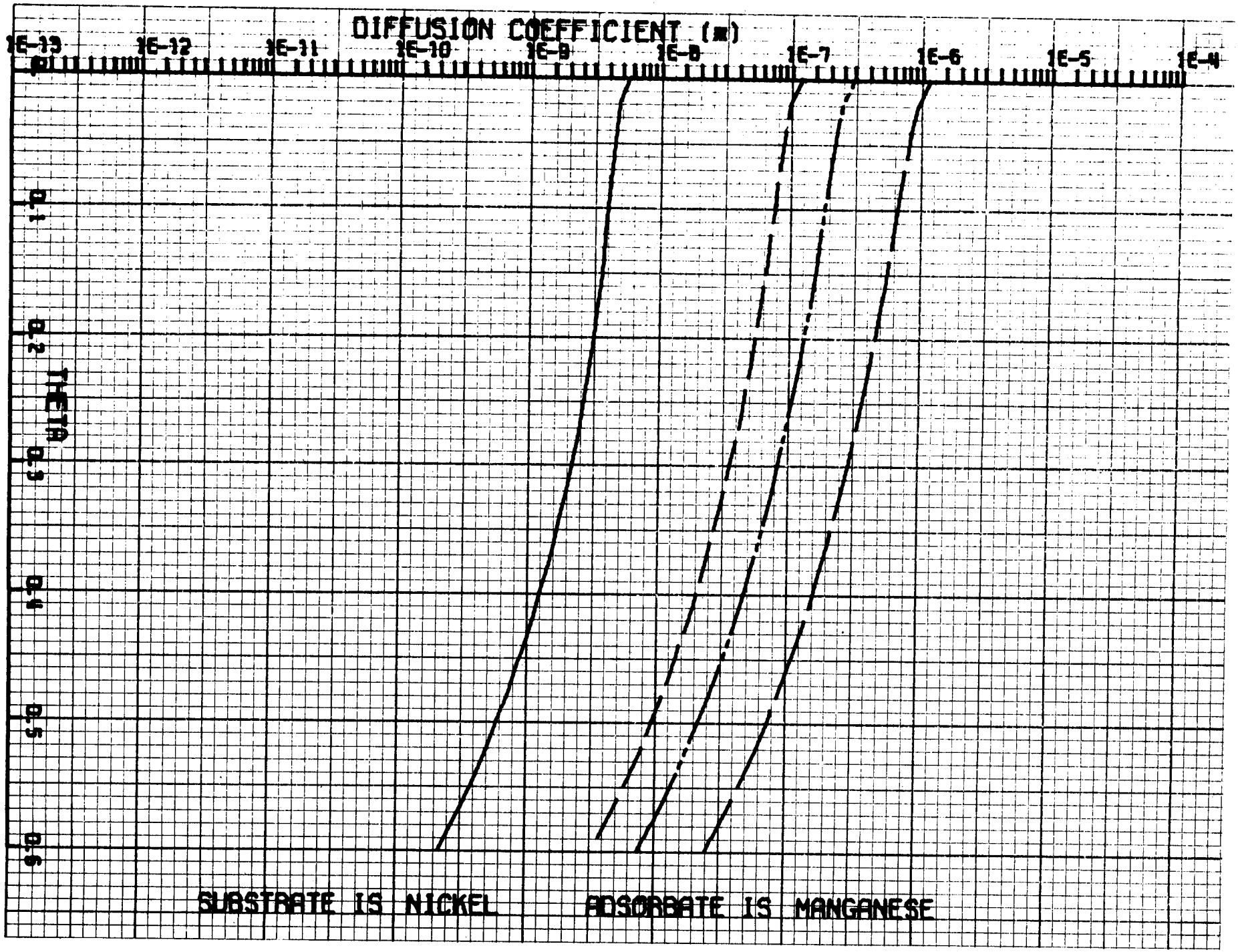
DIFFUSION COEFFICIENT (m)
1E-13
1E-12
1E-11
1E-10
1E-9
1E-8
1E-7
1E-6
1E-5
1E-4
THETA
0.1
0.2
0.3
0.4
0.5
0.6
SUBSTRATE IS NICKEL
ADSORBATE IS MANGANESE

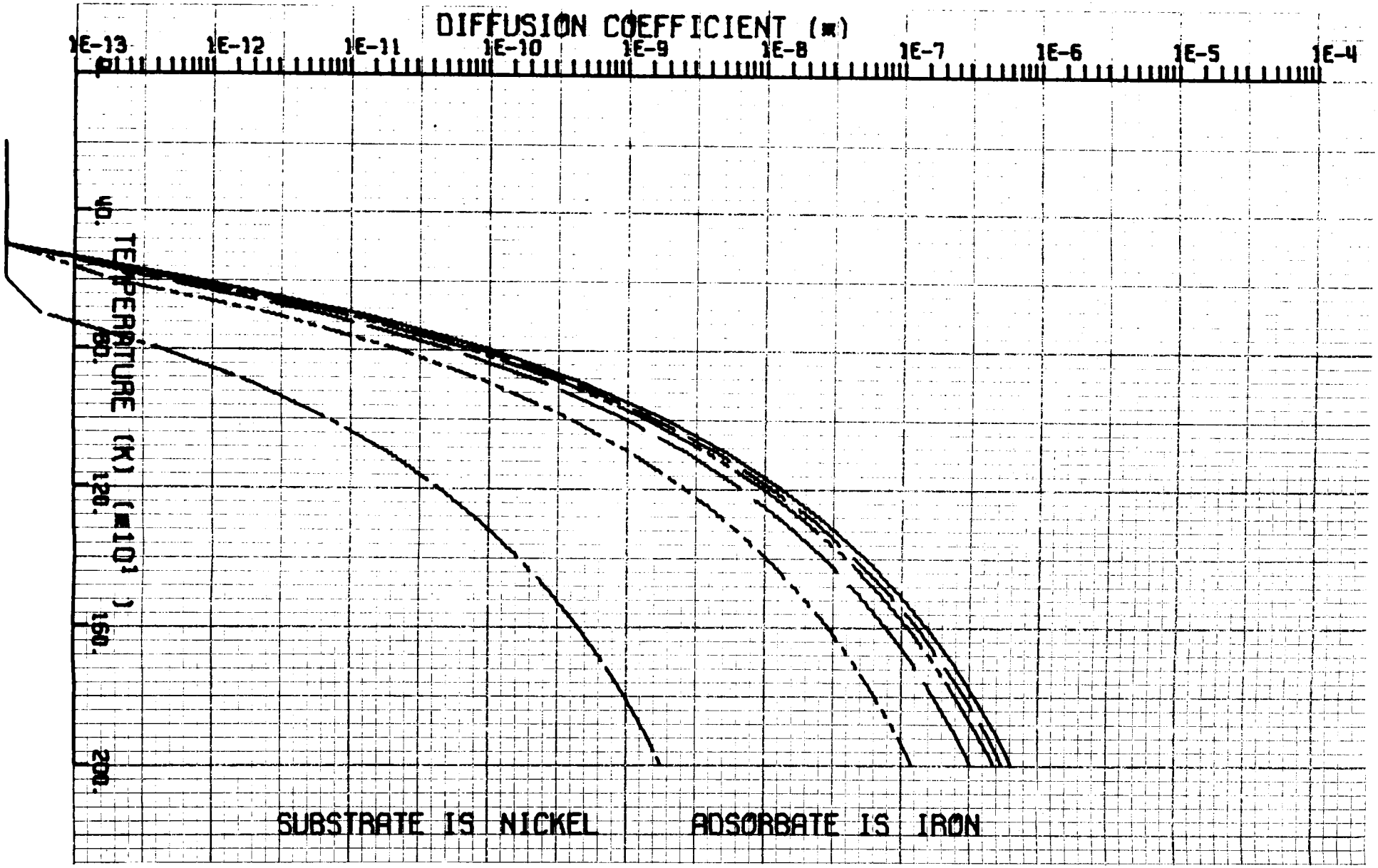
DIFFUSION COEFFICIENT (*)
1E-13
1E-12
1E-11
1E-10
1E-9
1E-8
1E-7
1E-6
1E-5
1E-4
40.
80.
120.
160.
200.
SUBSTRATE IS NICKEL
ADSORBATE IS IRON

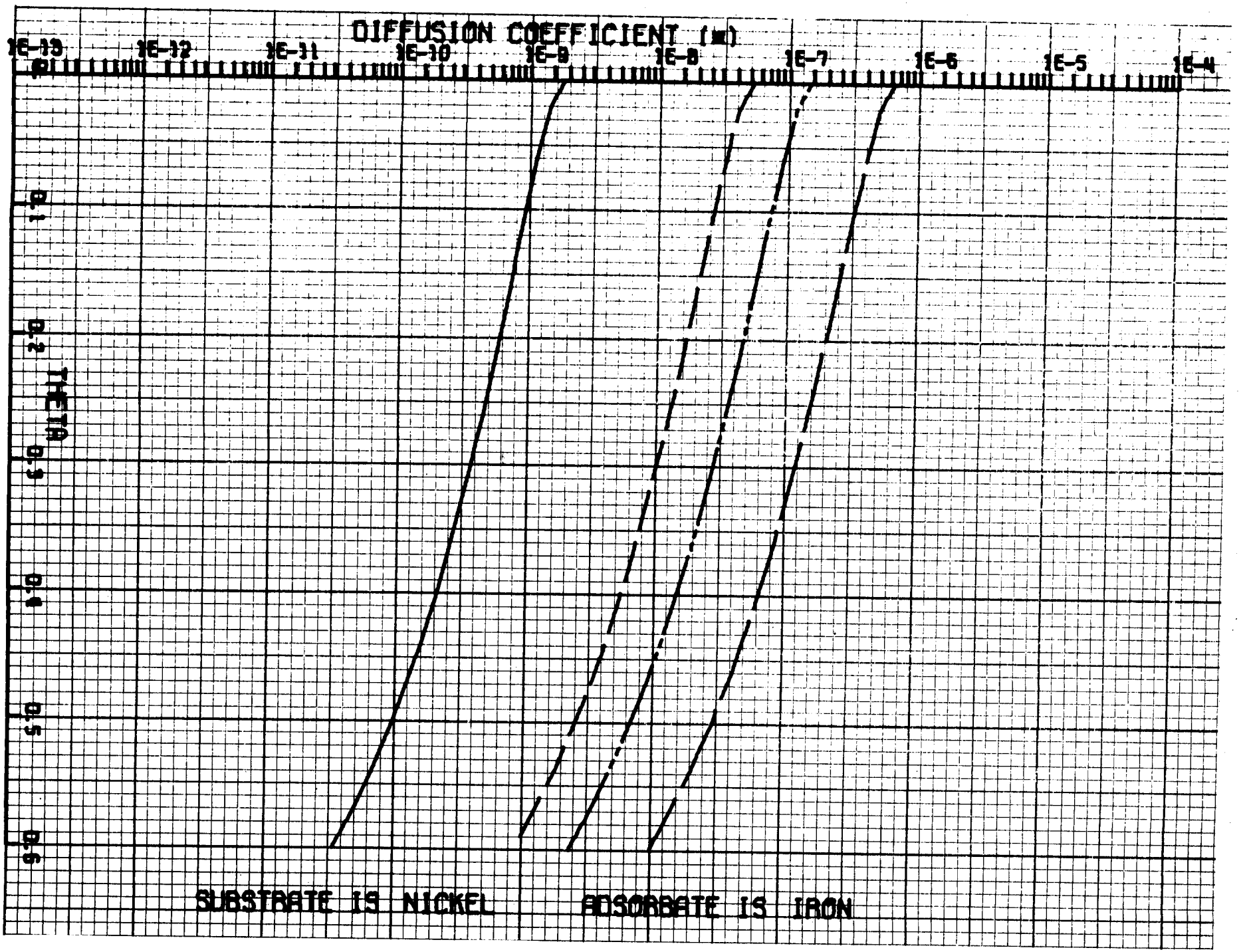
DIFFUSION COEFFICIENT (m)
1E-13
1E-12
1E-11
1E-10
1E-9
1E-8
1E-7
1E-6
1E-5
1E-4
THETA
0.1
0.2
0.3
0.4
0.5
0.6
SUBSTRATE IS NICKEL
ADSORBATE IS IRON

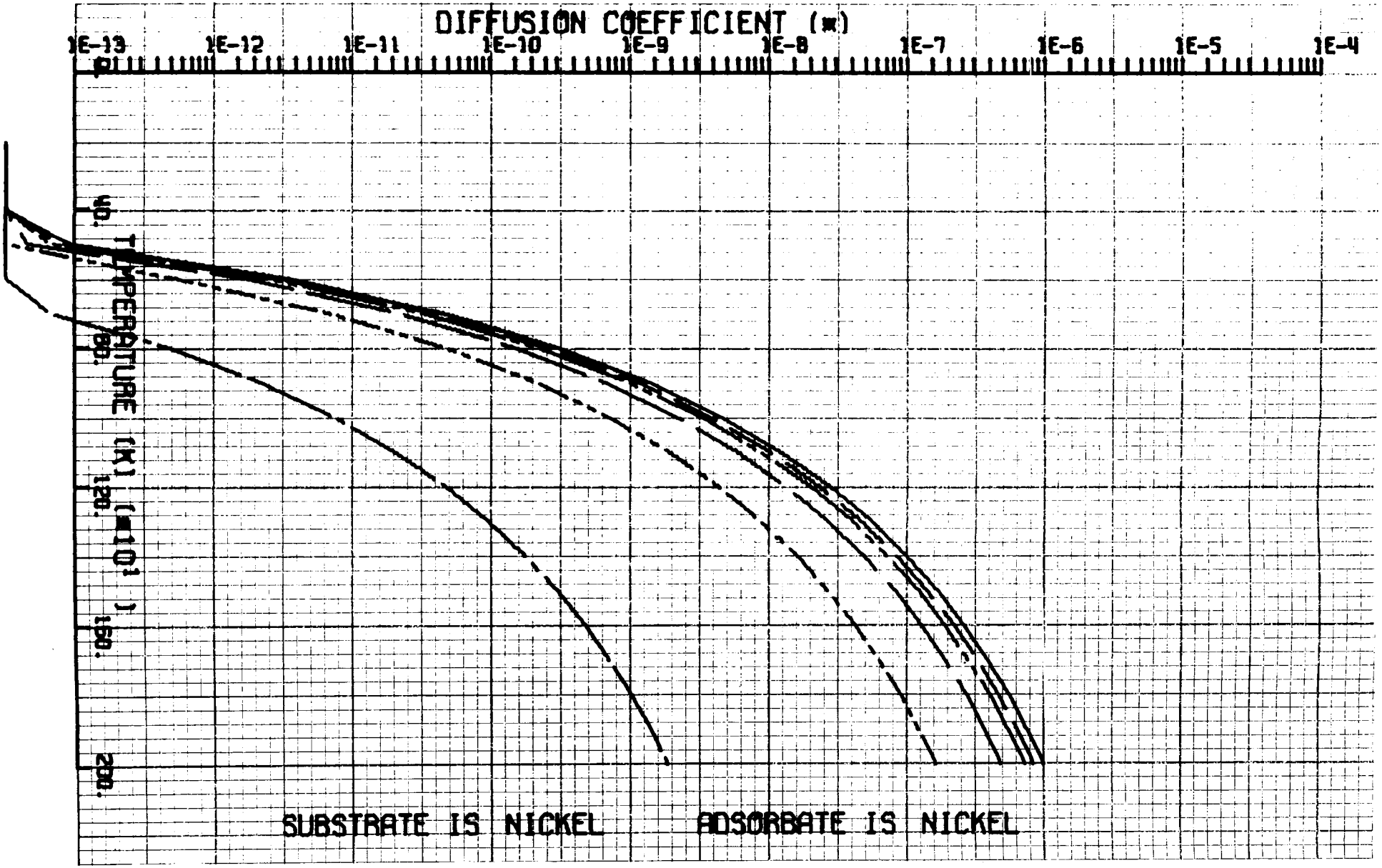
DIFFUSION COEFFICIENT (*)
1E-13
1E-12
1E-11
1E-10
1E-9
1E-8
1E-7
1E-6
1E-5
1E-4
TEMPERATURE (K) (*10¹)
90.
120.
150.
200.
SUBSTRATE IS NICKEL
ADSORBATE IS NICKEL

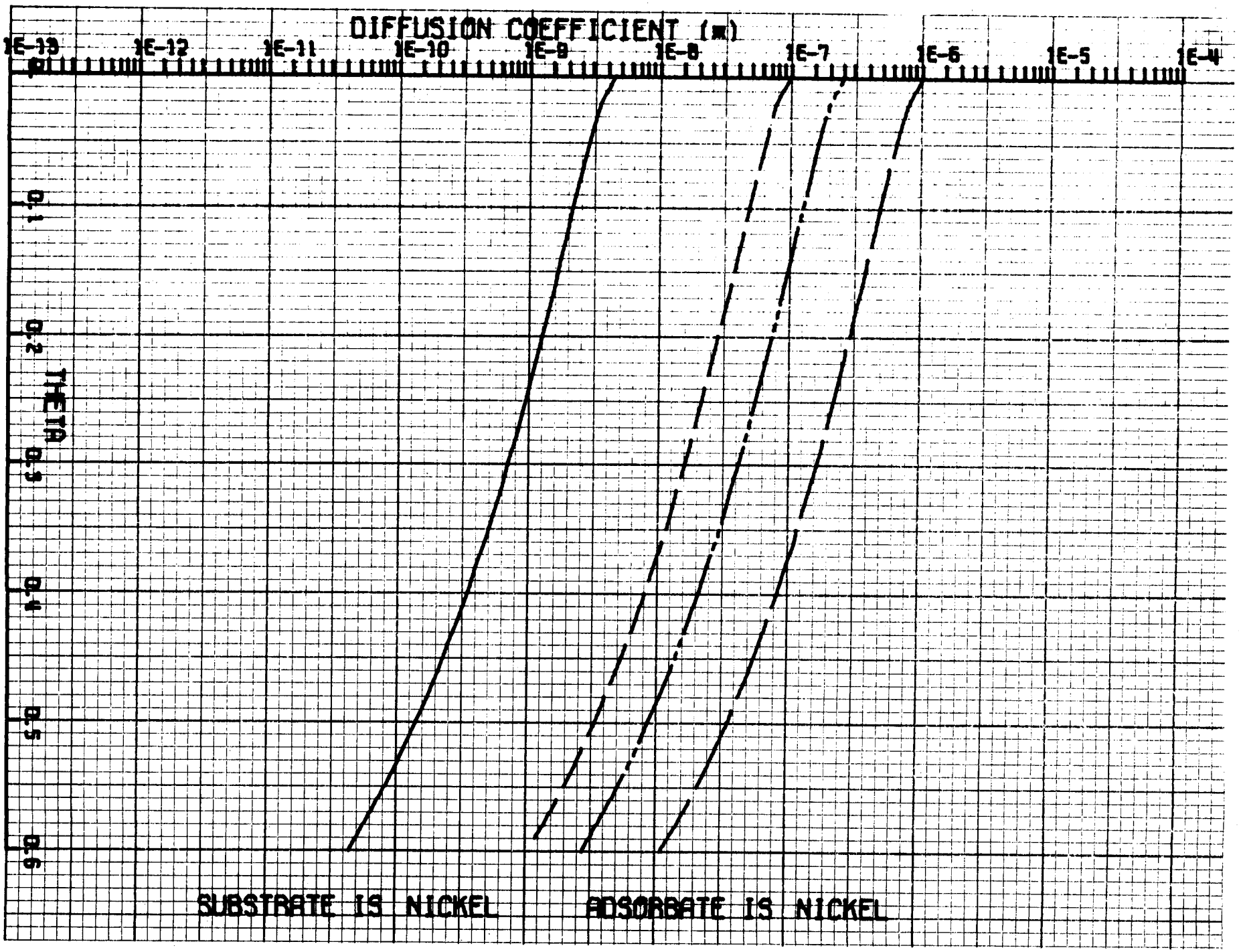
DIFFUSION COEFFICIENT (m)
1E-13
1E-12
1E-11
1E-10
1E-9
1E-8
1E-7
1E-6
1E-5
1E-4
0.1
0.2
THETA
0.3
0.4
0.5
0.6
SUBSTRATE IS NICKEL
ADSORBATE IS NICKEL

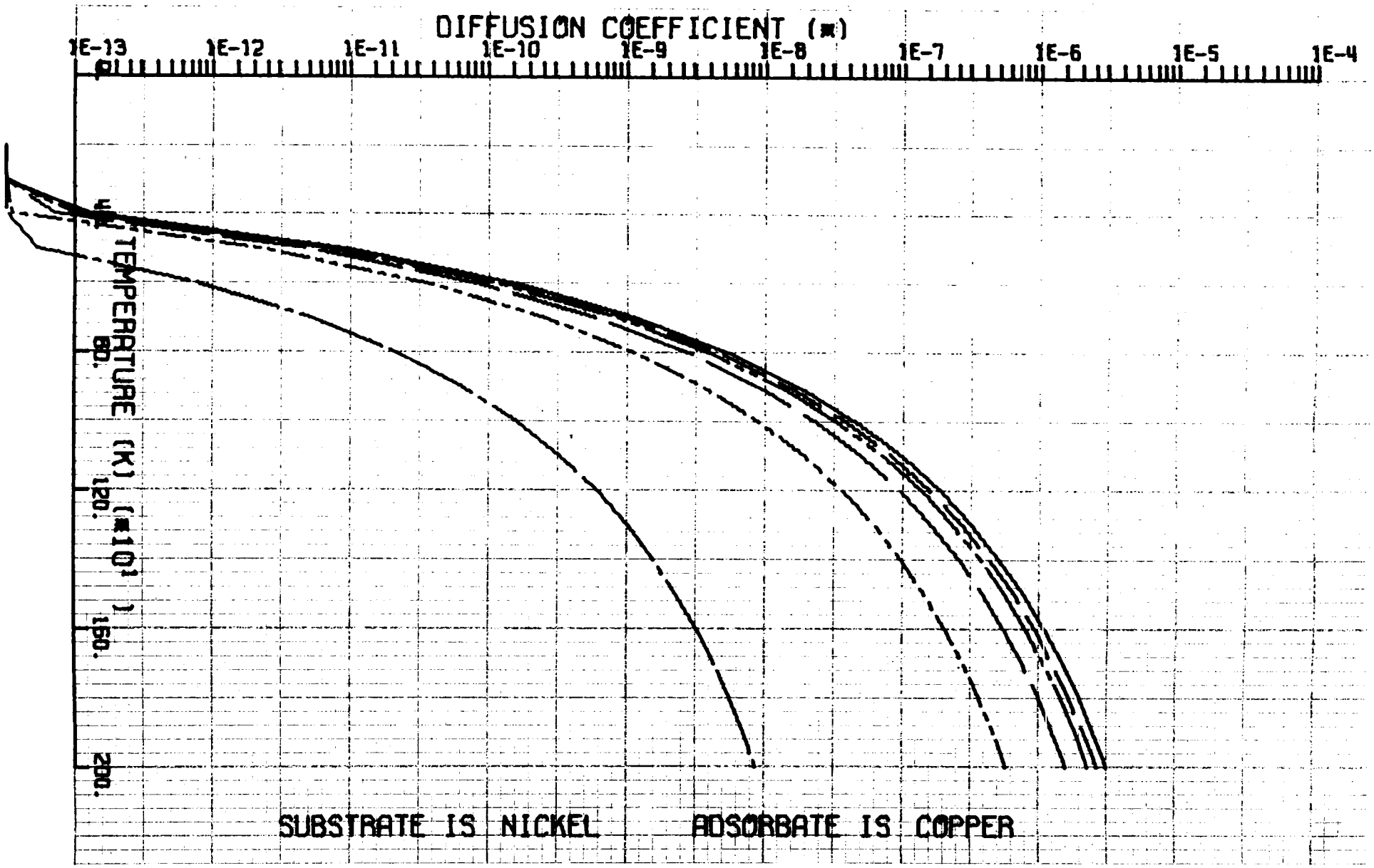
DIFFUSION COEFFICIENT (*)
1E-13
1E-12
1E-11
1E-10
1E-9
1E-8
1E-7
1E-6
1E-5
1E-4
TEMPERATURE (K) (*10¹)
80.
120.
150.
200.
SUBSTRATE IS NICKEL
ADSORBATE IS COPPER

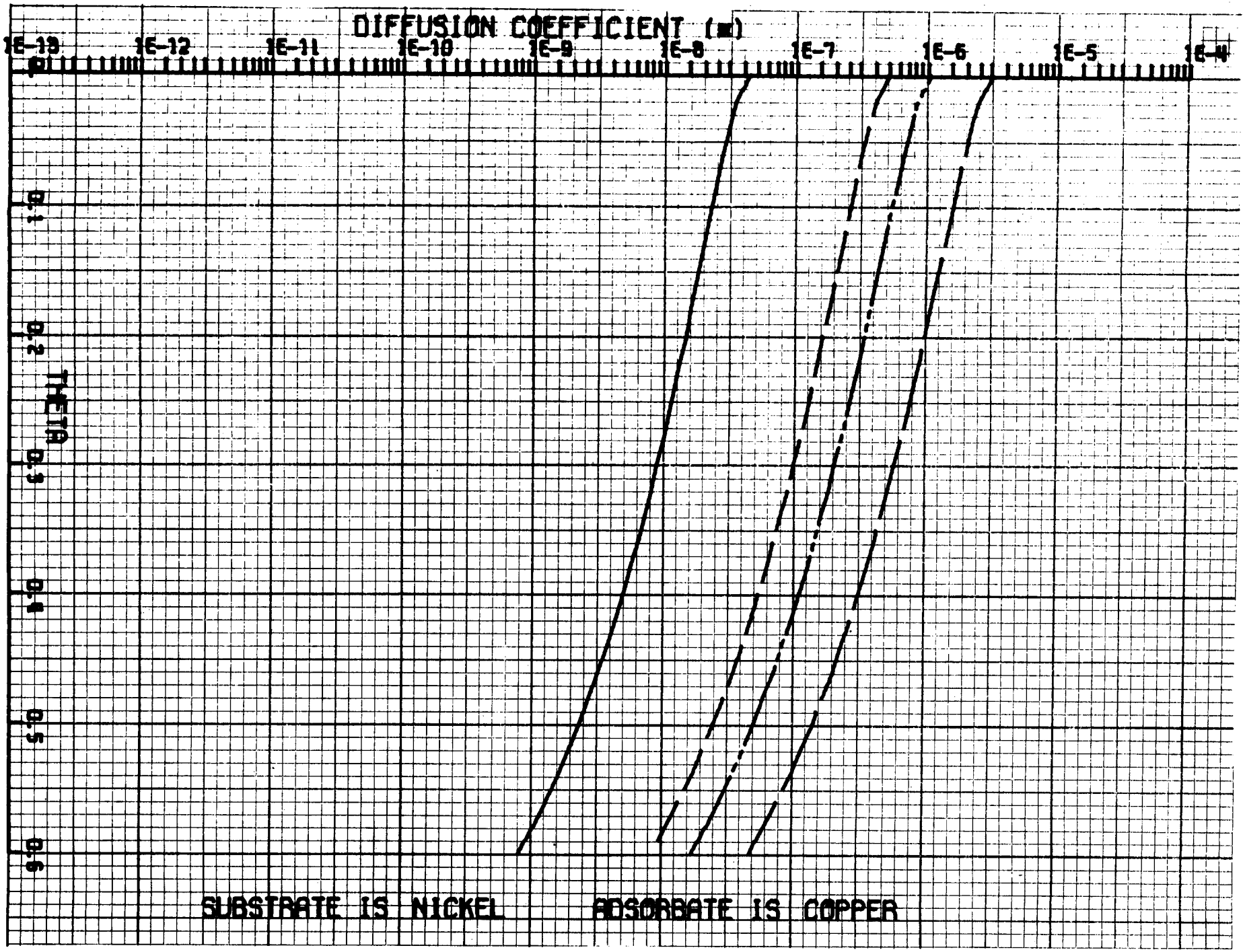
DIFFUSION COEFFICIENT (m)
1E-13
1E-12
1E-11
1E-10
1E-9
1E-8
1E-7
1E-6
1E-5
1E-4
THETA
0.1
0.2
0.3
0.4
0.5
0.6
SUBSTRATE IS NICKEL
ADSORBATE IS COPPER

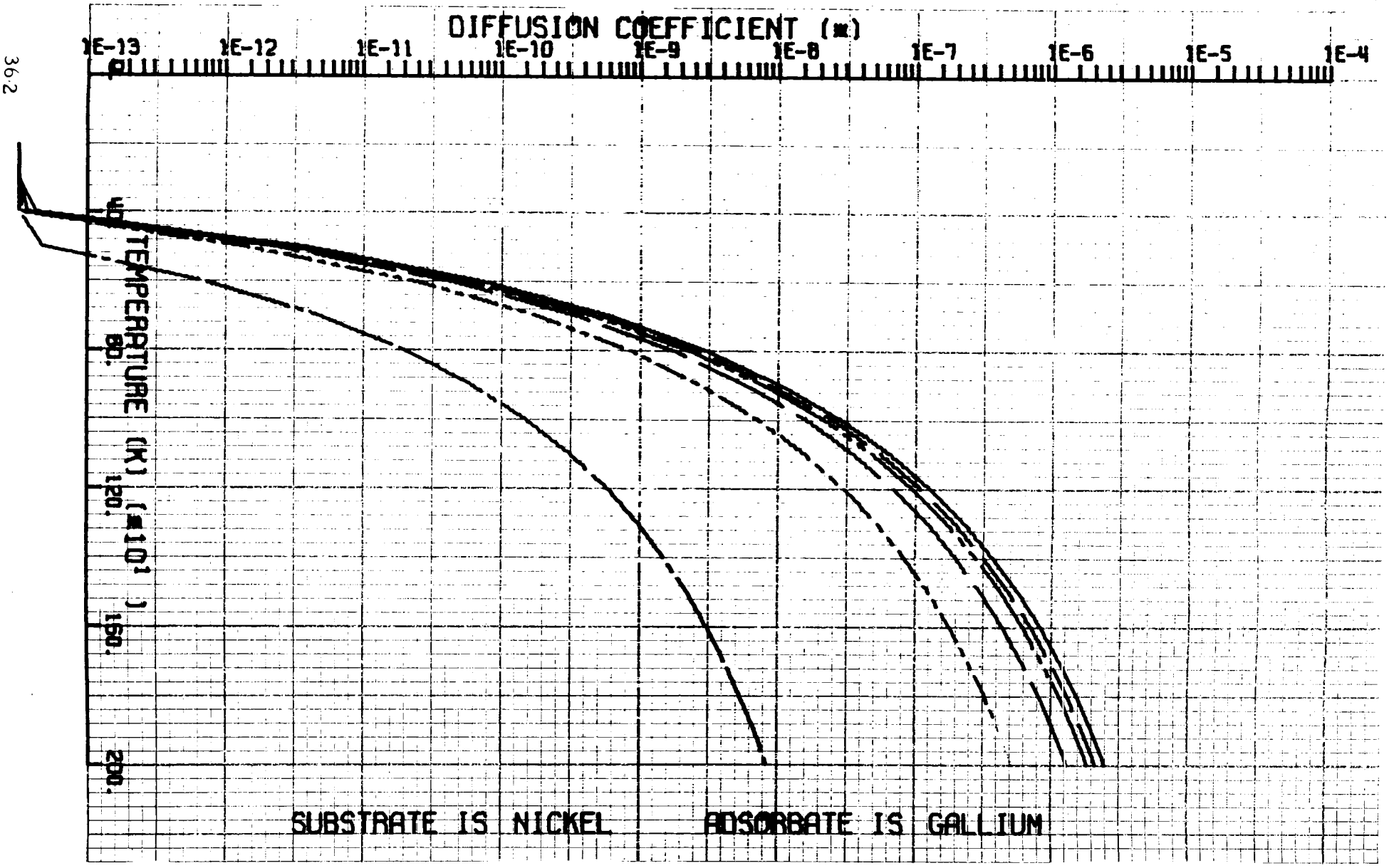
DIFFUSION COEFFICIENT (*)
1E-13
1E-12
1E-11
1E-10
1E-9
1E-8
1E-7
1E-6
1E-5
1E-4
TEMPERATURE (K) (*10^1)
40.
80.
120.
160.
200.
SUBSTRATE IS NICKEL
ADSORBATE IS GALLIUM

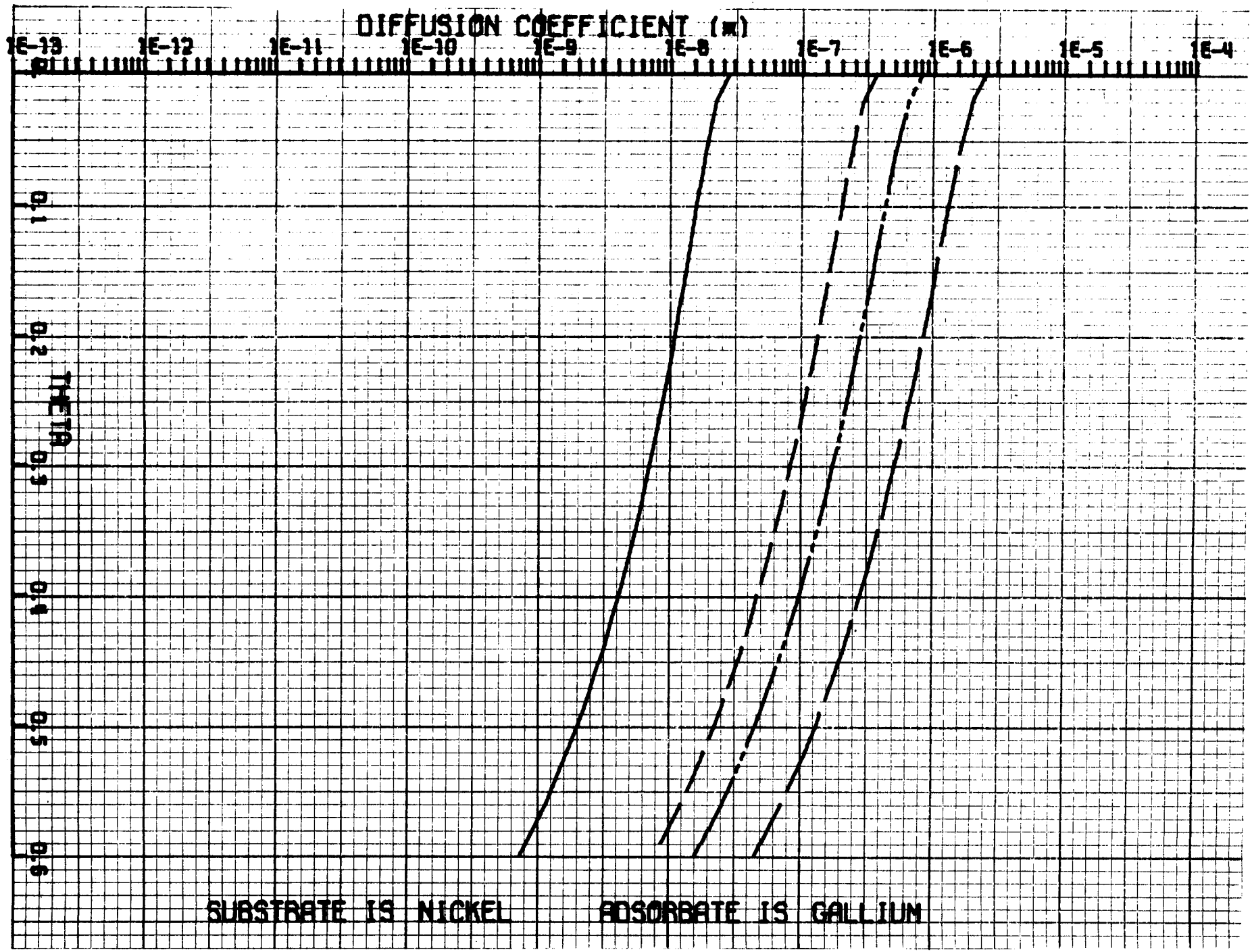
DIFFUSION COEFFICIENT (m)
1E-13
1E-12
1E-11
1E-10
1E-9
1E-8
1E-7
1E-6
1E-5
1E-4
0.1
0.2
0.3
0.4
0.5
0.6
THETA
SUBSTRATE IS NICKEL
ADSORBATE IS GALLIUM

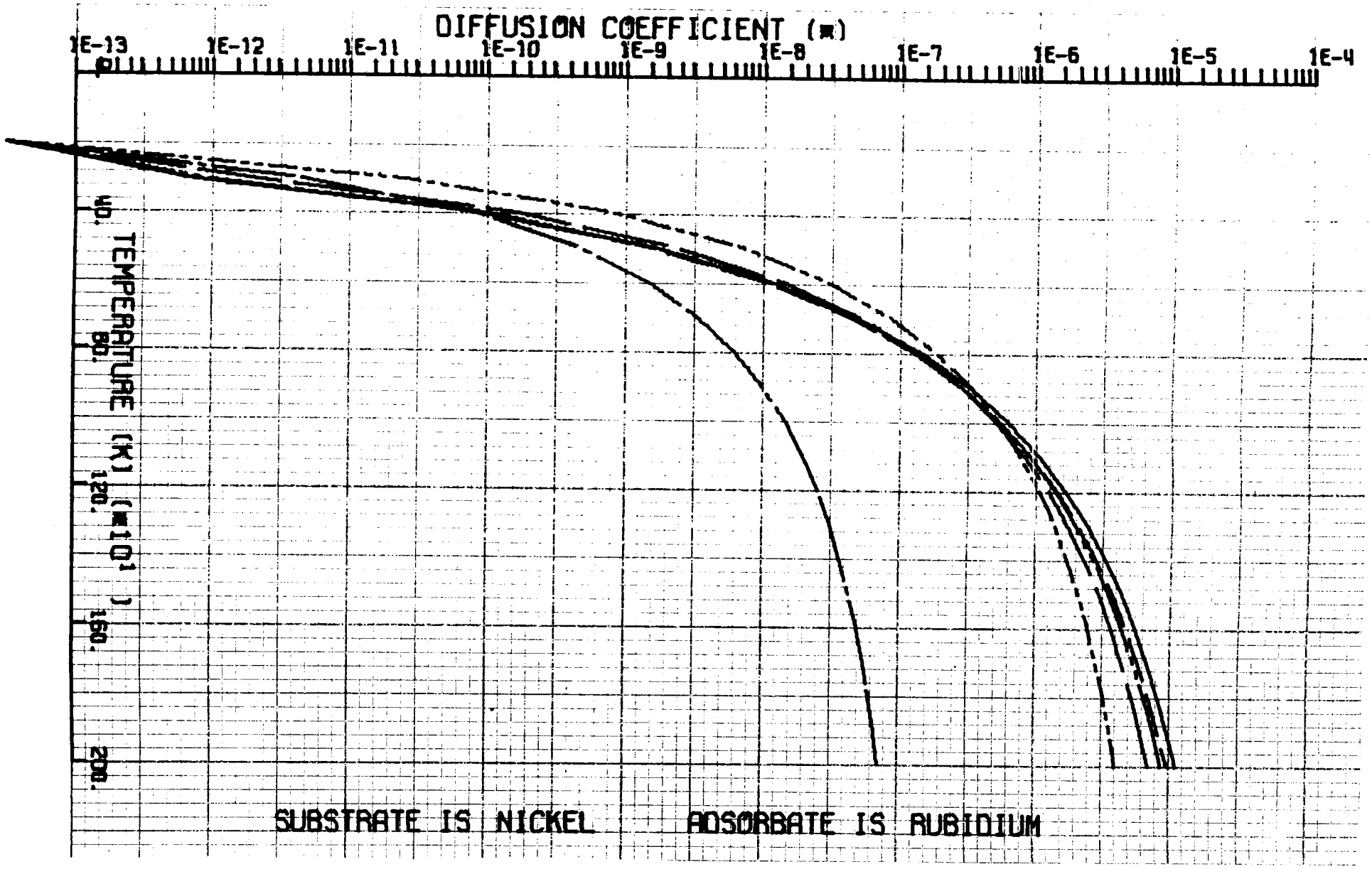
DIFFUSION COEFFICIENT (m)
1E-13
1E-12
1E-11
1E-10
1E-9
1E-8
1E-7
1E-6
1E-5
1E-4
40.
TEMPERATURE (K) (m10¹)
80.
120.
160.
200.
SUBSTRATE IS NICKEL
ADSORBATE IS RUBIDIUM

DIFFUSION COEFFICIENT (Dm)
1E-4
1E-5
1E-6
1E-7
1E-8
1E-9
1E-10
1E-11
1E-12
1E-13
0.1
0.2
0.3
0.4
0.5
0.6
THETA
SUBSTRATE IS NICKEL
ADSORBATE IS RUBIDIUM

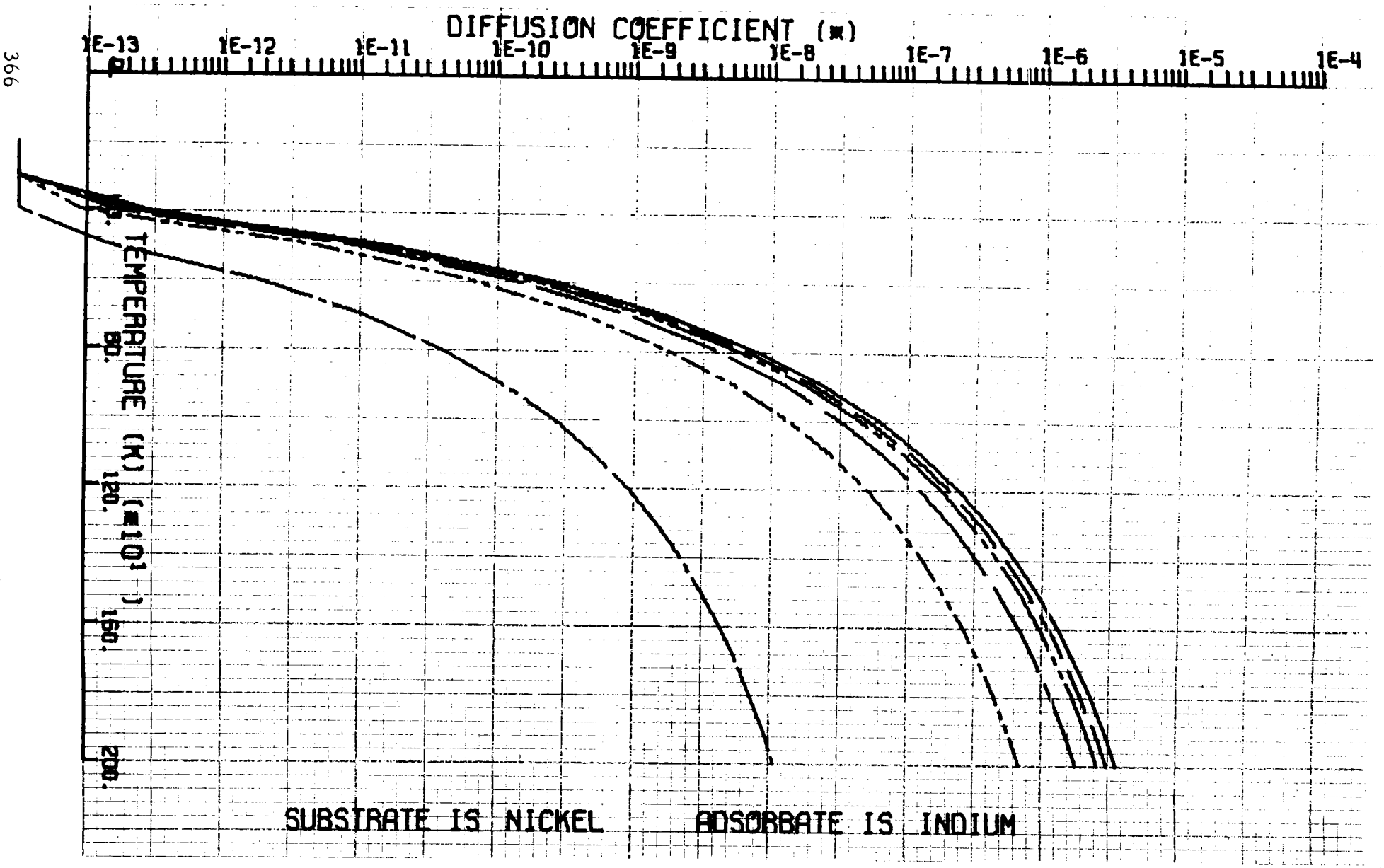
DIFFUSION COEFFICIENT (*)
1E-13
1E-12
1E-11
1E-10
1E-9
1E-8
1E-7
1E-6
1E-5
1E-4
TEMPERATURE (K) (*10¹)
80.
120.
160.
200.
SUBSTRATE IS NICKEL
ADSORBATE IS INDIUM

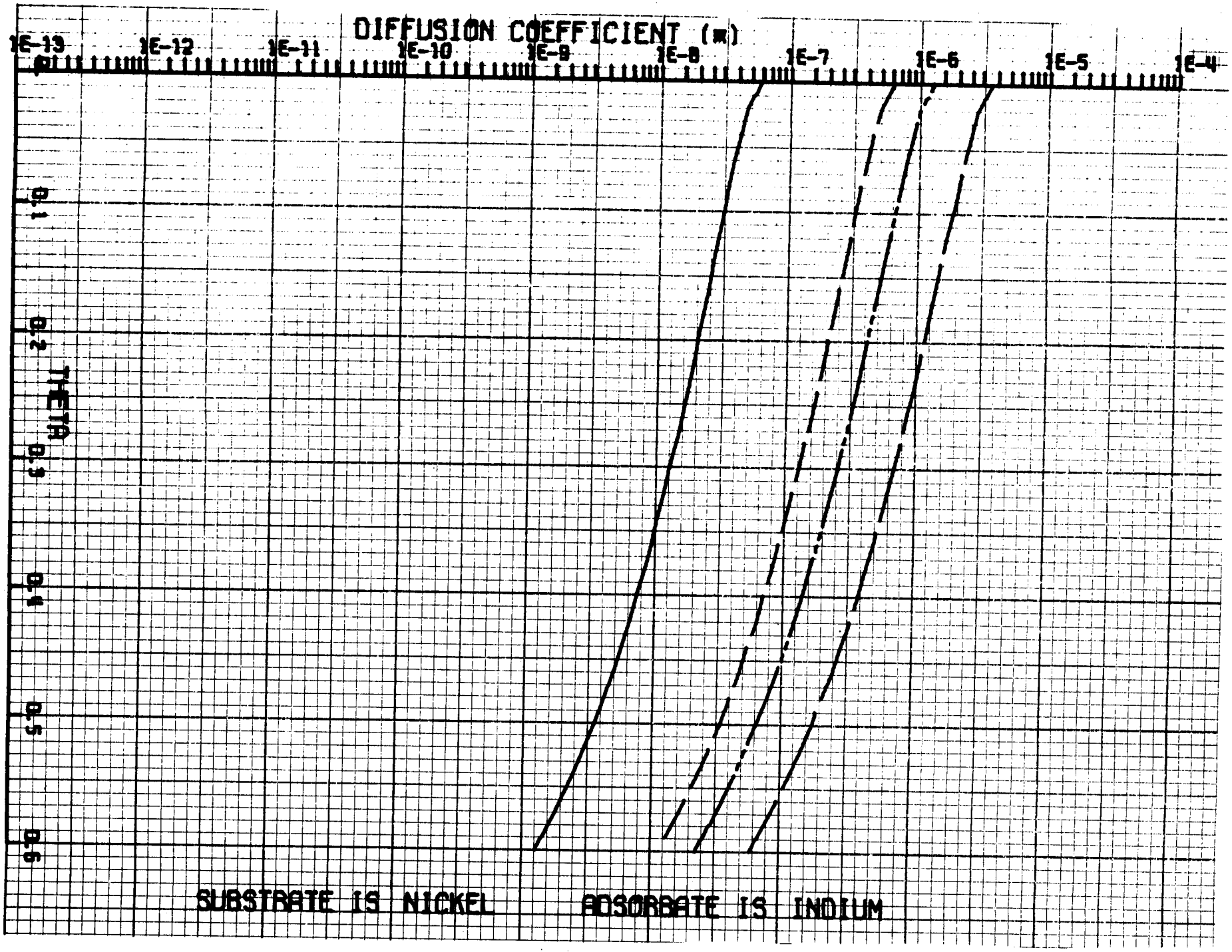
DIFFUSION COEFFICIENT (m)
1E-13
1E-12
1E-11
1E-10
1E-9
1E-8
1E-7
1E-6
1E-5
1E-4
THETA
0.1
0.2
0.3
0.4
0.5
0.6
SUBSTRATE IS NICKEL
ADSORBATE IS INDIUM

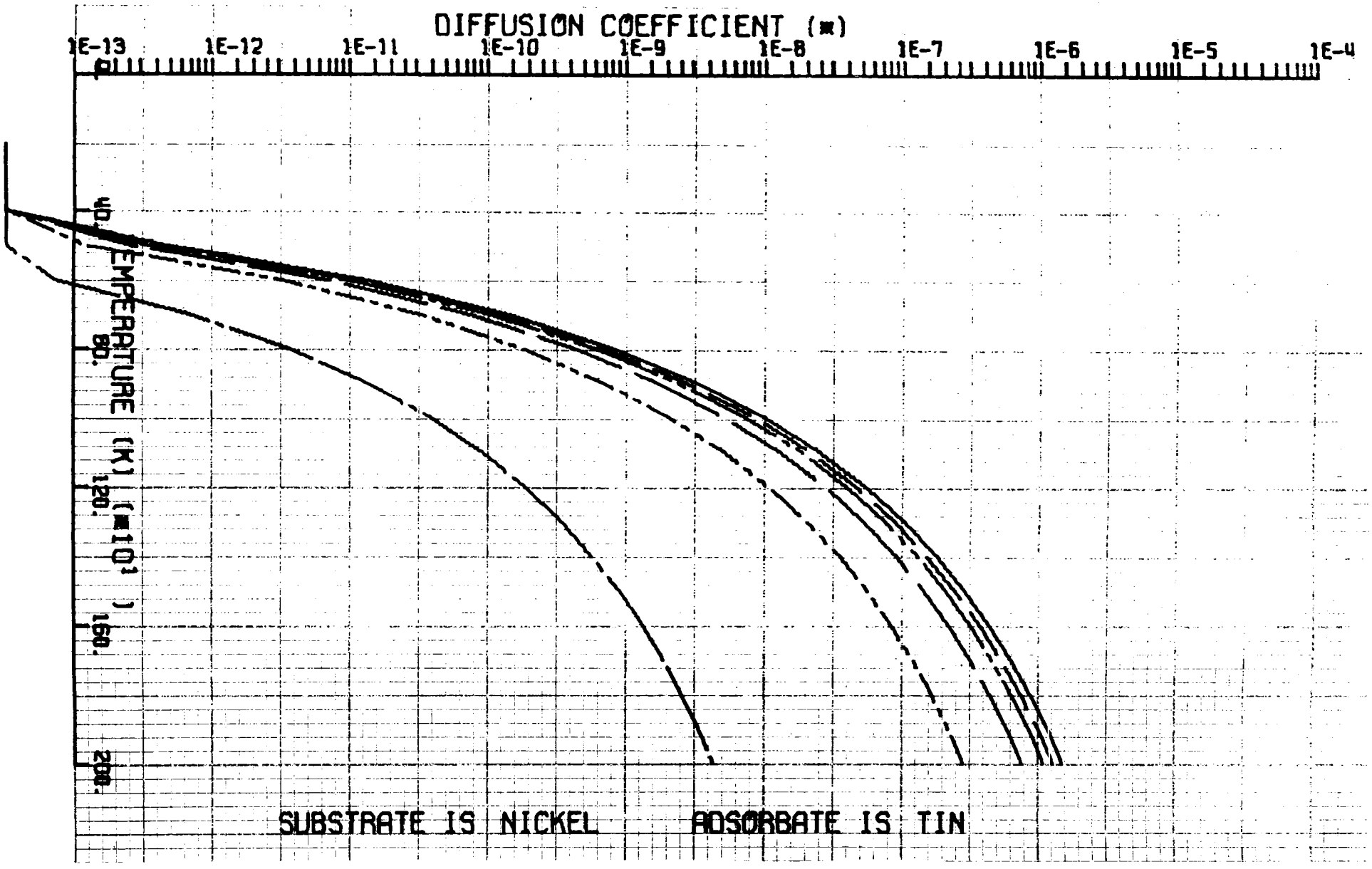
DIFFUSION COEFFICIENT (*)
1E-13
1E-12
1E-11
1E-10
1E-9
1E-8
1E-7
1E-6
1E-5
1E-4
TEMPERATURE (K) (*10)
40.
80.
120.
160.
200.
SUBSTRATE IS NICKEL
ADSORBATE IS TIN

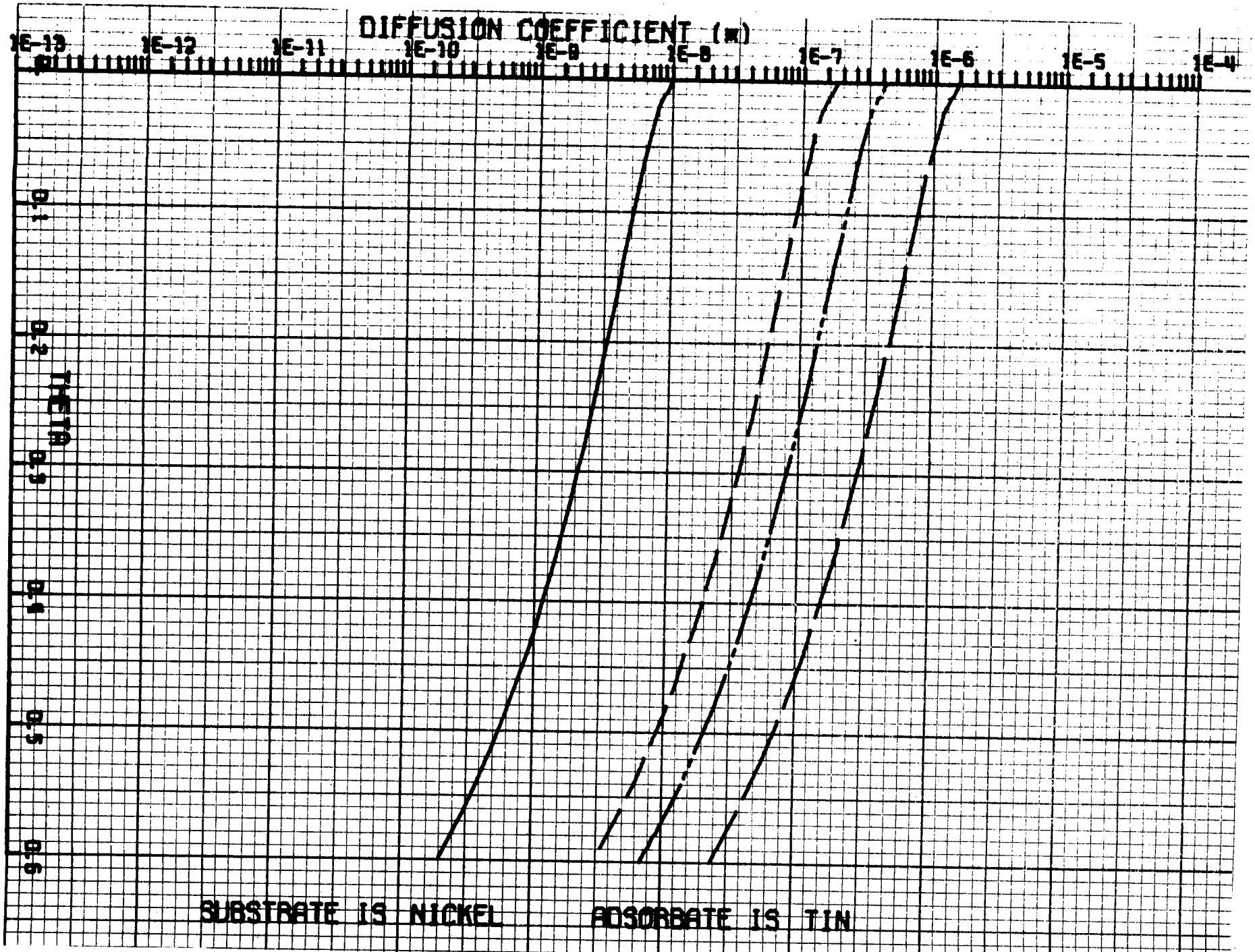
DIFFUSION COEFFICIENT (m)
1E-13
1E-12
1E-11
1E-10
1E-9
1E-8
1E-7
1E-6
1E-5
1E-4
0.1
0.2
0.3
0.4
0.5
0.6
SUBSTRATE IS NICKEL
ADSORBATE IS TIN

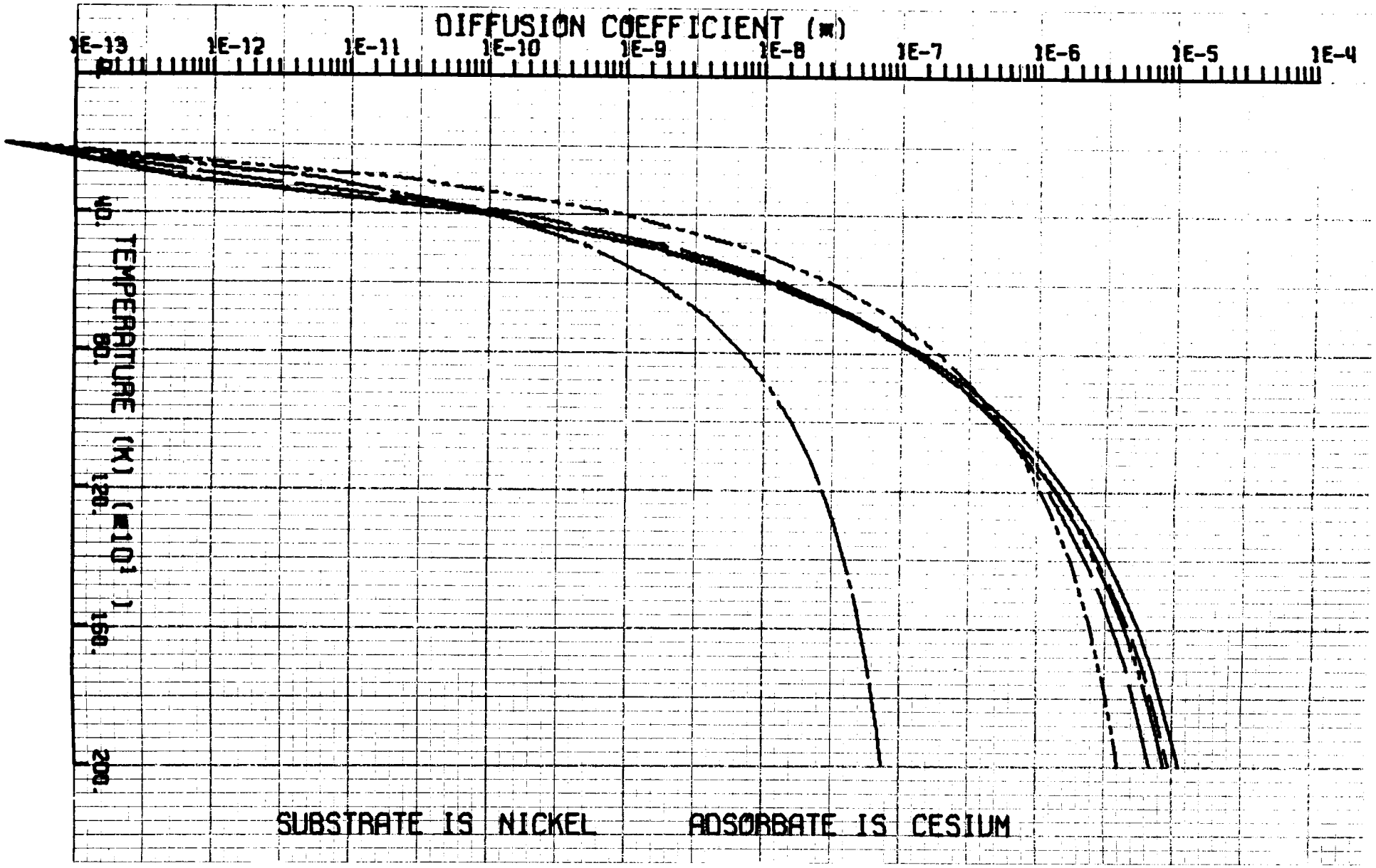
DIFFUSION COEFFICIENT (m)
1E-13
1E-12
1E-11
1E-10
1E-9
1E-8
1E-7
1E-6
1E-5
1E-4
40.
80.
120.
160.
200.
SUBSTRATE IS NICKEL
ADSORBATE IS CESIUM

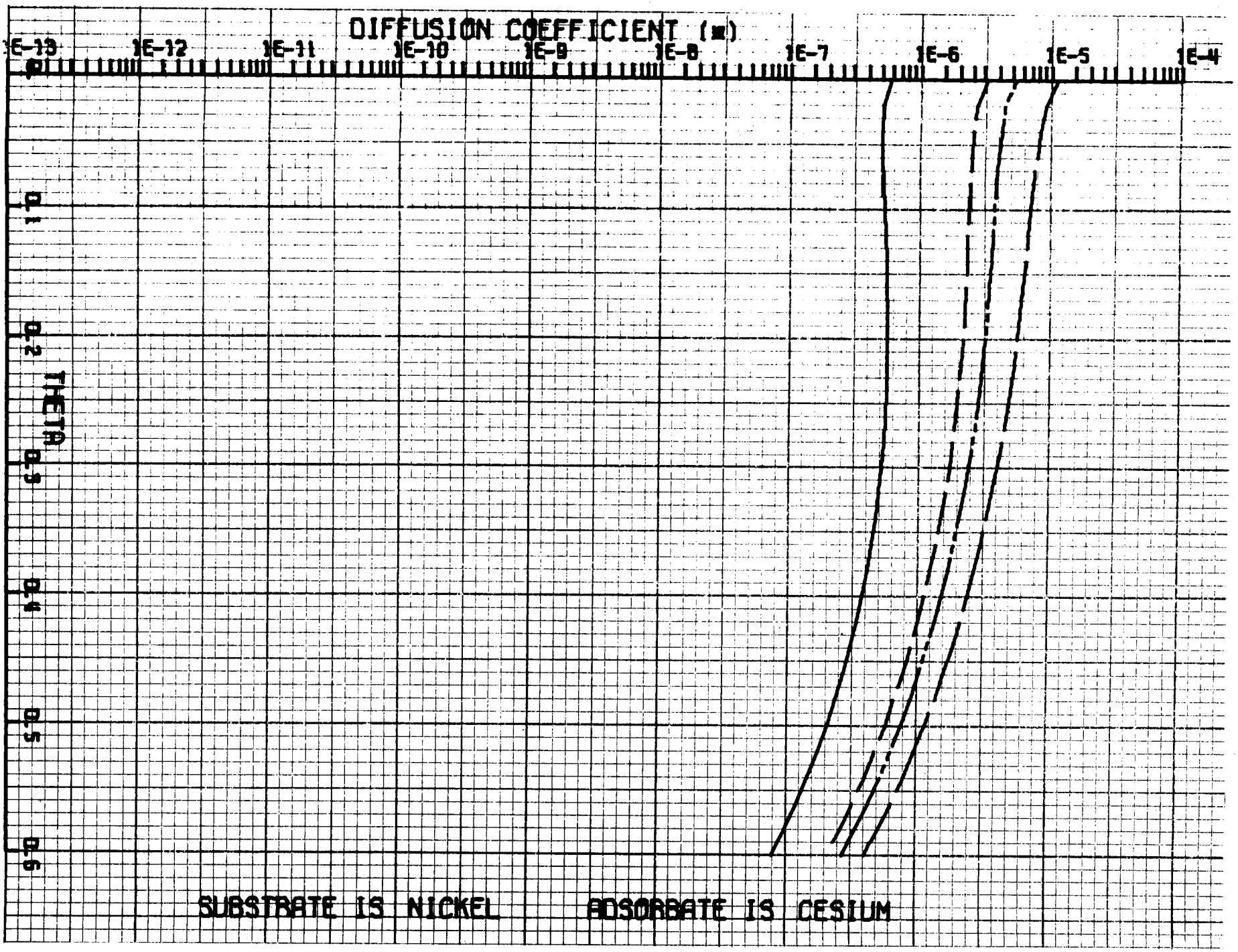
DIFFUSION COEFFICIENT (m)
1E-13
1E-12
1E-11
1E-10
1E-9
1E-8
1E-7
1E-6
1E-5
1E-4
THETA
0.1
0.2
0.3
0.4
0.5
0.6
SUBSTRATE IS NICKEL
ADSORBATE IS CESIUM

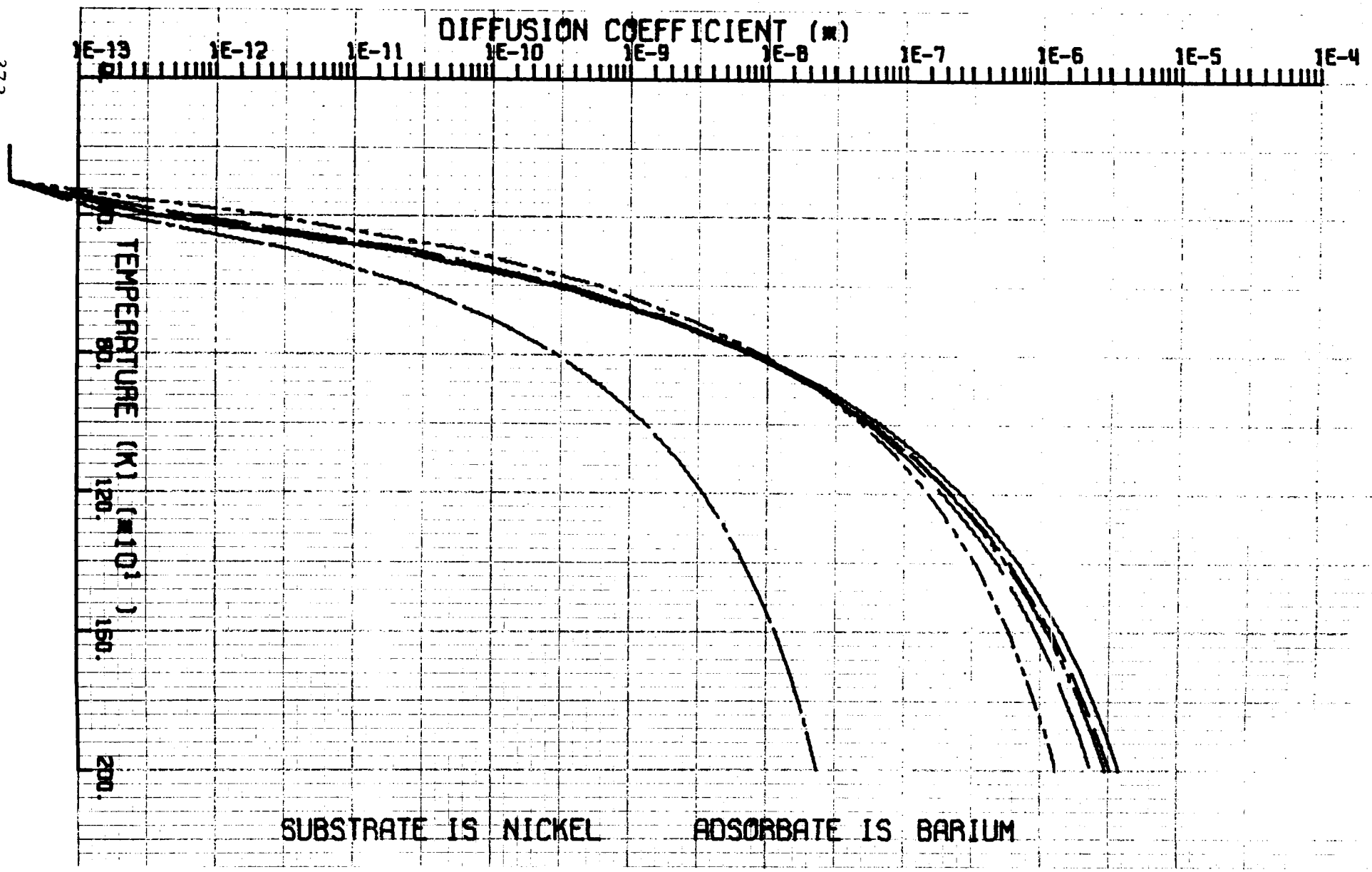
DIFFUSION COEFFICIENT (*)
1E-13
1E-12
1E-11
1E-10
1E-9
1E-8
1E-7
1E-6
1E-5
1E-4
TEMPERATURE (K) (*10¹)
80.
120.
160.
200.
SUBSTRATE IS NICKEL
ADSORBATE IS BARIUM

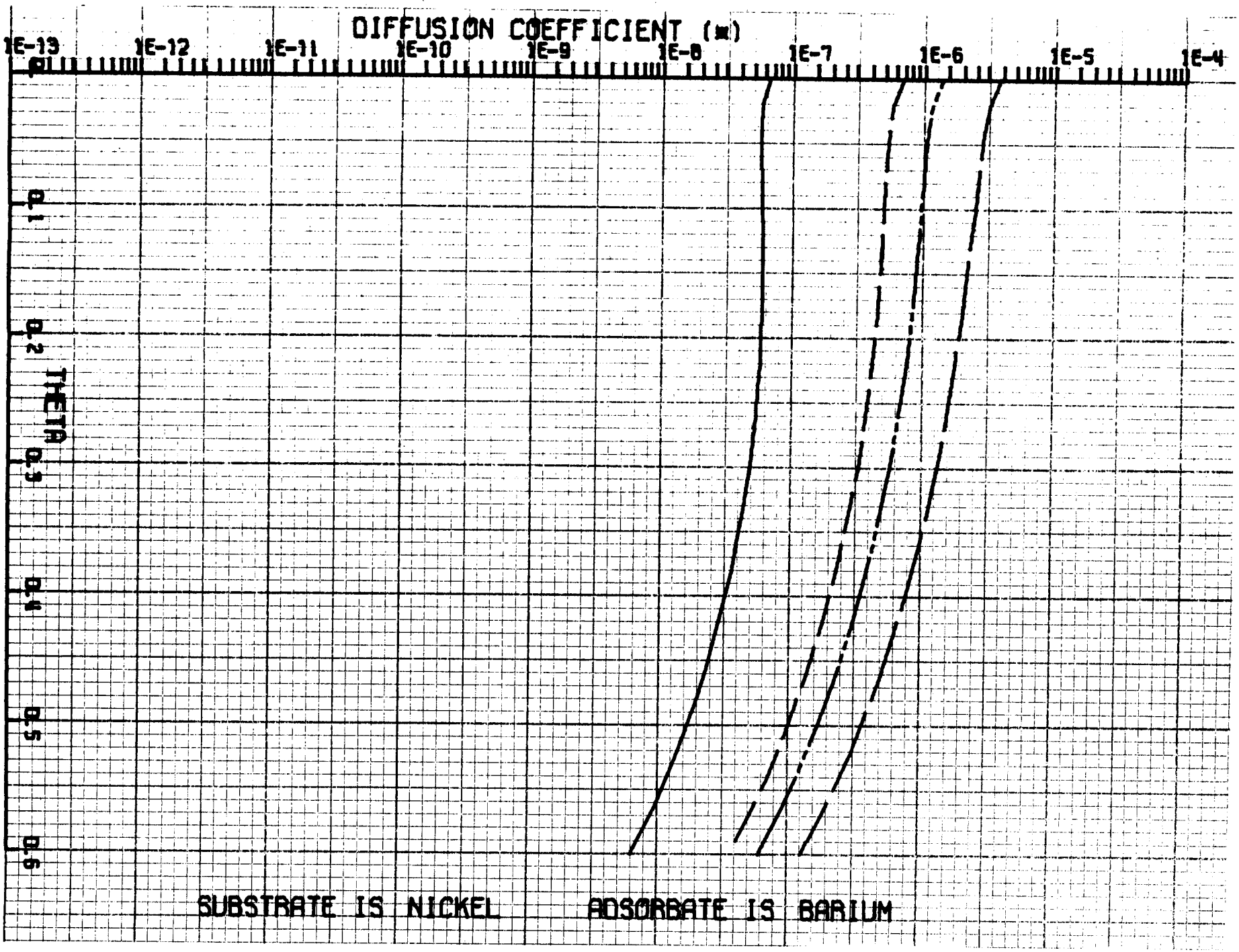
DIFFUSION COEFFICIENT (m)
1E-13
1E-12
1E-11
1E-10
1E-9
1E-8
1E-7
1E-6
1E-5
1E-4
0
0.1
0.2
0.3
0.4
0.5
0.6
THETA
SUBSTRATE IS NICKEL
ADSORBATE IS BARIUM

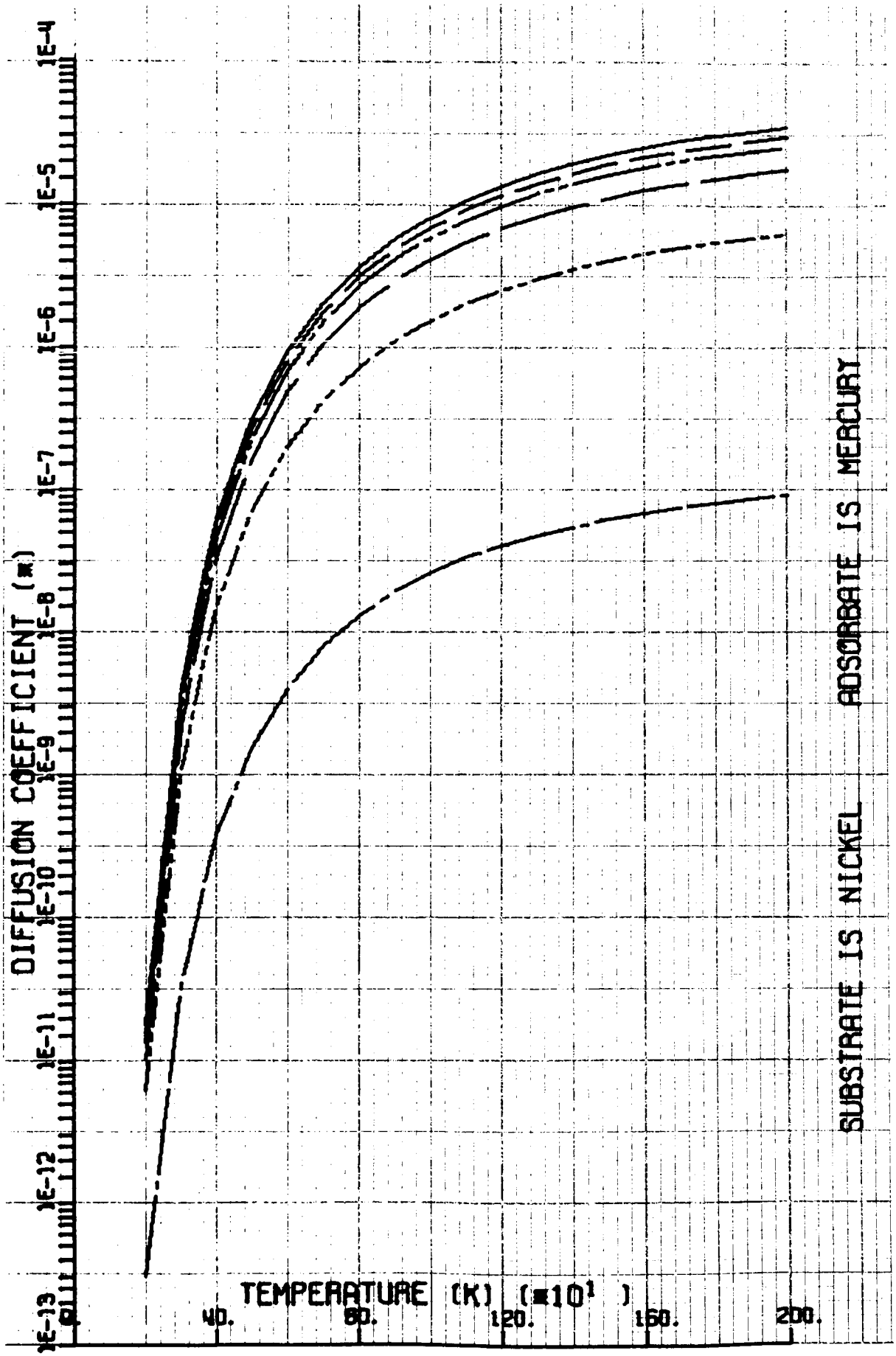
DIFFUSION COEFFICIENT (*)
1E-4
1E-5
1E-6
1E-7
1E-8
1E-9
1E-10
1E-11
1E-12
1E-13
TEMPERATURE (K) (*10^1)
40.
80.
120.
160.
200.
SUBSTRATE IS NICKEL ADSORBATE IS MERCURY

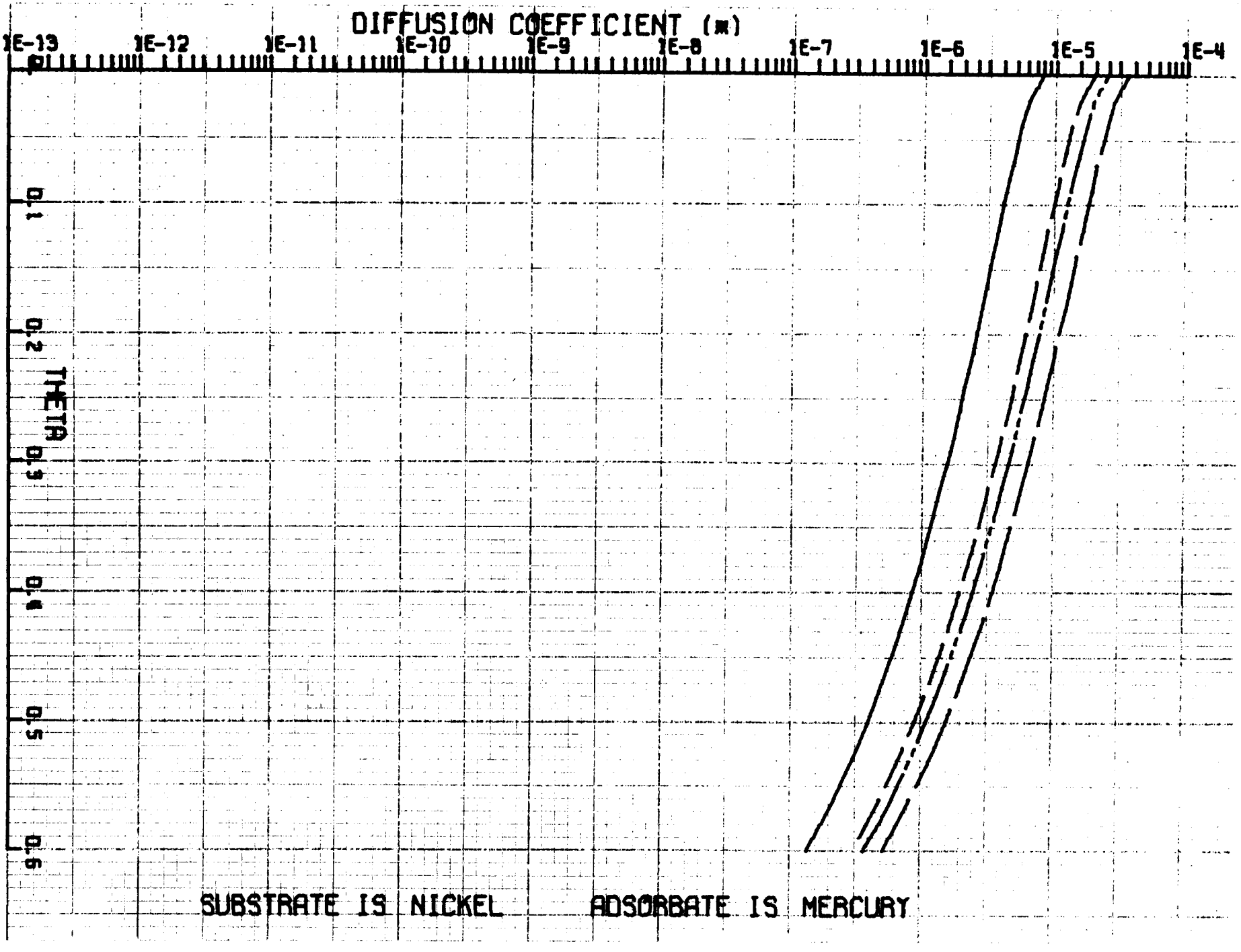
DIFFUSION COEFFICIENT (m)
1E-13
1E-12
1E-11
1E-10
1E-9
1E-8
1E-7
1E-6
1E-5
1E-4
THETA
0.1
0.2
0.3
0.4
0.5
0.6
SUBSTRATE IS NICKEL
ADSORBATE IS MERCURY